



**Photocatalytic Degradation of Pharmaceuticals in
Aqueous Solutions and Development of New Dye
Sensitised Photocatalytic Materials.**

Sharon Murphy (B.Sc.)

**A thesis submitted for the degree of
Doctor of Philosophy**

**Supervised by
Dr. Kieran Nolan
School of Chemical Sciences**

Dublin City University

January 2012

Declaration

I hereby certify that this material, which I now submit for assessment on the programme of study leading to the award of Doctor of Philosophy is entirely my own work, that I have exercised reasonable care to ensure that the work is original, and does not to the best of my knowledge breach any law of copyright, and has not been taken from the work of others save and to the extent that such work has been cited and acknowledged within the text of my work.

Signed: _____

ID No.: 53537102

Date: _____

Dedicated to the best Mum ever xxx

“What we have learned from others becomes our own reflection.”

Ralph Waldo Emerson

“You must be the change you want to see in the world”

Gandhi

Acknowledgements

Firstly, massive thanks are due to my supervisor Dr. Kieran Nolan. Kieran has been committed to my work at every stage, and changed my way of thinking about problems (of any kind) and ways of solving them. I really could not have completed this work without his vast knowledge, experience, wisdom, and immense positivity!

I would also like to thank my examiners Dr. Blánaid White and Dr. Leon Barron for their advice regarding corrections which I feel improved not only the thesis, but will also assist me greatly in my future endeavours! Sincere thanks are extended to the amazing NCSR technicians Maurice Burke and Stephen Fuller. Thanks also to all staff of the school of chemical sciences including all of the amazing technicians whom are the glue that holds the place together!

Thanks to all my colleagues in X249: especially Kieran, Declan, Brian and the previous members of our group Emma and Sonia who offered me much help, advice and alcohol when it was needed. Thanks to all my past visiting students (apprentices!): Juliana, Diego, Anais, David and Carla. Thanks also to Debbie, Áine, Donnack, Christopher, Melody, Kim, Mary, Ana, Ubaldo, Denis and Nadia for being great friends and for the many needed laughs throughout this experience! Thanks also to Rosemarie for the endless support, and amazing experiences we have shared for the last 8 years. You have been the greatest friend and I don't think you realise how much you have influenced my life in such a positive way, so thank you so much. Nora, thanks so much for everything: the amazing coffees, the nights out, the chats, the shopping trips and for the many laughs we have had over the years together. Thanks for always being there for me too.

Thanks so much to my dad for the calls, and the support. It was so nice to confide in a family member who was also trying to write a thesis. Thanks also so much for supplying me with a laptop to finish this work and for being there always. I love my family so much and could not have come this far without their support not only throughout this process but throughout my life. Mum and Tom thanks for believing in me, always thinking of me and helping me in every way you could. Thanks to my sisters Tamara and Thea and my brother Tom Jr. I have really enjoyed seeing you all grow up and spending time with you (it was such a welcome distraction to this PhD). You are such great people and I love you all so so much. I owe a significant amount of gratitude to Jamie. He has been a best friend, colleague, housemate and partner throughout this whole experience. Not only has he mastered all these roles but also achieved a PhD while being there for me with mine. Thank you for all your advice, love, respect, challenges, laughs etc. (I could write another thesis here...) so just thank you for everything.

Table of Contents

	<u>Page</u>
Declaration.....	I
Dedication.....	II
Acknowledgements.....	IV
Table of Contents.....	V
List of Conferences Attended, Poster Presentations and Papers Published/In preparation.....	IX
Abbreviations/ Acronyms/ Symbols.....	XI
Abstract.....	XIV
Chapter 1 - Literature Review.....	1
1.0 Introduction: Pharmaceuticals in the Environment.....	2
1.1 Current and Potential Methods for Removal of Pharmaceuticals.....	4
1.2 Advanced Oxidation Processes (AOPs).....	6
1.3 Heterogeneous Photocatalysis.....	11
1.4 Titanium Dioxide.....	16
1.5 Optimising the Photocatalytic Process.....	23
1.6 Literature Concerning the Pharmaceuticals Targets in this Work.....	26
1.7. Project Proposal.....	29
1.8 Thesis Outline.....	30
Chapter 2 - Experimental.....	32
2.1 General.....	33
2.2 Chromatographic Methods.....	34
2.3: Chapter 3: Photolytic and Photocatalytic Degradation Studies with Famotidine, Tamsulosin and Solifenacin.....	35
2.4: Chapter 4: Intermediate Analysis and Elucidation of Degradation Mechanism for Famotidine, Tamsulosin and Solifenacin.....	41
2.5: Chapter 5: Development and Characterisation of Visible Light Sensitised Photocatalytic Materials and Evaluation of their Photocatalytic Activity with Famotidine.....	42
Chapter 3 - Photolytic and Photocatalytic Degradation Studies of Famotidine, Tamsulosin and Solifenacin with TiO₂.....	51
3.1 Introduction.....	52
3.2 Results and Discussion.....	54
Heterogeneous Photocatalysis Part I: Famotidine.....	54
3.2.1 UV-vis Studies.....	54

3.2.2 Quartz Glassware: Photolysis Studies.....	55
3.2.3 Quartz Glassware: Photocatalysis Studies	56
3.2.4 Alternative Reactor Studies.....	57
3.2.5 Pyrex Glassware: Photolysis Studies.....	58
3.2.6 HPLC Analysis of Photolysis Studies.....	58
3.2.7 Famotidine Heterogeneous Photocatalysis: Pyrex.....	59
3.2.8 Famotidine Heterogeneous Photocatalysis: TiO ₂ Optimisation.....	60
3.2.9 Famotidine pH Adjustment Studies	63
3.2.10 Famotidine Hydrogen Peroxide Addition: P-25 TiO ₂	70
3.2.11 Adsorption Studies: Glassware and TiO ₂	76
3.2.12 Famotidine Concentration Variation Studies.....	78
3.2.13 Famotidine Heterogeneous Photocatalytic Degradation Conclusions.....	79
Heterogeneous Photocatalysis Part II: Tamsulosin.....	79
3.2.14 UV-vis Studies.....	79
3.2.15 Quartz Glassware: Photolysis Studies.....	80
3.2.16 Quartz Glassware: Photocatalysis Studies.....	81
3.2.17 Pyrex Glassware: Photolysis Studies.....	82
3.2.18 HPLC Analysis of Photolysis Studies.....	83
3.2.19 Tamsulosin Heterogeneous Photocatalysis: Pyrex.....	83
3.2.20 Tamsulosin Heterogeneous Photocatalysis: TiO ₂ Optimisation.....	84
3.2.21 Tamsulosin pH Adjustment Studies.....	86
3.2.22 Tamsulosin Hydrogen Peroxide Addition: P-25 TiO ₂	88
3.2.23 Adsorption Studies: Glassware	93
3.2.24 Tamsulosin Concentration Variation Studies.....	93
3.2.25 Tamsulosin Heterogeneous Photocatalytic Degradation Conclusions.....	93
Heterogeneous Photocatalysis Part III: Solifenacin.....	94
3.2.26 UV-vis Studies.....	94
3.2.27 Quartz Glassware: Photolysis Studies.....	95
3.2.28 Quartz Glassware: Photocatalysis Studies.....	96
3.2.29 Pyrex Glassware: Photolysis Studies.....	97
3.2.30 HPLC Analysis of Photolysis Studies.....	98
3.2.31 Solifenacin Heterogeneous Photocatalysis: Pyrex.....	98
3.2.32 Solifenacin Heterogeneous Photocatalysis: TiO ₂ Optimisation.....	100
3.2.33 Solifenacin pH Adjustment Studies.....	102
3.2.34 Solifenacin Hydrogen Peroxide Addition: P-25 TiO ₂	103
3.2.35 Adsorption Studies: Glassware.....	105
3.2.36 Solifenacin Concentration Variation Studies.....	107

3.2.37 Solifenacin Heterogeneous Photocatalytic Degradation Conclusions.....	107
Chapter 4 - Intermediate Analysis and Elucidation of Degradation Mechanisms for Famotidine, Tamsulosin and Solifenacin	109
4.1 Introduction.....	110
4.2 Results and Discussion.....	110
4.2.1 LC-MS/MS Method Transfer and Re-optimisation.....	110
4.2.2 Molecular Oxidation Analysis.....	113
4.2.3 Direct Infusion Mass Spectrometry Studies: Famotidine.....	114
4.2.4 Follow-Up Direct Infusion Mass Spectrometry Studies: Famotidine.....	119
4.2.5 LC-MS/MS Studies and Intermediate Analysis: Famotidine.....	122
4.2.6 Ions which could not be Elucidated.....	137
4.2.7 Famotidine Proposed Intermediates Structures Conclusions.....	141
4.2.8 Direct Infusion Mass Spectrometry Studies: Tamsulosin.....	144
4.2.9 Follow-Up Direct Infusion Mass Spectrometry Studies: Tamsulosin.....	147
4.2.10 LC-MS/MS Studies and Intermediate Analysis: Tamsulosin.....	148
4.2.11 Ions which could not be Elucidated.....	172
4.2.12 Tamsulosin Proposed Intermediates Structures.....	176
4.2.13 Direct Infusion Mass Spectrometry Studies: Solifenacin.....	179
4.2.14 Follow-Up Direct Infusion Mass Spectrometry Studies: Solifenacin.....	182
4.2.15 LC-MS/MS Studies and Intermediate Analysis: Solifenacin.....	183
4.2.16 Ions which could not be Elucidated.....	211
4.2.17 Solifenacin Proposed Intermediates Structures.....	213
4.2.18 Control Experiments.....	216
4.2.19 LC-MS/MS Analysis of the Optimised TiO ₂ /UV/H ₂ O ₂ Process.....	216
4.2.20 Intermediate Studies Conclusions.....	217
Chapter 5 - Development and Characterisation of Visible Light Sensitised Photocatalytic Materials and Evaluation of their Photocatalytic Activity with Famotidine	218
5.1 Introduction.....	219
5.2 Results and Discussion.....	220
5.2.1 Synthesis of TCPP-TiO ₂	220
5.2.2 Characterisation of TCPP-TiO ₂	221
5.2.3 Examination of the Photocatalytic Efficiency of TCPP-TiO ₂ in Famotidine Degradation with Visible Light.....	225
5.2.4 Synthesis of Zn-Hexadecafluorophthalocyanine-TiO ₂	236
5.2.5 Characterisation.....	237

5.2.6 Examination of the Photocatalytic Efficiency of ZnHFphthalocyanine-TiO ₂ in Famotidine Degradation with Visible Light.	239
5.2.7 Preparation of 1,4-(tetrabenzaldehyde)phthalocyanine-TiO ₂	241
5.2.8 Characterisation.....	242
5.2.9 Examination of the Photocatalytic Efficiency of β-(tetrabenzaldehyde)-phthalocyanine-TiO ₂ in Famotidine Degradation with Visible Light.	245
5.2.10 Synthesis of Acetylacetonate linker (3-[4-benzoic acid] pentane-2,4-dione)....	246
5.2.11 Immobilisation onto TiO ₂	246
5.2.12 Synthesis of TDI-TiO ₂	246
5.2.13 Characterisation of TDI-TiO ₂	247
5.2.14 Synthesis of APS-TiO ₂	248
5.2.15 Characterisation of APS-TiO ₂	248
5.2.16 Visible Light Sensitised Photocatalyst Development Conclusions.....	251
Chapter 6 - Thesis Conclusions and Future Work.....	253
References.....	258
Appendices.....	A1

List of Conferences attended, Poster presentations and Papers Published/In preparation

(Presenters starred)

International Conferences

Oxidation Technologies for Water and Wastewater Treatment AOP5 (5th IWA Specialist Conference / 10th IOA-EA3G-Conference) (Attendance Only) 30th March- 3rd April 2009 Berlin, Germany.

S. Murphy*, M. Oelgemöller, J. Tobin, A. Morrissey, K. Nolan "Photocatalytic Degradation of Pharmaceuticals in Aqueous Solutions" *Journées Européennes de la Photocatalyse (JEP)* 22-23rd September 2009, Bordeaux, France.

S. Murphy*, M. Oelgemöller, J. Tobin, A. Morrissey, K. Nolan "Photocatalytic Degradation of Pharmaceuticals in Aqueous Solutions" *CECP*, 7-11th February 2010 Bad Hofgastein, Austria.

Local Conferences

M. Cullen*, A. Deegan*, C. Lacey, S. Murphy*, A. Morrissey, M. Oelgemöller, J. Tobin "Pharmaceuticals in the Aquatic Environment" *ENVIRON* (DkIT) 1- 3rd February 2008, Dundalk, Ireland.

K. Joyce*, S. Murphy*, M. Oelgemöller "Green Photochemistry: From the Synthesis of Fine Chemicals to Water Treatment with Sunlight" EPA conference, Royal Hospital Kilmainham, 6th-7th February 2008, Dublin, Ireland.

S. Murphy, A. Deegan, M. Cullen, C. Lacey, A. Morrissey, M. Oelgemöller*, J. Tobin "Green Photochemistry" Detection and Sustainable Degradation of Pharmaceuticals" *Challenge of Sustainability Conference*, 20th June 2008, Dundalk (DkIT), Ireland.

S. Murphy*, M. Oelgemöller, J. Tobin, A. Morrissey, K. Nolan "Photocatalytic Degradation of Pharmaceuticals in Aqueous Solutions" *ENVIRON* (WIT) 15-17th January 2009, Waterford, Ireland.

S. Murphy*, M. Oelgemöller, J. Tobin, A. Morrissey, K. Nolan "Photocatalytic Degradation of Pharmaceuticals in Aqueous Solutions" SCI Green Chemistry Helix, DCU April 2010.

Colloquia

S. Murphy*, K. Nolan, A. Morrissey, J. Tobin, M. Oelgemöller "Water Treatment with Light: Photochemical Degradation of Pharmaceuticals in the Environment", *60th Irish Universities Chemistry Research Colloquium* (UCC) 11- 13th June 2008, Cork, Ireland.

61st Irish Universities Chemistry Research Colloquium (DIT) (Attendance Only) 17-19th June 2009, Dublin, Ireland.

Publications

Albarelli, J. Q., Santos, D. T., Murphy, S., Oelgemöller, M., (2009) "Use of Ca-Alginate as a Novel Support for TiO₂ Immobilization in Methylene Blue Decolorisation" *Water Science and Technology* 60, 1081-1087.

Murphy, S., Saurel, C., Morrissey, A., Tobin, J., Oelgemöller, M., Nolan, K., (2011) "Photocatalytic Activity of a Porphyrin/TiO₂ Composite in the Degradation of Pharmaceuticals" (*submitted to Applied Catalysis B: Environmental*)

Murphy, S., Oelgemöller, M., Tobin, J., Morrissey, A., Nolan, K., (2012) "Heterogeneous Photocatalytic Degradation of Famotidine in Aqueous Solutions with Suspended TiO₂ and Identification of its Degradation Products" (*in preparation*)

Abbreviations/Acronyms/ Symbols

1,4-TBpc	1,4-tetrabenzaldehyephthalocyanine
^1H NMR	Proton Nuclear Magnetic Resonance
^{13}C NMR	Carbon-13 Nuclear Magnetic Resonance
ACN	Acetonitrile
AOP	Advanced Oxidation Process
API	Active Pharmaceutical Ingredient
As	Asymmetry Factor
A_t/A_0	Absorbance at time(mins)/Absorbance at 0mins
CEC	Commission of the European Communities
CS	Compound Stability Parameter
C_t/C_0	Concentration at time(mins)/Concentration at 0mins
DI-MS	Direct Infusion Mass Spectrometry
DI-MS/MS	Fragmentation of parent ion from DI-MS
DR	Diffuse Reflectance (UV-vis spectroscopy)
DSSCs	Dye Sensitised Solar Cells
e^-	Electron from electron-hole pair
EAC	Extruded Activated Carbon
EDC	Endocrine Disrupting Chemical
EDX	Energy Dispersive X-ray Spectroscopy
EIC	Extracted Ion Current Chromatogram
ESI	Electrospray Ionisation
ESR	Electron Spin Resonance
F.A.	Formic Acid
FAM	Famotidine
FT-IR	Fourier Transform Infrared Spectroscopy
GAC	Granular Activated Carbon
h^+	positive hole from an electron-hole pair
HETP	Height Equivalent Theoretical Plate
HPLC	High Performance Liquid Chromatography
IUPAC	International Union of Pure and Applied Chemistry
k'	Capacity/Retention Factor, $k' = t_R'/t_0$
LC-MS/MS	Liquid Chromatography tandem Mass Spectrometry
LP Hg Lamp	Low Pressure Mercury Lamp
MeOH	Methanol
MO	Metal oxide

MPc	Metal Phthalocyanine
MP Hg Lamp	Medium Pressure Mercury Lamp
MS	Mass Spectrometry
MS/MS	Mass Spectrometry tandem Mass Spectrometry
Mw	Molecular Weight (g/mol)
m/z	Mass to Charge ratio
N	Column Efficiency, $N = 16(t_R/W_b)^2$
NF	Nanofiltration
NHE	Normal Hydrogen Electrode
NSAID	Non-Steroidal Anti-Inflammatory Drug
o	Overlap
PAC	Powdered Activated Carbon
Pc	Phthalocyanine
PCB	Polychlorobiphenyls
PDA	Photo-Diode Array (Detection)
PFP	Pentafluorophenyl
pnd	Present but not a dominant ion
PPCP	Pharmaceutical and Personal Care Products
PZC	Point Zero Charge
R _f	Retention factor
RO	Reverse Osmosis
ROS	Reactive Oxygen Species
RX _{ads}	Adsorbed organic substrate
SA	Sigma-Aldrich TiO ₂
SAT	Soil Aquifer Treatment
SC	Semiconductor
SOL	Solifenacin
TAMS/TAM	Tamsulosin
TIC	Total Ion Current Chromatogram
TDI	Toluenediisocyanate
T _f	Tailing Factor $T_f = W_b/2f$
TLC	Thin Layer Chromatography
TPP	Tetraphenylporphyrin
TCPP	Tetra-(4-carboxyphenyl)porphyrin
t _R	Retention Time
UV	Ultra Violet (Light)
UV-vis	Ultra Violet and Visible (Light)

UV-vis (DR)	Solid state UV-vis analysis
ν	wavenumbers (cm^{-1})
w/v	Weight by volume
ZnHFpc	Zn-hexadecafluorophthalocyanine

Abstract

This research examines the photocatalytic degradation of 3 active pharmaceutical ingredients (APIs) Famotidine (FAM), Tamsulosin Hydrochloride (TAM) and Solifenacin Succinate (SOL) using TiO_2 and UV light. Photocatalytic degradation studies were monitored with individual HPLC-PDA methods which were developed and validated. The optimum concentration of TiO_2 to treat 0.32 L of 0.083 mM drug solution was found to be 0.1 g or 0.2 g, and all three pharmaceuticals could be appreciably degraded within the 3 hour irradiation period (100% FAM and TAM, and ~80 % of SOL). Various parameters were also investigated on the process such as pH, oxidant addition etc. pH was not found to significantly affect the photocatalytic degradation process, although there was notably more adsorption of the drug to the TiO_2 surface at more alkaline pHs. This increase in adsorption of the drug at alkaline pH, in the case of SOL, did not lead to an enhanced photocatalytic degradation as is often reported by other authors.

Various intermediates (or degradation products) were observed in LC traces of photocatalytic studies and the addition of hydrogen peroxide to the TiO_2 /UV process was found to hinder the formation of these intermediates and eliminate them completely within the allotted irradiation time. Concentration studies examined the robustness of the proposed TiO_2 /UV process to varying concentrations of drug solution. These indicated that the process can completely eliminate concentrations up to 0.2 mM of FAM and TAM, and determined that in the case of SOL only low concentrations of drug can be completely eliminated (0.02 mM).

The intermediates of the optimised photocatalytic degradation experiments were analysed initially by DI-MS, allowing some initial intermediates being proposed. This data was later corroborated with LC-MS/MS data from photodegradation experiments and various intermediates were further proposed based on the masses and fragments obtained from this analysis. Including isomers, over 80 intermediates were discovered between the 3 APIs. Routes of degradation have also been postulated based on the intermediates proposed.

Further to this, composite materials based on TiO_2 and dye molecules have been developed in the hope of developing solar/visible light activated photocatalysts. A visible light sensitised photocatalyst based on the porphyrin tetra-(4-carboxyphenyl)porphyrin was successfully developed. This composite was prepared by a simple adsorption method of preparation and was compared in activity to a harsher literature reflux method. Other composites based on novel metallated and metal free phthalocyanine dyes (MPc and Pc) were also prepared and characterised by UV spectroscopy (solution and solid-state) and FT-IR spectroscopy. The photoactivity of these composites was examined with our pharmaceutical targets. These are the first composite materials, to our knowledge, to be tested with actual pharmaceuticals. The

porphyrin/TiO₂ composite showed good photoactivity in the degradation of FAM, although LC traces indicated that this degradation could merely be a selective conversion to an oxidised/reduced form of FAM. Tests with the other pharmaceuticals further indicated this selectivity toward FAM, as no degradation occurred with either TAM or SOL. MPc/TiO₂ and Pc/TiO₂ composites were also tested with Famotidine, however these exhibited a poor/negligible degradation compared to the porphyrin/TiO₂ composite.

Chapter 1- Literature Review

1.0 Pharmaceuticals in the Environment

In recent years, the presence of pharmaceuticals and personal care products (PPCPs) in the environment has become a serious cause for concern and the problem is continuing to grow with the on-going development of more potent and more metabolically resistant drugs. PPCPs are defined by other authors as *“a diverse group of chemicals comprising human and veterinary drugs...X-ray contrast media.....and other consumer chemicals such as cosmetics, fragrances and sun-screen agents as well as inert ingredients or excipients used in PPCP formulations and manufacture”*.¹ Even within these, there are many classes of pharmaceuticals which include analgesics, anti-depressants, contraceptives, antibiotics and also veterinary medicines and pesticides used in agriculture. Endocrine disrupting chemicals (EDCs) are another class of compounds causing further alarm and these chemicals include not only hormones and contraceptive drugs but also a number of phenolic compounds, dioxins and polychlorobiphenyls (PCBs) amongst others.^{2,3,4} All of these chemicals through various sources end up eventually in our environment and the effects of these bioactive molecules are, as of yet, still unknown.

There are a number of point-sources for the entry of drugs to the environment.⁵ At home, routes of entry include direct flushing of unused/ out-of-date pharmaceuticals down the toilet. In the majority of cases, while on drug therapy, pharmaceuticals pass through our bodies. These drugs can undergo transformations in the body such as oxidation, reduction etc. or end up in a conjugated form of the original drug. In some cases though, drugs can be mostly un-metabolised and thus, entry through human waste (urine and faeces) is another route of entry to the environment.^{139,152,153} Drugs that are discarded in household rubbish will inevitably end up in landfill and can leach into soil. Pesticides and veterinary drugs that are used in plants and animals respectively can be found in streams and soil. Un-metabolised drugs in animals are also a major issue and regular testing is sought to determine the quantities retained in their tissues to prevent harm through consumption by the public. Their additional excretion via animal faeces can result in the release of these compounds, in manure which is often used as a fertiliser, so entry in this manner is also possible.

Wastewater treatment plants and sewage treatment plants alike, potentially face the task of treating some of the discarded, transformed/conjugated and un-metabolised waste from each of these sources. Many studies worldwide have found that current treatment methods from these plants are insufficient in destroying these pharmaceuticals. The consequence of this is exposure of these potent chemicals to aquatic animals and they have the potential to reach drinking water. Many prescribed antibiotics such as ampicillin and ciprofloxacin have been detected in hospital effluents and their presence has provoked concern regarding bacterial resistance to these drugs.⁶ There are also worries concerning the effects on aquatic animals, particularly with the presence

of EDCs which can mimic or block certain hormones and potentially disrupt regular bodily functions. This is of huge concern as inhibition of regular reproductive cycles can occur in both aquatic and terrestrial organisms and thus can limit the numbers or deform the offspring of these animals.

Multiple studies across the United States, Canada and Europe have found traces of 'cocktails' of these pharmaceuticals in drinking water at relevant concentrations of $\mu\text{g/L}$.^{7,8,9,10,11} In 2007 Esplugas *et al.* reported the effects of EDCs in humans to cause increased incidence in testicle and prostate cancer in males along with a reduction in sperm count.¹² Other effects documented in a report by the Commission of the European Communities ((CEC) (also mentioned in this review) included the increased incidence of breast tissue in men and endometriosis. Various research groups worldwide are currently trying to tackle this issue and there are a number of projects that are looking into both the detection of pharmaceuticals and also at the degradation of pharmaceuticals using various treatment methods. There are a number of approaches to this problem, some of which are outlined in the next section (Section 1.1). These approaches are non-destructive and simply involve removal of the pollutants via various filtration or osmotic processes. It should be highlighted that there are also a number of destructive techniques which can be applied to remove these pollutants. These techniques involve the use of Advanced Oxidation Processes, which give rise to an unselective degradation of the pollutant until complete mineralisation is reached.

Mineralisation is the total conversion of the pharmaceutical and its intermediate compounds into products already abundant in our environment such as CO_2 , NO_3^- , SO_4^{2-} and H_2O . Complete mineralisation of PPCPs is desirable as while less is known about the ecotoxicity of these compounds once released into the environment, even less is known about their intermediate products. In photocatalytic studies, compounds undergo multiple oxidation and reduction reactions, so in cases where incomplete mineralisation occurs (i.e particularly stable intermediate compounds are formed) the potential lies therein for these compounds to bioaccumulate in the environment. The environmental implications of this are still largely unknown and can only be speculated to have numerous adverse effects not only to the environment (sorption to soil and sludge), but also to terrestrial/aquatic biota as is the case with parent pharmaceuticals.^{13,14,15} While some studies do exist to determine the toxicity of PPCPs and their intermediate products on organisms such as *Vibrio fishceri* and *Daphnia magna*, more studies are required to not only identify intermediate products from PPCPs and EDCs, but to also determine exactly their degree of toxicity in the environment to multiple organisms.^{15,16}

In the following review, various water treatment processes for the removal of pharmaceuticals are examined. The first section contains a brief background on current technologies in wastewater treatment, and evaluates their potential in the removal of pharmaceuticals. Section 1.2 describes the various Advanced Oxidation Technologies which exist to tackle environmental contaminants. Section 1.3-1.5 discusses the process of heterogeneous photocatalysis, its mechanisms, potential for solar applications, defines the characteristics for the ideal photocatalyst and also current methods to optimise the photocatalytic process. Finally, section 1.6-1.8 presents the chemical properties and current research involving the pharmaceuticals examined in this thesis and outlines the proposed research, its aims and this thesis chapter by chapter.

1.1 Current and Potential Methods for Removal of Pharmaceuticals

There have been a number of proposed methods to remove pharmaceuticals from wastewater and there are numerous processes already in place to treat raw wastewater. These methods comprise a number of filtration techniques, chlorination and advanced technologies which can be both destructive (i.e they completely decompose compounds present/disinfect the wastewater) or non-destructive (whereby the hazardous pollutants and organic matter are removed by either filtration or adsorption onto an adsorbent). The following is a list of these processes, their methodologies and their effectiveness in water treatment and in the removal of PPCPs among other micro-pollutants.

Removal methods (non-destructive)

1.1.1 Active Carbon Filtration:

This involves filtration of the contaminated water through activated carbon or charcoal. Activated carbon is highly porous and pollutants contained in the contaminated water can be effectively adsorbed onto its surface. However, like ozone and other removal methods, there are selectivity issues and more hydrophilic compounds have been found to de-sorb back into the water.¹⁷

1.1.2 (River)Bank Filtration/ Slow sand filtration

Bank Filtration is a technique which has existed in Europe since the 1870s. Bank Filtration involves digging wells in sandy sediment beds which are adjacent to a river or ground water source. Water is then extracted from these water sources by the wells, and in the process is filtered through the fine sandy sediments, leading to water of a much higher quality than from the original source. While this technique has been found to completely remove PPCPs such as antibiotics, oestrogens, cholesterol lowering drugs (bezafibrate) and NSAIDs such as indomethacin, other compounds such as carbamazepine were readily transported by bank

filtration.¹⁸ Slow sand filtration is a similar technique to bank filtration but works on a much smaller scale, about 1-2 metres in depth and is considered as both a chemical and a biological process due to the presence of algae, bacteria and other micro-organisms in the *schmutzdecke* which can digest organic material in the raw water.^{19,20,21} There are few disadvantages to this technique however, like other biological processes, it can be disrupted under certain conditions i.e certain climates such as very cold weather which may induce freezing and hence can affect the quality of the purified water. It is also important that the algae present are not upset by the presence of other toxic forms of algae which can cause ‘choking’ of the filtration device, and regular cleaning would be required.²¹

1.1.3 Membrane filtration: Nanofiltration (NF) and Reverse Osmosis (RO)

Nanofiltration (NF) and reverse osmosis (RO) are two membrane based techniques which are widely employed in wastewater treatment, and in drinking water treatment both in the developed and the developing world. In both NF and RO, the polluted water is forced through a narrow pore membrane at very high pressures, which forces only pure water through the membrane, with the contaminants retained on the membrane. NF is considered to lie somewhere between Ultrafiltration and Reverse Osmosis in terms of filtration capacity.^{22,23} RO can be considered more appropriate for complete removal of pollutants, however, purification comes at a high energy cost. The more contaminated the water the more pressure required. *Activated carbon* filters are also required to remove certain residual factors such as odour and taste and it is therefore a high maintenance system.

1.1.4 Soil Aquifer Treatment

Soil aquifer treatment (SAT) is a treatment method consisting of physical, chemical and biological processes. Like bank filtration, SAT is filtered by the earth. It comprises 3 main stages²⁴:

- (i) Infiltration of the partially treated water through a biologically active infiltration interface at the soil/water boundary.
- (ii) Percolation through a vadose zone (10-100ft in depth),
- (iii) Storage/Transport in the underlying aquifer. Once it is required, recovery wells pump the recharged water for supply.²⁵

Conditions such as flooding can be detrimental to SAT and anaerobic conditions which can adversely affect the efficiency of purification. Additionally, the efficacy of this treatment to remove trace organic pollutants, EDCs and PPCPs is still unknown.²⁶

Destructive

1.1.5 Ultra-Sound/Sonic Treatment

Although still in its infancy, ultrasound treatment has recently emerged as a new alternative to other wastewater treatment technologies.^{27,28,29} Ultrasound/Ultrasonic treatment is similar to other destructive advanced oxidative processes, in that hydroxyl radicals are generated which can degrade pollutants. Its method of activation is the formation of bubbles which resemble 'microreactors'. The 'microreactors' form, grow, pulsate and then collapse. The bubbles which are formed (adiabatically) contain extremely high temperatures (2000°C) and pressures (200 atm) and can be referred to as 'hot nuclei'. Pollutants can either enter within these bubbles and hence will be completely dissociated, or they can be indirectly dissociated via a hydroxyl radical based mechanism. Hydroxyl radicals are formed within the bubble by water and oxygen dissociation. In general, this process can be more effective in mineralising pollutants when used in combination with other treatment systems such as UV or Fe salts.²⁹

1.1.6 Chlorination

Chlorination is a standard method of disinfection in swimming pools, and is still employed in current wastewater treatment facilities. Chlorination is extremely effective in the elimination of micro-organisms such as bacteria and viruses, and thus prevents the spread of disease. It is, however, considered to be a non-green method. There are common drawbacks with evidence of its reaction with organic compounds to form lethally toxic intermediates.^{30,31} Thus, chlorination can be considered as a technique which should be only used exclusively for disinfection and not for the degradation of pharmaceuticals.

1.2 Advanced Oxidation Processes

An advanced oxidation process (AOP) is one where hydroxyl radicals are continuously generated: these hydroxyl radicals will then unselectively degrade pollutants. Research recognises a number of AOPs. In the following sections, a select number of unary, binary, ternary and quaternary systems are discussed which have been used in the degradation of pollutants.

1.2.1 Unary Processes

Ozonation, O_3

Ozonation is the most common advanced oxidation treatment currently employed in wastewater treatment although it is more common in the disinfection of drinking water. Ozone is mainly employed in wastewater treatment to assist in the mineralisation of organic compounds. Ozone has been shown to efficiently degrade organic compounds that possess amines, activated

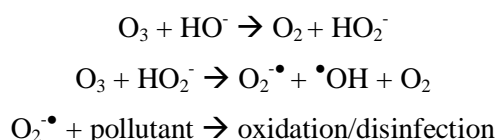
aromatic rings such as phenols, alkyl aromatics and olefinic moieties.³² It has also been shown to degrade antibiotics (ciprofloxacin), antiepileptics (carbamazepine), oral contraceptives (17R-ethinylestradiol), tranquilizers (diazepam) and anti-phlogisitics (diclofenac).^{33,34,35,36} However, there are a number of disadvantages to employing this technique in wastewater treatment:

(1) Formation of Bromate, (BrO_3^-): In the treatment of bromide containing water, this is a particular concern with Ozonation. Bromate is a suspected human carcinogen and in recent years contamination by this anion has led to extreme measures being taken. For example, in the Silver lake and Elysian reservoirs in California, 600 million gallons of water had to be drained due to bromate formation in the water and in one case in the United Kingdom, it managed to reach bottled water.^{37,38}

(2) Poor solubility: Relative to other oxidants.

(3) Selectivity Issues: Since it is an electrophile and only favours the mineralisation of compounds with the moieties listed above.³⁹

Oxidation using ozonation may undertake two pathways of degradation. Either direct reaction of the ozone with the pollutant, or indirectly with the reaction of radicals generated from the ozone with pollutants (below).⁴⁰



Although proven to be very effective as a unary process, ozonation is found to be enhanced when used with other advanced oxidation processes such as UV or H_2O_2 which help accelerate the formation of $\bullet\text{OH}$ radicals and thus increase its unselectivity towards pollutants.

UV – UV Irradiation

UV irradiation is also classed as photochemical degradation/ direct photolysis / homogeneous degradation. UV irradiation can be an effective treatment in water remediation studies however it is largely subjective to the pollutant studied and the configuration system employed. In studies which employ UV along with other AOPs, UV alone is always examined to determine its contribution to degradation.⁴¹ In the majority of cases, it has been found to be inferior to combinatory processes although this can be substrate dependant and also depends on the light source used e.g. UV/A, UV/C etc.^{41, 42, 43} The emission spectrum for a typical medium pressure mercury lamp is shown in Figure 1.1 with most of the emissions arising between 250-315 nm.

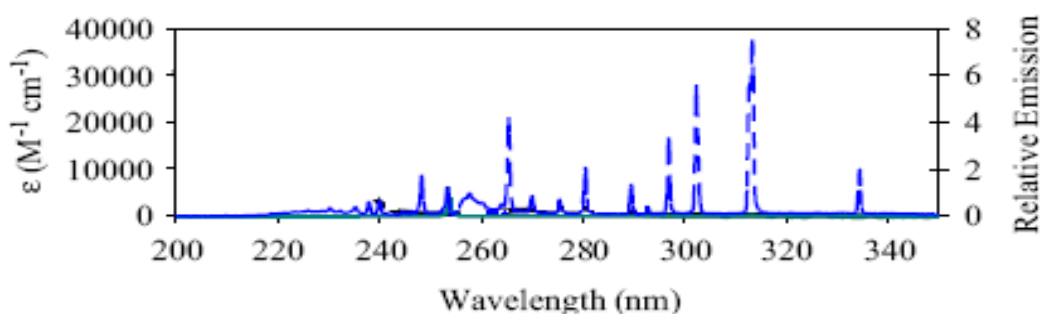


Figure 1.1: Wavelength Emissions from a Medium Pressure Lamp reproduced from Pereira 2007.⁵¹

Studies by Shemer *et al.* 2006 (degradation of Metronidazole) determined that UV alone is not effective in the elimination of pharmaceuticals and more favourable results can be achieved in combination with other AOPs.⁴⁴ Despite this, UV irradiation has been found to be extremely useful for waters which are infested with bacteria such as cryptosporidium and e.coli.

1.2.2 Binary Processes

UV/TiO₂ – Heterogeneous Photocatalysis

This technique is one of the most common AOPs for pharmaceutical abatement in the environment and will be discussed in more detail later. TiO₂ is an effective photocatalyst and is cheap, non-toxic, safe and regularly used in the pharmaceutical and cosmetic industries.⁴⁵ It can be employed both in a suspended form, but also in an immobilised form. There are advantages and disadvantages to both configuration systems. Although this process is quite effective alone, it is usually used in conjunction with an auxiliary oxidant to ensure complete mineralisation. Countless literature articles exist documenting its efficient degradation of organic compounds from dyes to antibiotics and NSAIDs to EDCs.^{88, 123}

H₂O₂/Fe²⁺ -Fenton Process with Hydrogen Peroxide

The Fenton Process is an AOP process which incorporates Ferrous salts along with hydrogen peroxide to generate hydroxyl radicals. The advantage is that it is very effective and only small concentrations of reagents are required. It has efficiently degraded pharmaceuticals including Penicillin, Metronidazole (antimicrobial agent) and Gemfibrozil (lipid-regulator) and many textile dyes.^{46,47,48} However, its efficiency is consistently compared to the *Photo*-Fenton process (see p10) which is more efficient again, producing both a higher degradation rate and a higher degree of mineralisation.

O₃/H₂O₂ – (Peroxone process)

The mechanism for formation of hydroxyl radicals with O₃ and H₂O₂ is by reaction of the two species together by a radical chain mechanism similar to the H₂O₂ process discussed later (see

1.5.4). In a study by Ternes in 2003 this binary system was found to be much more effective than sole ozonation.⁵⁴ An enhancement in the removal efficiency was found in all cases for iomeprol, diatrizoate, iopromide and iopamidol. Similarly, a study by De Witte *et al.* 2009, showed an enhanced degradation with the addition of peroxide. They also observed that at higher concentrations of peroxide, degradation can be inhibited by the scavenging of hydroxyl radicals.

UV/H₂O₂

Hydrogen Peroxide cannot be employed by itself as it is a poor oxidant for many organic pollutants. In all oxidation processes, it is part of a binary or ternary system with either UV light, metal salts or ozone.⁴⁹ In order for hydrogen peroxide to efficiently photolyse, UV light below 400 nm must be employed. UV/H₂O₂ has been studied in the degradation of ibuprofen, diphenylhydramine, phenazone, phenytoin with removal of < 40 % in all cases at relatively higher concentrations of H₂O₂ and low concentrations of pharmaceuticals (5 µM).⁵⁰ A similar study with carbamazepine, naproxen, clofibric acid and iohexol achieved removal efficiencies between 20-50 % with medium pressure lamps (see Figure 1.1 for wavelengths) at 100 mJ/cm³.⁵¹ It would appear that decomposition of pharmaceuticals with this process is very much substrate-dependant, and it can be seen to be inferior when compared to other AOPs such as Ozonation.⁵²

UV/O₃

The Ozonation process combined with UV improves the formation of unselective hydroxyl radicals by the decomposition of ozone. This AOP has been found to improve the standard O₃ process but not in all cases has it been found to mineralise more efficiently.^{53,54} An interesting study by Rivas *et al.* in 2009 compared the effects of a number of AOPs including UV/O₃ with TiO₂/UV in the removal of bisphenol A, a well-known EDC.⁵⁵ They found promising results with both processes. However, with an economic consideration of employing either AOP, it can be found that TiO₂ would be a far more feasible option with the stipulation that the photocatalyst could be regenerated and reused.

1.2.3 Ternary Processes

UV/H₂O₂/O₃

This method combines UV/H₂O₂ with Ozone and has been reported to be more efficient than either the UV/H₂O₂ or the UV/O₃ process. This is due to the increased flux of hydroxyl radicals from H₂O₂ and the additional effects of mineralisation by ozone. Most work with this method has been done on an industrial scale owing to its effectiveness, and very promising results have been obtained in terms of complete mineralisation after 1-2 h of very toxic substances such as

trichloroalkanes.⁷³ This method is considered as both the fastest and most efficacious of all the current processes in relation to industrial water treatment and is potentially the most employable.

UV/H₂O₂/ Fe³⁺ - Photo-Fenton Process

The photo-Fenton process is similar to Fenton, however light is incorporated along with iron (III) salts which are *photo*-active (Iron (II) can also be employed). Typical iron complexes which are used are FeCl₃, FeSO₄.7H₂O, and Fe(NO₃)₂. Numerous pharmaceuticals have been degraded using this process with very promising mineralisation efficiency with diclofenac, dipyrone, tetracycline, amoxicillin and gemfibrozil to name but a few.^{56,57,58,59,48} This process has great potential with regard to solar applications since the ferric-oxalate complex ([Fe(C₂O₄)₃]³⁻) allows more visible-light induced photocatalysis. In the majority of studies where solar light has been harnessed, oxalate complexes are utilised. As with the Fenton, major obstacles exist to its application in full scale water treatment including: the cost of required oxidant (H₂O₂), controlled pH to solubilise the iron salts and additionally, in this case, light is required.⁶⁰ Along with these drawbacks, the photocatalyst cannot be retained. On the contrary, very small amounts of iron salts (in some cases as low as 2 mg/L) can be used to achieve complete mineralisation.⁵⁷

1.2.4 Quaternary Processes

UV/O₃/H₂O₂/Fe³⁺

This process was used by Beltran-Heredia *et al.* in 2001 to degrade p-hydroxybenzoic acid.⁶⁰ They found that this was the best method among those tested (see Figure 1.2).

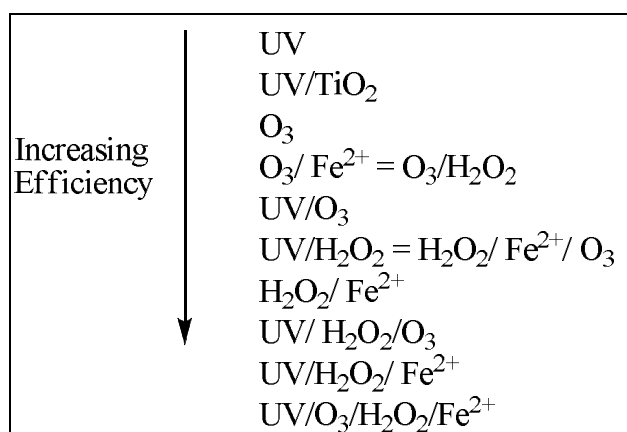


Figure 1.2: AOP Processes examined in the degradation of p-hydroxybenzoic acid.

The system of UV/O₃/H₂O₂/Fe²⁺ was determined predominantly to be a radical based mechanism of degradation. This process was found to be the most efficient ozone consumer with respect to the degradation achieved. Among the other processes examined by this group, various synergisms were noticed among the different combinatory processes, however, the

Fentons reagent ($\text{Fe}^{2+}/\text{H}_2\text{O}_2/\text{O}_3$) was found to have inhibitory effects on the action of ozone. No other reports of this system have been found in relation to the decomposition of organic compounds, however the combined effects of various AOPs in this study can be seen to be very efficacious in organic pollutant removal.

1.3 Heterogeneous Photocatalysis

1.3.1 Introduction

In recent years, the use of AOPs in the treatment and disinfection of wastewater has grown. Many countries including Canada (Figure 1.3), Germany, Ireland and other parts of Europe are now employing tertiary treatment steps to provide a higher quality of water.^{63,61} The most popular AOP employed is UV, which has been found to efficiently disinfect water and can effectively remove micro-pollutants depending on the lamp used. UV is one of the easiest treatments to integrate as it can be retrofitted into existing chlorine contact chambers and with the use of certain lamps, is only slightly greater in cost and more efficacious in disinfection than the chlorination/ dechlorination processes.⁶²

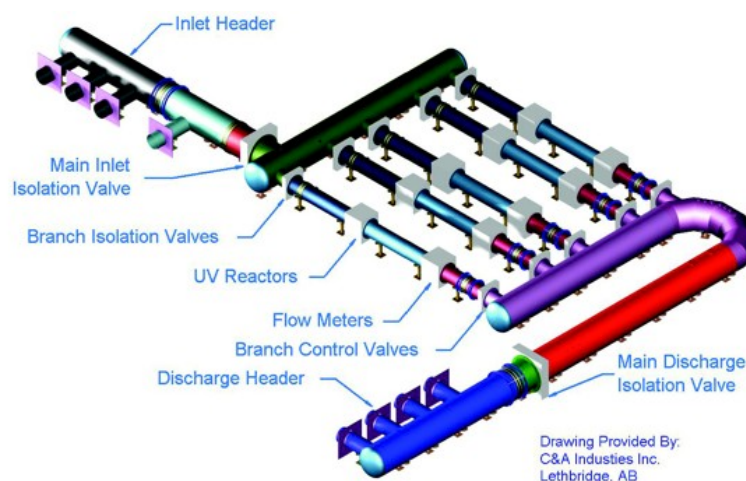


Figure 1.3: Lethbridge, Alberta's additional UV-treatment step to its water treatment facility, reproduced from environmental science and engineering magazine (ESEM).⁶³

At present, the application of photocatalytic AOPs (heterogeneous and homogeneous) in water treatment is still a work in progress despite hundreds of literature articles published every year documenting its efficiency for the elimination of various organic compounds. There are also numerous research centres worldwide which have large scale *solar* photocatalytic equipment namely the PSA in Spain, however it may be sometime before systems like these are introduced into actual water treatment facilities worldwide.

1.3.2 Heterogeneous Photocatalysis

IUPAC defines Heterogeneous catalysis, as catalysis “*in which the reaction occurs at or near an interface between phases*”.⁶⁴ The only difference with heterogeneous photocatalysis is that the catalyst is activated not by thermal methods but by photonic methods.⁶⁹ At present, there is no current definition by IUPAC for heterogeneous photocatalysis although it has been aptly described by authors as ‘photo-induced molecular transformations or reactions which take place at the surface of a catalyst’.⁶⁵

1.3.3 Descriptions and Applications

Heterogeneous photocatalysis is generally employed because of its versatility in that it can be carried out in both gas and aqueous or organic liquid phases.⁶⁹ Photoinduced redox reactions were sparked by Fujishima and Honda with the discovery of water splitting by a single crystal TiO₂ electrode.⁶⁶ Nowadays, heterogeneous photocatalysis can be used in various organic reactions: (oxidations, reductions, oxidative cleavages, polymerisations). TiO₂ also has potential uses in environmental decontamination: with the destruction of organic pollutants and the treatment of wastewater, furthermore TiO₂ also features in current solar cell models and self-cleaning window applications among other commercial uses.

1.3.4 Photocatalytic Materials

TiO₂ is the leading semiconductor photocatalyst in water detoxification studies. Some of its other metal chalcogenides such as ZnO, ZnS and CdS have been used in comparative studies alongside TiO₂ however, these semiconductors are generally less active under similar conditions and in some cases can be less stable under illumination.⁶⁷

1.3.5 Solar Light Harvesting of TiO₂

TiO₂ has a band gap energy, E_g , of 3.2 eV which corresponds to absorption in UVA/B and C regions of the electromagnetic spectrum. Table 1 below shows the wavelengths in the UV/vis regions that can be employed with TiO₂ photocatalysis and their corresponding energies in eV. The sun emits all energies i.e gamma, x-ray, UV-vis, however the light that reaches the earth is above 300 nm.⁶⁸ Since the majority of photocatalytic studies employ Pyrex glassware that contains a light filter (< 300 nm), these conditions can be considered to be optimum for solar heterogeneous photocatalysis.

Spectral Sub Category	Wavelength Range (nm)	E (in eV)
UV-A	400-315	3.09-3.93
UV-B	315-280	3.93-4.42
UV-C	280-100	4.42-12.39

Table 1.1: UV categories and corresponding energies in eV.

1.3.6 Fundamentals of Heterogeneous Photocatalysis

The fundamental processes of heterogeneous photocatalysis can be described by the classical heterogeneous catalysis process. The classical process consists of five stages.

The **first stage** comprises the transfer of the reactants to the surface of the semiconductor photocatalyst.

In the **second stage**, adsorption of at least one of the reactants or the sorbate occurs.

The **third stage** in classical heterogeneous catalysis is simple reaction of the adsorbed products, however in heterogeneous photocatalysis this stage is much more complex, and involves

- (i) the simultaneous absorption of photons by the semiconductor and also reaction in the adsorbed state,
- (ii) the creation of electron-hole pairs and
- (iii) various redox processes including radical propagation, charge neutralisation and radical recombination.

The **fourth stage** involves desorption of the products.

The final stage encompasses the removal of the products from the interface region.⁶⁹

1.3.7 Mechanism of Heterogeneous Photocatalysis

The basic principle of photocatalysis is the promotion of an electron from the valence TiO_2 band to the conduction band which is initiated by photon absorption. In order for this to occur, a photon with energy of 3.2 eV (in the case of TiO_2) or greater must be absorbed by the semiconductor.

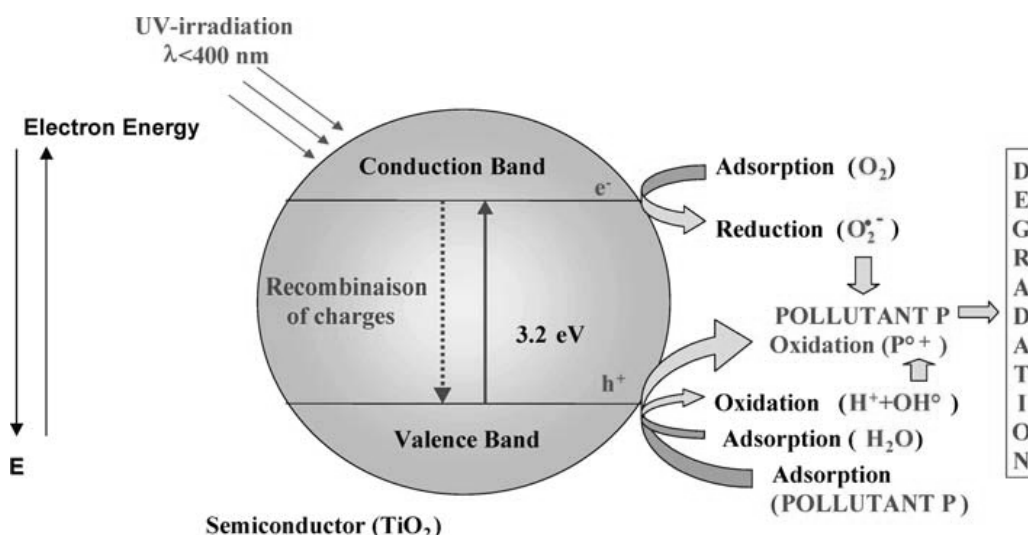


Figure 1.4: Irradiation of a TiO_2 particle reproduced from Herrmann 2004.⁶⁹

Upon promotion of an electron, a charged separated state is formed as shown in Figure 1.4 above, with an electron (e^-) in the conduction band and a hole (h^+) in the valence band. This can be referred to as an electron-hole pair. There are numerous processes which can then occur.⁷⁰

- The electron can fall back down to refill the valence band hole with the subsequent release of heat, known as recombination.
- The electron-hole pair can migrate and become trapped on the surface in meta stable states.⁷¹
- The electron-hole pair can react with adsorbed donors and acceptors such as H₂O and O₂, surface hydroxyls, H₂O₂ or pollutant molecules.

Electrons are powerful reductive species (-0.2 V), and likewise, holes are powerful oxidative species (+3.0 V). Figure 1.5 below shows the various band gap widths for a range of semiconductors with their corresponding redox potentials in Volts for electrons and holes in the valence and conduction bands.⁷² Comparatively, the oxidation potential of a hydroxyl radical (•OH) is 2.8 V relative to the normal hydrogen electrode (NHE). The potentials of other oxidative substances used for water disinfection are listed: Fluorine (3.03 V) Ozone (+2.07 V), H₂O₂ (+1.78 V), HOCl (+1.49 V) and chlorine (+1.36 V).⁷³

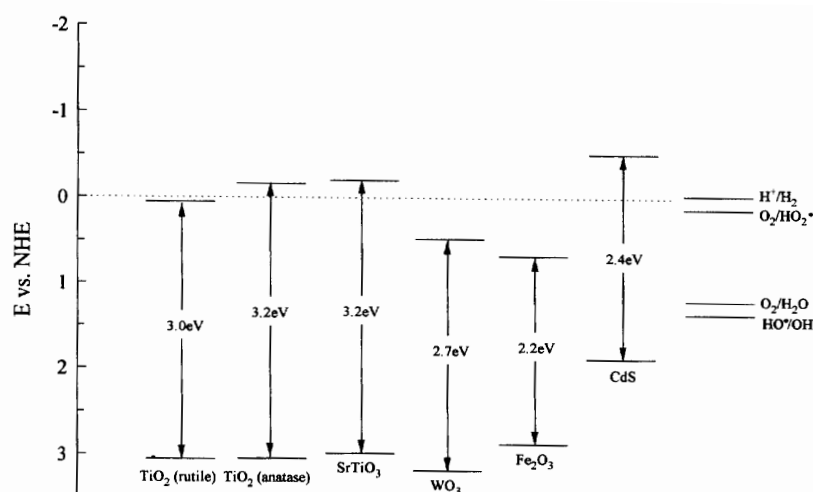
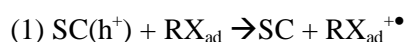
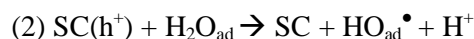


Figure 1.5: The band gaps of TiO₂ rutile and anatase amongst other semiconductors (reproduced from Mills *et al.*, 1997).⁷²

Of the possible pathways listed above, the most studied is the reaction of the electron-hole pair with donor and acceptor molecules on the semiconductor surface and the ensuing redox reactions that can occur. The equations below show the possible reactions of various donors and acceptors with h⁺ and e⁻:



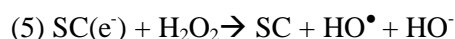
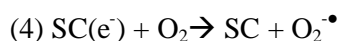
The above equation (1) shows the reaction of a positive hole on a semiconductor with an adsorbed substrate i.e an organic compound. The result is the transfer of an electron from the adsorbed substrate to the semiconductor valence band generating a charged radical species which can then further react or dissociate.



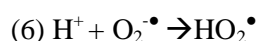
As seen in the previous equation, equation (2) shows the reaction of a hole with an adsorbed water molecule generating an adsorbed hydroxyl radical and a proton.



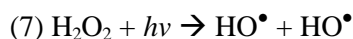
If the semiconductor is irradiated under basic conditions, whereby an abundance of HO^- species are present, these can adsorb to the semiconductor surface and reaction with holes can yield further hydroxyl radicals (3).



Reaction of an electron with oxygen or hydrogen peroxide can generate highly reactive superoxide anions and hydroxyl radicals respectively. These can then react with adsorbed pollutants and unselectively degrade them. Since all of the above reactions can effectively happen simultaneously, combination reactions can occur to further generate additional radical species. An example of this would be the following:



Combination of a proton and a superoxide anion gives rise to a hydroperoxyl radical. These can also be formed by the reaction of hydroxy radicals with an oxidant such as hydrogen peroxide. However, formation in this manner can be expected to be low since the predominant reactions of H_2O_2 are shown in equation (5) and (7).¹²⁹



The powerful redox chemistry associated with electron-hole pairs is the focal point of research in heterogeneous photocatalysis and its environmental application. The degradation of pollutants through direct oxidation via holes or indirectly via radicals (generated by electron-hole pairs) is still a subject of debate.⁷⁴

1.3.8 Characteristics of the Ideal Photocatalyst

The properties that an ideal photocatalyst must display for the unselective degradation of pharmaceuticals in the environment are listed below. TiO_2 can be seen as a good candidate for the ideal photocatalyst, and is currently the benchmark to which other photocatalysts are compared.⁷⁵

Stability and sustained photocatalytic activity: The photocatalyst should be chemically inert and should be uniform in its performance, it should also be stable upon illumination and have a high turnover frequency (molecules reacting per active site in unit time).⁶⁴

Good overlap of absorption cross-section with solar spectrum: In order to make use of more sustainable resources such as solar energy, the ideal photocatalyst should absorb a significant

portion of the solar spectrum. Although absorption in the visible range is not crucial, it is preferable so that a larger proportion of the sun's radiation can be converted.

High conversion efficiency and quantum yield: Conversion of photons to chemical energy needs to be an efficient process in photocatalysis, and a high quantum yield should be envisaged.

Ease of Recovery: For commercial applications of heterogeneous photocatalysis, immobilization is generally a preferred format, particularly in terms of cleaning, recovery and reuse. However, there are generally sacrifices made for this in terms of the photocatalytic efficiency and surface area. On the contrary, suspended systems are also recoverable, however further steps such as cleaning, centrifugation or filtration are required along with further illumination to rid the material of any remaining adsorbed contaminants. Whether the material is to be re-used or not, recovery of the material is a very important consideration.

Recycling: The whole principle of photocatalysis and catalysis in general is the potential for continuous reuse of the material. From a commercial viewpoint, continuous recycling of the photocatalyst is favourable rather than continual replacement. This is especially the case in terms of more expensive photocatalysts which use rare metals or are doped with expensive materials.

Low cost: In cases where the photocatalyst is non-recyclable, cost efficiency is another concern. Photocatalysts which use rare metals can be expensive, and obviously are in low abundance. Where photocatalysts are recyclable, it would be ideal for the process of retrieving and cleaning to be inexpensive.⁷⁵

Safety: Materials employed in wastewater treatment facilities should be non-toxic, therefore proposed photocatalytic materials should not be cytotoxic and should not accumulate in the environment if released. In cases where a material may bio-accumulate, the material in question should be filtered/settled from the wastewater prior to discharge and should be recycled or disposed of safely.

1.4 Titanium Dioxide

1.4.1 Semiconductor Profile

TiO₂ exists as three natural allotropes: brookite, anatase and rutile. Anatase and rutile have been proven as the most effective photocatalysts, with anatase showing a higher photocatalytic

efficiency over rutile.⁷⁶ Unit cells of both rutile and anatase are shown in Figure 1.6. Formulations of TiO₂ generally contain either a mixture of both rutile and anatase or just pure anatase. Two of the most common formulations now remain as standards in the field of heterogeneous photocatalysis: these are Degussa (now Evonik) P25 and Sachtleben's Hombikat UV100. These two formulations are widely used in photocatalytic degradation of organic compounds and have even competed with lab-prepared formulations in some cases. The photocatalytic activity of TiO₂ is dependent on both the particle size and the crystalline form it is in.⁷⁷ Anatase and brookite can be converted to rutile upon heating.

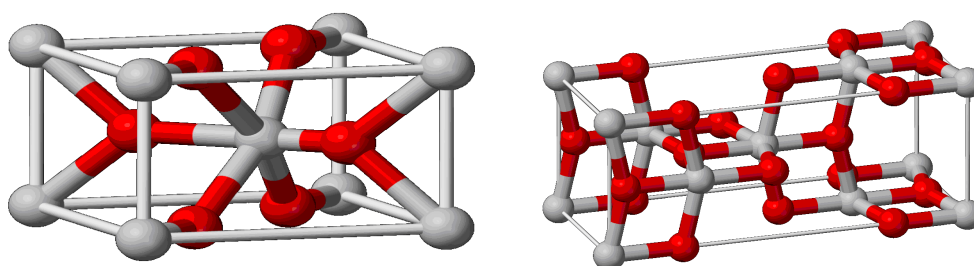


Figure 1.6: A 3-D image of rutile titania (Left) and Anatase titania (Right): in grey are Ti atoms and in red are oxygen atoms.^{78,79}

1.4.2 Sachtlebens Hombikat UV100 and Degussa P25

Sachtlebens formulation is 100 % of the anatase allotrope with a surface area of >250 m²/g and a particle size of 5 nm. Several studies have proposed that this particular TiO₂ has a greater tendency to degrade aliphatic species.⁸⁰ Degussa's P25 has a formulation of roughly 3:1 anatase: rutile with a surface area of 50 m²/g and a particle size of 20 nm. It has been postulated that this titania favours the destruction of aromatic and olefinic species unlike the Hombikat.⁸⁰

Since the majority of drugs on the market have an aromatic or heterocyclic ring within their structure, and/or olefinic components, it comes as no surprise that P25 is more widely applicable. Many studies have been conducted comparing both of these formulations, however more in depth studies which compare single versus mixed phase titania using ESR have been conducted. These studies have examined the benefits of mixed formulations and why.

One study by Hurum and Agrios compared P25 with anatase and rutile and concluded that mixed formulations of the two allotropes showed a greater photoeffectiveness based on three quintessential factors.⁸¹

1. Rutile, served to extend absorption into the visible region due to its slightly smaller band gap 3.0 eV.

2. Recombination of electron transfer processes was significantly controlled in P25 due to stabilisation of the charge separation from rutile to anatase.
3. The small size of the rutile crystals facilitate in electron transfer and create ‘catalytic hotspots’ at the rutile/anatase interface.

These results are evidence to the apparent synergistic relationship between anatase and rutile in mixed formulations and its efficacy in photocatalytic degradation of pharmaceuticals.

1.4.3 Limitations of Employing the TiO₂-Photocatalytic Process

There are two major challenges that face the field of TiO₂ photocatalysis and currently these issues can hamper its application in wastewater treatment.

(1) The first challenge is immobilisation of TiO₂ such that the material can be easily removed and recycled. Many immobilisation substrates are possible, although achieving the same removal rates and efficiency as suspended TiO₂ is the overall goal.

(2) The second challenge is the development of visible light sensitised photocatalytic materials such that cheaper visible light sources or solar light can be harnessed. Currently, UV light is required which heightens the cost of the process significantly. Achieving visible light sensitised photocatalysts can be done in many ways such as doping with metals, or coating with dyes.

Overcoming these drawbacks is the present focus of research in TiO₂ photocatalysis and some of this research is discussed in the following sections of this review.

1.4.4 Immobilisation on surfaces.

TiO₂ can be configured in either a suspended form or an immobilised form. There are obvious disadvantages to configuration in an immobilised form such as a decreased surface area, however there are notable advantages such as the prevention of light scattering, ease of removal, and easy reuse. TiO₂ has been immobilised on various stationary surfaces such as thin films, reticulated foam monoliths, fiber glass, glass/ceramic rings (Raschig rings), sand, glass beads, glass wool, silica fibres, titanium alloys, quartz, stainless steel and Pyrex glass tubes containing scratched polymeric fibres (to enhance the availability of light).^{82,83,84,85,86,87,129,88,89,90} There are other immobilisation substrates which are possible; however these have not been applied for the interest of water remediation and will therefore not be discussed. There are numerous methods for immobilisation of TiO₂ on surfaces and they all depend on the application required. Different immobilisation techniques include: dip coating, sol gel and electrophoretic coating, thermal, and aerosol powder coating among others.^{82, 89, 91}

1.4.5 TiO_2 doping with metals

Many studies have been performed in relation to metal or ion doping in order to enhance the photophysical properties of the semiconductor in heterogeneous photocatalysis. Doping with metals such as the Lanthanides, Fe, Pt, Ag and other noble metals may effectively enhance the photocatalytic efficiency.^{92,93,94} It has been postulated that doping the titania surface with various metals can reduce recombination processes by effectively trapping electrons and additionally extending absorption into the visible region (Figure 1.7).⁷⁰ It can also enhance the rate of the photocatalytic reaction, enhance the yield of a particular product or change the reaction products.⁹³

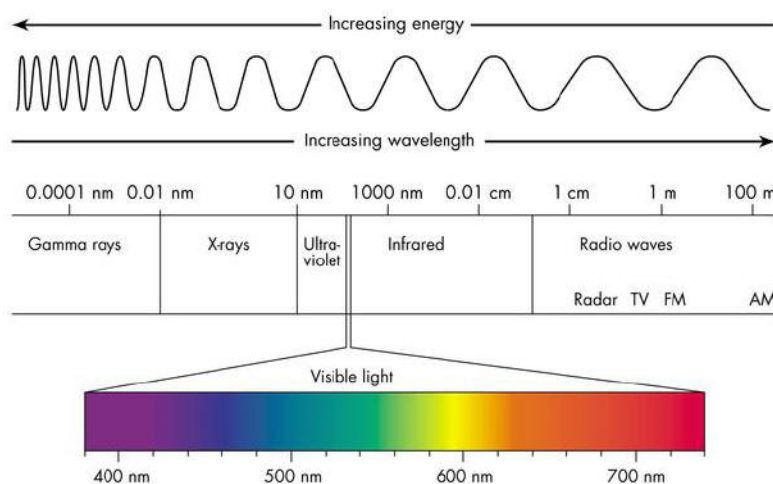


Figure 1.7: The electromagnetic spectrum of light showing the visible region.⁹⁵

One of the major challenges with TiO_2 photocatalysis has been electron-hole recombination as generally this process competes with photodegradation: doping with metals provides a solution to this problem. It prevents this process with migration of the electron to the metal, by the alignment of the Fermi levels of both the metal and the semiconductor. This not only suppresses the process but also the decrease in electron density causes an increase in hydroxyl acidity which affects the photocatalytic process. The major drawback with adding a dopant is that it heightens the cost of the process particularly when metals such as Ag or Pt are applied.

Selective oxidation/reduction can also be achieved by doping. Depending on the compound, TiO_2 -mediated photocatalysis can either preferentially oxidise or reduce the contaminant. In a study undertaken by Choi *et al.* they found that doping with Vanadium (IV) accelerated the oxidation of chloroform, and doping with Ruthenium accelerated the reduction of carbon tetrachloride. Doping with other species such as Silica-tungstic acid can effectively inhibit one of these processes also resulting in a potentially 'selective' decomposition.⁹⁶

1.4.6 Sensitisation of TiO_2 with visible light absorbing molecules

In recent years, TiO_2 has been coated with visible light sensitised materials that enable the harnessing of visible/solar light in photocatalysis. Research which has gained considerable momentum is the sensitisation of TiO_2 with various conjugated conducting polymers. Depending on the number of units, the absorbance of these polymers can be further red shifted, and modification of TiO_2 by these polymers allows sensitisation by visible light. Thusfar, these polymer modified TiO_2 materials show considerable promise in photo voltaic cells, and recent work by Qui *et al.*, Xu *et al.* and Liao *et al.* (opal crystal-polymer hybrid) have shown its potential for photocatalytic degradation of textile dyes and phenol.^{97,98,99} No literature yet exists on their potential for photocatalysis of pharmaceuticals. Other sensitising materials which have been considered are organic dyes such as methylene blue, rhodamine B, Chryosidine G and also macrocyclic sensitising molecules such as phthalocyanines and porphyrins.^{100,101,102}

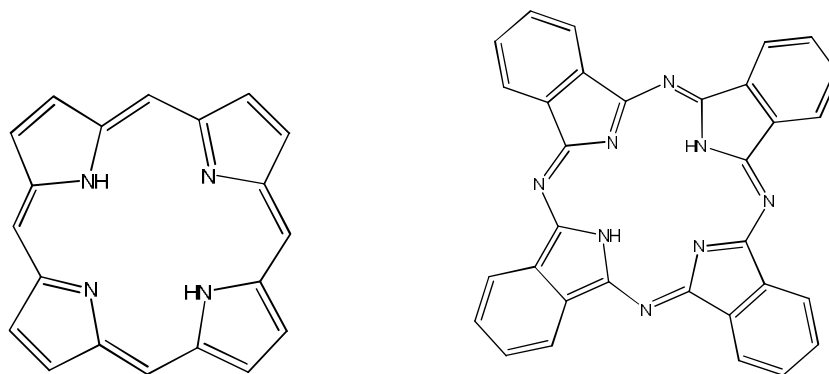


Figure 1.8: Structures of the simplest porphyrin (left) and phthalocyanine (right).

Porphyrins and phthalocyanines are well-known for their use as photosensitising molecules and their application stretches from PDT, photovoltaic cells, contrast/imaging agents, to non-linear optics.^{103,104} Structures of the simplest porphyrin and phthalocyanine are shown in Figure 1.8. In terms of their photo-sensitising ability, generally metal phthalocyanines and metal porphyrins are employed due to their higher stability and improved photocatalytic activity over the metal free form.¹⁰⁵ Attachment of sensitisers of this type to TiO_2 has been done in many ways via chemisorption, physisorption and covalent binding.¹¹¹ Thusfar, their use with TiO_2 in photocatalytic degradation has been limited to the degradation of various nitrophenols and chlorophenols, organic dyes and lignins.^{105, 106, 107, 108, 109}

1.4.7 Linkers for attachment of sensitising molecules to TiO_2

One strategy to covalently link a dye molecule to the surface of TiO_2 is to use a linking molecule that is initially bound to the TiO_2 surface. Many options exist for anchoring molecules to metal oxide surfaces and some of the most stable and commonly used linkers are discussed below. Figure 1.9 shows a schematic of a metal oxide with a dye attached via a linker composed

of an anchoring group and a bridging molecule. Work by Anderson *et al.* demonstrated the effects of longer bridging molecules with carboxylate anchoring groups.¹¹⁰ The longer the bridge (units of CH₂) length the shorter the injection time of electrons to the metal oxide surface, in this case SnO₂.

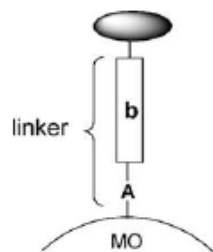


Figure 1.9: Metal Oxide (MO) with linker composed of an anchoring group (A) and a bridging group (b) to attach sensitising molecules. Reproduced from Galoppini 2004.¹¹¹

- **Carboxylates (COOH)**

In the most efficient DSSCs, Ruthenium complexes are anchored to TiO₂ via carboxylic acid groups which bind to surface hydroxyl groups on the TiO₂ surface (chemisorption).¹¹² These carboxylate anchors can bind in a variety of modes (Figure 1.10) from mono dentate to bi-dentate, ionic, hydrogen bonding and ester linkages. While these linkages are shown to exhibit a high stability in most anhydrous organic solvents their binding to TiO₂ is reversible and dyes can be easily desorbed in basic conditions (> pH 9).^{111,113}

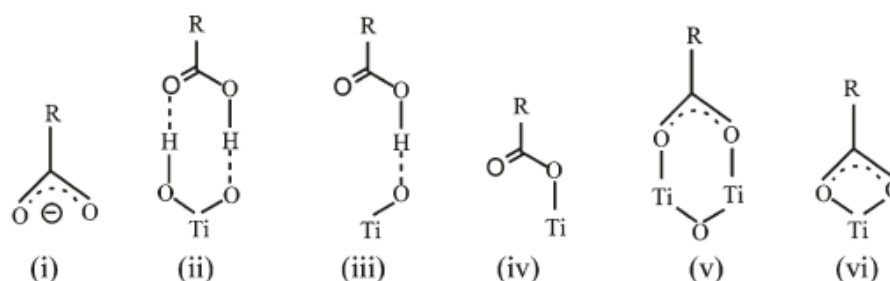


Figure 1.10: The six different possible binding modes of carboxylate groups on titanium dioxide.¹¹⁴

- **Phosphonate (PO₃H₂)**

The highly oxophilic phosphonic acid group has been reported to provide a strong chemical attachment, most probably because of its affinity to hard acid metals such as Ti(IV) in TiO₂. Phosphonate along with carboxylate are the most common linkers for binding sensitizers to metal oxide films. Work by Hupp *et al.* in 2007 compared phosphonate linked Ruthenium and Rhenium dyes with carboxylate linked onto TiO₂ films.¹¹³ Amongst their findings they discovered that phosphonate anchors facilitate faster electron injection and stronger electronic coupling (computer-modelled) with a CH₂ spacer group.

- **Silanes (SiOEt₃)**

Silane groups have been successfully grafted onto TiO₂ particles. Lin *et al.* in 2001 successfully grafted these groups onto silica gel and TiO₂ particles with the silane agent 3-glycidoxypopyl trimethoxy silane (GPS).¹¹⁵ A higher grafting percentage was found on Silica gel due to its higher H content. The grafting of GPS on TiO₂ was found to be 0.95% compared to 16% on Silica. They further grafted the Xanthene dye Rhodamine B onto the GPS modified silica gel. Other work in silane modified TiO₂ particles has been done by Ye *et al.* who successfully modified the metal oxide surface with APTS and further attached a biomolecule.¹¹⁶

- **Acetylacetonate ACAC:**

Heimer *et al.* in 1996 investigated the use of acetylacetonate (acac) as a linker for Ru(bpy) complexes to TiO₂.¹¹⁷ This linker has been found to be stable to hydrolysis over a range of pH's. In 2008, McNamara *et al.* reported a Mn-based catalyst bound to P-25-TiO₂.¹⁶³ Results showed an improved stability in water of the acac catalyst and also a good resistance to oxidation with oxone over a period of 24 h. They concluded that acac shows great potential in providing a versatile and robust linkage between metal oxide particles and sensitising molecules.

- **Toluene diisocyanate (TDI)**

TDI has been employed by Jiang *et al.* as both a linker and a sensitising molecule in the surface modification of TiO₂.^{100,118} The TDI modified TiO₂ was found to be superior over P-25 TiO₂ in the degradation of Methylene Blue. In later work, they further attached a dye (chrysidine G) which proved to be a better photocatalyst and showed great reproducibility upon recycling. Chen *et al.* in 2009 later adopted their TDI modified photocatalyst in the degradation of chlorophenol and a number of other organic molecules.¹¹⁹

- **Diols/Boronic Acids**

Notestein *et al.* in 2007 sensitised Hombikat TiO₂ with different derivatives of 'cone' calixarenes.¹²⁰ The calixarenes they employed were functionalised with diols which served to anchor the structures to the TiO₂ surface. Altobello *et al.* recently employed boronic acids as anchors in Ruthenium based DSSCs.¹²¹ These anchors can adsorb to the metal oxide surface like carboxylic acids. They demonstrated the potential of these acids as linkers, however they have since adopted phosphonic and carboxylic acid anchors in Ruthenium and Osmium based DSSCs.

1.5 Optimising the Photocatalytic Process

TiO₂ has been reported to successfully degrade contaminants all across the broad spectrum of pharmaceuticals. To achieve the most efficient degradation of pollutants, various parameters must be optimised. Numerous studies have employed TiO₂ under conditions such as varying pH, anion effects, concentration of catalyst, concentration of pollutant, lamp type, lamp intensity, addition of various oxidants etc. These parameters will be discussed in the next section and also the effect with which these parameters have on the photocatalytic process.

1.5.1 Anion Effects: CO₃²⁻ SO₄²⁻ Cl⁻

Various anions have been reported to be radical scavengers in the photocatalytic process, and many studies have shown an inhibited degradation by TiO₂ with the addition of these anions in solution.^{122,123} A study by Pujara *et al.* 2007, found that sulfates (SO₄²⁻), chlorides (Cl⁻) and carbonates (CO₃²⁻) had detrimental effects on the degradation of phenol-4-sulfonic acid. A significant decrease in mineralisation efficiency was reported by this group for this compound and they attributed not only radical scavenging but potential competitive adsorption to these effects.¹²⁴ It has also been thought that these compounds can filter light (inner filter effects) reaching the target analyte, and can therefore also competitively absorb light. These anions naturally appear amongst the flora and fauna of surface and ground waters and can be released in the photocatalytic process by compounds being studied in degradation. Studies into the effects of these anions on the degradation of pharmaceuticals can provide a more realistic evaluation of efficiency and robustness of degradation.

1.5.2 pH Effects

pH is another parameter which can be optimised in heterogeneous photocatalysis. TiO₂ has a point zero charge (pzc) or an isoelectric point at ~ pH 6.4 which gives rise to either a positive charge at acidic pHs and a negative charge at more alkaline pHs on the surface of the TiO₂ particle. This can potentially have an enhanced effect or a detrimental effect on the adsorption of the organic compounds and also on the rate of photocatalytic degradation.¹²⁵ The surface charge of TiO₂ or the zeta potential is largely affected by the pH and the ionic strength of the solution as work by Jiang *et al.* 2009 shows. Also, agglomeration of particles is found to be enhanced by an increase in pH close to the pzc for TiO₂.¹²⁶

1.5.3 Oxidants

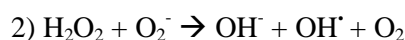
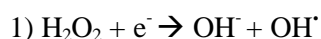
TiO₂ is usually used in conjunction with some sort of oxidant to achieve complete mineralisation of all pollutants. Mineralisation refers to the complete conversion of the pollutant into components or substances naturally abundant in the environment (i.e CO₂, O₂, nitrates,

sulfates and carbonates etc.) Oxidants generally employed are ozone (O₃), oxygen, potassium peroxydisulfate and hydrogen peroxide.

1.5.4 Hydrogen Peroxide-H₂O₂

Hydrogen Peroxide is the most common oxidant due to its solubility, and to its high generation of hydroxyl radicals. The role of hydrogen peroxide in the photocatalytic degradation of organic compounds is two-fold.

- 1) Upon electron excitation to the conduction band hydrogen peroxide accepts the photo-generated electron, promoting charge separation.
- 2) Hydroxyl radicals can also be formed from reaction with superoxide anions which can then unselectively degrade contaminants. See equations below:¹²⁷



Appropriate concentrations of H₂O₂ can considerably enhance degradation and mineralization of compounds.¹²⁸ Hydroxyl radicals unselectively degrade pollutants due to their high oxidation potential of 2.8 V.⁴⁹ They are extremely unstable species and are continuously produced throughout radical propagation and chain reaction mechanisms. Their mechanism of degradation of organic contaminants occurs either by a H-abstraction in the case of alkene/olefinic or alcohol functionalities. In the case of aromatic species, the general case is hydroxylation of the phenyl ring, and perhaps subsequent displacement of EWGs such as halides. In general, reactions of hydroxyl radicals can be summarized into H-abstraction, electrophilic addition and electron transfer.⁷³

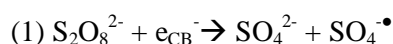
In the majority of studies, only one of the oxidants mentioned above is selected and used. If more than one is used or 'too much' is used, various inhibitory processes come into play and the efficiency of degradation is somewhat compromised. This is realised in reported studies by Adan *et al.* 2006 and Kaniou *et al.* 2005 where degradation efficiency decreases once a threshold of H₂O₂ is reached. Adan *et al.* 2006 performed studies using TiO₂ immobilised on Silica fibres with various oxidants.^{129,71} They found that after 300 mins irradiation 38% salicylic acid is removed using H₂O₂ at 29 mmol, and after 300 mins irradiation using oxygen 33% salicylic acid is removed. At this concentration Adan reported that various recombination processes start to compete with degradation. They also reported that the degradation rate limits

due to recombination of hydroxyl radicals with various other radical species such as hydroperoxyl radicals and peroxide.

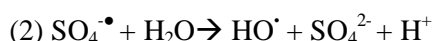
Kaniou *et al.* found, in the photocatalytic degradation of sulfamethazine, that concentrations above 200 mg/L resulted in a decrease in the reaction rate. This particular study examined both TiO₂ and ZnO on the degradation of sulfamethazine. Addition of H₂O₂ to ZnO, interestingly had no effect positive or negative on the reaction rate. Kaniou and co-workers explained this in relation to the negligible adsorption of H₂O₂ on the surface of ZnO which was also noticed by Carraway *et al.* in 1994 and Kormann *et al.* 1988.^{130,131} The adsorption of H₂O₂ on TiO₂ is much more photocatalytically favourable due to an increase in the reduction by photogenerated electrons of H₂O₂ and therefore a reduced e⁻/h⁺ recombination rate. All in all, optimum concentrations must be realised for the most efficient degradation.

1.5.5 Potassium peroxydisulfate K₂S₂O₈

Potassium Peroxydisulfate is commonly used in organic chemistry oxidations particularly the Elbs persulfate oxidation. Potassium Peroxydisulfate works in a similar fashion to hydrogen peroxide. It generates reactive sulfate radical ions SO₄^{•-}, comparable to hydroxyl radicals. The equations given below show the generation of the sulfate radical ions from the peroxydisulfate ion.¹³²



The nature of radical chemistry is that once one radical species is formed, this can then undergo various chain reactions or propagation stages which inherently generate further species of radicals. Equation 1, will thus undergo propagation to generate hydroxy radicals as follows:



1.5.6 Ozonation-O₃

Ozone is considered an effective pollutant treatment method by itself and is one of the advanced oxidation processes mentioned in other sections. In some cases it has been used in conjunction with TiO₂ and has shown to be effective, although there are some drawbacks to its utilisation.

Ozone can be generated from either oxygen or regular lab air with the initial irradiation of UV light or electrical discharge.⁴⁹ It is then passed into the reaction chamber via a porous diffuser and is then solubilised within the water. Using ozone as an oxidant requires a high energy input and the resulting yield of pure ozone is low comparatively. It also is much less soluble in water than conventionally used (cheaper) oxidants such as hydrogen peroxide. The nature of ozone is such that it cannot be stored and must be generated and kept in close proximity to the reaction set up.

1.6 Literature Concerning the Pharmaceutical Targets in this Work

The three APIs examined in this work are Famotidine, Tamsulosin Hydrochloride and Solifenacin Succinate. All three are manufactured by Astellas Pharmaceutical Ltd in Damastown, Dublin and have varying therapeutic action.

Famotidine:

Otherwise known as Pepcid, Famotidine is a histamine H₂-receptor antagonist.¹³³ It is commonly used in the treatment of peptic ulcer disease (or gastrointestinal ulcer prophylaxis) and functions in inhibiting stomach acid production. In 2010, Famotidine was the 3rd (Pepcid Complete) and 4th (Pepcid AC) most popular antacid with sales of over \$105 million.¹³⁴ In the last decade it has also appeared recurrently within the top 200 over the counter health care products annually (See Table 1.2). In patients that use Famotidine, it has been documented that 65-70% of the drug is recovered unchanged in the urine, thereby rendering this drug as one of the many that is released into the environment on a day-to-day basis.¹³⁵ Recent studies in Spain and Cyprus have also indicated that it is frequently present in both wastewater treatment plant influent and effluent and is only partially degraded.^{136,137,138}

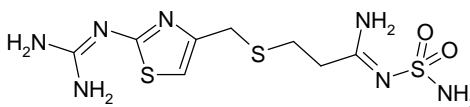


Figure 1.11. Famotidine: (3-[2-(diaminomethyleneamino)thiazol-4-ylmethylthio]-N-sufamoylpropionamide).

Much of the work done on this drug has been done with relevance to a medical or a synthetic/patentability application/benefit. To our knowledge, no comprehensive study has been done on the degradation of this compound by photolytic or photocatalytic degradation with TiO₂ in solution. One study by Kakinoki *et al.* examined the effect that TiO₂ had in formulation with Famotidine in the solid-state.¹³⁹ This study examined compacts of Famotidine and TiO₂ and found discoloration with irradiation of these compacts. They also found that Famotidine was quite photo-stable for the wavelengths tested (300-450 nm). Another study more recently examined Famotidine degradation using the photo-Fenton process.¹⁴⁰ Other work that has been done (with relevance to this work) involves stability studies by Wu *et al.* who found that in comparison to other similar drugs Famotidine resulted as the least stable in aqueous solutions at pH 2.0 at 25°C.¹⁴¹ Its stability was also found to be independent of exposure to light (fluorescent) and the presence of other drugs in the system did not influence its stability. It was apparent during the study that pH was the dominant factor contributing to the degradation of all drugs present. Famotidine was the most stable at pH 4.0 and the least at pH 2.0. Other work

includes identification of acid/base hydrolysis products for Famotidine oxidation (see Figure 1.12) and metabolite studies and various papers on High Performance Liquid Chromatography (HPLC)/ Liquid Chromatography tandem Mass Spectrometry (LC-MS/MS) methods.^{142, 143}

Famotidine (Pepcid AC)		Retail Sales (\$) OTC/HBC ranking of 200	
Mol. Wt. g/mol	337.44	2007	60,894,330 (111 th)
pK _a	6.9	2006	72,251,510 (46 th)
Log P	-0.4	2003	81,392,744 (31 st)
Log D _{7.4}	-1.02	2001	105,497,120 (37 th)

Table 1.2: Properties of Famotidine including sales data and product rank amongst other over the counter health and beauty care products.^{134,144}

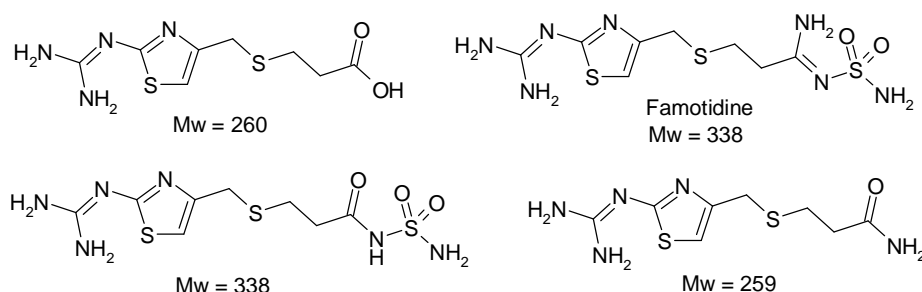


Figure 1.12: Famotidine and its reported acid and base hydrolysis products according to Junnarkar and Singh.^{142,143}

Tamsulosin Hydrochloride:

Tamsulosin HCl is an antagonist of alpha 1-adrenoreceptors and relieves the symptoms of benign prostatic hyperplasia.¹⁴⁵ Its structure is shown in Figure 1.13 and it is marketed under the name Flomax and is reported to be continually placed in the top 200 drugs in the last 4 years.¹⁴⁶ Sales figures and rankings are presented in Table 1.3 along with various properties for Tamsulosin including Log P, Log D etc. Of the administered dose of Tamsulosin, 75% is excreted as metabolites in the urine, with 10% excreted as the parent structure.¹⁴⁷ As with Famotidine, the majority of studies concerning Tamsulosin are its detection in human plasma and serum using various HPLC and LC-MS/MS methods.^{148,149} It has been used as an internal standard in other studies.¹⁵⁰ Currently, no work has been done in relation to photodegradation studies with this compound and likewise, no studies yet exist which show its presence in the environment.

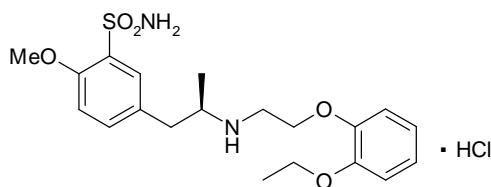


Figure 1.13. Tamsulosin: ((-)-(R)-5-[2-[[2-(o-Ethoxyphenoxy)ethyl]amino]propyl]-2-methoxybenzenesulfonamide, monohydrochloride).

Tamsulosin (Flomax)		Retail Sales (\$000)/Ranking of 200	
Mol. Wt. g/mol	444.98	2010	486,106 (69 th)
pK _a	8.4 (secondary amine), 10.2 (sulfonamide)	2009	1,556,273 (17 th)
Log P	2.24	2008	1,236,963 (27 th)
Log D _{7.4}	0.79	2007	1,002,163 (36 th)

Table 1.3: Properties of Tamsulosin including retail sales figures and ranking amongst other drugs.^{144,146}

Solifenacin Succinate:

Solifenacin succinate is an anticholinergic muscarinic receptor antagonist used in the treatment of overactive bladder.¹⁵¹ Its structure is shown in Figure 1.14 and it is marketed under the name Vesicare and like Tamsulosin, has been amongst the top 200 drugs sold annually in the past 4 years.¹⁴⁶ These data along with Log P, Log D and pK_a values for Solifenacin can be found in Table 1.4. Pharmacokinetic studies have found that Solifenacin is completely orally bioavailable and of the administered dose, 50% is excreted renally unchanged.^{152,153} Of all three compounds, this has the least amount of studies found in the literature, although HPLC and LC-MS/MS methods have been reported for its detection in plasma.^{154,151} Thusfar no photodegradation studies have been performed with this pharmaceutical. Similarly, no studies exist which have reported its presence in the environment.

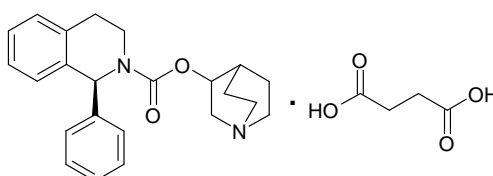


Figure 1.14 Solifenacin: ((+)-(1S,3'R)-quinuclidin-3'-yl 1-phenyl-1,2,3,4-tetrahydroiso quinoline-2-carboxylate monosuccinate.

Solifenacin (Vesicare)		Retail Sales (\$000)/Ranking of 200	
Mol. Wt. g/mol	480.55	2010	440,862 (82 nd)
pK _a	8.5	2009	379,283 (98 th)
Log P	3.7	2008	299,147 (115 th)
Log D _{7.4}	2.07	2007	205,637 (152 nd)

Table 1.4: Properties of Solifenacin including retail sales figures and ranking amongst other drugs ^{144,146}.

1.7 Project Proposal

The aim of the following work, in conjunction with the Astellas pharmaceutical plant in Damastown Dublin, is to develop photochemical methods to degrade 3 active pharmaceuticals from this plant: Famotidine, Tamsulosin Hydrochloride and Solifenacin Succinate. All 3 pharmaceuticals are regularly prescribed drugs and thus far, few studies are available on each and none in relation to their photocatalytic degradation. Total mineralisation of these compounds is envisaged, using current advanced oxidation processes which have been successfully applied in water treatment of pharmaceuticals.

Two photochemical methods will be examined; (1) direct photochemical degradation (the absence of a photocatalyst) and (2) heterogeneous photocatalysis. Homogeneous photocatalysis will be undertaken by a separate analyst in a similar project. Heterogeneous photocatalysis will comprise the use of TiO₂, while homogeneous photocatalysis will comprise the use of Fe-salts. The photochemical methods, in this work, will be compared in terms of their practicality, cost, and more importantly their degradation efficiency. All these factors will determine the feasibility of its commercial application.

Further comparisons will also be made regarding heterogeneous photocatalysis: Two commonly used standard TiO₂ formulations will be compared to see which is the most photocatalytically efficient: Sigma-Aldrich TiO₂ (Hombikat UV100 could not be obtained) and Degussa's P25 TiO₂. Various other conditions which will be optimised include pH, and concentrations of an oxidant. While the success of the degradation of the 3 pharmaceuticals is paramount to this project, identification of the intermediate products formed and the pathways of degradation are just, if not equally, as important. In some cases, the intermediate products formed in degradation can be more harmful than the initial pharmaceutical. LC-MS/MS analysis will be employed once the photodegradation studies have been optimised to determine the number and nature of the intermediates formed. From this analysis, mechanisms of degradation will then be proposed for each pharmaceutical.

In addition to this work, attempts will be made to develop visible light sensitised photocatalysts which can be used either indoor using cheap halogen lamps (or Laser Emitting Diodes (LEDs)) or outdoor using solar light. These will incorporate TiO₂ and will be applied in a suspended form. These novel photocatalysts will be characterised using various techniques such as Fourier Transform Infrared Spectroscopy (FT-IR), UV-vis Spectroscopy (UV-vis), Scanning Electron Microscopy (SEM), and Energy-Dispersive X-ray Spectroscopy (EDX). Their photocatalytic efficiency will then be tested on a model pollutant and compared against conventional P-25 TiO₂, currently the most efficient commercially available photocatalyst.

1.8 Thesis Outline

This section outlines this thesis chapter by chapter and describes in brief the research content within each chapter as follows:

Chapter 1 has presented the existing and potential methods used to eliminate pharmaceuticals (APIs) and discussed in detail the TiO₂ photocatalytic process, its mechanism of action, limitations and the current and future research in the field. Chapter 2 contains the detailed experimental procedures and methods for all research work contained within this thesis.

Chapter 3 focuses on the photolytic and photocatalytic degradation studies of the 3 pharmaceuticals. Initial UV-vis profile studies of each API are shown including studies at different pHs to determine any arising effects on the APIs. Preliminary photolysis studies with various lamps and reactors of different scales and configurations are also discussed. Chapter 3 also presents studies investigating the effect of various parameters on each API such as (i) TiO₂ concentration (using the titanium dioxide with the most superior performance), (ii) varying pH (iii) addition of hydrogen peroxide at various concentrations and (iv) varying concentrations of initial API to test the method robustness. These studies have been analysed using individual LC methods developed on a HPLC-PDA system.

Chapter 4 examines comprehensively the intermediates generated from the APIs in photodegradation studies. LC-PDA methods used in previous studies were adjusted and transferred to an ESI-LC-MS/MS instrument. These methods were used to detect and identify intermediate compounds generated from the APIs in the optimized photolytic and photocatalytic reactions. Intermediate structures were determined from analysis of the combined DI-MS and LC-MS/MS data attained in photolytic and photocatalytic studies. This data has been corroborated with a predictive oxidation analysis and further confirmed by the characterisation of their respective fragment ions. Degradation pathways are also presented showing the route of each pharmaceutical to these intermediate compounds.

Chapter 5 describes the development of new visible light sensitised photocatalytic materials. The most stable and popular linkers from those discussed in Chapter 1 were selected to anchor dyes to TiO_2 . Various sensitising molecules (phthalocyanines and porphyrins) were then selected to attach to these linkers and to TiO_2 . These composite materials were then characterised and their photoactivity was evaluated with our target APIs.

Finally, Chapter 6 presents the overall conclusions from the research discussed in this thesis and suggests future work which could be undertaken based on these conclusions.

Chapter 2 - Experimental

2.1 General

2.1.1 Materials and Instrumentation

Famotidine, Tamsulosin Hydrochloride and Solifenacin Succinate were donated by Astellas Ireland Pharmaceutical Limited (Dublin, Ireland). Millipore Milli-Q water was used in all experiments. HPLC and LC-MS/MS analysis were undertaken with respective HPLC grade and LC-MS grade solvents purchased from Fischer Scientific Ltd. Formic acid was mass spectrometry grade and purchased from Sigma Aldrich. FIXANAL buffers were purchased from Sigma-Aldrich and were comprised of citric acid, sodium tetraborate, potassium dihydrogen phosphate, disodium hydrogen phosphate, NaOH, HCl, NaCl depending upon the pH. P-25 TiO₂ was kindly donated by Degussa. Sigma Aldrich TiO₂ was purchased from Sigma Aldrich 99.8% Anatase. Hydrogen peroxide (27.5%) and sodium bisulfite were used as purchased from Sigma-Aldrich Chemicals. Nylon membrane filters were purchased from Millipore (Ireland) and used in filter housings to filter samples from photocatalytic experiments. Mobile phases were filtered with Pall nylon filters (0.2 µm pore size, 47 mm diameter) and for LC-MS/MS analysis regenerated cellulose filter membranes (0.2 µm pore size, 47 mm diameter). UV absorption profiles for the pharmaceuticals were undertaken using a UV-vis spectrophotometer (Cary 50 UV-vis, Varian). Chromatographic separations were performed on a 'reversed-phase' HPLC column: Phenomenex PFP (Luna) C₁₈ 150 mm x 4.6 mm 5 µm particle size for HPLC-UV(PDA), and 150 mm x 2.1 mm (5 µm) for LC-MS/MS analysis. Analysis of samples were performed on two HPLC systems: (1) a Varian Prostar HPLC-PDA (Varian Inc, Palo Alto, USA) with a Varian Prostar Solvent Delivery system(model 230), PDA detector (model 330) autosampler (model 410), (2) a Varian HPLC-UV (Varian Inc, Palo Alto, USA) with a Varian Inert 9012 Tertiary Pump system, Varian 9050 Variable wavelength UV-vis detector, and Rainin Dynamax auto-injector model AI-200. LC-ESI-MS/MS analysis was performed on an Agilent 1100 series high performance liquid chromatograph with a vacuum degasser, binary pump, ALS autosampler, and diode array detector. This LC was coupled to a Bruker Daltonics Esquire ESI-ion trap mass spectrometer. Agilent Chemstation version A.09.03 (Agilent Technologies, USA) and Bruker Daltonics esquire control version 4.0 (Bruker Daltonics, UK) were employed to control the system and data analysis was performed using Bruker Daltonics Data Analysis 3.0 (Bruker Daltonics, UK).

2.1.2 UV-vis Analysis Experimental Procedure

Dilutions of 1 mM stock solutions were undertaken and the most appropriate concentration for absorption was determined. These concentrations were also adopted in photocatalytic studies (0.028 g/L Famotidine, 0.037 g/L Tamsulosin), which can be found to be optimum for photocatalytic drug studies in literature (5-50 mg/L).^{155, 156} A 1 in 12 dilution (0.083 mM)

displayed an appropriate UV-vis profile for Famotidine and Tamsulosin. For Solifenacin a concentration of 1 mM was employed.

2.1.3 pH Effects Experimental Procedure

4 mL of each drug solution was prepared with 50:50 buffer: drug solution. Buffers were previously diluted with Millipore water in a 500 mL volumetric as per manufacturer's instructions. The final concentration of drug/buffer solution used in these studies was 50 μ M for Famotidine, 83 μ M for Tamsulosin and 500 μ M for Solifenacin. Solutions were then analysed by UV-vis spectroscopy.

2.2: Chromatographic Methods

2.2.1 Method Development Part II HPLC-UV Experimental Procedure

Stock solutions of 100 μ M were prepared in Millipore distilled water and dilutions were made with Millipore water with laboratory auto-pipettes. Mobile phases were filtered and sonicated prior to use. (Varian Prostar HPLC-PDA) Mobile Phase A: 100% MeOH 0.1% Formic Acid. Mobile Phase B: 100% H₂O 0.1% Formic Acid. Table 2.1 contains method development conditions with the methanol solvent phase system which were optimized from methods developed by A. Deegan.¹⁵⁷ See Table 2.2 for final methods.

API	Wavelength nm	Mobile Phase	Inj. Vol.	Run Time (mins)	t_R (mins)
FAM	265	25% MeOH: H ₂ O (0.1% F.A.)	50 μ L	10	4.0
TAM	280	65% MeOH: H ₂ O (0.1% F.A.)	50 μ L	10	4.7
SOL	220	70% MeOH: H ₂ O (0.1% F.A.)	50 μ L	10	7

Table 2.1: Chromatographic Conditions with Methanol on Varian-UV-vis instrument.

2.2.2 Method Development Part III HPLC-PDA Method Development

Stock solutions of 100 μ M were prepared in Millipore distilled water and dilutions for samples were made with Millipore water with laboratory auto-pipettes. Analysis was performed on the Varian Prostar HPLC-PDA previously described. See Table 2.2 for final methods and Table 2.3 for theoretical plate calculations, retention factor, and tailing and asymmetry factors.

API	Wavelength nm	Mobile Phase	Inj. Vol. μ L	Run Time (mins)	t_R (mins)
Famotidine	265	9% MeOH:H ₂ O 0.1% F.A	20	15	10.5
Tamsulosin	223	40% MeOH:H ₂ O 0.1% F.A	20	20	13.1
Solifenacin	220	30% ACN:H ₂ O 0.1% F.A	20	20	14.2

Table 2.2: Final methods on Varian HPLC-PDA system for analyte and intermediate detection

API	T _f	A _s	N	k'	HETP
Famotidine	0.94	0.92	3582	4.18	0.0418
Tamsulosin	1.08	1.2	2342	5.88	0.064
Solifenacin	1.1	1.23	3125	5.86	0.0479

Table 2.3: Tailing, asymmetry and capacity factors for the three pharmaceuticals along with column efficiency, and HETP values.

2.2.3 LC-MS/MS Method Transfer and Re-optimisation

Standards for each pharmaceutical and samples from a previous photocatalytic experiment were employed such that the retention times of intermediates could be adjusted. See Chapter 4 Table 4.1 for final methods. Table 2.4 shows the MS conditions for each pharmaceutical.

Settings	Famotidine	Tamsulosin	Solifenacin
Capillary, V	- 4500	-4500	-4451
End Plate Offset, nA	- 500	-1200	-752
Nebuliser, psi	50	50	50
Dry Gas, L/min	8	8	8
Dry Temp, °C	325	325	325
Skim 1, V	15	19.2	31.7
Skim 2, V	8.1	6.2	15
Cap Exit, V	65	76.2	81.7
Cap Exit Offset, V	50	95.4	50
Octopole, V	5	2.51	2.64
Octopole Δ, V	2.05	1.93	2.05
Oct RF, Vpp	177.1	201.6	205.7
Lens 1, V	- 2.2	-4.1	-4.7
Lens 2, V	- 49.5	-46.1	-50.7
Trap Drive	50.1	38.4	38.5

Table 2.4: ESI-MS method conditions for each pharmaceutical.

2.3: Chapter 3: Photolytic and Photocatalytic Degradation Studies with Famotidine, Tamsulosin and Solifenacin

2.3.1 Quartz Photolysis General Experimental Procedure

The MP Hg Lamp set-up was employed (Figure 2.1) and experiments were performed using a TQ-150 MP Hg lamp and under static flow conditions (unless otherwise stated). The reactor volume was 300 mL. The solution was cooled using a quartz immersion well and all solutions were irradiated for 1 h with samples taken at 5 minute intervals. Sample concentrations of 0.083 mM, (Solifenacin 1 mM) were used, and were monitored by UV-vis spectrophotometry.

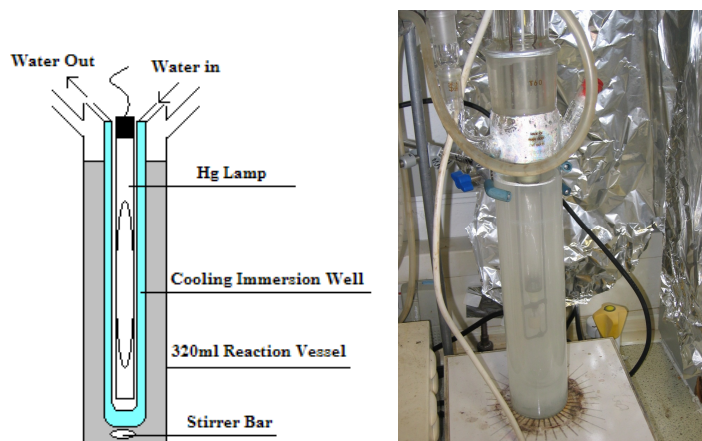


Figure 2.1: MP Hg Lamp Set-Up (Vol. 320 mL) schematic (left) and photograph (right).

2.3.2 Pyrex Photolysis Experimental Procedure

The general procedure was followed as outlined previously (2.3.1) with the incorporation of a Pyrex immersion well instead of Quartz. Irradiations were 1 h or 5 h. The reactor volume was also 320 mL in this case.

2.3.3 Enviolet Reactor Experimental Procedure

5 L of 0.083 mM drug solution (or 1 mM Solifenacin) was placed into the reactor (Figure 2.2). A 0 minute sample was taken at this point after pumping the solution through for 1 minute with no irradiation. Residual water can be left in the pumping system after cleaning and this sample represents the actual concentration in the reactor. The MP Hg lamp (600 W) was turned on and allowed to irradiate for 300 minutes. A cooling jacket in the main reservoir ensured the sample did not overheat. Samples were taken regularly at 0, 30, 60 minutes and every hour for 5 h and were monitored by UV-vis spectrophotometry.

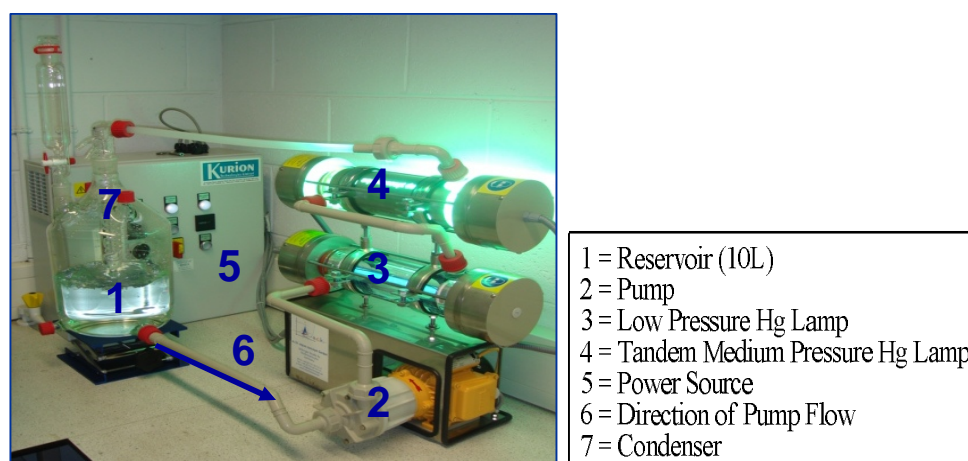


Figure 2.2: Custom built Enviolet Photoreactor for wastewater treatment.

2.3.4 Low Pressure Hg Lamp Experimental Procedure

Photolysis experiments were performed using a TQ-150 low pressure Hg lamp. The reactor volume was 800 mL. The solution was irradiated for 5 h using a quartz inner tube encasing the lamp with a Pyrex vessel (see Figure 2.3) to ensure filtration of light below 300 nm outside of the vessel. Samples were taken every 30 mins for one hour and then hourly after that. Sample concentrations of 0.083 mM were used (Solifenacin 1 mM), and were monitored by UV-vis spectrophotometry.

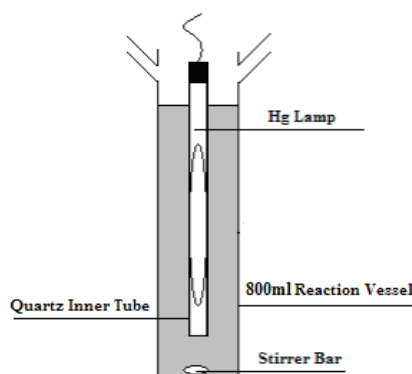


Figure 2.3: Schematic of the LP Hg Lamp Set-Up (Vol. 800 mL).

2.3.5 Pyrex and Quartz Photolysis with HPLC Analysis Experimental Procedure

The general procedure was followed (2.3.1 & 2.3.2). The concentration of pharmaceutical in each experiment was 0.083 mM. Analysis was undertaken with the final methods previously outlined (section 2.2.2). Degradation profiles are graphed with reaction (illumination) time on the x-axis (in minutes) and concentration is plotted on the y-axis in the form: C_t/C_0 where C_t is the concentration of pharmaceutical at time (in minutes) divided by the concentration of pharmaceutical at 0 minutes, C_0 . Degradation graphs are plotted thereafter in this manner.

2.3.6 Adsorption Experimental Procedure (orbital shaking experiments)

The adsorption experiments were performed with a varying substrate concentration of 0, 5, 10, 20, 50, 100 μM . A TiO_2 concentration of 0.25 g/L was applied to 50 mL volumes of drug solution in 250 mL conical flasks. Conical flasks were placed in an Orbital Mixer which was used to agitate and equilibrate the samples overnight in the absence of light (using tinfoil) unless otherwise stated. The following equation determined the amount of drug adsorbed by TiO_2 . pH experiments were conducted with buffers previously described.

$$q = \frac{C_f - C_i}{\text{TiO}_2(\text{g})} \times \text{Vol}(\text{L})$$

q = drug adsorbed(mg) per (g) of TiO_2

C_f = Concentration post-adsorption (mg/L)

C_i = Concentration pre-adsorption (mg/L)

Vol = Volume (L)

TiO₂ = Concentration of TiO₂ (g)

2.3.7 Heterogeneous Photocatalysis (Quartz) Experimental Procedure:

320 mL of drug solution was placed into the immersion well reactor at a concentration of 0.083mM (or 1mM for Solifenacin). A 0 minute sample was taken at this point. 0.05 g of TiO₂ (P25 or Sigma Aldrich) was then added into the reactor with washings from the solution in the reactor to ensure the entire amount was added. The lamp (TQ-150 Hg lamp) was turned on and allowed to illuminate for 60 minutes. A quartz immersion well ensured the sample mixture did not overheat. 5 mL samples were taken regularly at 0, 5, 10, 20, 30, 40 and 60 minutes.

2.3.8 Heterogeneous Photocatalysis (Pyrex) Experimental Procedure

The procedure, as previously outlined (2.3.7), was followed with the exception that a Pyrex immersion well was employed.

2.3.9 TiO₂ Optimisation (and general) Experimental Procedure

320 mL of solution (0.083 mM) was placed into the immersion well reactor. A 0 minute sample was taken at this point. TiO₂ (P25 or Sigma Aldrich) was then weighed out (0.1 g, 0.2 g, 0.4 g, 0.6 g) and added into the reactor with washings from the solution in the reactor to ensure the entire amount was added. The suspension was allowed to stir with a magnetic stirring bar and equilibrate for approximately 0.5 h without illumination. Once the equilibration time was reached, the lamp (TQ-150 Hg Lamp) was turned on and allowed to illuminate for 180 or 300 minutes. A Pyrex immersion well was used in all experiments to cool the sample mixture. Samples were taken regularly for the first hour and then hourly after this. Results were monitored using UV-vis spectroscopy and/or HPLC-UV/PDA instrumentation with methods previously described (2.2.2). Table 2.5 contains data relation to the physical and chemical properties of the two titanias used in photocatalytic studies.

Property	P-25 TiO ₂	SA-TiO ₂
Wt. Ratio (Anatase:Rutile)	80:20	100
Average Particle Size (nm)	21	130
Content	Al ₂ O ₃ 0.3%, SiO ₂ 0.2%, Fe ₂ O ₃ 0.01%, HCl 0.3%	0.2% trace metals
Specific Surface Area (m ² /g)	50±15	8.6
Moisture %	1.50	N/A
pH	3.5-4.5	N/A
Tapped Density (g/L)	130	N/A
Ref	158	159,160

Table 2.5: Characteristics of the two Titanias employed in photocatalytic studies.

2.3.10 pH Studies Experimental Procedure:

Stock solutions were prepared (0.083 mM) of each drug, and the pH adjusted accordingly with acids and bases to the appropriate pH (3, 5 or 8). In the case of Famotidine, a more extensive study was undertaken (pH 3-10). The solution was then made up to the mark and the pH measured with a pH meter. The pH of the solution was measured again post adsorption and readjusted if necessary. The general procedure, as outlined previously (2.3.9), was then followed.

2.3.11 Oxidant Addition Experimental Procedure:

The quantities of hydrogen peroxide doses used were 0.1 mM, 1 mM, 5 mM, 50 mM. Hydrogen peroxide was added prior to irradiation of the drug solution and post the 30 minute adsorption period. Stock solutions were prepared at concentrations taking into account the dilution factor from the hydrogen peroxide addition such that once added, the concentration of drug solution was 0.083 mM. The peroxide in each sample was quenched with 2 drops of sodium bisulfite (40% w/v, 3.84M).¹⁶¹ The general procedure, as outlined previously (2.3.9), was then followed. The final concentration of peroxide for each initial concentration added is given in Table 2.6.

$[\text{H}_2\text{O}_2]_{\text{init}}$ added (mM)	V_{total}	Dilution Factor	$[\text{H}_2\text{O}_2]_{\text{Final}}$ (mM)
0.1	320	3.75×10^{-5}	3.75×10^{-6}
1	320	3.75×10^{-4}	3.75×10^{-4}
5	320	1.875×10^{-3}	9.375×10^{-3}
50	320	1.875×10^{-2}	9.375×10^{-1}

Table 2.6 Final vs. initial concentration values for H_2O_2 addition experiments

2.3.12 Controls Experimental Procedure:

Control experiments were performed with a drug concentration of 0.083 mM. The control experiments which were conducted were as follows: (i) TiO_2 alone, (ii) H_2O_2 alone, (iii) UV alone, (iv) UV/ TiO_2 (v) $\text{H}_2\text{O}_2/\text{TiO}_2$ (vi) UV/ H_2O_2 . Hydrogen peroxide and TiO_2 concentrations were the optimum concentrations as determined in experiments. The general procedure, as outlined previously (2.3.9), was then followed.

2.3.13 Concentration Variation Experimental Procedure:

A stock solution was prepared of each pharmaceutical at 1mM. Dilutions were made from this stock to prepare 320 mL of 20 μM and 200 μM solution for irradiation experiments. A 1000 μM experiment was also performed. The general procedure, as outlined previously (2.3.9), was then followed. Table 2.7 shows the concentrations used in these studies in mg/L and μM .

μM	[FAM]mg/L	[TAM]mg/L	[SOL]mg/L
1000	337	444	480
200	67	88.8	96
83	28	37	40
20	6.7	8.88	9.6

Table 2.7: Concentrations employed in concentration variation studies in μM and mg/L.

2.3.14 Sodium Bisulfite Studies Experimental Procedure

UV-vis experiments were conducted with samples of API and API plus 2 drops of bisulfite per 4 mL of API solution. UV-vis analysis was conducted every minute for 10mins and then every 10 mins for 1 h. Further analysis was undertaken 19 h later. ^1H NMR experiments were performed in deuterated water and between 0.005-0.010 g of each API. 0.011 g of sodium bisulfite was added to each NMR tube. A further 0.030 g was added to each tube to see the effect of additional bisulfite. HPLC analysis of the effect of sodium bisulfite was undertaken on 100 μM samples of each API. 2 drops of sodium bisulfite were added per 4 mL of sample and the samples were then analysed via replicate injections on a HPLC as previously outlined in section 2.2.2.

2.3.15 Alternative Quencher Studies using Ethanol Experimental Procedure

1 mL solutions of Famotidine/ H_2O_2 were quenched with varying amounts of ethanol (0mL, 0.1 mL, 0.25 mL, 0.5 mL, 1 mL, 1.25 mL, 1.5 mL) as a quencher. The ethanol was cooled in a freezer to -18°C prior to use. Samples were taken after 5 mins and 10 mins reaction with H_2O_2 . Follow-up studies were performed with 0.5 mL ethanol as a quencher with solutions of Famotidine/ H_2O_2 with varying H_2O_2 concentrations. Samples were taken at 0mins, 0mins (after addition of H_2O_2) and 1 mins. The ethanol was cooled on ice prior to use and kept on ice as the sample was taken. As a control, 2 samples were not cooled on ice. The results from all experiments were analysed by HPLC as previously outlined in section 2.2.2.

2.3.16 Famotidine Hydrolysis Studies Experimental Procedure

UV-vis analysis was undertaken on 4 solutions: 2 of Famotidine (adjusted to pH 2, and an unadjusted sample) and 2 of Millipore water (adjusted to pH 2, and an unadjusted sample). 0.011 g of TiO_2 was added to 20 mL of each solution, and the solution filtered with Nylon filter membranes. UV-vis analysis of the resulting solutions was then undertaken. Sodium hydroxide was added to both original solutions of Famotidine (pH 2 and no pH adjustment) until a pH of 11 was obtained and the UVs were obtained and compared.

2.3.17 Adsorption of Pharmaceuticals to Immersion Reactor Experimental Procedure

320mL solutions of each pharmaceutical (0.083mM) were prepared and placed into the reactor which was stirred with a magnetic stirring bar for 3h. Samples were taken at regular intervals and analysed with UV-vis spectroscopy. Uv-vis profiles of samples were then compared to the UV-vis profile of the stock solution.

2.4: Chapter 4: Intermediate Analysis and Elucidation of Degradation Mechanism for Famotidine, Tamsulosin and Solifenacin

2.4.1 DI-Mass Spectrometry Studies

LC-MS/MS instrument details can be found in section 2.1.1 of this chapter. 100 μ L of each sample from a photolytic/photocatalytic experiment was placed in a glass syringe fitted to an automatic syringe pump. This sample was then slowly infused into the mass spectrometer at a rate of 300 μ L/h. For Famotidine and Tamsulosin, the optimised TiO₂ photocatalytic experiment was analysed with an initial drug concentration of 0.083 mM, and for Solifenacin, a photolysis experiment at 1 mM was analysed. Samples were run in positive mode only. MS/MS analysis was also employed on the parent ions of each pharmaceutical to establish and identify the daughter ions.

2.4.2 Follow up DI-Mass Spectrometry Studies

The same procedure as above was followed, however all samples were from photocatalytic experiments and were performed at much higher concentrations of 1 mM and with the optimised TiO₂ concentration for 0.083 mM experiments. Samples for these experiments were filtered with cellulose acetate syringe filters to prevent interferences. Cellulose acetate syringe filters (RC membrane, 0.2 μ m, 15 mm) were purchased from Phenomenex. The compound stability parameter was adjusted to 10%, 50% and 100% such that any additional unstable intermediates would arise.

2.4.3 LC-MS/MS Analysis Studies

Instrumentation and methods used can be found in sections 2.1.1 and 2.2.3 of this chapter. The optimised TiO₂ photocatalytic experiment for each drug was analysed at the optimum concentration of 0.083 mM and at 1 mM (with a 1 in 2 dilution pre-analysis). In addition, 3 further experiments were performed: photolysis experiments with Quartz and Pyrex (0.083 mM) and the optimised photocatalysis/H₂O₂ experiment with the optimum amount of peroxide. Experiments were run in positive mode only.

2.4.4 Control Experiments

Two control experiments were performed to ensure all ions detected in LC-MS/MS runs were from intermediates generated by each pharmaceutical. Control experiment 1: (Photolysis) Irradiation of 300 mL of pure Millipore water with quartz glassware and a medium pressure mercury lamp for 1 hour. Control experiment 2: (Photocatalysis) Irradiation of 320 mL of pure Millipore water with Pyrex glassware, and a medium pressure mercury lamp and 0.1 g TiO₂ for 1 h. Photocatalytic samples containing TiO₂ were filtered with cellulose acetate syringe filters. Samples were taken at least every 10 minutes. Samples were analysed by LC-MS/MS with a mobile phase of 40:60 MeOH: H₂O 0.1% Formic Acid, 10 µL injection volume and a run time of 70 mins.

2.5: Chapter 5: Development and Characterisation of Visible Light Sensitised Photocatalytic Materials and Evaluation of their Photocatalytic Activity with Famotidine

2.5.1 NMR Spectroscopy

NMR spectra were recorded on a Bruker 4- UltrashieldTM instrument (Bruker Daltonics, UK) (400 MHz for ¹H; 100 MHz for ¹³C). NMR spectra were recorded using Sigma Aldrich grade deuterated solvents.

2.5.2 IR- Spectroscopy

IR Spectra were recorded on a Perkin-Elmer Spectrum (Massachusetts, USA) 100 FT-IR spectrophotometer using ATR (diamond) or an FT-IR Perkin Elmer (GX –FTIR) with preparation using KBr discs.

2.5.3 SEM Imaging/EDX Spectroscopy

SEM images were obtained on a Hitachi S3400n Tungsten system (Tokyo, Japan). Accelerating voltages of 10 or 20 keV were applied for all samples.

2.5.4 Mass Spectrometry

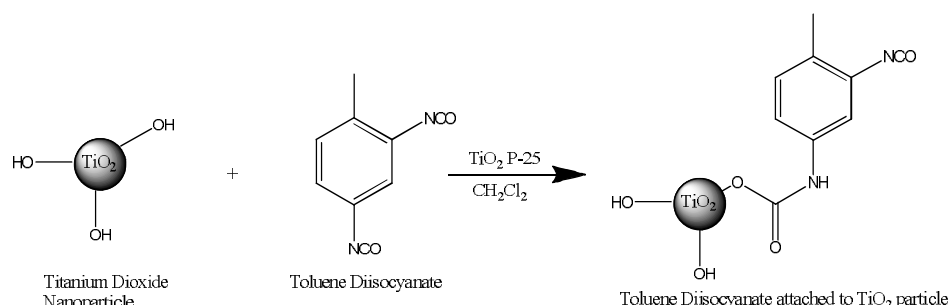
See section 2.1.1 of this chapter for full instrument details. Mass spectra were recorded in both positive and negative ion mode.

2.5.5 Diffuse Reflectance Spectroscopy

UV-vis profiles of coated TiO₂ materials were attained using a Jasco V-670 UV/Vis/NIR Spectrophotometer (Essex, UK) with a diffuse reflectance integrating sphere. Samples were

prepared into discs with KBr, and the scan range was between 200-900 nm. The reflectance was converted to absorbance using the software (Spectral Analysis), and plotted as the inv of % Reflectance.

2.5.6 Preparation of surface coated TiO₂ with TDI (toluene diisocyanate)



Reaction Scheme 1: Synthesis of TDI-TiO₂

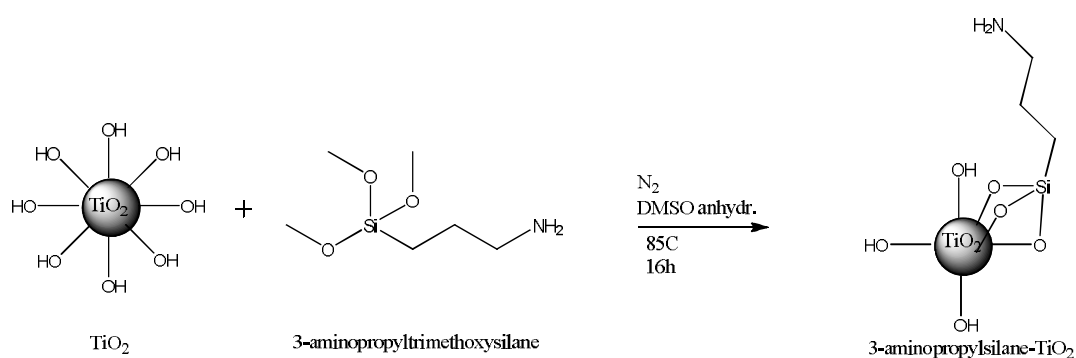
Procedure

A procedure from Jiang *et al.* 2008 was followed for the synthesis of TDI-TiO₂.¹⁰⁰ TiO₂ (1.6 g, 0.02 mol) was dispersed into CH₂Cl₂ under magnetic stirring and a white suspension was formed. TDI (1 mL, 0.007 mol) was then added drop wise into TiO₂/CH₂Cl₂ suspension under nitrogen. The suspension gradually turned yellow. The suspension was continually stirred for 2 h and subsequently filtered to obtain a yellow TDI-TiO₂ solid. The sample was washed 3 times with CH₂Cl₂ and left to vacuum dry. Analysis by FT-IR and UV-vis spectroscopy.

FT-IR: ν , cm⁻¹, 3300, 2280, 1644, 1600.

UV-vis (DR): nm, 408, 429 (λ_{max}), 470.

2.5.7 Aminosilanisation of TiO₂ particles.



Reaction Scheme 2: Synthesis of 3-aminopropylsilane-TiO₂

Procedure

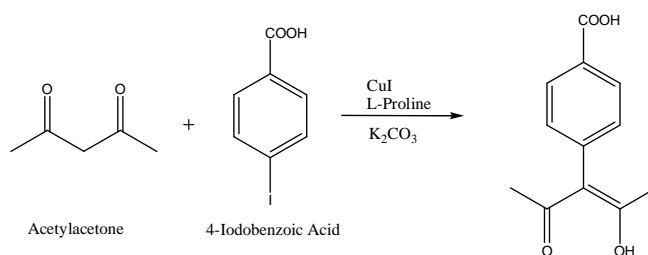
A procedure from Ye *et al.* was followed for the aminosilanisation of TiO₂ particles.¹⁶² A 500 mL round bottomed flask was degassed with N₂ and charged with TiO₂ (0.3 g). Anhydrous DMSO (210 mL) was then added. The particles were then dispersed into the anhydrous DMSO using ultrasonication for 10 min. APTS (1.5 mL) was then added into the flask. After stirring at

85°C for 16 h the solid particles were deposited by centrifugation and washed with anhydrous DMSO (3x180 mL). The TiO₂ particles were again dispersed in anhydrous DMSO (100 mL) using ultrasonication for 10 mins and were stirred under a nitrogen stream at 120°C for 20 h. The coated TiO₂ was then filtered once more and washed with anhydrous DMSO (3x180 mL). The product was then left to vacuum dry for 72 hours. Analysis was performed by FT-IR and EDX spectroscopy.

FT-IR: ν , cm⁻¹, 2937, 1666, 1138, 1055, 956 (Si-O-Ti).

EDX: keV, Si 1.8 keV, Ti 4.6, 5 keV.

2.5.8 Acetylacetonate linker synthesis



Reaction Scheme 3: Synthesis of Acetylacetonate Linker

Procedure

A procedure from McNamara *et al.* was followed for the synthesis of the acetylacetonate linker.¹⁶³ Iodobenzoic Acid (0.372 g, 0.0015 mol), acetylacetone (0.44 mL, 0.0045 mol), K₂CO₃ (1.036 g, 0.0075 mol), CuI (0.0285 g, 0.00015 mol) and L-Proline (0.0345 g, 0.003 mol) were dissolved in DMSO (15 mL) and heated at 90°C in a N₂ atmosphere for 24 h. The cooled solution was poured into 1 M HCl and extracted with ethyl acetate. The organic layer was dried over MgSO₄ and the solvent was removed under vacuum. The product was then purified using column chromatography with hexane: ethyl acetate (1:2) as eluant. The product eluted in the first 3 fractions.

Yield: Act (0.197 g, 60% Yield), Lit (0.205 g, 62%)

Appearance: Brown wax.

Mass Spec Analysis:

ESI positive mode: Molecular Ion at $m/z = 221(M+H)$,

ESI Negative mode: Molecular Ion at $m/z = 219(M-H)$

¹H NMR: ppm

Lit. 16.65 (s, 1H, OH) 8.08, (d, ³J_{H-H}) 8 Hz, 2H CH_{Ar}) 7.25, (d, ³J_{H-H}) 8 Hz, 2H CH_{Ar}) 1.84 (6H, CH₃) in CDCl₃

Act. 7.95 (d, ³J_{H-H} = 8.3 Hz, 2H CH_{Ar}) 7.3, (d, ³J_{H-H} = 8.2 Hz, 2H CH_{Ar}) 1.75 (6H, CH₃) in (CD₃)₂CO

¹³C NMR: ppm

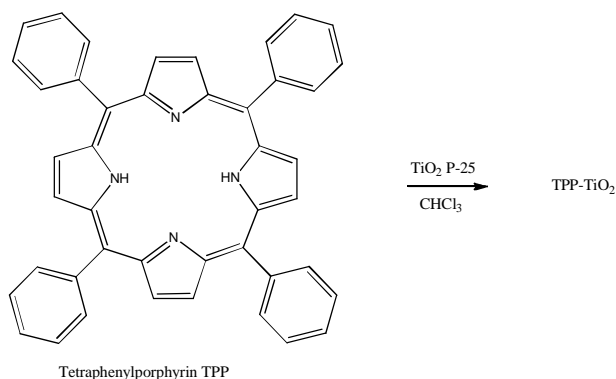
Lit. 190.7 (C-OH), 171.7 (COOH), 142.8 (C_{Ar}), 131.4 (CH_{Ar}), 130.8 (CH_{Ar}) 128.6 (C_{Ar}), 114.5 (C_{Enol}), 24.2 (CH₃).

Act. 191.58 (C-OH), 167.4179 (COOH), 142.78 (C_{Ar}), 132.34 (CH_{Ar}), 130.8391 (CH_{Ar}), 127.36 (very weak, C_{Ar}) 115.2917(C_{Enol}), 24.2117(CH₃) in (CD₃)₂CO

2.5.9 Determination of Loading Capacity Experimental Procedure

The loading capacity of the sensitizer onto TiO₂ in each composite was determined by the collection of the repetitive washings with solvent of each of the materials. In cases where exhaustive washings did not eventually become clear, a soxhlet extraction was undertaken. The material was placed inside an extraction thimble, and placed inside the extraction chamber of a soxhlet apparatus. The temperature was set to 30°C above the boiling point of the extraction solvent i.e. chloroform, methanol etc. The soxhlet extraction was complete once the solvent in the extraction chamber was completely clear. The thimble was removed and left to dry and the soxhlet extracted material removed from the chamber. The residual dye material in the extracted solvent was then rotary evaporated to dryness and the yield determined and added to the yield determined from washings. This total yield was then subtracted from the amount of material used in preparation of the composite. This amount was then determined to be the loading capacity for the composite and is quoted as g(dye)/g TiO₂.

2.5.10 Preparation of Tetraphenylporphyrin-TiO₂ (TPP-TiO₂).

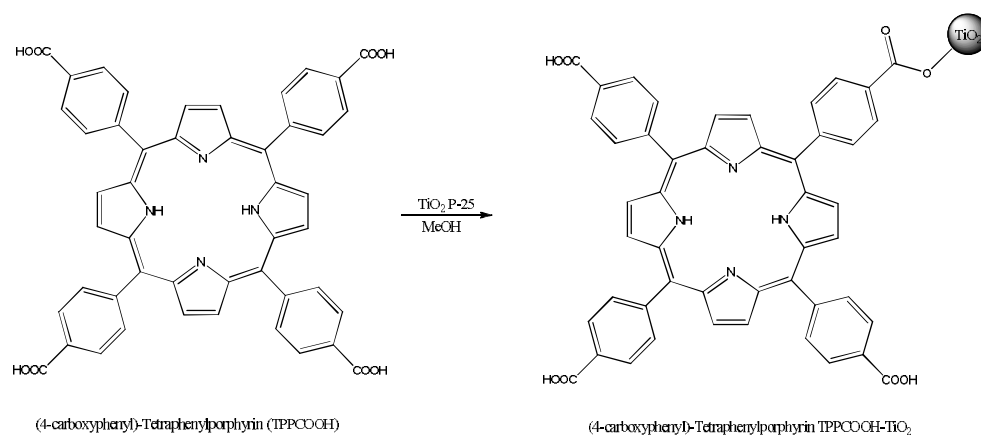


Reaction Scheme 4: Synthesis of TPP-TiO₂

Procedure

Tetraphenylporphyrin (0.038 g, 0.063 mmol) was added to a 100 mL round bottomed flask with a stirring bar. Chloroform (50 mL) was then added, along with TiO₂ (1 g). The solution was stirred at r.t for 4 h (foil covered). The product was filtered and washed with chloroform until washings ran clear. The product was additionally dried under vacuum overnight. The appearance of the product was a white solid powder, indicating that none of the TPP had been coated onto the TiO₂. No further analysis was conducted.

2.5.11 Preparation of Tetra(4-carboxy)phenylporphyrin-TiO₂ -A (TCPP-TiO₂-A)



Reaction Scheme 5: Synthesis of TCPP-TiO₂ via adsorbed method

Procedure

Methanol (50 mL) was added to a 100 mL round bottomed flask with a stirring bar. 1 g of TiO₂ was then added and the solution sonicated for 10 mins. 0.05 g of tetra(4-carboxy)phenylporphyrin was then added. The solution was stirred at room temperature for 4 h (foil covered). The product was then filtered and washed with copious amount of methanol until the washings ran clear. The colour of the composite was purple, however once ground via pestle and mortar, the appearance was a purple/brown powder.

TCPP

FT-IR: ν , cm⁻¹, 3014, 1685, 1604, 1400, 1222, 1174, 1099, 963.

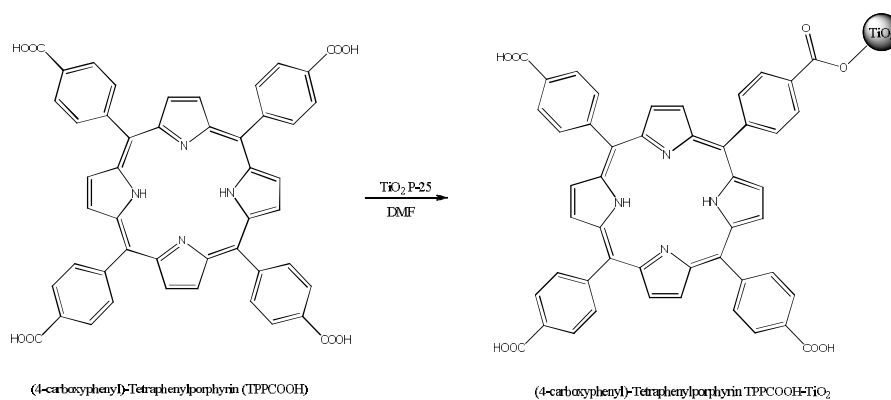
UV-vis: nm, 416(Soret), 512, 547, 589, 643.

TCPP-TiO₂-A

FT-IR: ν , cm⁻¹, 3740, 3391, 2923, 1614, 1383, 1263, 1176, 1110, 1054, 967, 636.

UV-vis (DR): nm, 408 (Soret), 523, 560, 597, 654.

2.5.12 Preparation of Tetra(4-carboxy)phenylporphyrin-TiO₂ -B (TCPP-TiO₂-B)



Reaction Scheme 6: Synthesis of TCPP-TiO₂ via bound method.

Procedure

DMF (50 mL) was added to a 100 mL round bottomed flask with a stirring bar. TiO₂ (1 g) was then added along with tetra(4-carboxy)phenylporphyrin (0.05 g, 0.63 mmol). The solution was sonicated for 10 mins and then heated to reflux for 5 h. The product was then filtered and washed with DMF. The filtrate remained pale pink after countless washings. Soxhlet extraction was then performed overnight with methanol as the extraction solvent. The product was then left to dry under vacuum and the product was collected. The appearance, as with the composite A was purple post-reaction, after grinding, it was a purple/brown colour.

TCPP

FT-IR: ν , cm⁻¹, 3014, 1685, 1604, 1400, 1222, 1174, 1099, 963.

UV-vis: nm, 416(Soret), 512, 547, 589, 643.

TCPP-TiO₂-B

FT-IR: ν , cm⁻¹, 3743, 3410, 2925, 1621, 1383, 1263, 1176, 1111, 1055, 966, 667.

UV-vis (DR): nm, 410 (Soret), 523, 561, 598, 655.

2.5.13 Preparation of Zn-Hexadecafluorophthalocyanine-TiO₂

The procedure (2.5.11) was employed with the following changes. Chloroform (50 mL) was employed as solvent and Zn-Hexadecafluorophthalocyanine (0.047 g, 0.054 mM) was employed as the sensitizer which was previously synthesized by B. Murphy in our group. Prior to immobilisation, the ZnHFphtalocyanine was analysed with TLC (hexane: ethyl acetate 6:1), UV-vis spectroscopy (in dichloromethane) and FT-IR. The ZnHFpc-TiO₂ product underwent a soxhlet extraction post reaction with chloroform. A further soxhlet extraction was performed on 0.42 g of the material with acetone as solvent. The ZnHFPC-TiO₂ product was analysed by FT-IR, and UV-vis spectroscopy.

ZnHFpc

TLC: R_f = 0

FT-IR: ν , cm⁻¹ 1491, 1313, 1266, 1144, 958.

UV-vis: nm, (B-bands) 349, (Q-bands) 643, 677.

ZnHFpc-TiO₂

FT-IR: ν , cm⁻¹ 1612, 1490, 1401, 1313, 1266, 1144, 958, 739.

UV-vis (DR): nm, (0.002 g/g TiO₂) (Q-bands) 647, 682.

(0.034 g/g TiO₂) (Q-bands) ~650, 689.

2.5.14 Preparation of 1,4-(tetrabenzaldehyde)phthalocyanine -TiO₂

The procedure (see 2.5.11) was employed with the following changes. Chloroform(50 mL) was employed as solvent and 1,4-(tetrabenzaldehyde)phthalocyanine (0.033 g, 0.054 mM) was employed as the sensitizer which was previously synthesized by V. Peters in our group. UV-vis

analysis of the phthalocyanine was conducted before use. The product was soxhlet extracted post reaction with chloroform. The photocatalyst product had a loading of 22 mg/1 g TiO₂. Analysis of the product was undertaken with FT-IR and diffuse reflectance UV-vis spectroscopy.

1,4-(tetrabenzaldehyde)phthalocyanine:

FT-IR: ν , cm⁻¹ 1720, 1601, 1506, 1237, 1165, 1094, 1014.

UV-vis: nm, (B-band) 329, (Q-bands) 666, 702.

1,4-(tetrabenzaldehyde)phthalocyanine -TiO₂:

FT-IR: ν , cm⁻¹ 1653, 1237, 1168, 1055, 679

UV-vis (DR): nm, (Q-bands) 638, 681, 709.

2.5.15 Alternative preparation of 1,4-(tetrabenzaldehyde)phthalocyanine -TiO₂

The same product as mentioned in 2.5.14 was prepared, although a method by Lu *et al.* 2010 was followed.¹⁶⁴ TiO₂ (1 g) was added to a 100 mL round bottomed flask along with chloroform (30 mL). 1,4-(tetrabenzaldehyde)phthalocyanine (0.006 g, 6 μ M or 0.008 g, 8 μ M) was then added and the reaction sonicated for 5 mins. The reaction solution was allowed to stir for 5 h, after which the solvent was removed under vacuum. The resulting product had a loading of either 6 mg/1 g TiO₂ or 8 mg/1 g TiO₂.

1,4-(tetrabenzaldehyde)phthalocyanine:

FT-IR: ν , cm⁻¹ 1720, 1601, 1506, 1237, 1165, 1094, 1014.

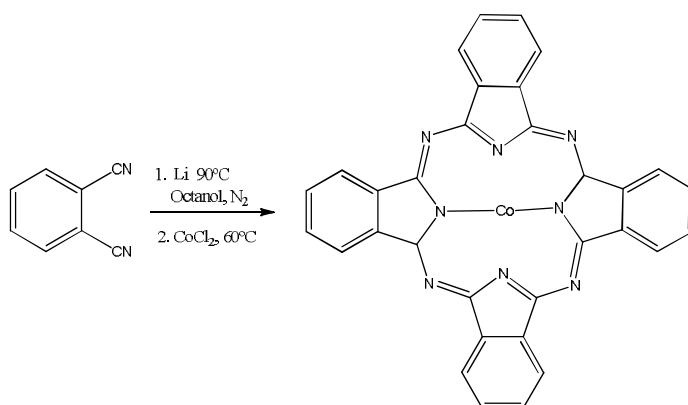
UV-vis: nm (B-band) 329, (Q-bands) 666, 702.

1,4-(tetrabenzaldehyde)phthalocyanine -TiO₂:

FT-IR: ν , cm⁻¹ 1650, 1237, 1167, 1116, 1096, 1056, 1015, 670.

UV-vis (DR): nm (Q-Bands) 621, 675, 708.

2.5.16 Synthesis of Cobalt Phthalocyanine



Reaction Scheme 7: Cobalt Phthalocyanine synthesis via condensation reaction.

Procedure

Octanol (2 mL) and Li (0.3 g) were added to a carousel synthesizer and heated to 90°C for 0.5 h until the solution became cloudy. Phthalonitrile was then added and the solution was purged with N₂ for 5 mins. A green/blue solution was obtained after addition of the phthalonitrile. The reaction mixture was allowed to stir under N₂ overnight. CoCl₂ (0.2 g) was then added and the temperature was set to 60°C and left for 3 h. An extraction of the product was attempted although it was not organic soluble, and the product was filtered and collected. No UV-vis analysis was conducted due to the insolubility of the phthalocyanine in any solvents. The product was then donated to another group for use.

2.5.17 General Procedure for Photocatalytic Reactions

Photocatalytic reactions were performed on aqueous solutions of Famotidine (100 mL) at a concentration of 0.083 mM. The solution was added to a schlenk flask (Figure 6.1) along with a previously weighed amount of photocatalyst (0.031 g) (or none for photolysis experiments). Prior to irradiation the reaction solution was sonicated for 10 mins, and the reaction was placed in a photochemical fume cupboard at a distance of 28 cm from a 500 W Halogen lamp (IQ Group). The irradiance spectrum for the halogen lamp can be found in the appendices (6A-2). The reaction was clamped to a stirring plate and a cooling cold finger inserted. Samples (2 mL) were taken regularly for the first hour and then hourly for 3 hours. Samples from all photocatalytic reactions were filtered using Nylon filter membranes straight into vials for HPLC analysis. Post reaction, the photocatalyst was recovered from the reaction solution via a centrifuge chamber. Once all the photocatalyst was collected from the reaction solution, it was washed with water (3 x 10 mL) and methanol (3 x 10 mL) to remove any impurities. Any remaining solvent was removed by rotary evaporator. HPLC analysis was employed on the samples taken from the photocatalytic experiments using methods detailed in section 2.2.2 of this chapter.

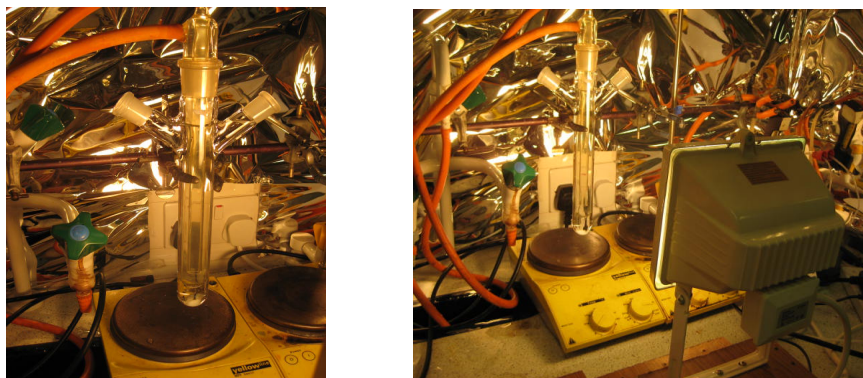


Figure 6.1: Indoor photocatalytic reaction set-up with Schlenk flask, and inserted cooling finger situated over a stirring plate with irradiation by a Halogen lamp.

2.5.18 Solar Photocatalytic Reactions Experimental Procedure

The general procedure (2.5.17) for photocatalytic reactions was followed and after sonication for 10mins the reaction was taken outside. In the case of these reactions the reaction set-up was the same with irradiation from sunlight instead of a halogen lamp. A lux meter recorded the intensity of the solar light throughout the reaction and was rotated frequently in line with the suns rotations to allow for an accurate reading.

2.5.19 Photocatalytic Reactions (Air Purged) Experimental Procedure

The general procedure (2.5.17) for photocatalytic reactions was followed. Air purging was undertaken with standard air pumps throughout the reaction (Hagen Elite aquarium pumps). A sparger at the air inlet allowed generation of a consistent flow of small air bubbles. These reactions were performed with a reduced volume of reaction solution (50 mL) to prevent overflow. The amount of photocatalyst was also halved in this case (0.0155 g). Air purged controls were also performed with no photocatalyst.

2.5.20 Controls Experimental Procedure (TCPP-TiO₂)

The general procedure (2.5.17) for photocatalytic reactions was followed. The control experiments performed were: (1) TCPP (0.001 g) with no TiO₂, and (2) both TCPP (0.001 g) and TiO₂ (0.031 g) together (3) No photocatalyst i.e photolysis (4) dark experiment with TCPP-TiO₂ (adsorption only).

2.5.21 Evaluation of TCPP-TiO₂ with Tamsulosin and Solifenacin Experimental Procedure

The general procedure (2.5.17) was followed with the pharmaceutical Tamsulosin or Solifenacin at a concentration of 0.083 mM. Control experiments were also performed: (1) photolysis and (2) TiO₂ alone.

Chapter 3 – Photolytic and Photocatalytic Degradation Studies of Famotidine, Tamsulosin and Solifenacin using TiO₂

3.1 Introduction

Preliminary photodegradation tests with sole irradiation must first be performed in any pharmaceutical photodegradation study. This should give an indication of the light sensitivity of each compound and also serve as a comparative control for photocatalytic experiments. The emission spectrum for a typical medium pressure (MP) mercury lamp is shown in Figure 3.1. It emits moderately at 254 nm. It also emits at many wavelengths between 250 nm and 320 nm, and also has some intense but scarce emissions between 400 nm and 600 nm. Low pressure mercury lamps emit exclusively at 254 nm (Figure 3.1). Depending on the lamp employed, the type of glassware used should be considered. The importance of using different types of glassware is shown in Figure 3.2. Pyrex has a cut off filter at 300 nm, which Quartz glassware does not. Employing Quartz glassware allows light below 300 nm into the reaction solution.

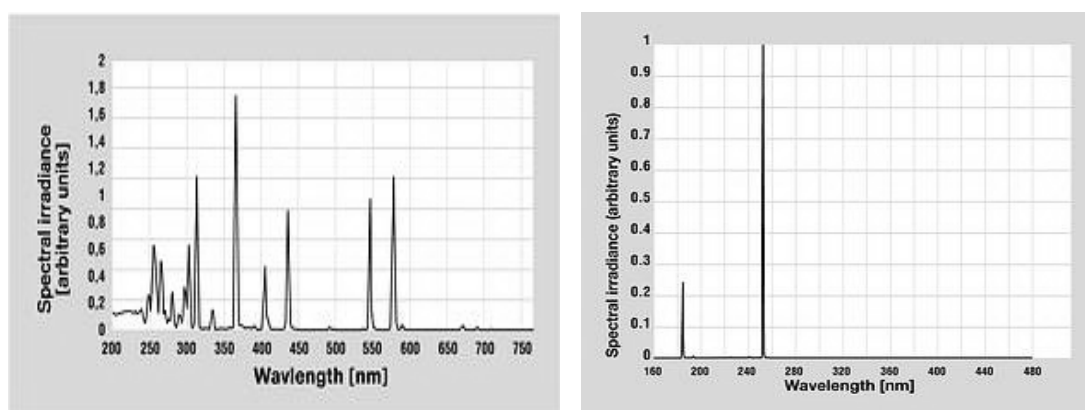


Figure 3.1: Typical emission spectrum of a medium pressure Hg lamp (left) and a low pressure Hg lamp (right).^{165,166}

The effects of different lamps and reactors have been examined in this chapter. Photolysis experiments were conducted with both low and medium pressure lamps and also with two types of immersion wells (Pyrex or Quartz). The typical set-up for photolysis and photocatalytic experiments is shown in the experimental chapter (section 2.3.1). In addition to the photolysis studies with different lamps and glassware, studies were conducted with a variety of reactor set-ups: 0.32 L immersion well vs. 0.8 L batch reactor vs. 5 L Enviolet reactor (10 L capacity, see section 2.3.2). Since all the compounds absorb light below 300 nm, irradiation with low pressure lamps should provide sufficient excitation to dissociate each of the pharmaceuticals leading to complete elimination.

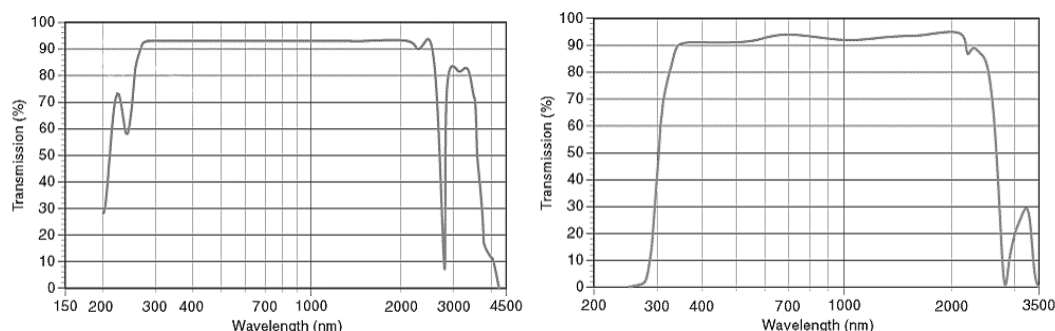


Figure 3.2: Transmittance spectrum of Quartz glassware >250 nm (left) and Pyrex glassware >300 nm (right).¹⁶⁷

Also in this chapter, the heterogeneous photocatalysis using TiO_2 of each of the three APIs is examined. Adsorption has been considered by many research groups to be an important prerequisite to photocatalytic degradation by titanium dioxide.^{168,125} However, there is some evidence to suggest that photocatalytic degradation can occur with little or negligible adsorption to the surface of the photocatalyst.^{169,170,171} Adsorption of the pharmaceuticals onto the surface of TiO_2 is also discussed.

Photocatalytic experiments conducted in this chapter involve the use of two types of Titania, (P-25 and Sigma-Aldrich) and a medium pressure lamp. Photocatalytic experiments were conducted with both Pyrex and Quartz glassware to determine the importance of the penetration of light below 300 nm in the case of Quartz. Various other parameters on the photocatalytic degradation have been investigated such as:

- (i) varying the concentration of TiO_2 to determine the optimum concentration required.
- (ii) the effect of pH,
- (iii) the effect of the addition of an oxidant to see if both a faster rate of degradation could be achieved and if intermediates generated from the APIs could be mineralised within the irradiation period,
- (iv) concentration variation studies to test the robustness of the photocatalytic method over different concentration ranges of the pharmaceuticals.
- (v) various control experiments were also performed to confirm that light is required for activation of TiO_2 and to see the effect of hydrogen peroxide alone on each of the drugs.

3.2 Results and Discussion

Heterogeneous Photocatalysis Part I: Famotidine

3.2.1 UV-vis Studies

Figure 3.1 shows the UV-vis absorbance profiles for Famotidine at 100 μM . Famotidine has absorbances at 208 and 265-280 nm (λ_{max}) depending on the pH of the solution (see pH studies). In water, Famotidine has a pH within the range of 7.5-7.7 and the UV-vis profile below, Figure 3.1, corresponds to this pH range. The molar extinction coefficient for Famotidine was calculated in standard curve experiments to be $10,000 \text{ M}^{-1}\text{cm}^{-1}$ at 267 nm at pHs 3-6. However at pH 7.5 and above, it has a 33% higher value as reported by Anzenbacherova *et al.* in 2003.¹⁷³

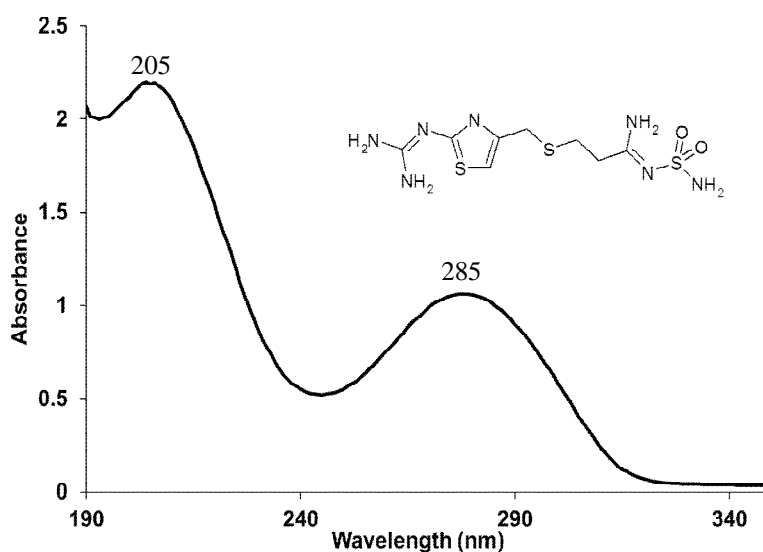


Figure 3.1: UV-vis analysis of of Famotidine 100 μM (pH 7.5-7.7).

Famotidine's absorption profile is affected by pH as seen in Figure 3.2. (Under conditions of STP and at pH 2 it is very unstable.¹⁴¹) A hypsochromic shift is observed on going from alkaline pH (8) where the λ_{max} is 285 nm to pH 6 where the λ_{max} is 265 nm. This type of shift is common for compounds possessing heterocyclic rings.¹⁷²

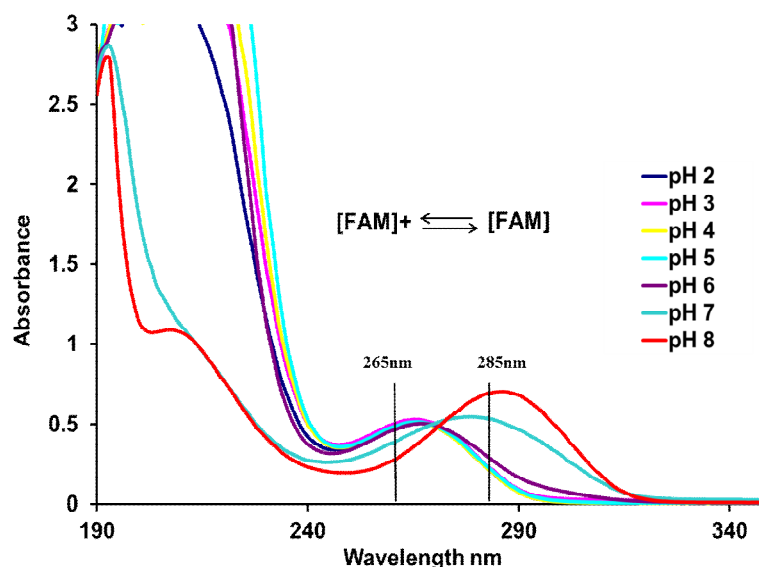


Figure 3.2: UV-vis analysis of Famotidine at different pHs (pH 2-8).

This change in pH also gives rise to a 33% decrease in the molar extinction coefficient as determined in the work by Anzenbacherova *et al.* in 2003.¹⁷³ They successfully manipulated this observation by developing a method to detect Famotidine using HPLC-UV at a wavelength of 285 nm in an alkaline mobile phase and developed a much more sensitive method. Absorbances below 250 nm can be ignored in these profiles as these are contributions by the different buffer components. Two other studies were performed with pH adjustment by NaOH and HCl (*no buffers*). In these studies, slight fluctuations were noticed which were due to a subtle dilution in the adjustment to each required pH. Nonetheless, the shifts obtained with the buffered studies were also observed in these studies.

3.2.2 Quartz Glassware: Photolysis Studies

Photolysis of Famotidine showed a steady decomposition of the absorbance at 260 nm and 210 nm even after only 1h of irradiation (Figure 3.3). A strong smell of sulfur compounds was noticed during sampling after approximately 10 minutes of irradiation. This was a clear sign of the evolution of gaseous sulfur compounds and thus indicated the dissociation of the molecule.

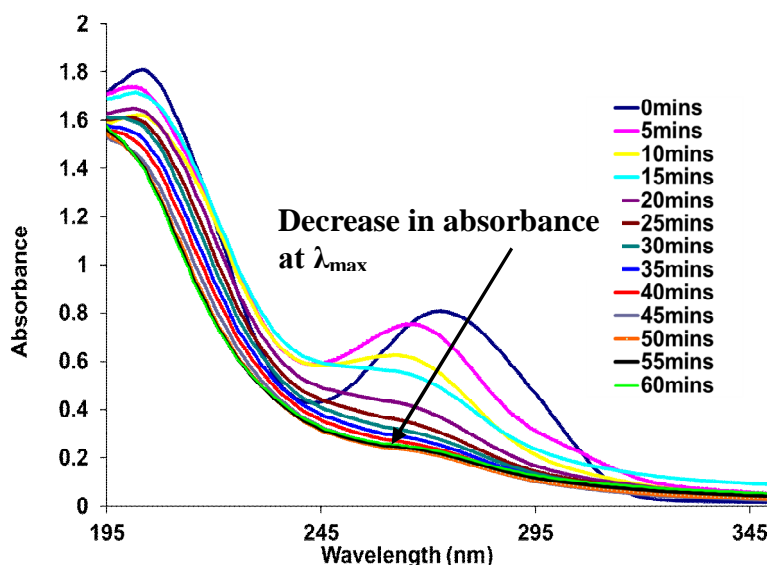


Figure 3.3: UV-vis spectroscopic analysis of the photodegradation (photolysis) of Famotidine with Quartz glassware. [FAM] = 0.083 mM, Time = 1 h.

3.2.3 Quartz Glassware: Photocatalysis Studies

TiO₂ can utilize both UV-A and UV-B light and also some UV-C light. In these studies the effects of TiO₂ with Quartz glassware are investigated using small amounts of TiO₂. All of the compounds absorb between 200-300 nm with the main absorbances occurring between 222-280 nm. Quartz photolysis studies had quite an effect on the compounds, because of this fact and also the effect of transmission of light above 250 nm, so TiO₂ addition should accelerate the rate of decomposition of the compound. Photocatalytic degradation with both Titanias (P25 and Sigma Aldrich) and Quartz glassware seemed to produce similar UV-vis degradation profiles although when the UV-vis data was plotted in degradation profile graphs, differences between the two titanias were observed (Figure 3.4). When comparing these profiles of either titania to photolysis with quartz, the results are quite poor indicating no real contribution to the photodegradation of Famotidine by photocatalysis. It is well known that photolysis and photocatalysis both occur to achieve the decomposition of any pharmaceutical. The only way to examine the effects purely contributed by photocatalysis is to cut off the effects by photolysis. This can be done with the use of Pyrex glassware which will then allow for a proper examination of the contribution by photocatalysis to degradation of the pharmaceutical.

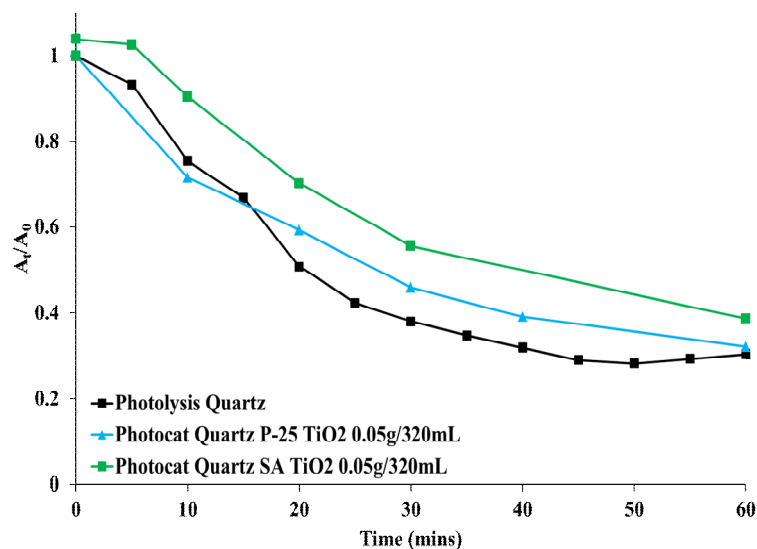


Figure 3.4: UV-vis degradation profiles showing the photocatalytic degradation of Famotidine with Quartz and SA and P-25 TiO_2 (0.05 g/320 mL) vs. Photolysis Quartz.

3.2.4 Alternative Reactor Studies

Additional Studies were conducted with different reactor set-ups, namely the Enviolet Reactor (5 L) and the Low Pressure mercury Lamp set up (800 mL). Larger scale studies in the Enviolet reactor showed a poorer result than was expected and the configuration of the lamp modules was attributed to this i.e solutions passing to and from the lamp modules and not experiencing consistent irradiation. In addition, some fundamental flaws were found with this reactor including the rise in temperature of the reaction solution which was found to be due to the rather ineffective cooling set-up. The larger volume employed may have given rise to the slower rate of degradation which can be the case in large scale studies. Further studies with the Enviolet reactor will be abandoned as this reactor was also considered to be unsuitable for photocatalysis due to the potential for build-up of residual TiO_2 over time throughout the reactor. The design of this reactor also makes cleaning an arduous process, and damage could occur to the reactor. Studies with the Low pressure lamp set-up were conducted to demonstrate the effects of 254 nm irradiation on each pharmaceutical. Since all of the pharmaceuticals absorb in this region, total destruction of all pharmaceuticals occurred within less than an hour. However, similar problems occurred with this reactor as with the Enviolet, with the lack of temperature control potentially affecting results. Experiments conducted with these reactors are presented in the Appendices for all APIs (3A-10 - 3A-11).

3.2.5 Pyrex Glassware: Photolysis Studies

The results of the photolysis using Pyrex are shown in Figure 3.5. It is evident that removing wavelengths below 300 nm shows a marked decrease in the degradation observed. Famotidine's maximum absorbance tails just over the 300 nm mark, so it is not surprising that some slight degradation is observed.

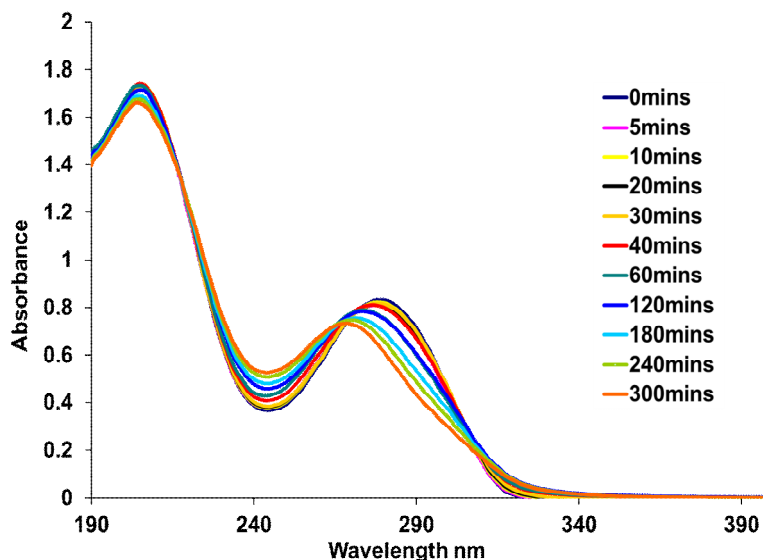


Figure 3.5: UV-vis spectroscopic analysis of the photodegradation (photolysis) of Famotidine for 5 h. [FAM] = 0.083 mM, Time = 5 h.

Lengthening of the illumination time to 5 h did not achieve a notable enhancement on Famotidine degradation although a rather interesting hypsochromic shift was observed which is due to a pH change in the solution over irradiation. Any slight decomposition of a pharmaceutical could give rise to organic acid formation which can result in a decrease of the pH of the solution. This observation has been reported in other photolysis studies and in photocatalytic studies of other pharmaceuticals and EDCs.^{174,175,176}

Although poorer degradation is achieved by using Pyrex glassware, from an application viewpoint it can be integrated more easily into an industrial photochemical water treatment reactor due to its low maintenance requirements and its inexpensiveness relative to quartz glassware.

3.2.6 HPLC Analysis of Photolysis Studies

Once suitable methods had been developed, HPLC analysis was then undertaken of the photolysis experiments for Famotidine. Both Quartz and Pyrex photolysis studies were analysed and the results are shown in Figure 3.6. As predicted, photolysis with quartz can eliminate Famotidine within an hour. Previous quartz photolysis studies conducted and analysed with UV-

vis spectroscopy (Figure 3.3) showed a small absorbance still at the λ_{max} so it is clear that despite the total elimination shown by HPLC analysis, photodegradation products may persist. In the case of photolysis with Pyrex, Famotidine showed more than 25% elimination in these studies after 3 h.

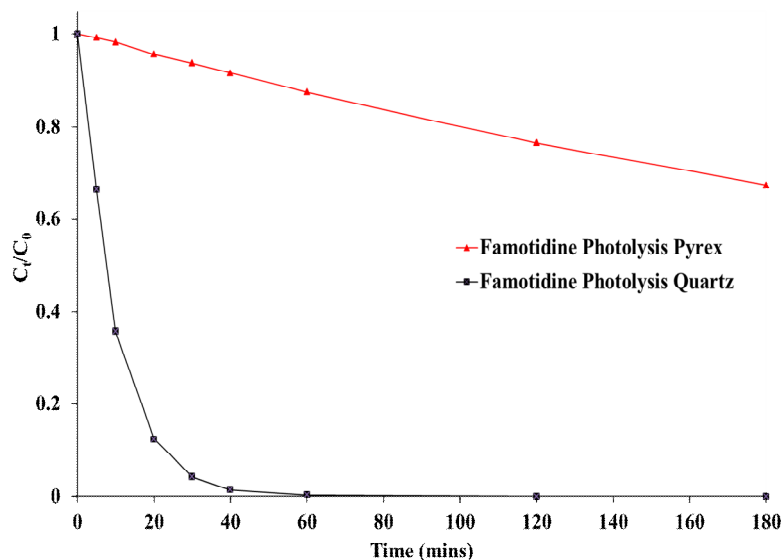


Figure 3.6: HPLC Analysis of photolysis experiments with Quartz and Pyrex glassware for Famotidine. [FAM] = 0.083 mM, Time = 3 h.

3.2.7 Famotidine Heterogeneous Photocatalysis: Pyrex

In the following experiments, the effects of the addition of TiO_2 were examined on the photocatalytic degradation of Famotidine. The Pyrex filtration effect allows for the examination of the effects of photocatalysis only. Initial photocatalytic studies with Famotidine, TiO_2 and Pyrex after 1 h did not significantly improve the degradation of Famotidine when compared to photolysis studies. Low amounts of TiO_2 were used in these studies (0.050 g/320 mL). Results are shown in Figure 3.7 and show a poor degradation of Famotidine for both titanias relative to photolysis. P-25 shows the most superior performance of the two although it is evident from these studies that the concentration of photocatalyst is too low.

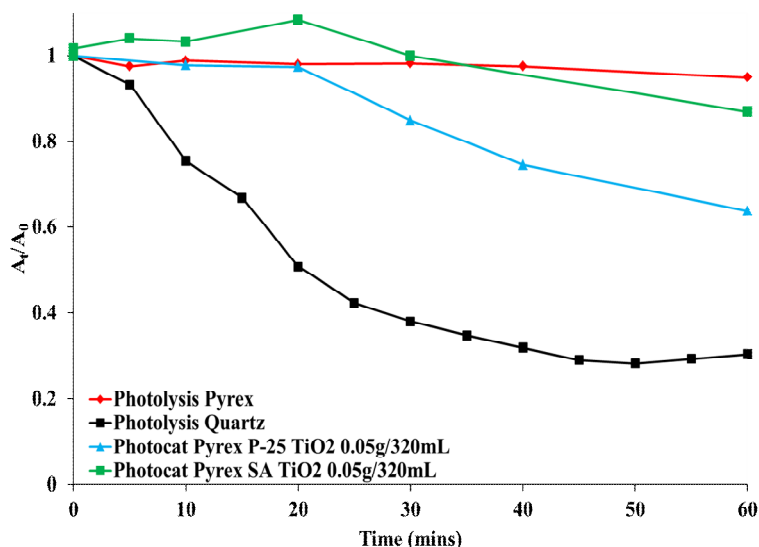


Figure 3.7: UV-vis degradation profile for Pyrex photocatalysis studies with SA and P-25 TiO_2 vs. Photolysis with Quartz and Pyrex.

3.2.8 Famotidine Heterogeneous Photocatalysis: TiO_2 Optimisation

In order to determine the optimum concentration of the photocatalyst, TiO_2 , experiments were performed with varying concentrations of TiO_2 . The aim of the following experiments was to determine the optimum concentration of titanium dioxide in the immersion well reactor system. All results analysed in this section were analysed by HPLC analysis or in early experiments where HPLC analysis could not be employed, UV-vis analysis was used to determine the optimum TiO_2 concentration. Table 3.1 below shows a list of experiments performed, their conditions and degradation achieved.

API	C_0 mM	TiO_2 Phase	TiO_2 g/320 mL	Irradiation Time h	100% reached HPLC	UV Data
Famotidine	0.083	Sigma	0.05	1	N/A	17
		Sigma	0.1	3	60 mins	90
		Sigma	0.2	3	60 mins	90
		Sigma	0.4	3	60 mins	91
		Sigma	0.6	3	60 mins	92
		P-25	0.05	1	N/A	35
		P-25	0.1	5	N/A	94
		P-25	0.2	5	N/A	33
		P-25	0.4*	5	N/A	91*

*400W Lamp

Table 3.1 List of conditions used in Famotidine TiO_2 optimisation photocatalytic degradation experiments

A titanium dioxide range of 0.05-0.6 g/320 mL was studied in these experiments. The results of HPLC analysis for Sigma TiO_2 are shown in Figure 3.8. Optimisation of P-25 TiO_2 concentration was undertaken with UV-vis analysis and degradation profiles using this data are

shown in Figure 3.9. In UV-vis analysis studies doubling the concentration from 0.05 g/320 mL to 0.1 g/320 mL for P-25 gave rise to a 96% elimination based on the A_t/A_0 ratio after 300 mins. Sigma TiO_2 similarly showed a marked increase, with 88% elimination based on the A_t/A_0 ratio.

In further studies, 0.1 g/320 mL was found to be the optimum concentration for Degussa P25. HPLC analysis used for the Sigma Aldrich studies confirmed that for Sigma TiO_2 , 0.1 g/320 mL was also superior over other concentrations used 0.2-0.6 g/320 mL. By increasing the concentration of TiO_2 in the photocatalytic process should, in theory, double the rate of degradation. However, realistically this cannot be a linear relationship as many factors come into account from the further addition of more catalyst. In degradation studies with 0.4 g – 0.6 g/320 mL, a 'saturated' effect could be seen, whereby TiO_2 could be seen to deposit around the top of the reactor. There are also other factors, whereby if there is too much photocatalyst present, enhanced light scattering occurs and light penetration into the reactor becomes more difficult. Since photocatalysis is essentially a radical generating process there effectively becomes a point where the degradation rate competes with the radical recombination rate, which is also the case for oxidant addition.¹²⁹ Figure 3.10 shows the UV-vis profile of degradation for the optimised P-25 TiO_2 photocatalytic reaction with 0.1 g TiO_2 /320 mL, with Figure 3.11 showing LC traces of this reaction also. The chromatogram shows other peaks more polar than Famotidine eluting early in the chromatogram which are intermediate products of the photocatalytic reaction. These intermediates are seen to be in quite low concentrations relative to the Famotidine peak and are identified later in Chapter 4.

Sigma-Aldrich TiO₂

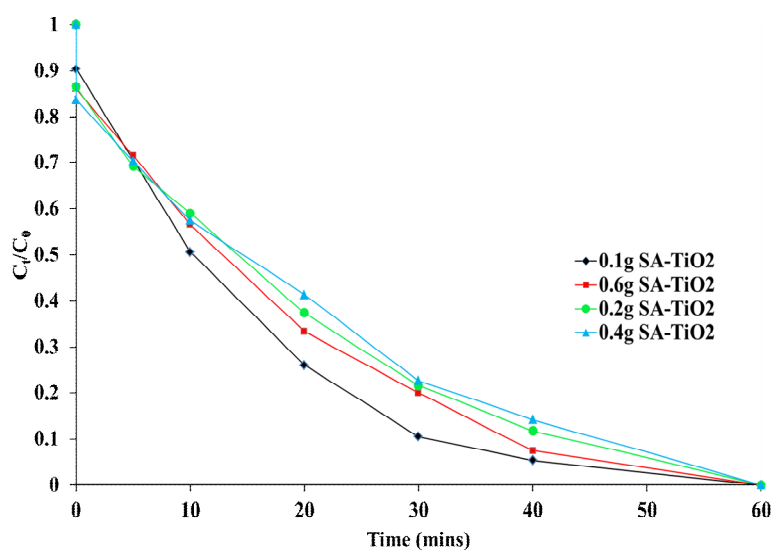


Figure 3.8: HPLC analysis of the photocatalytic degradation of Famotidine with varying SA-TiO₂ concentrations. [FAM] = 0.083 mM, TiO₂ = (0.1-0.6 g), Time = 3 h. Analysis undertaken with methods in appendices (2A-1).

Degussa P25 TiO₂

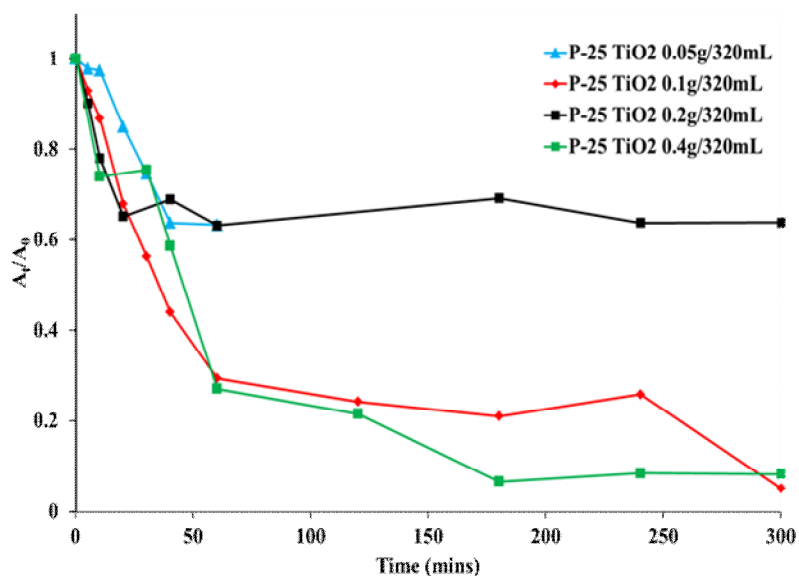


Figure 3.9: UV-vis degradation profiles of the photocatalytic degradation of Famotidine with varying amounts of P-25 TiO₂. [FAM] = 0.083 mM, TiO₂ = 0.05 g – 0.4 g/320 mL, Time = 1 h/5 h.

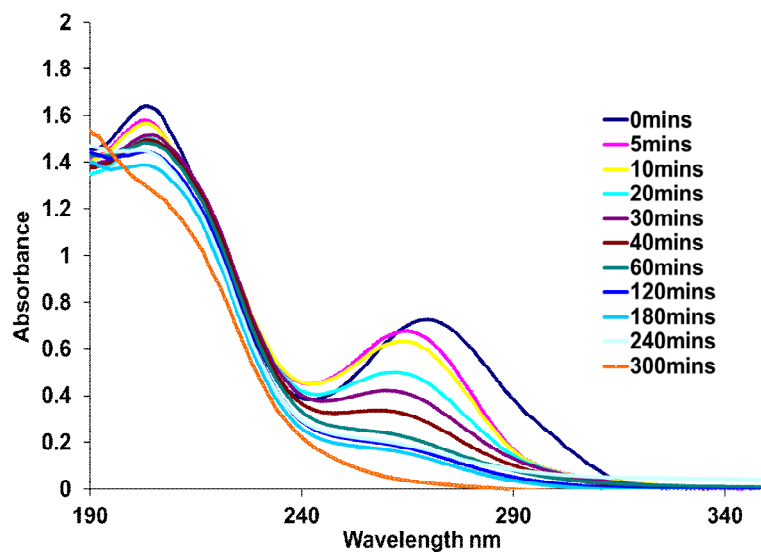


Figure 3.10: UV-vis spectroscopic analysis of the photocatalytic degradation of Famotidine with 0.1 g P-25 TiO_2 . [FAM] = 0.083 mM, TiO_2 = 0.1 g, Time = 5 h.

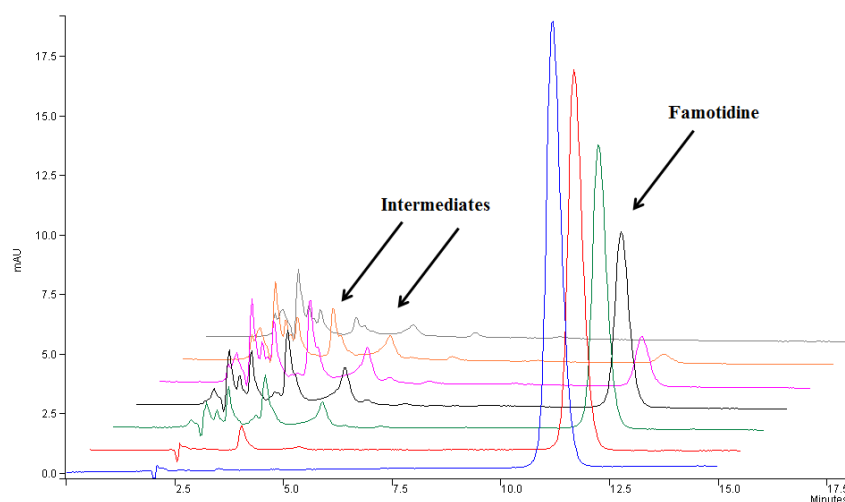


Figure 3.11: HPLC chromatogram of Famotidine with TiO_2/UV at 0mins, 0mins P_{ads} , 5, 10, 20, 30 and 40 mins. [FAM] = 0.083 mM, P-25 TiO_2 0.1 g/320 mL.

3.2.9 Famotidine pH Adjustment Studies

Photocatalytic degradation at various pHs was undertaken to examine whether this parameter had a positive or negative effect on the disappearance of the analytes. Buffers have been known to cause interferences with photocatalysis and the pH was adjusted using acids and bases in a procedure used by many other research groups.^{177,178} The pH range of 3-8 was adopted based on the PFP column selection (pH 2.5-8). In the case of P-25 TiO_2 , photocatalysis at pH 9 and pH 10 were also examined, which were monitored by UV-vis spectroscopy only. pH changes were

monitored throughout degradation and were found to decrease upon irradiation. The following studies incorporated the conditions listed in Table 3.2. UV-vis analysis was used to analyse all pH photodegradation experiments. HPLC analysis was employed only in P-25 TiO₂ photocatalytic experiments.

API	C ₀ mM	TiO ₂ Phase	pH	TiO ₂ g/320mL	Irradiation Time h	100% reached HPLC	UV data % Degradation
Famotidine	0.083	P-25	3	0.1	5	40mins	95
		P-25	4	0.1	5	N/A	88
		P-25	5	0.1	5	60mins	93
		P-25	6	0.1	5	N/A	81
		P-25	7.4	0.1	5	60mins	96
		P-25	8	0.1	5	40mins	98
		P-25	9	0.1	5	N/A	95
		P-25	10	0.1	5	N/A	94
		Sigma	3	0.1	3	N/A	69
		Sigma	4	0.1	3	N/A	62
		Sigma	5	0.1	3	N/A	67
		Sigma	6	0.1	3	N/A	85
		Sigma	7.4	0.1	3	N/A	90
		Sigma	8	0.1	3	N/A	60

Table 3.2 List of conditions used in Famotidine pH photocatalytic degradation experiments

Sigma-Aldrich TiO₂

Degradation profiles of the UV-vis data for Sigma Aldrich TiO₂ pH photocatalytic degradation experiments are presented in Figures 3.12. No change in pH (Figure 3.13) was found to be superior over experiments conducted with a pH change. Additional UV monitoring graphs from these experiments can be found in the appending data. These data showed varying results in relation to the initial adsorption of Famotidine onto TiO₂. Little or no adsorption was attained for pH 3 and a greater deal of adsorption was attained for pH 8. Despite these differences, both achieved poor degradation with the most superior degradation occurring for the unadjusted photocatalytic experiment.

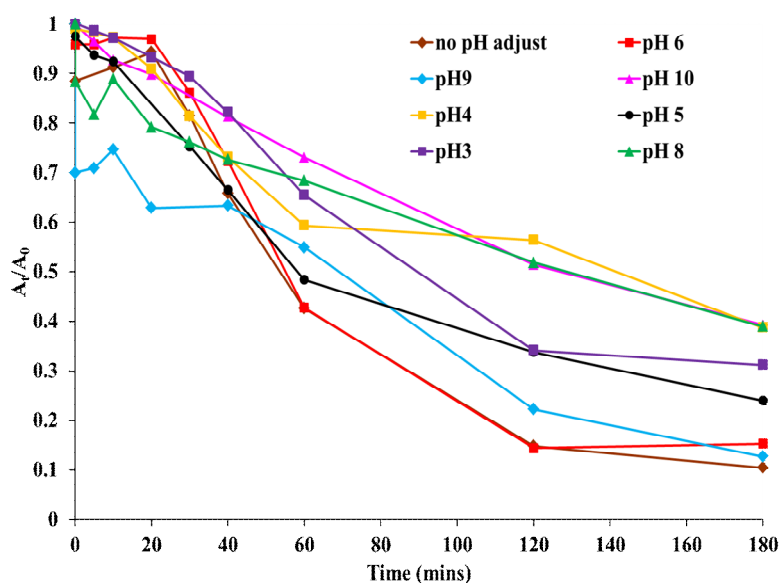


Figure 3.12 UV-vis degradation profiles of the photocatalytic degradation of Famotidine with 0.1 g SA TiO_2 at various pHs. [FAM] = 0.083 mM, TiO_2 = 0.1 g, Time = 3 h, pH = 3-10.

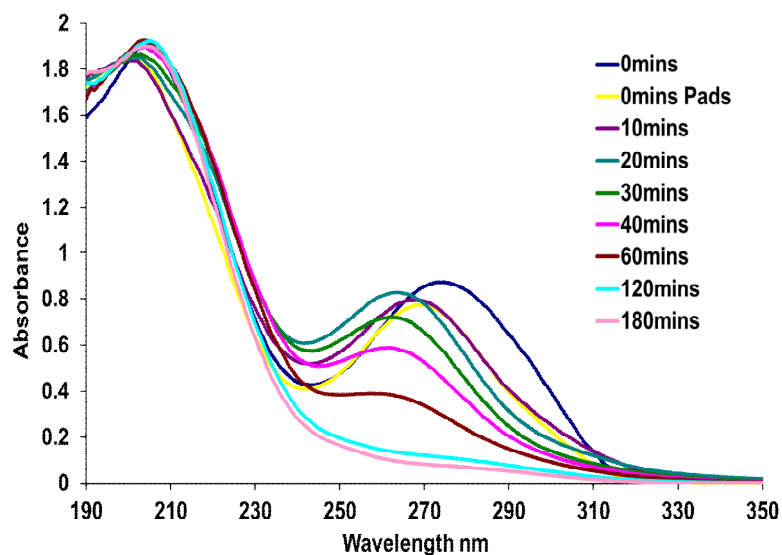


Figure 3.13 UV-vis spectroscopic analysis of the photocatalytic degradation of Famotidine with 0.1 g SA TiO_2 . [FAM] = 0.083 mM, TiO_2 = 0.1 g, Time = 3 h, no pH adjustment.

P-25 TiO_2

Figure 3.14 shows the results obtained for P-25 TiO_2 photocatalysis pH studies with Famotidine. Results showed that Famotidine degradation with this TiO_2 was enhanced in all cases by a change in pH. The most efficient degradation occurred at pH 8, followed closely by pH 3. The experiments shown in Figure 3.14 were repeats conducted by C. Saurel and the trend observed in earlier studies was also observed in these repeats. With both P25 and Sigma Aldrich TiO_2 , a decrease in the pH of the solution was observed throughout degradation as found with

non-adjusted pH degradation. The final pH observed for pH photocatalytic experiments (3-8) was between pH 3 and 4. A graph of the pH variation can be seen in Figure 3.17.

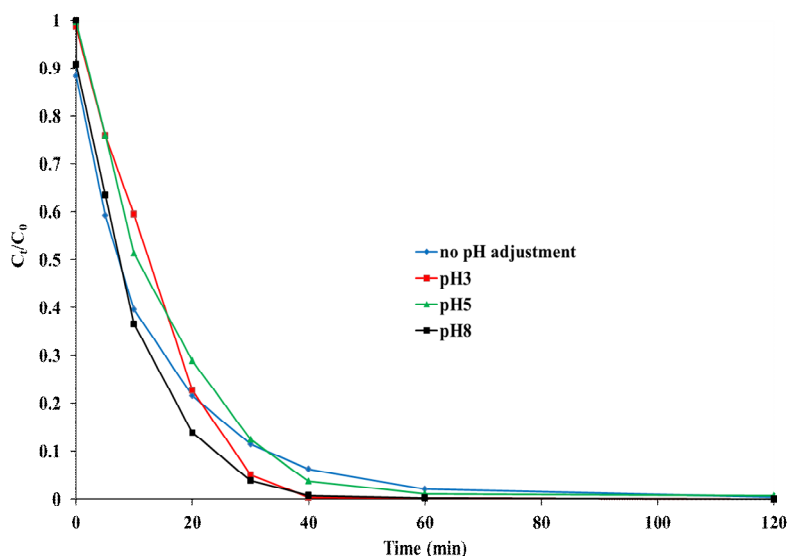


Figure 3.14: HPLC-UV analysis of Famotidine photocatalytic degradation with P-25 TiO₂ at varying pHs. [FAM] = 0.083 mM, P-25 TiO₂ = 0.1 g/320 mL, pH = 3,5,7,4,8, Time = 3, 5 h. Performed and analysed by C. Saurel.

Most of the pH decline occurred within the first hour of the photocatalytic experiment, which makes it consistent with the degradation of Famotidine. The pH tended to level off after the first hour in all cases. This would indicate that acidic intermediates are being generated from the degradation of Famotidine. These will occur via multiple oxidations of Famotidine, and an example of this already mentioned is with the hydrolysis products of Famotidine Mw = 259 g/mol and 260 g/mol. Figures 3.15 - 3.16 show the UV-vis monitoring for Famotidine degradation for pH 3 and 7 for Degussa P-25. Additional graphs of UV-vis monitoring at other pHs can be found in the appendices section (3A-4 - 3A-7).

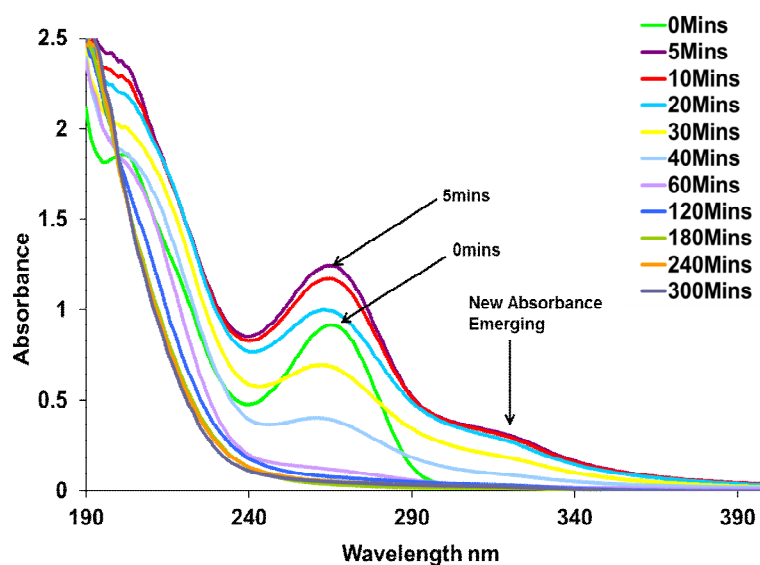


Figure 3.15: UV-vis analysis of the photocatalysis of Famotidine using P25 TiO₂ at pH 3. [FAM] = 0.083 mM, P-25 TiO₂ = 0.1 g/320 mL, pH = 3, Time = 5 h.

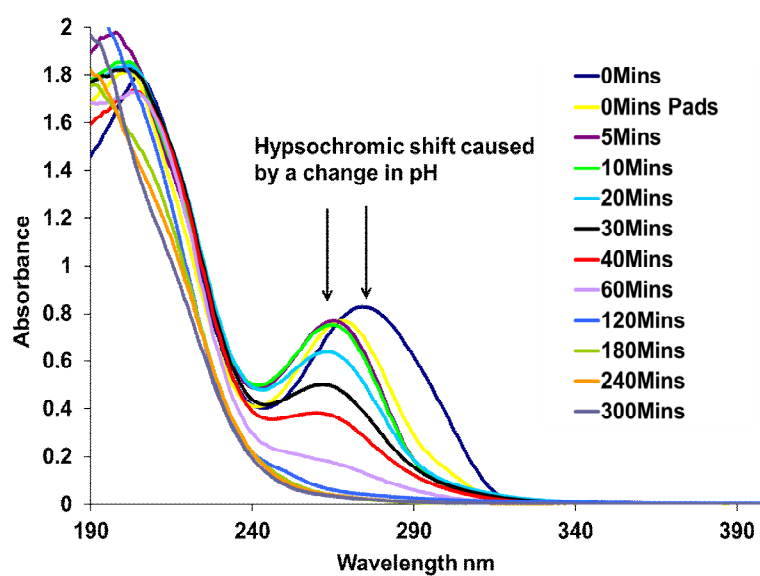


Figure 3.16: UV-vis analysis of the photocatalysis of Famotidine using P25 TiO₂ at pH 7. [FAM] = 0.083 mM, P-25 TiO₂ = 0.1 g/320 mL, pH = 7, Time = 5 h.

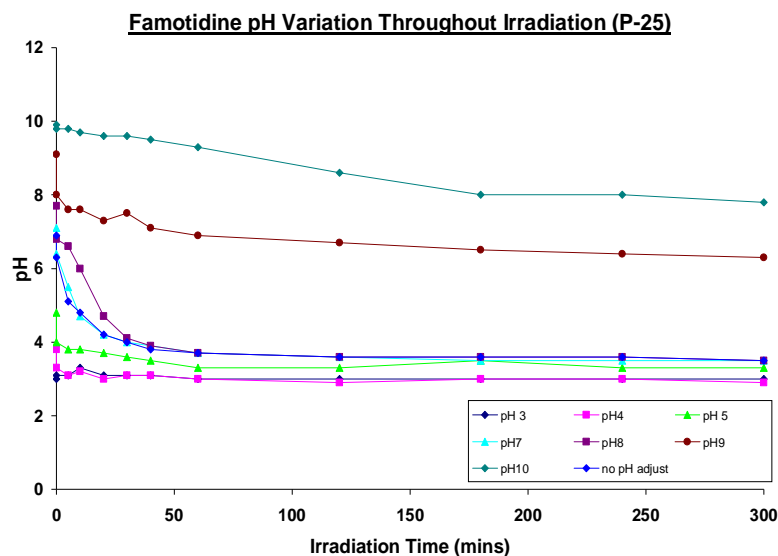


Figure 3.17: pH monitoring post photocatalysis for pH experiments showing the consistent decrease in pH throughout irradiation for Famotidine.

UV-vis Analysis

It was noticed that at acidic pHs i.e 3-5, a new absorbance was found to emerge at 320 nm (see Figures 3.15 and 3.18) which was thought to be hydrolysis products of Famotidine (already mentioned in Chapter 1 section 1.6) and was only found with P-25 TiO₂. This was later found to be due to the nylon filter membranes which are unstable at low pHs. Figure 3.18 shows the UV-vis studies which were performed with Famotidine at pH 2, Famotidine no pH adjustment and controls (Millipore water) at pH 2 and no pH adjustment. Of the three samples which were filtered (FAM pH 2, FAM no pH adjust, and Control pH 2), there is significant changes in the UV-vis for those samples at pH 2: a broad absorbance stretching as far as 320 nm. For unfiltered samples no such absorbance at 320 nm is observed, and the control sample, which was not pH adjusted and was filtered demonstrated that the filters show good stability at neutral pH. Further analysis was also undertaken to determine the stability of Famotidine at pH 2.

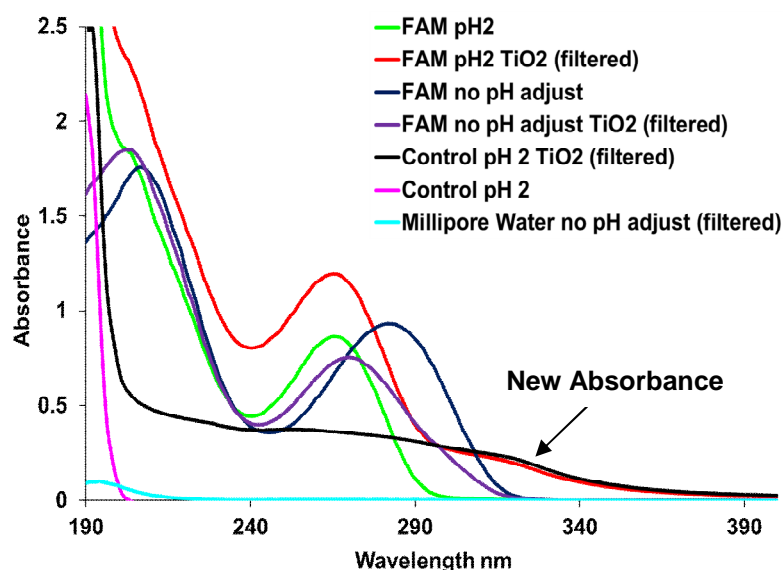


Figure 3.18: UV-vis spectroscopic analysis of the effect of instability of Nylon membrane filters at pH 2.

Figure 3.19 shows UV-vis experiments conducted with Famotidine at pH 2, no pH adjustment and controls (Millipore water) at pH 2 and no pH adjustment. After the UV-vis experiments were carried out at pH 2, the pH of the Famotidine solutions (pH 2 and non-adjusted) were adjusted with NaOH to pH 11. The two UV-vis profiles shown at pH 11 are identical aside from a slight decrease in the solution adjusted from pH 2, which required the addition of more base for adjustment to pH 11. It was concluded from these experiments that Famotidine is more stable than initially thought. In addition, this experiment proves that the shifts observed in the Famotidine UV-vis spectra are due to the protonation/deprotonation of the molecule and that protonation is a reversible process.

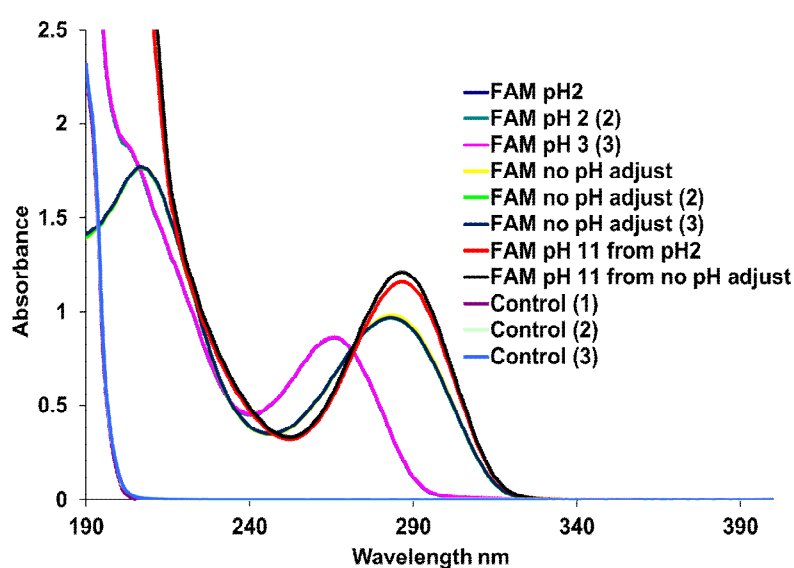


Figure 3.19: UV-vis spectroscopy analysis of the effect of the stability of Famotidine at pH 2. Controls = Millipore water at pH 2.

3.2.10 Famotidine Hydrogen Peroxide Addition: P-25 TiO₂

Hydrogen peroxide was employed as an oxidant in photocatalytic studies to enhance the degradation of Famotidine and its intermediates. In these studies, radicals are continually generated from the peroxide during the photocatalytic reaction, and can also continue to generate radicals from residual peroxide in the sample taken post reaction. The residual peroxide is usually quenched with a quenching agent and in our hydrogen peroxide studies sodium bisulfite (40% w/v) was used to quench the reaction. However, when a Famotidine photocatalytic experiment with H₂O₂ (quenched with bisulfite) was re-analysed at a later date, it was noticed that no Famotidine remained in any samples even at 0 minutes. This led us to believe that perhaps the sodium bisulfite was not an inert quencher and that it continued to degrade residual Famotidine in the samples post analysis. Various control tests were conducted to examine the effect of sodium bisulfite on Famotidine and on the other two pharmaceuticals. These included UV-vis analysis, HPLC analysis and ¹H NMR analysis.

UV-vis Analysis

UV-vis analysis of the effects of bisulfite was undertaken on Famotidine over the course of 1h and follow-up analysis after 19 h. The results are shown in Figure 3.20 including the UV-vis of bisulfite in water alone. Bisulfite absorbs in the same region as Famotidine, and upon addition of the bisulfite there is a significant hypsochromic shift and increase in absorbance. After 19 h there was a further increase in absorbance. Since the UV-vis of bisulfite interfered somewhat in a region where all three APIs absorb no solid conclusions could be drawn from this study, except the fact that over the course of time, some effect was occurring.

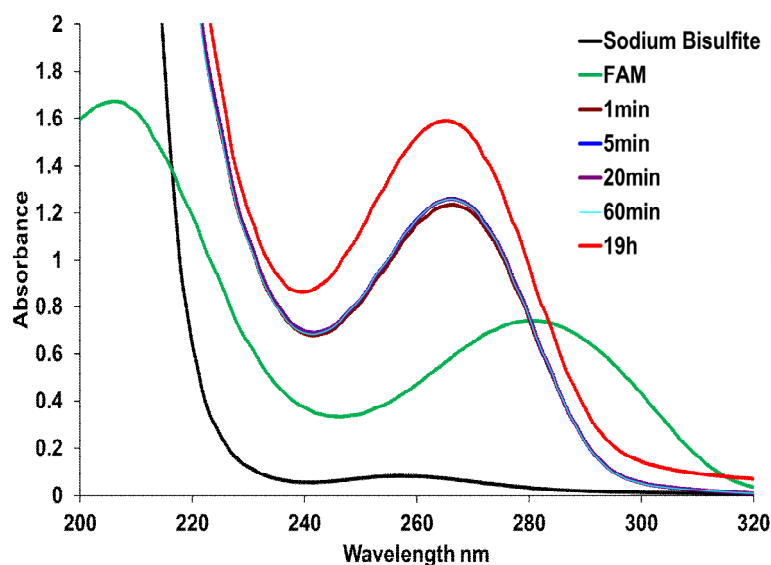


Figure 3.20: UV-vis spectroscopic analysis of the effect of sodium bisulfite (NaHSO₃) on Famotidine.

¹H NMR Analysis

¹H NMR analysis was performed on Famotidine in D₂O. NMRs were obtained of Famotidine alone in D₂O and with the addition of sodium bisulfite (0.011 g/2.5 mL). If any sort of oxidation/reduction is occurring in the reaction of sodium bisulfite with the APIs, there will be significant changes in the ¹H NMR spectrum.

The ¹H NMR spectra for Famotidine and Famotidine plus bisulfite are shown in Figure 3.21. Four types of proton exist in Famotidine (non-exchangeable) and these protons are highlighted in colour in Figure 3.22. Shifts arise in the Famotidine plus bisulfite spectrum for the heterocyclic proton (red) and the CH₂S protons (green). No significant shifts are observed for the two triplet signals at 2.4 ppm and 2.65 ppm which concludes no significant changes have occurred to their environment. The shifts observed for the other two types of proton, would indicate a change to the heterocyclic ring in Famotidine. The downfield shift observed would indicate a modification to the thiazole ring.

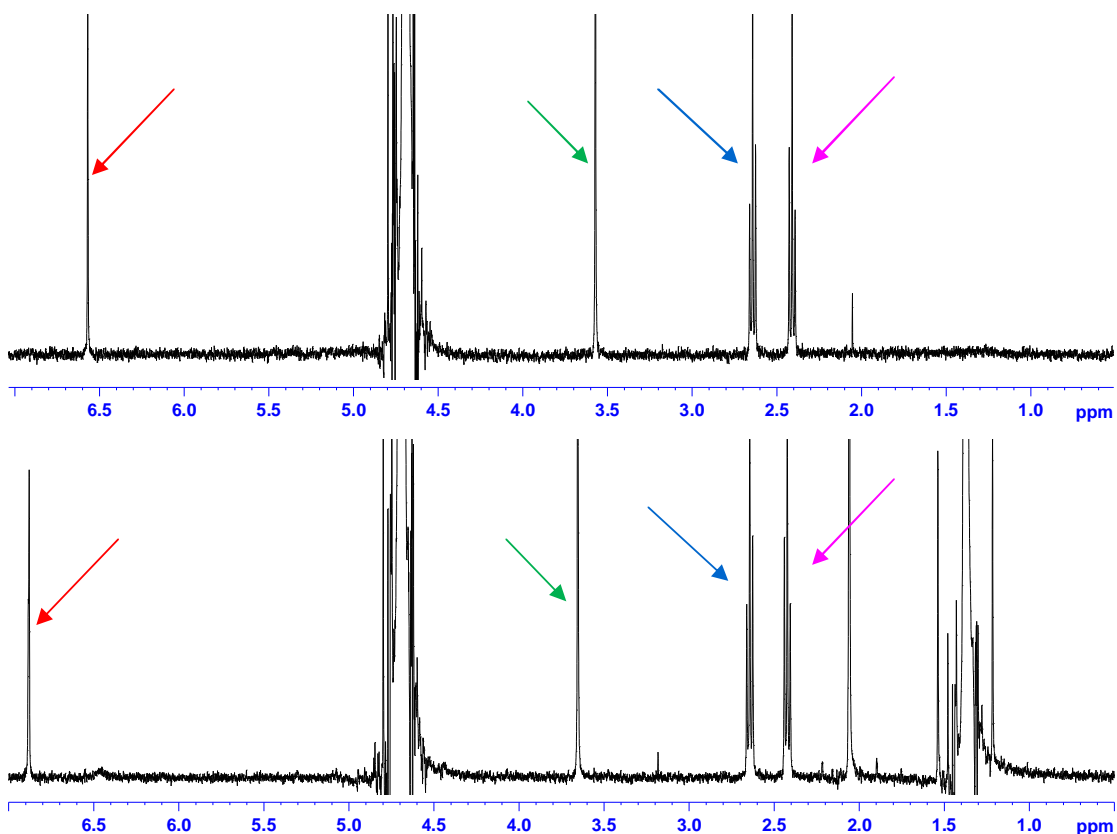


Figure 3.21: ¹H NMR in D₂O of Famotidine (Top) versus the addition of sodium bisulfite (Bottom) with analysis at approximately 25 mins. Coloured arrows relate to the coloured protons shown in Figure 3.22.

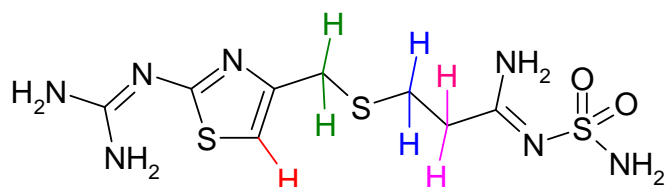


Figure 3.22: Structure of Famotidine with assigned protons highlighted in different colours.

HPLC Analysis

HPLC analysis of the effects of bisulfite were undertaken with repeat injections of Famotidine and Famotidine plus bisulfite. The results are shown in Figure 3.23 and show a consistent decrease in Famotidine for the first set of injections (every 0.5 h) and then a later injection approximately 48 h later shows a further decrease of Famotidine. This study along with previous ^1H NMR studies confirmed that the sodium bisulfite quencher was degrading Famotidine. Considering this, an alternative quencher was sought. An experiment was performed with various concentrations of ethanol (0.1 mL – 1.5 mL) and they were then used to quench 1mL samples of a FAM/ H_2O_2 reaction. However, upon HPLC analysis of the samples, it was noticed that the ethanol was causing considerable effects to the Famotidine peak shape. This effect was most noticeable at concentrations of ethanol above 0.5 mL. A further experiment was conducted with a number of concentrations of peroxide and sampling straight after addition of peroxide. These reactions were all quenched with 0.5mL of ethanol. The results were analysed and then re-analysed 24 h later. The results showed ethanol to be an ineffective quencher for peroxide.

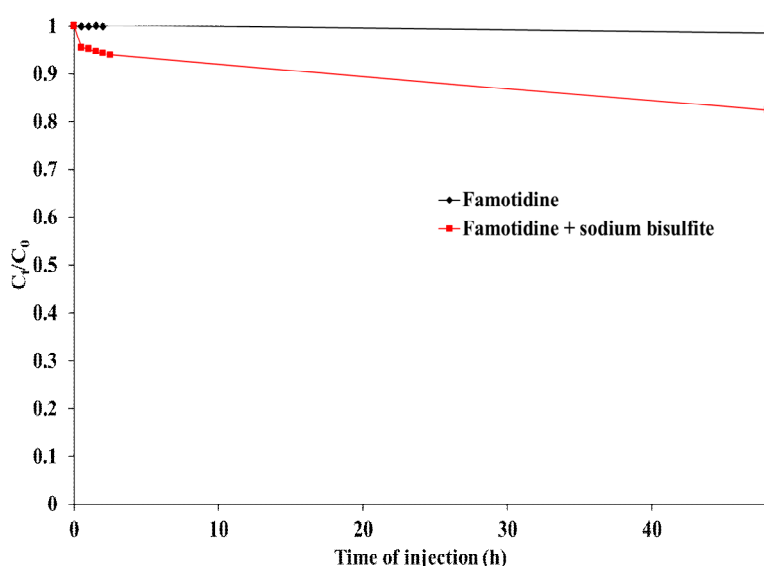


Figure 3.23: HPLC analysis with repeat injections of samples of Famotidine and Famotidine plus bisulfite.

A suitable quencher could not be found for Famotidine. The hydrogen peroxide photocatalytic experiments shown in Figure 3.24 were conducted prior to the testing of the effects of bisulfite and ethanol as a quencher. Despite the fact that bisulfite does indeed have an effect on Famotidine, the reaction is quite slow with approximately 15% eliminated after 48 h. It should also be considered that sodium bisulfite quenches hydrogen peroxide, and they do in essence quench one another. No equation could be found for the reaction of hydrogen peroxide with sodium bisulfite although hydrogen peroxide is known to oxidise sulfites to sulfates.¹⁷⁹ So products of this reaction would be likely to be:



So in reality the 15% elimination is possibly much less than this value in the experiments below. Experiments shown below contain analysis information in the legend stating the time elapsed between implementation of the experiment and follow-up analysis by HPLC of that experiment. While it is acknowledged that these experiments do not represent fully accurate information on the effect of different concentrations of H_2O_2 on Famotidine, valuable information can still be derived from them anyway, particularly in relation to intermediate formation, and intermediate elimination/ mineralisation. Figure 3.25 presents control experiments conducted with Famotidine including with TiO_2 in the absence of UV light, photolysis, with peroxide in the dark and with peroxide and TiO_2 in the absence of UV light. Control experiments with UV light alone have already been discussed. In the absence of UV light, adsorption of Famotidine to TiO_2 is hardly 15%, and no further adsorption is seen over the remainder of the experiment.

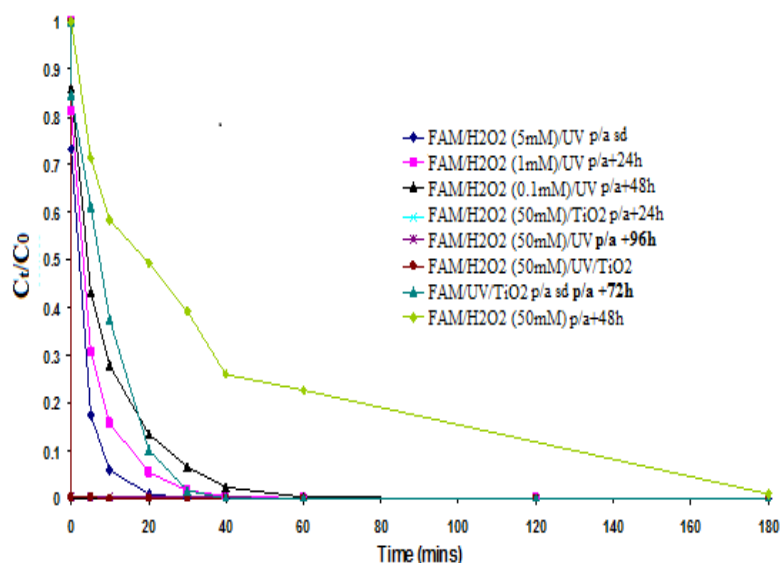


Figure 3.24: HPLC analysis of the photocatalytic degradation of Famotidine with varying additions of H_2O_2 . P-25 TiO_2 0.1 g/320 mL, $[\text{H}_2\text{O}_2]$ 0.1 mM-50 mM, $[\text{FAM}] = 0.083$ mM. (p/a= performed/analysed, sd = same day).

Chromatograms from two of the experiments in Figure 3.24 are shown in Figures 3.26 - 3.29. The chromatograms show the effect of 50 mM of hydrogen peroxide versus 5 mM hydrogen peroxide on the TiO_2/UV process. A number of intermediates can be seen early in the chromatogram and in the case of 50 mM H_2O_2 , after the addition of peroxide to the reaction solution there is complete disappearance of the Famotidine peak prior to any irradiation of the sample (Figure 3.26) and significant quantities of intermediates are now present. This is shown more clearly in Figure 3.27 whereby only the later samples (60 – 180 mins) are shown with the initial samples (0 Mins, 0 Mins P_{ads}). The significant quantities of the 2 main intermediate peaks would indicate that the 50 mM hydrogen peroxide is initially completely oxidizing Famotidine (at one or numerous positions). Subsequent samples shown in Figure 3.26 then show a reduction in the quantities of these intermediates and the development of more intermediates, which would imply that oxidation of the two principle intermediates is then occurring (since no Famotidine remains from 0 mins P_{ads}).

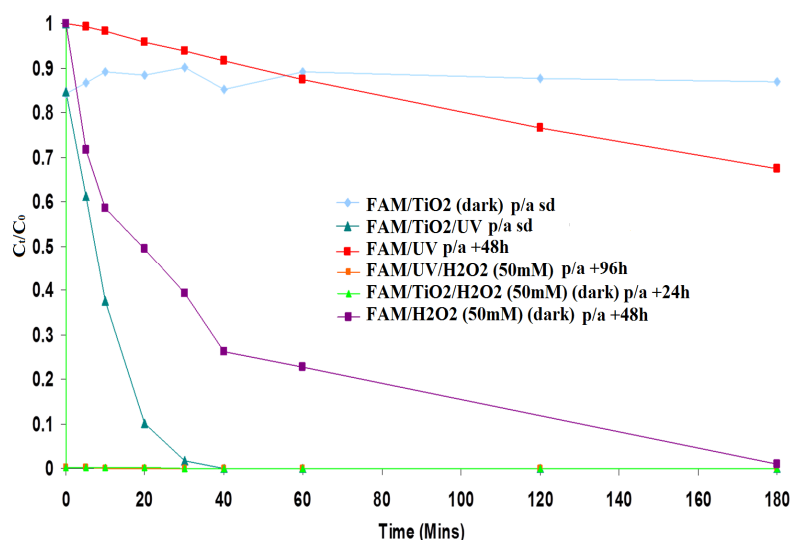


Figure 3.25: HPLC analysis of control experiments for Famotidine. P-25 $\text{TiO}_2 = 0.1 \text{ g}/32 \text{ mL}$, $\text{H}_2\text{O}_2=50 \text{ mM}$, $[\text{FAM}] = 0.083 \text{ mM}$. (p/a= performed/analysed, sd = same day).

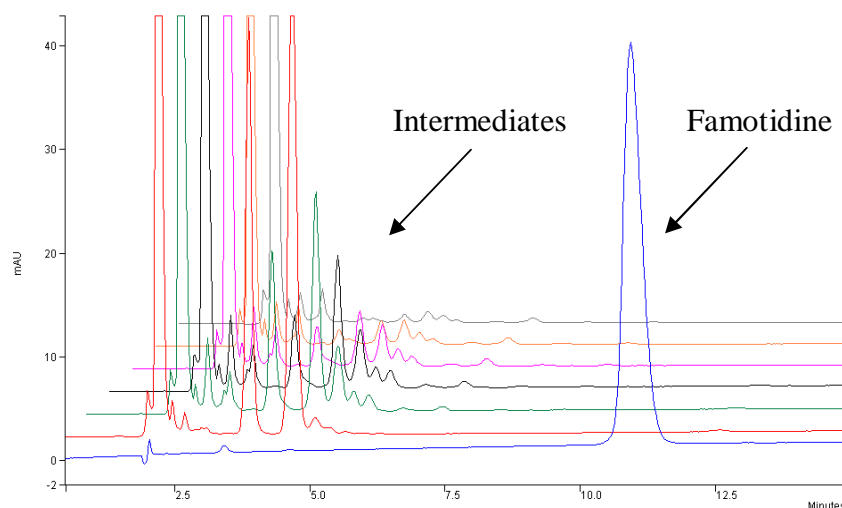


Figure 3.26: HPLC chromatogram of Famotidine with $\text{TiO}_2/\text{UV}/\text{H}_2\text{O}_2$ (50mM) at 0 mins, 0 mins P_{ads} , 5, 10, 20, 30 and 40 mins. $[\text{FAM}] = 0.083 \text{ mM}$, $\text{H}_2\text{O}_2 = 50 \text{ mM}$, P-25 TiO_2 0.1 g/320 mL.

Later samples (60-180 mins) show the complete disappearance of the initial intermediates and their oxidation products with remnants of oxidation products which may potentially not be able to undergo further oxidation or are simply more recalcitrant compounds. The chromatograms shown in Figure 3.28 - 3.29 are from the lower concentration of peroxide photocatalytic experiment (5 mM H_2O_2). These chromatograms tell a slightly different story to the previous ones and a very different degradation pathway can be observed.

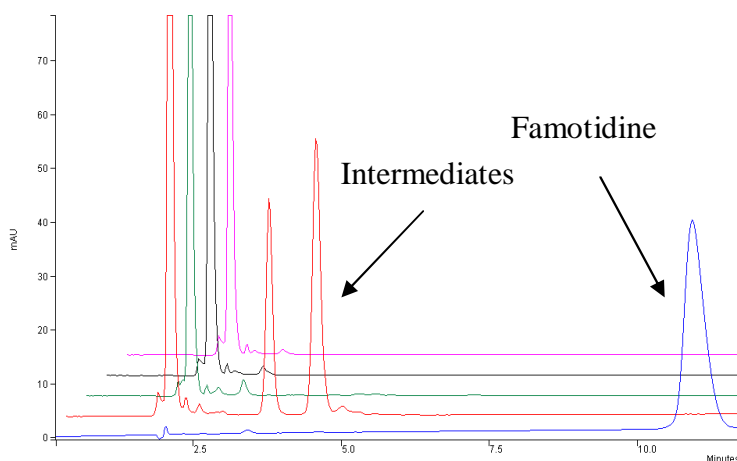


Figure 3.27: HPLC chromatogram of Famotidine with $\text{TiO}_2/\text{UV}/\text{H}_2\text{O}_2$ (50 mM) at 0 mins, 0 mins P_{ads} , 60, 120 and 180 mins. $[\text{FAM}] = 0.083 \text{ mM}$, $\text{H}_2\text{O}_2 = 50 \text{ mM}$, P-25 TiO_2 0.1 g/320 mL.

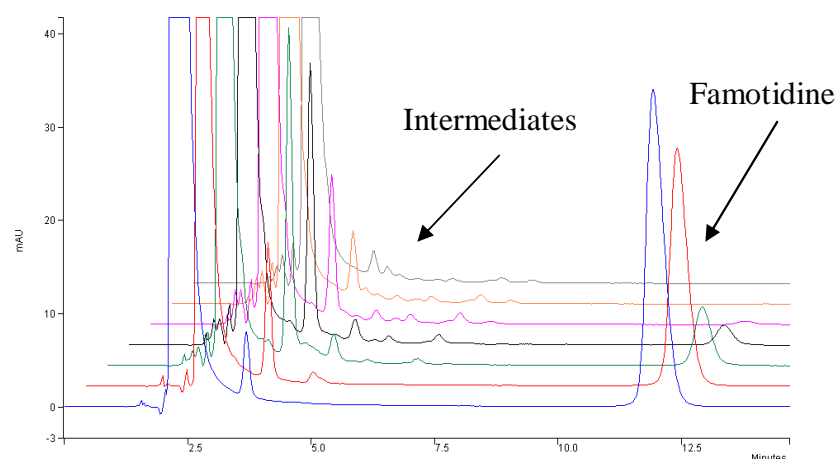


Figure 3.28: HPLC chromatogram of Famotidine with $\text{TiO}_2/\text{UV}/\text{H}_2\text{O}_2$ (5 mM) at 0 mins, 0 mins P_{ads} , 5, 10, 20, 30 and 40 mins. $[\text{FAM}] = 0.083 \text{ mM}$, $\text{H}_2\text{O}_2 = 5 \text{ mM}$, P-25 TiO_2 0.1 g/320 mL.

The lower concentration of peroxide in this case, shows obviously a slower photocatalytic degradation of Famotidine and the development of large quantities of the two initial intermediates is not observed in the first case with the higher concentration of peroxide (50 mM). Low quantities of these intermediates are seen and in general the quantities of all intermediates present appear to be lower in this case. This scenario would be preferred, as assuming intermediates are toxic, low quantities would be thus desired.

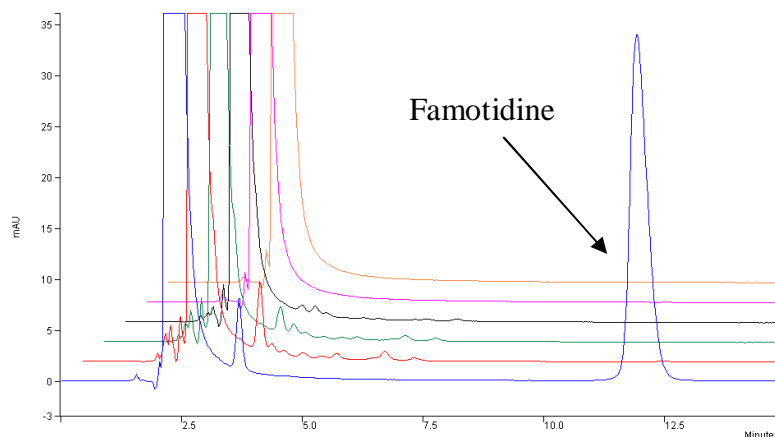


Figure 3.29: HPLC chromatogram of Famotidine with $\text{TiO}_2/\text{UV}/\text{H}_2\text{O}_2$ (5 mM) at 0 mins, 30, 40, 60, 120 and 180 mins. $[\text{FAM}] = 0.083 \text{ mM}$, $\text{H}_2\text{O}_2 = 5 \text{ mM}$, TiO_2 P-25 0.1 g/320 mL.

3.2.11 Adsorption Studies: Glassware and TiO_2

Further control experiments were conducted to investigate whether adsorption to the reactor glassware was potentially a large influence in photodegradation studies. Control experiments indicated that over the typical irradiation period studied of 3 h, 0.9% of Famotidine adsorbed to the reactor glassware (reactor, immersion well and stirring bar).

Some adsorption isotherm experiments were conducted at an early stage with Famotidine and with SA-TiO₂ which has a surface area of 8.6 m²/g.¹⁶⁰ These studies are presented in the Appendices section (3A-12 – 3A-15) and showed that Famotidine gave relatively poor adsorption: 3 mg FAM /g TiO₂ after 16 h and 8 mg FAM /g TiO₂ after an extended contact time of 48 h. This clearly represents very little adsorption by Famotidine onto the TiO₂ surface. A contact time of 48h, even though a greater adsorption is achieved, is not a feasible option for photocatalysis in the application for industry. In photocatalytic degradation experiments, 30 mins stirring time was allowed prior to irradiation for contact of the drug solution with the TiO₂. This was in accordance with results of control experiments and literature procedures, which can leave up to a maximum of 1 h for adsorption equilibrium to be obtained.⁸⁰

Despite the minimal adsorption achieved with these experiments, efficient photocatalytic degradation is seen to occur which indicates that perhaps a great amount of adsorption of drug to TiO₂ is not required for photocatalytic degradation to occur. Data from UV-vis spectroscopy studies of pH photocatalytic studies presented in the appendices also (3A-14) show bar chart graphs of the maximum adsorption of Famotidine reached after 0.5 h at various pHs along with the contribution by photocatalysis. In the case of acidic pH degradation experiments performed with Degussa TiO₂, adsorption after 30 mins resulted in higher absorbances than the 0 min sample so these results could not be comparatively evaluated. These problems were later found to be due to nylon filter membranes employed (see pH degradation section and appendices). Despite these problems, a general trend was observed with the maximum adsorption occurring at pH 7-8 for both titanias.

Adsorption at acidic pHs would be predicted to be unfavourable since Famotidine can be protonated and the surface of TiO₂ is also positively charged at this pH which would lead to an electrostatic repulsion. Famotidine has a pK_a of ~7 and TiO₂ has a pzc (point of zero charge) at ~6.4.¹⁹⁵ So adsorption can theoretically be presumed to be favoured at a pH above the pzc, and below the pK_a whereby the TiO₂ is negatively charged and Famotidine is positively charged. This is certainly the case in terms of Sigma-Aldrich TiO₂. In the case of P25, there is a similar adsorption observed at the natural pH of Famotidine (can vary dependent on Millipore water pH). However the max adsorption was achieved at a pH of 8. It should be noted that in lower pH experiments (pH 3 etc) it was observed that a good suspension was not obtained initially after adding the TiO₂ (although overcome after a period of stirring). At normal pH/no pH adjustment, a good suspension was always obtained initially. This effect was considered to be due to the zeta potential effect of TiO₂.

Jiang *et al.* found for their formulations of TiO₂, an increase in the ionic strength of the solution was proportional to a decrease in the zeta potential corroborating with an increase in the particle size. Their work also found that at pHs close to the isoelectric point (pzc) of TiO₂ that the zeta potential was found to tend to zero, with a simultaneous increase in hydrodynamic diameter. Optimum conditions based on their research for TiO₂ with a small hydrodynamic diameter would be low ionic strength (0 - 10⁻³M), and low or high pH (3-4, 8-9). In addition to the effects found on the suspension formed, hydrodynamic size and zeta potential effects may also be contributing to the adsorption of the analytes on the TiO₂ surface. In reality, a combined effect of surface charge (on the TiO₂ and the API), and zeta potential/hydrodynamic size is most likely.

3.2.12 Famotidine Concentration Variation Studies

Concentration variation experiments were performed to determine the robustness of the proposed photocatalytic method for Famotidine. Four different concentrations were studied in these experiments 20 µM, 83 µM, 200 µM and 1000 µM. (Dilutions were undertaken of higher concentrations so as not to overload the column.) These experiments were performed with TiO₂ alone. The results are shown in Figure 3.30.

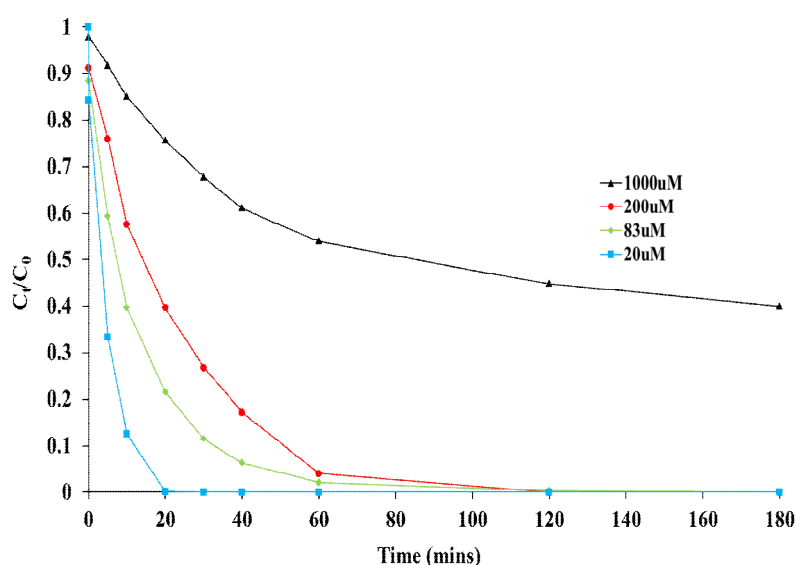


Figure 3.30: Concentration Variation Experiments for Famotidine. P-25 TiO₂ = 0.1 g/320 mL, [FAM] = 20 µM, 83 µM, 200 µM, 1000 µM. Dilutions of 1 in 2 for 200 µM and 1 in 10 for 1000 µM were undertaken for analysis.

Complete removal of Famotidine was seen after 20 mins in the case of 20 µM (6.7 mg/L) and even under increased concentrations of 200 µM (67 mg/L) complete degradation is seen at 120 mins. An additional experiment at 1000 µM (337 mg/L) was performed showing a much slower degradation profile due to Famotidine 'saturation'. Realistically, concentrations of Famotidine

in the environment would be in the order of $\mu\text{g/L}$ - ng/L , however, these experiments show that in situations where there may be a possibility of higher concentrations i.e from pharmaceutical production wastewater plant facilities, the method would be robust enough to be applied.

3.2.13 Famotidine Heterogeneous Photocatalytic Degradation Conclusions

Famotidine can be successfully degraded by TiO_2 -photocatalysis as all of the above studies under the various conditions have shown. It is a pharmaceutical which is stable to light $>300\text{ nm}$ as proven by the minimal degradation achieved in control studies with UV alone (photolysis). Additional control experiments showed that light is required to photocatalytically degrade Famotidine and that a 'thermal degradation' does not occur. Some adsorption to TiO_2 does occur, although this was found to be rather minimal in orbital shaking experiments, and was not greater than 15% in dark control experiments. It is particularly sensitive to pH changes, and the drop in pH throughout photocatalysis causes a shift in its absorption profile as shown in UV-vis monitoring studies.

P-25- TiO_2 was shown to be the superior formulation in all studies over the Sigma Aldrich TiO_2 . pH photocatalytic degradation studies determined the best pHs for Famotidine degradation to be pH 3 or pH 8. HPLC analysis of Famotidine photocatalytic experiments showed the presence of numerous intermediates in chromatograms. These are identified via LC-MS/MS analysis in the next chapter. These intermediates were found to be effectively mineralised with the addition of hydrogen peroxide to the photocatalytic process. Also, it was found in examining HPLC chromatograms that depending on the concentration of peroxide employed different mechanisms of intermediate formation and thus degradation are observed. In addition to these studies, concentration variation studies showed that the TiO_2 -photocatalytic process is still very effective for elimination of Famotidine at much higher concentrations ($200\text{ }\mu\text{M}$), and can eliminate 50% of $1000\text{ }\mu\text{M}$ concentrations after 180 mins proving the robustness of the process.

Heterogeneous Photocatalysis part II: Tamsulosin

3.2.14 UV-vis Studies

The UV-vis spectrum of Tamsulosin has 3 major absorbances in the UV region of the spectrum at 200 nm , 223 nm (λ_{max}) and 280 nm (Figure 3.31). Tamsulosin also decomposes with light and predictably should respond well to both photolysis and photocatalysis. The molar absorptivity coefficient calculated from standard curves was found to be $15000\text{ M}^{-1}\text{cm}^{-1}$ at 223 nm .

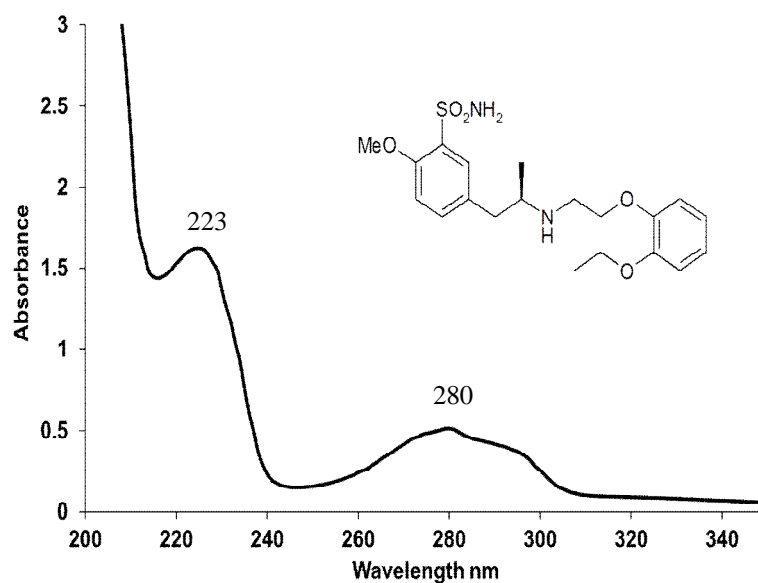


Figure 3.31: UV-vis analysis of Tamsulosin (100 μM).

Tamsulosin is unaffected by changes in pH. The variations in the UV-vis spectra shown in Figure 3.32 around 235 nm are due to various components of the buffers used. No shifts or changes in the absorbance at 280 nm were observed at different pHs which would indicate that Tamsulosin is relatively stable at varying pHs. Two initial studies were performed with pH adjustment by HCl and NaOH which corroborated well with these buffered studies.

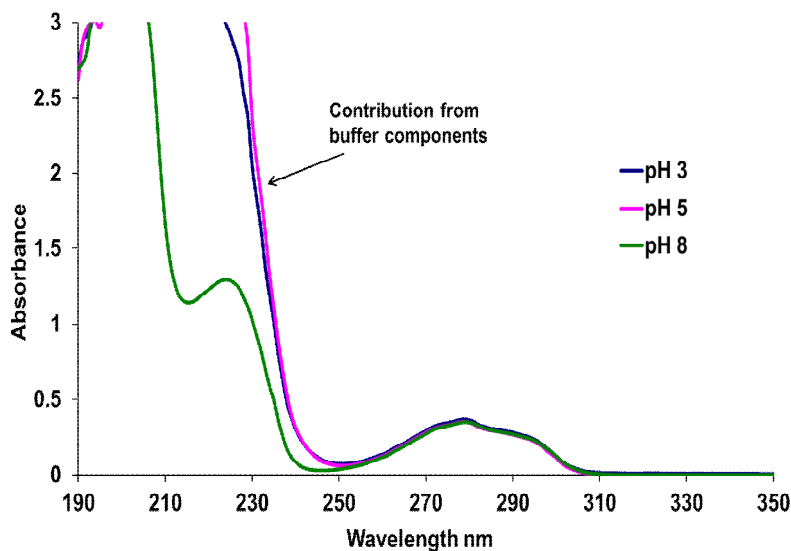


Figure 3.32: UV-vis analysis of Tamsulosin at different pHs (pH 3, 5, 8).

3.2.15 Quartz Glassware: Photolysis Studies

Photolysis of Tamsulosin with Quartz shows a clear step-wise degradation. This is shown with the obvious decrease in intensity of its 3 main absorption peaks in Figure 3.33. Also shown are the changes in shape and resolution of each peak with respect to time. This is thought to be due

to the conversion of Tamsulosins' parent structure and its transformation into secondary reaction products and intermediates. A slight yellow tinge could be observed from the Tamsulosin reaction mixture which could be due to the formation of coloured intermediate product(s). This would explain the shape shifting and stretch above 300 nm.

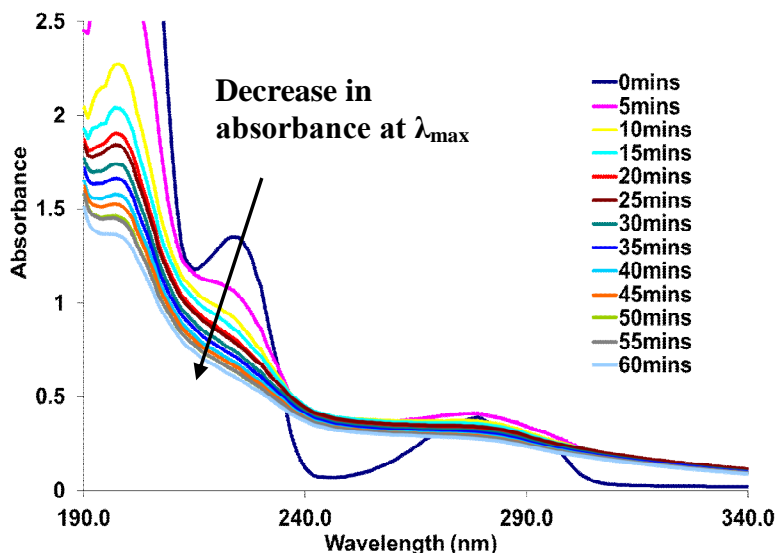


Figure 3.33: UV-vis spectroscopic analysis of the photodegradation (photolysis) of Tamsulosin with Quartz glassware. [TAM] = 0.083 mM, Time = 1 h.

3.2.16 Quartz Glassware: Photocatalysis Studies

The effects of both P25 and Sigma TiO_2 are almost equivalent with respect to degradation with Quartz (Figure 3.34). Considering the small amount of TiO_2 added and the time of only 1h irradiation, the results for decomposition of Tamsulosin are exceptional. It should be considered that the enhancement in degradation by photocatalysis was only ~30%. It should also be noted that photocatalysis with Quartz glassware comprises both photolysis and photocatalysis. It could be argued that with the presence of TiO_2 , there are transparency and light scattering issues which could affect the degradation achieved by photolysis. In any case, the switch from Quartz to Pyrex glassware should eliminate most of the effects of direct photolysis, and allow for an evaluation of degradation purely by the photocatalytic process.

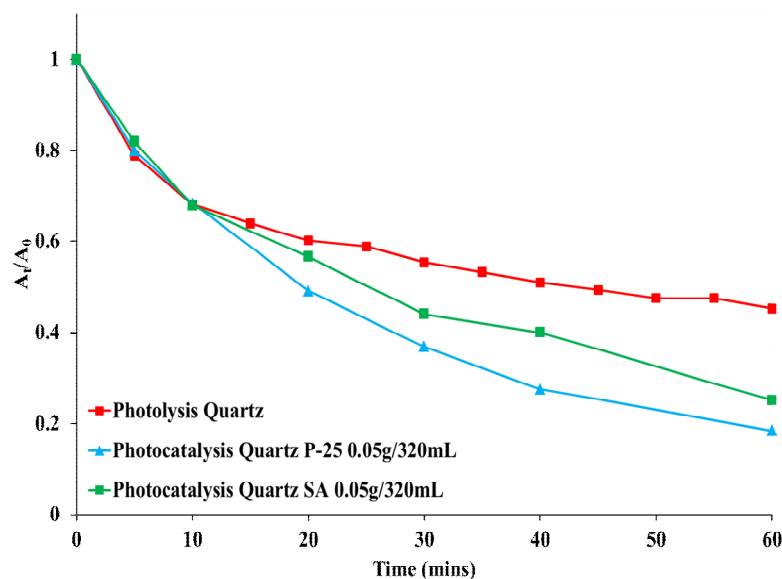


Figure 3.34: UV-vis degradation profiles showing the photocatalytic degradation of Tamsulosin with Quartz and SA and P-25 TiO_2 (0.05 g/320 mL) vs. Photolysis Quartz.

3.2.17 Pyrex Glassware: Photolysis Studies

Photolysis using Pyrex showed slightly poorer results compared to quartz, although some decomposition of Tamsulosin was achieved as shown in Figure 3.35. An increase in the absorbance was observed in some samples and a change in peak shape was observed in the UV-vis spectrum. Larger scale studies in the Enviolet also showed a straw-yellow coloured solution being produced, which was also detected in these studies. Yellow organic compounds tend to absorb below 400 nm and it is in this region that Tamsulosins' intermediates products are absorbing.

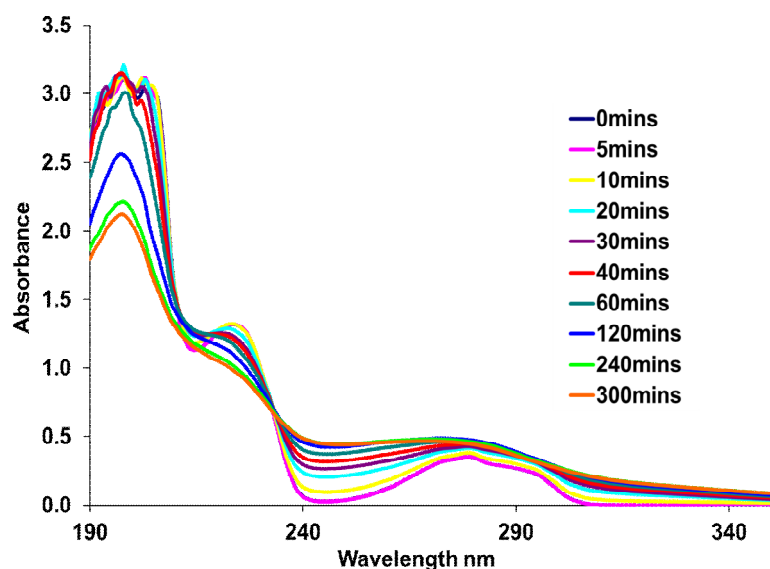


Figure 3.35: UV-vis spectroscopic analysis of the photodegradation (photolysis) of Tamsulosin with Pyrex for 5 h. [TAM] = 0.083 mM, Time = 5 h.

3.2.18 HPLC Analysis of Photolysis Studies

HPLC analysis was then undertaken of the photolysis experiments for Tamsulosin. Both Quartz and Pyrex photolysis studies were analysed and the results are shown in Figure 3.36. As predicted, photolysis with quartz can eliminate Tamsulosin within 30 mins. Previous quartz photolysis studies conducted and analysed with UV-vis spectroscopy (Figure 3.33) showed absorbances remaining at the λ_{max} after 1 h, so it is clear that despite the total elimination shown by HPLC analysis, photodegradation products may persist. In the case of photolysis with Pyrex, Tamsulosin showed a complete elimination also in these studies after the total 3 h irradiation period. Despite this intermediates may also be remaining as after 5 h of photolysis (Figure 3.35) absorbances still remain. Quartz glassware photolysis studies (including those of the Enviolet and LP studies in appendices 3A-10 - 3A-11) with Tamsulosin generated significant quantities of coloured intermediates which is obviously not a desirable result as these intermediates appeared to be quite photo-stable. The effect of photocatalysis of Tamsulosin will be interesting to examine, as an alternative route of degradation may prevent the formation of these intermediates.

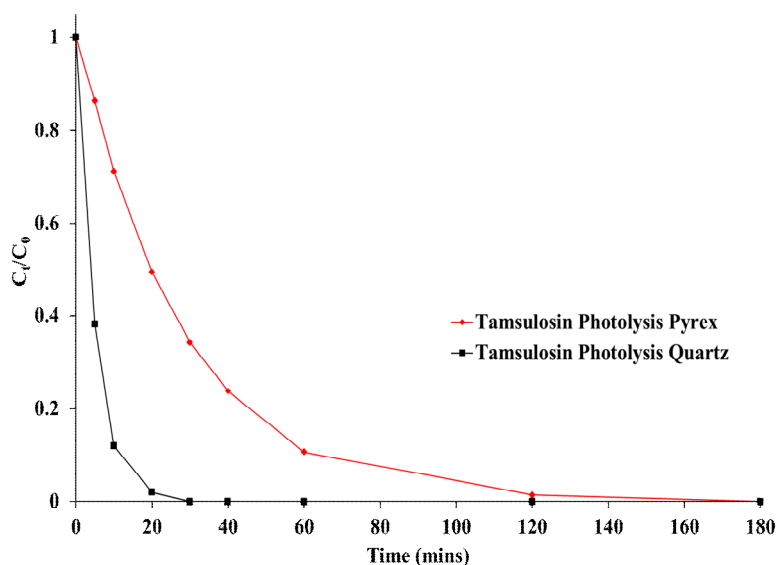


Figure 3.36: HPLC Analysis of photolysis experiments with Quartz and Pyrex glassware for Tamsulosin. [TAM] = 0.083mM, Pyrex or Quartz glassware, Time = 3 h.

3.2.19 Tamsulosin Heterogeneous Photocatalysis: Pyrex

Preliminary photocatalytic studies were conducted with concentrations of TiO_2 at 0.05 g/320 mL. The UV-vis degradation data obtained in these studies is shown in Figure 3.37. Determining the A_t/A_0 value using $\text{UV}_{223\text{nm}}$ spectroscopy showed a contribution by photolysis of ~10%, and contributions by photocatalysis to be 35% and 45% with P-25 and Sigma TiO_2 respectively. Neither SA- TiO_2 or P-25 TiO_2 achieved superior results compared to photolysis

studies with quartz. It can therefore be determined from these studies that 0.05 g/320 mL (0.15 g/L) is clearly a low amount of photocatalyst and a higher concentration is needed.

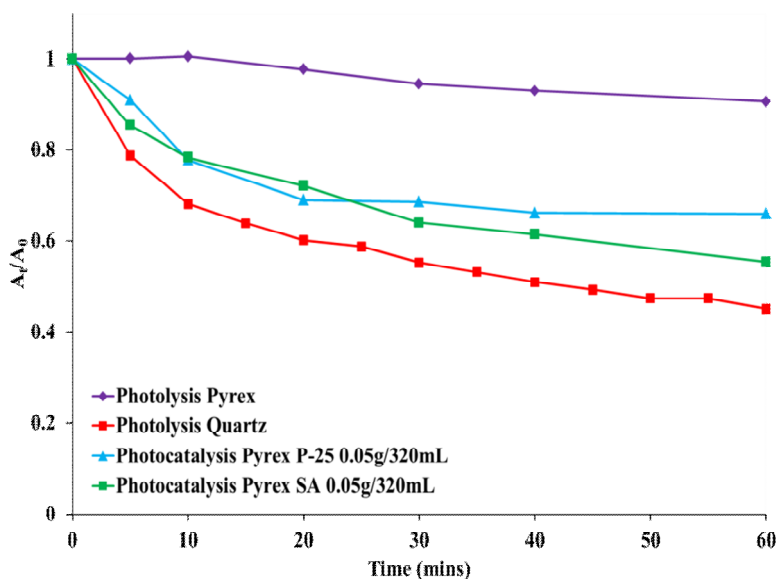


Figure 3.37: UV-vis degradation profiles showing the photocatalytic degradation of Tamsulosin with Pyrex and SA and P-25 TiO_2 (0.05 g/320 mL) vs. Photolysis Quartz and Pyrex.

3.2.20 Tamsulosin Heterogeneous Photocatalysis: TiO_2 Optimisation

API	C_0 mM	TiO_2 Phase	TiO_2 g/320 mL	Irradiation Time h	100% reached HPLC	UV data % Degradation
Tamsulosin	0.083	P-25	0.05	1	N/A	32
		P-25	0.1	3	120mins	71
		P-25	0.2	3	60mins	68
		P-25	0.4	3	120mins	63
		P-25	0.6	1	N/A	62
		Sigma	0.05	1	N/A	43
		Sigma	0.1*	3	N/A	67*
		Sigma	0.2*	5	N/A	72*
		Sigma	0.4*	5	N/A	75*

*400 W Lamp

Table 3.3 List of conditions used in Tamsulosin TiO_2 optimisation photocatalytic degradation experiments

Degussa P-25 TiO_2

For P-25 TiO_2 optimisation experiments, the best concentration was determined as 0.2 g/320 mL (0.6 g/L) by HPLC-UV analysis (see Figure 3.38) with 100% disappearance after 1 h. There did not appear to be an exceptional difference between the concentrations studied shown in the HPLC analysis. The initial rate was the same for all three, however after 30 mins irradiation, there is noticeable differentiation between the optimum 0.2 g/320 mL and 0.1 and 0.4 g/320 mL. This was also apparent in the UV-vis monitoring profiles for each experiment even though the concentration was effectively doubled each time.

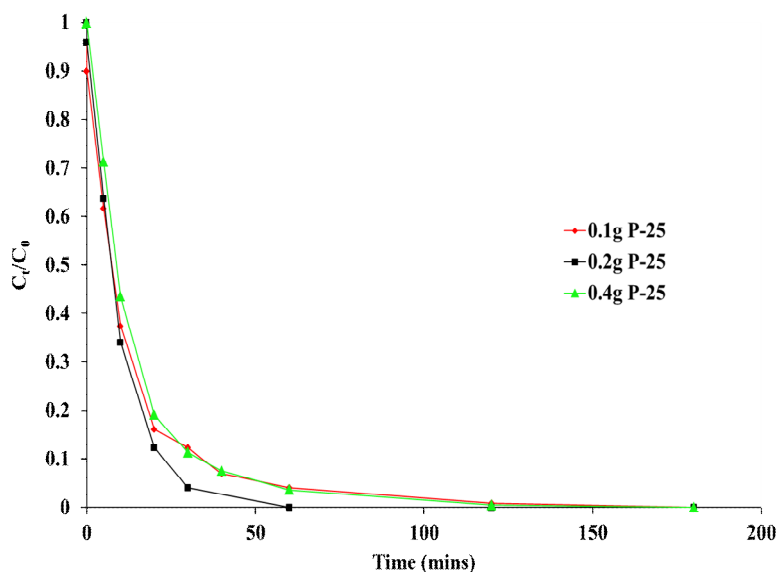


Figure 3.38: HPLC-UV analysis of photocatalysis of Tamsulosin with varying TiO_2 amounts. Order of degradation achieved: $0.2 \text{ g} > 0.1 \text{ g} > 0.4 \text{ g}/320 \text{ mL}$. $[\text{TAM}] = 0.083 \text{ mM}$, Time = 3 h, P-25 $\text{TiO}_2 = 0.1\text{-}0.4 \text{ g}/320 \text{ mL}$. Analysis undertaken with methods in appendices (2A-1).

Sigma-Aldrich TiO_2

Sigma TiO_2 optimum was determined by UV-vis analysis and the results are shown in Figure 3.39. The following order was determined $0.2 \text{ g} = 0.4 \text{ g} > 0.1 > 0.05 \text{ g}/320 \text{ mL}$ with $0.2 \text{ g}/320 \text{ mL}$ being determined as the optimum amount in these studies. $0.4 \text{ g}/320 \text{ mL}$ achieved an almost identical degradation profile to $0.2 \text{ g}/320 \text{ mL}$ however ideally the least amount of photocatalyst is ideal for cost effectiveness.

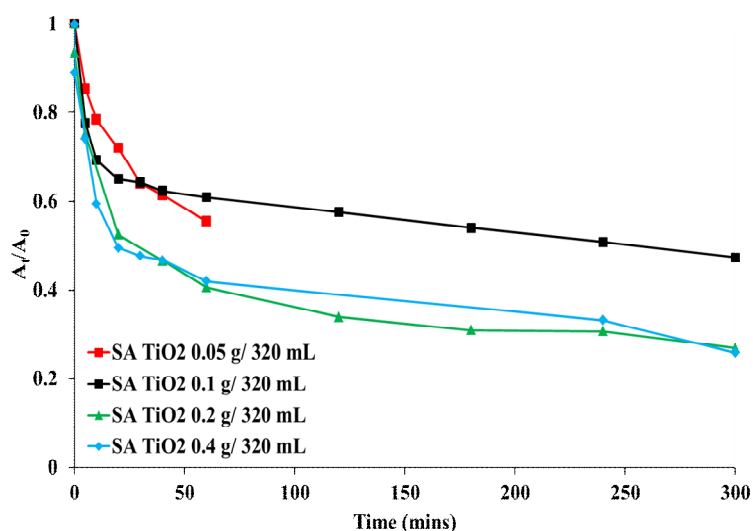


Figure 3.39: UV-vis degradation profiles showing the photocatalytic degradation of Tamsulosin with varying amounts of TiO_2 . $[\text{TAM}] = 0.083 \text{ mM}$, SA- $\text{TiO}_2 = 0.05 - 0.4 \text{ g}/320 \text{ mL}$, Time = 5 h (*400 W Lamp).

3.2.21 Tamsulosin pH Adjustment Studies

API	C ₀ mM	TiO ₂ Phase	pH	TiO ₂ g/320 mL	Irradiation Time h	100% reached HPLC	UV data % Degradation
Tamsulosin	0.083	P-25	3	0.1	3	92% (180 mins)	28
		P-25	5	0.1	3	120mins (96% (60 mins))	76
		P-25	8	0.1	3	120mins (99% (60 mins))	82
		Sigma	3	0.1	3	N/A	53
		Sigma	5	0.1	3	N/A	72
		Sigma	8	0.1	3	N/A	82

Table 3.4 List of conditions used in Tamsulosin pH photocatalytic degradation experiments.

P-25 TiO₂

Only pHs 3, 5 and 8 were examined with Tamsulosin as this drug is formulated as a hydrochloride salt and only acidic, moderately acidic and alkaline pHs were chosen to be examined. The order of the most efficient degradation with different pHs can be seen in Figure 3.40 and was as follows: pH 8 > pH 5 ≥ no pH adjust > pH 3. Degradation at pH 8 with Tamsulosin was far superior over other pHs, even the UV-vis spectroscopic profile Figure 3.41 shows an excellent degradation over time.

Although pH 8 can be considered to be mildly alkaline, there would be an additional abundance of [OH] ions present in solution, which can enhance the degradation process as these ions provide a source for OH radical generation. Tamsulosin at regular pH is ~pH 5 and has a pK_a of 8.4 (secondary amine) and 10.2 (sulfonamide).¹⁸⁰ At pH 8 TiO₂ is negatively charged and both protonatable sites of Tamsulosin are positively charged, building an electrostatic attraction which enhances adsorption and can consequently favour the photocatalytic degradation of the molecule. Similar effects have been reported by other authors.¹⁸¹ Tamsulosin also showed an effective degradation at pH 3 which would not be expected due to the potential electrostatic repulsion between the drug and the TiO₂ since adsorption is considered an important process and necessary for efficient degradation.

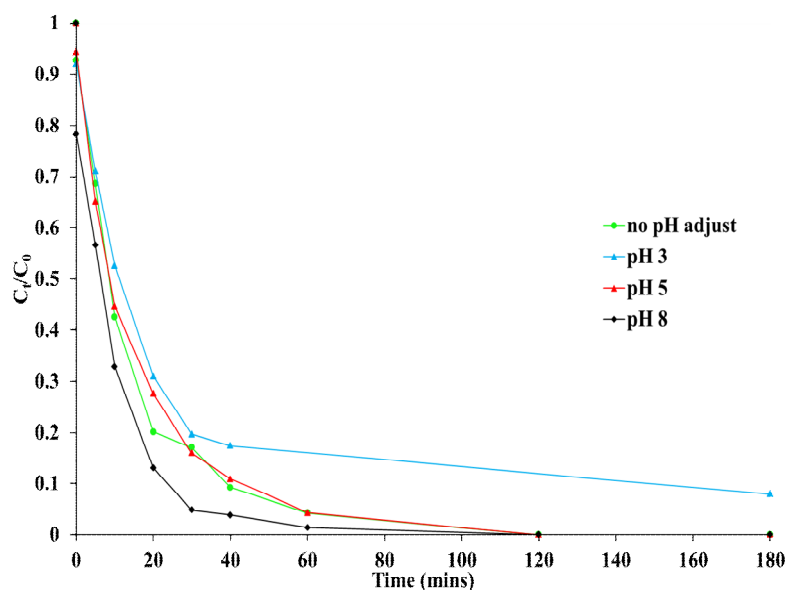


Figure 3.40: HPLC analysis of the photocatalytic degradation of Tamsulosin with varying pHs. [TAM] = 0.083 mM, P-25 0.1 g/TiO₂, Time = 3 h, pH = 3-8. Analysis undertaken with methods in appendices (2A-1)

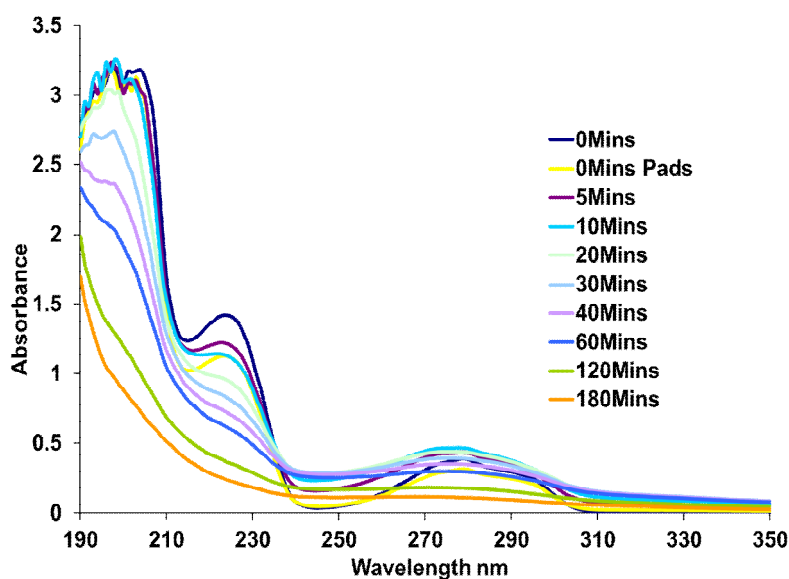


Figure 3.41: UV-vis spectroscopic analysis of the photocatalytic degradation of Tamsulosin with P-25 at pH 8. [TAM] = 0.083 mM, pH = 8, P- 25 TiO₂ = 0.1 g/320 mL, Time = 3 h.

Sigma Aldrich TiO₂

Figure 3.42 shows UV-vis data obtained from Sigma TiO₂ photocatalytic pH experiments and indicate that the following order of Tamsulosin photodecomposition is achieved pH 8 = pH 5 > no pH adjustment > pH 3. UV-vis analysis also showed a good clean disappearance of the absorbance at 223 nm for pH 5 and pH 8. pH tended to decrease most in the early stages of irradiation (Figure 3.43) and then flattened to a plateau although in some cases, pH did not fluctuate that much.

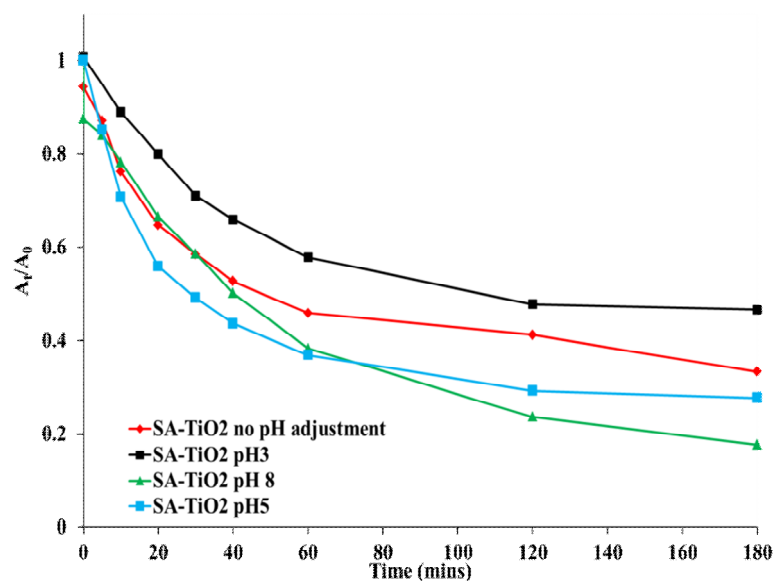


Figure 3.42: UV-vis degradation profiles showing the photocatalytic degradation of Tamsulosin with SA TiO₂ at varying pHs. [TAM] = 0.083 mM, pH = 3-8, SA TiO₂ = 0.1 g/320 mL, Time = 3 h.

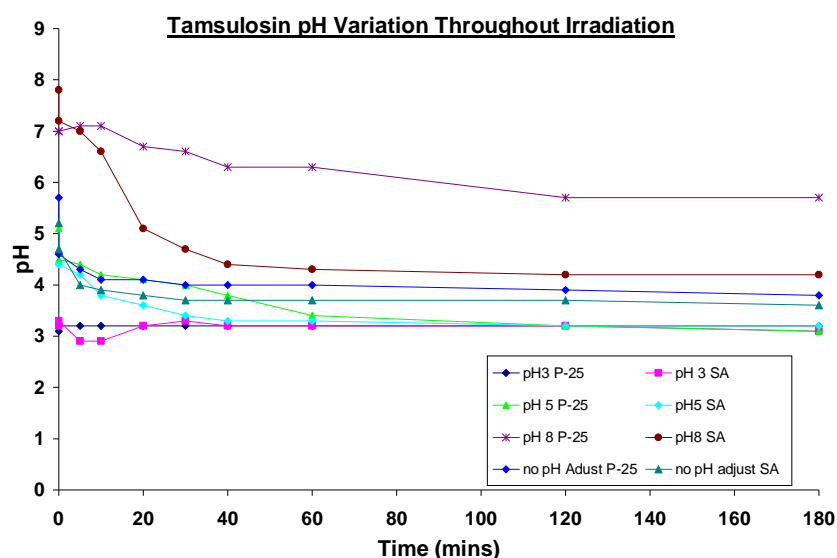


Figure 3.43: pH monitoring of samples post photocatalysis for Tamsulosin pH experiments showing the fluctuation/decrease in pH throughout irradiation.

3.2.22 Tamsulosin Hydrogen Peroxide Addition: P-25 TiO₂

As previously discussed, after hydrogen peroxide additions experiments were conducted, experiments were then performed to see the effect of the sodium bisulfite quencher individually on each of the pharmaceuticals. UV-vis analysis studies were not conducted in the case of Tamsulosin as sodium bisulfite was shown to absorb in the region of the λ_{max} of Tamsulosin (223 nm).

¹H NMR Analysis

In the case of Tamsulosin, no shifts were seen with the addition of bisulfite (Figure 3.44). In fact, there are very little changes to the spectra whatsoever. Signals arising at 4.7 ppm are due to solvent peaks and contributions from exchangeable protons. Spectra obtained within hours of one another showed no change and two days later again no shifts were observed. An addition of more bisulfite with immediate analysis yielded again no significant change in the spectra. This study would therefore conclude that sodium bisulfite is an inert quencher in the case of Tamsulosin. Predicted multiplicity assignments are shown in Figure 3.45.

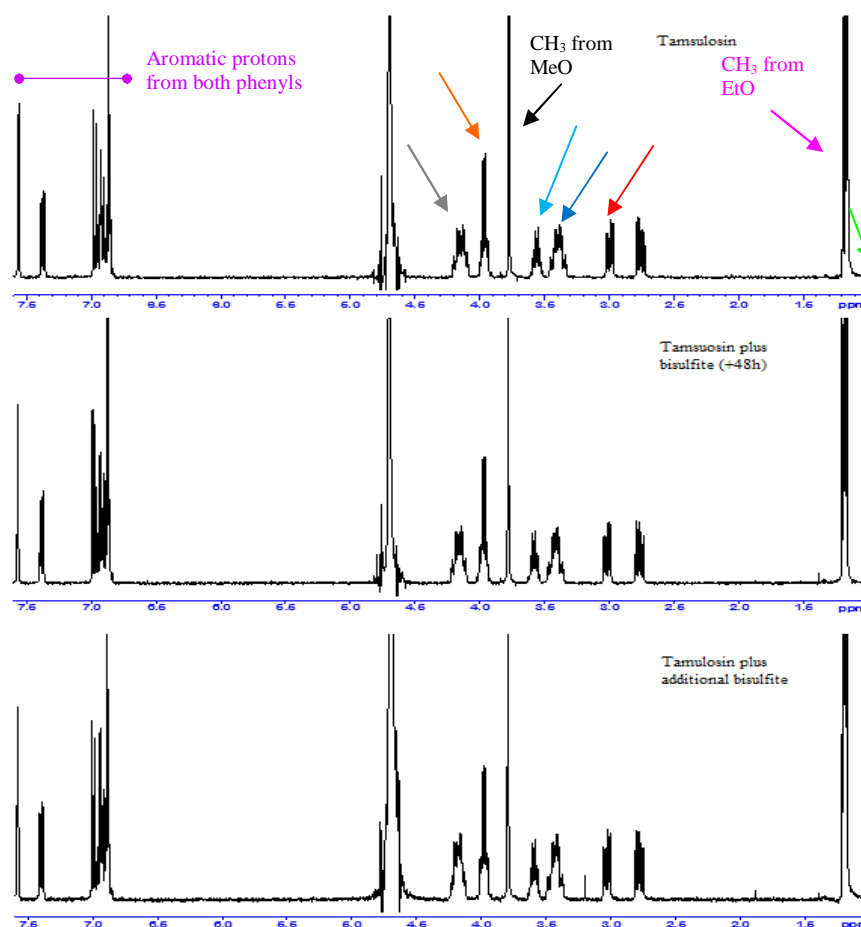


Figure 3.44: ¹H NMR spectra for Tamsulosin in D₂O (Top), Tamsulosin + Bisulfite (2 days) (Middle) and with additional bisulfite added (Bottom).

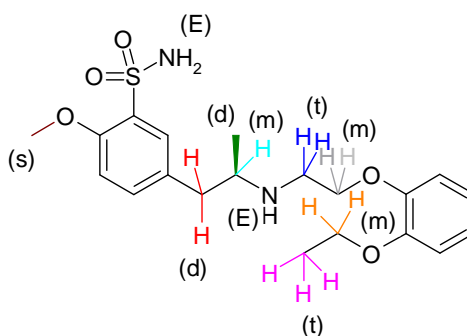


Figure 3.45: Tamsulosin, highlighted in colour are all protons which should show in ^1H NMR. s = singlet, d = doublet, t = triplet m = multiplet, E = exchangeable proton.

HPLC Analysis

HPLC analysis was conducted with Tamsulosin and bisulfite and the results are shown in Figure 3.46. No elimination of Tamsulosin was detected by HPLC. Any decrease can be considered to be due to the dilution effect of the addition of sodium bisulfite solution to Tamsulosin initially. There is no subsequent decrease after 30 h. These results combined with the ^1H NMR studies show that sodium bisulfite is an inert quencher and can be reliably used in hydrogen peroxide studies with Tamsulosin.

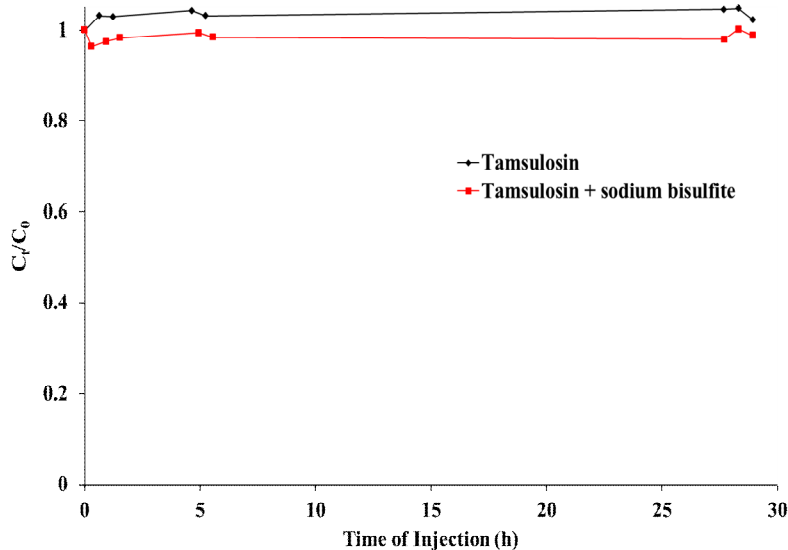


Figure 3.46: HPLC analysis with repeat injections of samples of Tamsulosin and Tamsulosin plus bisulfite.

Figure 3.47 shows experiments conducted with Tamsulosin and various concentrations of peroxide. Control experiments are shown for comparison and additional control experiments can be found in Figure 3.48. The optimum concentration of peroxide found for the photocatalytic degradation of Tamsulosin was found to be 5 mM. 50 mM also showed a similar degradation to 5 mM, although this amount of peroxide combined with 0.2 g TiO_2 (0.1 g is the

optimum for Famotidine) would perhaps produce significantly more radicals than 5mM. At high concentrations of peroxide, as discussed previously, radical recombination can come into effect and competes with the photodegradation process. Control experiments showed that peroxide on its own has little effect on the degradation of Tamsulosin. It was also evident that peroxide in the presence of TiO_2 in the dark showed a slight improvement compared to H_2O_2 alone. It was thought that this may just be the combined effect of degradation by peroxide plus the adsorption of Tamsulosin to TiO_2 , however, as indicated by control experiments, Tamsulosin in the presence of TiO_2 (dark) has no effect/adsorption in this case.

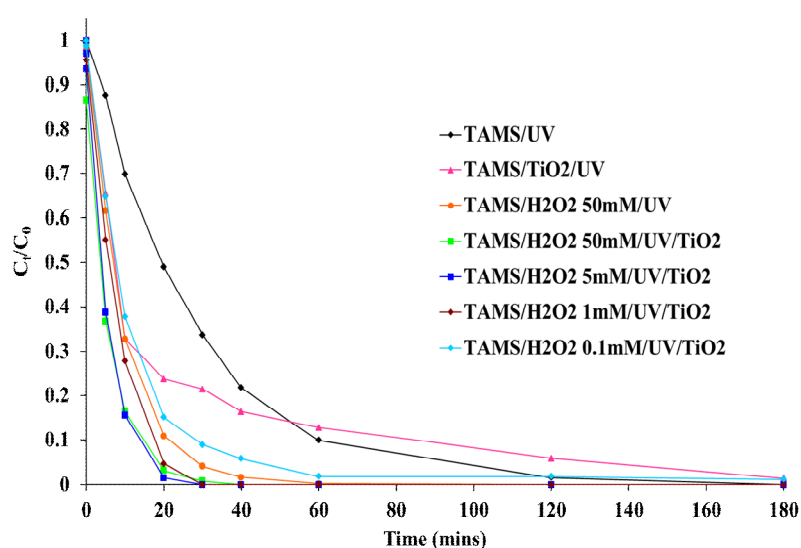


Figure 3.47: HPLC analysis of the photocatalytic degradation of Tamsulosin showing varying additions of H_2O_2 . P-25 TiO_2 0.2 g/320 mL, $[\text{H}_2\text{O}_2] = 0.1 \text{ mM} - 50 \text{ mM}$, $[\text{TAM}] = 0.083 \text{ mM}$.

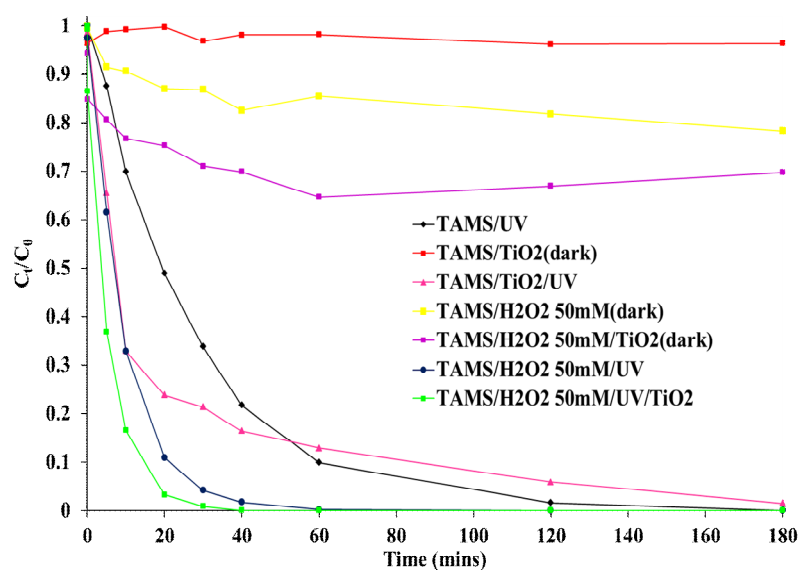


Figure 3.48: HPLC analysis of control experiments for Tamsulosin. P-25 $\text{TiO}_2 = 0.2 \text{ g/320 mL}$, $\text{H}_2\text{O}_2 = 50 \text{ mM}$, $[\text{TAM}] = 0.083 \text{ mM}$.

Control experiments also indicated that UV/H₂O₂ can efficiently eliminate Tamsulosin. However, the TiO₂/UV/(5 mM) H₂O₂ photocatalytic process was superior even to this, eliminating Tamsulosin completely in 20 mins. Chromatograms of peroxide additions showed fewer intermediates for Tamsulosin (see Figure 3.49). A chromatogram from a photocatalytic experiment without peroxide is shown in Figure 3.50 and the presence of intermediates can be clearly seen. Intermediates were found to be more prominent in the 280 nm wavelength channel. This would be predicted since previous UV-vis monitoring of photolysis studies showed that intermediates from Tamsulosin had extended absorption up to 340 nm.

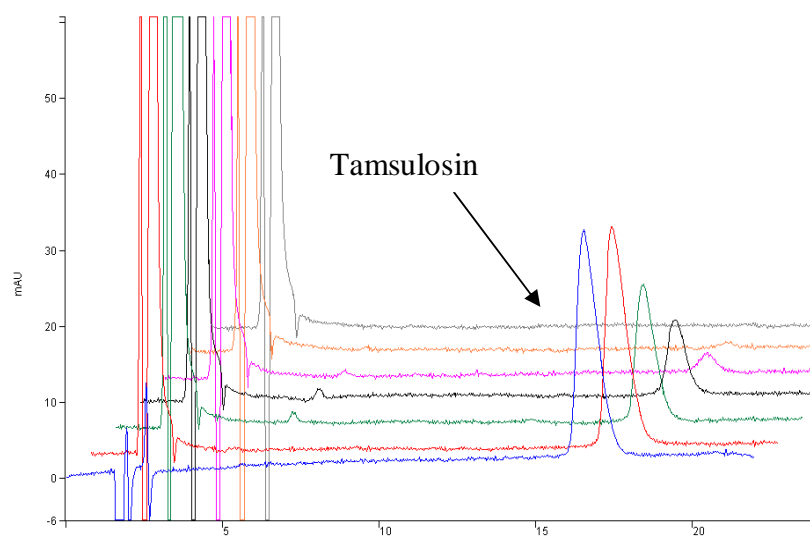


Figure 3.49: HPLC Chromatogram of Tamsulosin at 0Mins, 0mins P_{ads}, 5, 10, 20, 30, 40 mins. TiO₂ 0.2 g/320 mL, [H₂O₂] = 0.1 mM, [TAM] = 0.083 mM, Wavelength = 223 nm.

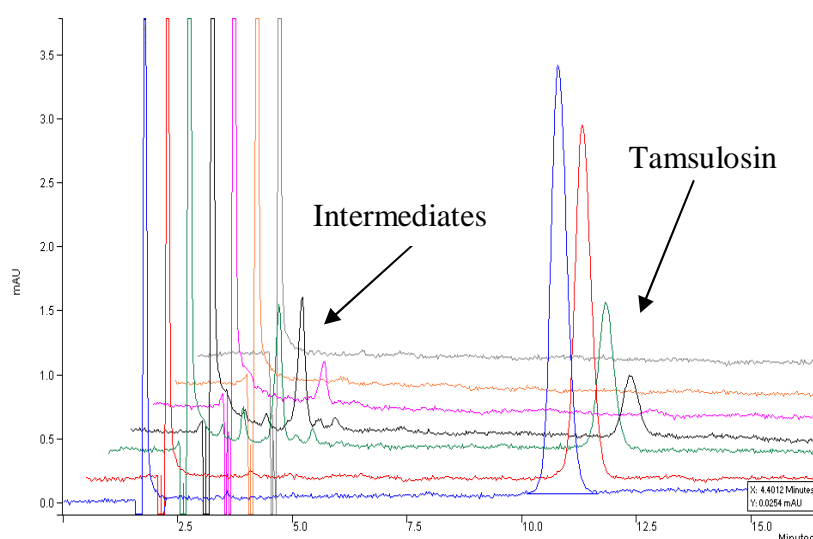


Figure 3.50: HPLC Chromatogram of Tamsulosin at 0Mins 0mins P_{ads}, 5, 10, 20, 30, 40mins. TiO₂ 0.2 g/320 mL, [TAM] = 20 µM, Wavelength = 280 nm.

3.2.23 Adsorption Studies: Glassware

Further control experiments were conducted to investigate whether adsorption of Tamsulosin to the reactor glassware was potentially a factor to skew any of the results in photodegradation or control studies. Control experiments indicated that over the typical irradiation period studied of 3 h, 0.9% of Tamsulosin adsorbed to the reactor glassware (reactor, immersion well and stirring bar). Therefore adsorption of Tamsulosin to the reactor glassware and apparatus was ruled out as a factor which may skew any of the results in these studies.

3.2.24 Tamsulosin Concentration Variation Studies

The results for Tamsulosin concentration studies are shown in Figure 3.51. Complete removal of Tamsulosin was seen after 20 mins in the case of 20 μM (8.8 mg/L) and even under increased concentrations of 200 μM (88.8 mg/L) almost complete degradation is seen after 3 h. An additional experiment at 1000 μM (444 mg/L) was performed showing predictably a much slower degradation profile however, almost 50% of Tamsulosin is eliminated after 3 h. These experiments show that the TiO_2/UV process is quite robust for Tamsulosin.

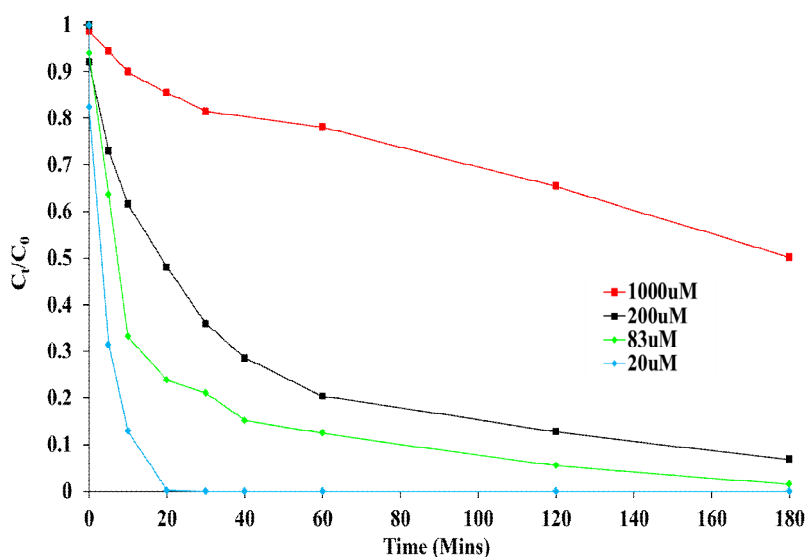


Figure 4.51: Concentration Variation Experiments for Tamsulosin. P-25 TiO_2 = 0.2 g/320 mL, [TAM] = 20 μM , 83 μM , 200 μM , 1000 μM . Dilutions of 1 in 2 for 200 μM and 1 in 10 for 1000 μM were undertaken for analysis.

3.2.25 Tamsulosin Heterogeneous Photocatalytic Degradation Conclusions

Tamsulosin is a light sensitive pharmaceutical and the effects of photolysis studies in this chapter showed this. These studies produced coloured photo-stable intermediates, which would be extremely undesirable in water treatment. The photocatalytic studies conducted in this chapter show that Tamsulosin can be efficiently degraded with TiO_2 and that intermediates

generated by this process, can also be eliminated. pH photocatalytic studies showed that pH 8 (mildly alkaline) or pH 5 gave the best results.

Peroxide addition studies demonstrated that Tamsulosin can be efficiently degraded in approximately 20 mins with 5 mM H₂O₂/TiO₂/UV. No significant quantities of intermediates were seen in chromatogram traces with peroxide studies which may indicate that intermediates are being efficiently mineralised. Follow-up LC-MS/MS studies with peroxide will conclude this. Concentration variation studies also demonstrated the robustness of the photocatalytic method at higher concentrations and even at 1000 µM, 50% of Tamsulosin could be eliminated.

Heterogeneous Photocatalysis Part III: Solifenacin

3.2.26 UV-vis Studies

The concentration used to attain the profile in Figure 3.52 was 1 mM, much higher than the other pharmaceuticals. Solifenacin has a very weak absorption in the UV region with a λ_{max} of 264 nm. It has no absorption above 300 nm which may result in poor degradation by photolysis when using Pyrex. No literature could be found in relation to an absorptivity coefficient for Solifenacin. A UV-vis profile of standards resulted in the lower concentrations dropping below the baseline. From single absorbance profiles at concentrations of 1mM, the average molar extinction coefficient was found to be 550 M⁻¹cm⁻¹ at 263 nm.

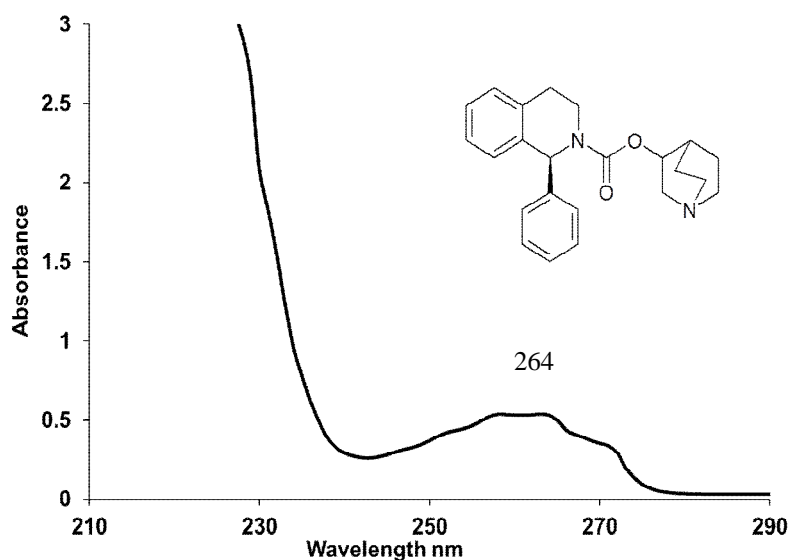


Figure 3.52: UV-vis analysis of Solifenacin Succinate (1 mM).

Solifenacin is formulated as a succinate salt and like Tamsulosin is unaffected by changes in pH. Once again, the differences seen between 220-250 nm in Figure 3.53 are due to buffer components as a fairly wide range was used (pH 2-8). Results were comparable with those done without buffers, using HCl and NaOH.

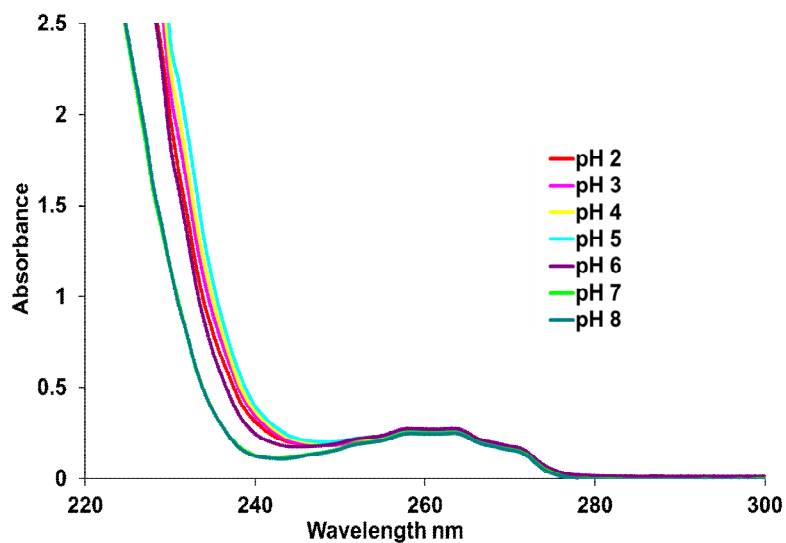


Figure 3.53: UV-vis analysis of Solifenacin at different pHs (pH 2-8).

3.2.27 Quartz Glassware: Photolysis Studies

Under photolytic conditions, Solifenacin undergoes a rapid transformation into its decomposition products, and unlike the other two compounds shows an increase in absorbance. Figure 3.54 shows the UV-vis monitoring and absorbance can be seen stretching into the near visible region of the spectrum. Irradiation after one hour yielded a solution which was a slight straw colour, indicating formation of a coloured intermediate product(s). Other cases in the literature have displayed a similar increase in absorbance, but not as drastic.¹⁸² This rapid increase with Solifenacin can be attributed to its much higher concentration relative to the other compounds, in order to analyse its decomposition by UV-vis spectroscopy. Photolysis with quartz for all three compounds can be seen to be quite substantial considering no photocatalyst is present.

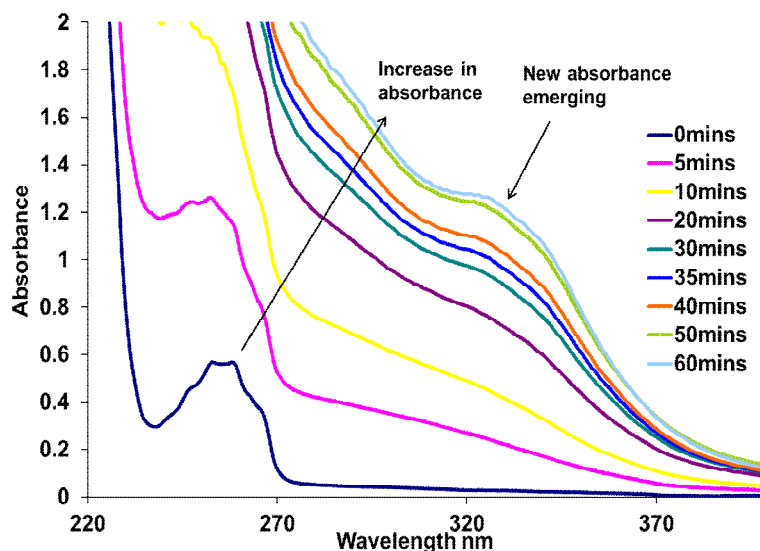


Figure 3.54: UV-vis spectroscopic analysis of the photodegradation (photolysis) of Solifenacin with Quartz glassware. [SOL] = 1 mM, Time = 1 h.

3.2.28 Quartz Glassware: Photocatalysis Studies

Photocatalytic studies with quartz and both titanias was undertaken with Solifenacin (1 mM) and the results were monitored by UV-vis spectroscopy. As with photolysis studies in the previous section, photocatalytic degradation with TiO_2 gave rise to intermediates of higher molar extinction coefficients than Solifenacin. There is also a clear emergence of a new absorbance at ~ 340 nm also seen in the direct photolysis with Quartz. Photocatalysis with quartz compared with photolysis appears to disrupt the effects of photolysis, since a slower increase in absorbance is seen in these studies. Initial results would indicate that SA- TiO_2 was superior to the P-25 formulation in these studies (Figure 3.55-3.56).

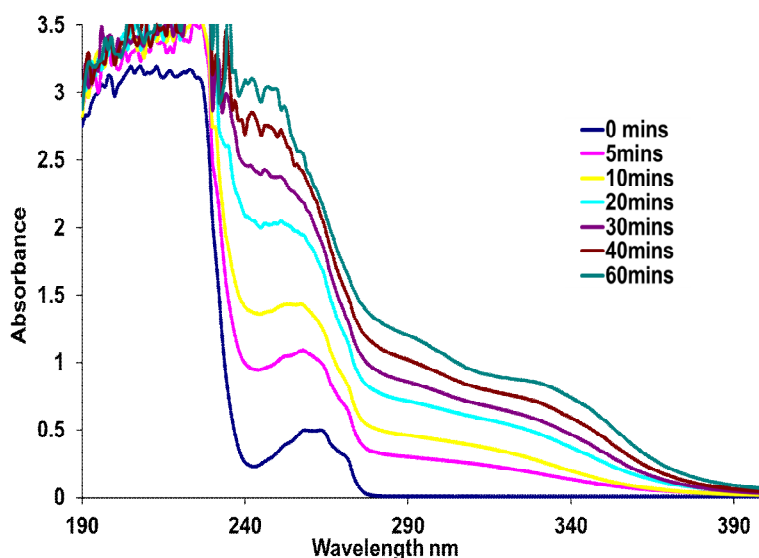


Figure 3.55: UV-vis analysis of the photocatalysis of Solifenacin with quartz glassware and P-25 TiO_2 . [SOL] = 1 mM, Time = 1 h.

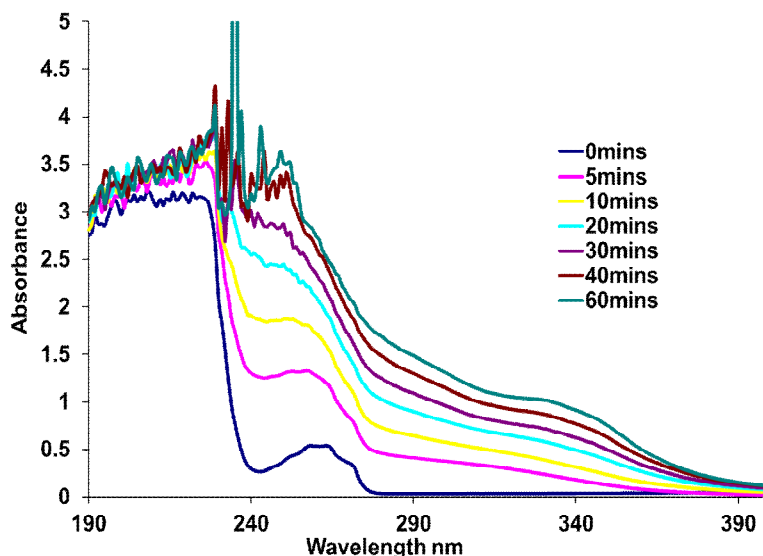


Figure 3.56: UV-vis spectroscopic analysis of the photocatalytic degradation of Solifenacin with SA TiO_2 and quartz glassware. $[\text{SOL}] = 1 \text{ mM}$, $\text{TiO}_2 = 0.05 \text{ g/320 mL}$.

3.2.29 Pyrex Glassware Studies

Photolysis of Solifenacin with Pyrex glassware showed no significant change in the UV-vis monitoring even after 300 mins of irradiation as shown in Figure 3.57. This result is in stark contrast to the previous results with photolysis using quartz glassware. Since Solifenacin does not absorb above 300 nm it can be expected that little or no degradation will be observed as seen here. After 5 h there is a slight rise in the absorbance, however photolysis with Pyrex can be deemed to be insignificant for the degradation of Solifenacin.

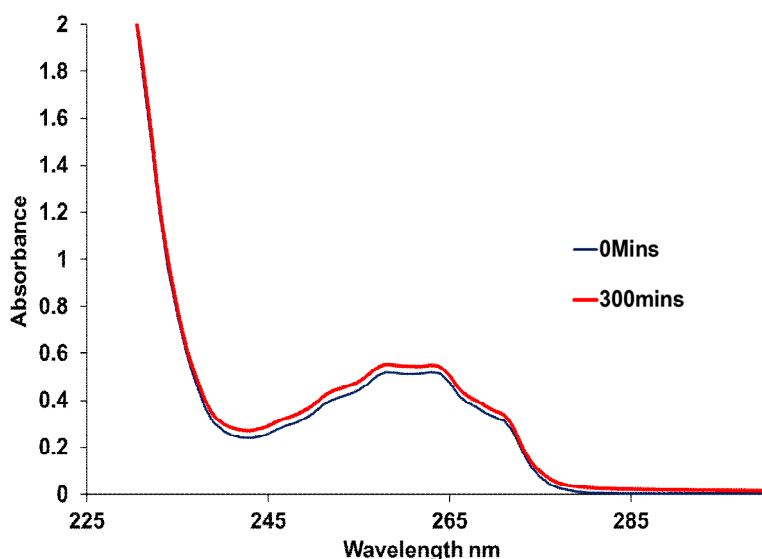


Figure 3.57: UV-vis spectroscopic analysis of the photodegradation (photolysis) of Solifenacin with Pyrex for 5 h. $[\text{SOL}] = 1 \text{ mM}$, Time = 5 h.

3.2.30 HPLC Analysis of Photolysis Studies

HPLC analysis was then undertaken of the photolysis experiments for Solifenacin. It should be noted that these HPLC studies were conducted at the concentration relative to the other pharmaceuticals i.e 0.083mM. Both Quartz and Pyrex photolysis studies were analysed and the results are shown in Figure 3.58. As with the other two APIs, photolysis with quartz can eliminate Solifenacin within 30 mins. Previous quartz photolysis studies conducted and analysed with UV-vis spectroscopy (Figure 3.54) showed intermediate formation giving rise to an increase in absorbance at Solifenacin's λ_{max} , so it is clear that despite the total elimination shown by HPLC analysis, photodegradation products may still be persistent. In earlier studies of the photolysis of Solifenacin with Pyrex glassware, very poor results were observed with a very small rise in absorbance occurring after the total 3 h irradiation period. HPLC analysis indicated that less than 20% elimination occurs in photolysis with Pyrex which would reinforce earlier results obtained with sole UV-vis analysis. Similar to Tamsulosin, Solifenacin Quartz glassware photolysis studies (and those of the Enviolet and LP studies in appendices 3A-11) generated significant quantities of coloured intermediates which appeared to be very photo-stable. The effects of the photocatalytic degradation of Solifenacin will be interesting to examine to see if both it and its coloured intermediate products can be eliminated.

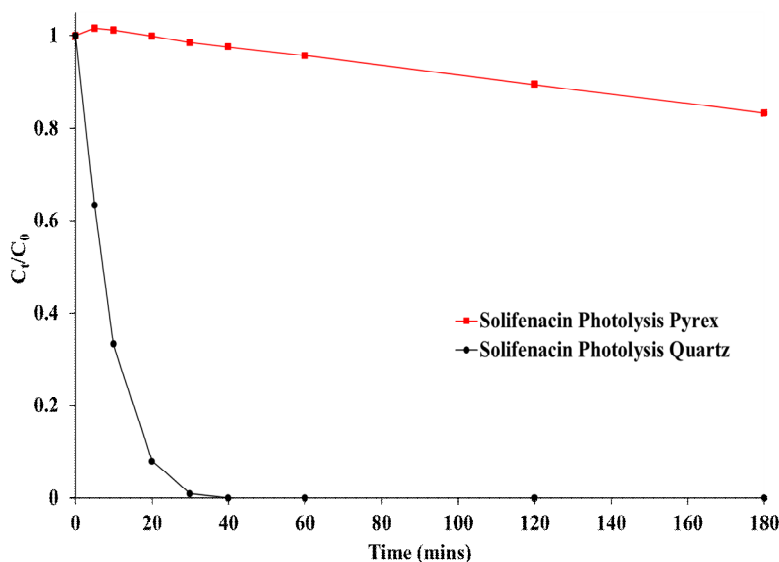


Figure 3.58: HPLC Analysis of photolysis experiments with Quartz and Pyrex glassware for Solifenacin.[SOL] = 0.083mM

3.2.31 Solifenacin Heterogeneous Photocatalysis: Pyrex

The changeover from Quartz to Pyrex glassware showed that photocatalytic degradation of Solifenacin was reduced. A slight increase in absorbance was observed indicating slight degradation by UV-vis monitoring (Figure 3.59-3.60). In the previous studies with Quartz

glassware, there is a large contribution from photolysis due to the lack of a light filter (as with Pyrex). It may be the case that 0.05 g/320 mL may be too little an amount of photocatalyst also to see an effective result.

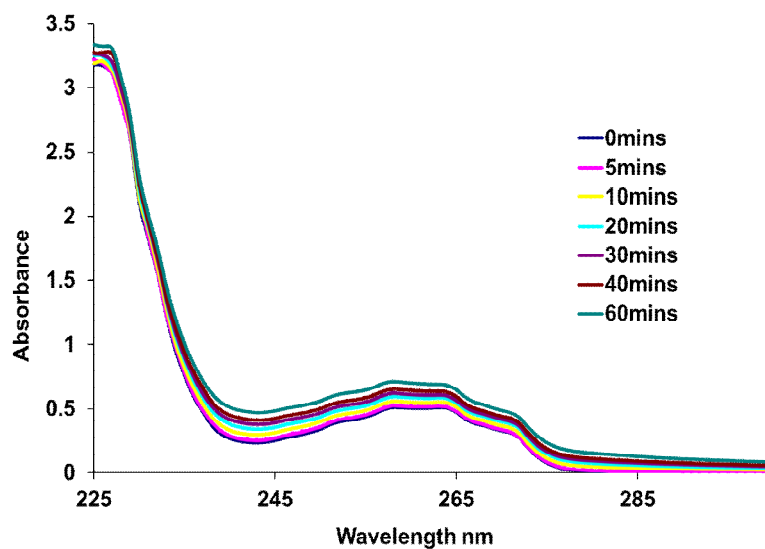


Figure 3.59: UV-vis spectroscopic analysis of the photocatalytic degradation of Solifenacin with P-25 TiO₂ and Pyrex glassware. [SOL] = 1mM, TiO₂ = 0.05 g/320 mL.

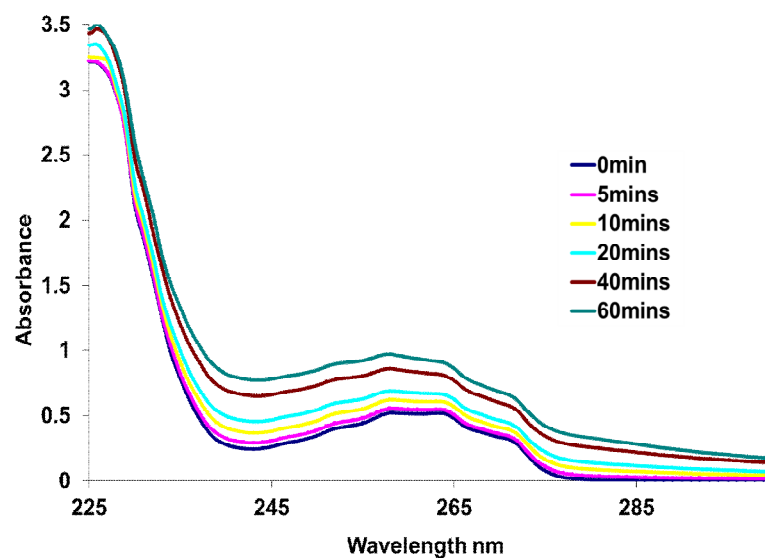


Figure 3.60: UV-vis spectroscopic analysis of the photocatalytic degradation of Solifenacin with SA TiO₂ and Pyrex glassware. [SOL] = 1 mM, SA-TiO₂ = 0.05 g/320 mL

3.2.32 Solifenacin Heterogeneous Photocatalysis: TiO₂ Optimisation

API	C ₀ mM	TiO ₂ Phase	TiO ₂ g/320 mL	Irradiation Time h	100% reached at (HPLC)
Solifenacin	0.083	P-25	0.05	1	N/A
		P-25	0.1	3	180mins (81%)
		P-25	0.2	3	180mins (82%)
		P-25	0.4	3	180mins (86%)

Table 3.5: List of conditions used in Solifenacin TiO₂ optimisation experiments.

In studies thus far with Solifenacin, higher concentrations of the drug have been used compared to the other APIs. This was in order to see the effects by UV-vis spectroscopy due to Solifenacin's weak absorption profile. Thus similar concentrations of TiO₂ (as with the other pharmaceuticals) are not having similar decomposition effects as can be seen from Figure 3.61-3.62 below. These studies will provide a further insight into later concentration studies where concentration of the analyte is varied against the optimum photocatalyst concentration. The addition of more SA-TiO₂, as shown in these studies, despite the much higher concentration of Solifenacin gives rise to an improved degradation profile to that observed previously and there is some conversion to intermediate products. P-25 TiO₂ gave poorer results compared to SA-TiO₂ with little or no affect even after 5 h.

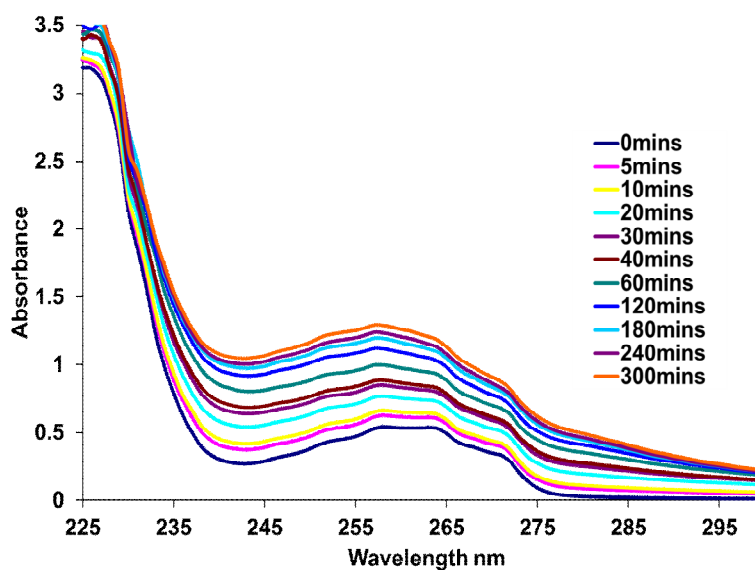


Figure 3.61: UV-vis Analysis of the photocatalysis of Solifencin with 0.1 g SA-TiO₂. [SOL] = 1 mM, SA-TiO₂ = 0.1 g/320 mL, Time = 5 h.

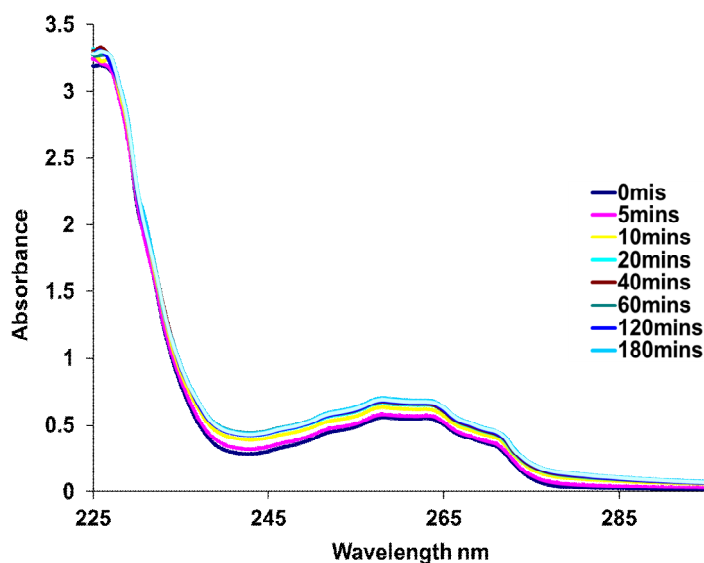


Figure 3.62: UV-vis Analysis of the photocatalysis of Solifenacin with 0.1 g P-25-TiO₂. [SOL] = 1 mM, P-25 TiO₂ = 0.1 g/320 mL, Time = 5 h.

HPLC methods were developed after these initial TiO₂ optimisation studies and our studies proceeded with only the P-25 TiO₂ due to this titania being the literature standard. These studies are presented in Figure 3.63. From these studies, it was clear that Solifenacin is not completely eliminated by TiO₂ photocatalysis with approximately 80% eliminated after the 3 h irradiation period. Additional amounts of TiO₂ (0.2 and 0.4 g/320 mL) did not improve the degradation of Solifenacin. These studies showed the optimum concentration of TiO₂ to be 0.1 g/320 mL and also concluded that the addition of an oxidant may be required for complete removal of Solifenacin.

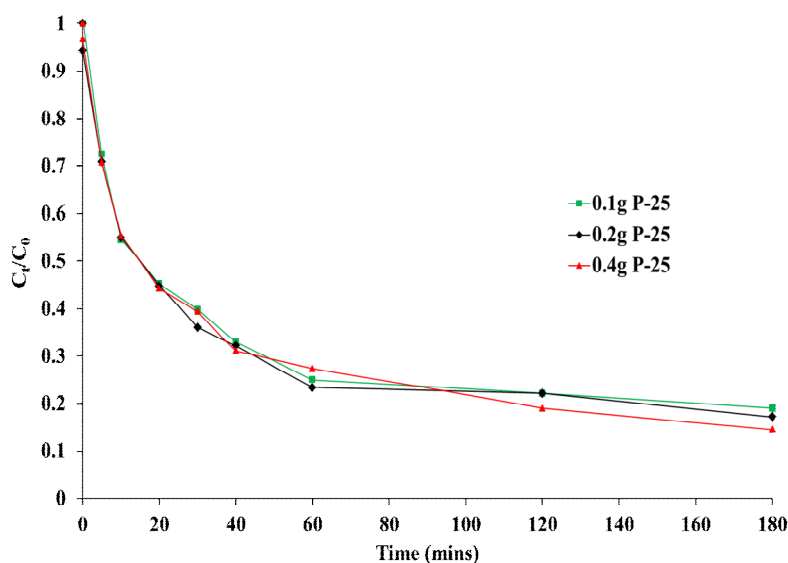


Figure 3.63: HPLC analysis of the photocatalytic degradation of Solifenacin with varying TiO₂ concentrations. [SOL] = 0.083 mM, P-25 TiO₂ = 0.1 g, 0.2 g or 0.4 g/320 mL, Time = 3 h.

3.2.33 Solifenacin pH Adjustment Studies

API	C ₀ mM	TiO ₂ Phase	TiO ₂ g/320 mL	pH	Irradiation Time h	100% reached at (HPLC)
Solifenacin	0.083	P-25	0.1	3	3	180mins (84%)
		P-25	0.1	No pH adjust	3	180mins (81%)
		P-25	0.1	8	3	180mins (79%)

Table 3.6: List of conditions used in Solifenacin pH optimisation experiments.

Unlike Famotidine, and like Tamsulosin, Solifenacin is unaffected by pH as shown in earlier pH studies with UV-vis analysis. Photocatalytic degradation studies, where pH was adjusted, were somewhat inconclusive with Solifenacin. These studies are shown in Figure 3.64. pH 5 was not conducted as the Solifenacin non pH adjusted experiment was already at a pH of 5. There was no major enhancement to the photodegradation process by a change in pH. Since no buffers were employed, the pH decreased (to pH 5) as with the previous pharmaceuticals for the pH 8 experiment. For pH 3, the pH tended to vary between pH 3-3.5. pH 8 showed a high adsorption initially, however a poor photodegradation followed this, with only 75% elimination achieved after 3 h. pH 3 achieved an elimination of 84% which surpassed the non pH adjusted experiment albeit only slightly. The plateau that can be seen in these experiments has been reported with other drugs, and can be associated with the formation of coloured intermediate products.¹⁸³ These products can compete for degradation and for light absorption so inhibition of the degradation of the parent compound can occur and seems to be what was observed here with Solifenacin.

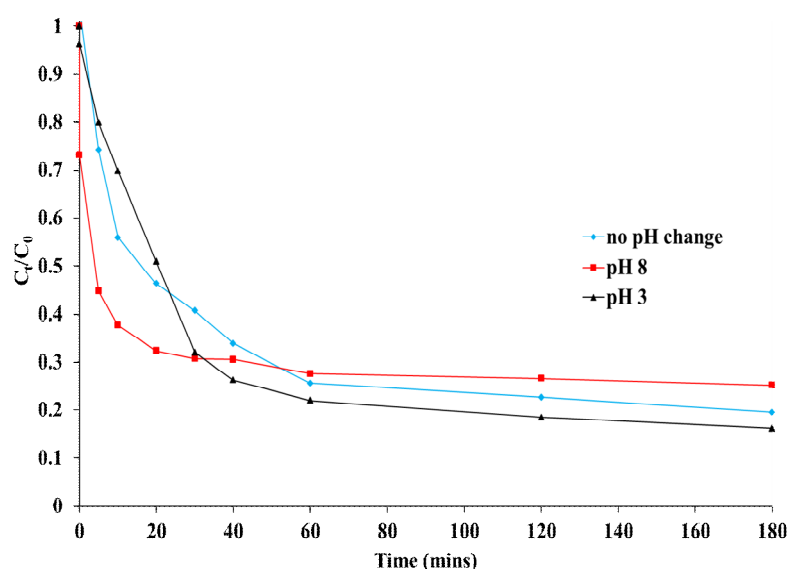


Figure 3.64: HPLC analysis of the photocatalytic degradation of Solifenacin with varying pH. [SOL] = 0.083 mM, pH = 3, 8, and no pH adjustment, TiO₂ = 0.1 g/320 mL.

3.2.34 Solifenacin Hydrogen Peroxide Addition: P-25 TiO₂

Evaluation of the effect of sodium bisulfite with Solifenacin was undertaken. UV-vis analysis could not be conducted due to Solifenacin's poor absorption in the UV-vis as earlier studies have shown. ¹H NMR and HPLC analysis were chosen to investigate whether bisulfite was contributing to Solifenacin degradation.

¹H NMR

Spectra of Solifenacin compared to Solifenacin plus bisulfite show no significant shifts 48 h later (Figure 3.65). The addition of further bisulfite appeared to have effects on the shape of some signals, although still no shifts, as were seen in the case of Famotidine. The higher concentration of bisulfite was a higher amount than that used to quench reactions in peroxide experiments. It was concluded that HPLC analysis may provide further information in relation to the elimination of Solifenacin by bisulfite.

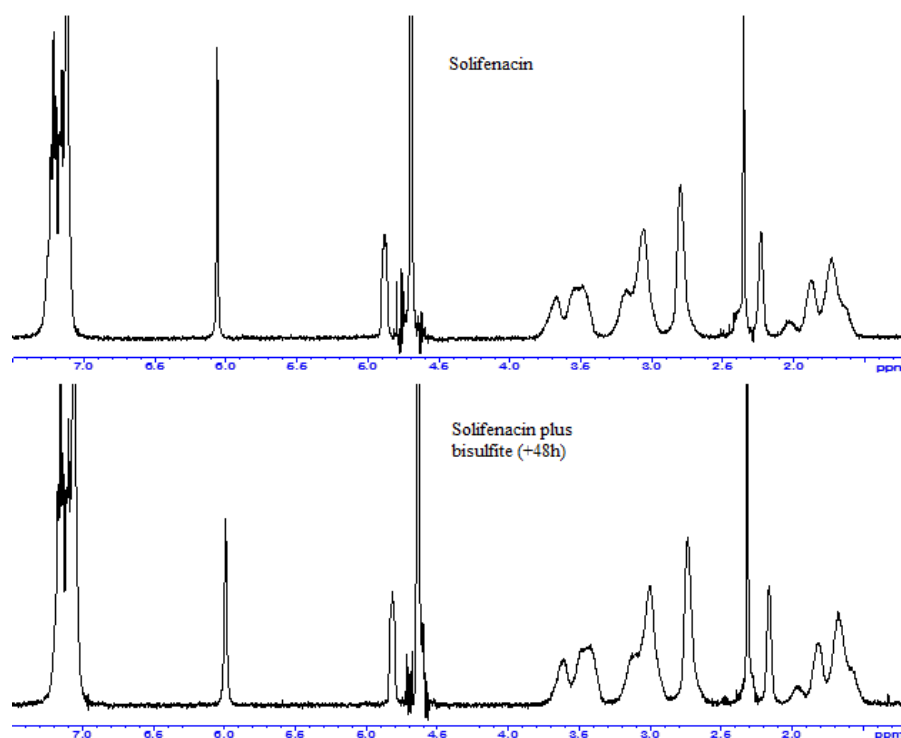


Figure 3.65: ¹H NMR spectra for Solifenacin in D₂O (Top), Solifenacin + bisulfite (2 days) (Middle) and with additional bisulfite added (Bottom).

HPLC Analysis

HPLC analysis was conducted with Solifenacin and Solifenacin plus bisulfite, in a manner that was identical to the quenching studies with peroxide (Figure 3.66). 4 mL of Solifenacin was added to a sample tube with 2 drops of sodium bisulfite solution. Multiple injections of

Solifenacin (control) and Solifenacin plus bisulfite were performed. There was no indication of any significant degradation effect after 24 h.

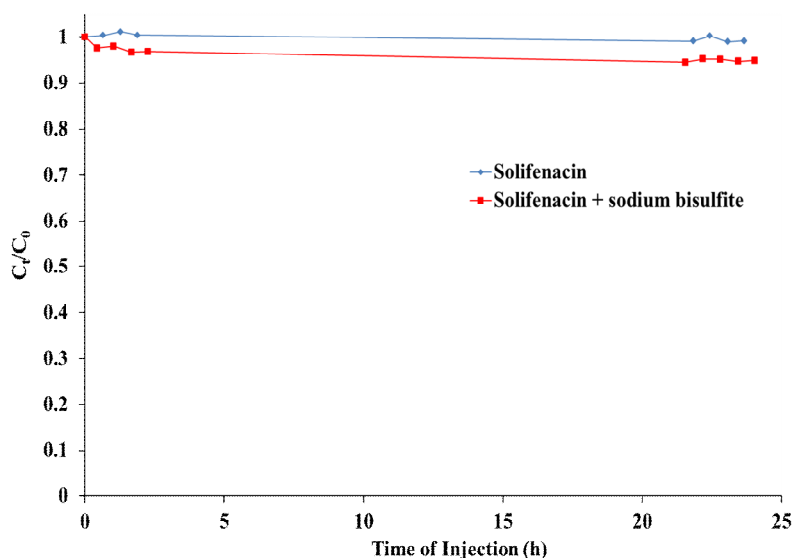


Figure 3.66: HPLC analysis with repeat injections of samples of Solifenacin and Solifenacin plus bisulfite.

Figure 3.67 outlines the studies conducted with varying concentrations of peroxide on the photocatalytic degradation of Solifenacin. In these studies a range of 0.1 mM-5 mM of peroxide was studied. Control experiments indicated the limited effect of UV alone and TiO_2 alone in the elimination of Solifenacin. A control experiment with 1 mM H_2O_2 /UV and Solifenacin showed a good elimination of Solifenacin but could not eliminate Solifenacin completely within the duration of the experiment. Additional controls included the effect of $\text{TiO}_2/\text{H}_2\text{O}_2$ in the dark and H_2O_2 in the dark with Solifenacin shown in Figure 3.68.

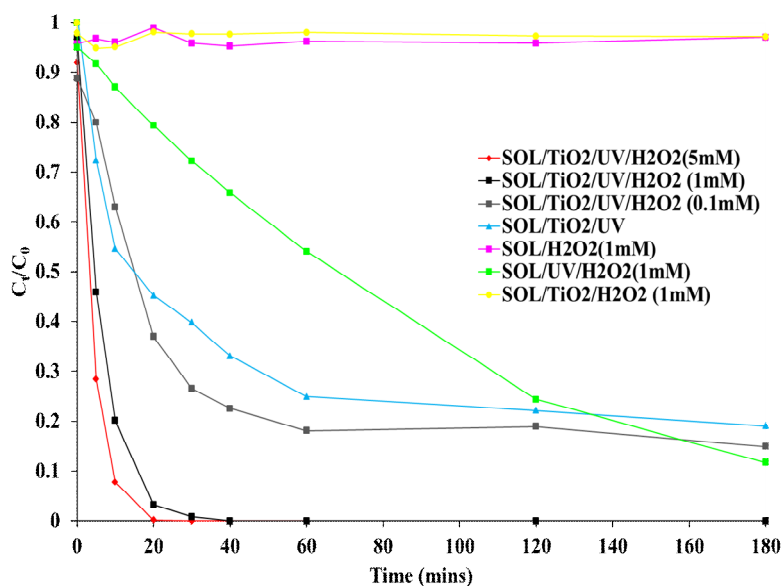


Figure 3.67: Degradation chart for Solifenacin showing varying additions of H_2O_2 . TiO_2 (opt)/320 mL, $[\text{H}_2\text{O}_2] = 0.1 \text{ mM}-50 \text{ mM}$, $[\text{SOL}] = 0.083 \text{ mM}$.

The most effective concentration of peroxide in the $\text{TiO}_2/\text{UV}/\text{H}_2\text{O}_2$ process was 5 mM, however 1 mM was also extremely effective even though it was 5 times less concentrated. This concentration was selected as the optimum. Few intermediates were observed in chromatograms with $\text{TiO}_2/\text{UV}/\text{H}_2\text{O}_2$ experiments, and those that were present were in extremely low concentrations (Figure 3.69 (260 nm) - 3.70 (260 nm)).

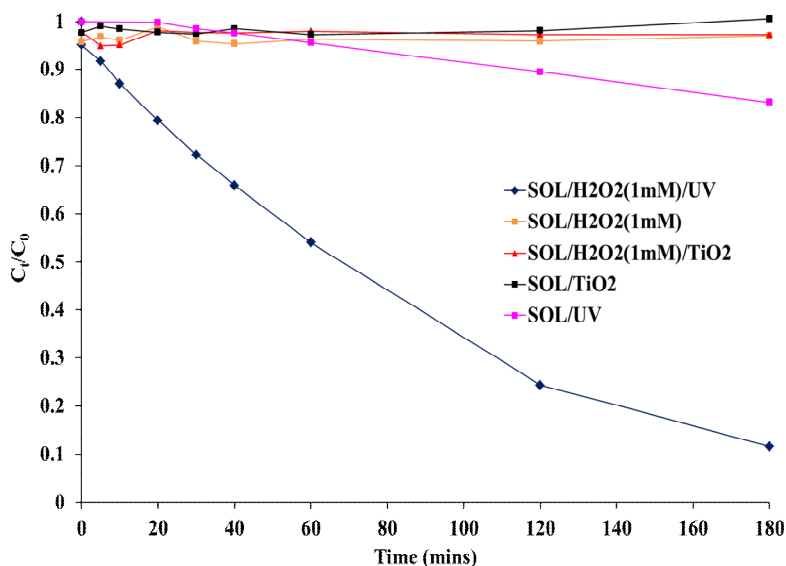


Figure 3.68: Control Experiments performed with Solifenacin. P-25 $\text{TiO}_2 = 0.1 \text{ g}/320 \text{ mL}$, $1 \text{ mM } \text{H}_2\text{O}_2$, $[\text{SOL}] = 0.083 \text{ mM}$.

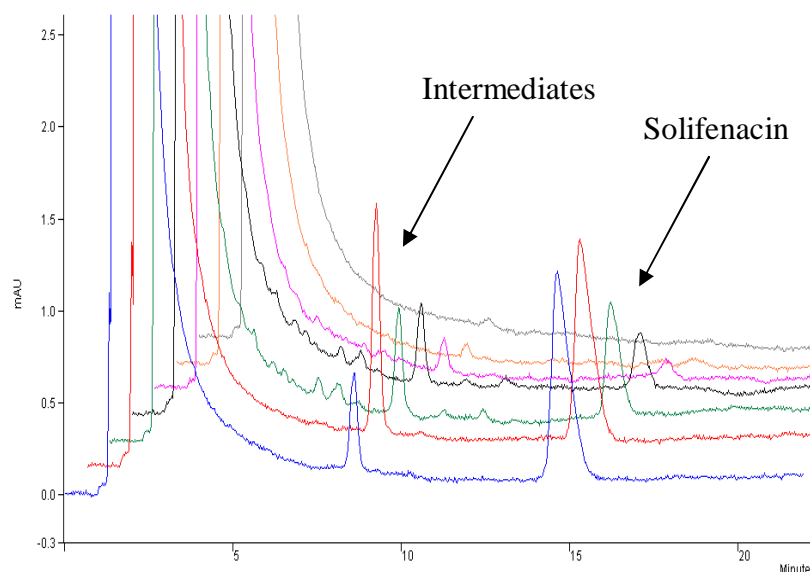


Figure 3.69: HPLC Chromatogram of Solifenacin (14.5 mins) with 0 mins, 0 mins P_{ads} , 5 mins – 40 mins. TiO_2 0.1 g/320 mL [SOL] = 0.083 mM, H_2O_2 = 1 mM, Wavelength = 260 nm.

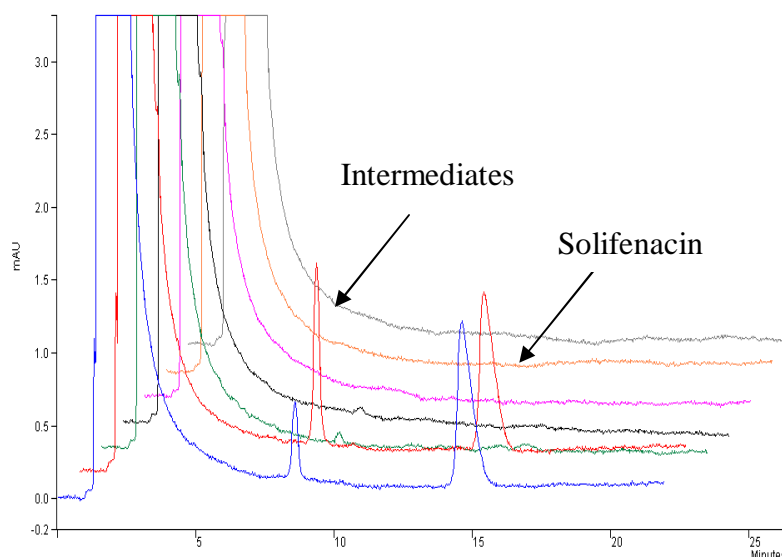


Figure 3.70: HPLC Chromatogram of Solifenacin (14.5 mins) with 0 mins, 0 mins P_{ads} , 30 mins – 180 mins. TiO_2 0.1 g/320 mL [SOL] = 0.083 mM, H_2O_2 = 1 mM, Wavelength = 260 nm.

3.2.35 Adsorption Studies: Glassware

Further control experiments were conducted to investigate whether adsorption of Solifenacin to the reactor glassware was potentially an influence in photodegradation studies. Control experiments indicated that over the typical irradiation period studied of 3 h, 0.3% of Solifenacin adsorbed to the reactor glassware (reactor, immersion well and stirring bar). Therefore adsorption of Solifenacin to the reactor glassware and apparatus was ruled out as a factor which may skew any of the results in these studies.

3.2.36 Solifenacin Concentration Variation Studies

The results for Solifenacin concentration studies are shown in Figure 3.71. These studies show that the TiO₂/UV process is effective only for low concentrations of this drug 20 µM (9.6 mg/L).

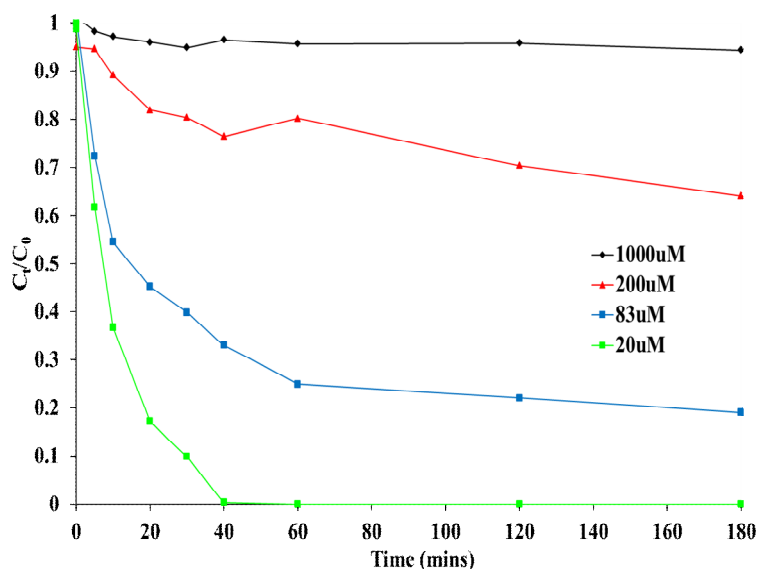


Figure 3.71: Concentration Variation Experiments for Solifenacin. P-25 TiO₂ = 0.1 g/320 mL, [SOL] = 20 µM, 83 µM, 200 µM, 1000 µM. Dilutions of 1 in 2 for 200 µM and 1 in 10 for 1000 µM were undertaken for analysis.

The process starts to reach a limit and becomes barely effective with only 84% - 35% elimination of Solifenacin after 180 mins for 83 µM (40 mg/L) – 200 µM (96 mg/L) respectively. Both Famotidine and Tamsulosin showed at least 90% elimination for concentrations of 200 µM after 180 mins irradiation. At even a higher concentration of 1000 µM (480 mg/L) there is little or no elimination, which is in line with earlier photocatalysis studies which were monitored by UV-vis spectroscopy.

3.2.37 Solifenacin Heterogeneous Photocatalytic Degradation Conclusions

It was initially thought that Solifenacin would be the most challenging of the pharmaceuticals to eliminate. UV-vis studies indicated that an increase as opposed to a decrease in its absorbance was occurring in photodegradation studies which may indicate formation of stable photodegradation products. Photocatalytic studies initially showed poor photodegradation when monitored by UV-vis analysis. These studies were undertaken at high concentrations of Solifenacin. However, at lower concentrations and with HPLC analysis, Solifenacin was shown to be effectively degraded, albeit not completely, achieving approximately 80% removal after

the 3h irradiation period. The optimum TiO_2 concentration was found to be similar to that of Famotidine at 0.1 g/320 mL.

pH photocatalytic studies showed good adsorption at pH 8 for Solifenacin, and both pH 3 and pH 8 achieved fast rates for the first 20 mins of irradiation, however a general plateau was reached after 40 mins. It was concluded from these studies that the production of intermediates was inhibiting complete degradation as seen by other groups with other pharmaceuticals.¹⁸³ Peroxide studies were shown to effectively eliminate Solifenacin within 30-40 mins, and very few intermediates were detected in these studies. LC-MS/MS analysis will be more conclusive in the identification of intermediates and the effectiveness of elimination of these by the combined $\text{TiO}_2/\text{UV}/\text{H}_2\text{O}_2$ process. Concentration variation studies showed that the TiO_2/UV process is limited to eliminating only low concentrations of the drug effectively and concentrations above this gave much poorer degradation profiles.

Chapter 4 - Intermediate Analysis and Elucidation of Degradation Mechanisms for Famotidine, Tamsulosin and Solifenacin

4.1 Introduction

Following our optimised photocatalytic studies for each of the pharmaceuticals, we were interested in identifying the intermediates generated from this process. Pharmaceuticals treated by advanced oxidation processes (AOP) can undergo various types of reactions to generate these intermediates which can include oxidations, reductions, cyclisations, oxidative cleavages, reductive cleavages, desmethylations etc.¹⁸⁹ Consequently, in the oxidation/reduction reactions which these pharmaceuticals can undergo in photocatalysis, toxic intermediates can be formed. In certain circumstances, these can be more toxic than the original pharmaceutical.^{184, 185} Oftentimes, it is also reported by authors that some intermediate products are identical to some of the *in vivo* metabolites excreted by patients and animals administered with these pharmaceuticals.^{57,155}

Liquid chromatography coupled to mass spectrometry (LC-MS) is a powerful tool which has been used by many authors to characterise intermediate products from photocatalytic studies.^{186, 187} LC-MS/MS is often required for full characterisation and high resolution instruments with accurate mass measurement can allow the generation of molecular formulae for both the parent mass and fragment ions.^{189,188}

This chapters aims are to (i) identify these intermediates, (ii) determine the effectiveness of photocatalysis in eliminating these intermediates and (iii) propose a degradation pathway for each of the pharmaceuticals. LC-MS/MS, being the instrument of choice in the elucidation of intermediate structures in the literature, has been employed and we have corroborated this data with DI-MS studies to further confirm the presence of intermediates generated and their structures. In addition to this we have performed a thorough literature search on reported phase 1 metabolites from these pharmaceuticals as these metabolites would predictably be similar to those generated from photocatalysis. We have also further predicted what we believe would be typical vulnerable sites for photocatalytic oxidation and used these predictions in the analysis and interpretation of all data.

4.2 Results and Discussion

4.2.1 LC-MS/MS Method Transfer and Re-optimisation

The HPLC methods previously used to monitor and determine the APIs in previous photodegradation studies were transferred to a Bruker LC-MS/MS system. These methods were also further re-optimised to try to further resolve any intermediates for their identification. Longer run times were employed in these studies (up to 1h) and further changes in mobile phase composition assisted this. For Famotidine, the methanol phase was reduced to 1%, and for

Tamsulosin and Solifenacin an additional mobile phase was prepared consisting of 10% methanol and 10% acetonitrile respectively. Varying percentages of each phase were attempted in optimisation, and the optimum compositions including a method summary are displayed in Table 4.1.

API	Famotidine	Tamsulosin	Solifenacin
Column	PFP 150 mm x 2.1 mm 5 μ m	PFP 150 mm x 2.1 mm 5 μ m	PFP 150 mm x 2.1 mm 5 μ m
Mobile Phase A	1:99 MeOH:H ₂ O 0.1% F.A	40:60 MeOH:H ₂ O 0.1% F.A	30:70 ACN:H ₂ O 0.1% F.A
Mobile Phase B	N/A	10:90 MeOH:H ₂ O 0.1% F.A	10:90 ACN:H ₂ O 0.1% F.A
Injection Volume μL	10	10	10
Pump Composition (A:B)	N/A	(75:25)	(65:35)
Wavelengths scanned (nm)	265, 205, 254, 280, 300	223, 280, 300, 205, 254	215, 220, 205, 254, 280
Flow Rate (mL/min)	0.15	0.2	0.2
Run Time (mins)	63	70	70
Retention Time t_R (mins)	47	37	58

Table 4.1: Method summary of each API for LC-MS/MS method transfer

MS ion signals were also optimised using the Bruker system software automated optimisation function. Optimised parameters include capillary voltage, endplate, skim 1, skim 2 cap exit offset, octopole, octopole RF, octopole delta, lens 1, lens 2 and the trap drive. These conditions are listed in the experimental section of this chapter. Nebuliser, dry gas and temperature were unchanged. A series of standards from 0.1 μ M to 100 μ M were run with each method and standard curves were generated. In general, good linearity was obtained without the incorporation of the 100 μ M standard, with R^2 values of 0.997 for Famotidine and Tamsulosin and 0.996 for Solifenacin. Considering the development and validation of a combined method by A. Deegan *et al.* for these three pharmaceuticals, and our use of the LC-MS/MS only for *qualitative* analysis of the intermediates, no further work in validation of these methods were carried out.

Figures 4.1 - 4.3 show the EICs (extracted ion current) of standards run on each method and also the mass spectra attained from the analytes. The mass spectrum showing the molecular ion is displayed and in addition the MS/MS of the parent ion is shown. For Famotidine the molecular ion is $m/z = 338$, with daughter ions $m/z = 259$ and $m/z = 189$. For Tamsulosin, the molecular ion is $m/z = 409$ with daughter ions, $m/z = 271$, 228, 200, and 148. For Solifenacin, the molecular ion is $m/z = 363$, with daughter ions $m/z = 236$, 193, 153, and 110.

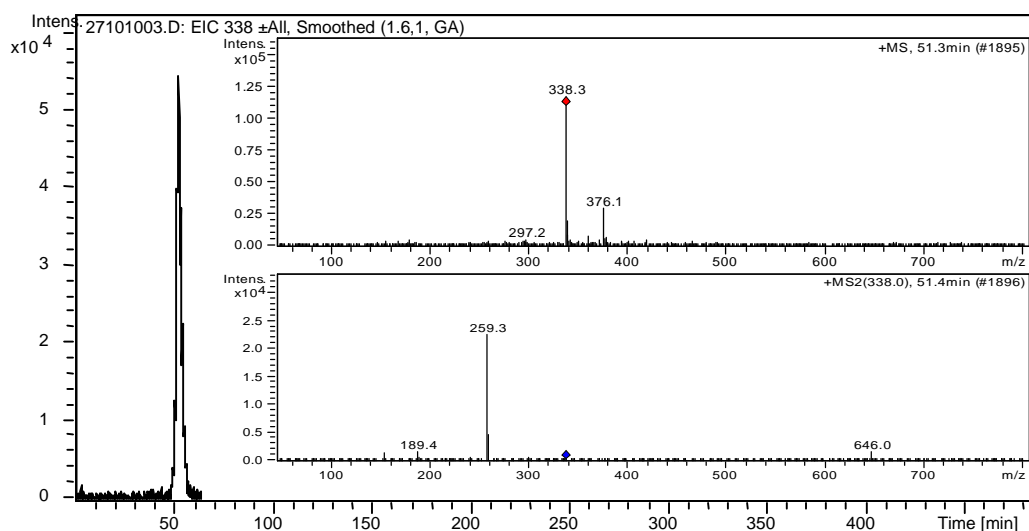


Figure 4.1: EIC Chromatogram of Famotidine 50 μ M standard inset MS (top) and MS/MS spectra (below).

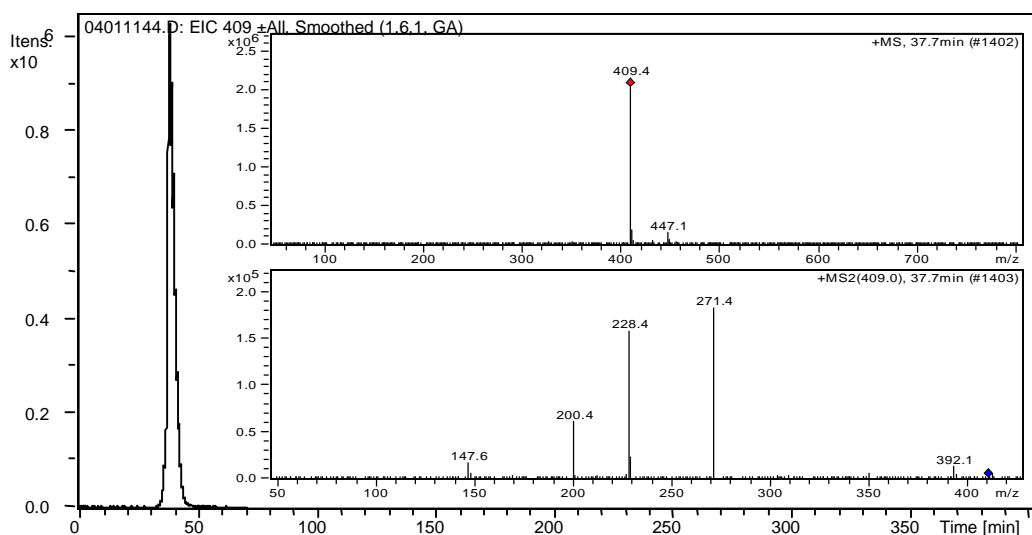


Figure 4.2: EIC chromatogram of Tamsulosin 50 μ M Standard, and inset MS (top) and MS/MS spectra (below).

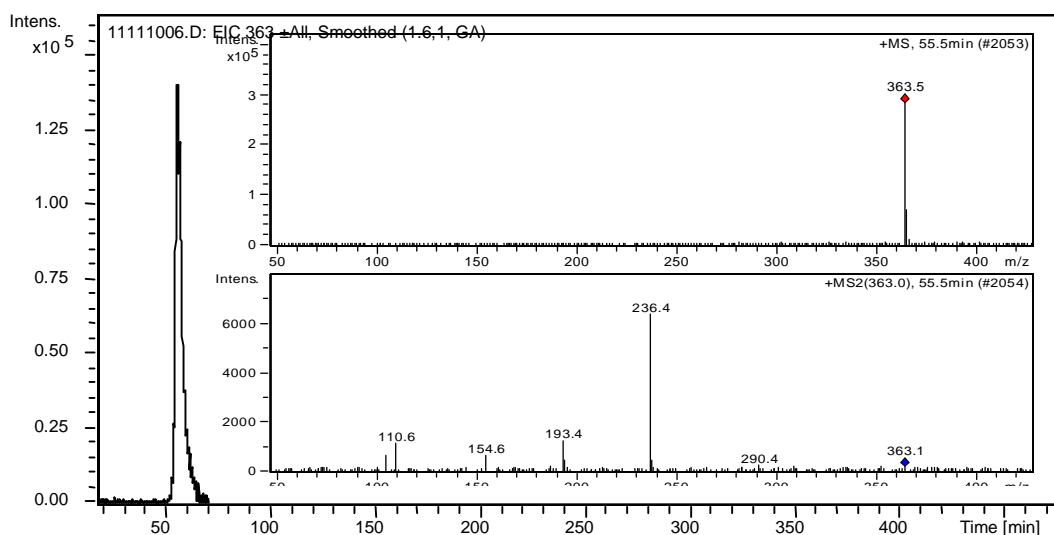


Figure 4.3: EIC chromatograms of Solifenacin 10 μ M standard and inset MS (top) and MS/MS spectra (below).

4.2.2 Molecular Oxidation Analysis

A molecular oxidation analysis of each of the pharmaceuticals was undertaken to identify vulnerable points in each molecule whereby oxidation/hydroxyl radical attack might occur. Figure 4.4 shows these points highlighted in red. Since the mechanism of photocatalytic degradation typically follows a H-abstraction followed by a hydroxyl radical addition, any vulnerable hydrogen atoms will be removed and essentially substituted with a hydroxyl group. Good examples of removable protons are the two benzylic carbons in Solifenacin which form particularly stable radicals. In Tamsulosin, the ethoxy group (on the second aromatic ring), can be predicted to be substituted by a hydroxyl radical in this case. Additional oxidations can be predicted on this secondary ring due to the stable radicals that would result from H-abstraction. This stability would arise from activation of certain positions due to the electron donating groups on this ring. For Famotidine, one of the most predictable sites for oxidation is the thioether moiety, which can be readily oxidised to the sulfoxide, and further to the sulfone. In addition, carbons alpha to a heteroatom may also be easily oxidised, which can also be seen in work by Radjenovic *et al.* for Ranitidine, a related H_2 -receptor antagonist (Figure 4.5).¹⁸⁹ In addition, metabolites are shown for Ebrotidine, a fellow H_2 -receptor antagonist which is similar in structure to Famotidine.^{190 191}

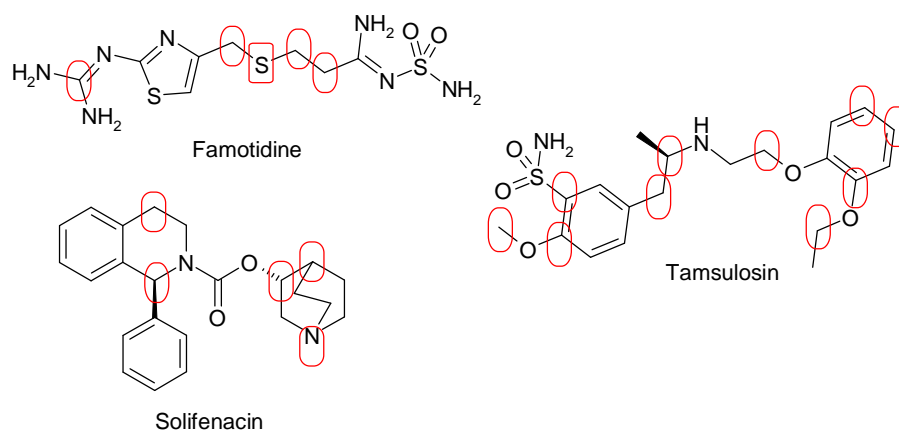


Figure 4.4: The three pharmaceuticals showing vulnerable positions for oxidation/hydroxyl radical attack.

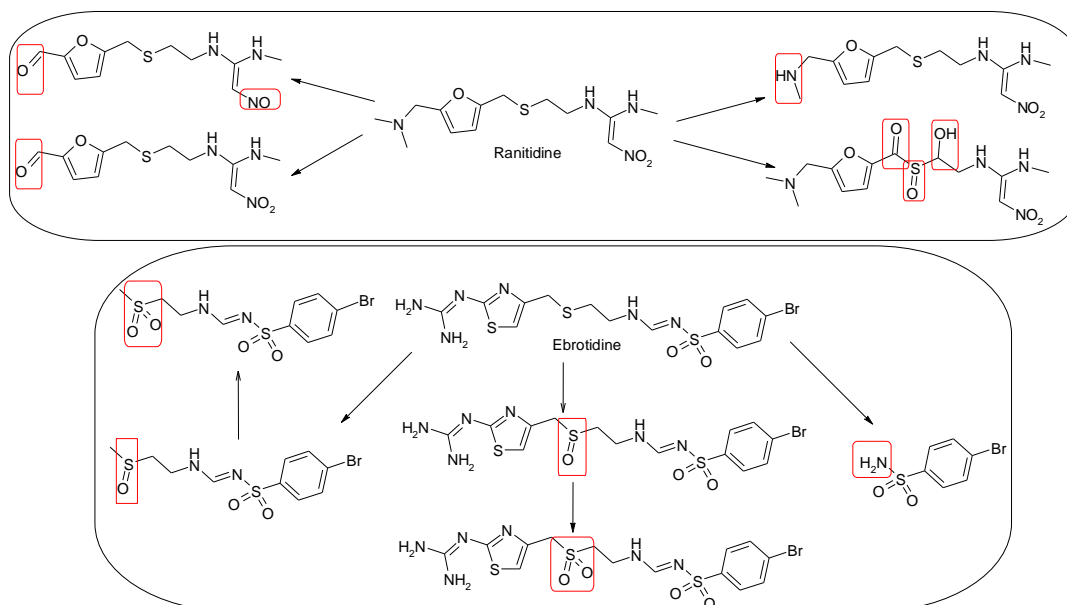


Figure 4.5: Ranitidine intermediates reported by Radjenovic *et al.* 2010 and Ebrotidine metabolites found by Sentellas *et al.* and Rozman *et al.* showing similar sites of oxidation as those predicted for Famotidine.^{189,190,191}

4.2.3 Direct Infusion Mass Spectrometry Studies: Famotidine

Initial direct infusion studies of photo-degradation experiments used quite low concentrations of drug (0.083 mM). Increasing this concentration substantially and doing subsequent mass spectrometric analysis should result in more pronounced signals for the main intermediates. These studies were performed once the photocatalytic degradation process had been completely optimised for all 3 pharmaceuticals. Figure 4.6 displays a HPLC-PDA (265 nm) chromatogram of a photocatalytic degradation experiment for Famotidine in concentration variation studies. The appearance of numerous intermediates can be seen clearly in the chromatogram as well as the disappearance of Famotidine.

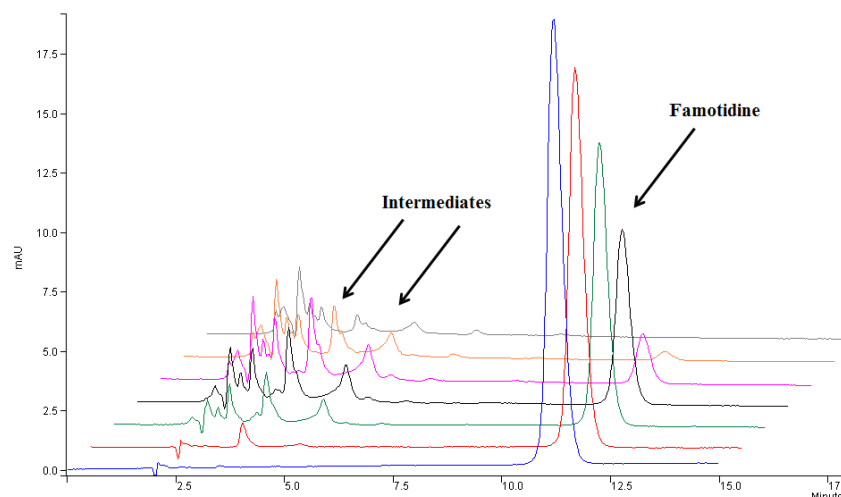


Figure 4.6: Famotidine photocatalytic degradation experiment showing intermediate formation and disappearance over time. 0 Mins, 0 Mins P_{ads} , 5 mins, 10 mins, 20 mins, 30 mins, 40 mins. [FAM] = 83 μ M, TiO_2 = 0.1 g/320 mL P-25 TiO_2 .

Mass spectrometric analysis of a photocatalytic degradation experiment of Famotidine was undertaken and the appearance of various new masses could be seen after only 10mins of irradiation. Nylon membranes were used to filter all samples from photocatalytic degradation experiments prior to analysis. A variety of masses were observed in DI-MS spectra which were seen to be caused by these filters. These signals were noticeably absent from photolysis experiments where these filters were not used. Tran *et al.* reported interferences in LC-MS analysis caused by these filters.¹⁹² In addition, once these filters were replaced with more stable filters in later DI-MS studies, these masses were not observed. The signals m/z = 227, 453 and 679 in Figure 4.9 and 4.10 can be seen to be a contribution by these Nylon filters in each spectrum and thus should be ignored.

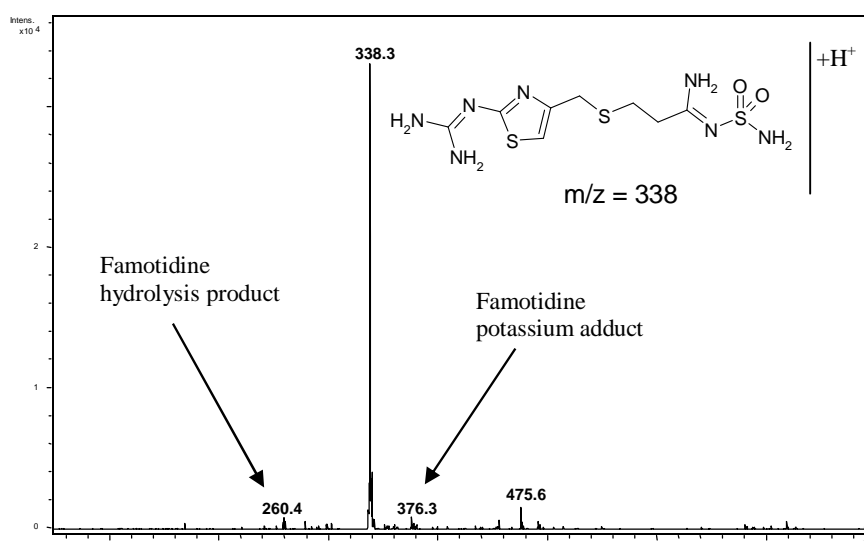


Figure 4.7: DI-Mass spectrum of a 0 mins P_{ads} sample of a photocatalytic degradation experiment for Famotidine. Photocatalysis, [FAM] = 0.083 mM, 0.1 g/320 mL SA TiO_2 ,

Figure 4.7 shows the Famotidine mass spectrum at 0mins (post adsorption) and aside from the base peak (also the molecular ion in this case) there are some low abundance masses which can be seen. m/z 260 is a Famotidine hydrolysis product, the structure of which is identified amongst other intermediates in Figure 4.11. The molecular ion of Famotidine is at m/z =338, although its molecular weight is 337, so the ion of highest abundance is a protonated form of the drug [FAM+H⁺].

Figure 4.8 shows the fragments of Famotidine's molecular ion under MS/MS and the structures of these daughter ions, the formation of which entails two alpha cleavages for m/z = 242 and 259 and a basic aliphatic fragmentation of m/z = 189 at the thioether moiety. m/z 259 is the most abundant ion due to the resonance stabilisation at the alpha carbon to both amines. The positive charge at this site is stabilised by an inductive effect spread over both the C-N bonds. Additional minor fragments can also be found, although the structure and formation of these fragments was too complex to decipher, and so these fragments are reported here only for potential aid in the identification of intermediates later.

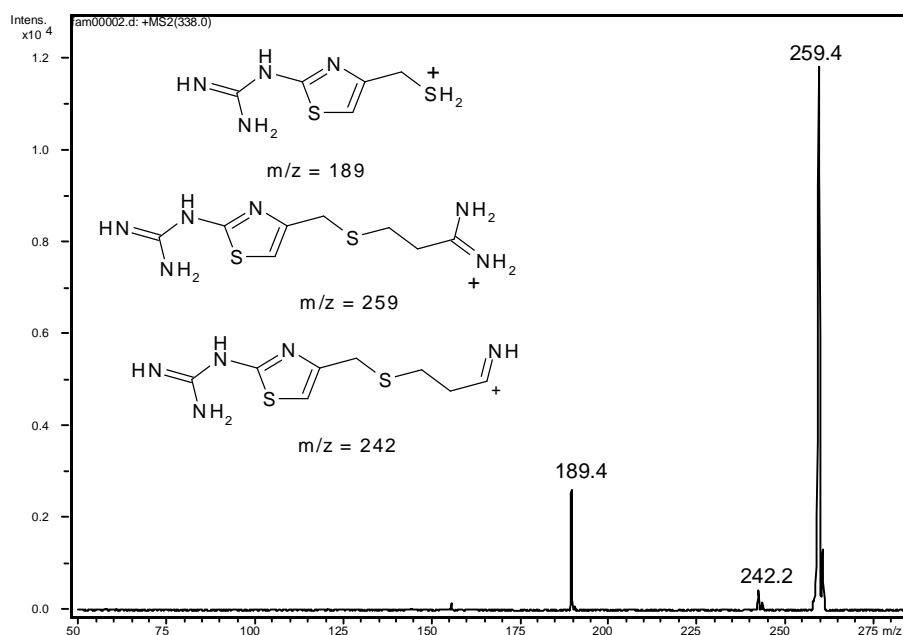


Figure 4.8: DI-MS/MS spectrum in a 0Mins P_{ads} sample showing fragments from the Famotidine parent molecule: m/z = 259, m/z = 242, m/z = 189 (inset) structures.¹⁹³ Photocatalysis 0.1 g/320 mL TiO₂ SA TiO₂, [FAM] = 0.083 mM

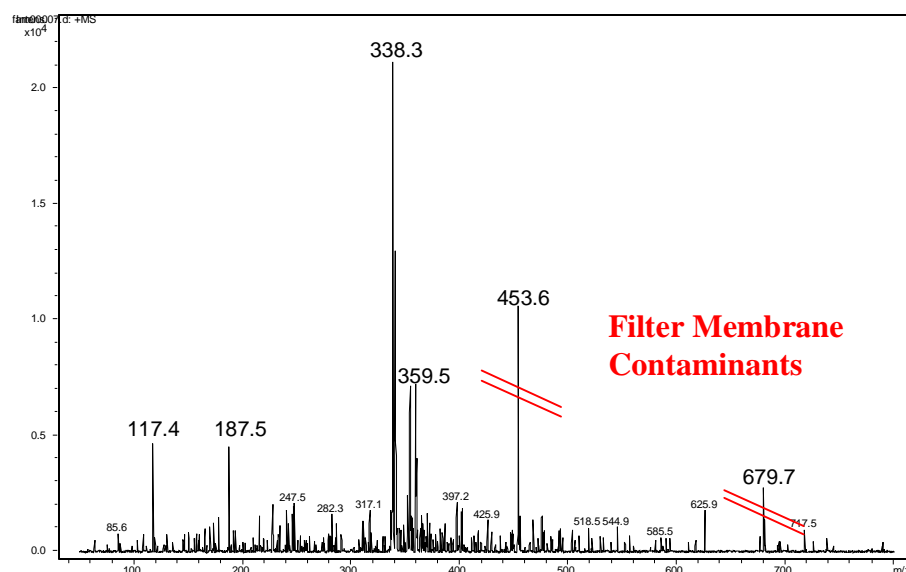


Figure 4.9: DI-mass spectrum of a 30 mins sample in a photocatalytic degradation experiment for Famotidine. Photocatalysis 0.1 g/320 mL SA TiO₂, [FAM] = 0.083 mM.

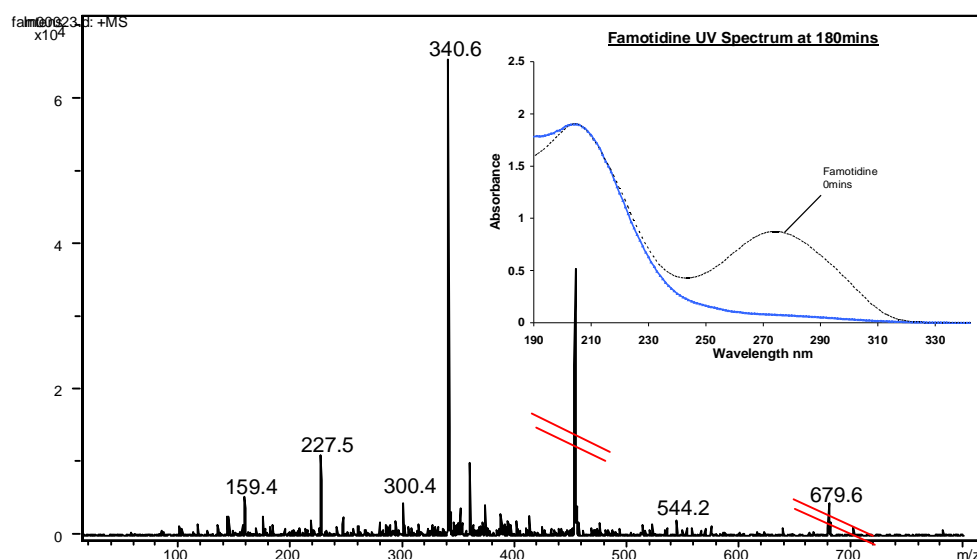


Figure 4.10: DI-Mass spectrum of a 180 mins sample in a photocatalytic degradation experiment of Famotidine (inset) UV-vis spectra showing absorbance at 0mins and 180mins. Photocatalysis 0.1 g/320 mL SA TiO₂, [FAM] = 0.083 mM

Figure 4.9 and 4.10 show the mass spectrum of photocatalysis of Famotidine after 30 mins and 180 mins using the optimum amount of TiO₂ (0.1 g). Figure 4.10 also shows the UV-vis spectra after 180 mins of irradiation. The UV-vis spectrum indicates that little or no Famotidine remains after 3 h. A significant absorbance remains at ~220 nm which can be due to low molecular weight degradation products. The thiazole ring and guanidine functionalities respectively can absorb at these wavelengths. From the UV-vis spectra alone, it can be deduced therefore that Famotidine is not effectively mineralized by photocatalysis with TiO₂ alone. A table of masses found and their respective intensities is shown in appendix 4A-1 (Masses highlighted in colour

showed up consistently and with high intensities relative to the base peak.). Initially the base peak in the spectra is $m/z = 338$ (Figure 4.7, Figure 4.9), however after 60mins, this changes to $m/z = 340$ (Figure 4.10).

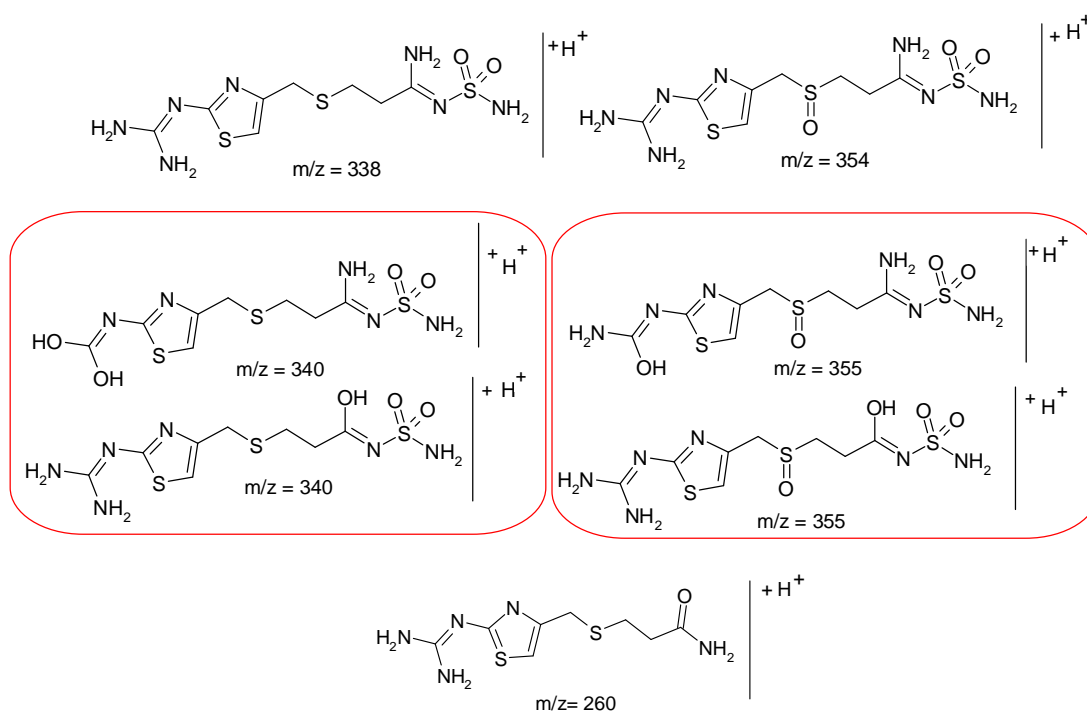


Figure 4.11: Famotidine and proposed structures for high abundance masses found.

Plausible intermediates have been elucidated based on masses in Table 4A-1 (appendices) of Famotidine with Sigma TiO_2 (0.1 g) and are shown in Figure 4.11 and Figure 4.12. Many of the higher masses could have quite complex fragmentation patterns so further analysis on these must be undertaken to confirm or rule out any of the proposed structures. As expected one of the main oxidation sites would occur at the thioether moiety. This is in line with an oxidation study with $KMnO_4$ on Famotidine by Rahman and Kashif 2003 and is also reported as an *in vivo* oxidation site in phase 1 metabolism.^{194, 195}

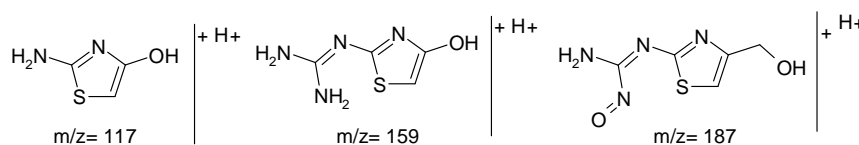


Figure 4.12: Proposed structures in initial DI-MS studies for masses in high abundance in mass spectra.

While the guanidine functionality is quite photo-stable it can be predicted that it will undergo at least a partial oxidation within the irradiation period of the degradation experiments.¹⁹⁶ Complete oxidation of guanidine has been determined to be within irradiation periods of 70+ h by Calza *et al.* 2004. Figure 4.13 shows the various transformations steps reported in Calza's

work for the guanidine moiety. Figure 4.14 and Figure 4.15 show the equivalent structures from masses found in Famotidine mass spectra and the pathway for this oxidation.

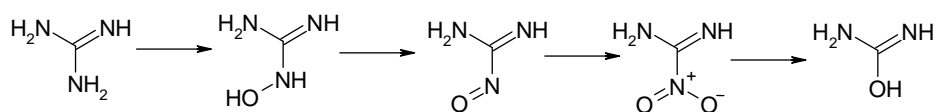


Figure 4.13: Guanidine transformation pathway reported by Calza *et al.* 2004.

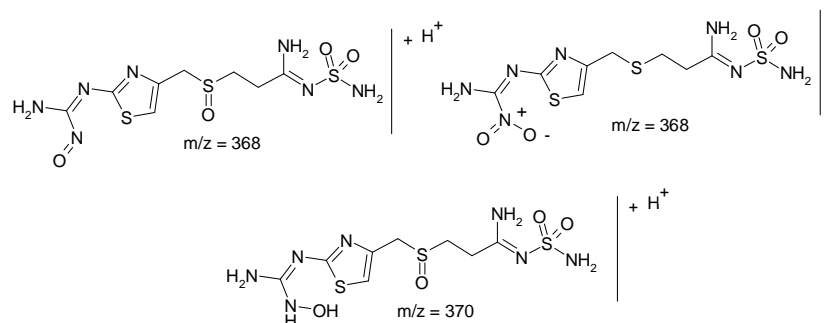


Figure 4.14: $m/z = 370$ and 368 were found in low abundances in Famotidine mass spectra.

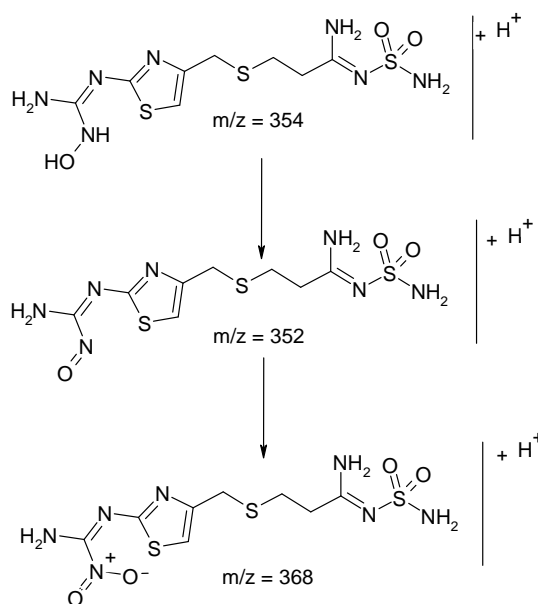


Figure 4.15: Masses detected at low intensities and proposed pathway to a partial oxidation of guanidine.

4.2.4 Follow-Up Direct Infusion Mass Spectrometry Studies: Famotidine

Further direct infusion studies were undertaken using cellulose acetate filters. These studies were performed with a much higher concentration of Famotidine (1 mM) and the photocatalytic experiment was undertaken with the optimised concentration of 0.1 g/320 mL P-25 TiO₂. MS/MS analysis was performed for various ions found in this experiment and the compound stability parameter (CS) was adjusted to either 10, 50 or 100% to see if any other intermediates would appear. Figure 4.16 shows samples 0 Mins (10% CS), 300 Mins (10% CS), 300 Mins (50% CS), and 300 Mins (100% CS). The effect of the CS parameter can be seen on $m/z = 338$

which in the case of 100% CS is now less dominant in the spectra. The most dominant ion is now $m/z = 189$ a fragment of $m/z = 338$.

Aside from this difference, there are some other ions that are merely less intense ($m/z = 354$) or no longer present ($m/z = 370$) when compared to 300mins (10% CS). Some new ions can be seen in 50% CS: $m/z = 286$ and in 100% CS: $m/z = 221$. These are most probably the fragments of intermediate ions as interestingly, examination of the MS/MS for $m/z = 370$ showed a fragment $m/z = 221$ (Table 4.2). Ions are shown twice in this table where multiple MS/MS analysis of an intermediate ion may have shown additional fragments. Selected mass spectra from this study can be found in the appendices (Appendix 4A2 - 4A9). Two fragments of Famotidine are also shown along with their respective fragments for reference where an intermediate may share some of these ions. The ion $m/z = 675$, with fragments $m/z = 338$ and 259, were found in spectra at 10% CS. This ion indicates that famotidine can dimerise under ESI conditions. Although ionisation at 100% CS is enough to significantly reduce the appearance of this dimer.

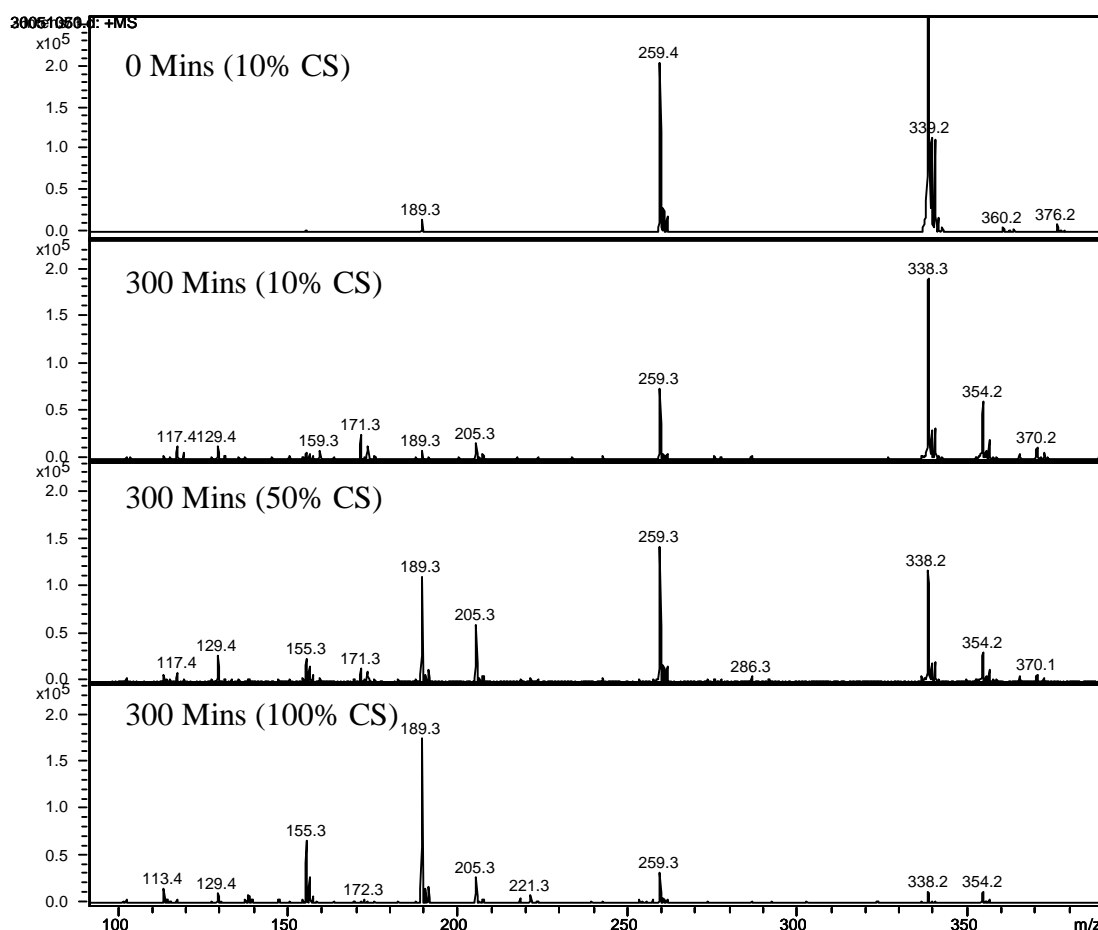


Figure 4.16: Famotidine direct infusion mass spectra at 0 Mins (10% CS), 300 Mins (10% CS), 300 Mins (50% CS), and 300 Mins (100% CS). Photocatalysis [FAM] = 1 mM, 0.1 g/320 mL TiO_2 .

DI-MS studies with no interferences from filters and MS/MS analysis allowed some intermediate structures to be confirmed at this stage. Figure 4.17 shows the parent and daughter ions for $m/z = 352$ and 171. Figure 4.18 shows the parent ion and daughter ions for $m/z = 354$ and $m/z = 370$. Additional ions were found at this stage (found in Table 4.2) however the absence of these masses in LC-MS/MS data meant that structural identification was not attempted for these masses.

Mass m/z	Fragments m/z	Mass m/z	Fragments m/z
675	<u>338</u> , 259	350	333, 271, 189, <u>155</u> , 138
403	385, <u>324</u> , 245	286	<u>207</u> , 150, 137
402	323, <u>253</u> , 156, 116	281	264, <u>239</u> , 211, 194, 169
392	351, 313, <u>243</u> , 188, 172, 149	221	<u>156</u> , 114
392	313, <u>243</u> , 189, 113	173	<u>155</u> , 144, 138, 129, 102
370	291, <u>221</u> , 157	171	155, 154, <u>129</u> , 113, 102
370	352, 291, 282, <u>221</u> , 203, 187, 173, 156, 114	147	<u>113</u> , 88
365	<u>286</u> , 216, 207, <u>182</u> , 165, 137, 119	259	242, <u>189</u> , 155, 138, 113, 102, 85
354	275, <u>205</u> , 155	155	<u>138</u> , 113
352	<u>273</u> , 238, 214, 203, 113		

Table 4.2: Table of masses found in follow-up DI-MS studies and their fragments. (DI-MS/MS). Ions in bold and underlined denote the base peak found in that mass spectrum. In grey are two of famotidines' fragments found in this study.

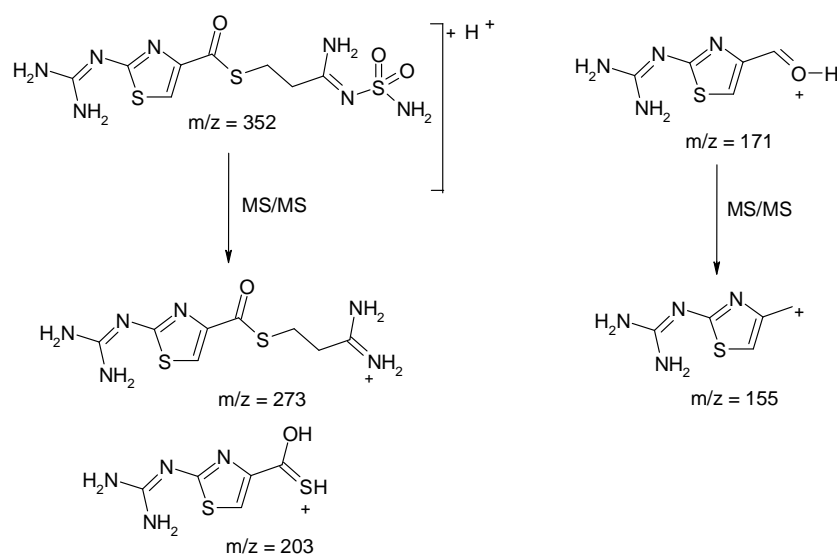


Figure 4.17: Intermediate $m/z = 352$ ($M_w = 351$) and intermediate $m/z = 171$ ($M_w = 170$) and fragments based on DI-MS/MS analysis.

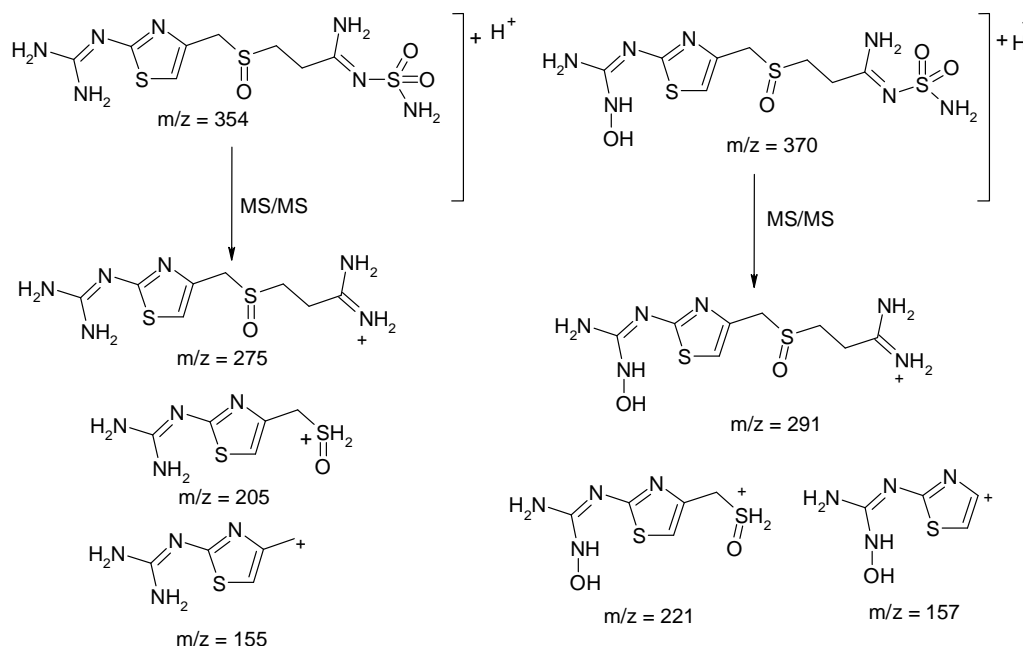


Figure 4.18: Intermediate $m/z = 354$ ($M_w = 353$) and intermediate $m/z = 370$ ($M_w = 369$) and fragments identified by DI-MS/MS analysis.

4.2.5 LC-MS/MS Studies and Intermediate Analysis: Famotidine

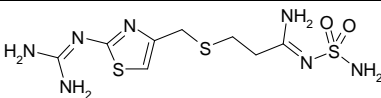
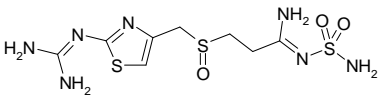
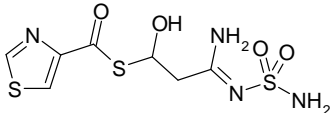
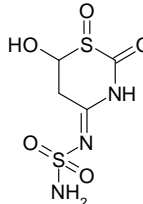
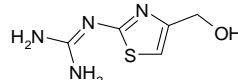
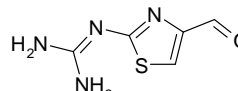
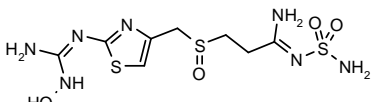
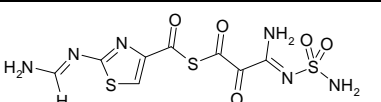
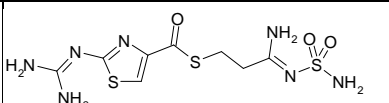
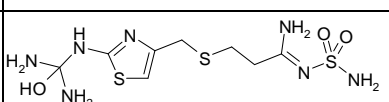
LC-MS/MS analysis of four Famotidine photo-degradation experiments were performed. The first experiment was the optimized photocatalysis with 0.1 g/320 mL TiO_2 and 0.083 mM Famotidine. An additional photocatalytic experiment was performed at a much higher concentration of 1mM Famotidine and 0.1 g/320 mL TiO_2 . (The higher concentration experiment was performed in order to see intermediates which may be formed at much lower concentrations.) Photolysis experiments with both Quartz and Pyrex were also analysed using LC-MS/MS at the optimum concentration of 0.083 mM Famotidine. Tables 4.3 and 4.4 show all of the ions found in each chromatogram for each sample in each experiment. At an early stage in data analysis some of the ions in these tables were ruled out as intermediates for a number of reasons: 1) the ion was present at too low an intensity, 2) the ion was present at a good intensity but did not give a successful MS/MS fragmentation or 3) the ion appeared at erratic retention times. This was the case for ions detected for each pharmaceutical throughout this chapter. Beside each ion in the table is the retention time that ion appears at in the chromatogram. Table 4.5 and 4.6 summarise all intermediate ions found in these experiments including their fragments, retention times, Mol. Wt. and calculated Log P values. Following these tables are individual EIC chromatograms for each significant intermediate ion found including their mass spectra and the MS/MS for that ion and the proposed intermediate structure.

	Photocatalysis (0.083mM)	Photocatalysis (1mM)
0Mins	338 (39.6), 392 (10.6)	338 (49.7), 392 (12.9), 354 (13.2),
0Min P.	338 ,(47.2) 392 (11.3), 129 (7.7)	338 (49.7), 392 (13.1), 354 (13.0),
5Mins	403 (25.8), 392 (12.7), 365 (25.9), 354 (12.4), 338 (51), 299 (3.9), 242 (10.9)	338 (49.3), 392 (13.1), 354 (13.0), 366 (2.8), 365 (27), 403 (26.6), 306 (23.2), 205 (13.3), 356 (13.1)
10Mins	403 (24.6), 392 (12.1), 365 (24.5), 354 (12.3), 338 (48.4), 299 (3.9), 205 (12.3), 356 (12.1), 117 (4.6)	405 (27.3), 403 (27.1), 392 (13.1), 370 (4.4), 365 (26.9), 354 (13.2), 338 (49.2), 336 (7.1), 299 (3.9), 286 (6.5), 207 (3.4), 205 (12.9), 356 (13.1)
20Mins	403 (23.9), 392 (11.7), 365 (24.2), 354 (11.8), 338 (46.6), 299 (3.8), 205 (11.7), 173 (9.5), 171 (12), 356 (11.7), 407 (9.2)	405 (26.6), 403 (26.7), 392 (13.1), 365 (27), 354 (12.9), 338 (49.9), 325 (7.3), 311 (3.9), 299 (4.2), 286 (6.5), 242 (11.4), 205 (12.7), 173 (9.9), 171 (12.6), 117 (4.9), 356 (13)
30Mins	403 (23.7), 392 (11.3), 366 (4.9), 365 (23.5), 354 (11.1), 338 (44.6), 336 (15.8), 311 (6.3), 299 (3.8), 356 (6.8)	407 (9.8), 403 (26.8), 392 (13.5), 365 (27.5), 356 (13.3), 354 (13.1), 338 (49.9), 336 (31.7), 325 (15.5), 324 (14.8), 311 (3.9), 306 (pnd), 299 (4) 286 (6.4), 242 (11.3), 205 (13.3), 173 (10), 171 (12.9), 117 (4.7)
40Mins	403 (22.7), 392 (11.1), 365 (22.5), 354 (11.1), 338 (39.7), 336 (15.3), 299 (3.7), 356 (6.7), 205 (11.1), 117 (4.5)	407 (9.6), 405 (27.4), 403 (27.6), 392 (13.2), 370 (4.4), 366 (27), 365 (27.2), 356 (13.4), 354 (13.1), 340 (24.3), 338 (), 336 (32.5), 311 (4), 306 (7.2, 17.1), 299 (4), 286 (6.5), 242 (11.5), 232 (4), 205 (13.4), 173 (9.9), 171 (12.2), 117 (4.9)
60Mins	403 (26), 392 (12.3), 365 (25.6), 354 (12.2), 338 (52.4), 336 (17.4), 299 (4.1), 356 (7.2)	405 (27), 403 (27), 392 (13.2), 365 (27), 356 (13.1), 354 (13.2), 340 (24.7), 338 (50.8), 336 (31.9), 325 (7.1), 311 (4.1), 306 (7.3, 16.9), 299 (4), 286 (6.6), 242 (11.4), 205 (13.3), 173 (pnd), 171 (12.7), 117 (4.9)
120Mins	403 (26.6), 392 (13.4), 365 (26.4), 354 (12.9), 338 (52.9), 336 (18.1), 325 (3.4), 286 (6.5), 173 (9.6), 356 (7.5)	405 (26.6), 403 (27.1), 392 (13.8), 365 (26.8), 356 (7.3, 4.5), 354 (13.4), 338 (49.5), 336 (31.1), 325 (6.8), 311 (4), 306 (7.4, 17), 299 (4.3), 286 (6.5), 242 (11.8), 205 (13), 173 (9.5), 171 (13.3)
180Mins	403 (26.2), 392 (12.7), 366 (4.9), 365 (26.7), 354 (13.1), 338 (53.2), 336 (17.7), 299 (4), 173 (9.5)	407 (9.8), 405 (26), 403 (26), 392 (12.8), 370 (21.1), 365 (26), 356 (6.9), 354 (12.5), 338 (48.5), 336 (30.1), 325 (6.7), 311 (3.9), 306 (6.8), 299 (4.2), 286 (6.2), 284 (32.3), 282 (8.1), 242 (11.3), 205 (12.6), 173 (9.3).

Table 4.3: Table of Ions present in the LC-MS/MS chromatographic runs of two photocatalytic experiments at 0.083 mM and 1 mM. In brackets after each ion is the retention time (in minutes) at which this ion was found in each EIC. (pnd= present however not a dominant ion)

	Photolysis (Quartz)	Photolysis (Pyrex)
0Mins	338(43.6), 392(11.4)	338(43.6), 392(pnd), 354(pnd), 306(3.9), 171(25.7)
0Min P.	N/A	N/A
5Mins	403(24.1), 392(11.4), 354(11.4), 338(47.2), 306(14.7, 6), 286(5.6), 173(8.3), 324(3.5)	338(46), 392(11.4)
10Mins	403(24.9), 392(11.4), 354(11.6), 338(48), 306(6.2, 14.9), 286(5.6), 299(2.7), 173(8.5), 324(3.5)	392(11.6), 354(11.4), 338(46.9), 117(4.3)
20Mins	392(11.5), 354(11.2), 306(15.3), 286(5.6), 324(3.5), 338(47.2), 299(3.4), 242(10.7), 207(2.6)	354(11.5), 392(11.4), 338(46.7), 324(20.8)
30Mins	392(11.5), 306(14.5), 173(8.5), 311(0.6), 207(2.6), 324(3.6), 338(47.8), 299(3.3)	354(11.5), 392(11.4), 338(46.9)
40Mins	299(3.3), 306(14.9), 366(4.4), 207(2.7), 324(3.4)	403(23.8), 354(11.5), 173(8.5), 392(11.5), 338(46.9)
60Mins	nothing significant, too much noise present	403(24.2), 354(11.4), 173(8.3), 392(11.3), 338(47.1)
120Mins	299(3.4), 207(2.1), 328(3.7)	403(24.2), 354(pnd), 392(11.4), 338(47.3), 306(14.7), 365(24.4), 173(8.3)
180Mins	311(3.8), 328(3.7)	407(8.3), 403(24.6), 354(11.4), 173(8.4), 392(11.6), 338(47.9), 306(14.5, 6.2), 365(25)

Table 4.4: Table of ions present in the LC-MS/MS chromatographic runs of two photolysis experiments at 0.083 mM with Quartz and Pyrex. In brackets after each ion is the retention time at which this ion was found in each EIC. (pnd= present however not a dominant ion)

Name	Structure	Mass m/z	Daughter Ions m/z	Mol. Wt. g/mol	t _R mins	cLog P
Famotidine		338	259, 242, 189	337	43	-0.2
S-oxide Famotidine, P354		354 (392 K ⁺ adduct)	275, 205	353	13	-1.37
P311		311	293, 232, 214	310	4	-0.11
P242		242	224, 145	241	11.5	-1.10
P173		173	155	172	9.5	-1.53
P171		171	154	170	12.2	-1.75
P370		370	291, 221	369	4.3	-1.63
P365		365 (403 K ⁺ adduct)	286, 207, 182	364	27.2	0.29
P352		352	273, 203	351	N/A*	-0.72
P356		356	277, 207	355	7.6	-0.72

* Found in DI-
MS Studies only

Table 4.5: Table of Famotidine's confirmed intermediates (degradation products), their fragments, retention times, molecular weight and calculated Log P values.^{197, 198}

Intermediate $m/z = 354$

The ion $m/z = 354$ was found in each photodegradation experiment analysed and generally appeared in the first few samples taken for each experiment. From this we can conclude that it is one of the first breakdown products of Famotidine. Additionally, this ion appeared in initial and follow-up mass spectrometry studies and can be confirmed as an intermediate. It appears in each experiment at a retention time of 11.5 mins although in the higher concentration experiment it appeared at 13 mins (seen in the chromatogram in Figure 4.19). This was in line with a similar apparent shift in the retention time of Famotidine (49 mins) appearing in other experiments at 47 mins. This shift was due to the high loading of sample on the column of Famotidine (1mM) and its intermediates. The 40 mins sample is shown below, it was at this time period the maximum concentration of $m/z = 354$ was found. This intermediate co-elutes with $m/z = 392$ which can be clearly seen in the inset mass spectrum at a lower intensity. This may be an indication of a relationship between these two ions. The fragments for $m/z = 354$ are $m/z = 275$ and $m/z = 205$. This fragmentation is similar to that of Famotidine with a difference of 16 mass units between fragments (Famotidine: $m/z = 259$ and $m/z = 189$). This, combined with analysis of fragments would indicate that oxidation has likely occurred at the thioether functionality. Previous studies by other authors confirm the oxidation of thioethers and propose a mechanism of oxidation via positive holes on the TiO_2 surface.¹⁹⁹ The structure proposed for this fragment along with its daughter fragments are shown in figure 4.20.

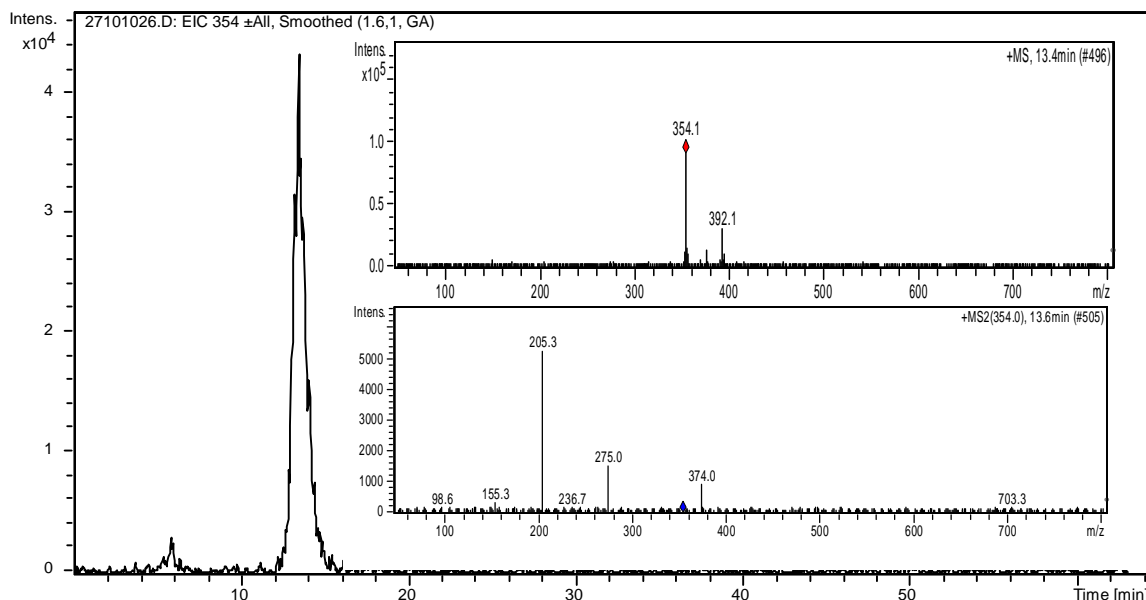


Figure 4.19: EIC of intermediate $m/z = 354$ in a 40 mins sample at a t_R of 13.1 mins. Inset MS (top) and MS/MS (bottom) spectra. Photocatalysis, [FAM] = 1mM, 0.1 g TiO_2 /320 mL.

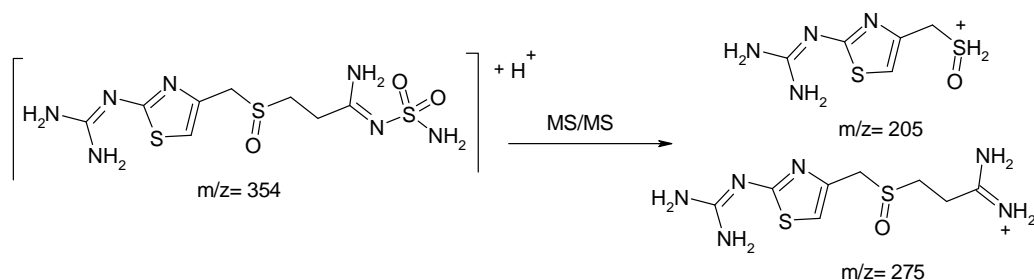


Figure 4.20: Structure proposed for $m/z = 354$ and its daughter ions according to LC-MS/MS data.

Intermediate $m/z = 392$

The intermediate $m/z = 392$ appeared in all experiments analysed, co-eluting with $m/z = 354$ at a t_R of 13.5 mins (Figure 4.21). A small amount of this ion was present in the 0 mins sample, although it was also seen to develop throughout the experiment. EICs showing the $m/z = 392$ throughout each sample can be found in Appendix 4A-11 for the 1 mM photocatalytic experiment. For experiments at 0.083 mM, the concentration of this ion in the 0mins samples was significantly lower than in the 1mM experiment. Fragments from $m/z = 392$ are $m/z = 313$ (loss of 79), $m/z = 243$ (loss of 149), and $m/z = 188$ (loss of 204). A similar pattern is observed with the parent ion for $m/z = 354$ with fragments $m/z = 275$ (loss of 79), $m/z = 205$ (loss of 149). The difference of 38 mass units between the parent mass and fragments implies a possible adduct of the intermediate $m/z = 354$ with K^+ which has an atomic mass of 39 amu. Structures for the parent ion and daughter ions for $m/z = 392$ are shown in Figure 4.22. It should be noted that the potassium adduct for Famotidine, $m/z = 376$, was also observed in LC-MS/MS data (see appendix 4A-12). This ion was fragmented in DI-MS studies, resulting in $m/z = 297$ which is the potassium adduct for the fragment $m/z = 259$ of Famotidine.

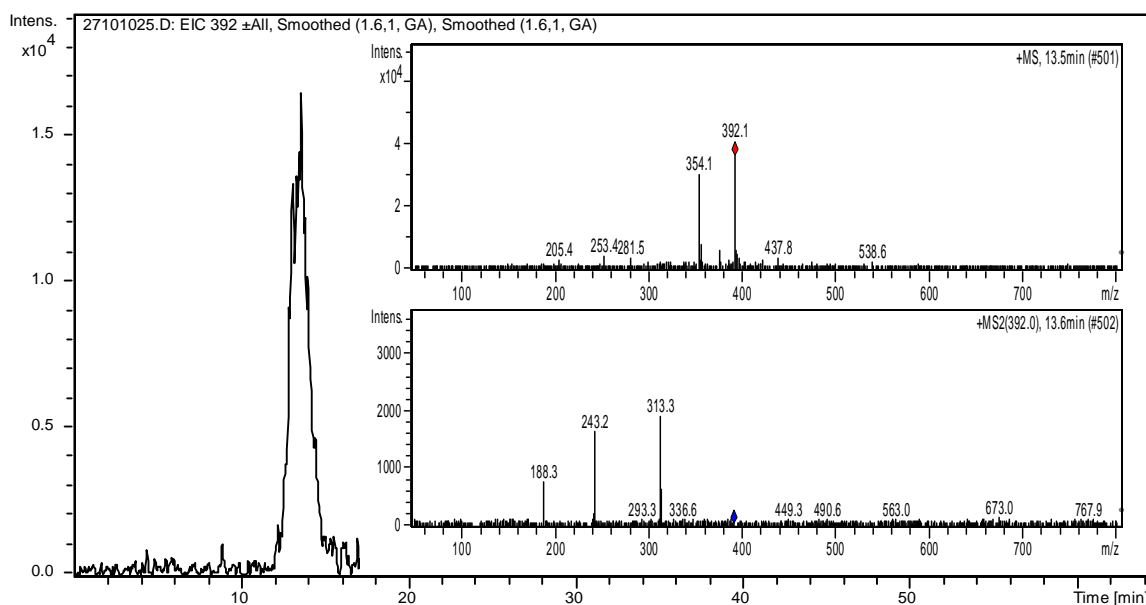


Figure 4.21: EIC of intermediate $m/z = 392$ in a 30 mins sample at a t_R of 13.5 mins. Inset MS (top) and MS/MS (bottom) spectra. Photocatalysis, [FAM] = 1 mM, 0.1 g TiO_2 /320 mL.

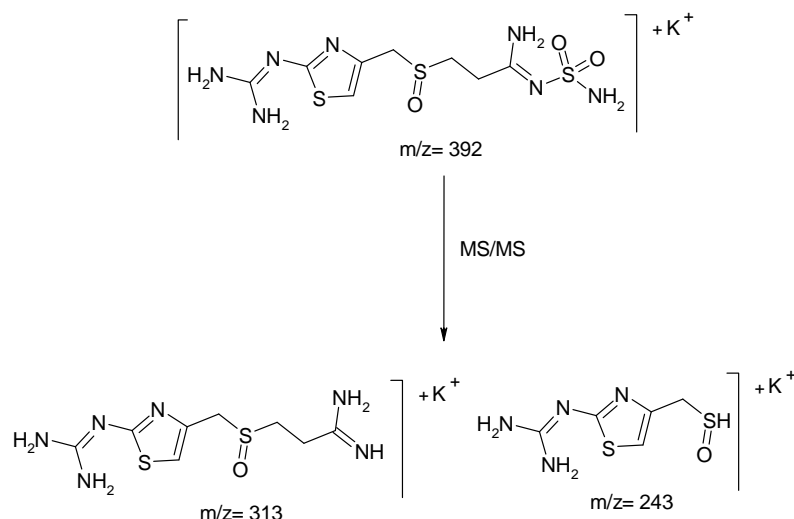


Figure 4.22: Structure of $m/z = 392$ and its fragments $m/z = 313$ and $m/z = 243$.

Intermediate $m/z = 242$

The intermediate $m/z = 242$ was found in the concentrated 1mM photocatalytic experiment and also in the Quartz photolysis experiment from approximately 20mins onwards. Its low signal intensity would imply a less favoured fragmentation pathway and thus very little is formed even at increased concentration. The alternative to this is that it is a favoured intermediate but is however unstable and/or further oxidized to another intermediate quite quickly. The fragments for $m/z = 242$ are $m/z = 224$ and $m/z = 145$. $m/z = 145$ is the most intense fragment (base peak) and is therefore the most stable fragment of the two. $m/z = 224$ is an M-18 fragment which can conclusively be assigned as a loss of H_2O from the parent structure. The difference between the two fragments is 79 mass units. This would indicate the loss of a sulfonamide and based on the molecular weight would tell us that the famotidine molecule has been effectively split up, losing the thiazole-guanidine moiety. Its appearance quite early in the chromatogram would signify that it is quite a polar compound. In figure 4.24, a cyclic intermediate has been proposed for this mass. Work by Buth *et al.* in 2007 examined the products of chlorination of cimetidine in water treatment processes.²⁰⁰ One of the products they found in their study was a δ -sultam which was formed after chlorination of the cimetidine sulfoxide leading to the cleavage of the imidazole. They proposed the formation of a cyclic δ -sultone. Further reaction with hypochlorite led to the δ -sultam as an intermediate (see Figure 4.25).

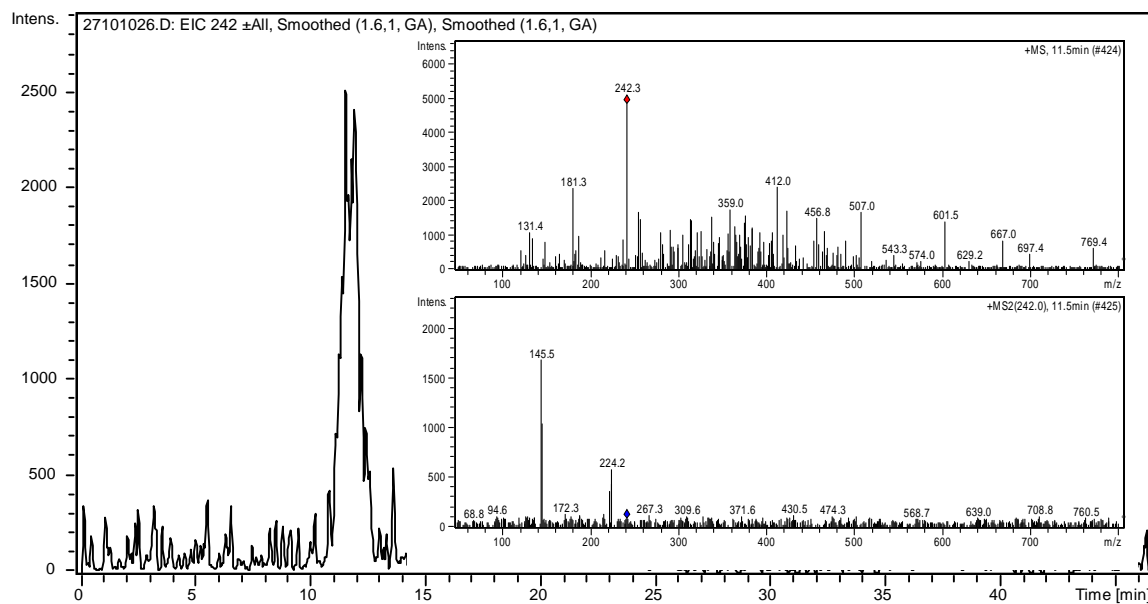


Figure 4.23: EIC of intermediate $m/z = 242$ in a 40 mins sample at a t_R of 11.5 mins. Inset MS (top) and MS/MS (bottom) spectra. Photocatalysis, [FAM] = 1 mM, 0.1 g TiO_2 /320 mL.

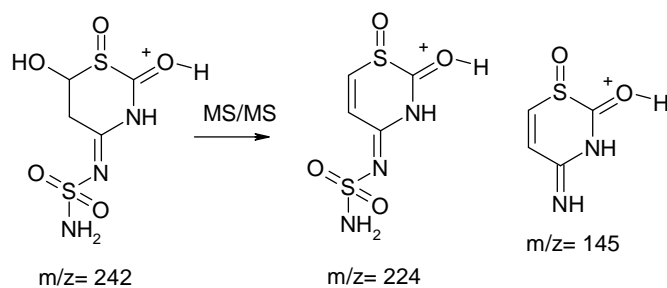


Figure 4.24: Structure proposed for $m/z = 242$ and its daughter ions $m/z = 224$ and $m/z = 145$ according to LC-MS/MS data.

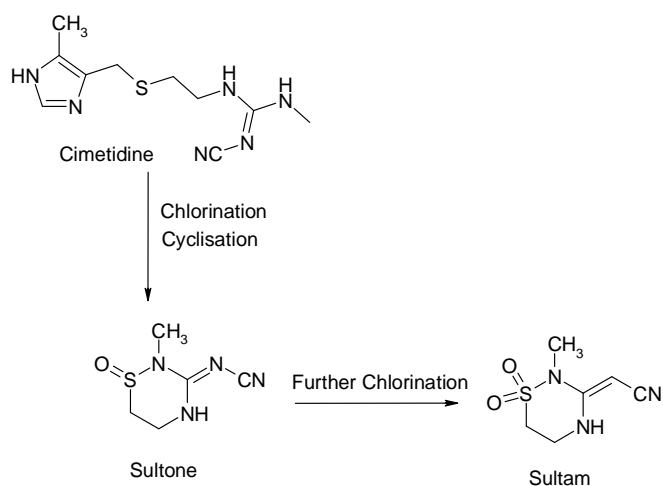


Figure 4.25: Proposed cyclic chlorination products for Cimetidine from Buth *et al.* 2007.

Intermediate $m/z = 173$

The intermediate at $m/z = 173$ was found in all experiments analysed and appeared at 8.4 mins in photolysis experiments and 9.5 mins in photocatalysis experiments. It should be noted that photolysis experiments were run on a different occasion to photocatalytic experiments. The only fragment found for $m/z = 173$ was $m/z = 155$. This fragment is also a minor fragment for famotidine and indicates a split of the famotidine molecule, with the oxidation occurring on the thiazole-guanidine region of the molecule. Earlier DI-MS studies (Table 4.2) show that $m/z = 155$ fragments to give one mass $m/z = 138$. This mass was observed in the MS/MS for $m/z = 173$ in Figure 4.26 at a lower intensity relative to $m/z = 155$. What this indicates is that $m/z = 155$ is indeed the same structure to the fragment for Famotidine. The proposed structure for $m/z = 173$ and its fragment is shown in Figure 4.27.

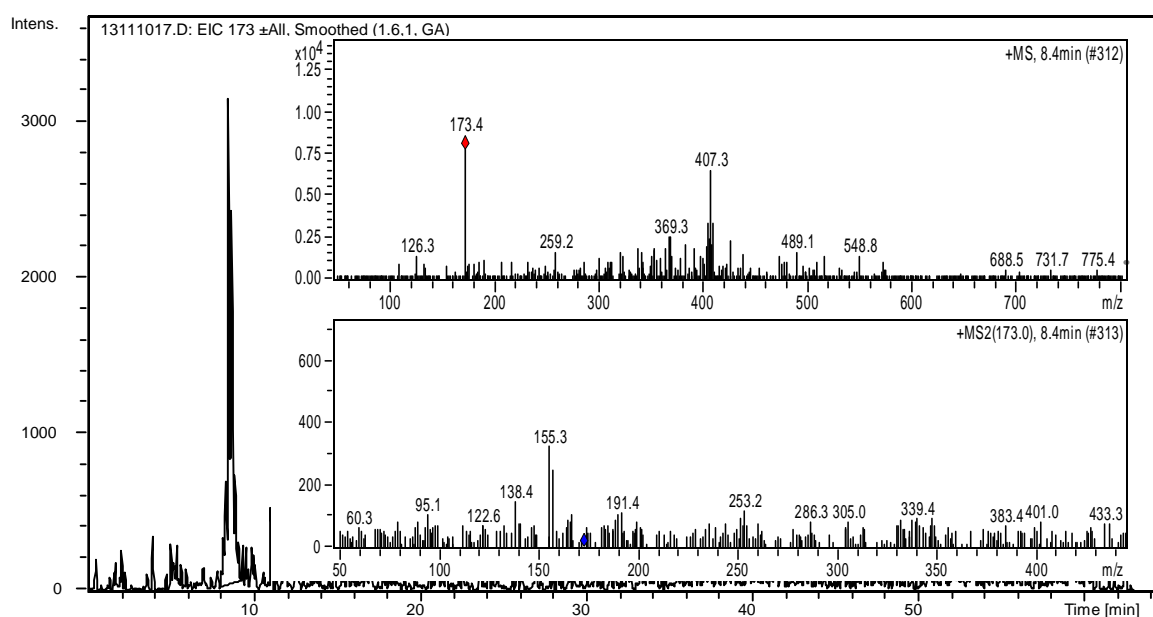


Figure 4.26: EIC of intermediate $m/z = 173$ in a 180 mins sample at a t_R of 8.4 mins. Inset MS and MS/MS spectra. Photolysis Pyrex, [FAM] = 0.083 mM.

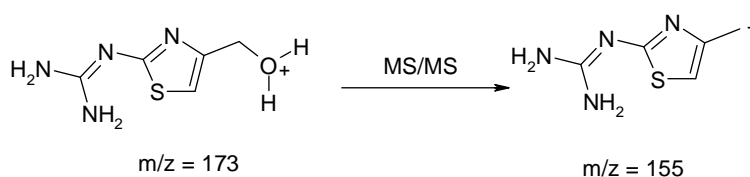


Figure 4.27: Structure proposed for $m/z = 173$ with daughter ion $m/z = 155$

Intermediate $m/z = 311$

The intermediate $m/z = 311$ was found in the Quartz photolysis experiment and also in the 1 mM photocatalysis experiment. It appeared in all experiments at a retention time of around 3.8 - 4 mins. It was found to appear later in the experiment for quartz photolysis (180 mins), whereas in higher concentration photocatalysis, 1 mM, it was detected earlier (20 mins-onwards). Three fragments were detected from MS/MS analysis of $m/z = 311$: $m/z = 293$ (loss of 18), $m/z = 232$

(loss of 79), and $m/z = 214$ (loss of 97). A loss of 79 mass units from the parent $m/z = 311$ as with the other intermediates, would indicate possible loss of the sulfonamide. This loss gives rise to the fragment $m/z = 232$, and separately, loss of water from the parent intermediate gives rise to $m/z = 293$. A loss of water in addition to loss of the sulfonamide leads to the fragment $m/z = 214$. Two possible structures have been put forward for $m/z = 311$. These are structural isomers and are indistinguishable based on their fragments. Both structures proposed show that numerous oxidations have occurred to the Famotidine molecule through loss of the guanidine, and oxidations to the aliphatic chain in the molecule. One of the oxidations on the aliphatic chain is to a ketone at the carbon between the thiazole ring and the thioether. A second oxidation is proposed along the aliphatic chain neighbouring the amidine group and this oxidation is likely on either carbon. Both isomers and their proposed fragments are shown in Figure 4.29 and Figure 4.30. In this case, oxidation of numerous moieties and loss of the guanidine moiety are likely.

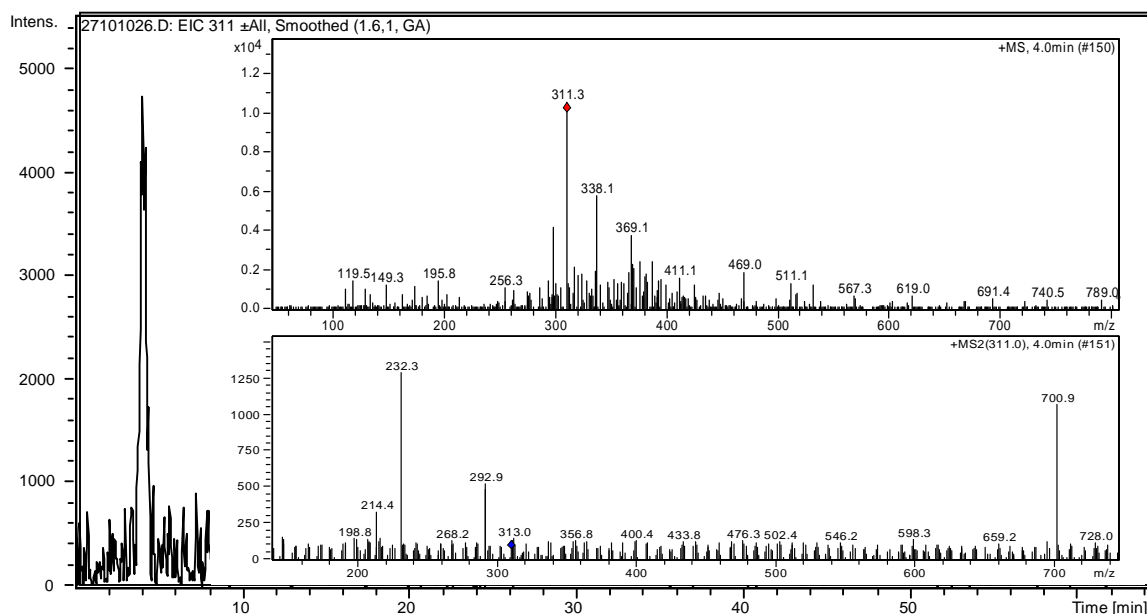


Figure 4.28: EIC of intermediate $m/z = 311$ in a 40 mins sample at a t_R of 4 mins. Inset MS and MS/MS spectra. Photocatalysis, [FAM] = 1mM, 0.1 g TiO_2 /320 mL.

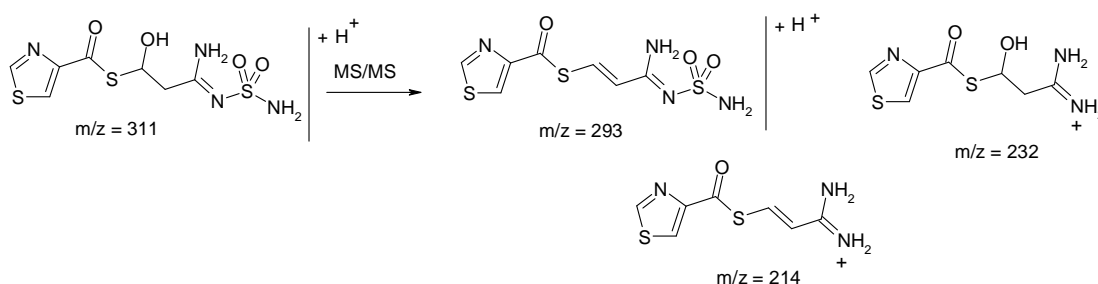


Figure 4.29: Proposed structure for $m/z = 311$ and its fragments $m/z = 293$, $m/z = 232$ and $m/z = 214$.

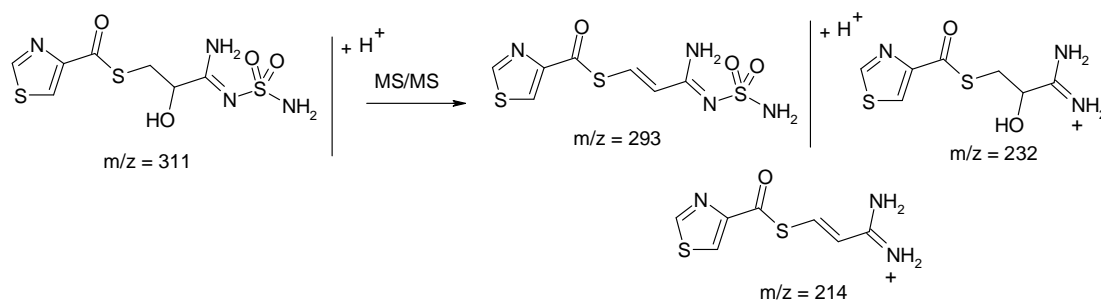


Figure 5.30: Proposed isomer for $m/z = 311$ with fragments $m/z = 293$, $m/z = 232$ and $m/z = 214$.

Intermediate $m/z = 171$

The intermediate $m/z = 171$ was found exclusively in the 1 mM photocatalytic experiment. We believe this is because it is not produced in large quantities and could only be detected at the increased concentration. $m/z = 171$ is closely related to the previous intermediate at $m/z = 173$ in that oxidation of the same carbon occurs. It is thought that due to the differing fragments for $m/z = 173$ and $m/z = 171$ it is likely that the oxidation mechanism for both these intermediates are different. Famotidine may first undergo oxidation of the thioether resulting in cleavage of the molecule with a resulting radical on the carbon alpha to the sulfur atom. A hydroxyl radical may then combine with this radical to give $m/z = 173$. The fragment from MS/MS analysis of $m/z = 173$ ($m/z = 155$) supports this mechanism (Figure 4.26). $m/z = 171$ could be formed by a slightly different mechanism of H-abstraction and hydroxyl radical attack would result in $m/z = 154$ in the case of $m/z = 171$. Another possible mechanism which is reported in the literature is the abstraction of H by a hydroxyl radical and addition of oxygen to give a peroxy radical.¹⁹⁹ This will decompose to give the resulting ketone, $m/z = 171$. The structure for $m/z = 171$ is shown in Figure 4.32. The fragments for $m/z = 171$ could not be proposed, so molecular formula are presented in this case.

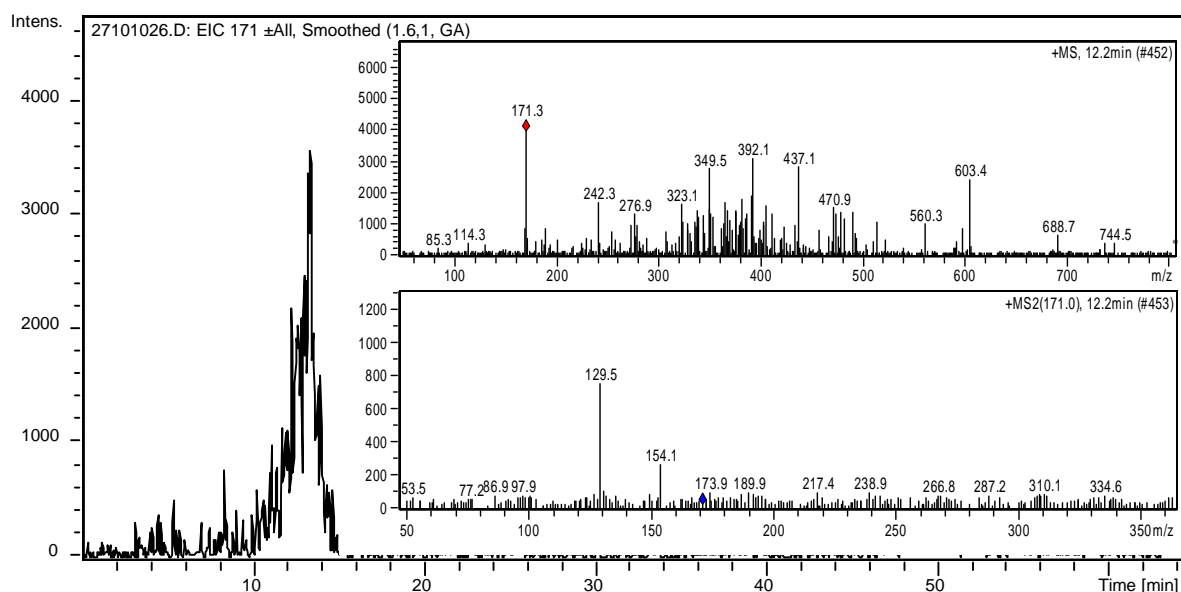


Figure 4.31: EIC of intermediate $m/z = 171$ in a 40 mins sample at a t_R of 12.2 mins. Inset MS (top) and MS/MS (bottom) spectra. Photocatalysis, [FAM] = 1 mM, 0.1 g TiO_2 /320 mL.

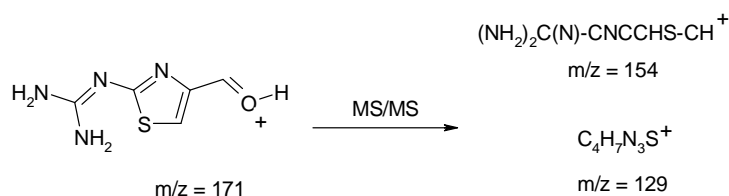


Figure 4.32: Structure proposed for $m/z = 171$ and molecular formula for $m/z = 154$, and $m/z = 129$.

Intermediate $m/z = 370$

Intermediate $m/z = 370$ was found in earlier MS/MS studies and a structure was proposed for this ion. However, upon initial examination by LC-MS/MS, this ion was not found. Upon further examination of the data, in only one sample (20 mins), did this ion dominate over others and was thus detected with subsequent MS/MS analysis. It was found at a retention time of 4.3 mins after 20 mins of irradiation in the higher concentration photocatalytic experiment. LC-MS/MS data show only two fragments for $m/z = 370$; $m/z = 291$ and $m/z = 221$. Two structures are proposed for intermediate $m/z = 370$ and its fragments (Figure 4.34). LC-MS/MS data and a literature search would indicate that the sulfone is the most likely intermediate (Santellas *et al.*). However, DI-MS studies showed an additional fragment $m/z = 157$ (Table 4.2, Figure 4.18) which is additional evidence for the proposal of the sulfoxide/hydroxylamine intermediate (upper structure).

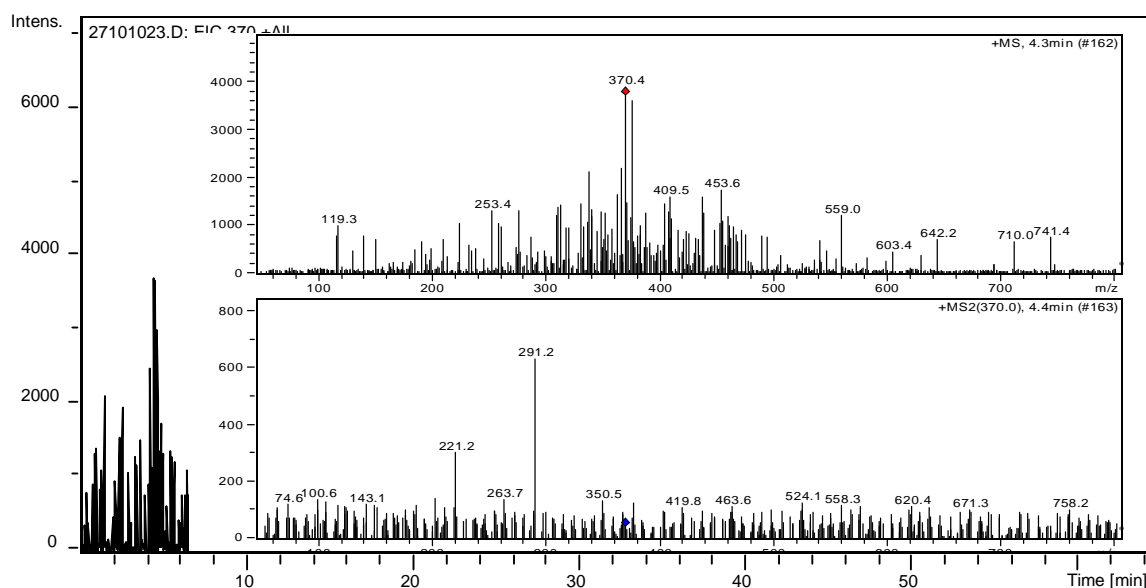


Figure 4.33: EIC of intermediate $m/z = 370$ in a 20 mins sample at a t_R of 4.3 mins. Inset MS (top) and MS/MS (bottom) spectra. Photocatalysis, [FAM] = 1 mM, 0.1 g $\text{TiO}_2/320\text{ mL}$.

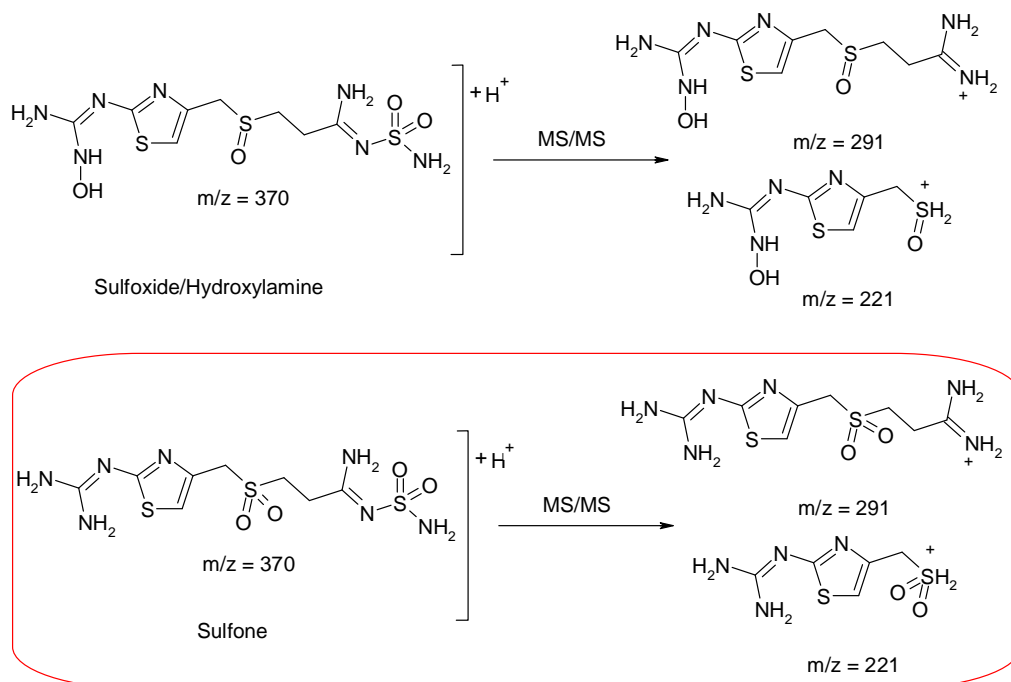


Figure 4.34: Structure of $m/z = 370$ and its fragments $m/z = 291$ and $m/z = 221$.

Intermediate $m/z = 365$

Intermediate $m/z = 365$ was found in both photocatalytic experiments (1 mM and 0.083 mM) and found in the photolysis of Famotidine with Pyrex but not with quartz. It appeared at a t_R of 27 mins. Similar to intermediate $m/z = 354$, it features an ion in its mass spectrum (inset Figure 5.32) which is 38 mass units higher than $m/z = 365$. This would imply that a potassium adduct is also formed for this intermediate with $m/z = 403$. $m/z = 365$ has 3 fragments', $m/z = 286$ (loss of 79), $m/z = 207$ (loss of 158) and $m/z = 182$ (loss of 183). Loss of 79 would imply loss of the

sulfonamide. The difference in mass units between $m/z = 365$ and famotidine $m/z = 338$ is 27 mass units. Cyclic structures and various other oxidations on the molecule were predicted although a viable structure for $m/z = 365$ could not be proposed. One structure has been put forward in Figure 4.36 which entails the oxidation of numerous carbons on the molecule and a loss of $-NH_2$ from the guanidine moiety. This was the only possible structure that fits a mass of 364 ($m/z = 365$) and fragment of $m/z = 286$. EICs showing the development of this intermediate throughout samples in the photocatalytic experiment can be found in appendix 4A-10.

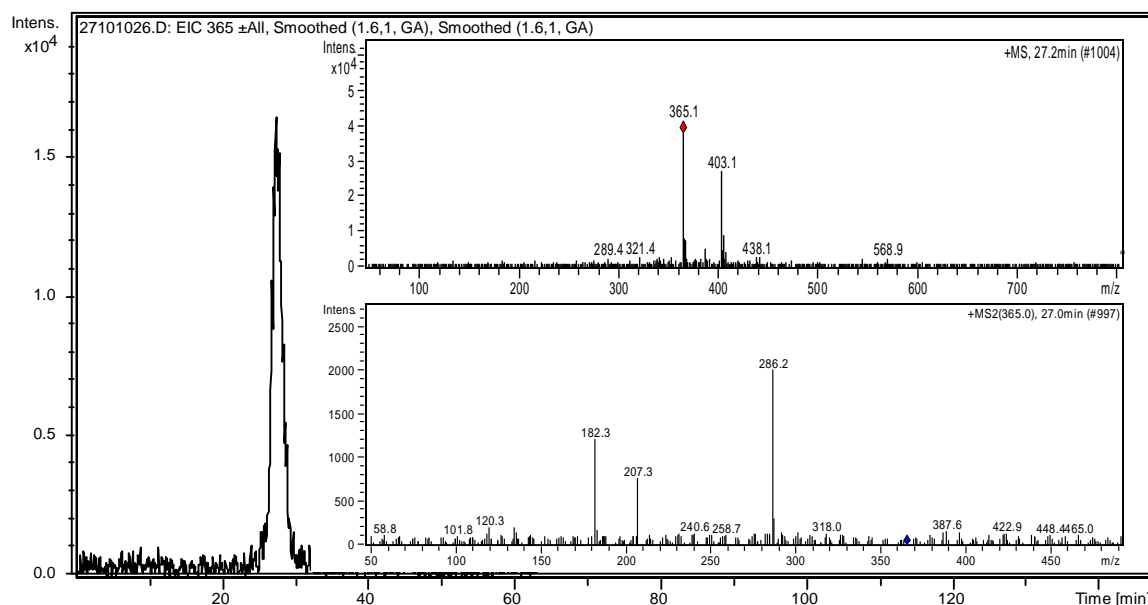


Figure 4.35: EIC of intermediate $m/z = 365$ in a 40 mins sample at a t_R of 27.2 mins. Inset MS (top) and MS/MS (bottom) spectra. Photocatalysis, [FAM] = 1 mM, 0.1 g TiO_2 /320 mL.

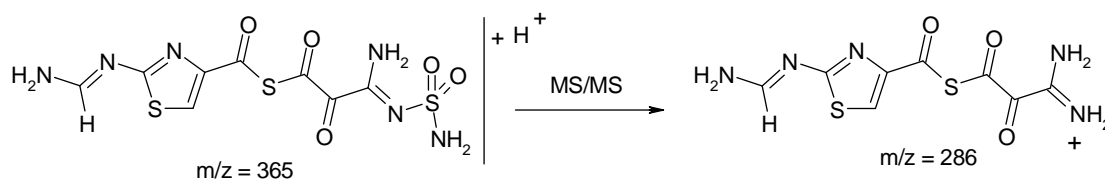


Figure 4.36: Proposed structure of $m/z = 365$ and its main fragment $m/z = 286$.

Intermediate $m/z = 403$

The intermediates $m/z = 403$ appeared in all experiments analysed (photolysis and photocatalysis), co-eluting with $m/z = 365$ at a t_R of 27.6 mins (Figure 4.37). Fragments from $m/z = 403$ are $m/z = 324$ (loss of 79), and $m/z = 245$ (loss of 158). A similar pattern to this is observed for $m/z = 365$ with fragments $m/z = 286$ (loss of 79), $m/z = 207$ (loss of 158). The difference of 38 mass units between the parent mass and fragments again implies a possible adduct of the intermediate $m/z = 365$ with K^+ . Structures for the parent ion and daughter ions for $m/z = 403$ are shown in Figure 4.38.

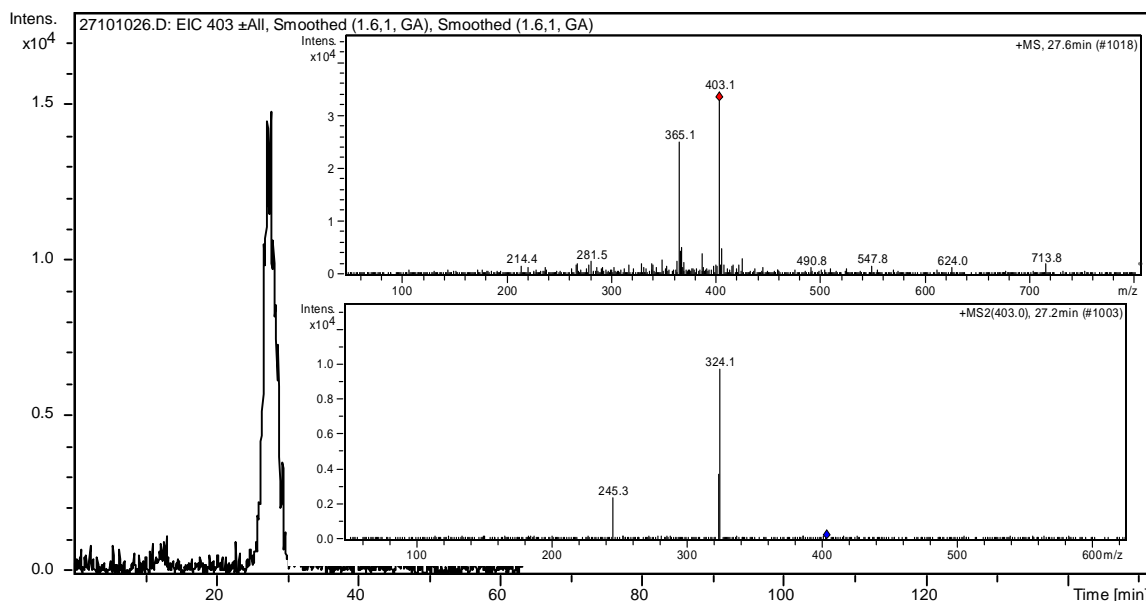


Figure 4.37: EIC of intermediate $m/z = 403$ in a 40 mins sample at a t_R of 27.6 mins. Inset MS (top) and MS/MS (bottom) spectra. Photocatalysis, [FAM] = 1 mM, 0.1 g TiO_2 /320 mL.

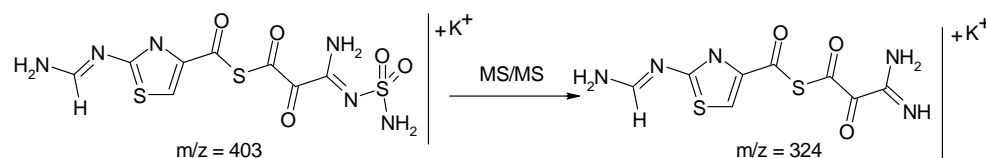


Figure 4.38: Structure of $m/z = 403$ and its main fragment $m/z = 324$.

Intermediate $m/z = 356$

Intermediate $m/z = 356$ was only found in the 1mM photocatalysis experiment at a t_R of 7.6 mins and was detected initially after 20 mins of irradiation and was present until 180 mins. Its fragment ions are $m/z = 277$ (loss of 79) and $m/z = 207$ (loss of 149). This fragmentation pattern was also seen for ions $m/z = 392$, $m/z = 338$ (Famotidine), $m/z = 354$ and $m/z = 324$. The EIC for $m/z = 356$ showed two peaks one at 7.6 mins and one at 13.4 mins. The second peak was found at the same retention time of $m/z = 354$. For this intermediate two possible structures are proposed (Figure 4.40). In line with the fragmentation pattern, oxidation must have occurred on the thiazole-guanidine fragment of the molecule.

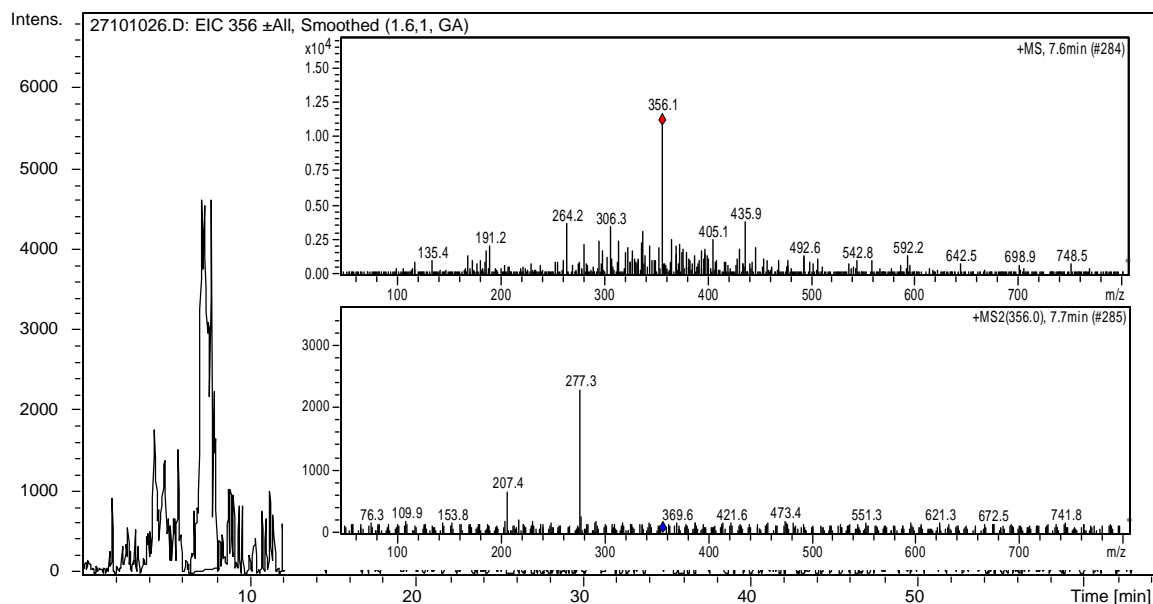


Figure 4.39: EIC for 356 at 40 mins at a t_R of 7.6 mins and 13.4 mins. Photocatalysis, [FAM] = 1 mM, 0.1 g TiO_2 /320 mL.

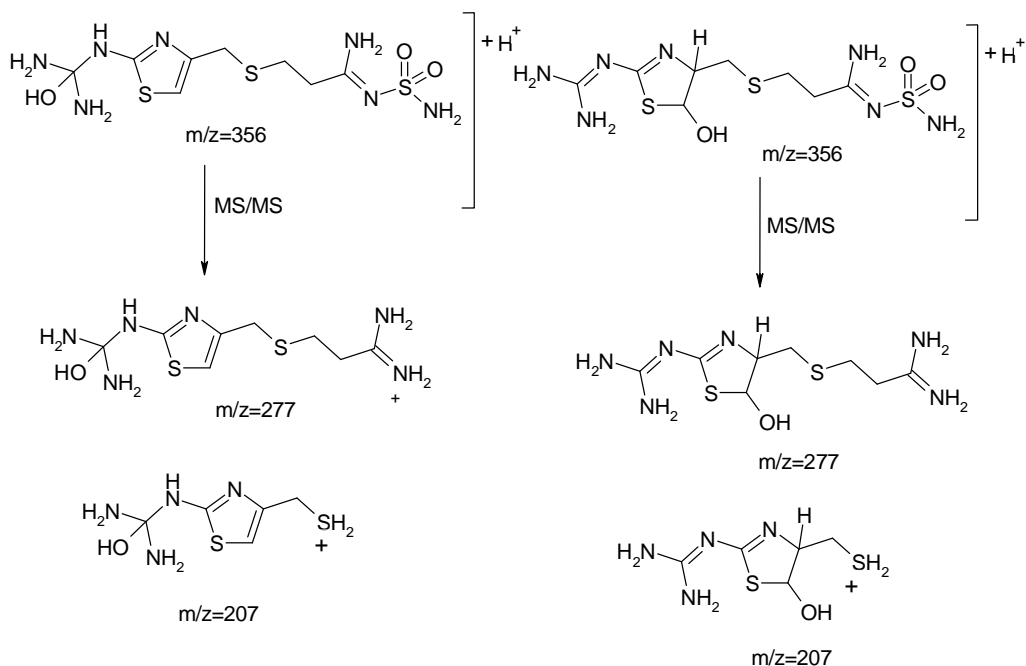


Figure 4.40: Structures proposed for $m/z = 356$ and its fragments $m/z = 277$ and $m/z = 207$.

4.2.6 Ions which could not be Elucidated

A number of intermediates detected in samples throughout photodegradation experiments could not be elucidated. These intermediates are presented in Table 4.6 along with their retention times, fragments and the experiments in which they were present. EIC chromatograms are presented along with MS and MS/MS spectra in Figures 4.41-4.46.

Intermediate m/z	Fragments	t _R (mins)	Experiment
324	307(306), 227, 175, 157(158)	3.4	Quartz Photolysis
306	227, 157, 125	6.2, 16	Photocat 1mM
336	273, 202 (319, 257, 238)	15.3, 32.3	Photocat (1mM, 0.083mM)
299	265, 231	4	Photocat (1mM, 0.083mM) Photolysis (Quartz)
286	206, 197, 177, 129	6.6	Photocat (1mM, 0.083mM) Photolysis (Quartz)
325	308, 284, 206, 155	6.6	Photocat 1mM

Table 4.6 Table of intermediates for which structure could not be proposed.

Although structures could not be elucidated for intermediates $m/z = 324$ and $m/z = 306$, we believe that these intermediates may be related as they share two common ions: $m/z = 227$ and $m/z = 157$ and differ only in mass by 18 (a loss of water). Based on the fragmentation pattern, we would speculate strongly that oxidation has occurred at the thiazole-thioether moiety. Fragmentation of the aliphatic chain would then likely occur with the usual loss of the sulfonamide. The intermediate $m/z = 286$, which has the same mass of one of the main fragments of the intermediate $m/z = 365$, does not indicate that it is in any way related to $m/z = 365$.

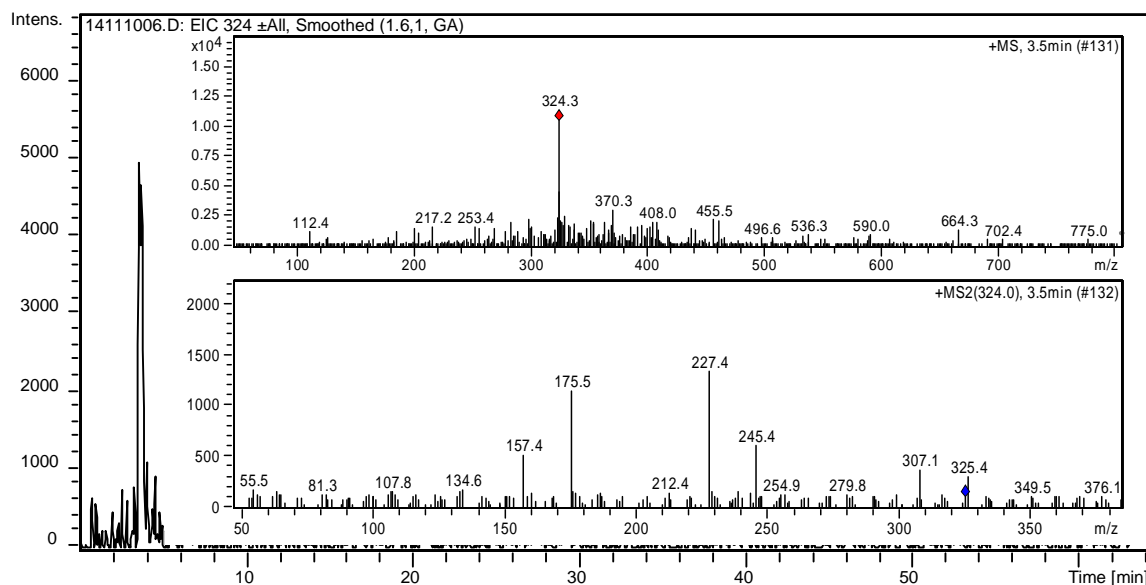


Figure 4.41: EIC of intermediate $m/z = 324$ in a 20 mins sample at a t_R of 3.5 mins. Inset MS and MS/MS spectra. Photolysis Quartz, [FAM] = 0.083 mM.

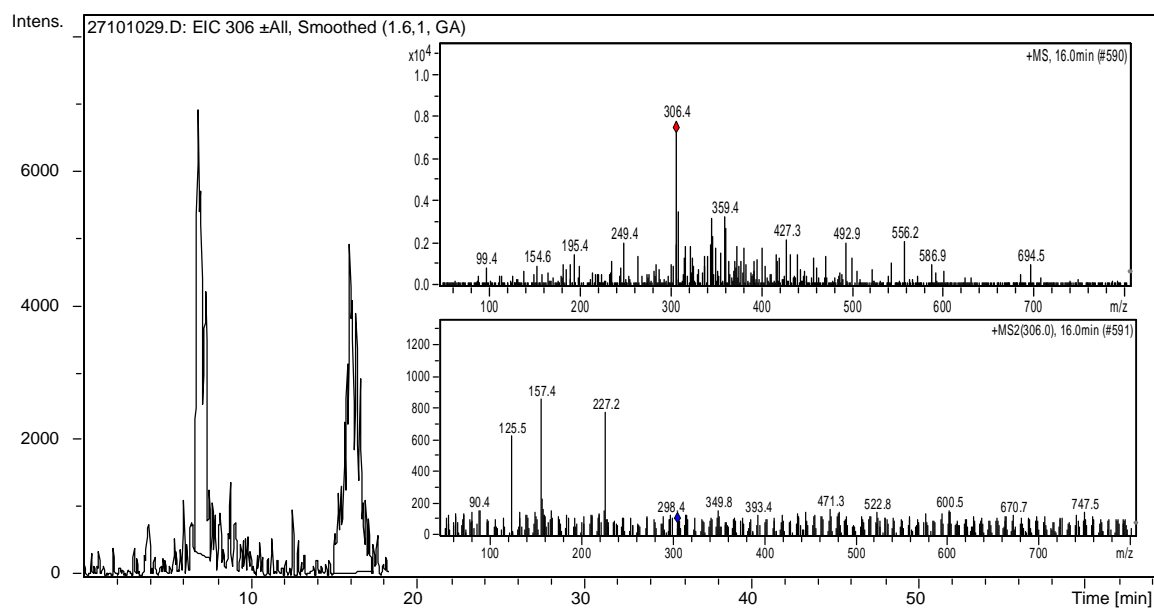


Figure 4.42: EIC of intermediate $m/z = 306$ in a 180 mins sample at a t_R of 16 mins. Inset MS and MS/MS spectra. Photocatalysis, [FAM] = 1 mM, 0.1 g TiO_2 /320 mL.

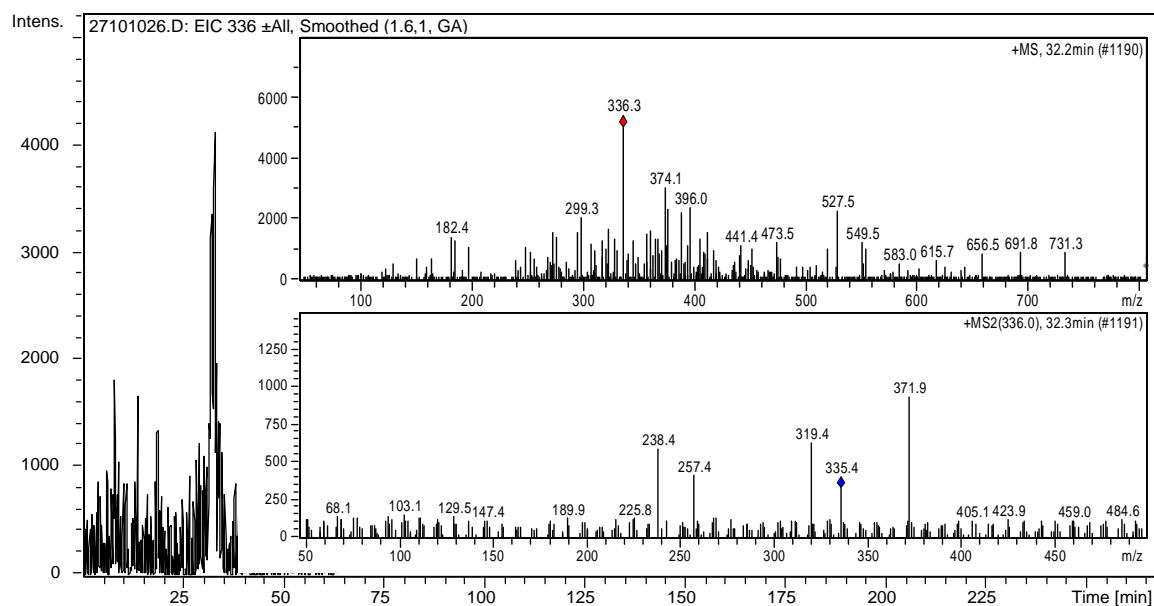


Figure 4.43: EIC of intermediate $m/z = 336$ in a 180 mins sample at a t_R of 32.3 mins. Inset MS and MS/MS spectra. Photocatalysis, [FAM] = 1 mM, 0.1 g TiO_2 /320 mL.

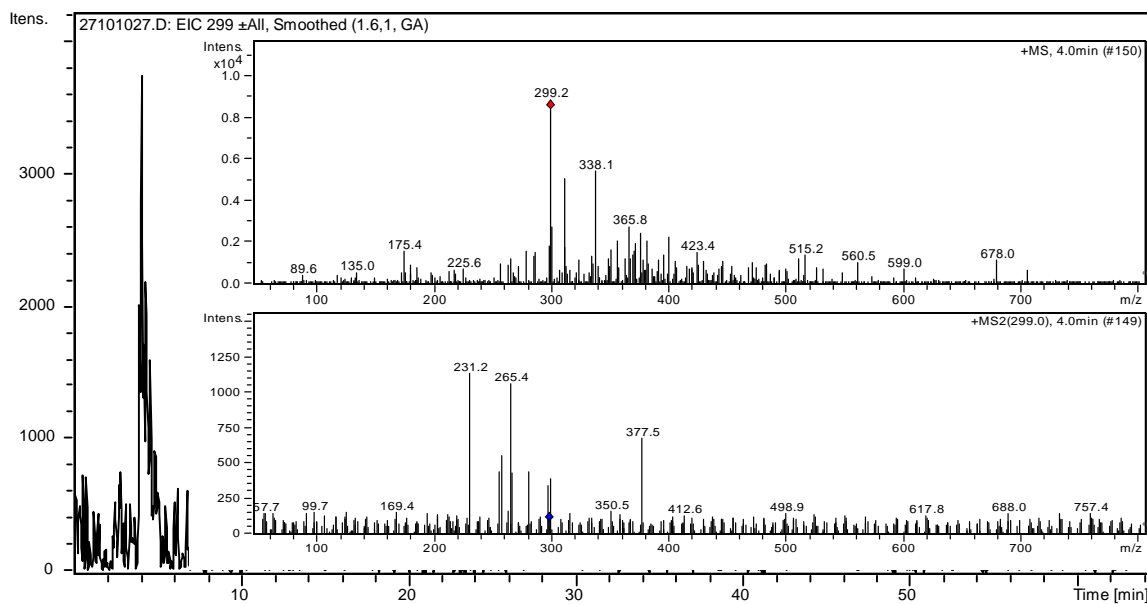


Figure 4.44: EIC of intermediate $m/z = 299$ in a 60 mins sample at a t_R of 4 mins. Inset MS (top) and MS/MS (bottom) spectra. Photocatalysis, [FAM] = 1 mM, 0.1 g TiO_2 /320 mL.

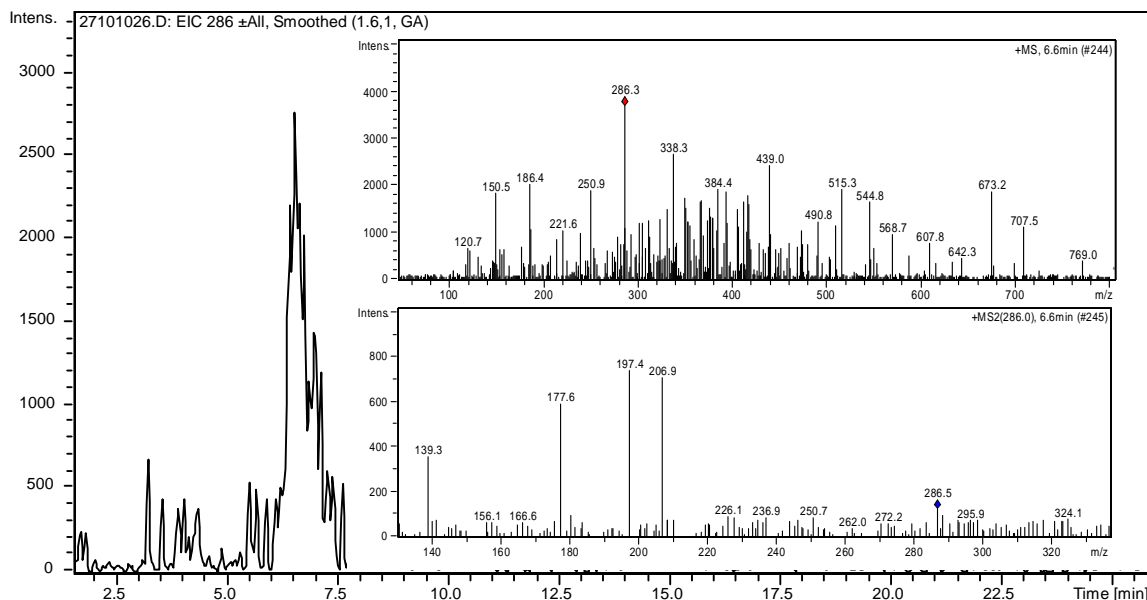


Figure 4.45: EIC of intermediate $m/z = 286$ in a 40 mins sample at a t_R of 6.6 mins. Inset MS (top) and MS/MS (bottom) spectra. Photocatalysis, [FAM] = 1 mM, 0.1 g TiO_2 /320 mL.

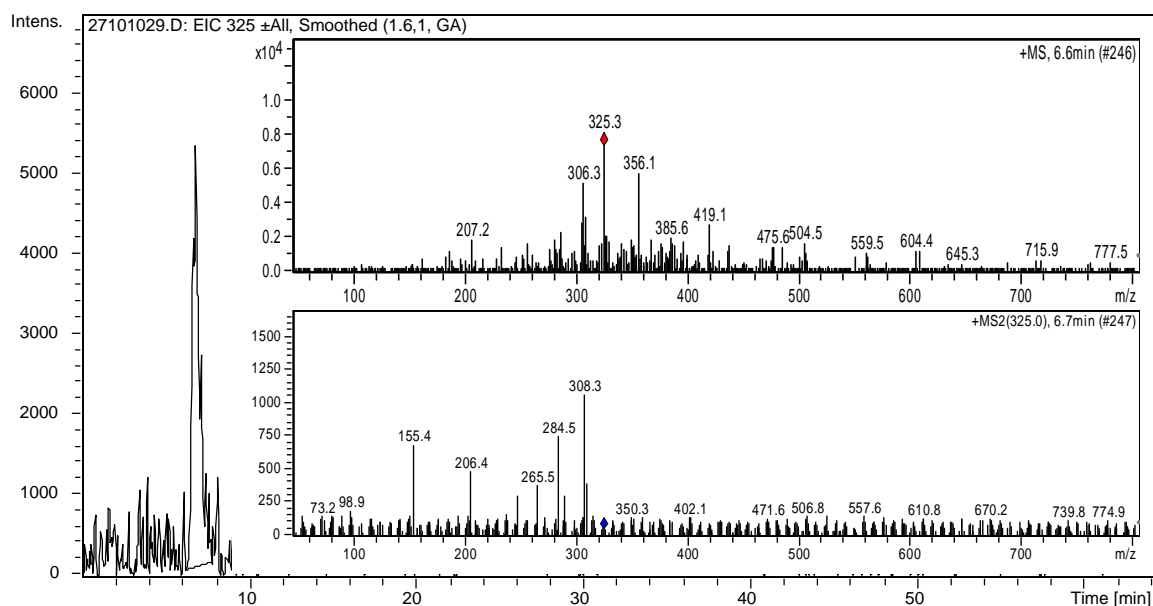


Figure 4.46: EIC of intermediate $m/z = 325$ in a 180 mins sample at a t_R of 6.6 mins. Inset MS and MS/MS spectra. Photocatalysis, [FAM] = 1 mM, 0.1 g TiO_2 /320 mL.

4.2.7 Famotidine Proposed Intermediates Structures Conclusions

A total of 15 intermediates were discovered collectively in LC-MS/MS and DI-MS data for Famotidine. Of these 15, structures for 9 intermediates have been proposed, based on molecular oxidation analysis, careful study of fragments and corroboration with literature data where available. A further two have been analysed and positions of oxidation have been proposed, although structures have not. The remaining 4 intermediates could not be assigned structures. Structures of intermediates which have been proposed can be found in Figure 4.47 along with their molecular mass. A likely degradation pathway is also shown in Figure 4.48. Ion monitoring graphs for all ions monitored in each experiment can be found in the appendices (4A-13 – 4A-16).

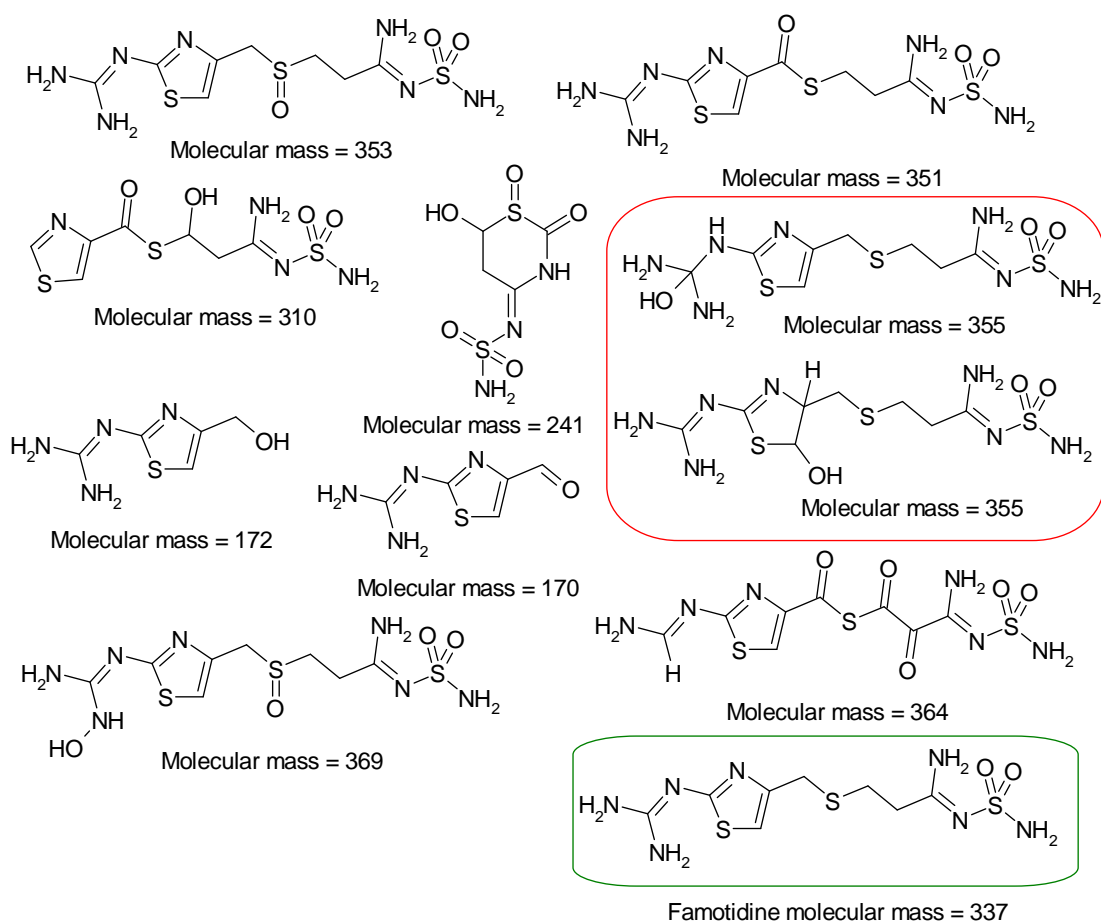


Figure 4.47: Final structures and molecular masses for intermediates proposed for Famotidine, Famotidine's structure is highlighted in the green box.

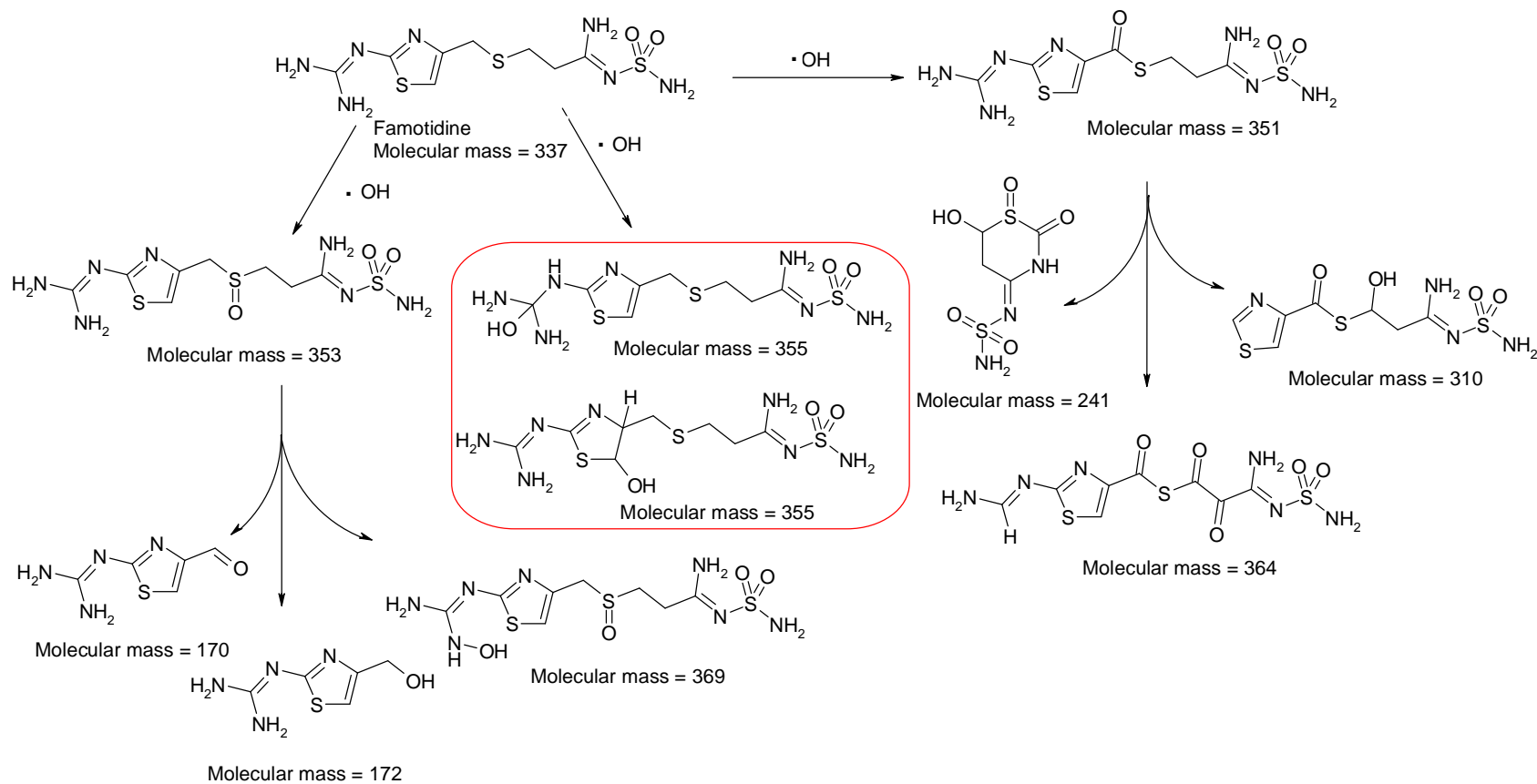


Figure 4.48: Proposed Degradation Pathway for Famotidine and intermediates which were detected via LC-MS/MS and DI-MS.

4.2.8 Direct Infusion Mass Spectrometry Studies: Tamsulosin

Figure 4.49 displays a HPLC-PDA (280 nm) chromatogram of a photocatalytic degradation experiment for Tamsulosin. The appearance of numerous intermediates can be seen clearly in the chromatogram as well as the disappearance of Tamsulosin.

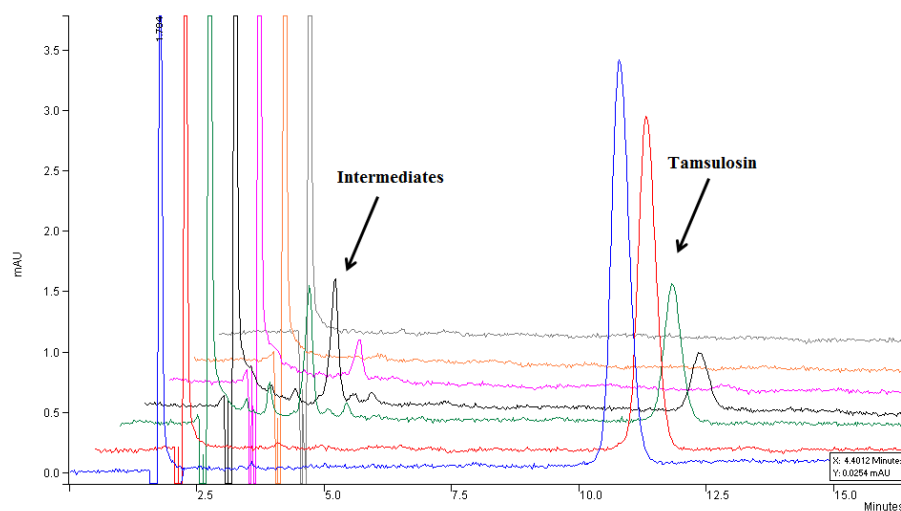


Figure 4.49: Tamsulosin photocatalytic degradation experiment showing intermediate formation over time. 0 Mins, 0 Mins P_{ads} , 5 mins – 40 mins. [TAM] = 20 μ M, TiO_2 = 0.2 g/32 0mL P-25 TiO_2 , 280 nm.

DI-MS analysis of a photocatalytic degradation experiment of Tamsulosin was undertaken and the appearance of various new masses could be seen particularly after only 10 mins of irradiation. Figure 4.50 shows the mass spectrum of the 0 Mins sample from this experiment. The parent ion of Tamsulosin, $[M+H]^+$, is at m/z 409 which can be clearly seen in the spectrum, however it has a molecular weight of 444.48 g/mol. The loss of 35 mass units upon ionisation means that the chlorine from the hydrochloride salt of Tamsulosin is lost. MS/MS analysis of Tamsulosin's parent ion at m/z 409 yielded the daughter ions listed in Table 4.7.

Generation of these daughter ions is mainly via cleavage at a carbon alpha to any sort of heteroatom such as N, S or O. Both $m/z = 228$ and 271 have very high abundances. In $m/z = 228$, the positive charge is stabilised by the secondary carbon and in $m/z = 271$, the positive charge can be considered to be stabilised by the neighbouring olefinic functionality. Structures for the molecular ion of Tamsulosin and its daughter ions can be found in Figure 4.51.

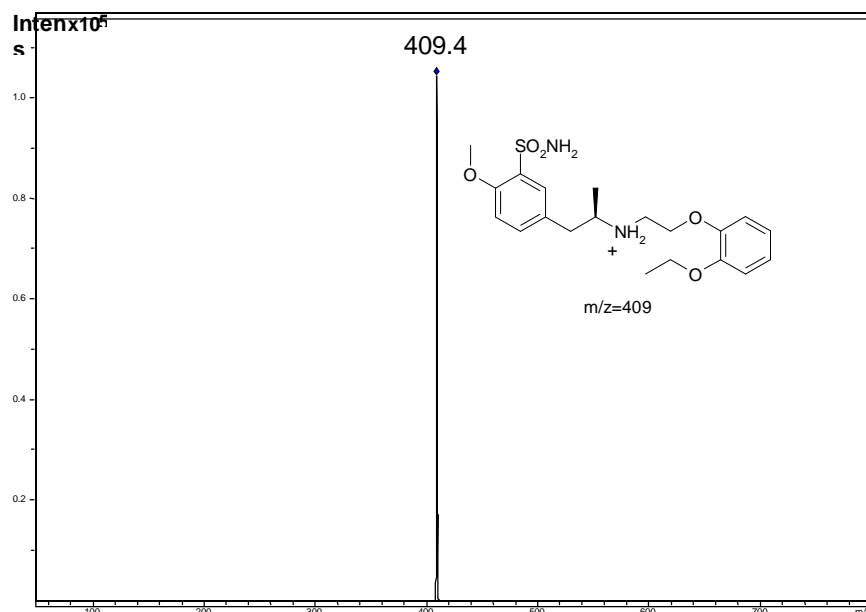


Figure 4.50: DI-MS of a 0 Mins sample of a photocatalytic degradation experiment showing the parent ion of Tamsulosin, $m/z = 409$. Photocatalysis, [TAM] = 0.083 mM, 0.2 g TiO_2 /320 mL.

Parent Ion m/z	Daughter Ion m/z
409	271
	228
	200
	148

Table 4.7: MS/MS analysis of Tamsulosin's parent ion.

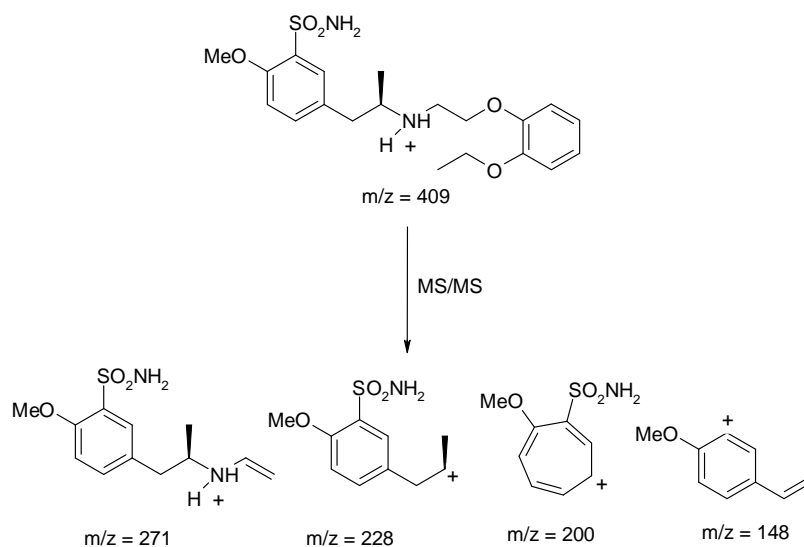


Figure 4.51: Tamsulosin parent ion $m/z = 409$ and its daughter ions $m/z = 271$, $m/z = 228$, $m/z = 200$ and $m/z = 148$.

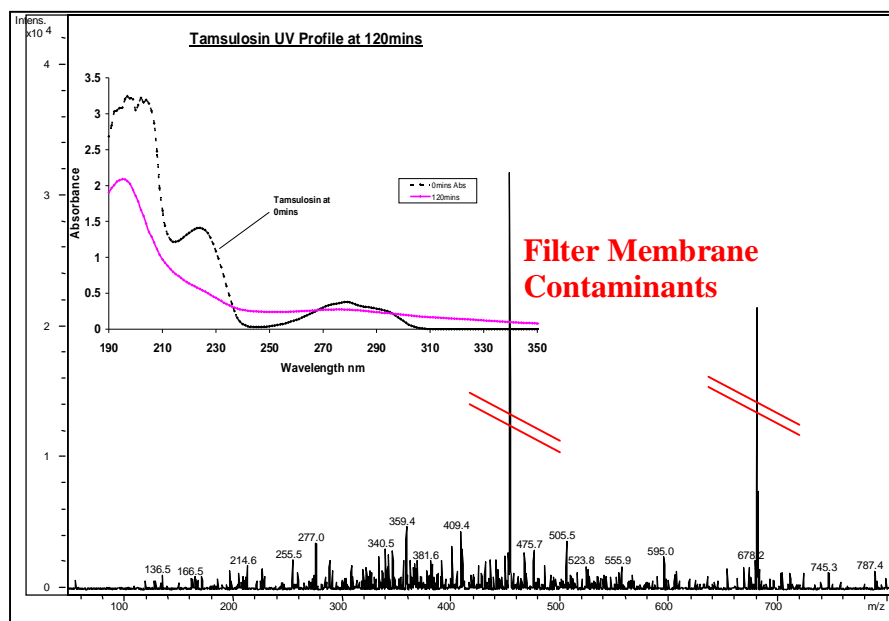


Figure 4.52: DI-MS of a 120 mins sample of a photocatalytic degradation experiment, (inset) UV-vis spectra at 0 mins and 120 mins. Photocatalysis, [TAM] = 0.083 mM, 0.2 g TiO₂/320 mL.

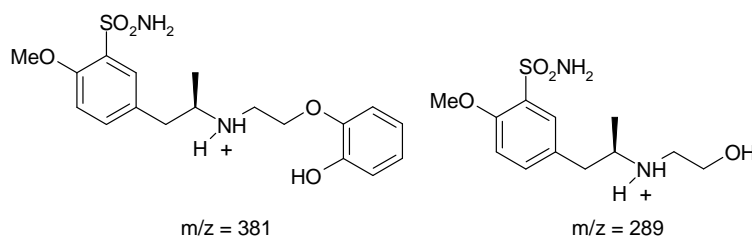


Figure 4.53: Intermediates proposed for $m/z = 381$ and $m/z = 289$ ions found in DI-MS spectra.

Mass spectra were attained for several samples of a photocatalytic degradation experiment of Tamsulosin. A table of various ions found throughout the course of the experiment and their intensities can be found in the appendices 4A-17. Figures 4.53 & 4.54 show structures which have been proposed for some of the consistent ions identified in this table. These are plausible structures based mainly on the formation of hydroxylated species.

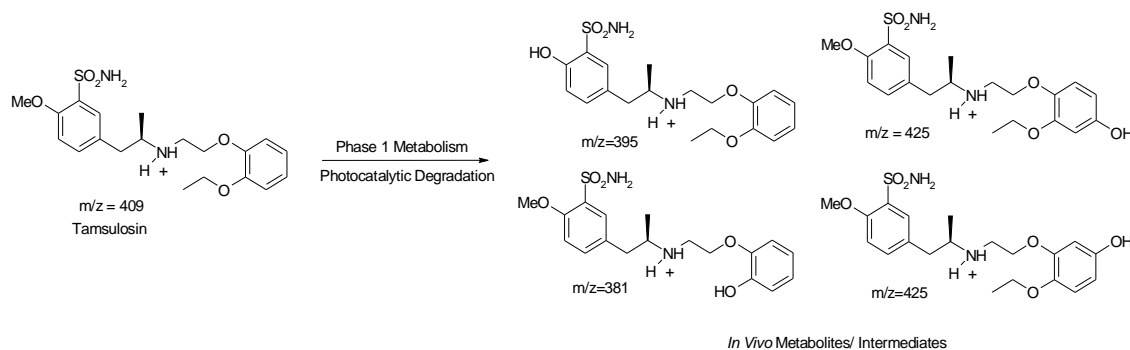


Figure 4.54: Tamsulosin proposed intermediates from its *in vivo* metabolites.²⁰¹

The presence of Nylon membrane contaminants, once again interfered with identification of intermediates. As can be observed in the mass spectrum in Figure 4.52 the two most intense

signals in the mass spectrum are due to these contaminants with $m/z = 453$ and 679 . Excluding these, there is little else of significant intensity in the spectra. There is a weak peak for Tamsulosin ($m/z = 409$) which is the next most intense peak. Figure 4.54 shows *in vivo* metabolites which were identified by Taguchi *et al.* in 1997. Since phase 1 metabolism consists of hydroxylations similar to the action of photocatalysis, it is highly likely that these compounds will be generated in photocatalytic degradation experiments.

4.2.9 Follow-Up Direct Infusion Mass Spectrometry Studies: Tamsulosin

Follow up DI-MS studies were undertaken using cellulose acetate filters and at a higher concentration of 1mM. Some additional ions were observed such as $m/z = 346$, 328 and 285 and are listed in Table 4.8. It was noticed that the MS/MS of these ions all contain the common ion $m/z = 239$. Also, $m/z = 285$ was common to $m/z = 346$ and $m/z = 328$, so these ions may be all from the same intermediate. The ion $m/z = 817$ when fragmented yielded the parent ion for Tamsulosin ($m/z = 409$), so it can dimerise under ESI conditions. Numerous other ions were observed by DI-MS although these ions were not observed by LC-MS/MS. The intermediate ion $m/z = 346$ was found by LC-MS/MS along with its main fragment ion $m/z = 285$, which corroborates with this data. Previously proposed intermediate ions such as $m/z = 381$, 395 and 425 were also confirmed in this study and can be found in the 180 mins mass spectrum shown in Figure 4.55. (Isotopes for Tamsulosin can also be seen, $m/z = 410$ and $m/z = 411$.)

Mass m/z	Fragments m/z	Mass m/z	Fragments m/z
817	<u>409</u> , 271	328	<u>285</u> , 271, 239
447	429, 363, 318, 222, 137	328	285, <u>272</u> , 239, 176
447	418, 254	289	271, <u>228</u> , 200
431	414, <u>293</u> , 202	285	271, 257, <u>239</u> , 227, 211, 196, 183, 148
425	408, 287, <u>271</u> , 244, 228, 216, 200, 148	285	270, 257, <u>239</u> , 211, 179
425	408, 396, 287, <u>271</u> , 260, 244, 228, 200, 148	257	<u>239</u> , 229, 214, 197, 183
425	<u>408</u> , 360, 287, 271, 228, 200	239	224, <u>211</u> , 196, 183, 179, 172
425	408, 360, 287, 271, 244, 228, 208, 200, 183, 151	185	153
394	<u>375</u> , 322, 220, 195, 163, 149	409	<u>271</u> , 228, 200, 148, 392
394	376, 349, <u>327</u> , 257, 220, 197, 169, 153	271	<u>228</u> , 200, 148
346	<u>285</u> , 239, 165, 142	228	<u>200</u> , 148, 117
346	<u>285</u> , 224, 209, 165	200	<u>169</u> , 120, 104, 92
346	294, <u>285</u> , 257, 239, 211, 165, 137	148	133, 117, <u>91</u>
330	240, 175, <u>149</u> , 121		

Table 4.8: Table of masses found in follow-up DI-MS studies and their fragments. (DI-MS/MS). Ions in bold and underlined denote the base peak found in that mass spectrum. In grey are Tamsulosin's parent ion and fragments found in this study.

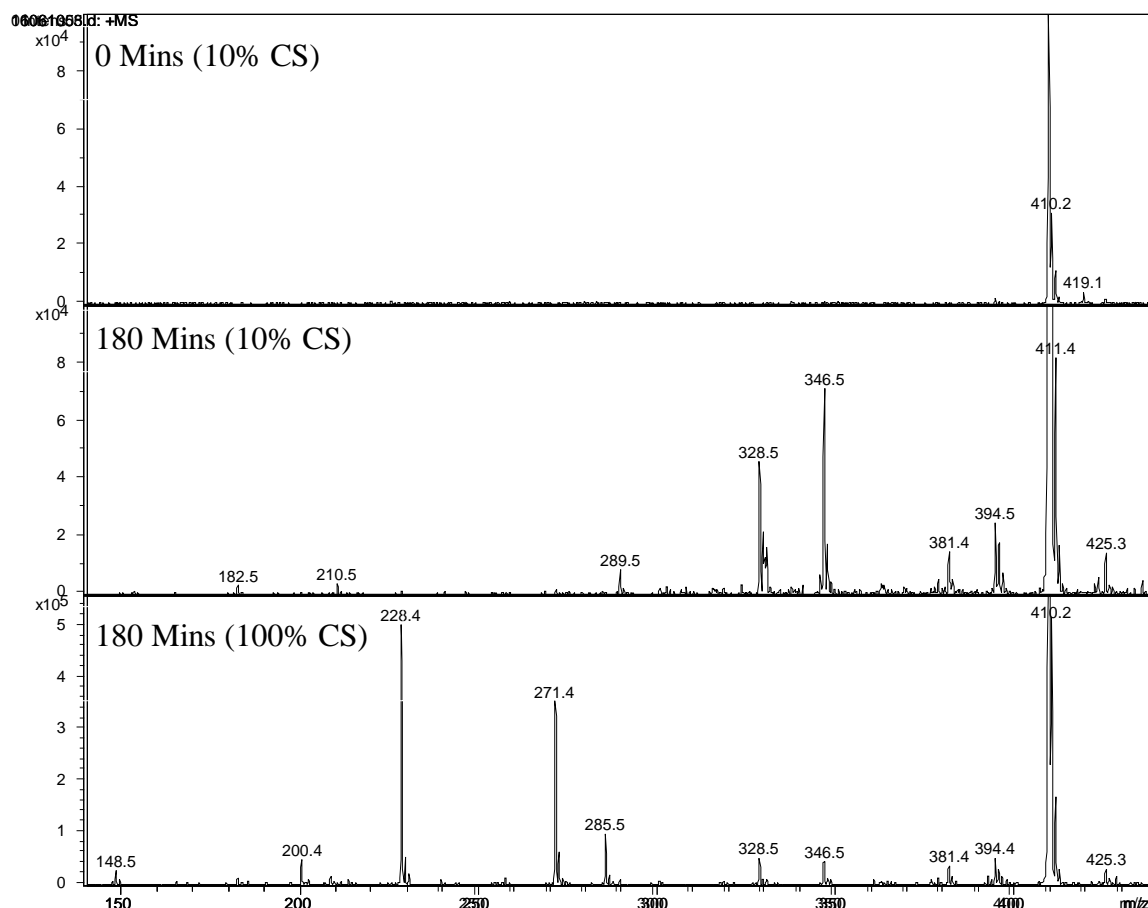


Figure 4.55: Tamsulosin direct infusion mass spectra at 0 Mins (10% CS), 180 Mins (10% CS), and 180 Mins (100% CS). Photocatalysis [TAM] = 1 mM, 0.2 g/320 mL.

4.2.10 LC-MS/MS Studies and Intermediate Analysis: Tamsulosin

LC-MS/MS analysis of four Tamsulosin photodegradation experiments were performed. Firstly, the optimized photocatalysis with 0.2 g/320 mL TiO_2 and 0.083mM Tamsulosin. An additional photocatalytic experiment was performed at a much higher concentration of 1 mM Tamsulosin and 0.2 g/320 mL TiO_2 . This heightened concentration was performed in order to see intermediates at much lower concentrations. Photolysis experiments with both Quartz and Pyrex were also analysed using LC-MS/MS at the optimum concentration of 0.083 mM Tamsulosin. Two tables 4.9 and 4.10 are presented showing all of the ions found in each chromatogram. Beside each ion in the table is the retention time that ion appears at in the chromatogram. Table 4.11 and 4.12 summarise all intermediate ions found in these experiments including their fragments, retention times, Mol. Wt. and calculated Log P values. Following these tables are individual EIC chromatograms for each significant intermediate ion found including their mass spectra and the MS/MS for that ion and the proposed intermediate structure.

	Photocat (0.083mM)	Photocat (1mM)
0Mins	425 (19.1, 12.8), 409 (37.4), 289 (2.3)	481 (3.4), 473 (2.9), 425 (5.9, 10.2, 11.8, 16.8), 409 (30.5), 381 (8.8), 346 (25.5), 289 (2.2)
0Min P.	425 (19.6, 13.9), 409 (38.7), 381 (10.2), 289 (2.3),	425 (6.3, 11.8, 16.3), 409 (29.6), 289 (2.3)
5Mins	441 (15.5), 425 (11.6, 13.4, 18.6), 423 (5.3, 17.9), 409 (38.2), 400 (7.8), 395 (27.3), 381 (10), 289 (2.3),	481 (3.4), 479 (13.9), 441 (2.6, 13.9), 425 (10.1, 11.5, 16, 21.9), 423 (4.8, 15.6, 25.7), 413 (5.7), 409 (30.3), 400 (7.3), 395 (23.5), 381 (8.7), 289 (2.3)
10Mins	441 (15.5), 425 (11.4, 13.5, 18.7), 423 (5, 17.6, 29.9), 409 (38.4), 400 (7.9), 396 (14, 15.3), 395 (27.5), 381 (9.8), 346 (33.6), 289 (2.3), ,	481 (3.3), 479 (13.9), 441 (13.6), 425 (10, 11.4, 16.1, 21.9), 423 (4.8, 15.4, 25.6) 413 (5.8), 409 (29.4), 400 (7.4), 395 (23.2), 381 (8.7), 355 (5.9), 346 (17.6), 289 (2.3),
20Mins	425 (13.1, 18.7), 423 (5.1, 17.6, 30.8), 413 (6.2), 409 (38.5), 395 (27.4), 381 (9.8), 289 (2.3),	479 (3.3, 13.7), 459 (4.1), 441 (2.7, 13.9), 425 (9.7, 11.4, 15.8, 21.3), 423 (4.8, 15.3, 25.3), 413 (5.7), 409 (29.3), 400 (7.3), 395 (23), 381 (8.7), 355 (5.9), 346 (17.4), 289 (2.3)
30Mins	441 (2.7), 425 (11, 13, 18.6), 423 (5.2, 17.6, 30.3) 409 (38.8), 395 (27.5), 381 (9.7), 318 (23.1), 289 (2.3)	479 (3.3pnd), 441 (2.6, 13.1), 425 (9.6, 10.8, 15, 20.5), 423 (4.6, 14.6, 24.3), 414 (3.2), 413 (5.3), 409 (28.2), 400 (7.2), 395 (22.1), 381 (8.3), 355 (5.7), 346 (13.9), 328 (17.1), 289 (2.3),
40Mins	479 (3.3), 441 (2.7), 425 (11.3, 12.9, 18.6), 423 (17.6, 30.7), 409 (38.9), 395 (27.6), 381 (9.5), 346 (32.3), 289 (2.3),	479 (3.3), 473 (3.5), 441 (14.7, 15.1), 425 (10.9, 12.5, 17.6), 423 (4.9, 17, 28.4), 414 (3.4), 409 (32.9), 400 (7.6), 395 (26.2), 381 (9.4), 346 (21.1), 328 (21.4), 289 (2.3)
60Mins	441 (2.8), 425 (11.1, 12.9, 18.3, 25), 423 (17.3, 30.6), 409 (38.9), 395 (27.6), 381 (9.8), 289 (2.3),	481 (6.2), 479 (3.3), 473 (3.5), 425 (11, 12.7, 17.9), 423 (17.2), 414 (3.5) 409 (33.8), 400 (7.7), 395 (26.5), 381 (9.6), 346 (29.6), 328 (28.7), 289 (2.3)
120Mins	425 (11, 12.7, 18.7, 25.2), 423 (17.6), 409 (39), 395 (27.9), 381 (9.7), 346 (21.6), 318 (22.8), 289 (2.3),	481 (3.9), 479 (pnd), 473 (3.8), 441 (5.8), 425 (12.9, 11.1, 18), 423 (29.4, 17.1, 4.1), 414 (3.4), 409 (34.1), 400 (5.1, 7.8), 395 (26.5), 381 (9.6), 346 (43.3), 289 (2.3)
180Mins	425 (11.1, 12.9, 18.9, 24.9), 423 (17.8), 409 (38.1), 395 (27.4), 381 (9.7), 318 (23.1), 289 (2.3)	481 (4), 425 (17.9, 12.7, 10.9), 423 (17.2), 414 (3.4), 409 (34.5), 400 (5.4), 395 (26.9), 381 (9.7), 346 (pnd), 328 (30.7), 318 (22.3), 289 (2.3)

Table 4.9: Table of Ions present in the LC-MS/MS chromatographic runs of two photocatalytic experiments at 0.083 mM and 1 mM. In brackets after each ion is the retention time (in minutes) at which this ion was found in each EIC. (pnd= present however not a dominant ion)

	Photolysis (Quartz)	Photolysis (Pyrex)
0Mins	409 (37.3), 381 (10), 289 (2.3)	409 (34.7), 381 (9.1), 289 (2.3)
0Min P.	N/A	N/A
5Mins	479 (13.4), 441 (15.6, 13.7), 414 (7.9), 409 (38.9), 400 (2), 396 (3.2, 10.4), 395 (27.6), 381 (10.2), 380 (3.5, 5.4), 378 (4.2, 8.1, 22.9), 368 (11.7), 362 (6.1), 346 (4.8) , 336 (18.2), 318 (9.9), 289 (2.3),	479 (15.5), 441 (15.9), 414 (8), 409 (36.9), 396 (3.2, 10.6), 395 (27.1), 381 (9.8), 378 (4.1), 362 (6.1), 348 (4), 346 (45.8), 289 (2.3),
10Mins	479 (13.4), 441 (15.7, 18.7), 414 (3.8), 409 (39.6), 400 (1.9), 396 (5.6, 10.5), 395 (27.8), 380 (3.4, 7.4, 9.7), 378 (4.2, 8, 15.9, 22.9) 368 (11.8), 362 (6.3), 336 (2.5, 18), 346 (45.2) , 318 (9.9), 289 (2.3),	479 (13), 441 (15.3), 425 (12.9, 18), 423 (17.4), 414 (7.9), 409 (37.5), 400 (2), 396 (3.2, 10.1), 395 (27.6), 381 (9.7), 378 (4.2), 368 (11.4), 362 (6.1), 348 (3.9), 346 (44.6), 336 (18.1), 318 (9.9), 289 (2.3),
20Mins	409 (36.4), 395 (26.6), 380 (2.8, 5.6), 378 (4.1), 368 (11), 348 (3.9), 346 (42.7), 289 (2.3)	441 (13.6, 15.5), 425 (18.1, 25.9), 423 (17.3), 414 (8), 409 (37.9), 400 (1.9), 396 (3.2, 10.4), 395 (27.9), 381 (9.8), 380 (3.6), 378 (4.3, 8.2, 16.4, 22.8) 368 (11.4), 362 (6.2), 348 (4), 346 (45.2), 336 (18.1), 318 (10), 289 (2.3)
30Mins	414 (2.1), 396 (2.5, 3.4, 8.4), 380 (5.9, 9.8), 378 (4.1),	479 (17.9, 21.1, 30.4), 441 (18.5, 26.2), 423 (23.9), 414 (9.4), 409 (54.7), 400 (2), 396 (3.4, 13.2), 395 (37.4), 381 (12.5), 380 (3.9), 378 (4.9, 10.3, 21.6, 31), 368 (15.4), 318 (12.4), 348 (4.5), 336 (6.8, 24.6), 289 (2.4),
40Mins	380 (9.4), 378 (4.1)	479 (18.1), 441 (17.8, 20.4, 25.4, 28.9), 414 (9.5), 409 (53.9), 400 (2), 396 (3.5, 13) 395 (36.9), 381 (12.1), 378 (4.8, 10, 21.7, 30.3), 368 (15.4), 348 (4.5), 346 (60.8), 336 (6.5, 24), 318 (12.1), 289 (2.4),
60Mins	396 (2.5), 378 (4),	479 (18.9, 21.9), 441 (22.2, 27.2), 414 (5.9, 9.5, 14.4), 409 (60.6), 400 (2), 396 (3.5, 13.8), 395 (40.4), 381 (12.8), 380 (3.9, 6.8), 378 (4.8, 10.2, 22.1, 33.1), 348 (4.5), 346 (67.8), 336 (25.3), 318 (12.7), 289 (2.4),
120Mins	378 (4)	479 (20.1, 24, 29.3), 441 (21.2, 23.9, 28.7, 34), 413 (7.2), 409 (64.6), 400 (2.1), 395 (43), 378 (5.1, 10.6, 23.5, 35), 368 (17), 348 (4.8), 346 (67.7), 289 (2.4), 318 (13.9), 336 (2.7, 27.3)
180Mins	No significant ions present	441 (15.1, 19.3, 21.6, 29.4), 409 (40), 400 (1.9), 396 (2.8, 14.3), 395 (28.1), 380 (3.6), 378 (4.2, 8.2, 15.9, 23.6), 348 (34.2), 346 (45.9), 336 (2.4, 18.8), 318 (10), 289 (2.4),

Table 4.10: Table of ions present in the LC-MS/MS chromatographic runs of two photolysis experiments at 0.083 mM with Quartz and Pyrex. In brackets after each ion is the retention time at which this ion was found in each EIC. (pnd= present however not a dominant ion)

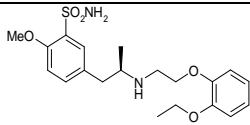
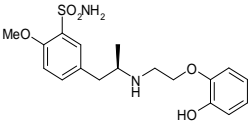
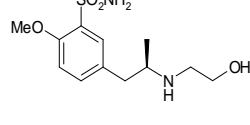
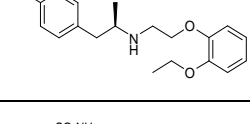
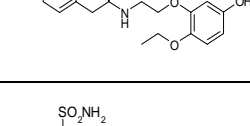
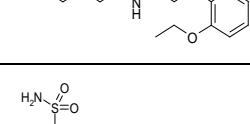
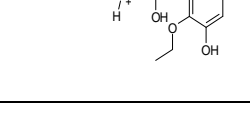
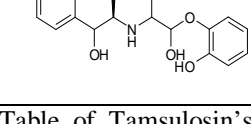
Name	Structure	Mass m/z	Daughter Ions m/z	Molecular Weight g/mol	<i>t_R</i> mins	cLog P
Tamsulosin		409	271, 228, 200, 148	444.45 (hydrochloride salt)	37	3.05
P381		381	271, 228, 200	380	10	1.88
P289		289	271, 228, 199	288	2.4	0.15
P395		395	257, 214, 197, 182	394	22	2.72
P425		425	408, 271, 228, 200, 148	424	Numerous	2.53(m-) 2.59(o-)
P425		425	408, 264, 245, 228	424	20.5	2.17
P473		473	427, 289, 271, 228,	472	3.6	1.42
P352		352	334, 238	351	4.8	-0.09

Table 4.11: Table of Tamsulosin's confirmed intermediates (degradation products), their fragments, retention times, molecular weight and calculated Log P values.^{197,198}

Name	Structure	Mass m/z	Daughter Ions m/z	Molecular Weight g/mol	<i>t_R</i> mins	cLog P
P346		346	285, 257	345	45.2	3.72
P423		423	405, 377, 285, 228	422	4.8	2.79
P423		423	381, 313, 271, 228	422	15.3	2.69
P423		423	377, 285	422	23.3	2.53
P441		441	395, 271, 228, 200	440	Numerous	2.37-2.41
P275		275	257, 214, 197	274	2.2	1.01
P378		378	360, 242, 161	377	Numerous	0.5
P415		415	271, 228	414	2.8	0.24
P413		413	271, 228	412	5.7	1.49
P419		419	271, 229	418	3.7	-0.24

Table 4.12: Table of Tamsulosin's confirmed intermediates (degradation products), their fragments, retention times, molecular weight and calculated Log P values (continued).^{197,198}

Intermediate $m/z = 381$

The intermediate $m/z = 381$ appeared at a retention time of 10 mins, although the retention time did tend to vary slightly between 9.6 mins and as high as 12 mins. It was also found in every photo-degradation experiment analysed and generally appeared in the first few samples (5 mins onwards) taken for each experiment. From this we can conclude that it is one of the first breakdown products from Tamsulosin. This intermediate was also proposed in previous preliminary studies where it was found in DI-mass spectra. It was also found in follow-up studies where a higher concentration of Tamsulosin was used. The fragment ions for this particular intermediate are identical to those for Tamsulosin, so from this we can deduce that oxidation takes place on the ethoxybenzene ring with loss of the ethoxy group by attack of a hydroxyl radical. This sort of hydroxyl radical attack incurs a break in the aromaticity of the phenyl ring, which is restored with the subsequent loss of the ethoxy group. The proposed structure and daughter ions are shown in Figure 4.57.

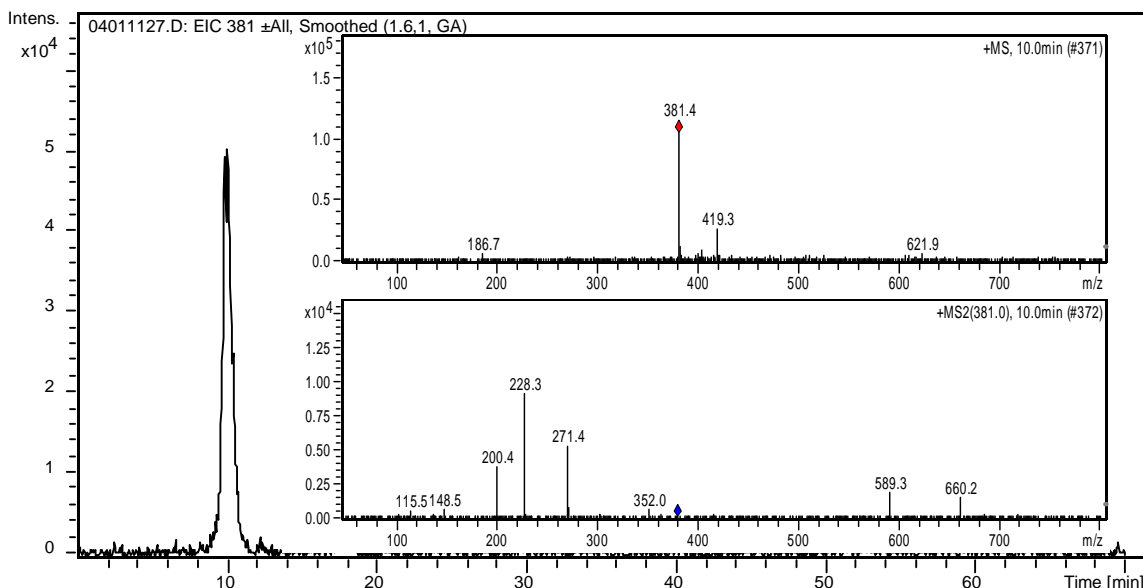


Figure 4.56: EIC of intermediate $m/z = 381$ in a 5 mins sample at a t_R of 10 mins. Inset MS and MS/MS spectra. Photocatalysis, [TAM] = 0.083 mM, 0.2 g TiO_2 /320 mL.

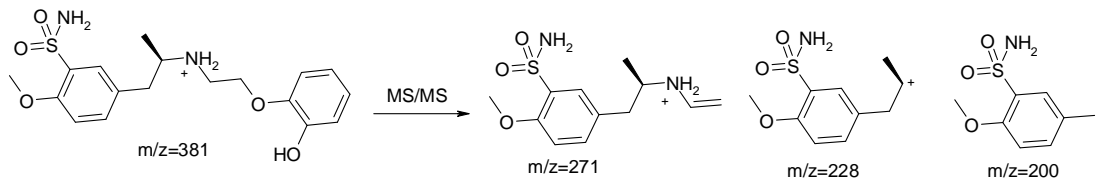


Figure 4.57: Structure of Intermediate $m/z = 381$ and its daughter ions $m/z = 271$, 228 and 200.

Intermediate $m/z = 289$

The intermediate $m/z = 289$ had one of the highest abundances in DI-MS studies. In follow-up studies with higher concentrations of Tamsulosin it also appeared and was also observed in all experiments analysed by LC-MS/MS. It was generally the first eluted compound at 2.3 mins

(Figure 4.58), and was found to be a persistent intermediate, although in photolysis with Quartz it was not observed after 20 mins. Since this intermediate showed identical fragments to Tamsulosin we can deduce that oxidation occurs on the carbon β to the secondary amine. The proposed structure is shown in Figure 4.59 along with its proposed daughter ions.

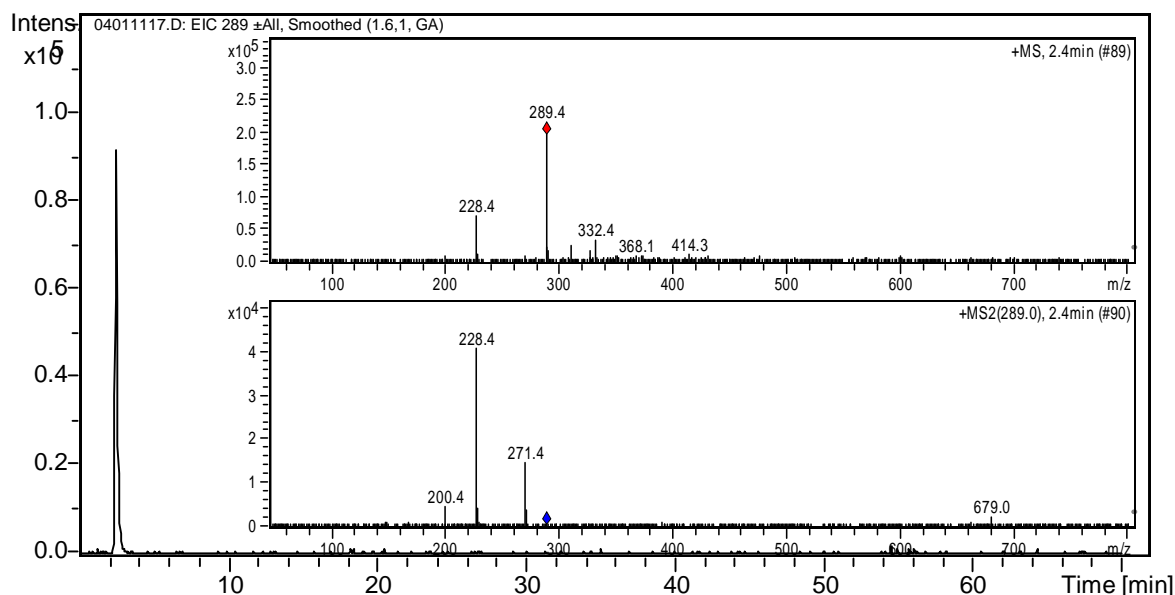


Figure 4.58: EIC of intermediate $m/z = 289$ in a 10 mins sample at a t_R of 2.4 mins. Inset MS and MS/MS spectra. Photolysis Pyrex, [TAM] = 0.083 mM.

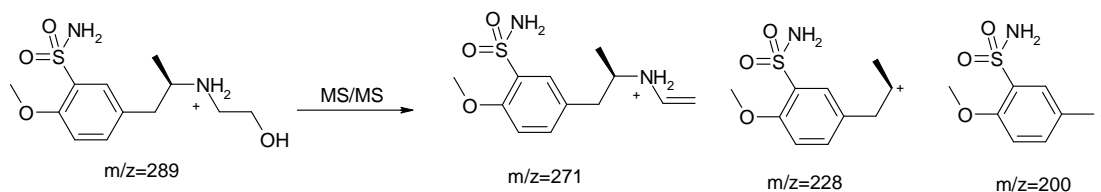


Figure 4.59: Structure of Intermediate $m/z = 289$ and its daughter ions $m/z = 271$, 228 and 200 .

Intermediate $m/z = 395$

The ion $m/z = 395$ was also found in all of the photo-degradation experiments and in preliminary work with DI-MS studies. This intermediate was eluted before Tamsulosin generally at a t_R of 27 mins, although for the higher concentration photocatalytic experiment it was eluted earlier at 22 min (Tamsulosin was also eluted earlier in this case). The daughter fragments for this intermediate differ from the parent drug Tamsulosin, which would indicate that an oxidation has taken place on the methoxy sulfonamide aromatic ring with the loss of the methoxy group via hydroxyl radical attack. Proposed structures for the daughter ions are shown in Figure 4.61.

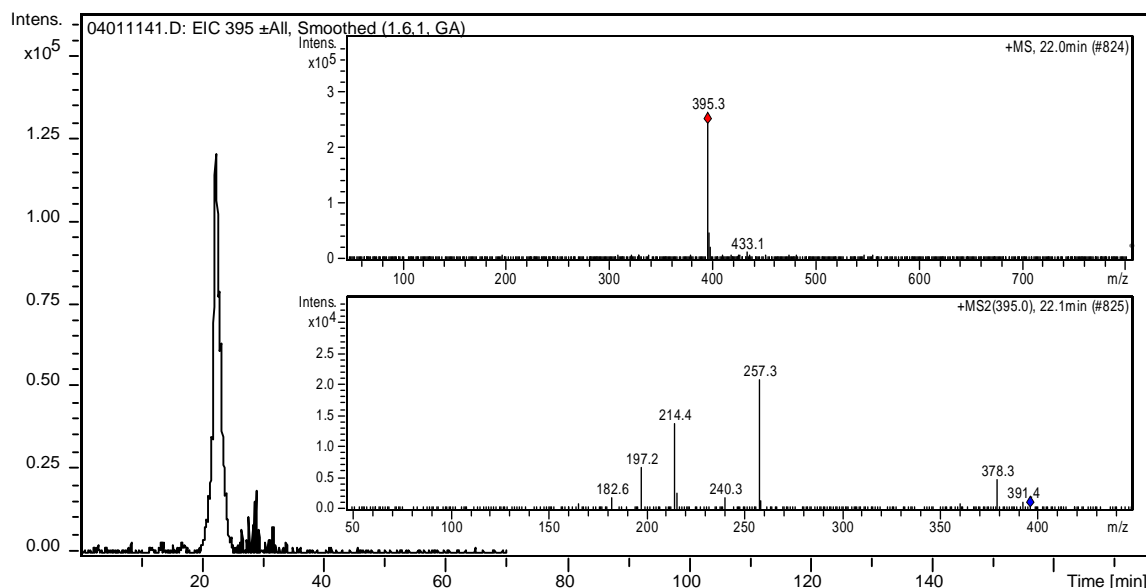


Figure 4.60: EIC of intermediate $m/z = 395$ in a 30 mins sample at a t_R of 22 mins. Inset MS and MS/MS spectra. Photocatalysis, [TAM] = 1 mM, 0.2 g TiO_2 /320 mL.

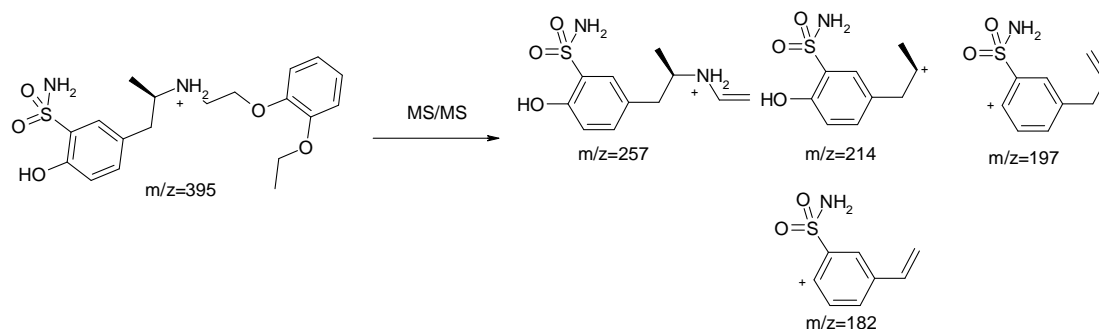


Figure 4.61: Structure of Intermediate $m/z = 395$ and its daughter ions $m/z = 257$, 214, 197 and 182.

Intermediate $m/z = 425$

The ion $m/z = 425$ is composed of the Tamsulosin ion ($m/z = 409$) + 16 amu, which results from the addition of oxygen indicating that an oxidation has taken place. The EIC for 425 contained 4 distinct peaks as shown in Figure 4.62 with another 2 peaks co-eluting with Tamsulosin (their masses were not dominant enough to be identified). Of the other peaks, 3 had identical fragmentation patterns exhibiting the exact fragments of Tamsulosin $m/z = 271$, 228 and 200 with an additional fragment of 408 which we believe is loss of the hydroxyl group (gained via photocatalytic oxidation). The final 4th intermediate had only one of the fragments for Tamsulosin, $m/z = 228$, and other fragments of $m/z = 245$, 264 and 408.

Single oxidation can take place on the ethoxy phenyl ring (catechol ring) or alpha to the amine. In the case of oxidation of the catechol ring, there are four possible sites for oxidation leading to four positional isomers (Figure 4.66). In Figure 4.68 an intermediate resulting from oxidation on

the aliphatic chain adjacent to the secondary amine is shown although without assignment of the other fragments for this intermediate, the exact site of this oxidation cannot be confirmed.

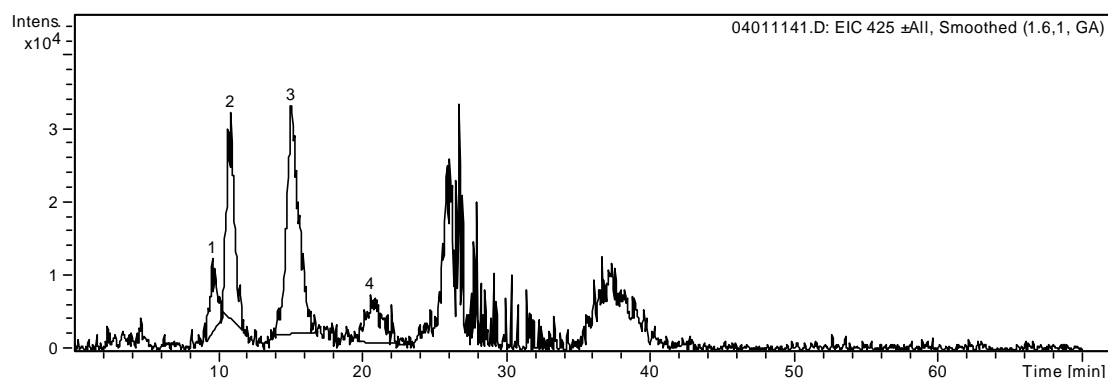


Figure 4.62: EIC chromatogram for $m/z = 425$ showing four peaks and two additional peaks whose ions were not dominant enough in chromatograms to be determined. Photocatalysis, $[TAM] = 1$ mM, 0.2 g $TiO_2/320$ mL.

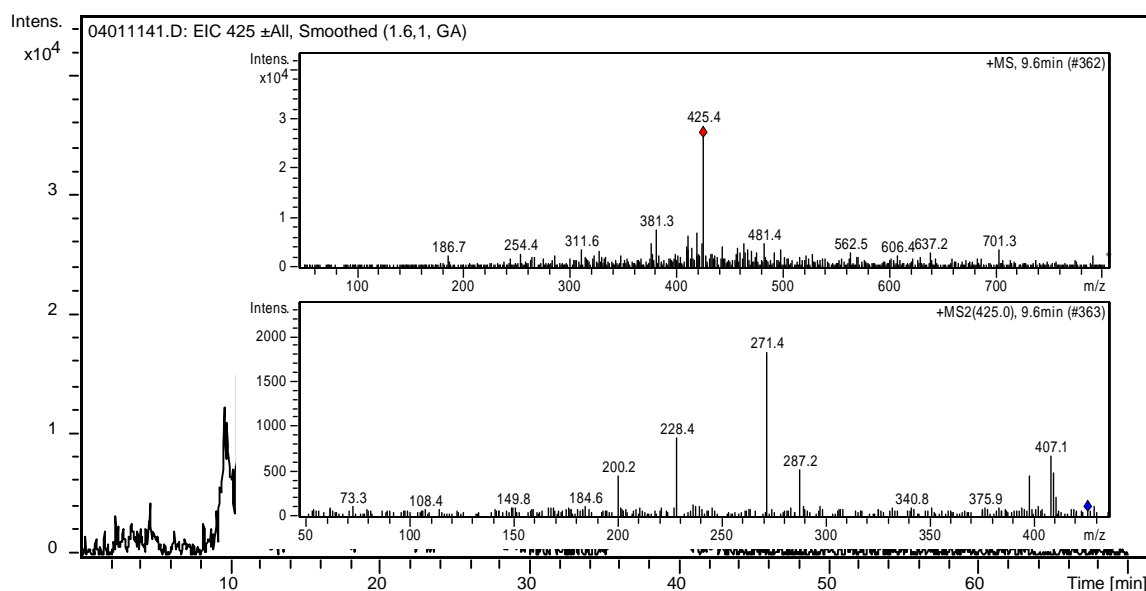


Figure 4.63: EIC of intermediate $m/z = 425$ in a 30 mins sample at a t_R of 9.6 mins. Inset MS and MS/MS spectra. Photocatalysis, $[TAM] = 1$ mM, 0.2 g $TiO_2/320$ mL.

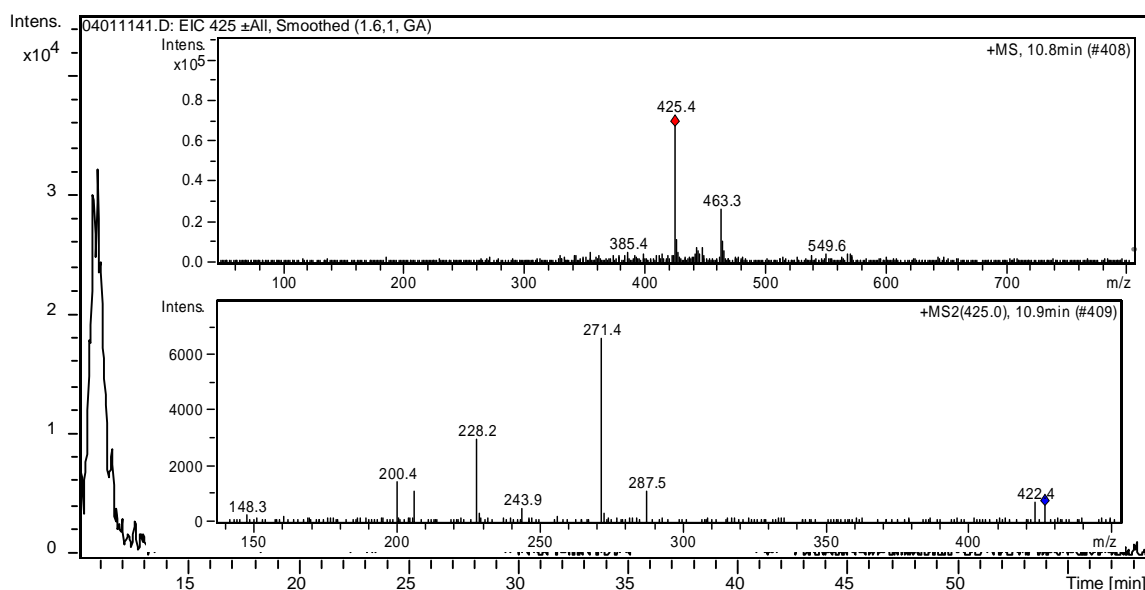


Figure 4.64: EIC of intermediate $m/z = 425$ in a 30 mins sample at a t_R of 10.9 mins. Inset MS and MS/MS spectra. Photocatalysis, [TAM] = 1 mM, 0.2 g TiO_2 /320 mL.

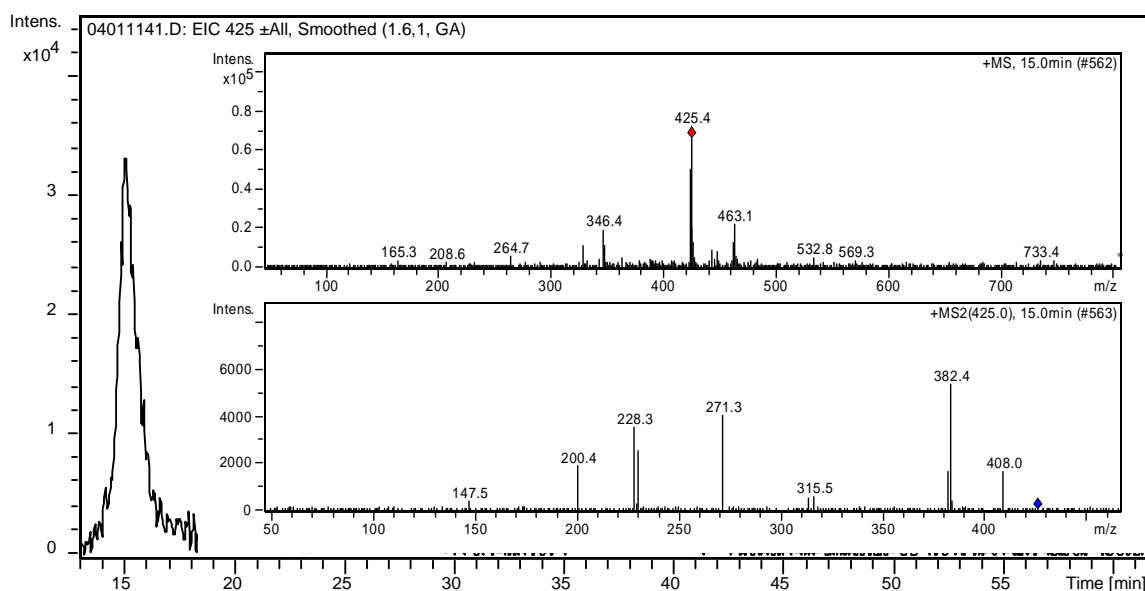


Figure 4.65: EIC of intermediate $m/z = 425$ in a 30 mins sample at a t_R of 15 mins. Inset MS and MS/MS spectra. Photocatalysis, [TAM] = 1 mM, 0.2 g TiO_2 /320 mL.

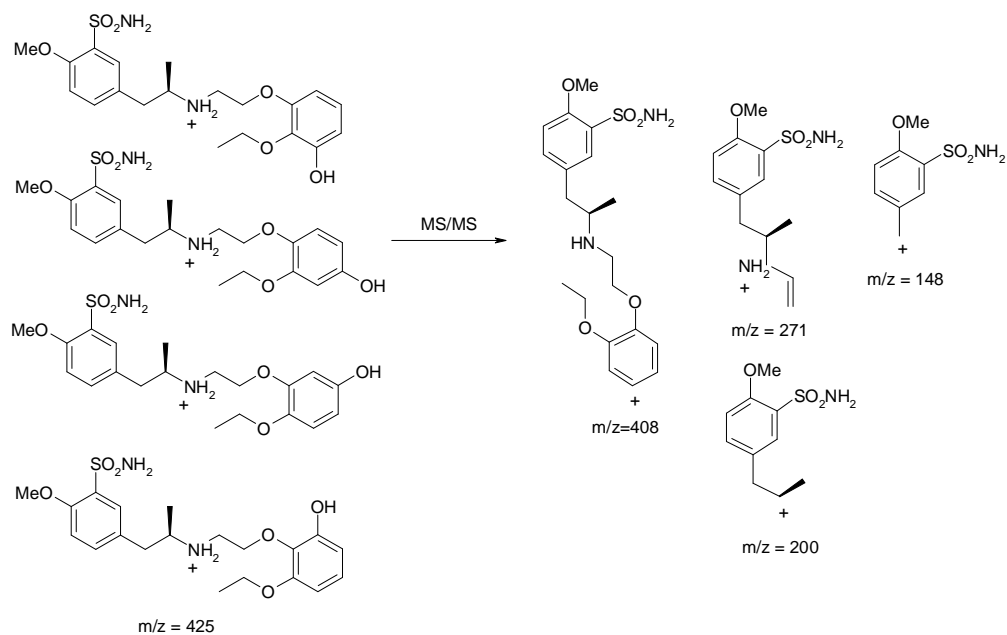


Figure 4.66: Structures of possible isomers for $m/z = 425$, and the common fragments found for each: $m/z = 408, 271, 228, 200$.

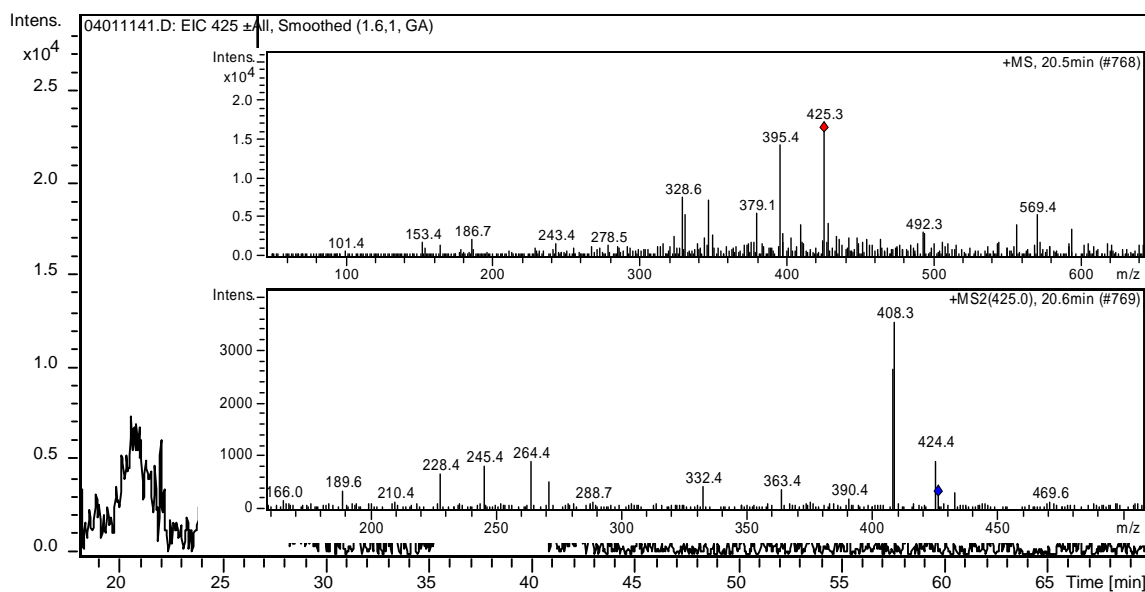


Figure 4.67: EIC of intermediate $m/z = 425$ in a 30 mins sample at a t_R of 20.5 mins. Inset MS and MS/MS spectra Photocatalysis, [TAM] = 1 mM, 0.2 g TiO_2 /320 mL.

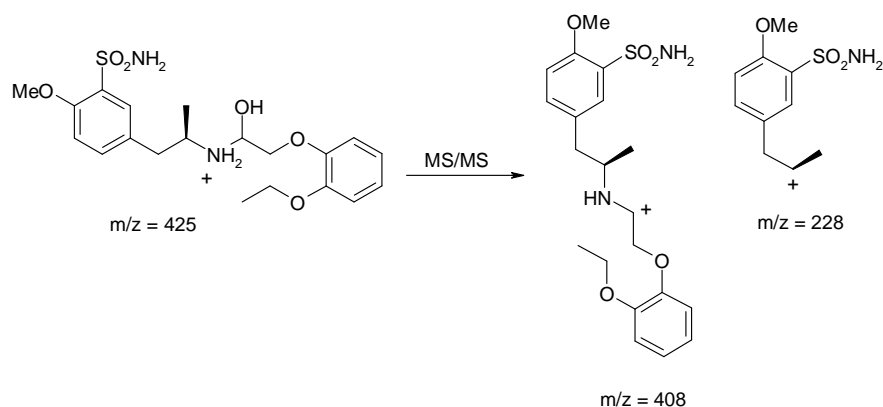


Figure 4.68: Structure proposed for $m/z = 425$ and proposed structure for two of its fragments $m/z = 408$ and 228.

Intermediate $m/z = 441$

EICs for the intermediate $m/z = 441$ contained either one or more peaks depending on the photo-degradation experiment analysed. Of the peaks attained, only two appeared in a large enough abundance that would allow identification. A m/z of 441 is composed of the Tamsulosin ion ($m/z = 409$) + 32amu, which indicates two sites of oxidation. As was observed for $m/z = 425$, at least 4 isomers are possible when oxidation occurs on the catechol ring. This number of isomers increases to six when a second oxidation is possible. In addition, oxidation of the aliphatic chain is also possible which would lead to further isomers for $m/z = 441$. The total number of isomers possible as a result of oxidation on the catechol ring are shown in Figure 4.69. Figure 4.72 shows proposed structures for $m/z = 441$ and its fragments.

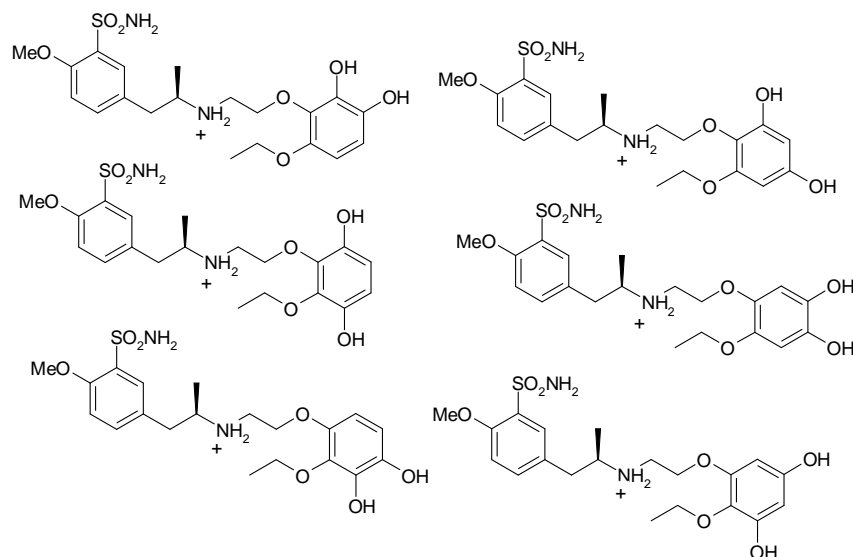


Figure 4.69: Possible isomers for $m/z = 441$, where two oxidations occur on the catechol ring.

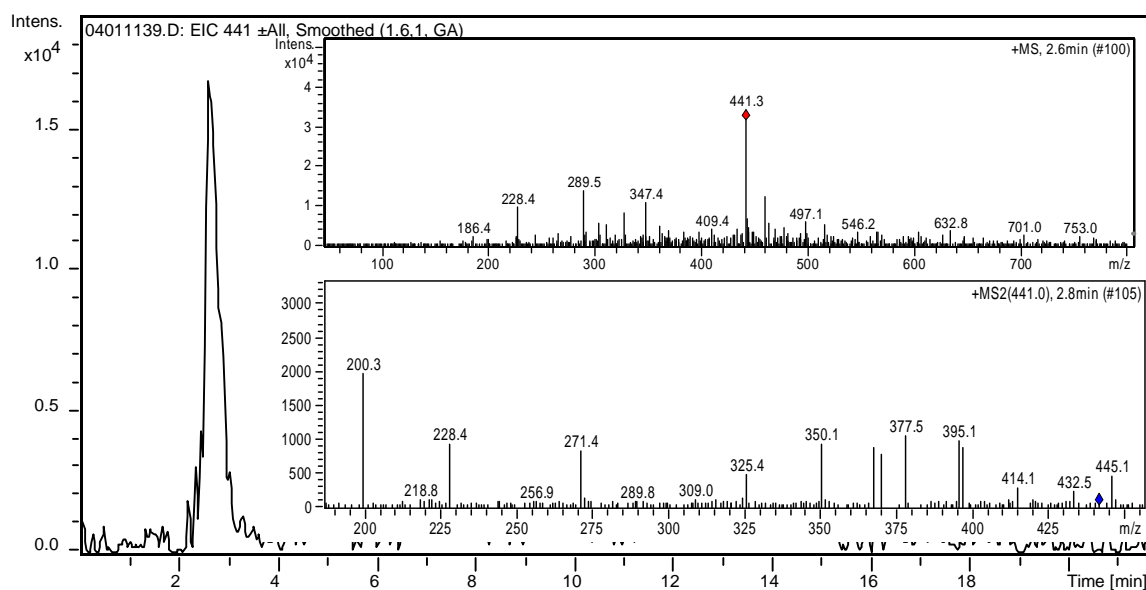


Figure 4.70: EIC of intermediate $m/z = 441$ in a 10 min sample at a t_R of 2.7 min. Inset MS and MS/MS spectra. Photocatalysis, [TAM] = 1 mM, 0.2 g TiO_2 /320 mL.

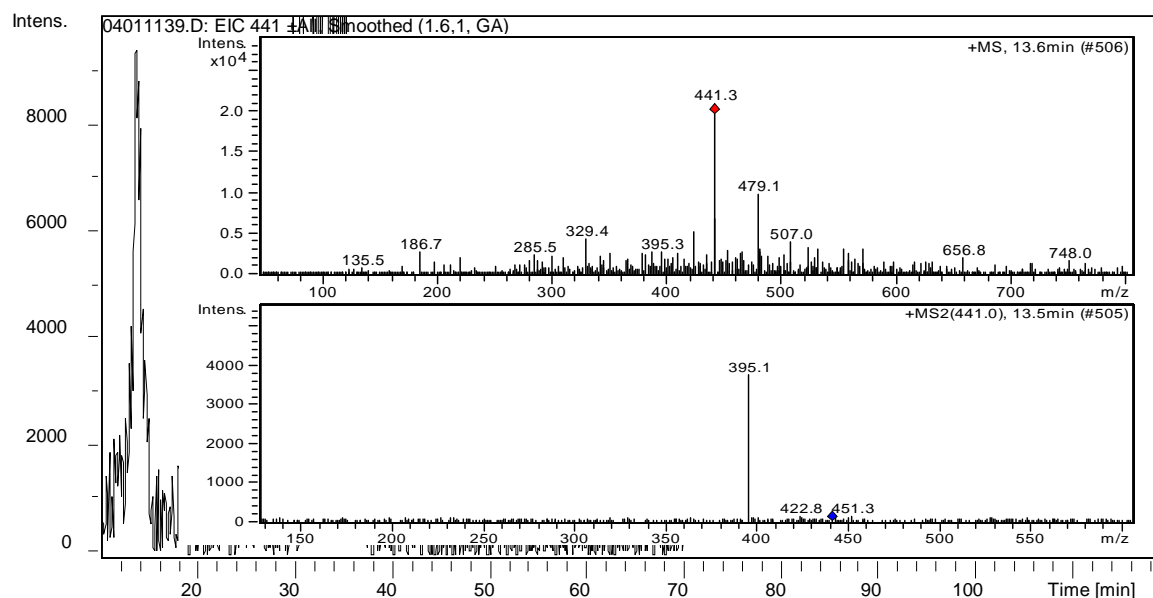


Figure 4.71 EIC of intermediate $m/z = 441$ in a 10 min sample at a t_R of 13.6 min. Inset MS and MS/MS spectra. Photocatalysis, [TAM] = 1 mM, 0.2 g TiO_2 /320 mL.

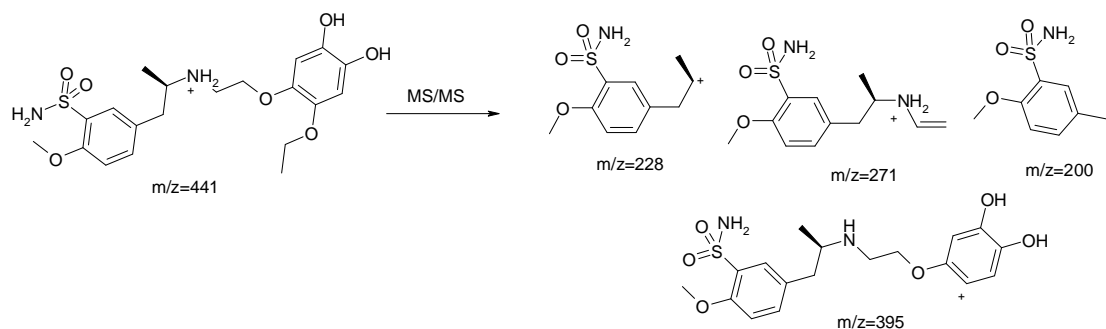


Figure 4.72: Structure of one of the possible isomers for $m/z = 441$, and the common fragments found for each isomer: $m/z = 395$, 271 , 228 , 200 .

Intermediate $m/z = 423$

The intermediate $m/z = 423$ was found exclusively in both the photocatalytic experiments and appeared at three retention times in the chromatogram at $t_R = 4.8$ mins, 15.4 mins, and 25.3 mins indicating the presence of three isomers. $m/z = 423$ is composed of Tamsulosin ($m/z = 409$) + 14amu which indicates that oxidation to a carbonyl has occurred and not an alcohol as in previous cases. The most likely oxidation sites for oxidation to a carbonyl are any of the sp^3 hybridised carbons located on the aliphatic chains of Tamsulosin since an oxidation of one of these carbons will result in the addition of 14 mass units. Oxidation at any of the six sp^3 hybridised carbons on the aliphatic chains in Tamsulosin should result in different fragmentation patterns and allow us to distinguish between isomers. Based on the fragmentation pattern for $m/z = 423$ (4.8 mins) an oxidation at the carbon β to the secondary amine has been proposed. This site of oxidation is also confirmed in fragments $m/z = 285$ (Tamsulosin's $m/z = 271 + 14$) and $m/z = 228$ (Tamsulosin fragment).

The proposed structure for $m/z = 423$ (4.8 mins) and its fragments are shown in Figure 4.74. For $m/z = 423$ (15.4 mins) an oxidation at the peripheral ethoxy group has been proposed. This is supported by the fragments $m/z = 228$ and $m/z = 271$ which indicate that the main aliphatic chain is still intact. $m/z = 313$ is an addition of 42 mass units to $m/z = 271$. For this mass we are proposing a fragmentation which involves an attack of the newly formed ester functional group by the neighbouring secondary amine with the simultaneous loss of the secondary aromatic ring and splicing of the main aliphatic chain. The proposed structure for this mass and its' fragments are shown in Figure 4.76. For $m/z = 423$ (25.3 mins), no original Tamsulosin fragments were attained, which would imply that oxidation must occur on the aliphatic chain closest to the primary aromatic ring. Only two of the three fragments for this intermediate could be elucidated shown in Figure 4.78.

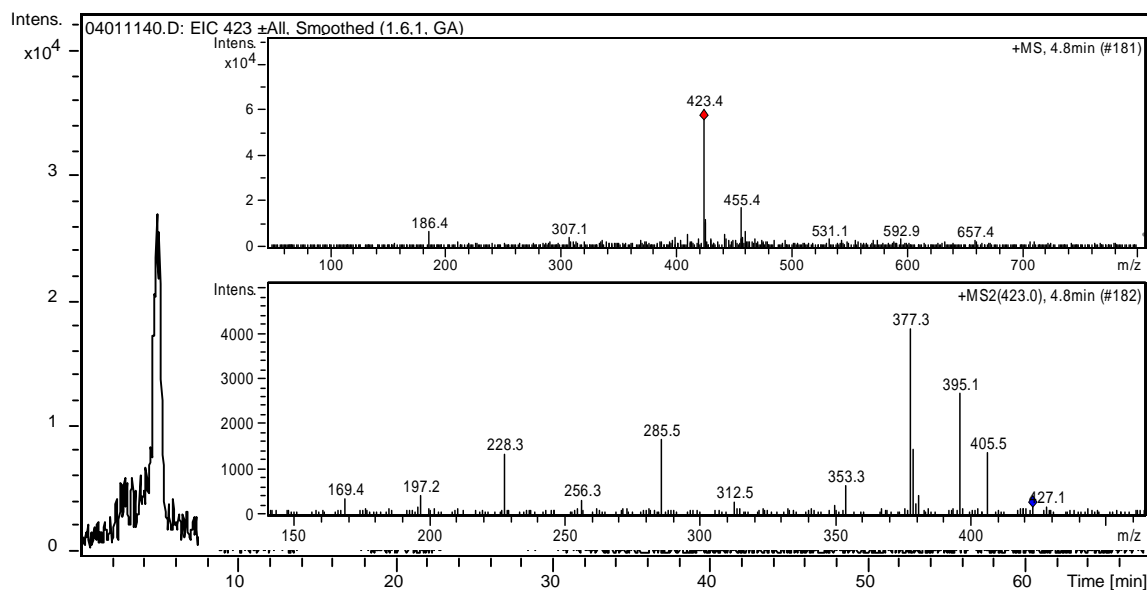


Figure 4.73: EIC of intermediate $m/z = 423$ in a 20 mins sample at a t_R of 4.8 mins. Inset MS and MS/MS spectra. Photocatalysis, [TAM] = 1 mM, 0.2 g TiO_2 /320 mL.

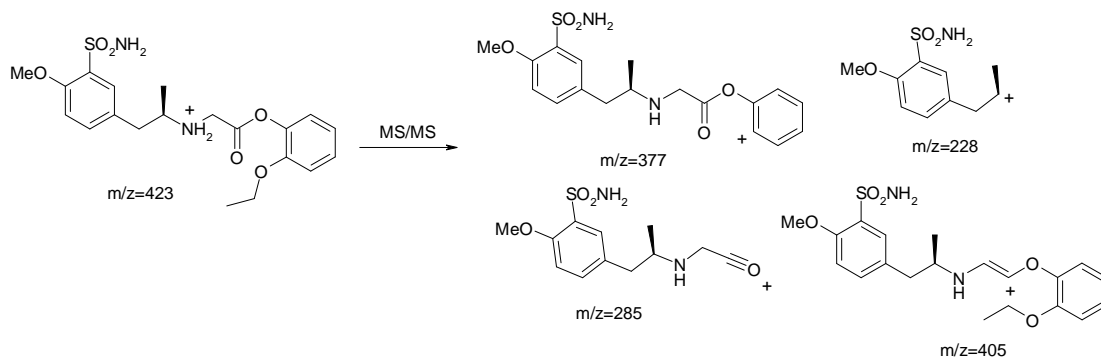


Figure 4.74: Structure proposed for $m/z = 423$, and fragments $m/z = 405$, 377 , 285 , and 228 .

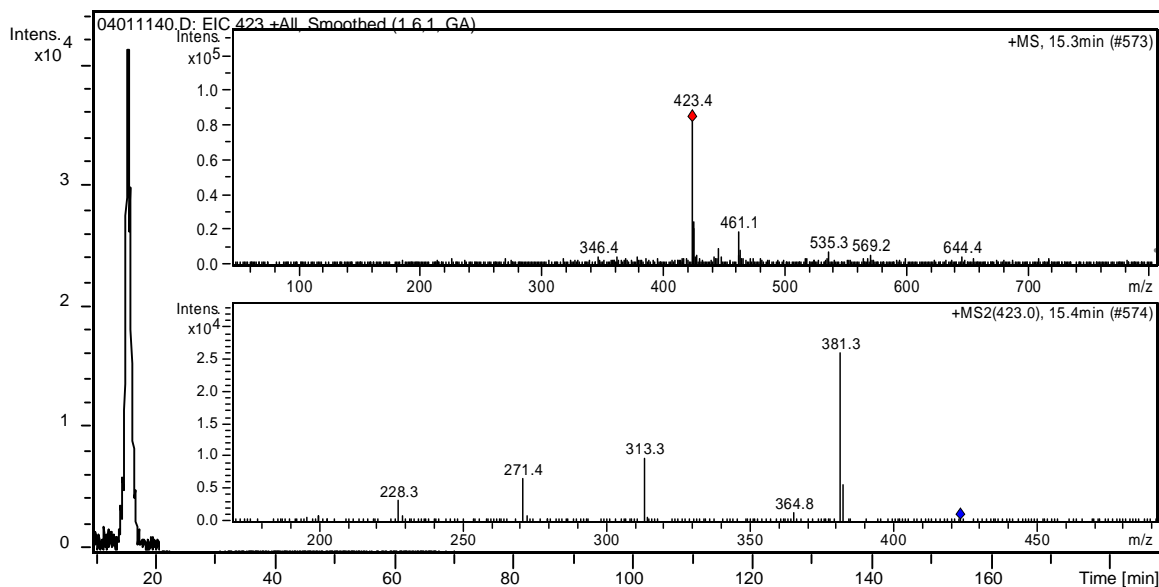


Figure 4.75: EIC of intermediate $m/z = 423$ in a 20 mins sample at a t_R of 15.3 mins. Inset MS and MS/MS spectra. Photocatalysis, [TAM] = 1 mM, 0.2 g TiO_2 /320 mL.

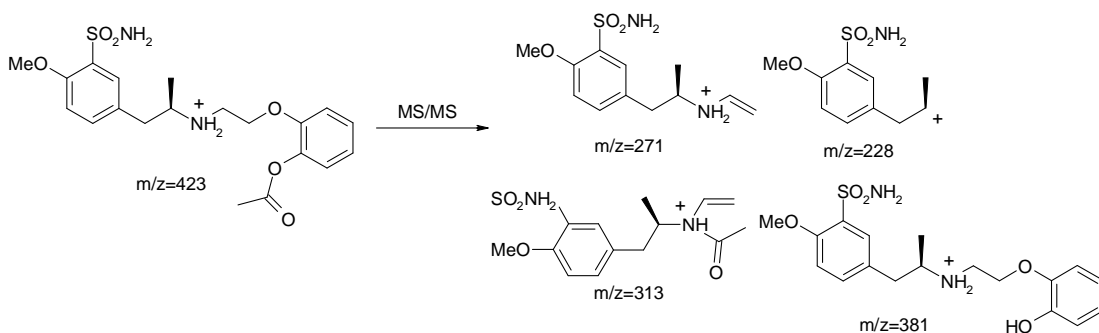


Figure 4.76: Structure proposed for $m/z = 423$, and fragments $m/z = 381$, 313 , 271 and 228 .

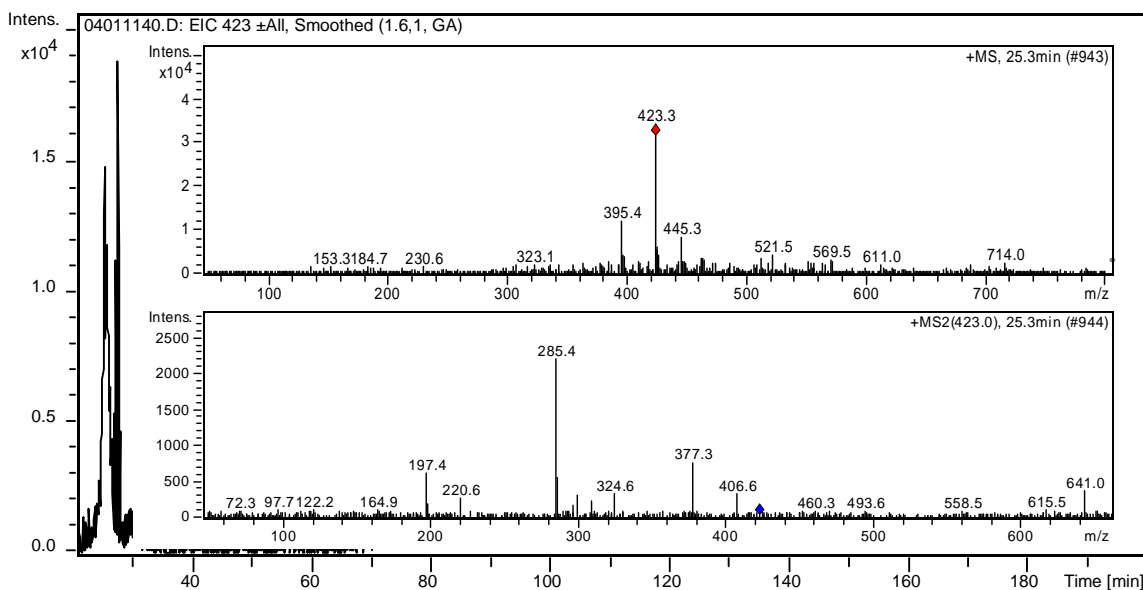


Figure 4.77: EIC of intermediate $m/z = 423$ in a 20 mins sample at a t_R of 25.3 mins. Inset MS and MS/MS spectra. . Photocatalysis, [TAM] = 1 mM, 0.2 g $\text{TiO}_2/320$ mL.

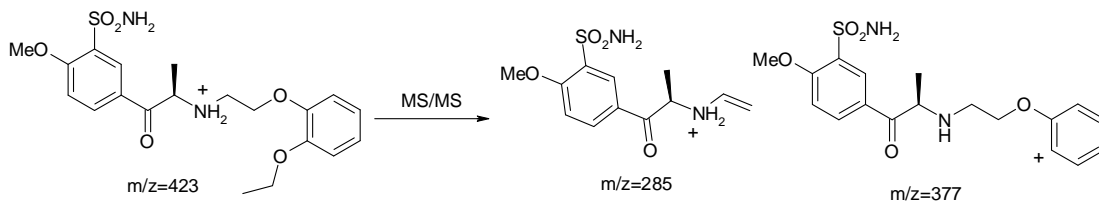


Figure 4.78: Structure proposed for $m/z = 423$, and fragments $m/z = 377$ and 285 .

Intermediate $m/z = 352$

Intermediate $m/z = 352$ was found exclusively in both of the photolysis experiments at a t_R of 4.8 mins. Two main fragments were observed for this ion, $m/z = 334$ (loss of 18) and $m/z = 238$ (loss of 114). Figure 4.80 shows the structure we have proposed for $m/z = 352$ and the various possible isomers of its fragments $m/z = 334$. The early elution time of $m/z = 352$ would indicate a highly polar compound, so for this reason we have proposed possible oxidation at numerous points in the molecule. No structure could be elucidated for the fragment $m/z = 238$.

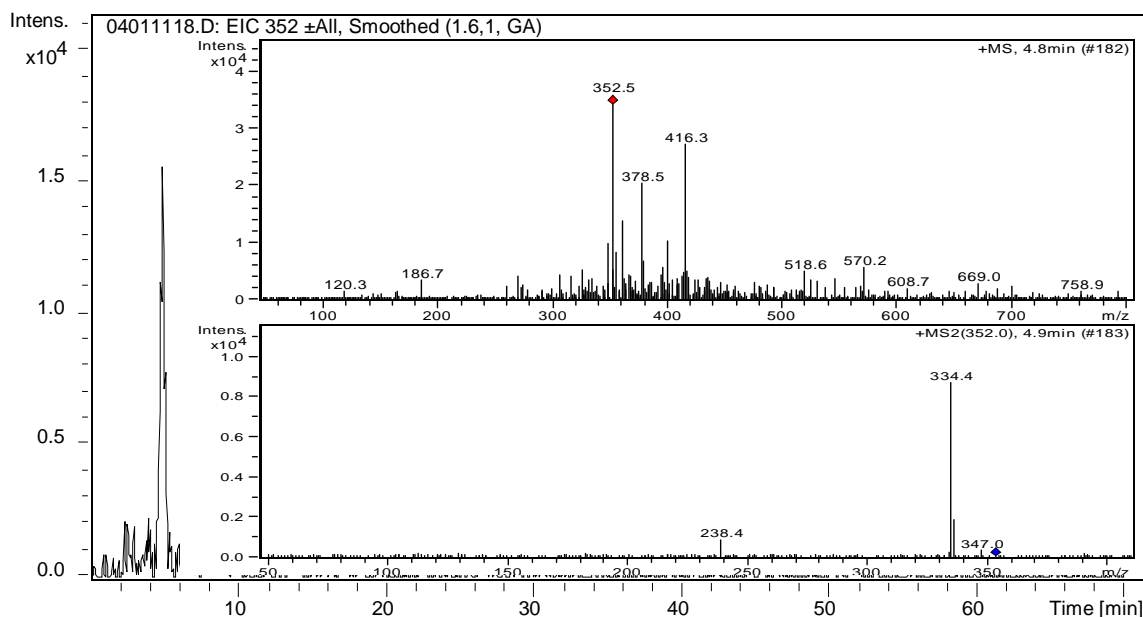


Figure 4.79: EIC of intermediate $m/z = 352$ in a 20 mins sample at a t_R of 4.8 mins. Inset MS and MS/MS spectra. Photolysis Pyrex, [TAM] = 0.083 mM.

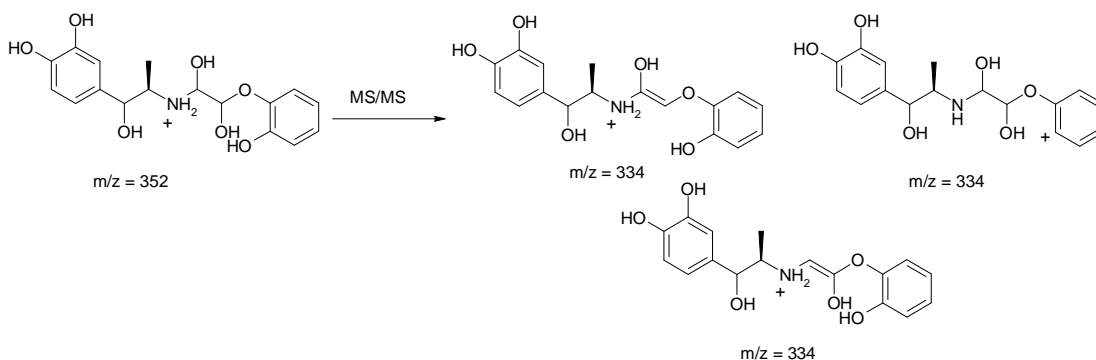


Figure 4.80: Structure proposed for $m/z = 352$, and the isomers possible for fragment $m/z = 334$.

Intermediate $m/z = 378$

This ion was found exclusively in both of the photolysis experiments at a t_R of 4.9, 10.4, 21.6, 31 mins. Various fragments were found for each peak and these are presented in Table 4.13. The chromatogram of the most intense isomer is shown in Figure 4.82. Only one structure could be proposed for one of the isomers, and this structure is presented in Figure 4.83. Two isomers of its main fragments are also presented.

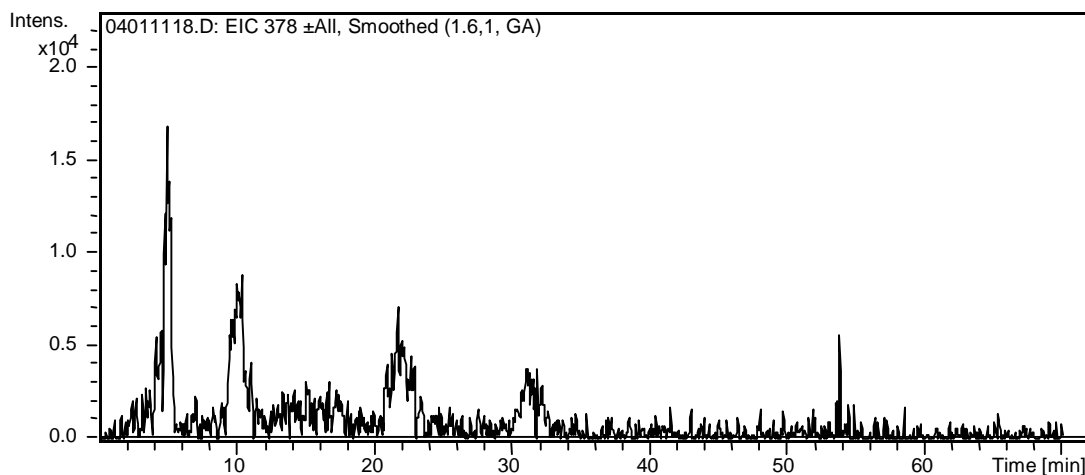


Figure 4.81: EIC of ion $m/z = 378$ in a 20 mins sample at retention times of 4.9, 10.4, 21.6, 31 mins. Photolysis Pyrex, $[TAM] = 0.083$ mM.

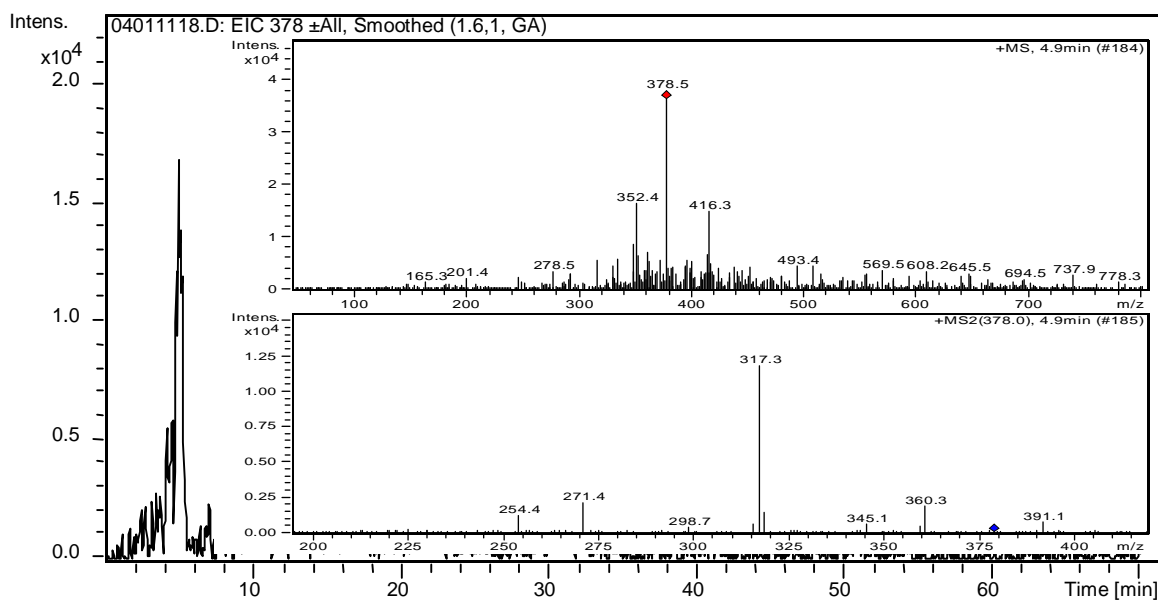


Figure 4.82: EIC of intermediate $m/z = 378$ in a 20 mins sample at a t_R of 4.5 mins. Inset MS and MS/MS spectra. Photolysis Pyrex, $[TAM] = 0.083$ mM.

m/z	MS/MS	t_R
378	<u>317</u> , 271, 254	4.9
378	<u>303</u> , 233, 215, 145	10.4
378	<u>360</u> , 242, 161	21.6
378	317, <u>271</u> , 157	31

Table 4.13: Daughter ions found at different retention times for $m/z = 378$. Highlighted in grey is the ion for which a structure has been proposed.

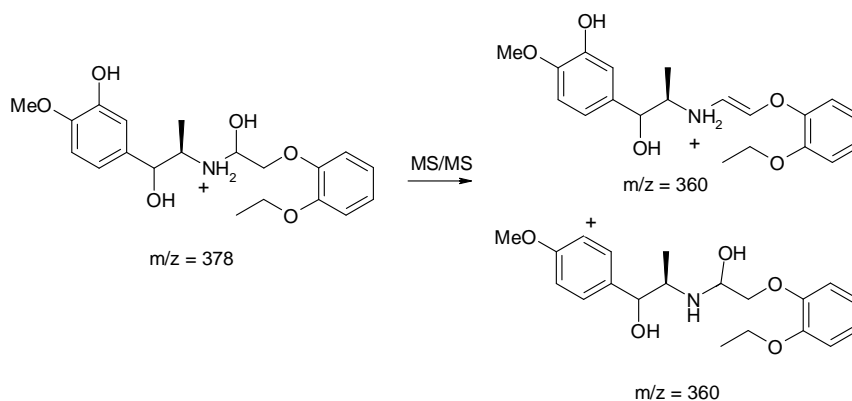


Figure 4.83: Possible Structure proposed for $m/z = 378$ and two possible isomers for its major fragment $m/z = 360$.

Intermediate $m/z = 346$

The intermediate with mass $m/z = 346$ was found in all experiments carried out, eluting after Tamsulosin at a t_R of 45.2 mins. Two fragments were observed for this intermediate $m/z = 285$ (loss of 61), and $m/z = 257$ (loss of 89). Considering its close proximity to Tamsulosin in the chromatographic run, it was considered that a structure similar to Tamsulosin was likely. Loss of the sulfonamide group and replacement with a hydroxyl group yielded a mass of $m/z = 346$ although no predictable fragmentation yielded the fragments which were obtained by LC-MS/MS. However, a search of fragments for this ion found in DI-MS studies yielded two fragments which matched this proposed structure, $m/z = 165$ and $m/z = 137$.

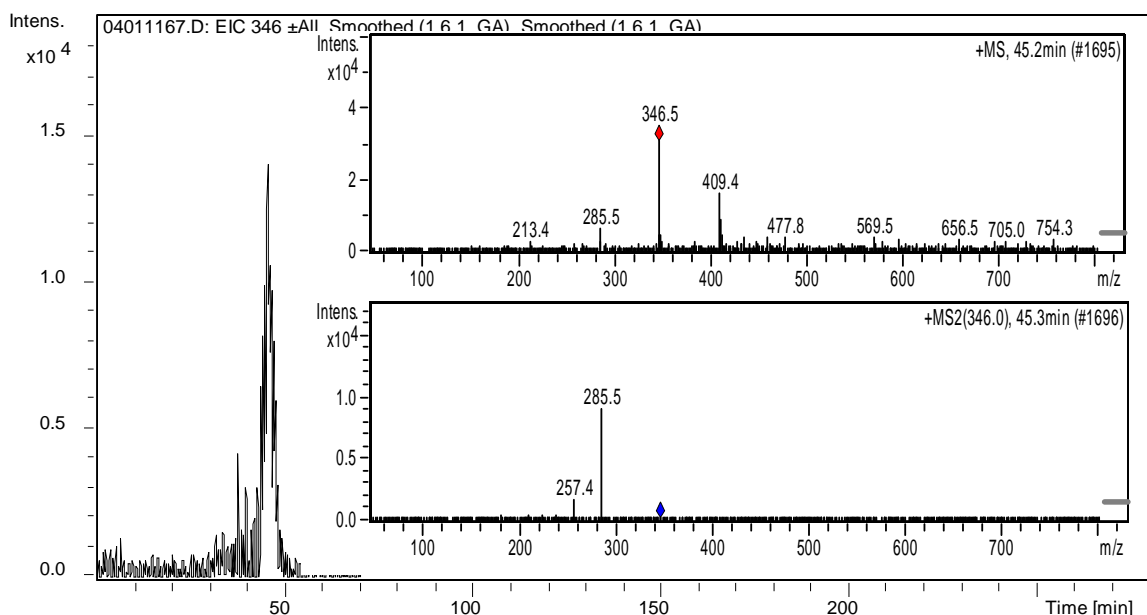


Figure 4.84: EIC of intermediate $m/z = 346$ in a 20 mins sample at a t_R of 45.2 mins. Inset MS and MS/MS spectra. Photolysis Pyrex, [TAM] = 0.083 mM.

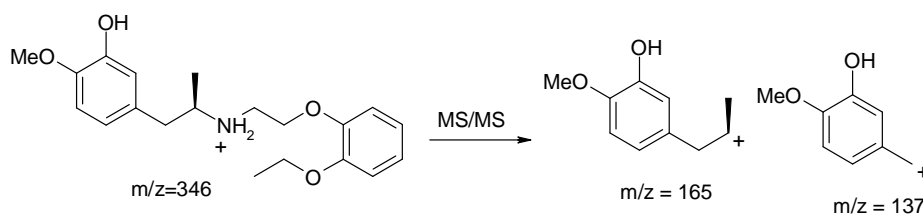


Figure 4.85: Structure proposed for $m/z = 346$ and fragments found in DI-MS studies $m/z = 165$ and $m/z = 137$.

Intermediate $m/z = 275$

The intermediate $m/z = 275$ was found in both photocatalytic experiments at a retention time of 2.2 mins. Three main fragments were discovered for this intermediate, which were similar to earlier reported fragments for the intermediate $m/z = 395$. Considering this relationship with $m/z = 395$, we initially proposed oxidation on the sulphonamide ring with the loss of the methoxy group (as with $m/z = 395$). The low mass of this intermediate would indicate the loss of a significant portion of Tamsulosins' structure through multiple oxidations. We have therefore proposed a carbamic acid derivative for this intermediate. This would occur through oxidation of the alpha carbon to Tamsulosins' secondary amine, with further oxidation resulting in cleavage of the alpha-beta carbon bond. Loss of H_2O through alpha cleavage of the OH group results in the fragment at $m/z = 257$, although the principle fragmentation, $m/z = 214$, is through loss of the entire carbamic acid group. The structure proposed for the intermediate $m/z = 275$ and its fragments is shown in Figure 4.87.

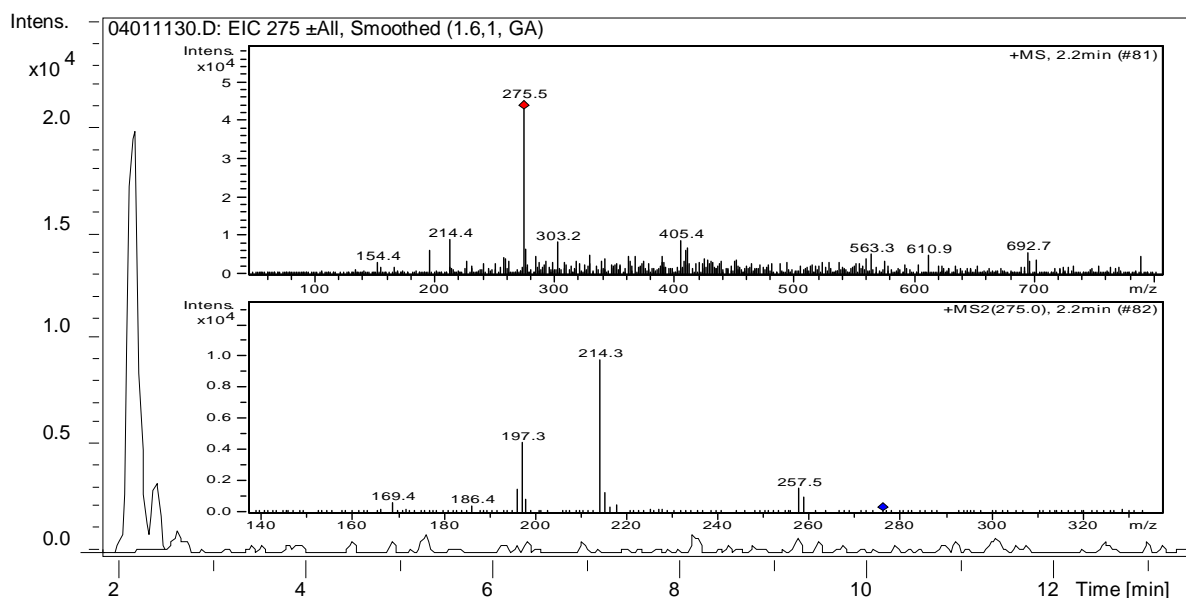


Figure 4.86: EIC of intermediate $m/z = 275$ in a 30 mins sample at a t_R of 2.2 mins. Inset MS and MS/MS spectra. Photocatalysis Pyrex, [TAM] = 0.083 mM, 0.2 g TiO_2 /320 mL.

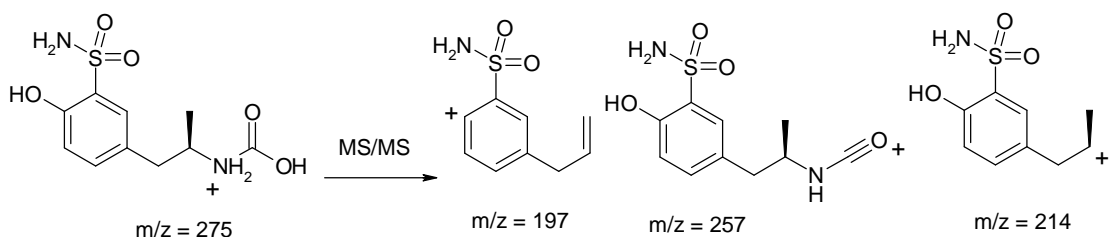


Figure 4.87: Structure proposed for $m/z = 275$ and fragments $m/z = 197$, $m/z = 214$ and $m/z = 257$.

Intermediate $m/z = 415$

The intermediate $m/z = 415$ was found in trace quantities in the 1 mM photocatalytic experiment. The only fragments obtained for this intermediate were Tamsulosins' own fragments ($m/z = 271$ and $m/z = 228$). We can therefore conclude that oxidations for this intermediate occur principally on the catechol ring with the aliphatic chain and the sulphonamide ring remaining intact. Oxidation at two positions on the catechol ring, combined with a break in aromaticity caused by a photo-reduction would result in the mass of $m/z = 415$. An alternative structure could be a ring opened structure which is often proposed and identified in pharmaceutical degradation pathways. These ring openings tend to form after a number of hydroxylations have occurred to the aromatic ring. The structures proposed for $m/z = 415$ and its fragments are shown in Figure 4.89. Due to the number of ketone and carboxylic acid moieties present more fragments would be expected for the ring opened structure such as loss of COOH , CO , and H_2O .

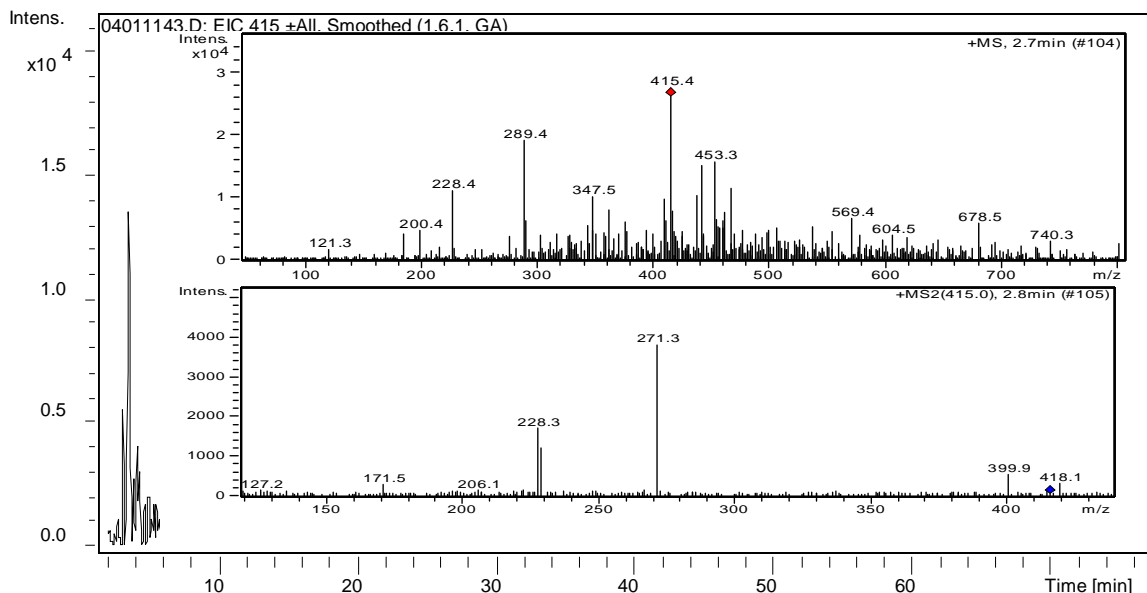


Figure 4.88: EIC of intermediate $m/z = 415$ in a 60 mins sample at a t_R of 2.8 mins. Inset MS and MS/MS spectra. Photocatalysis, $[\text{TAM}] = 1 \text{ mM}$, $0.2 \text{ g TiO}_2/320 \text{ mL}$.

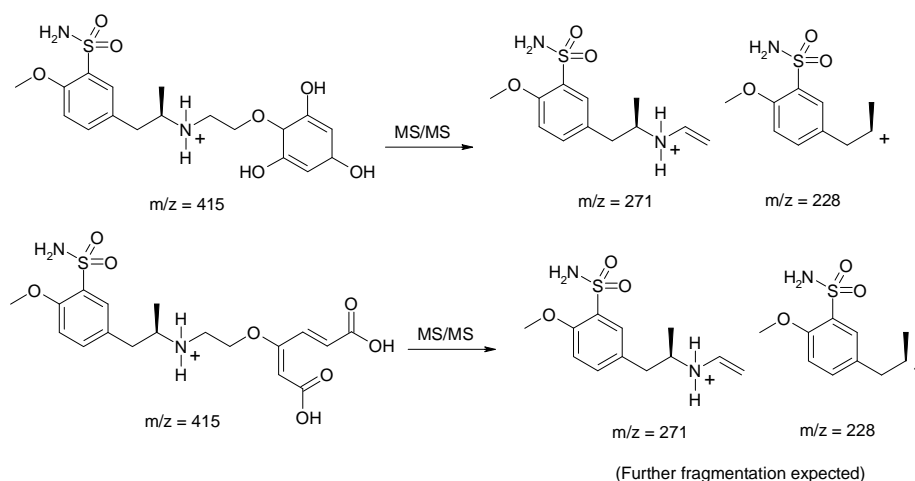


Figure 4.89: Structures proposed for $m/z = 415$ and fragments $m/z = 271$ and $m/z = 228$.

Intermediate $m/z = 473$

The intermediate $m/z = 473$ was found in trace quantities in the 1 mM photocatalytic experiment. The high mass of this intermediate would indicate a series of oxidations have occurred. $409 + 64$ means that a total of 4 oxidations have occurred on the Tamsulosin structure. The fragments obtained for this intermediate included Tamsulosins' fragments $m/z = 271$, and 228 which would indicate that the oxidations are likely to have occurred mainly on the catechol ring of Tamsulosins' structure. In addition to these fragments, $m/z = 289$ and $m/z = 427$ were also observed more intensely. The fragment at $m/z = 289$ would indicate a single oxidation on the aliphatic chain of Tamsulosin, similar to the previously reported intermediate (intermediate $m/z = 289$). This would mean that the remaining 3 oxidations occur on catechol ring of Tamsulosin. The fragment at $m/z = 427$ is due to the loss of the ethoxy group. The remaining fragments as well as the structure for the intermediate $m/z = 473$ are shown in Figure 4.91.

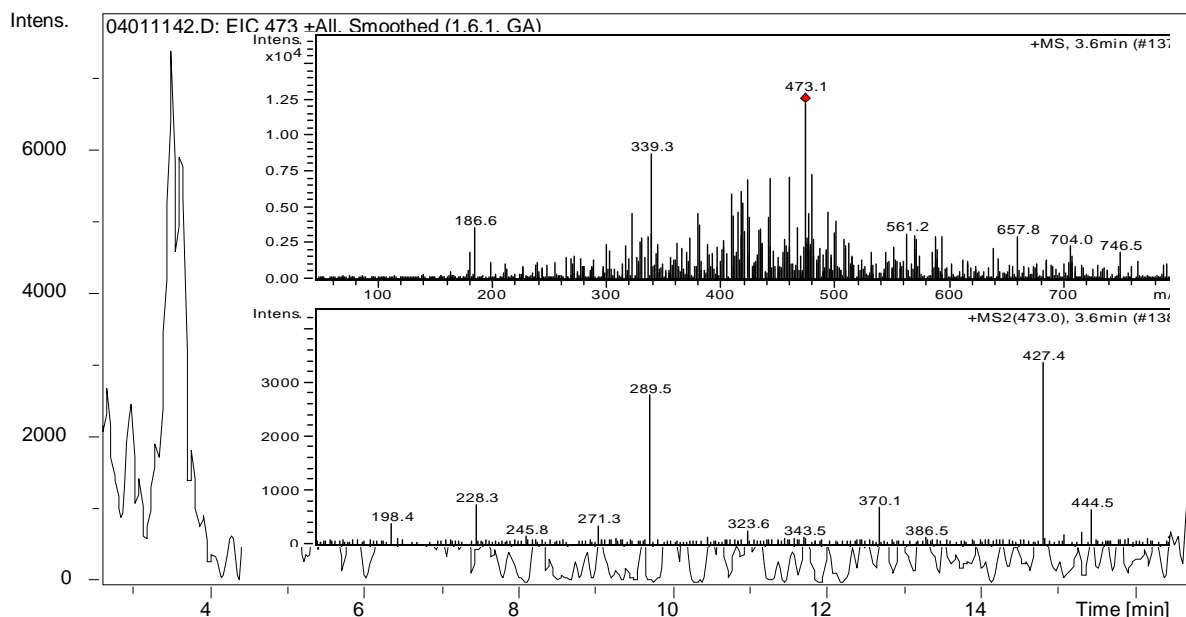


Figure 4.90: EIC of intermediate $m/z = 473$ in a 40 mins sample at a t_R of 3.6 mins. Inset MS and MS/MS spectra. Photocatalysis, [TAM] = 1 mM, 0.2 g $\text{TiO}_2/320$ mL.

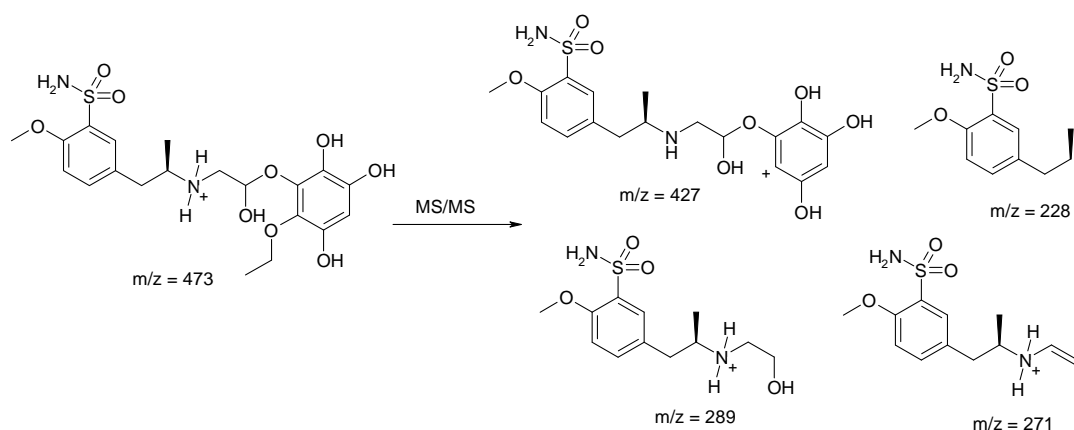


Figure 4.91: Structure proposed for $m/z = 473$ and fragments $m/z = 427$, 289, 271 and 228.

Intermediate $m/z = 419$

The intermediate $m/z = 419$ was found in trace amounts in the 1 mM photocatalytic experiment at a t_R of 3.7 mins. The fragments obtained for $m/z = 419$ were $m/z = 271$ and $m/z = 228$. Since the fragments of this intermediate are shared with Tamsulosin, it can be predicted that the oxidations which occur are exclusively on the catechol ring. Since this mass is 4 units higher than the intermediate $m/z = 415$, we have proposed a similar structure with 2 photo-reductions also occurring. These steps would give rise to a break in aromaticity leading to an aliphatic ring. An alternative structure could also be a ring opened structure however further fragmentation would be expected in this case. Both structures are proposed in Figure 4.93.

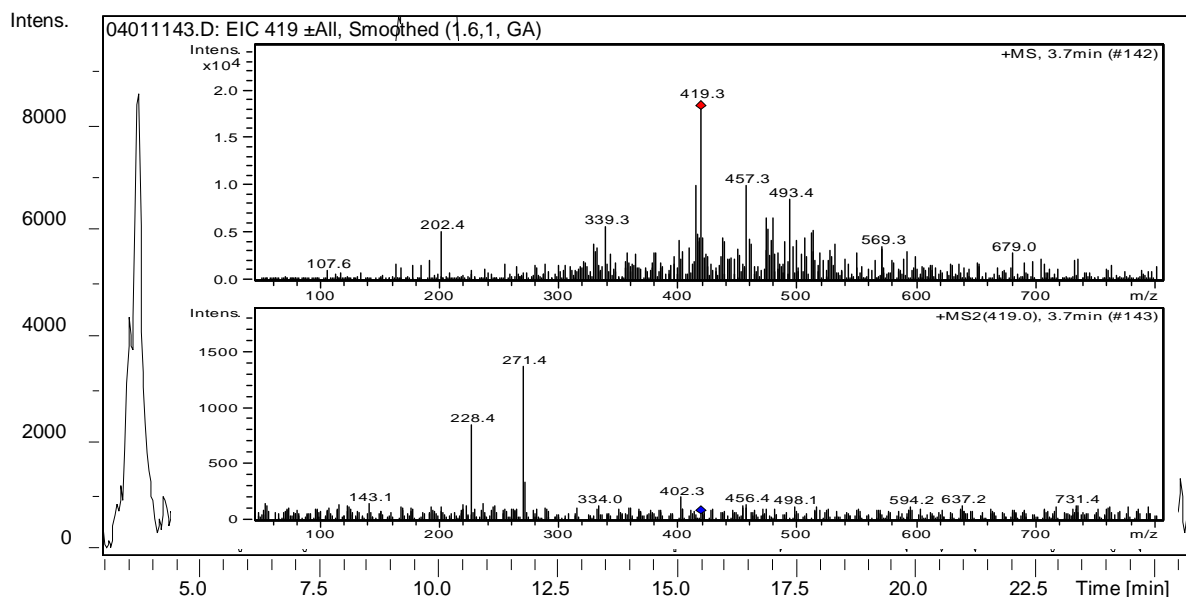


Figure 4.92: EIC of intermediate $m/z = 419$ in a 60 mins sample at a t_R of 3.7 mins. Inset MS and MS/MS spectra. Photocatalysis, [TAM] = 1 mM, 0.2 g $\text{TiO}_2/320$ mL.

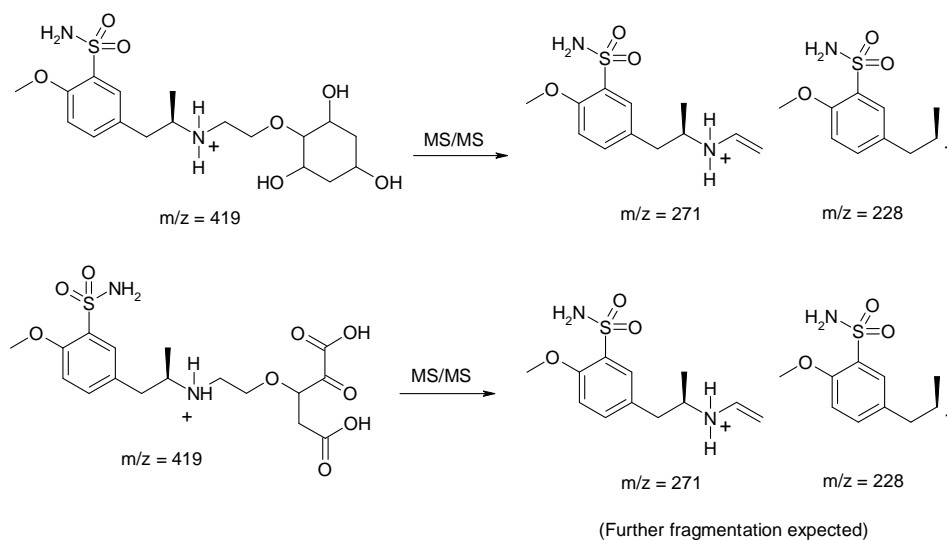


Figure 4.93: Structure proposed for $m/z = 419$ and fragments $m/z = 271$ and $m/z = 228$.

Intermediate $m/z = 413$

The intermediate $m/z = 413$ was found in trace amounts in the 1 mM photocatalytic experiment at a t_R of 5.7 mins. The fragments obtained for $m/z = 413$ were $m/z = 313$, $m/z = 271$ and $m/z = 228$. As with the previous intermediates $m/z = 419$ and $m/z = 415$, this fragmentation pattern would indicate that the oxidations which have occurred are on the catechol ring of Tamsulosin. The structure proposed for $m/z = 413$ and its fragment ions is shown in Figure 4.95.

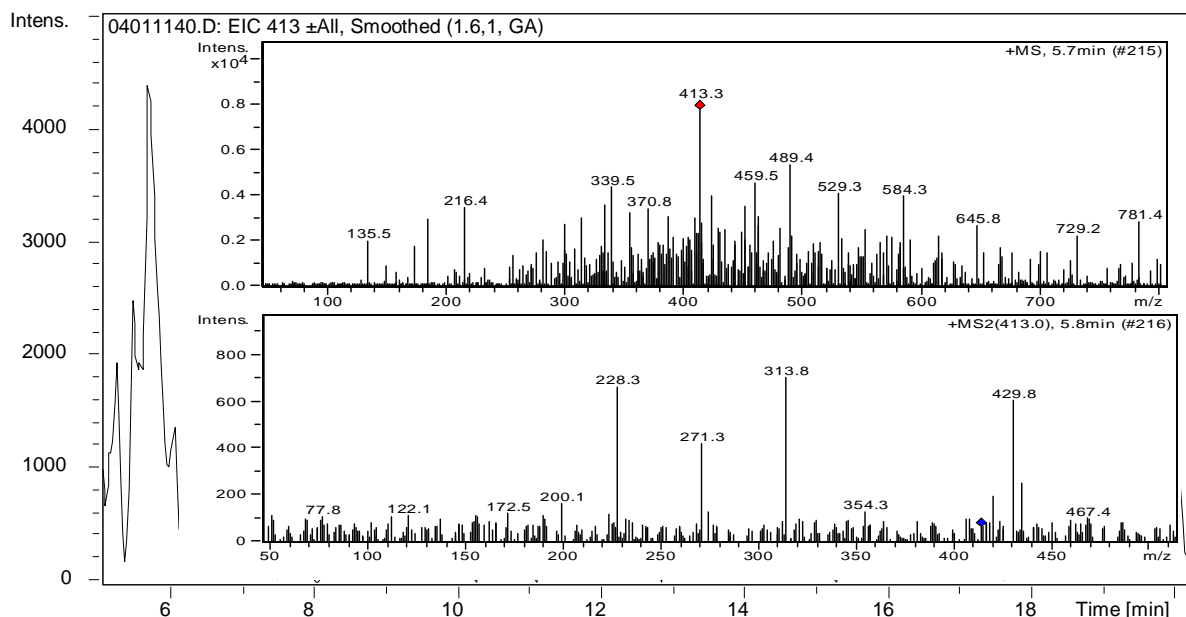


Figure 4.94: EIC of intermediate $m/z = 413$ in a 20 mins sample at a t_R of 5.7 mins. Inset MS and MS/MS spectra. Photocatalysis, [TAM] = 1 mM, 0.2 g TiO₂/320 mL.

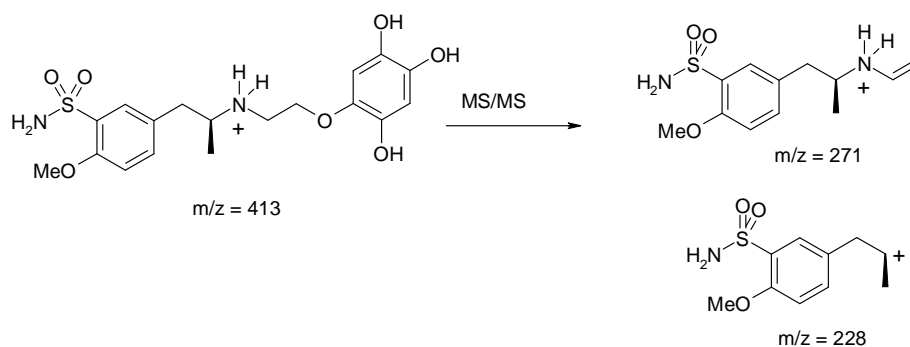


Figure 4.95: Structure proposed for $m/z = 413$ and its fragments $m/z = 271$ and $m/z = 228$.

4.2.11 Ions which could not be Elucidated

For Tamsulosin, there were also a number of intermediates which could also not be elucidated. These intermediates can be found in Table 4.14 below along with their retention times, fragments and the experiments in which they were present.

Intermediate m/z	Fragments	t_R (mins)	Experiment
318	257, 239	10	Photolysis (Pyrex and Quartz)
348	330, 287, 199	3.9	Photolysis (Pyrex and Quartz)
362	301, 227, (181)147	7.6, 8.4	Photolysis (Pyrex and Quartz)
350	332, 322, 187	5.5	Photolysis (Pyrex and Quartz)
414	396, 334, 316, 254, 227	3.6	Photocat 1mM
400	382, 364, 276	7.2	Photocat (1mM, 0.083)

Table 4.14 Table of Tamsulosin intermediates which could not be elucidated.

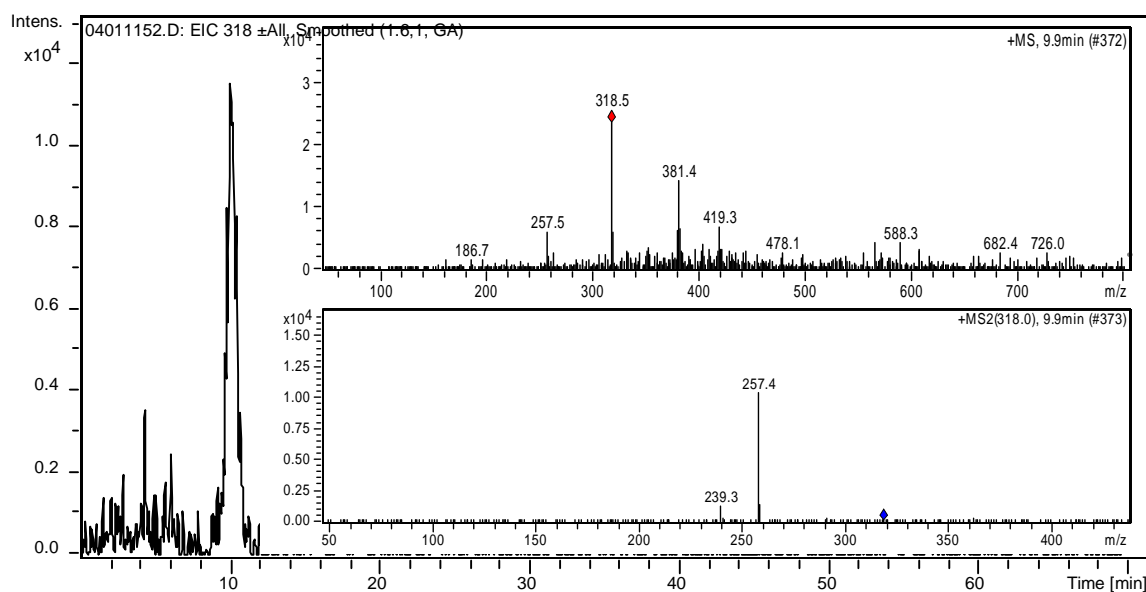


Figure 4.97: EIC of intermediate $m/z = 318$ in a 5 mins sample at a t_R of 10 mins. Inset MS and MS/MS spectra. Photolysis Quartz, [TAM] = 0.083 mM.

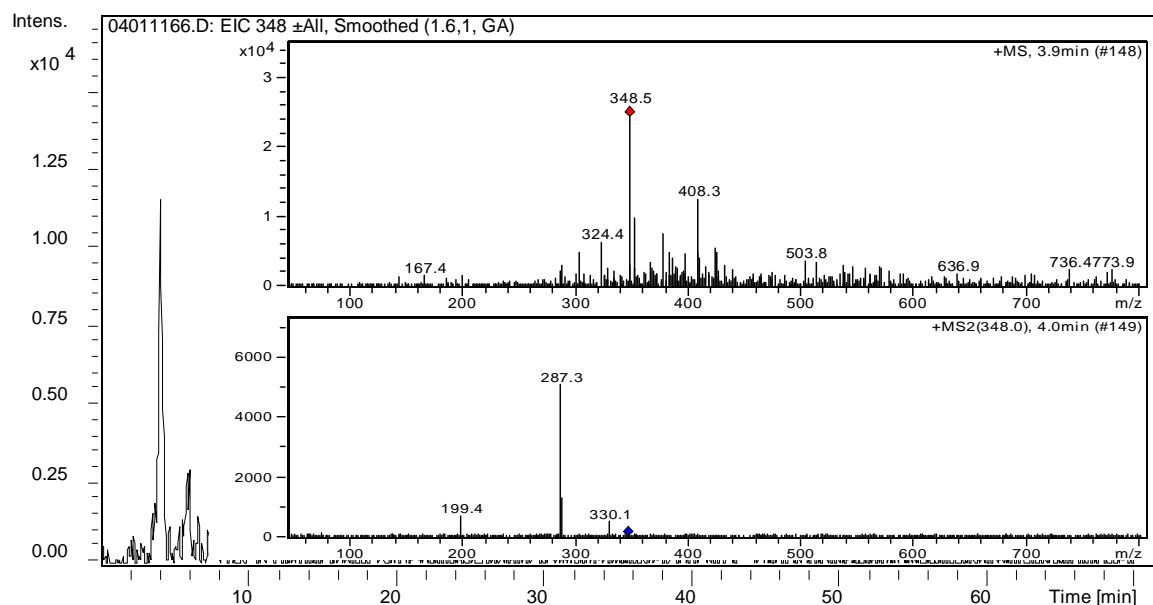


Figure 4.98: EIC of intermediate $m/z = 348$ in a 10 mins sample at a t_R of 3.9 mins. Inset MS and MS/MS spectra. Photolysis Pyrex, [TAM] = 0.083 mM.

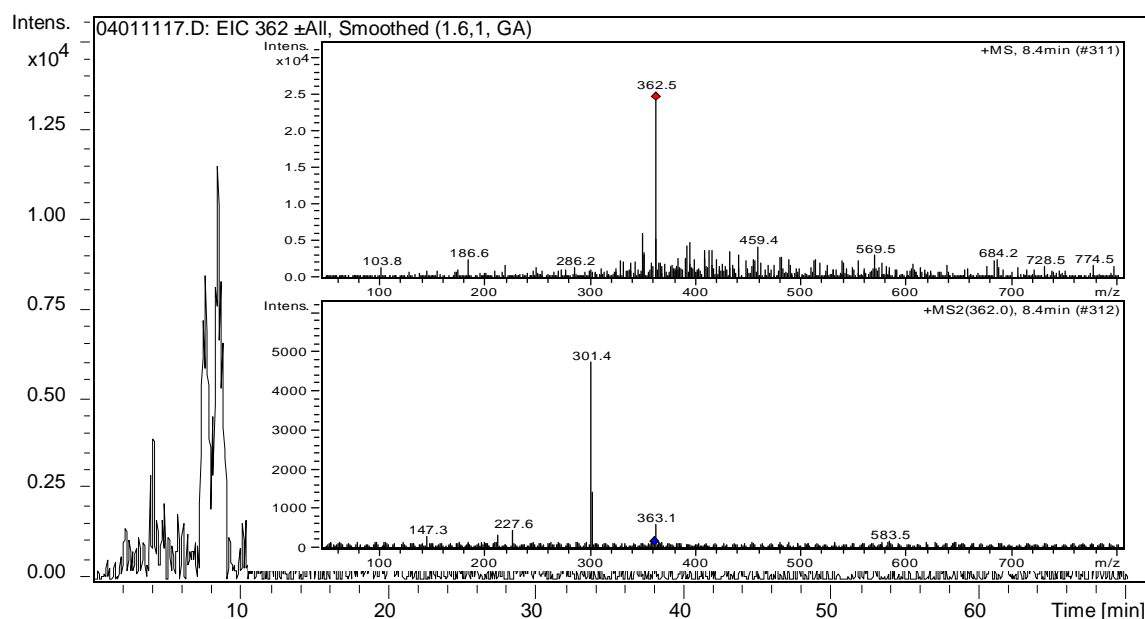


Figure 4.99: EIC of intermediate $m/z = 362$ in a 10mins sample at a t_R of 8.4 mins. Inset MS and MS/MS spectra. Photolysis Pyrex, [TAM] = 0.083 mM.

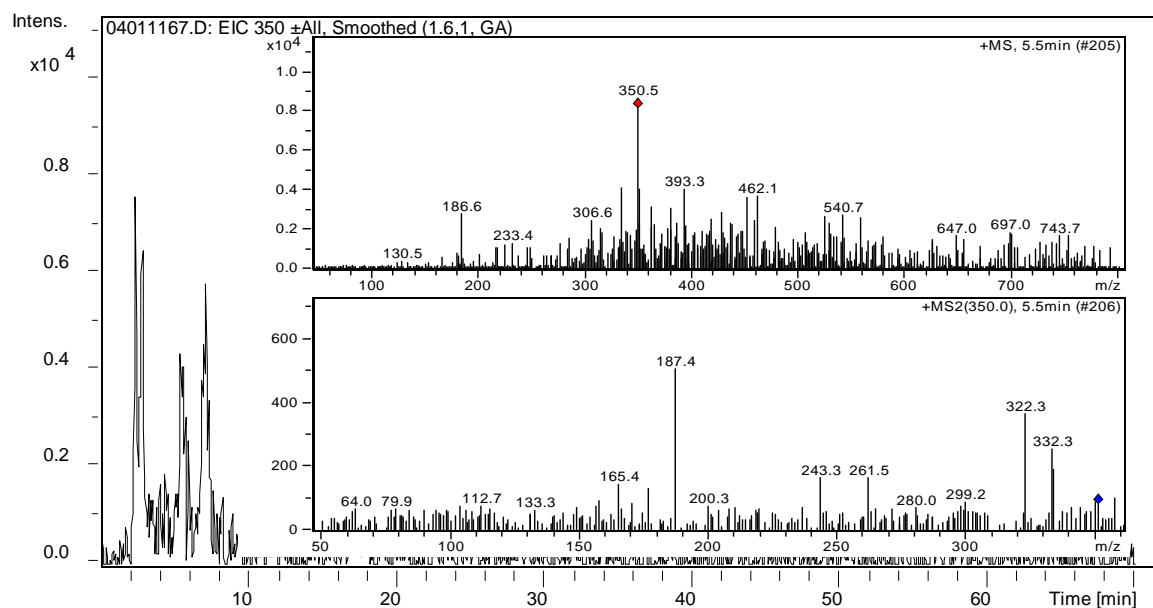


Figure 4.100: EIC of intermediate $m/z = 350$ in a 20 mins sample at a t_R of 5.5 mins. Inset MS and MS/MS spectra. Photolysis Pyrex, [TAM] = 0.083 mM.

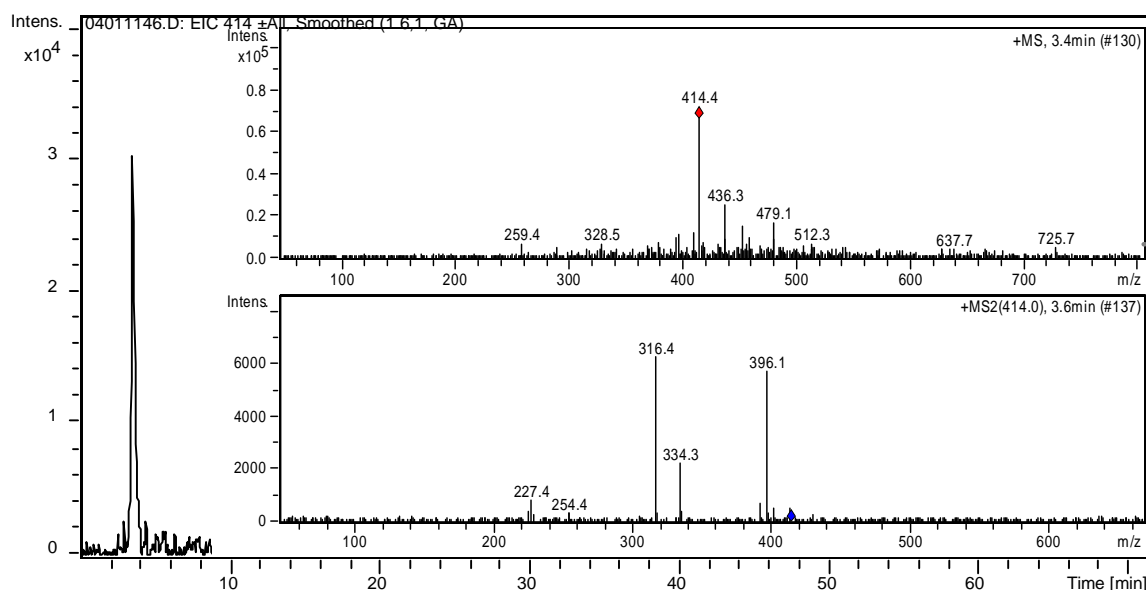


Figure 4.101: EIC of intermediate $m/z = 414$ in a 180 mins sample at a t_R of 3.6 mins. Inset MS and MS/MS spectra. Photocatalysis [TAM] = 1 mM, 0.2 g/320 mL.

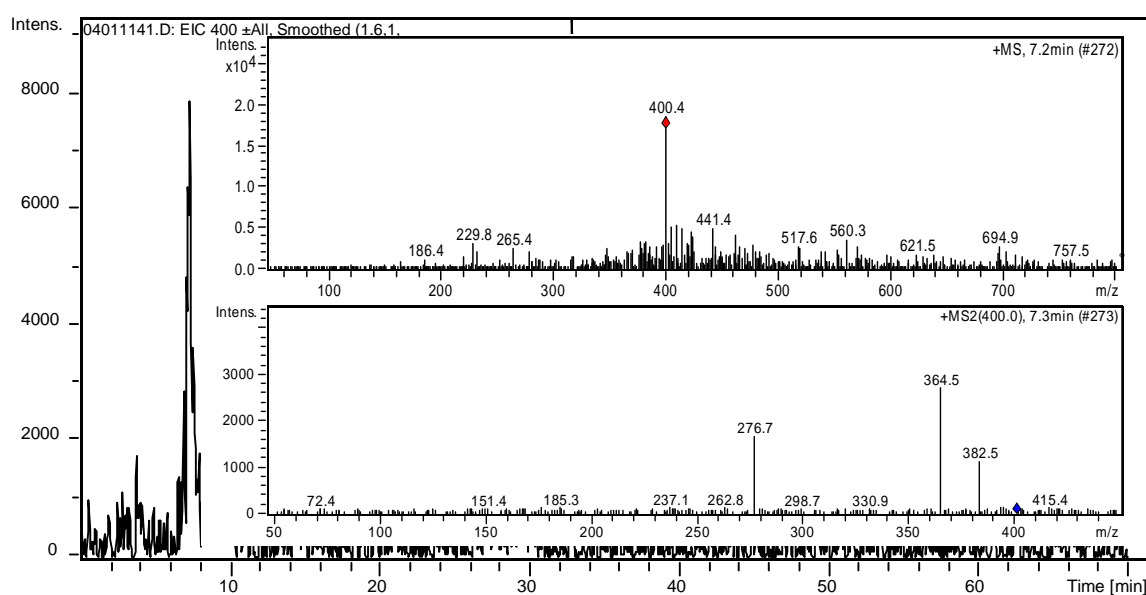


Figure 4.102: EIC of intermediate $m/z = 400$ in a 30 mins sample at a t_R of 7.2 mins. Inset MS and MS/MS spectra. Photocatalysis, [TAM] = 1 mM, 0.2 g TiO_2 /320 mL.

4.2.12 Tamsulosin Proposed Intermediates Structures

A total of 30 intermediates (20 different intermediate ions) were discovered collectively in LC-MS/MS and DI-MS data for Tamsulosin. (This number includes the isomers of intermediates) Of these, 20 structures have been proposed. The structures of the remaining 10 intermediates could not be elucidated and 5 of these have the same molecular mass. The structures which have been proposed can be found in Figure 4.103 along with their molecular mass. A plausible

degradation pathway is also shown in Figure 4.104 Ion monitoring graphs for all ions monitored in each experiment can be found in the appendices (4A-18 – 4A-21).

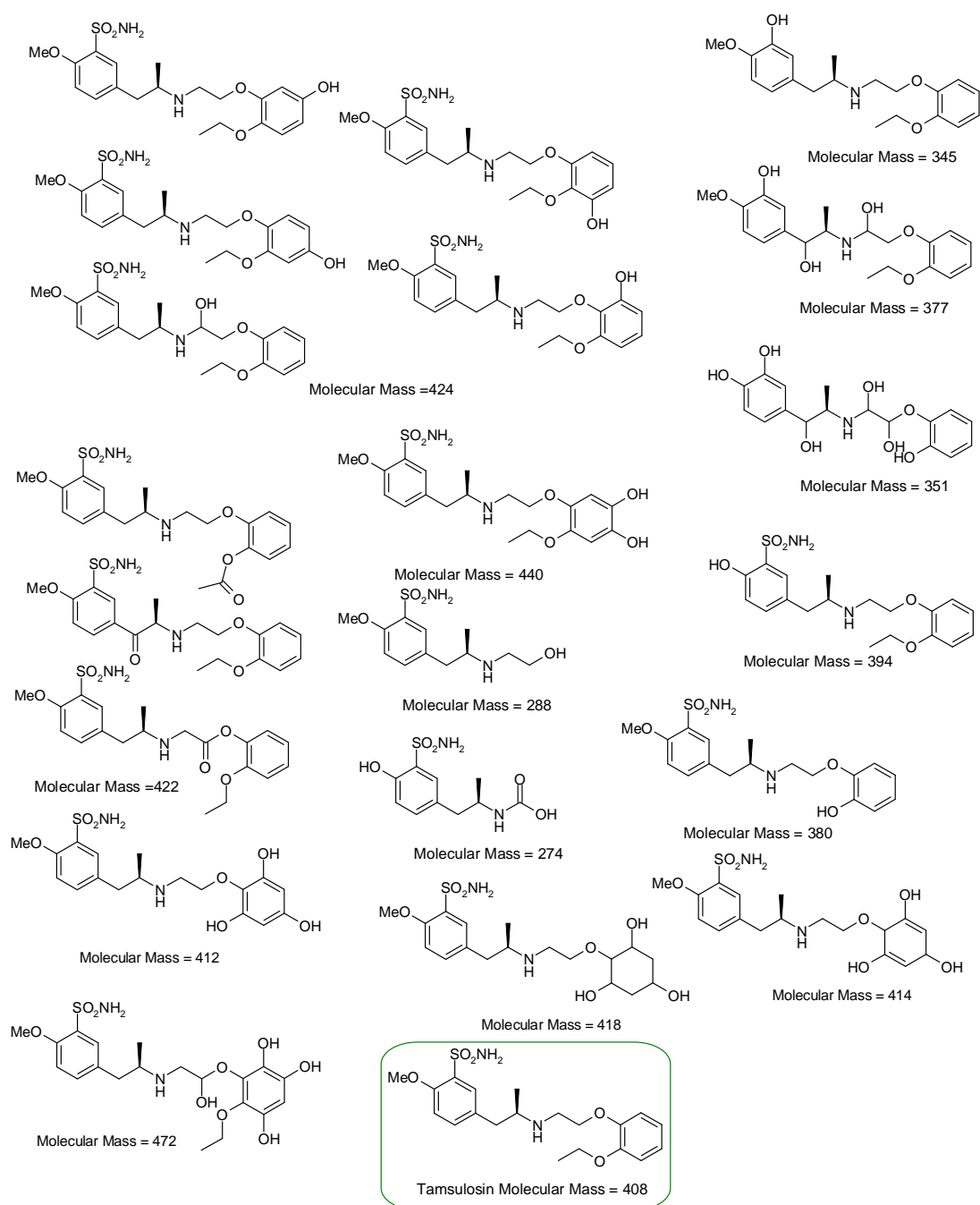


Figure 4.103 Final structures and molecular masses for intermediates proposed for Tamsulosin. Tamsulosin's structure is highlighted in the green box.

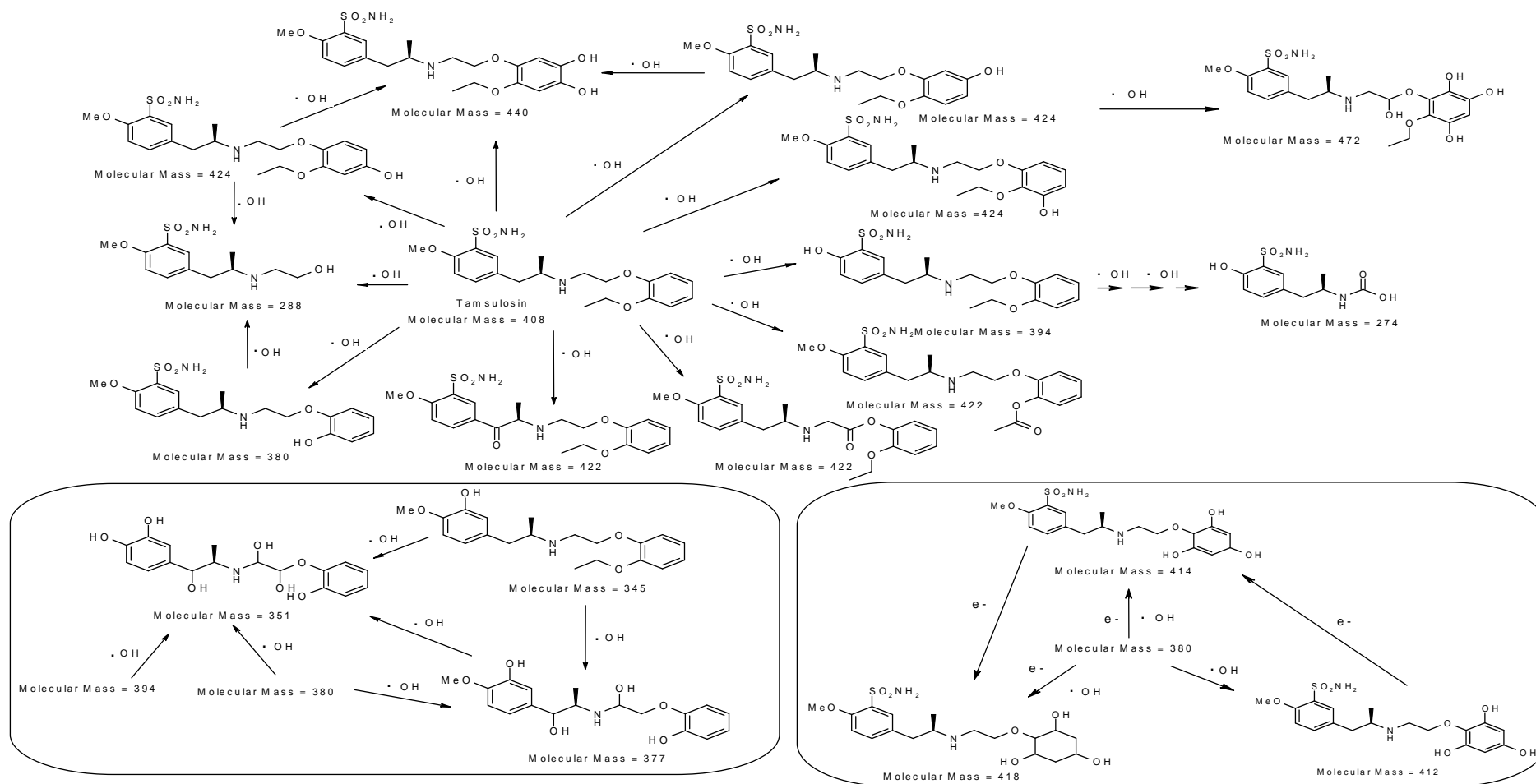


Figure 4.104: Proposed Degradation Pathway for Tamsulosin and intermediates which were detected via LC-MS/MS and DI-MS.

4.2.13 Direct Infusion Mass Spectrometry Studies: Solifenacin

Figure 4.105 displays a HPLC-PDA (260 nm) chromatogram of a photocatalytic degradation experiment for Solifenacin. The appearance of numerous intermediates can be clearly seen in the chromatogram as well as the disappearance of Solifenacin.

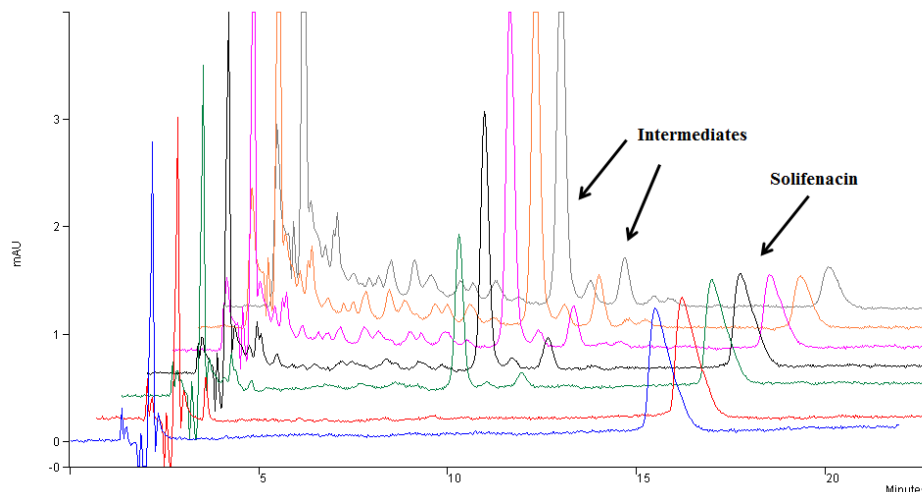


Figure 4.105: HPLC Chromatogram (260 nm) of a Solifenacin photocatalytic experiment showing degradation of Solifenacin and appearance of intermediates. Photocatalysis, [SOL] = 0.083 mM 0.1 g TiO_2 /320 mL (pH 3).

DI-MS analysis of a photolysis experiment of Solifenacin was analysed to examine intermediates that were formed. Figure 4.106 shows the 0 Mins sample from this experiment. The molecular ion of Solifenacin appears at $m/z = 363$. The molecular weight of Solifenacin is 480.55 g/mol which means a loss of 117 g/mol from the molecule. Solifenacin, like Tamsulosin, is formulated as a salt, and its counter anion is succinate which has a molecular weight of 117 g/mol. An MS/MS study of Solifenacin showed the daughter ions in Figure 4.107.

Structures for these daughter ions are shown in Figure 4.108. The presence of the carbamate moiety in Solifenacin makes fragmentation of the molecule relatively simple; however a further break-up of the molecule is less likely due to the high conjugation and stability of the resulting fragments. The mass at $m/z = 193$ is the second most stable fragment in the spectra. A structure was elucidated and is based on the formation of a tropylium ion on the peripheral phenyl ring and cleavage of the alpha C to the N of the carbamate.

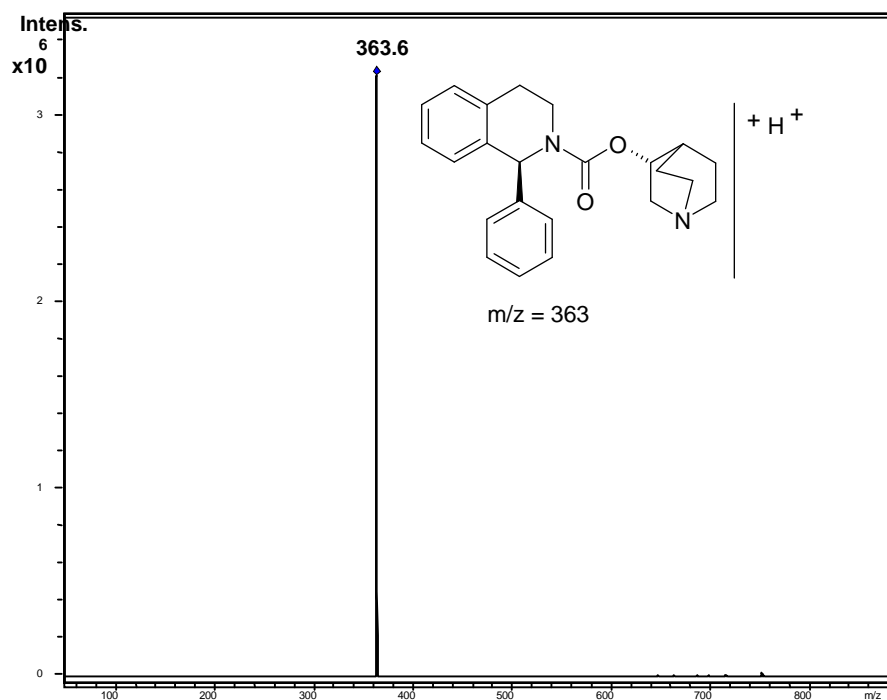


Figure 4.106: DI-MS of a 0 Mins sample of a Solifenacin photolytic degradation experiment showing the parent ion of Solifenacin, m/z= 363. Photolysis, (Enviolet Quartz), [SOL] = 1 mM.

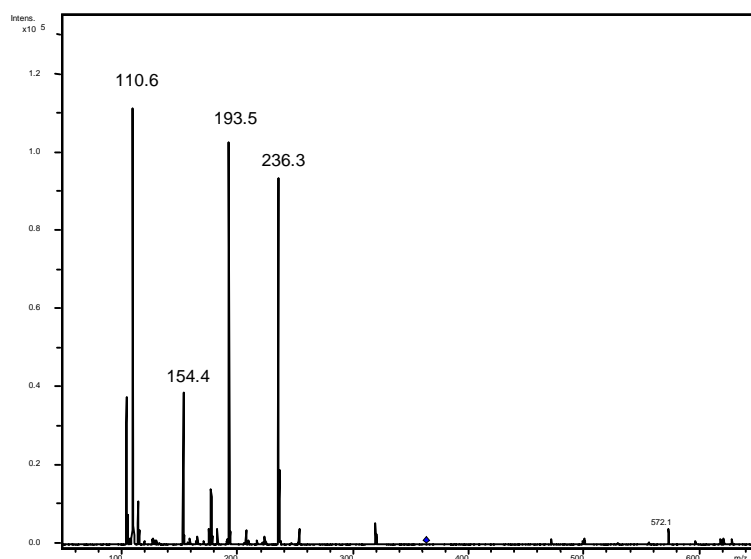


Figure 4.107: DI-MS/MS of m/z = 363 showing the fragment ions for Solifenacin: m/z 236, 193, 154, 110.

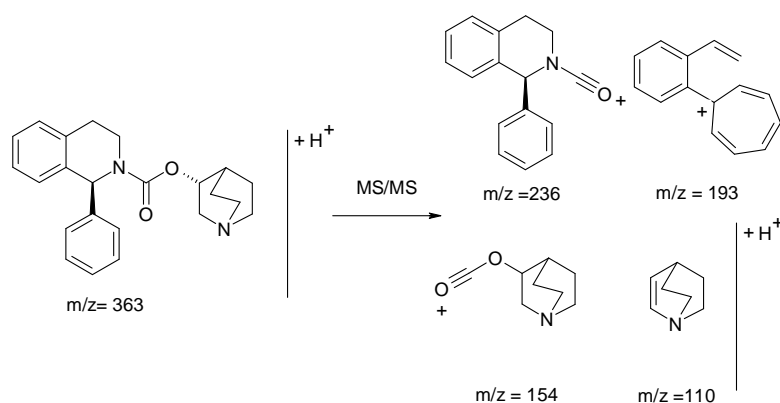


Figure 4.108: Solifenacin's parent ion $m/z = 363$ and its daughter ions $m/z = 236$, $m/z = 193$, $m/z = 154$ and $m/z = 110$.

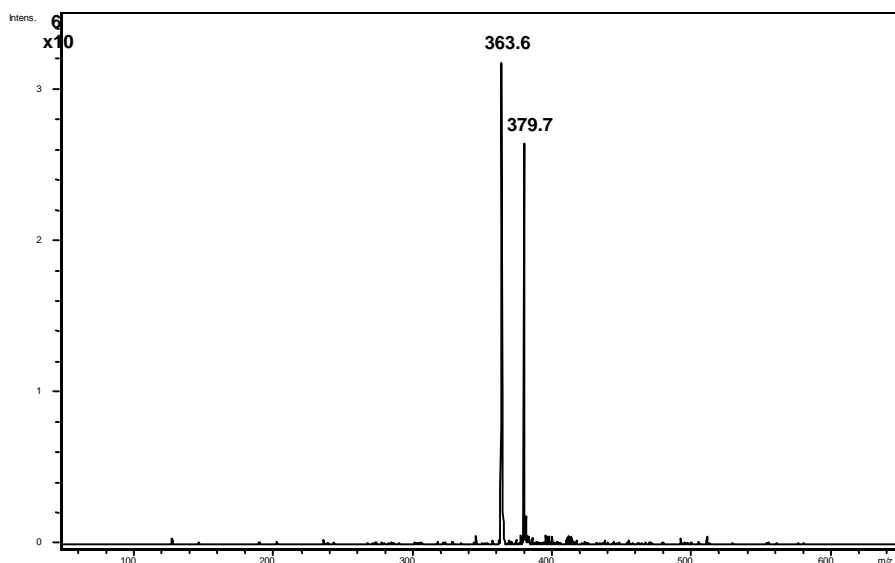


Figure 4.109: DI-MS of a 300 mins sample of a photolysis experiment. Showing $m/z = 363$ (Solifenacin's parent ion) and the intermediate $m/z = 379$. Photolysis, (Enviolet Quartz), [SOL] = 1 mM.

In the mass spectra of the photolysis of Solifenacin, Figure 4.109, after 300 mins only two main signals are in the spectra. The signal at $m/z = 363$ which is Solifenacin and a structure giving a signal at $m/z = 379$. Both signals are at quite a high intensity and have a high abundance in the sample. 379 is the addition of a +16 mass to Solifenacin, which means that at some point on the molecule an oxidation has occurred.

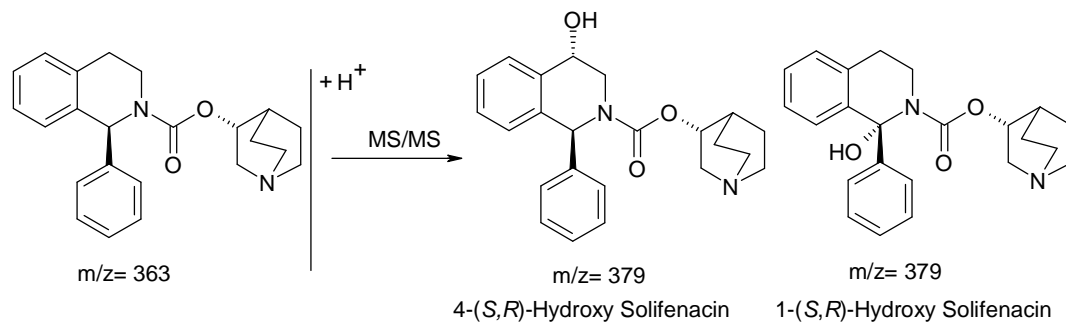


Figure 4.110: Solifenacin possible hydroxylation sites from photolysis.

Figure 4.110 shows two possible hydroxylation sites for Solifenacin which involve oxidation at the two benzylic carbons. It can be assumed that the most likely product is 1-(*S,R*)-hydroxy-Solifenacin since a hydroxylation at this site will be much more stable due to the extended conjugation provided by the two phenyl rings. 4(*S,R*)-hydroxy-Solifenacin has been determined as a well-known metabolite of Solifenacin and was used in work by Yanagihara 2007.¹⁵¹ Since enzymes are enantioselective, this is the exclusive metabolite of Solifenacin in vivo however, in photocatalysis studies, hydroxyl radicals are unselective species so a mixture of these two compounds is expected, however, a much larger amount of the 1-(*S,R*)-hydroxy is likely.

4.2.14 Follow-Up Direct Infusion Mass Spectrometry Studies: Solifenacin

Follow-up DI-MS studies were performed using a 1 mM Solifenacin photocatalytic experiment. This data was corroborated with later LC-MS/MS data, however due to our suspicions of isomers with Solifenacin, these data alone were of limited use.

Mass m/z	Fragments m/z	Mass m/z	Fragments m/z
469	<u>451</u> , 425, 414, 396, 365, 340, 284	421	<u>403</u> , 362, 315, 251, 193, 128
467	448, <u>423</u> , 378	415	<u>397</u> , 362, 317, 288, 252, 226, 154
461	443, <u>371</u> , 273, 259	413	395, 379, <u>363</u> , 353, 329, 307, 250, 224, 154
454	435, <u>391</u> , 334, 317	411	393, <u>377</u> , 342, 285, 254, 128
454	435, 316, 119, 102, <u>93</u>	410	400, 365, <u>229</u> , 75
454	<u>435</u> , 392, 366, 291, 217, 68, 55	402	<u>365</u> , 58
451	<u>433</u> , 414, 391, 280, 198, 133	400	380, 363, <u>280</u> , 252
451	<u>433</u> , 389, 361, 280, 154	395	377, <u>349</u> , 301, 259, 213, 194, 154, 128
445	<u>427</u> , 399, 381, 300, 153,	395	<u>377</u> , 351, 301, 268, 209, 154
439	421, 403, 380, <u>363</u> , 237	395	<u>377</u> , 362, 349, 268, 224, 154, 142
436	417, 363, 330, 309, 290, <u>282</u> , 272, 248	388	380, <u>369</u> , 350, 327, 285, 180
435	391, 361, <u>308</u> , 290, 248, 205, 172, 154, 128	388	379, <u>369</u> , 217, 154
431	<u>411</u> , 395, 367, 286, 154	388	411, <u>369</u> , 274, 154
426	<u>407</u> , 383, 363, 287, 239	385	<u>381</u> , 366, 184
423	<u>405</u> , 364, 254	379	<u>363</u> , 361, 252, 209, 154, 110

Table 4.15: Table of masses found in follow-up DI-MS studies and their fragments. (DI-MS/MS). Ions in bold and underlined denote the base peak found in that mass spectrum.

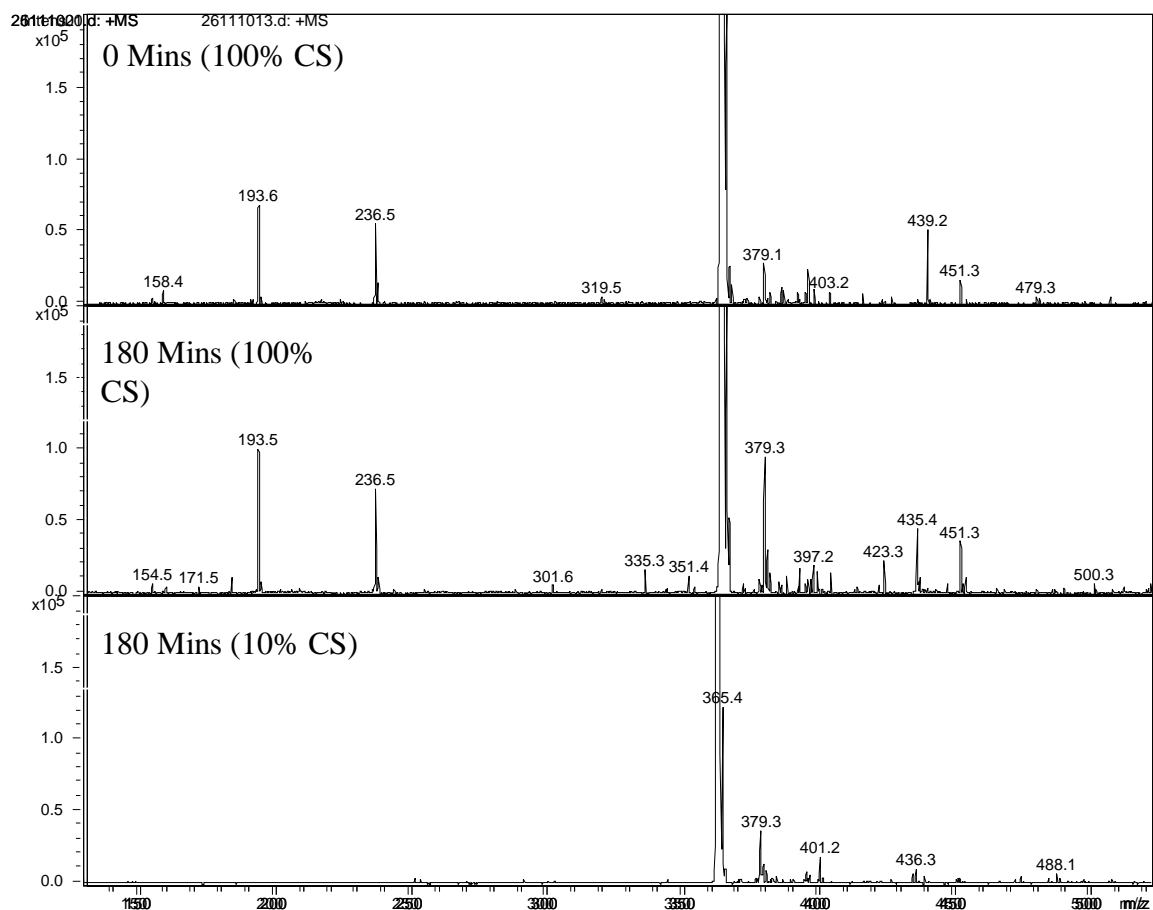


Figure 4.111: Solifenacin direct infusion mass spectra at 0 Mins (100% CS), 180 Mins (100% CS), and 180 Mins (10% CS). Photocatalysis [SOL] = 1 mM, 0.1 g/320 mL TiO₂.

4.2.15 LC-MS/MS Studies and Intermediate Analysis: Solifenacin

LC-MS/MS analysis of four Solifenacin photo-degradation experiments were performed: (1) firstly, the optimized photocatalysis with 0.1 g/320 mL TiO₂ and [0.083 mM] Solifenacin. (2) an additional photocatalytic experiment was performed at a much higher concentration of [1 mM] Solifenacin and 0.1 g/320 mL TiO₂. This heightened concentration was performed in order to see intermediates with higher sensitivity. (3) and (4) photolysis experiments with both Quartz and Pyrex were also analysed using LC-MS/MS at the optimum concentration of [0.083 mM] Solifenacin. Two tables (Table 4.16 and 4.17) are presented showing all of the ions found in each chromatogram for all experiments. Beside each ion in the table is the retention time that ion appears at in the chromatogram. Table 4.18 and 4.19 summarise all intermediate ions found in these experiments including their fragments, retention times, Mol. Wt. and calculated Log P values. Ranges of Log P values are shown where isomers exist and underlined in bold is the log P values of the isomer presented. Following these tables are individual EIC chromatograms for each significant intermediate ion found including their mass spectra and the MS/MS for that ion and the proposed intermediate structure.

	Photocat (1mM)	Photocat (0.083mM)
0Mins	363 (47.6), 275 (2.4)	363 (52.7), 275 (2.4)
0Min P.	363 (47.6), 275 (2.4)	363 (53.5), 275 (2.4)
5Mins	463 (2.5), 445 (2.7), 413 (3.9), 395 (19.1,28.6), 379 (14.8, 18.5, 20.9, 25.1, 38.1) 377 (31.3pnd, 25.6pnd), 363 (46.7), 303 (3.9 pnd), 301 (5.1 pnd), 275 (2.4)	463 (2.4), 445 (2.9), 433 (2.5), 415 (3.4, 26.2), 413 (4.8), 411 (7.4), 399 (4.3), 397 (4.6), 395 (6, 7.9, 10.7, 11.6, 19.5pnd, 28.1), 379 (12.2, 14.4,15, 18.7, 20.9, 25.7, 39.2), 377 (26, 31.5), 363 (54.1), 343 (4.1), 303 (3.9), 301 (5.1pnd)
10Mins	463 (2.5), 445 (2.6), 415 (25.6pnd,18.8pnd) 413 (3.9pnd), 397 (3.9), 395 (10.7, 18.9, 28.1, 7.7pnd, 15.9pnd), 379 (12, 14.3, 15, 16.3, 18.4, 20.8, 25, 38.2) 377 (26, 31.2), 363 (46.5), 303 (3.9pnd), 301 (5.2), 275 (2.4)	445 (2.6), 433 (2.6), 415 (3.2, 26.5), 411 (7.2), 395 (5.9, 7.9, 10.7, 16.1, 19.1, 27.9), 379 (12.1, 14.4, 15, 18.9, 21, 25.4, 39.6), 377 (26.1, 31.8), 363 (54.9), 303 (4), 301 (5.1),
20Mins	463 (2.5), 445 (2.7), 429 (2.6), 415 (3.3pnd, 24.5pnd), 413 (3.6), 397 (3.8), 395 (7.4,10.2, 15.5, 18.4 25.8, 21.4), 379 (11.6, 14.2, 13.5, 14.2, 15.8, 17.7,19.7, 23.9, 35.9), 377 (24.4, 29.5), 363 (44.1), 303 (3.9pnd), 301 (5.1pnd), 275 (2.5)	445 (2.9), 433 (2.5), 415 (3.3, 26.6), 413 (3.5), 411 (7.1, 8.7), 399 (4.4, 6), 395 (4.8, 5.9, 10.8, 28), 379 (12.1, 14.3, 15.1, 16.7, 18.9, 21.2, 25.3, 39.7), 377 (26.1, 32), 363 (55.2), 343 (4.2pnd), 303 (3.9), 301 (5)
30Mins	445 (2.6, 3.6), 435 (26.7), 429 (2.5), 415 (3.3, 23.7pnd), 413 (3.3), 397 (3.4), 395 (7.2, 9.9, 25.6), 363 (43), 379 (11.4, 13.1, 14, 15.2, 17, 19, 23.7, 34.7), 377 (23.7, 28.5), 303 (3.9), 301 (4.9), 275 (2.4)	445 (2.9), 433 (2.6), 415 (3.4, 26.7), 413 (3.2), 411 (7.6), 397 (3.5), 395 (4.9, 6, 8, 10.8, 28.2), 379 (12.1, 14.5, 15.1, 16.8, 18.9, 21, 25.4, 39.5), 377 (26.2, 31.9) 363 (55.1), 343 (4.2pnd), 303 (4pnd), 301 (5.1).
40Mins	445 (2.7), 435 (20.4, 26.7, 30.8 pnd), 429 (2.8), 415 (3.2pnd, 24.3pnd), 413 (3.1), 395 (7.3, 9.9, 25.2pnd, 21pnd), 379 (11.4, 13, 13.9, 15.2, 17, 18.8, 23.4, 35), 377 (23.8, 28.6), 363 (43), 303 (3.9pnd), 301 (4.9pnd)	445 (2.9), 433 (2.5), 429 (2.6), 415 (3.3, 26.2pnd), 411 (7.4), 399 (4.4), 397 (3.5), 395 (4.9, 5.8,7.9, 10.9, 27.9), 379 (12.2, 14.9, 15.1, 16.6, 18.9, 21.2, 25.5, 39.5), 377 (26.5, 32), 363 (55), 303 (3.9), 301 (5.1), 243 (1.7pnd), 128 (1.6pnd)
60Mins	435 (5.5pnd, 20.4pnd, 26.9pnd), 429 (2.5pnd), 415 (3.1pnd, 23.8pnd), 413 (3.2), 397 (3.8), 395 (7.3pnd, 9.9 pnd, 14.8pnd, 20.9pnd 24.9pnd), 379 (11.4, 13.1, 13.7, 15.5, 16.9, 19.1, 23.3, 34.5), 377 (24pnd, 28.3), 363 (42.8), 303 (3.9pnd), 301 (5pnd), 275 (2.4)	445 (2.9), 433 (2.5), 429 (2.7), 413 (3.2), 411 (8.5), 397 (3.6), 395 (4.8, 5.9, 7.8, 10.8, 28.3), 379 (12.1, 14.3, 15.2, 16.7, 18.9, 20.3, 21, 25.6, 39.7), 377 (26.6, 32), 363 (55.3), 303 (3.9pnd), 301 (5.1), 243 (1.8pnd), 128 (1.7pnd).
120Mins	435 (19.2, 25.4), 433 (2.5), 415 (3.3pnd, 22.7pnd), 413 (3.4), 397 (3.6pnd), 395 (7pnd, 9.3pnd, 23.5pnd), 379 (11.1, 13.3, 14.9, 16, 17.8 22.1, 32.1), 377 (22.3pnd, 26.2pnd), 363 (39.4), 303 (3.8pnd), 301 (4.9), 275 (2.4)	429 (2.6), 415 (5.3, 26.2pnd), 413 (2.9), 411 (7.5), 399 (4.5), 397 (3.6), 395 (5, 6, 7.8, 11, 28.3), 379 (12.3, 14.3, 15, 16.7, 18.9, 21.1, 25.7, 39.6), 377 (26.4pnd, 32.5), 363 (56.5), 303 (4.1), 301 (5.1), 243 (1.9)
180Mins	435 (21.6pnd, 24.9pnd, 28.7), 429 (2.5), 413 (2.9), 397 (3.6pnd), 395 (7.6pnd, 10.4pnd), 379 (11.8, 14.6, 16.2, 17.9, 19.4, 20.3, 24.6, 37.2), 377 (25.4pnd,30.3pnd), 363 (45.6), 303 (4pnd), 301 (5.2), 275 (2.4)	429 (2.5), 413 (2.7), 397 (3.5), 395 (4.9, 5.7, 6.5, 7.7, 10.5, 27.2), 379 (12, 14.1, 14.8, 16.5, 18.3, 20.5, 25, 38.5), 377 (25.7, 31.3), 363 (53.6), 303 (3.9), 301 (5.1), 128 (1.6)

Table 4.16: Table of Ions present in the LC-MS/MS chromatographic runs of two photocatalytic experiments at 0.083 mM and 1 mM. In brackets after each ion is the retention time (in minutes) at which this ion was found in each EIC. (pnd= present however not a dominant ion)

	Photolysis (Quartz)	Photolysis (Pyrex)
0Mins	363 (53.1), 275 (2.4)	363 (50.7), 275 (2.3)
5Mins	413 (2.6), 395 (9, 4.7, 23.8), 381 (4.7, 29.5, 41.5, 42.3), 379 (25.7, 21.3, 15.4,12.0,14.5), 363 (35.7, 53.9), 128 (1.7),	379 (19.3, 24.9), 363 (50), 275 (2.3)
10Mins	413 (2.6), 397 (11.1), 395 (4.7, 23.7, 7.8, 9.5), 381 (4.7, 29.4, 41.6), 379 (39.5(pnd),25.5, 21.1, 18.8, 14.5, 12.4), 363 (54.8, 35.9 63.3), 303 (3.9), 279 (2.5), 275 (pnd), 243 (1.8), 128 (1.7)	379 , 363 (51.1), 275 (2.4)
20Mins	397 (5.5, 6.9, 8.2, 12), 395 (11.5, 23.8), 381 (42.3, 29.6, 4.7), 379 (14.3, 15.3, 18.8, 21.2, 25.7, 40.3), 363 (35.9, 56.7, 63.7), 303 (4), 243 (1.9), 275 (2.4), 128 (1.6)	379 (25., 18.8), 363 (54), 275 (2.4)
30Mins	395 (24, 11.4, 5.1, 7.8), 381 (42.3, 29.4, 4.7), 379 (40, 25.7, 21.5, 19, 14.7), 363 (56.8 64.5), 303 (4.1) , 275 (2.4), 243 (1.8), 128 (1.7)	379 (12.2, 15.5,19.3, 21.2), 363 (54.5), 445 (2.5)
40Mins	381 (29.5, 42.7), 379 (25.6, 21.1, 19), 363 (57.2), 303 (4.1), 243 (1.8), 128 (1.6),	395 (20.3, 29.7), 379 (12.3, 15.2, 19.3, 21.8, 26.1), 363 (54.9), 275 (2.4), 303 (4.1), 445 (3.1)
60Mins	303 (4), 275 (pnd), 243 (1.9), 128 (1.7),	445 (2.7), 395 (29.2), 379 (12.3, 15.7, 19.5, 21.6, 26.2, 40.6), 363 (54.4), 431 (2.5), 275 (2.4)
120Mins	275 (2.4), 243 (1.8)	395 (28.6, 16.1), 379 (12.2, 15.1, 18.7, 21.1, 25.9, 39.4), 363 (53.5), 431 (2.4), 413 (4.9), 411 (7.4), 429 (2.6), 303 (4), 445 (2.8)
180Mins	275 (2.4), 243 (1.7), 171 (2), 128 (1.6)	395 (11.4, 28.5), 379 (12.2, 15, 16.4, 18.8, 21.1, 25.6, 39.6), 363 (53.9), 431 (2.4), 415 (26.3), 411 (7.2), 275 (2.4), 429 (3.4), 445 (2.9), 303 (3.9)

Table 4.17: Table of Ions present in the LC-MS/MS chromatographic runs of two photolytic experiments at 0.083 mM and 1 mM. In brackets after each ion is the retention time (in minutes) at which this ion was found in each EIC. (pnd= present however not a dominant ion.

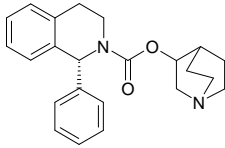
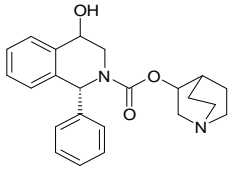
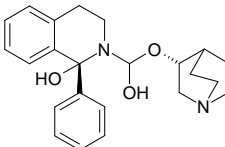
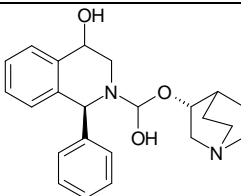
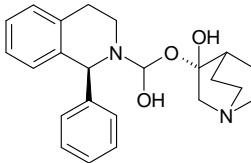
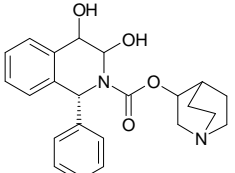
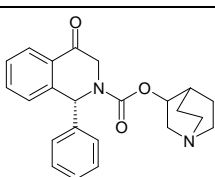
Name	Structure	Mass m/z	Daughter Ions m/z	Molecular Weight g/mol	<i>t_R</i> mins	cLog P
Solifenacin		363	236, 193, 154, 110	480	55	3.37
P379		379	361, 252, 154, 128	378	Numerous	(2.21)- (2.57)(2.37)
P381-A		381	254, 154, 110	380	4.7	2.40
P381-B		381	363, 351, 207, 154	380	29.5	2.04
P381-C		381	363, 351, 236	380	41.5	(2.2)-(2.4)
P395		395	377, 268, 250, 154, 128	394	Numerous (Isomers)	(1.4)- (2.1)(1.97)
P377		377	250, 110	376	31.2	(2.7) -(3.0)

Table 4.18: Table of Solifenacin's confirmed intermediates (degradation products), their fragments, retention times, molecular weight and calculated Log P values.^{197,198} Ranges of Log P values are shown where isomers exist and underlined in bold is the log P values of the isomer presented.

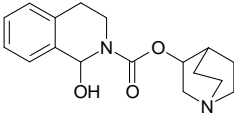
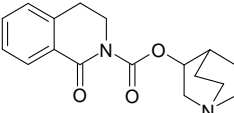
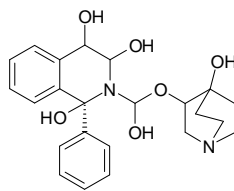
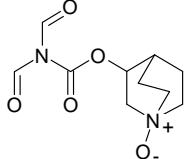
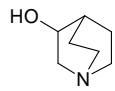
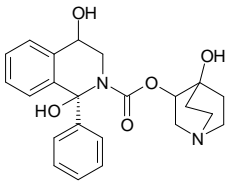
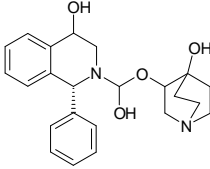
Name	Structure	Mass m/z	Daughter Ions m/z	Molecular Weight g/mol	<i>t_R</i> mins	cLog P
P303		303	154	302	4	1.34
P301		301	154	300	5	1.55
P429		429	411, 395, 284	428	2.5	(-0.04) – (0.29) (0.05)
P243		243	154, 128	242	1.7	-0.74
P128		128	No successful MS/MS	127	1.7	0.05
P411		411	393	410	7.4	(0.82) - (1.37) (0.93)
P397		397	379, 329, 252	396	3.9	(1.1) - (1.58) (1.39)

Table 4.19: Table of Solifenacin's confirmed intermediates (degradation products), their fragments, retention times, molecular weight and calculated Log P values (continued).^{197,198} Ranges of Log P values are shown where isomers exist and underlined in bold is the log P values of the isomer presented.

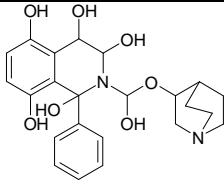
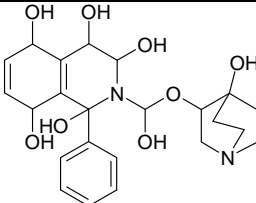
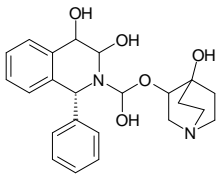
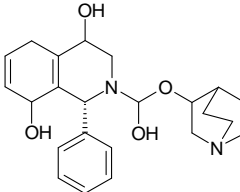
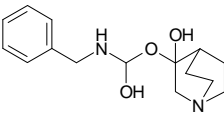
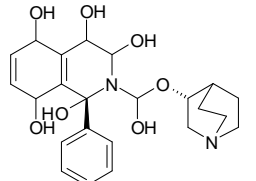
Name	Structure	Mass m/z	Daughter Ions m/z	Molecular Weight g/mol	<i>t_R</i> mins	cLog P
P445		445	427, 399, 154	444	2.8	0.36
P463		463	445, 427, 399, 381	462	2.5	-1.13
P413		413	395, 379, 363, 355	412	3.9	<u>(0.4)</u> (0.6)
P399		399	381, 211, 184, 154	398	4.4	0.68 <u>(0.93)</u>
P279		279	154, 128, 110	278	2.5	0.38
P447		447	429, 383, 353, 154	446	2.4	-0.57

Table 4.20: Table of Solifenacin's confirmed intermediates (degradation products), their fragments, retention times, molecular weight and calculated Log P values (continued).^{197,198} Ranges of Log P values are shown where isomers exist and underlined in bold is the log P values of the isomer presented.

Intermediate $m/z = 395$

The intermediate $m/z = 395$ was found in the all experiments analysed at various retention times, shown in Figure 4.112, which would indicate that various isomers of this ion are possible. Table 4.13 presents the isomers and their observed fragments. Numerous fragments were observed for each intermediate ion (presented in Table 4.21) with many of the same fragment ions appearing for most of the isomers. The ion $m/z = 395$ is composed of Solifenacin ($m/z = 363$) + 32 amu implying oxidation at two points on the molecule. Figure 4.113 shows the Solifenacin molecule with numbered positions where oxidations are possible. Two oxidations can generate up to 15 isomers. These isomers are presented in the appendices. Attempts were made to assign different isomers based on their fragmentation patterns, however some of these isomers have identical fragmentation patterns so it is not possible to distinguish between them. Figure 4.114 presents one of the isomers for $m/z = 395$ and structures for the various proposed isomers and their respective fragments. Additional isomers can be found in Appendix 4A-22. MS and MS/MS spectra for one isomer are shown in Appendix 4A-23.

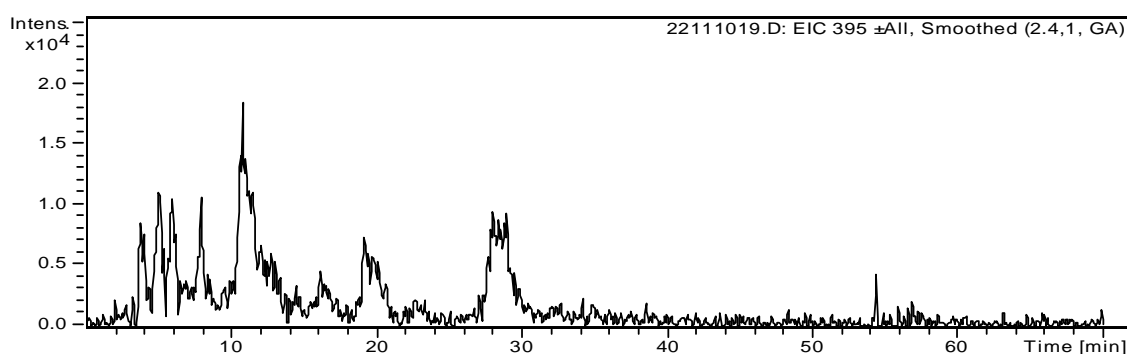


Figure 4.112: EIC of the intermediates $m/z = 395$ in 10 mins sample of a Solifenacin photocatalytic experiment. [SOL] = 0.083 mM, $\text{TiO}_2 = 0.1 \text{ g/320 mL}$.

#	m/z	MS/MS	t_R (mins)
A	395	377, 154	4.9
B	395	377, 154, 128	6
C	395	377, 250, 154	6.7
D	395	377, 268, 154, 128	8
E	395	377, 268, 250, 154, 128	10.8
F	395	377, 361, 349, 154	19
G	395	351, 154	28

Table 4.21: Daughter ions found at different retention times for $m/z = 395$.

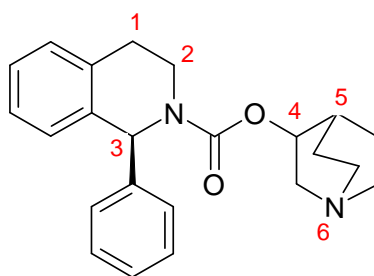


Figure 4.113 Structure of Solifenacin showing 6 of the most likely sites for oxidation. Oxidation at two positions would result in 15 possible isomers.

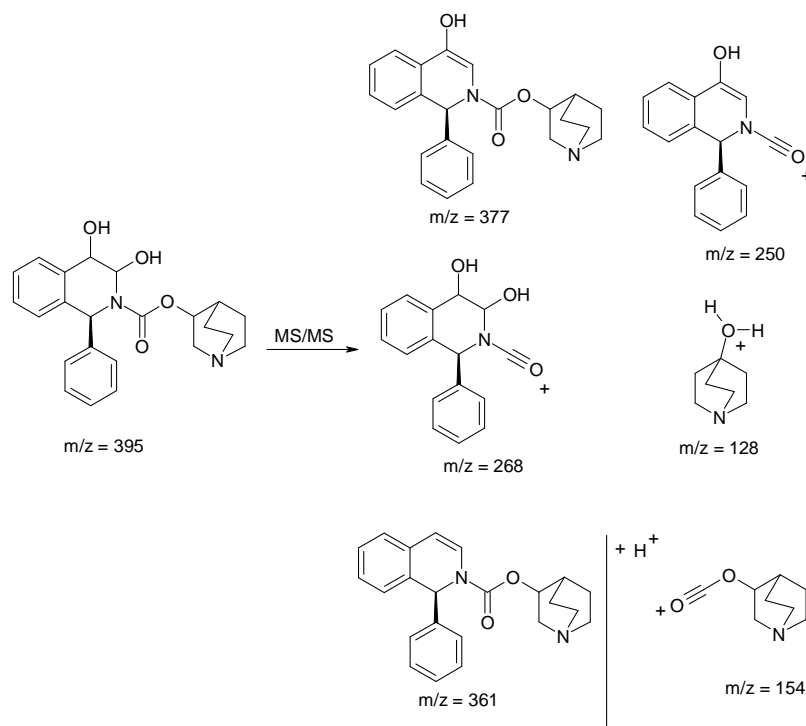


Figure 4.114: One of the isomers of $m/z = 395$ and the structures of all fragment ions detected for isomers. Additional isomers can be found in Appendix 4A-22.

Intermediate $m/z = 379$

The intermediate $m/z = 379$ was found in the all experiments analysed at various retention times, shown in Figure 4.115, which would indicate that various isomers of this ion are possible. Numerous fragments were observed for each ion, presented in Table 4.22, with many of the same ions appearing for most of the isomers. The ion $m/z = 379$, as previously discussed, is the parent ion of Solifenacin $m/z = 363 + 16$ implying oxidation at one point on the molecule. Attempts were made to assign different isomers based on their fragmentation patterns (although some isomers would have the same fragmentation patterns). Some ions presented in Table 4.13 could not be assigned at all and in general the fragments at each retention time tended to vary consistently. Figure 4.116 - 4.119 present structures for the various proposed isomers and their respective fragments. MS and MS/MS spectra are presented in the appendices (4A-24) for two of these intermediates

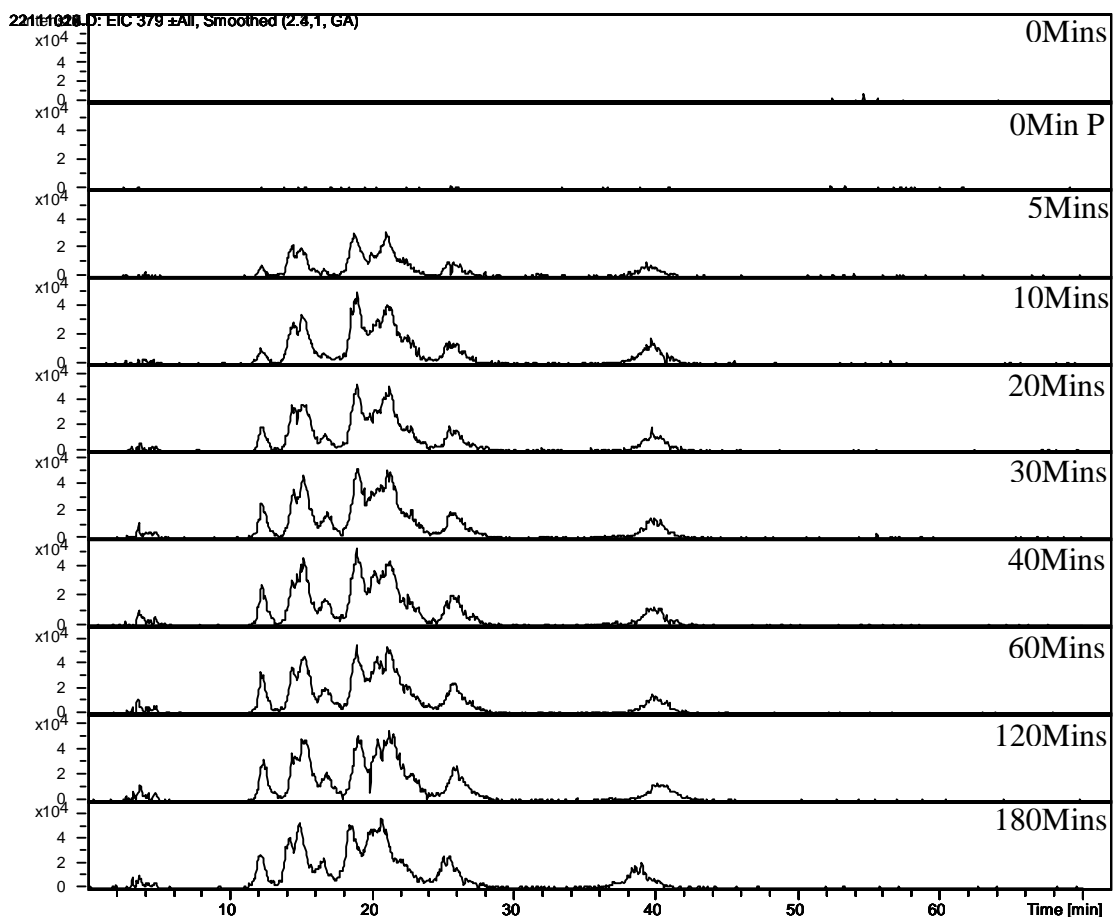


Figure 4.115: EICs of intermediates $m/z = 379$ in various samples of the optimized photocatalytic reaction. [0.083 mM Solifenacin] 0.1 g/320 mL

#	m/z	MS/MS	t_R (mins)
1	379	361, 154	11.8
2	379	361, 252, 154	14.6
3	379	361, 154	15.9
4	379	335, 252, 154, 128	17.9
5	379	375, 252, 154, 128	19.4
6	379	335, 251	20.3
7	379	208, 154, 128, 119, 110	24.6
8	379	387, 361, 239, 154, 128	37.2

Table 4.22: Daughter ions found at different retention times for $m/z = 379$. Highlighted in grey are the ions for which structures have been proposed.

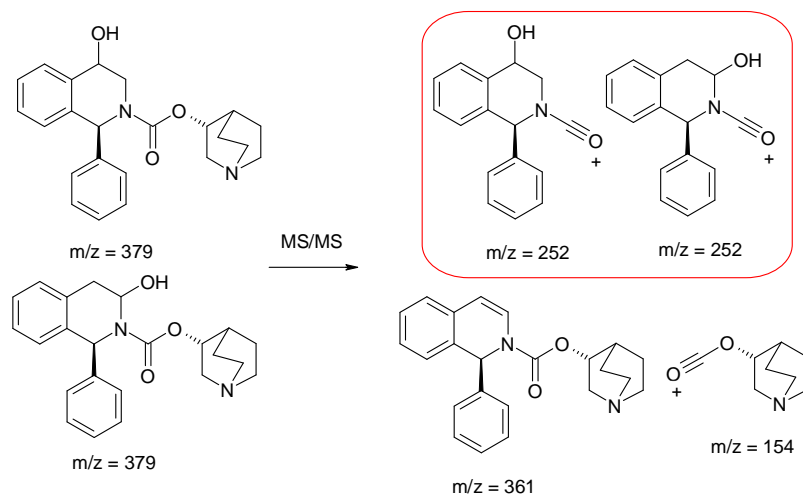


Figure 4.116: Structures proposed for $m/z = 379$ # 1 # 2 and #3 with fragments $m/z = 361$ and $m/z = 154$. The additional fragment which appeared for # 2 is also shown, possible for both.

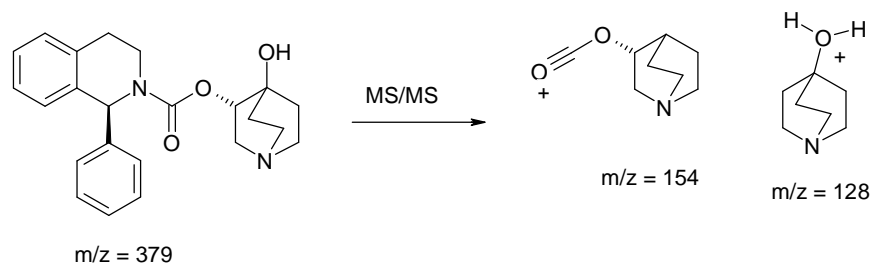


Figure 4.117: Structure proposed for $m/z = 379$ # 4 with fragments $m/z = 154$, $m/z = 128$.

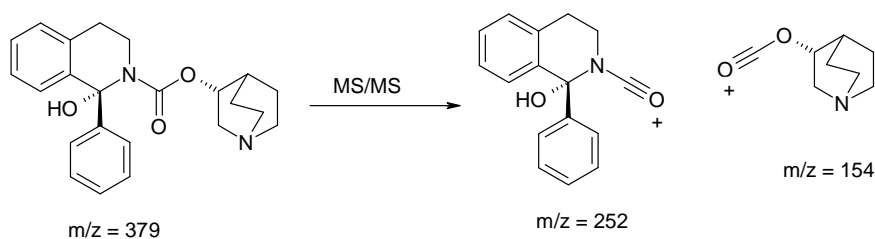


Figure 4.118: Structure proposed for $m/z = 379$ # 5 with fragments $m/z = 252$ and $m/z = 154$.

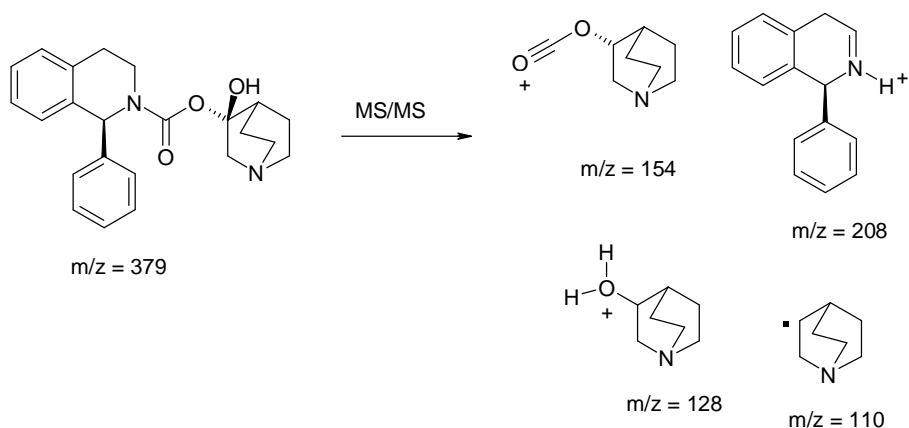


Figure 4.119: Structure proposed for $m/z = 379$ # 7 with fragments $m/z = 208$, $m/z = 154$, $m/z = 128$ and $m/z = 110$.

Intermediate $m/z = 377$

Intermediate $m/z = 377$ was found in both of the photocatalytic experiments at two retention times of 26 mins and 31.2 mins. $m/z = 377$ is the parent mass of Solifenacin $m/z = 363 + 14$, which would indicate an oxidation of an sp^3 hybridised carbon (in this case a benzylic carbon) to an sp^2 hybridised carbon (ketone). Fragments for these two peaks tended to vary consistently. In some samples, $m/z = 154$ was the only fragment for the first eluting peak. For the second peak, some fragments were common with $m/z = 207$ appearing frequently along with $m/z = 250$. The chromatograms below were taken from the sample where this ion was most abundant, and the MS and MS/MS spectra were taken from the apex of each peak. Based on these spectra two very different fragmentation patterns are shown. For the first eluting peak, the fragments were $m/z = 319$, 230 and 154. For the second peak, the fragments were $m/z = 250$ and 110. A structure for the first eluting peak could not be proposed, however, we would estimate that the oxidation must have occurred on the isoquinoline ring based on the fragment $m/z = 154$. For the second intermediate, $m/z = 377$, two structures have been proposed and are shown in Figure 4.122.

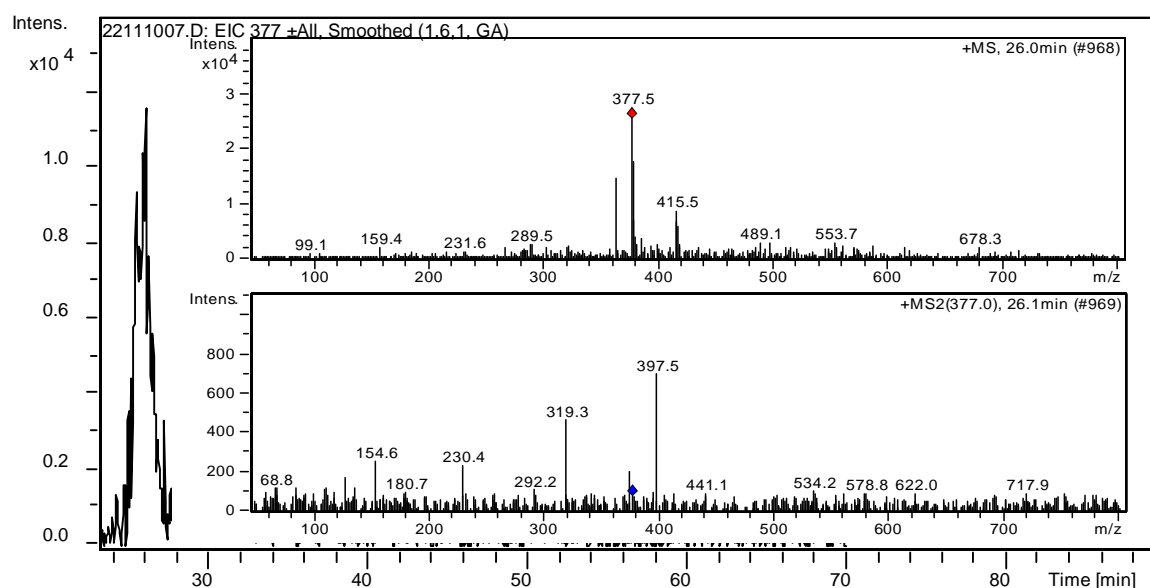


Figure 4.120: EIC of intermediate $m/z = 377$ in a 10 mins sample at a t_R of 26 mins. Inset MS and MS/MS spectra. Photocatalysis, [SOL] = 1 mM, 0.1 g TiO_2 /320 mL.

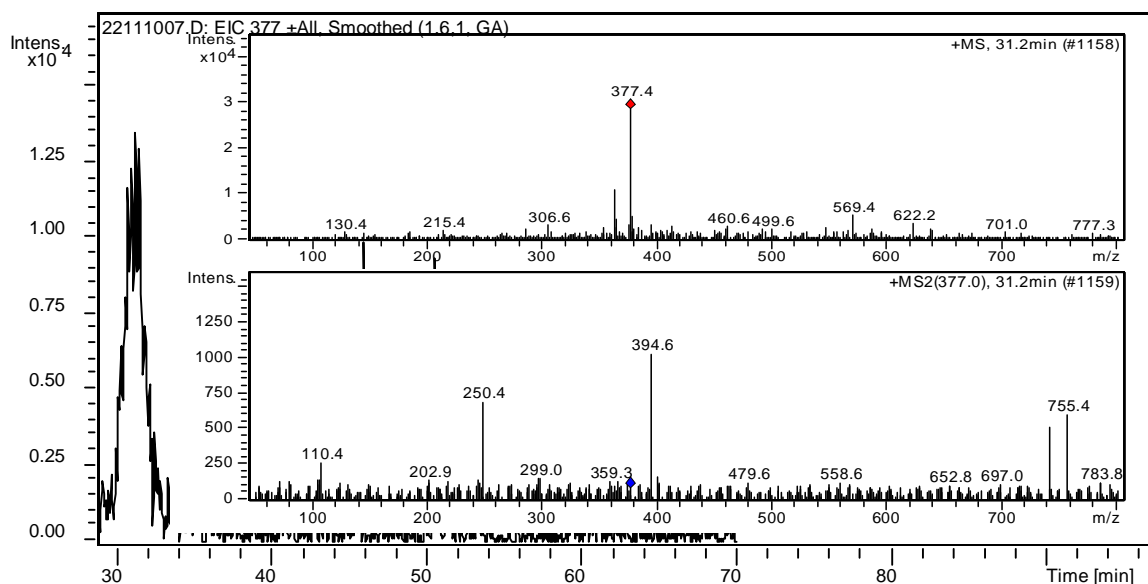


Figure 4.121: EIC of intermediate $m/z = 377$ in a 10 mins sample at a t_R of 31.2 mins. Inset MS and MS/MS spectra. Photocatalysis, [SOL] = 1 mM, 0.1 g $\text{TiO}_2/320$ mL.

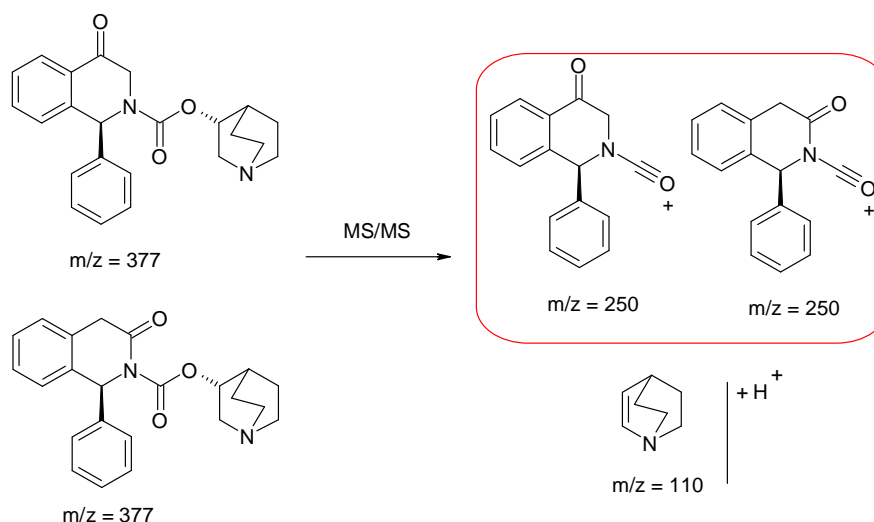


Figure 4.122: Structure proposed for $m/z = 377$ and its fragments $m/z = 250$ and $m/z = 110$. Two structures are possible and both are shown.

Intermediate $m/z = 303$

The intermediate $m/z = 303$ was found in both the photolysis and the photocatalytic experiments and was found at a retention time of 4mins. Only one fragment ion appeared for this intermediate $m/z = 154$. This would indicate that oxidation must occur on the tetrahydroisoquinoline part of the structure. The mass of 303 would also indicate a loss of something significant to the molecule. We have proposed hydroxyl radical attack on one of the primary benzylic carbons with subsequent loss of the neighbouring phenyl group. Figure 4.124 shows the structure proposed for intermediate $m/z = 303$ and its fragment $m/z = 154$.

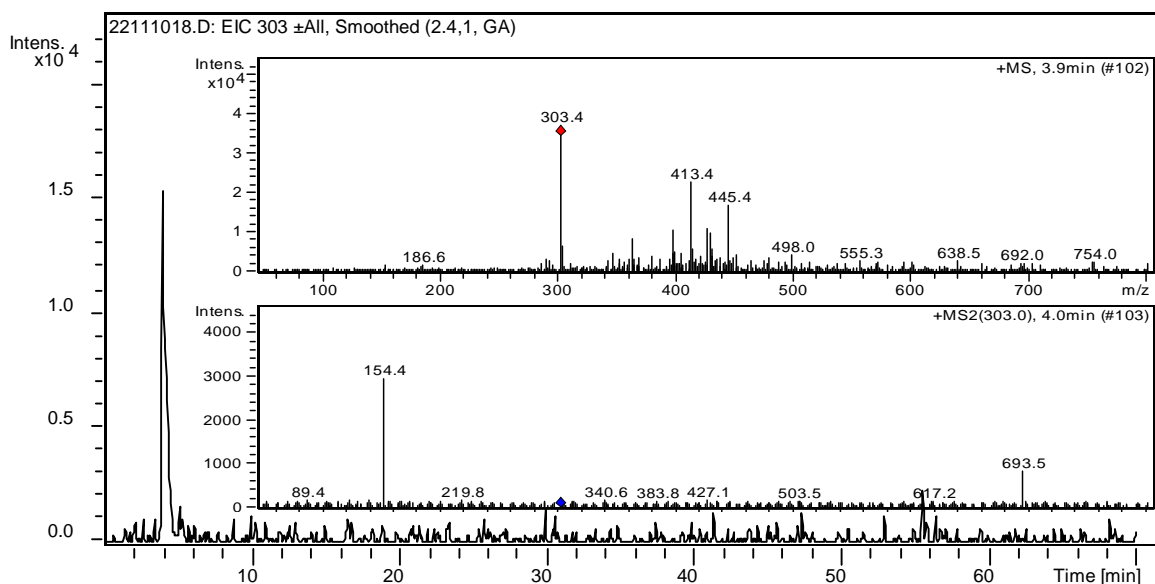


Figure 4.123: EIC of intermediate $m/z = 303$ in a 5 mins sample at a t_R of 4.0 mins. Inset MS and MS/MS spectra. Photocatalysis, [SOL] = 0.083 mM 0.1 g TiO_2 /320 mL.

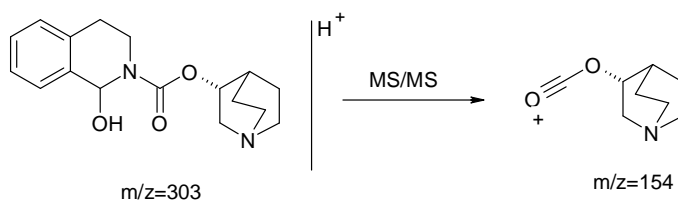


Figure 4.124: Structure proposed for $m/z = 303$ and its fragment $m/z = 154$

Intermediate $m/z = 301$

The intermediate $m/z = 303$ was found in both photolysis and photocatalytic experiments analysed and was found at a retention time of 4.9 mins. Similar to the previous intermediate, differing only by 2 mass units, this intermediate also had only one fragment ion appearing at $m/z = 154$. This would again indicate that oxidation must occur on the tetrahydroisoquinoline part of the structure as with $m/z = 303$. For this intermediate we have proposed a ketone. Figure 4.126 shows the structure proposed for intermediate $m/z = 301$ and its fragment $m/z = 154$.

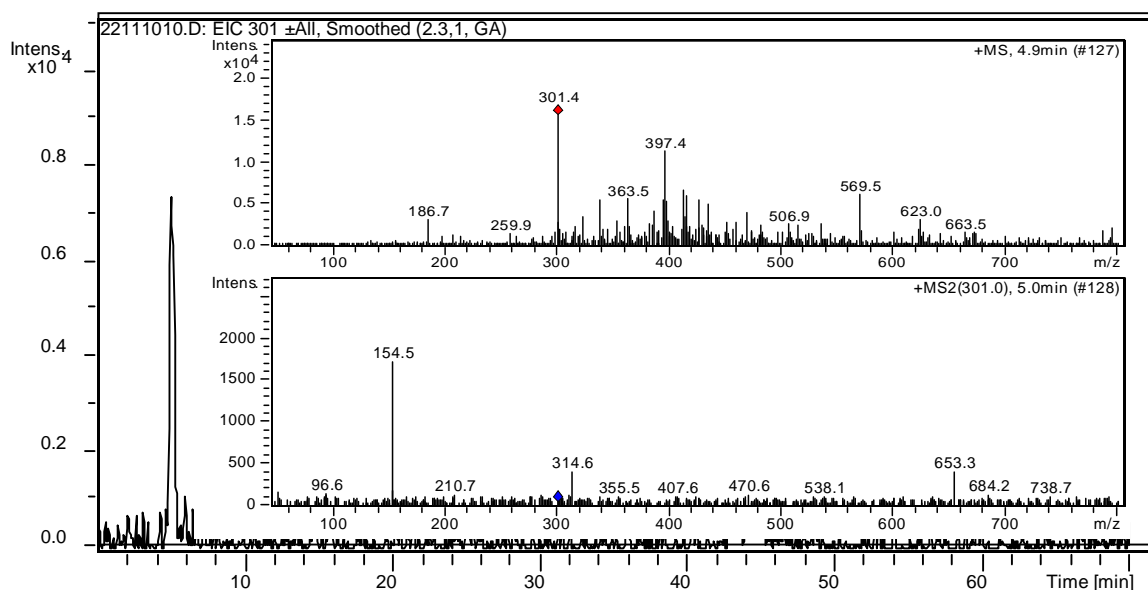


Figure 4.125: EIC of intermediate $m/z = 301$ in a 30 mins sample at a t_R of 5 mins. Inset MS and MS/MS spectra. Photocatalysis, [SOL] = 1 mM, 0.1 g TiO_2 /320 mL.

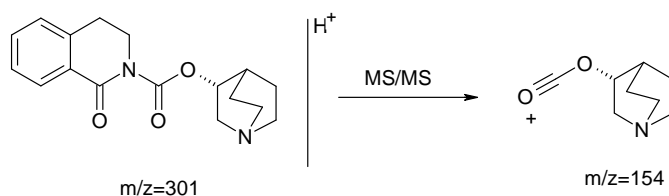


Figure 4.126: Structure proposed for $m/z = 301$ and its fragment $m/z = 154$

Intermediate $m/z = 429$

The intermediate $m/z = 429$ was found in the 1mM photocatalytic experiment at a t_R of 2.5 mins and its early retention time indicates that it is a highly polar compound. Numerous fragments appeared for this intermediate $m/z = 411$, 395, 370, 283, 224 and 172. The mass $m/z = 429$ is the parent ion for Solifenacin $m/z = 363 + 66$. This would indicate oxidation at four sites and a photo-reduction of the carbamate moiety. Only one other isomer is possible for $m/z = 429$ which is the oxidation of the alternative tertiary carbon in the quinuclidin ring. Both intermediate isomers and four of their fragments have been proposed and can be found in Figure 4.128.

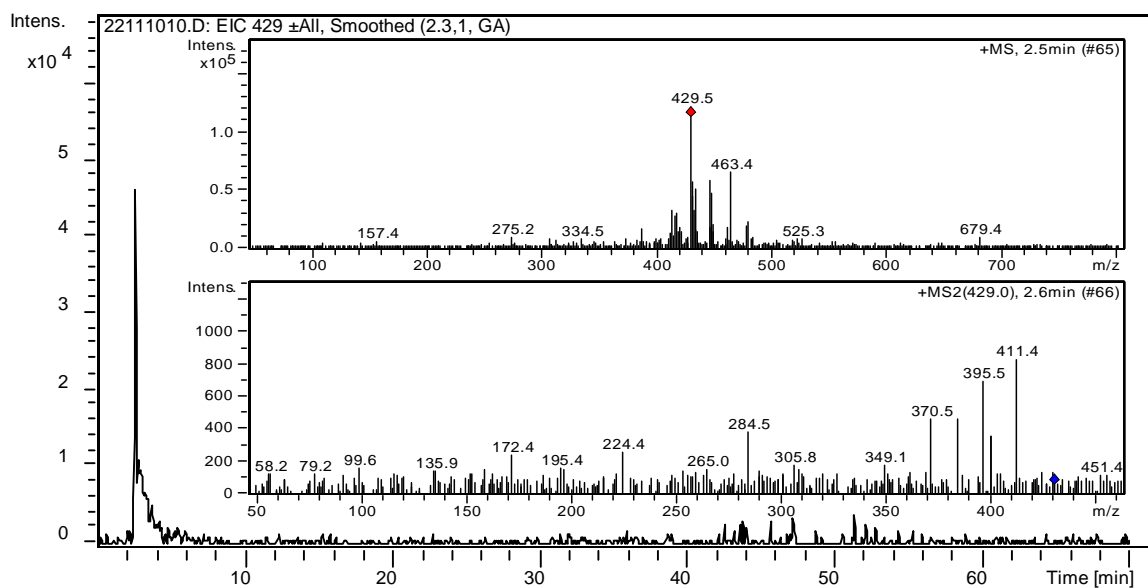


Figure 4.127: EIC of intermediate $m/z = 429$ in a 30 mins sample at a t_R of 2.5 mins. Inset MS and MS/MS spectra. Photocatalysis, [SOL] = 1 mM, 0.1 g TiO_2 /320 mL.

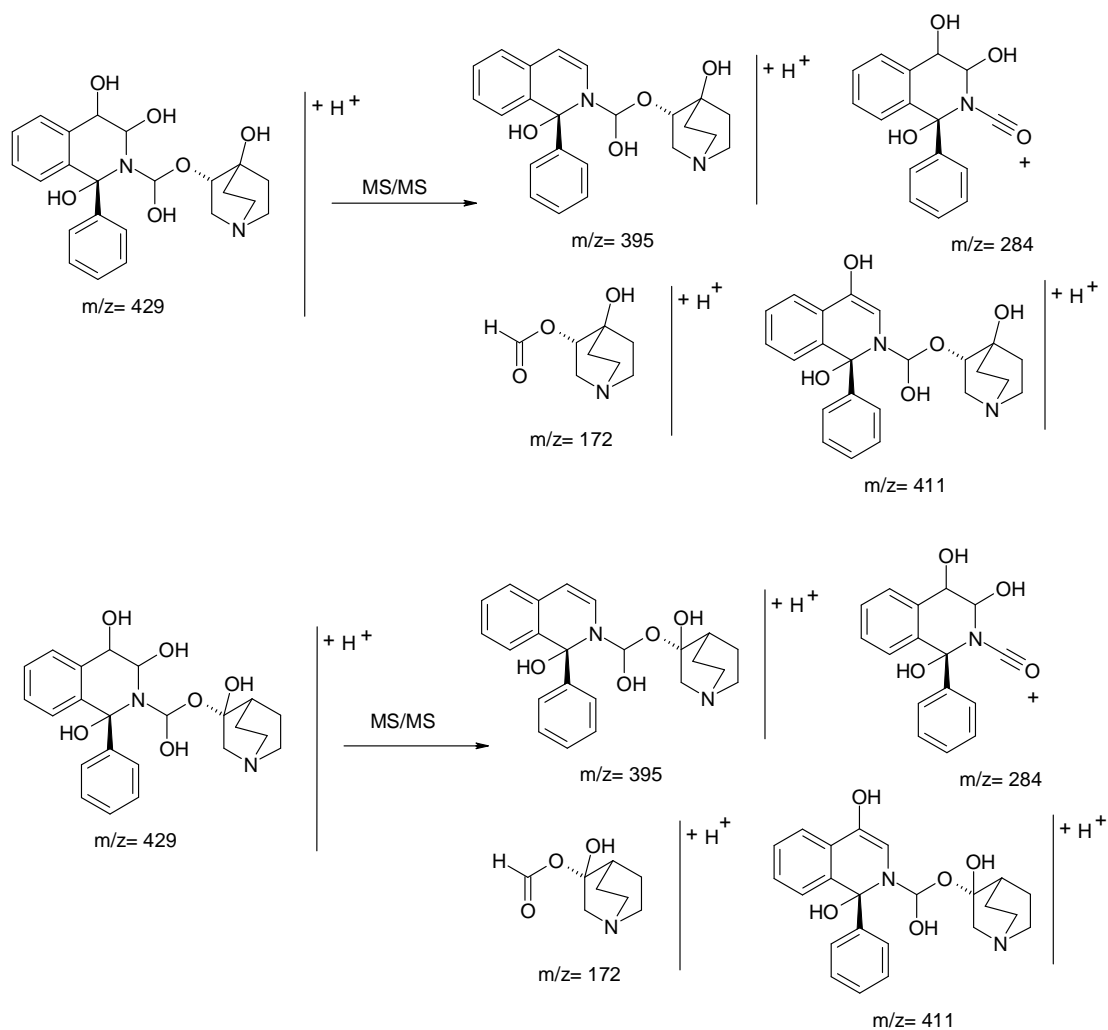


Figure 4.128: Structure proposed for the two possible isomers of $m/z = 429$ and their respective fragments $m/z = 411$, $m/z = 395$, $m/z = 284$ and $m/z = 172$.

Intermediate $m/z = 243$

The intermediate $m/z = 243$ was found in the 0.083 mM photocatalysis experiment and in the photolysis with quartz. It was present but not a dominant ion in the 1 mM photocatalysis. It was found in all experiments very early in the chromatogram at a retention time of 1.8 mins, signifying a highly polar compound. The fragments obtained for this intermediate were $m/z = 172$, 154 and 110. A structure has been proposed for this intermediate and two of its fragments are shown in Figure 4.130.

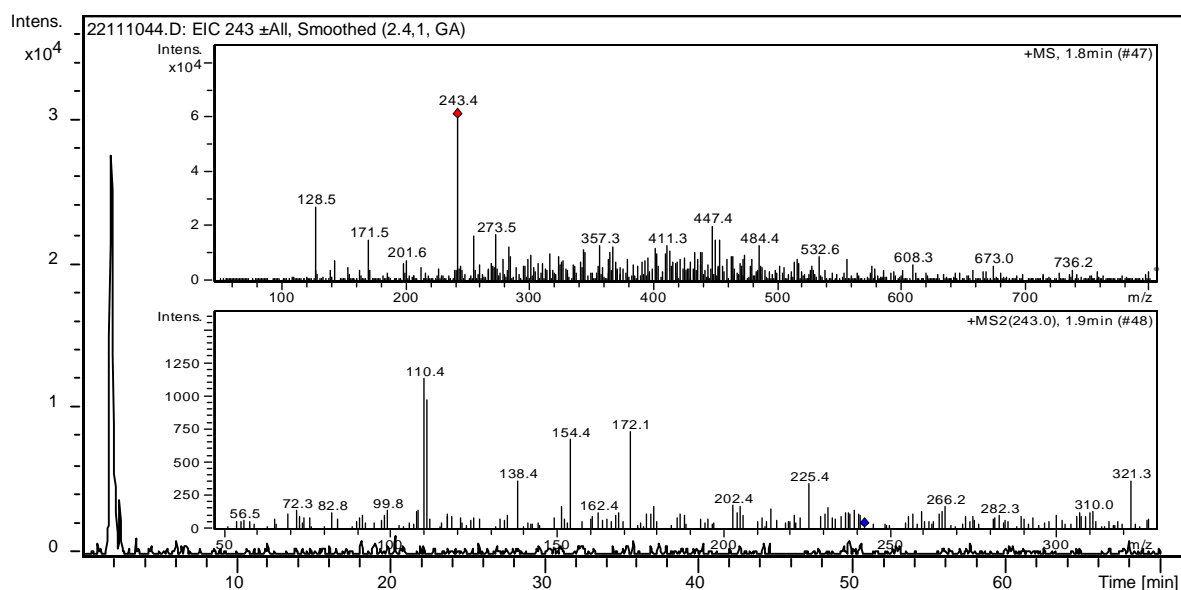


Figure 4.129: EIC of intermediate $m/z = 243$ in a 40 mins sample at a t_R of 1.7 mins. Inset MS and MS/MS spectra. Photolysis Quartz [SOL] = 0.083 mM.

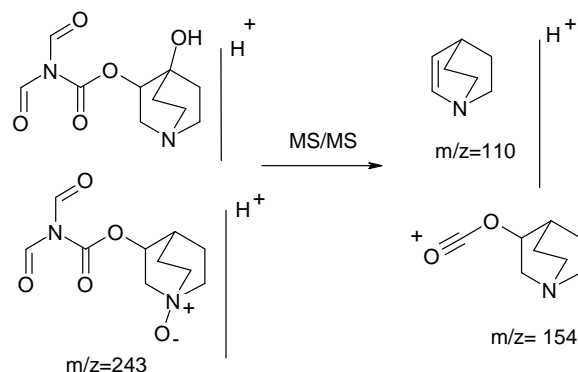


Figure 4.130: Structure proposed for $m/z = 243$ and its fragments $m/z = 154$ and $m/z = 110$.

Intermediate $m/z = 128$

The intermediate $m/z = 128$ was found in both photolysis (quartz) and in photocatalysis (0.083 mM) experiments at a retention time of 1.7 mins or 1.6 mins. No daughter ions were identified due to too low an intensity. This ion was also found in follow-up DI-MS studies. In addition, $m/z = 128$ was also found as a fragment in numerous other intermediates and its low mass would indicate an oxidation on the aliphatic amine ring ($m/z = 110 + 18$). A structure has been proposed in Figure 4.132 with the most likely fragment, $m/z = 110$, resulting from the loss of water.

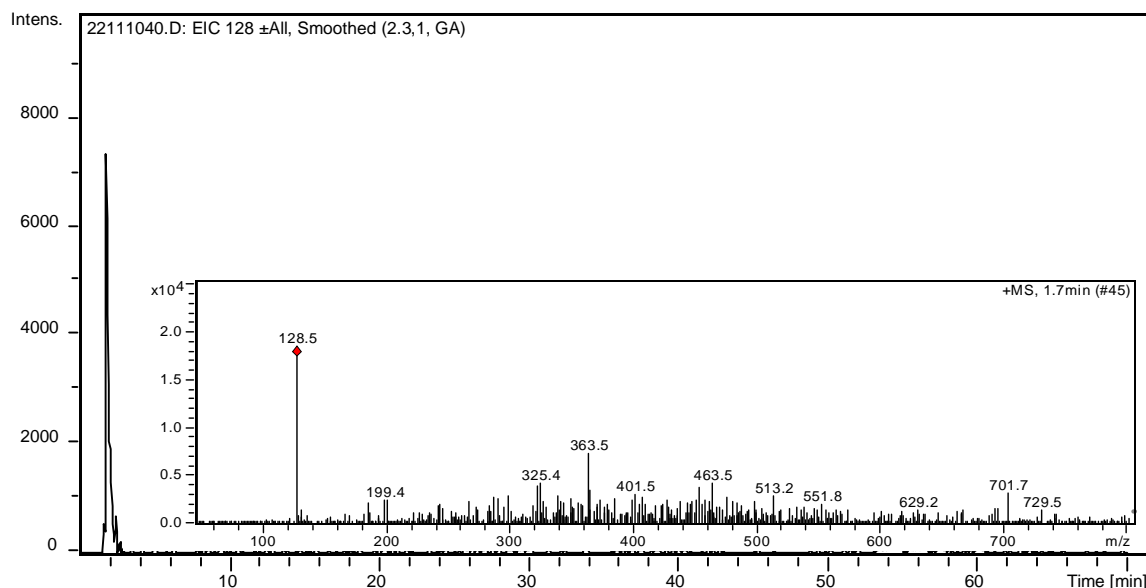


Figure 4.131: EIC of intermediate $m/z = 128$ in a 5 mins sample at a t_R of 1.7 mins. Inset MS spectrum. Photolysis Quartz, [SOL] = 0.083 mM.

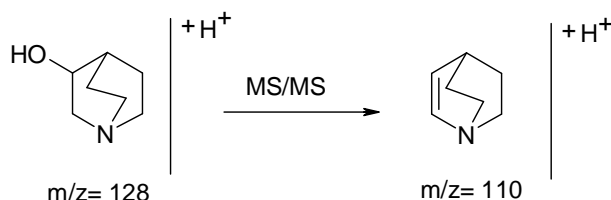


Figure 4.132: Structure proposed for $m/z = 128$ and a proposed fragment $m/z = 110$.

Intermediate $m/z = 381$

The ion $m/z = 381$ appeared at 3 different retention times 4.7 mins, 29.5 mins and 41.5 mins (Figure 4.133). This ion was only detected in the photolysis Quartz experiment. $m/z = 381$ is 2 mass units in difference to the intermediates $m/z = 379$. In addition there is an 18 mass unit difference between both parent ions and its main fragment ion (loss of water). A relationship between these ions can therefore be predicted. We believe that an identical oxidation to $m/z = 379$ is also occurring with $m/z = 381$ with hydroxyl radical attack of the benzylic carbons, and an additional photolysis (photo-reduction) of the sp^2 hybridised carbon of the carbamate. This photolysis can be initiated by light below 300 nm supplied by the absence of the filter in quartz glassware.

For the first eluting intermediate (4.7 mins), no fragment with $m/z = 363$ was detected, which would indicate a loss of water is not possible from the site of oxidation and oxidation at the benzylic carbon (tertiary carbon) is proposed (Figure 4.135). A cross sectional analysis of the MS/MS for each $m/z = 381$ intermediate was examined in each sample and additional fragments were found for each intermediate, although in general the most intense fragments were always observed. For $m/z = 381$ (4.7 mins), $m/z = 363$ was observed in some cases and for $m/z = 381$

(29 mins) an additional fragment which appeared at $m/z = 128$ did not appear in the MS/MS of the other fragments. This additional fragment would indicate that an oxidation for this intermediate is possible on the quinuclidine ring, the $m/z = 363$ fragment would further indicate that oxidation must allow a loss of water. We have thus proposed oxidation at either of the tertiary carbons in the quinuclidine ring which would facilitate a loss of water (Figure 4.137). Finally, for $m/z = 381$ (41.5 mins), we have proposed oxidation at the benzylic carbon (secondary carbon), although this or the neighbouring carbon is possible (Figure 4.139). Oxidation at the alternative benzylic carbon (tertiary carbon) is unlikely, as a loss of water (which is observed with $m/z = 363$ and $m/z = 236$) is not facilitated by this site of oxidation.

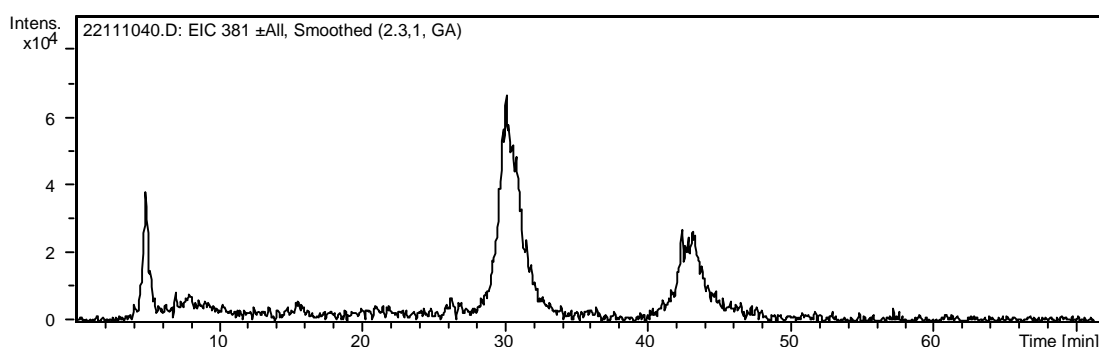


Figure 4.133: EIC for $m/z = 381$ showing 3 peaks at t_R of 4.7 mins, 29.5 mins and 41.5 mins.

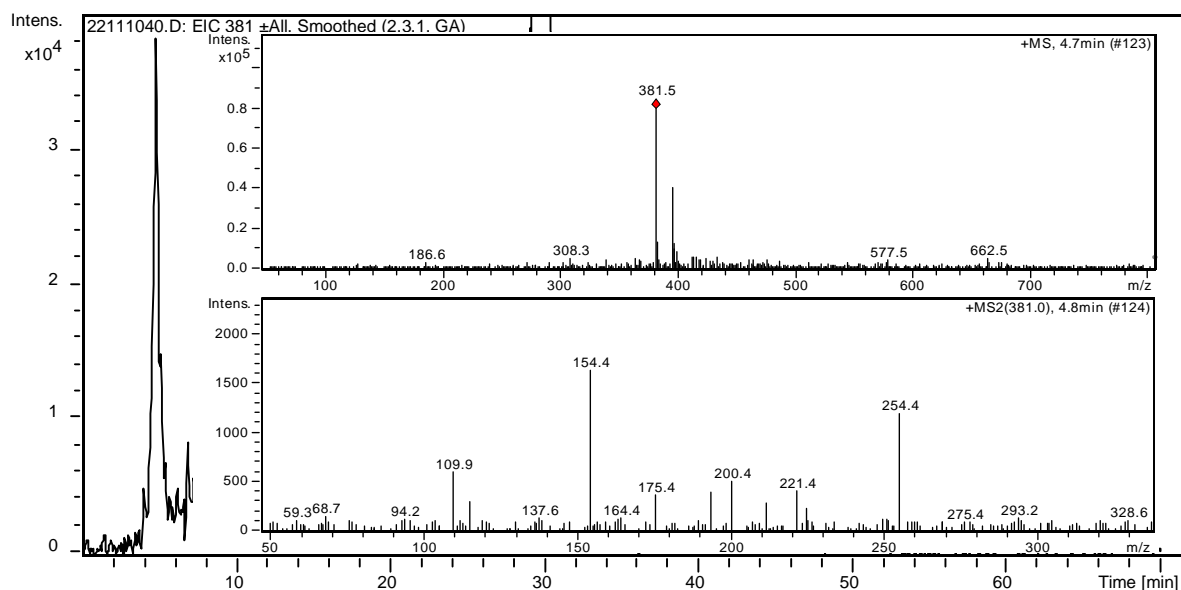


Figure 4.134: EIC of intermediate $m/z = 381$ in a 5 mins sample at a t_R of 4.7 mins. Inset MS and MS/MS spectra. Photolysis Quartz, [SOL] = 0.083 mM.

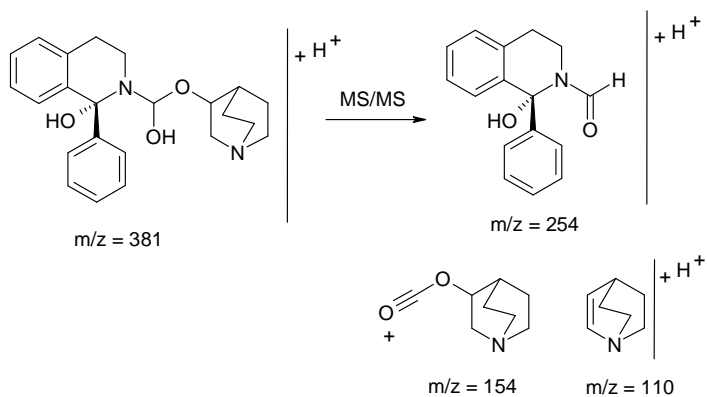


Figure 4.135: Structure proposed for $m/z = 381$ and its fragments $m/z = 254$, $m/z = 154$ and $m/z = 110$.

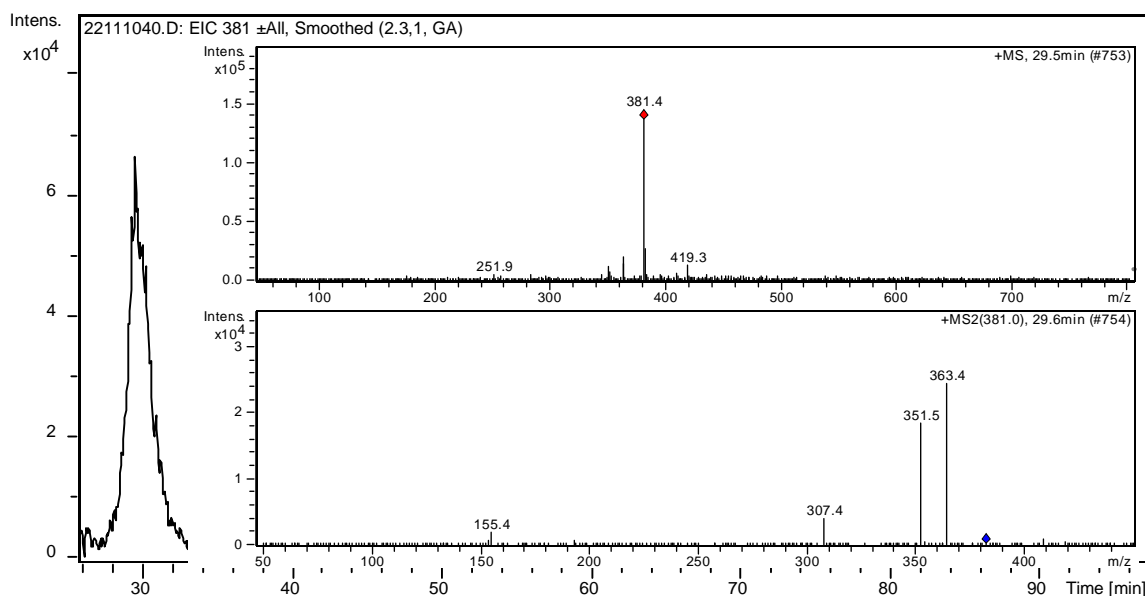


Figure 4.136: EIC of intermediate $m/z = 381$ in a 5 min sample at a t_R of 29.5 min. Inset MS and MS/MS spectra. Photolysis Quartz, [SOL] = 0.083 mM.

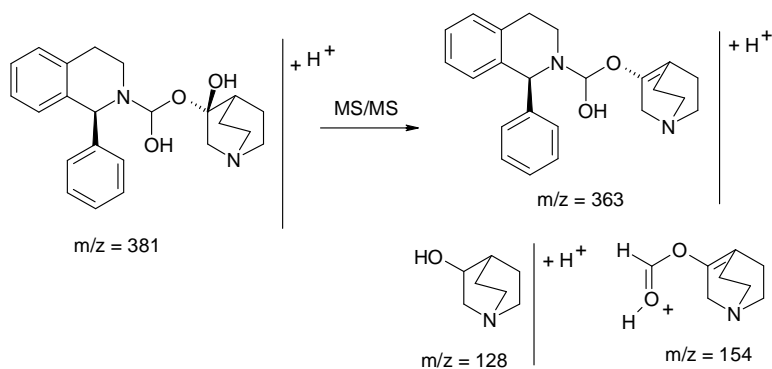


Figure 4.137: Structure proposed for $m/z = 381$ ($t_R = 29$ min) and its daughter ions $m/z = 363$, $m/z = 154$ and $m/z = 128$.

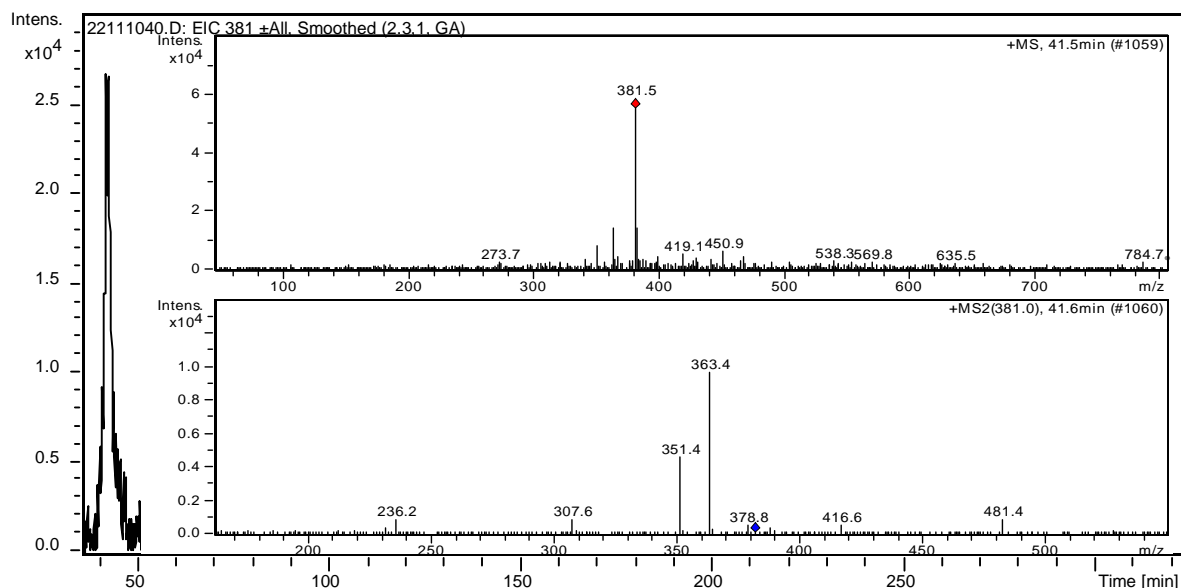


Figure 4.138: EIC of intermediate $m/z = 381$ in a 5 mins sample at a t_R of 41.6 mins. Inset MS and MS/MS spectra. Photolysis Quartz, [SOL] = 0.083 mM.

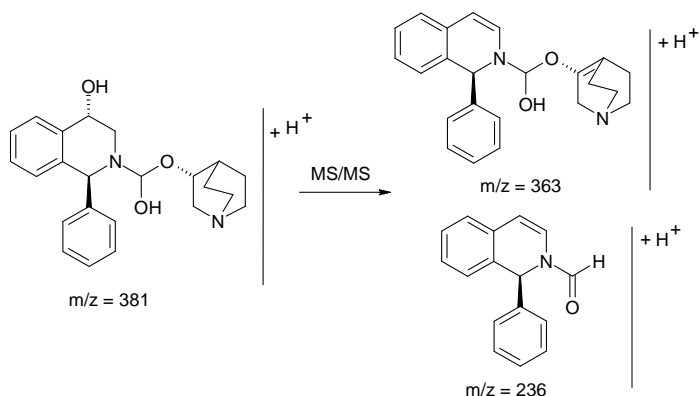


Figure 4.139: Structure proposed for $m/z = 381$ ($t_R = 41.6$ mins) and its daughter ions $m/z = 363$, and $m/z = 236$.

Intermediate $m/z = 411$

The intermediate $m/z = 411$ was found in the photocatalysis and photolysis pyrex experiments. It was present but not a dominant ion in the higher concentration experiment due to other more dominant ions in the chromatogram at that retention time. The intermediate $m/z = 411$ is $m/z = 363$ plus 48, which indicates oxidation at 3 points in the molecule. Various isomers are therefore possible for this mass. Only one fragment was detected for this ion $m/z = 393$ which is a loss of 18 mass units (water) from the parent ion. Based on this fragmentation, structures of the various possible isomers have been proposed in Figure 4.141. It should be noted that 3 other isomers are possible whereby oxidation occurs at the other tertiary carbon on the aliphatic ring in the molecule with the other two occurring on the benzylic carbons. These isomers are also shown in Figure 4.141.

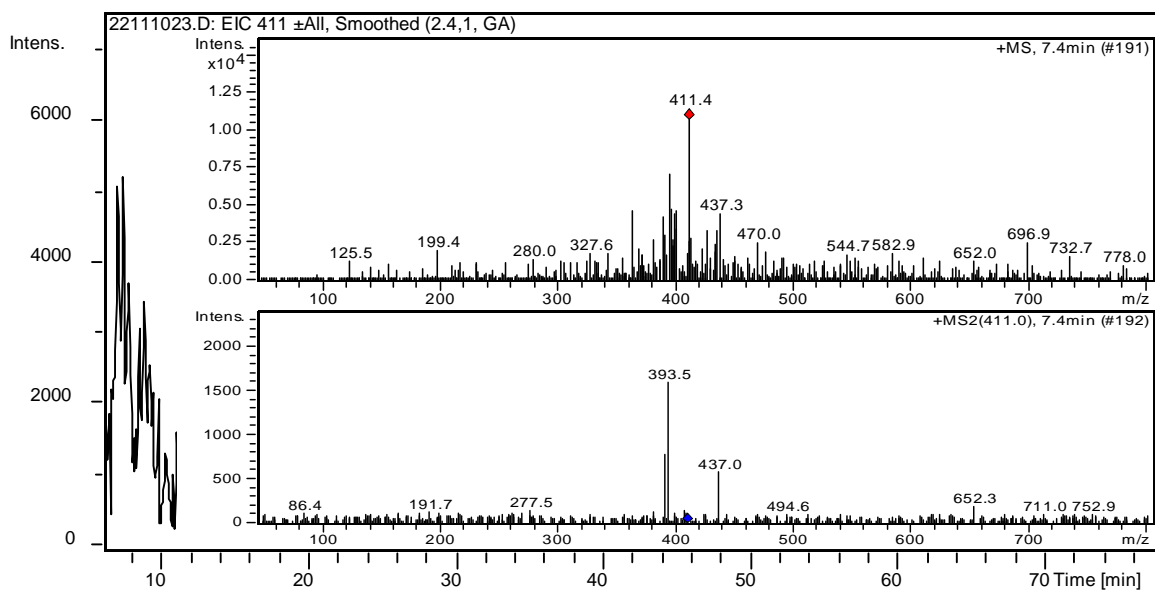


Figure 4.140: EIC of intermediate $m/z = 411$ in a 40 mins sample at a t_R of 7.4 mins. Inset MS and MS/MS spectra. Photocatalysis, [SOL] = 0.083 mM, 0.1 g TiO_2 /320 mL.

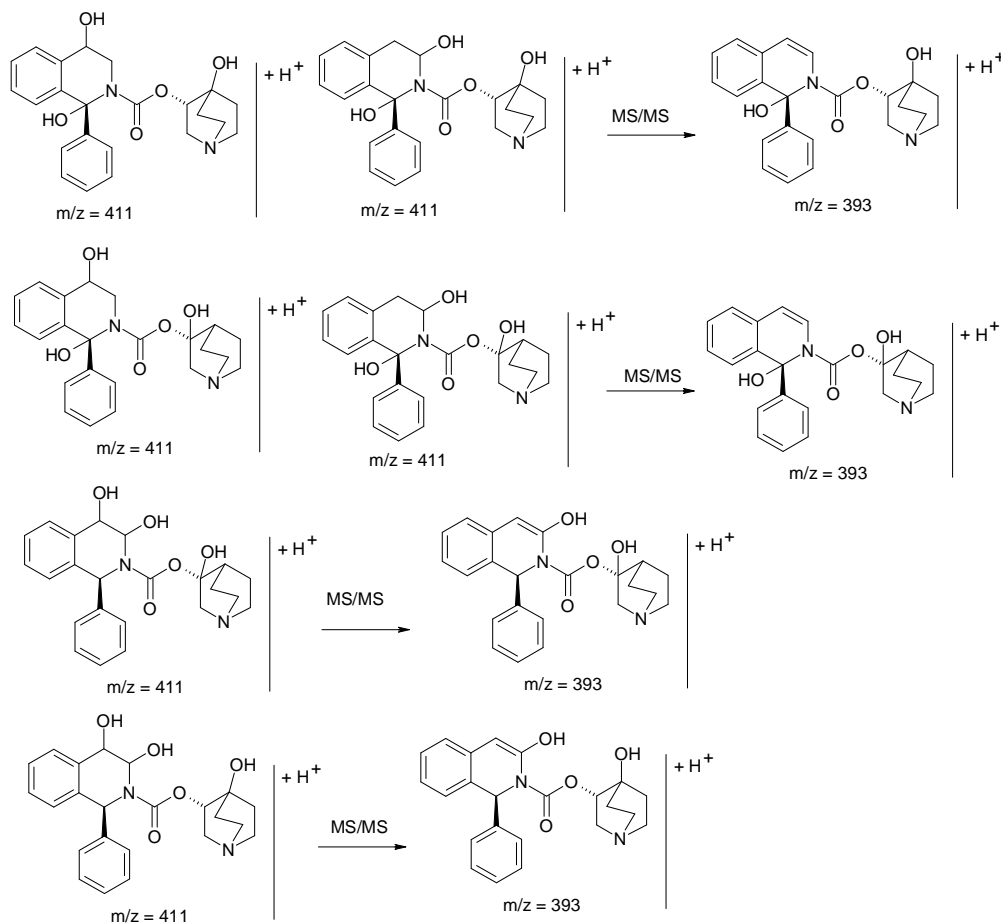


Figure 4.141: Structures of the isomers possible for $m/z = 411$ and its fragment $m/z = 393$.

Intermediate $m/z = 397$

The intermediate $m/z = 397$ was detected in both the photocatalytic experiments only at a retention time of 3.9 mins. This mass is exactly two units more than the intermediate $m/z = 395$ and we believe similar oxidations are likely with this intermediate. $m/z = 397$ is $m/z = 363 + 34$ mass units. We have proposed that oxidation of one of the benzylic carbons and one tertiary carbon in the molecule are likely in addition to the photo-reduction of the keto moiety which would account for the additional mass units in this case. The fragments from $m/z = 397$ are $m/z = 379$ (loss of water) and $m/z = 252$ which is the fragment of Solifenacin $m/z = 236 + 16$. This would signify one oxidation on the tetrahydroisoquinoline ring and one of the tertiary carbons on the quinuclidine ring in addition to the photo-reduction. In this case, four isomers are possible for this intermediate and all are shown in Figure 4.143 along with the respective proposed fragments for each isomer.

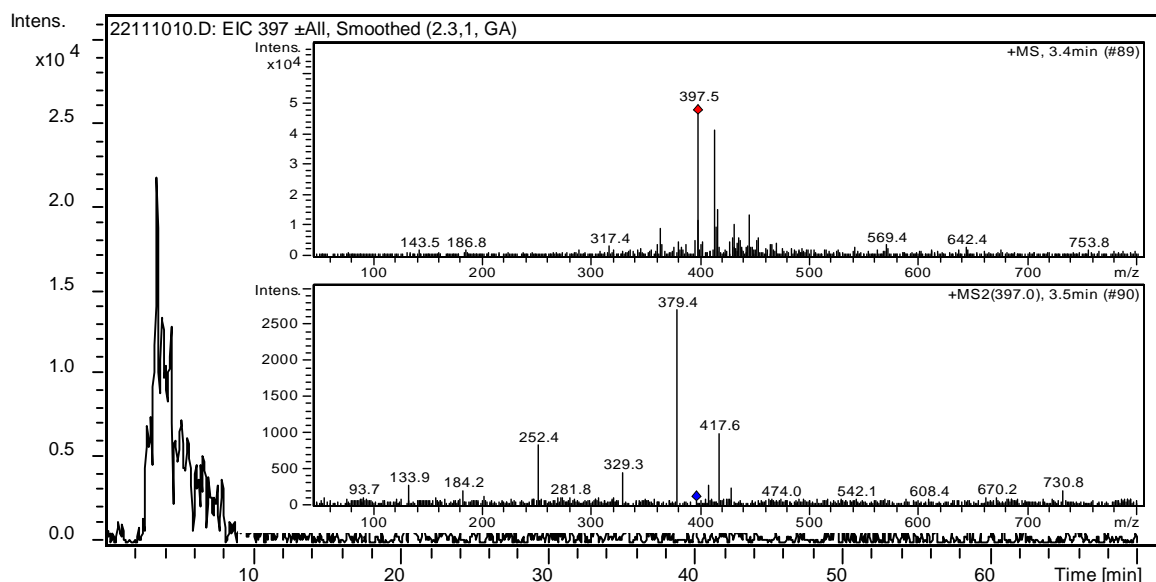


Figure 4.142: EIC of intermediate $m/z = 397$ in a 30 mins sample at a t_R of 3.9 mins. Inset MS and MS/MS spectra. Photocatalysis, [SOL] = 0.083 mM, 0.1 g TiO_2 /320 mL.

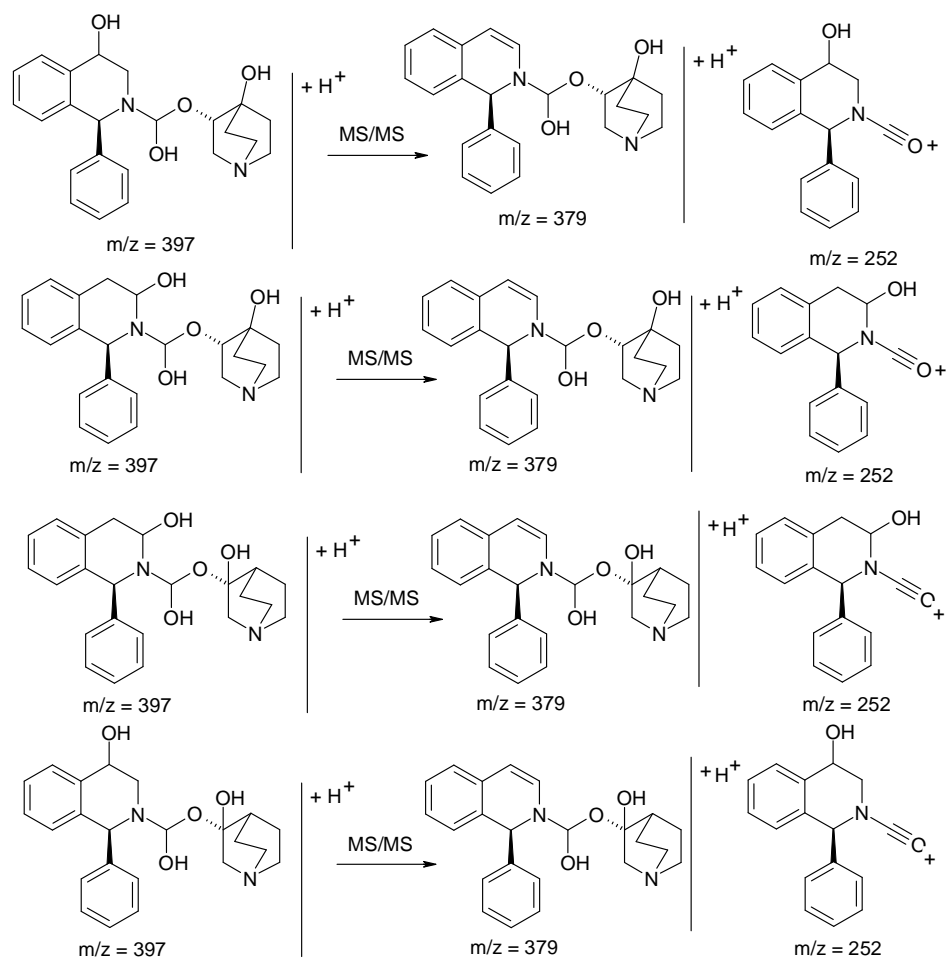


Figure 4.143: Structures of the isomers proposed for $m/z = 397$ and its fragments $m/z = 379$ and $m/z = 252$.

Intermediate $m/z = 447$

The intermediate $m/z = 447$ was found in all experiments analysed except the photolysis quartz experiment. $m/z = 447$ is $m/z = 363 + 84$ mass units, which would indicate at least 5 oxidations and a series of reductions at certain locations. The fragments obtained for this mass were $m/z = 429$ (loss of 18), 383 (loss of 64), 353 (loss of 94), 282 (loss of 165), 204 (loss of 243) and 154 (loss of 293). $m/z = 429$ has already been determined as an intermediate with multiple oxidations having occurred and we believe that the $m/z = 429$ fragment for $m/z = 447$ is an isomer of this previously determined intermediate. Although a structure could not be proposed for the fragment $m/z = 353$, its mass would indicate the loss of a monosubstituted phenyl and a hydroxyl group. The structure proposed for $m/z = 447$ and two of its fragments are shown in Figure 4.145.

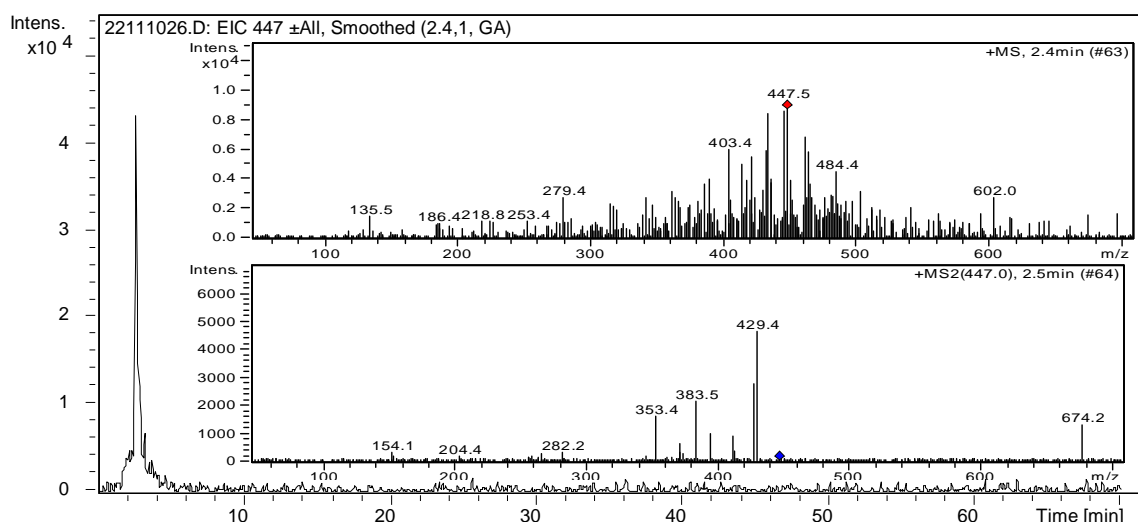


Figure 4.144: EIC of intermediate $m/z = 447$ in a 180 mins sample at a t_R of 2.4 mins. Inset MS and MS/MS spectra. Photocatalysis, [SOL] = 0.083 mM, 0.1 g TiO_2 /320 mL.

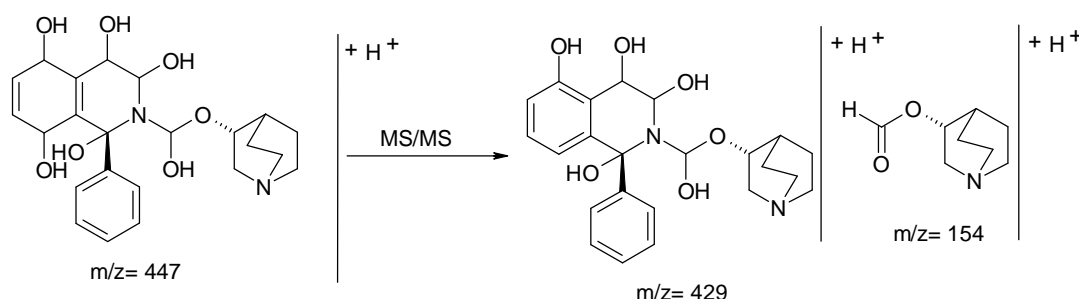


Figure 4.145: Structure proposed from $m/z = 447$ and its fragments $m/z = 429$ and $m/z = 154$.

Intermediate $m/z = 445$

The intermediate $m/z = 445$ was found in all experiments analysed except the photolysis quartz experiment. The EIC chromatogram in Figure 4.146 identifies 3 chromatographic peaks which elute as one peak and look to be irresolvable. These three peaks are isomers of $m/z = 445$ indicating that three isomers of this intermediate ion are formed and have similar polarity to one another. The fragments for this intermediate ion were $m/z = 427$, $m/z = 399$, $m/z = 381$ and $m/z = 226$. Similar to the previous mass, $m/z = 445$ is $m/z = 363 + 82$ mass units which would indicate that at least 5 oxidations and a photo-reduction is occurring. Two structures have been proposed in Figure 4.147 along with the respective isomers for the fragment $m/z = 427$ and the fragment $m/z = 154$.

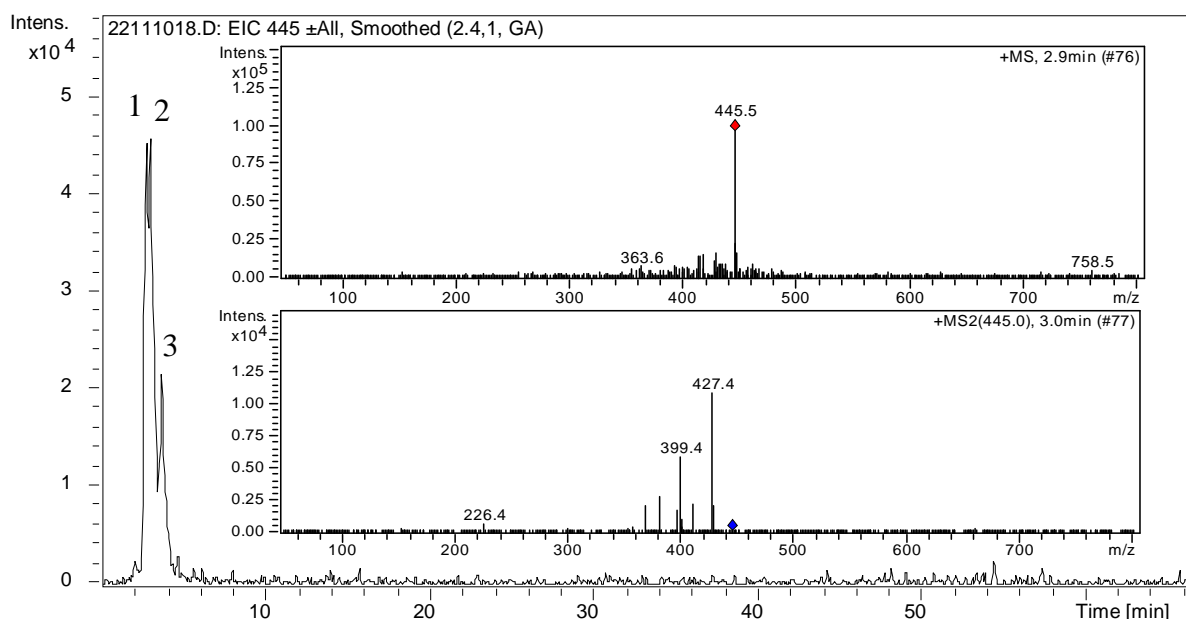


Figure 4.146: EIC of intermediate $m/z = 445$ in a 5 mins sample at a t_R of 2.9 mins. Inset MS and MS/MS spectra. Photocatalysis, [SOL] = 0.083 mM, 0.1 g $\text{TiO}_2/320$ mL.

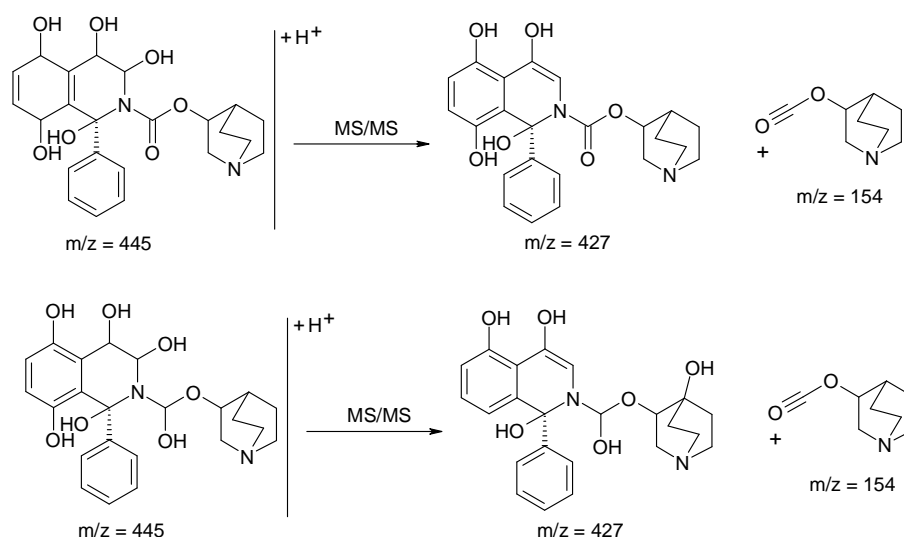


Figure 4.147: Structures of the isomers proposed for $m/z = 445$ and its fragments $m/z = 427$ and $m/z = 154$.

Intermediate $m/z = 463$

The intermediate $m/z = 463$ was found in both photocatalytic experiments eluting at a time of 2.5 mins. The high mass of this intermediate would indicate that again multiple oxidations have occurred to the parent Solifenacin structure. $m/z = 463 = 363 + 100$ which would indicate 6 oxidations and 2 sites of photo-reduction. Fragments for this intermediate were $m/z = 445$, 427, 399 and 381 amongst others. These fragments will result in multiple losses of water from the parent intermediate. A structure has been proposed for $m/z = 463$ and its fragments and is found in Figure 4.149.

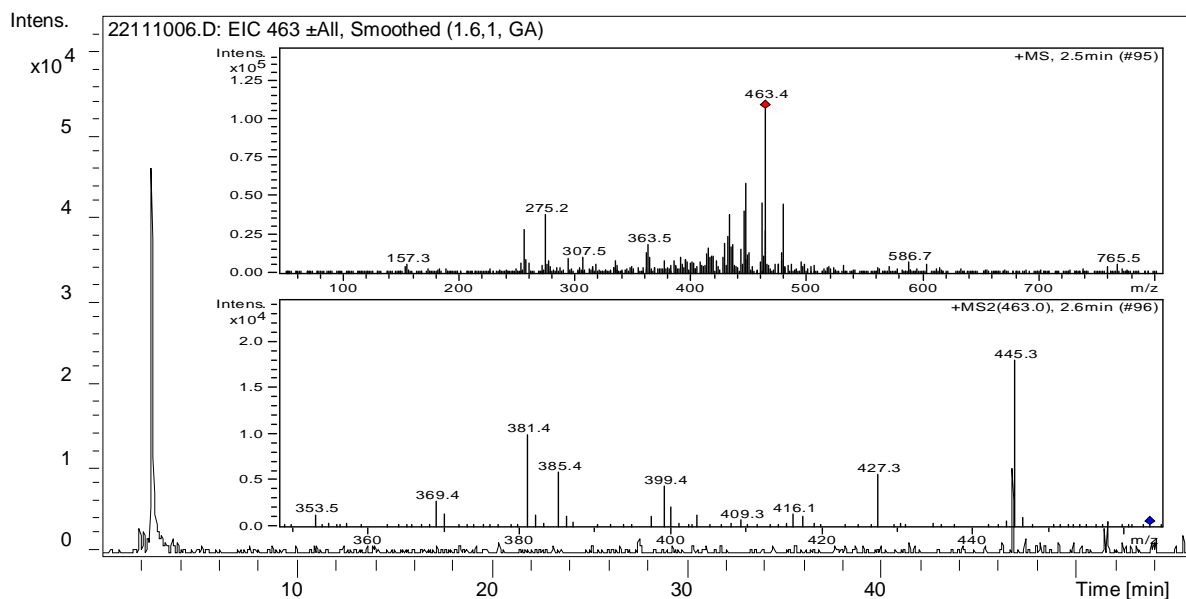


Figure 4.148: EIC of intermediate $m/z = 463$ in a 5 mins sample at a t_R of 2.5 mins. Inset MS and MS/MS spectra. Photocatalysis, [SOL] = 1 mM, 0.1 g TiO_2 /320 mL.

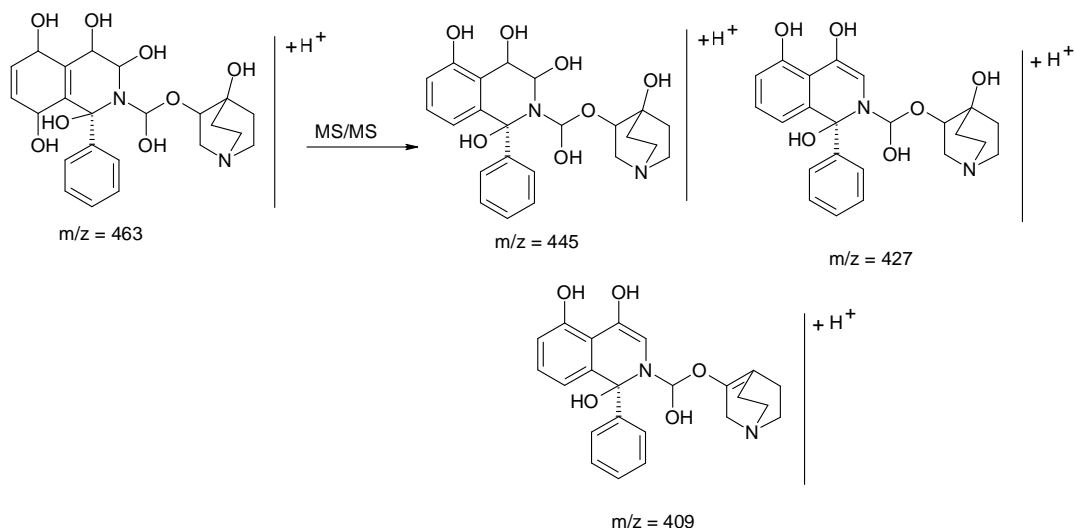


Figure 4.149: Structure proposed for $m/z = 463$ and its fragments $m/z = 445$, $m/z = 427$ and $m/z = 409$.

Intermediate $m/z = 413$

The intermediate $m/z = 413$ was detected at 3.9 mins in the 0.083 mM photocatalytic experiment. The mass $m/z = 413$ is Solifenacin's parent ion $m/z = 363 + 50$ and is also 2 mass units more than $m/z = 411$. This would indicate that oxidation occurs at 3 points in the molecule in addition to a photo-reduction which would account for the 2 extra mass units. The two main fragments detected for $m/z = 413$ are $m/z = 395$ and 379 and two possible structures have been elucidated for this mass and its fragments in Figure 4.151. It should be noted that earlier numerous isomers were proposed for $m/z = 411$. However, in the case of $m/z = 413$ certain isomers have been eliminated due to the fragment $m/z = 379$ which requires two neighbouring

hydroxyl groups which, when lost, allow the resulting radicals to combine and form the double bond.

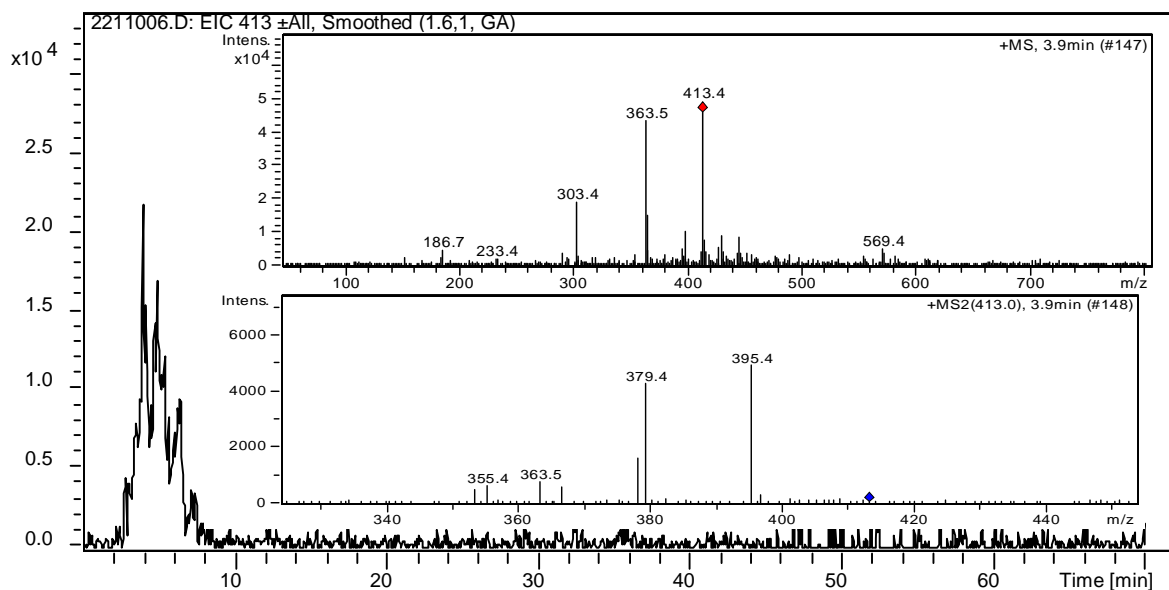


Figure 4.150: EIC of intermediate $m/z = 413$ in a 5 mins sample at a t_R of 3.9 mins. Inset MS and MS/MS spectra. Photocatalysis, [SOL] = 0.083 mM, 0.1 g $\text{TiO}_2/320\text{ mL}$.

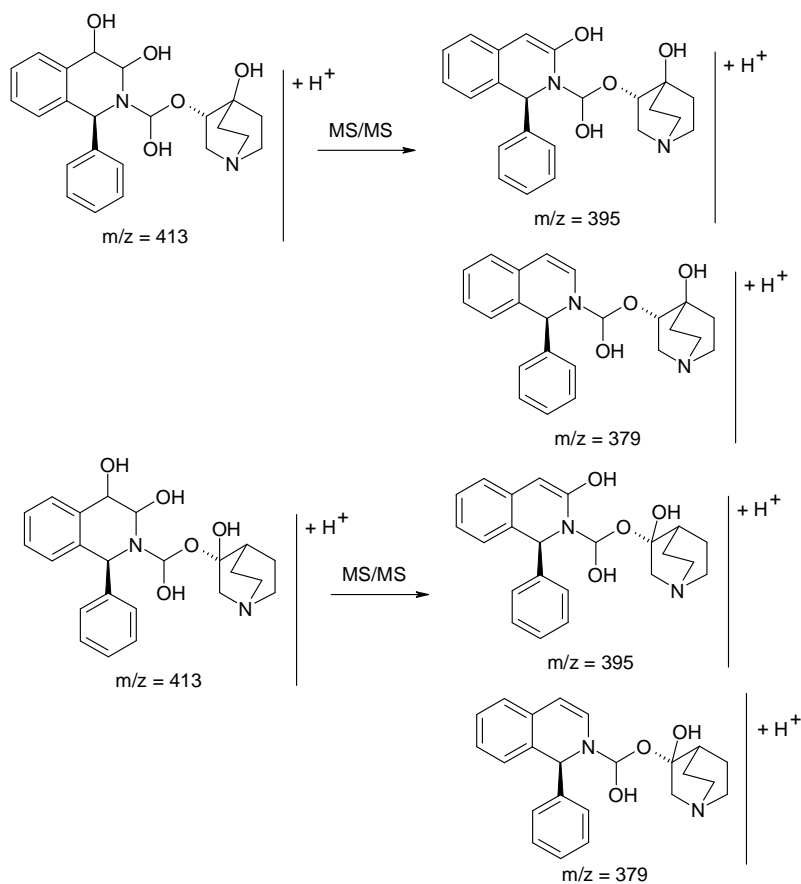


Figure 4.151: Structure proposed for $m/z = 413$ and its fragments $m/z = 395$ and $m/z = 379$

Intermediate $m/z = 399$

The intermediate $m/z = 399$ was detected only in the 0.083 mM photocatalytic experiment at a retention time of 4.4 mins. The fragments for this ion were $m/z = 381$, 211, 184 and 154. Since one of the fragments for this intermediate is $m/z = 381$ and another intermediate at this mass was determined previously, a relationship between these ions is expected. However, for the previous intermediate $m/z = 381$ a photo-reduction product was proposed, and for $m/z = 399$, a second photo-reduction must occur to achieve a mass of $m/z = 399$. The only other moieties in Solifenacin which can be photocatalytically reduced are the aromatic rings, so two possible structures have been proposed which incorporate a further photo-reduction. Both these structures can be found in Figure 4.153.

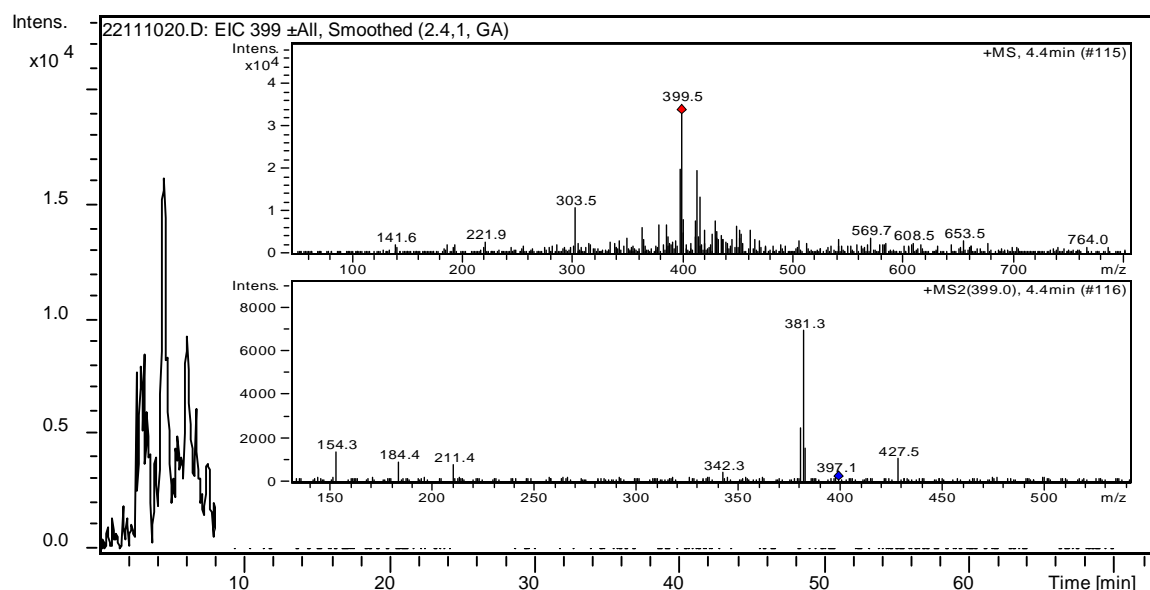


Figure 4.152: EIC of intermediate $m/z = 399$ in a 20 mins sample at a t_R of 4.4 mins. Inset MS and MS/MS spectra. Photocatalysis, [SOL] = 0.083 mM, 0.1 g TiO_2 /320 mL.

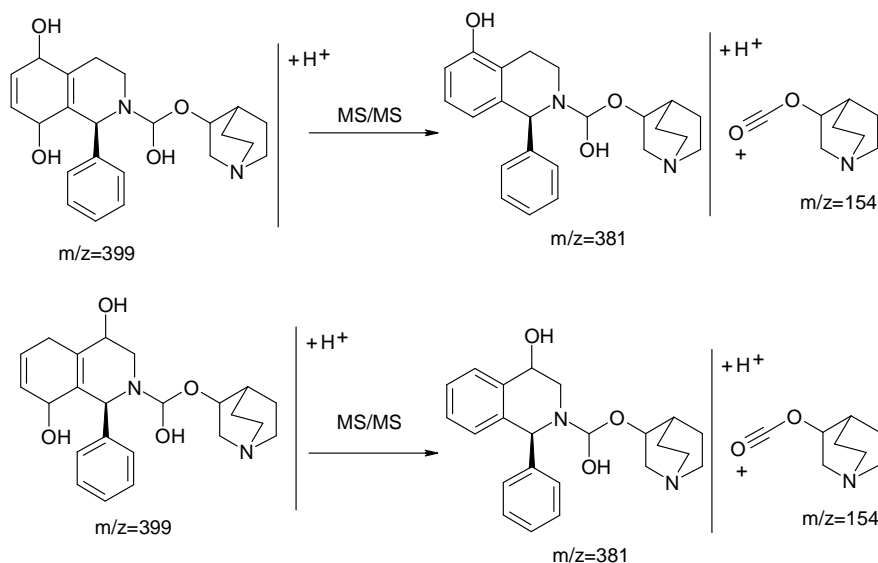


Figure 4.153: Structure proposed for the isomers possible for $m/z = 399$ and its fragments $m/z = 381$ and 154.

Intermediate $m/z = 279$

The intermediate $m/z = 279$ was detected at 2.5 mins in every experiment analysed. The low mass of this intermediate would indicate that a loss of something significant has occurred. However, the three fragments of this intermediate $m/z = 154$, 128 and 110, would imply that the quinuclidin portion of the structure is relatively intact. The structure proposed in Figure 4.155 is due to cleavage of the phenyl group of the tetrahydroisoquinoline ring through a series of photo-oxidations and photo-reductions.

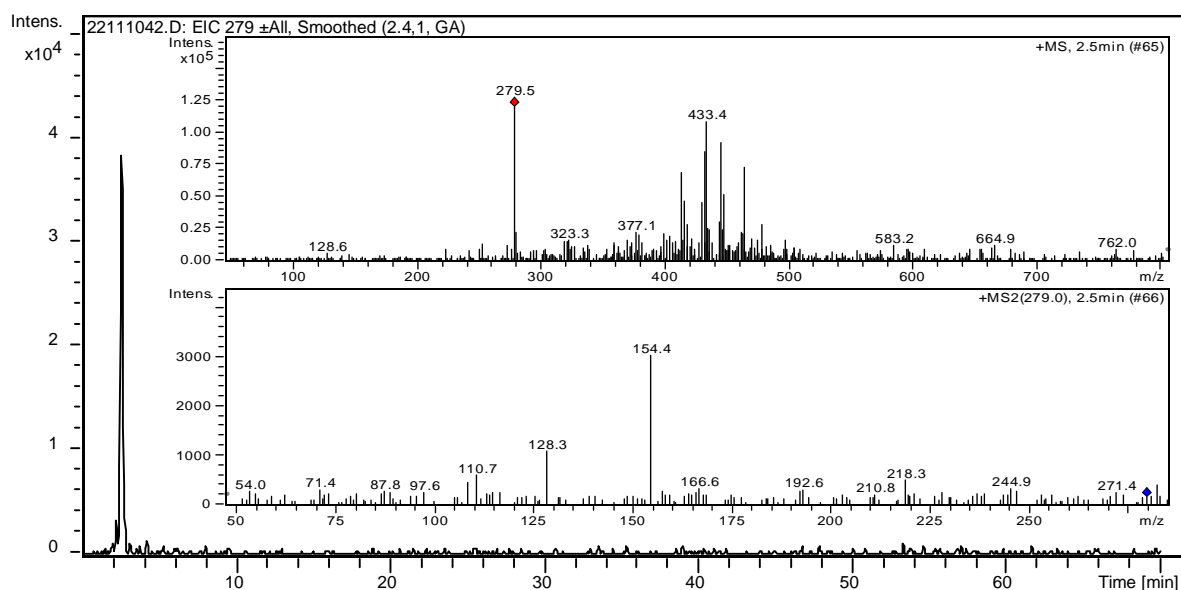


Figure 4.154: EIC of intermediate $m/z = 279$ in a 10 mins sample at a t_R of 2.5 mins. Inset MS and MS/MS spectra. Photolysis Quartz, [SOL] = 0.083 mM.

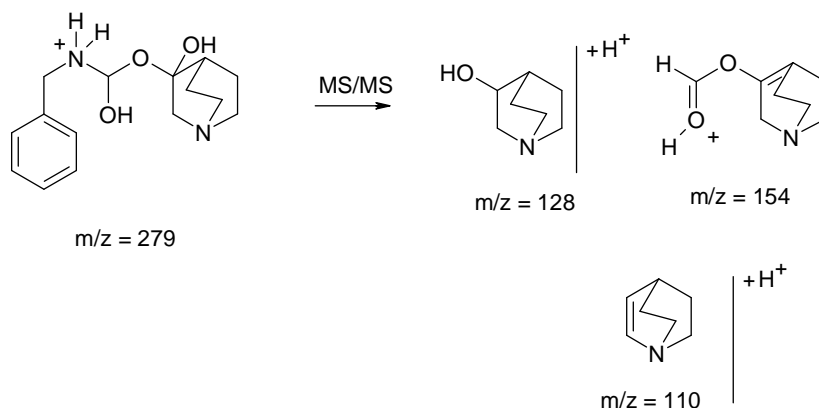


Figure 4.155: Structure proposed for the intermediate $m/z = 279$ and its fragments $m/z = 154$, 128, 110.

4.2.16 Ions which could not be Elucidated

The following chromatograms, Figure 4.156 - 4.158, show ions which were observed in experiments however no structure could be proposed for their mass or fragments. The ion $m/z = 275$ was detected at 2.4 mins in every experiment and every sample analysed including 0mins samples. It was suspected that due to its occurrence in every experiment that this may be a

contaminant and not an intermediate. $m/z = 273$ was found exclusively in photolysis experiments at a retention time of 10 mins. Fragments obtained for this intermediate were $m/z = 251$ and 229 . $m/z = 433$ was observed in both photocatalytic experiments and eluted with a number of other very polar intermediates determined earlier. Earlier DI-MS studies found an ion $m/z = 431$ which when extracted from data, overlapped with this intermediate. No structure could be proposed for this intermediate however fragment $m/z = 154$ suggests the quinuclidin ring remains intact and multiple oxidations and reductions are likely.

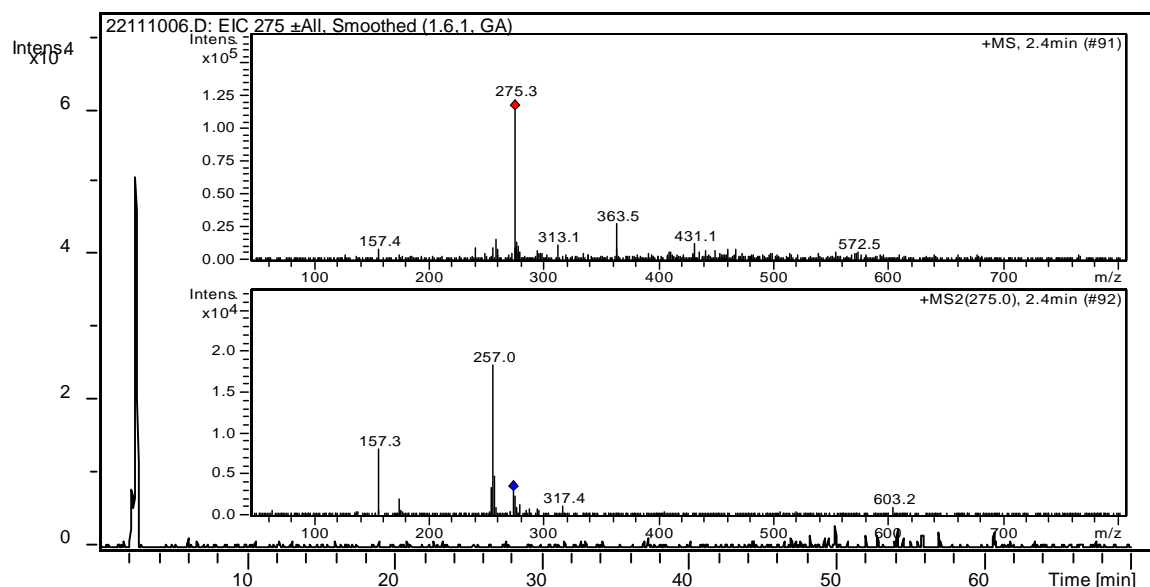


Figure 4.156: EIC of intermediate $m/z = 275$ in a 5 mins sample at a t_R of 2.4 mins. Inset MS and MS/MS spectra. Photocatalysis, [SOL] = 1 mM, 0.1 g $\text{TiO}_2/320$ mL.

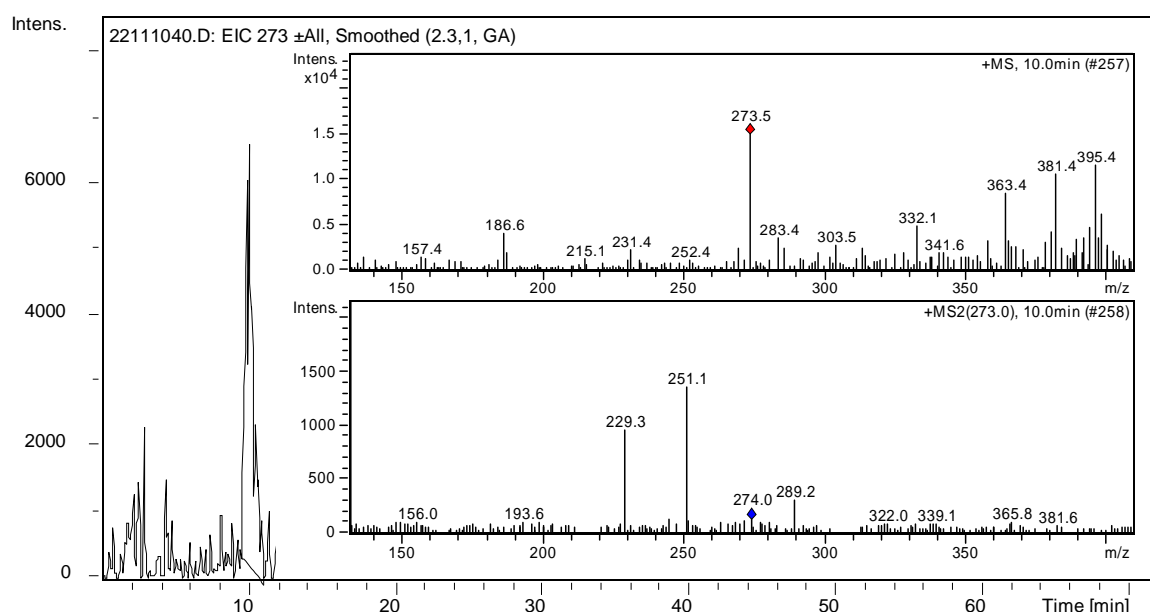


Figure 4.157: EIC of intermediate $m/z = 273$ in a 5 mins sample at a t_R of 10 mins. Inset MS and MS/MS spectra. Photolysis Quartz, [SOL] = 0.083 mM, 0.1 g $\text{TiO}_2/320$ mL.

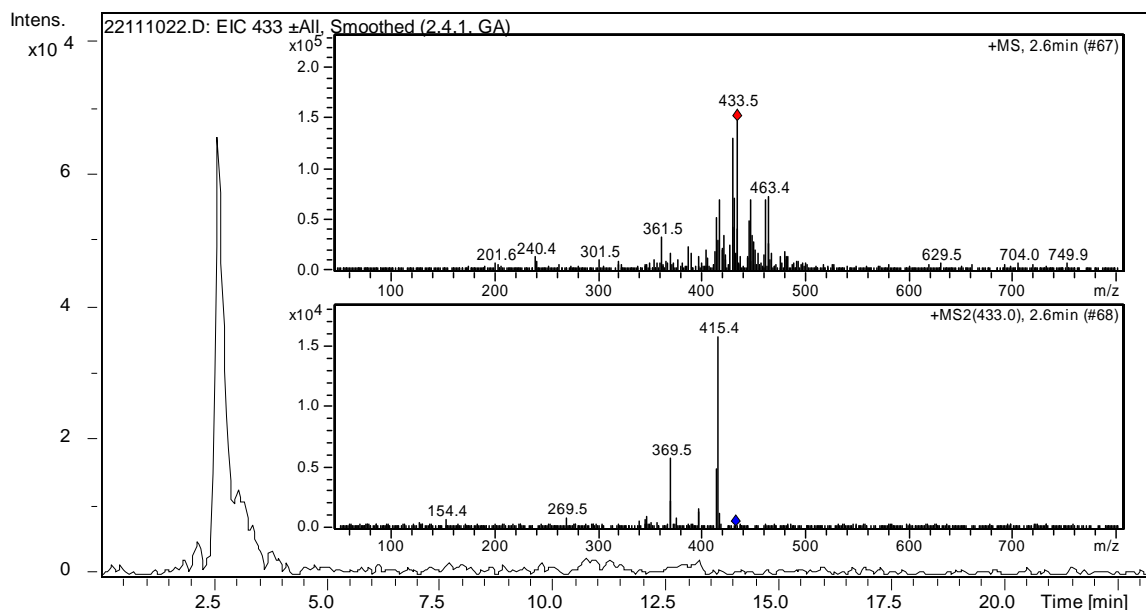


Figure 4.158: EIC of intermediate $m/z = 433$ in a 30 mins sample at a t_R of 2.6 mins. Inset MS and MS/MS spectra. Photocatalysis, [SOL] = 0.083 mM, 0.1 g TiO_2 /320 mL.

4.2.17 Solifenacin Proposed Intermediates Structures

17 different intermediate ions were detected for Solifenacin. Including all isomers, this amounts to a total of 36 intermediates for this pharmaceutical. Structures have been proposed for all of these ions. A total of 19 structures are presented in Figure 4.159, which also includes the 3 isomers for $m/z = 381$. Red coloured atoms and bonds represent where a photocatalytic reduction has occurred and blue colour atoms and bonds represent where a photocatalytic oxidation has occurred. Figure 4.160 presents likely degradation pathways for Solifenacin. Ion monitoring graphs for all ions monitored in each experiment can be found in the appendices (4A-25 – 4A-28).

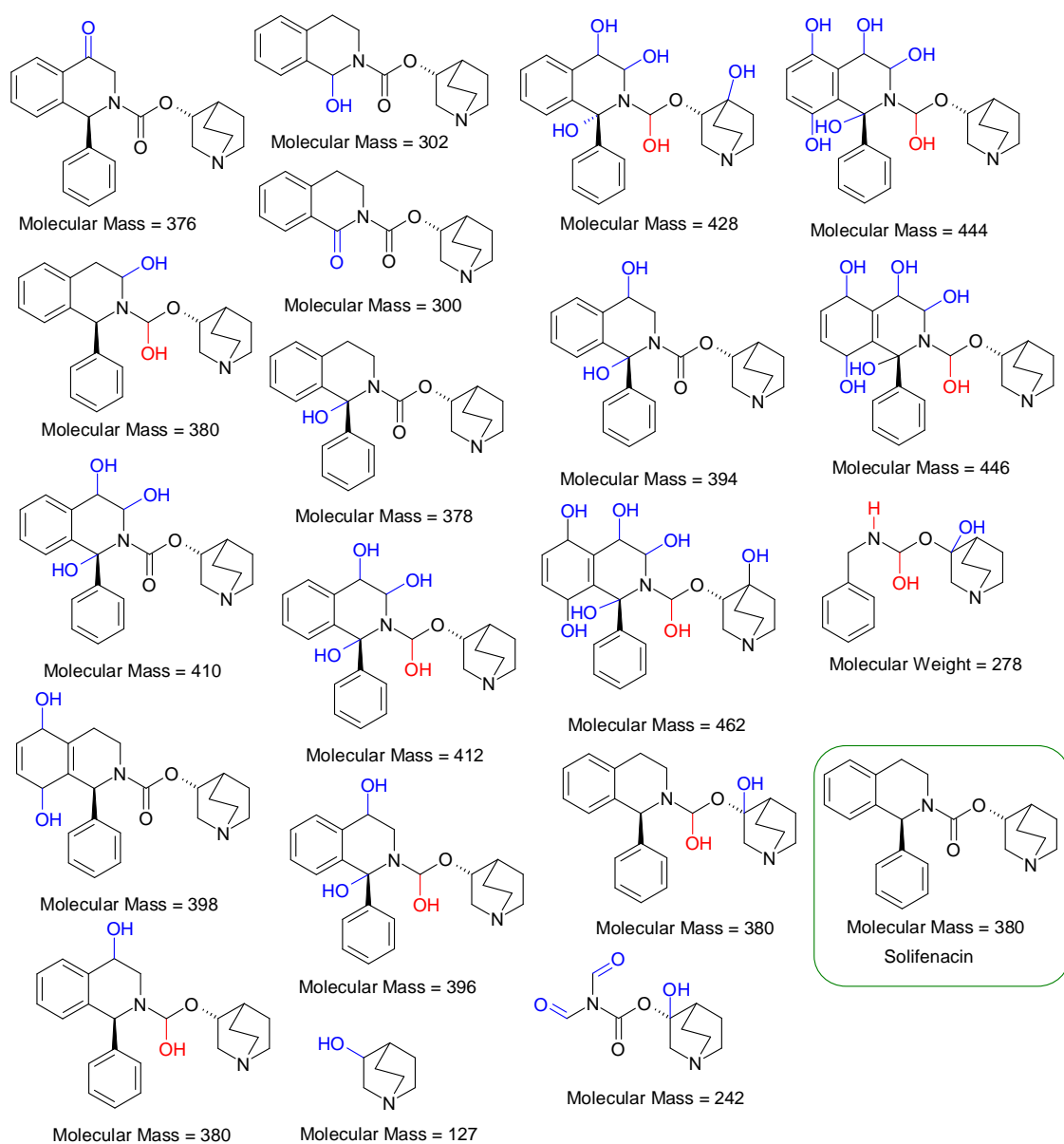


Figure 4.159: Final structures and molecular masses for intermediates proposed for Solifenacin. Solifenacin's structure is highlighted in the green box. (Blue atoms/bonds indicate where an oxidation has occurred. Red atoms/bonds indicate where a photo-reduction has occurred).

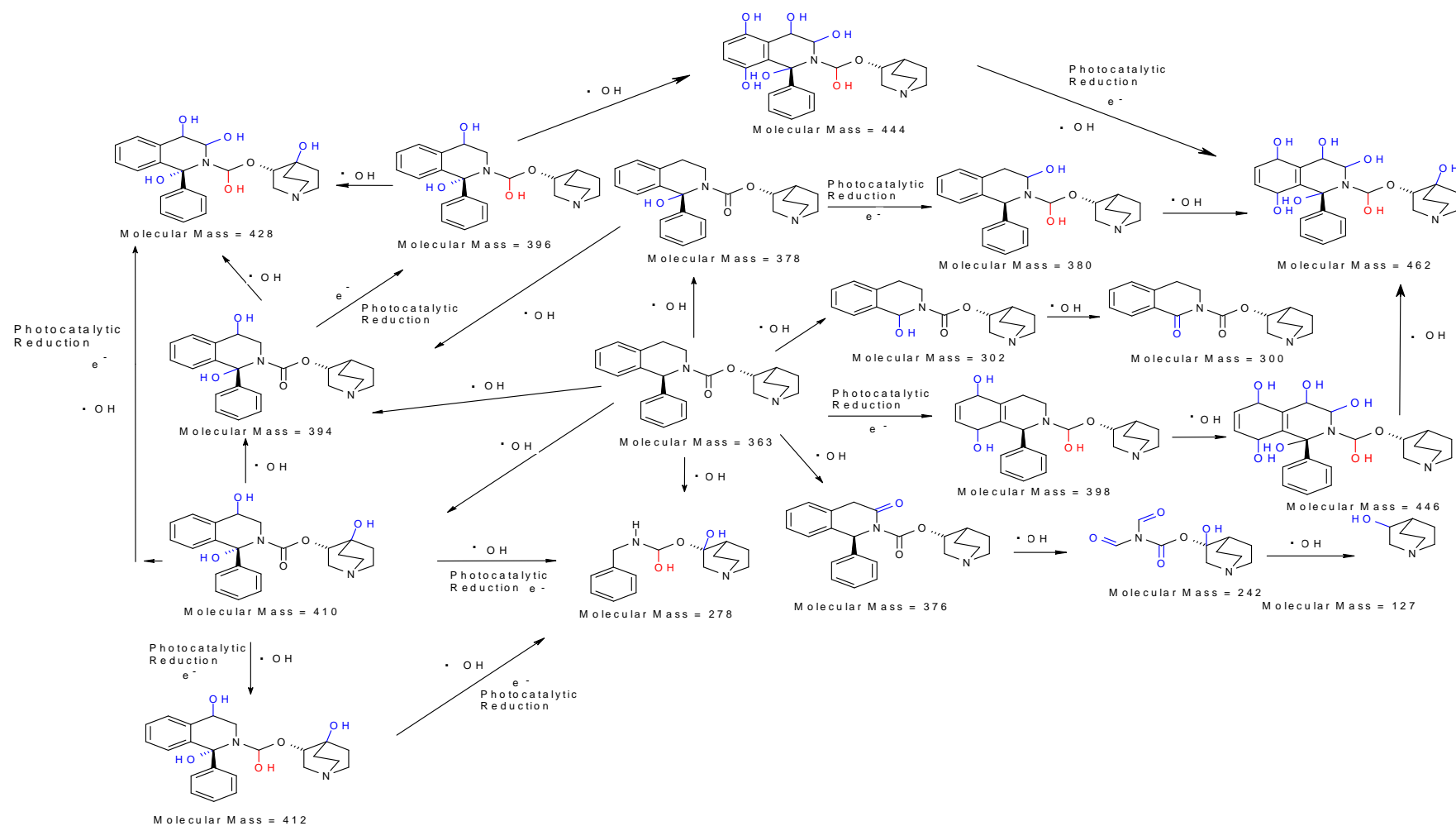


Figure 4.160: Proposed Degradation Pathway for Solifenacin and intermediates which were detected in LC-MS/MS and DI-MS studies.

4.2.18 Control Experiments

LC-MS/MS experiments were conducted to ensure that the intermediates which have been reported here were as a result of degradation of the pharmaceuticals and not from the Millipore water or any other possible source. Two control experiments were conducted, the first was a photolysis control in which Millipore water was irradiated using quartz glassware. The second experiment was a photocatalytic control whereby Millipore water was irradiated in the presence of 0.1 g of P-25 TiO_2 . Samples from this control experiment were filtered ensuring that they underwent the same procedure as photocatalytic samples for each of pharmaceuticals. Both experiments were run and the results showed only three ions throughout all samples ($m/z = 186$, $m/z = 569$ and $m/z = 137$). These ions were consistent throughout all samples and $m/z = 186$ was found also in our previous intermediate studies but was ruled out as an intermediate at a very early stage in data analysis. These ions were also noticed in background noise prior to the running of samples, and were considered to be instrumental contaminants. All intermediate ion masses were extracted from chromatograms, however, none of these ions were present concluding that all intermediates proposed therein were generated from the pharmaceuticals.

4.2.19 LC-MS/MS Analysis of the Optimised $\text{TiO}_2/\text{UV}/\text{H}_2\text{O}_2$ Process

The final intermediate analysis experiments involved examining whether the optimized $\text{TiO}_2/\text{UV}/\text{H}_2\text{O}_2$ process for each pharmaceutical eliminated all intermediates generated by the optimised TiO_2/UV process. In the case of Famotidine, the optimized photocatalytic experiment was re-run with the optimized $\text{TiO}_2/\text{UV}/\text{H}_2\text{O}_2$ (5 mM) experiment. These experiments were conducted more recently after previous intermediate studies and after instrumental downtime and replacement of a number of parts on the instrument. Samples run during this period showed a lower intensity in chromatograms and the parent ion for Famotidine also differed by approximately 0.5 Da. In previous intermediate studies the mass of Famotidine was $m/z = 338.3$, whereas in these studies it was $m/z = 337.8$. In MS/MS analysis, the instrument does not consider decimal digits and isolates only significant mass numbers. In these experiments $m/z = 337$ was thus isolated instead of $m/z = 338$. This error was found to vary between 0.3-0.5 Da for other intermediate masses in chromatograms. Since the purpose of these experiments was to confirm the elimination of all intermediates by the peroxide photocatalytic process, we decided to proceed with analysis.

Upon analysis of the data, few ions were present after the addition of peroxide and 5mins of irradiation ($m/z = 354$ was the main ion present). No Famotidine was detected after 10mins of the optimised peroxide photocatalytic experiment. The presence of only one peak was dominant throughout samples and eluted early in chromatograms. This was identified as sodium bisulfite.

Further instrumental problems ensued before work could continue with the optimised peroxide photocatalytic process for Tamsulosin and Solifenacin and unfortunately time constraints did not allow these analyses to be performed prior to submission of this thesis.

4.2.20 Intermediate Studies Conclusions

The photodegradation intermediates of Famotidine, Tamsulosin and Solifenacin have been identified in this chapter. LC-MS/MS analysis was central to identifying the intermediate structures. Tamsulosin and Solifenacin were found to be the toughest to photo-degrade (when compared to Famotidine in previous chapters). They are mostly aromatic in nature, so oxidations on these rings can result in countless isomers, particularly positional isomers as already mentioned.

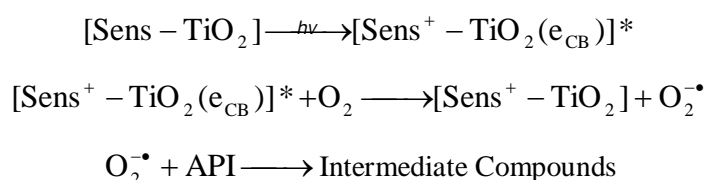
Although photo-reductions were found in these studies, the dominating degradation mechanisms were found to be photo-oxidative with the vast majority of intermediates being found to be hydroxylations occurring on aromatic rings. Some examples of oxidative aliphatic C-C bond cleavage were observed, and these were shown to occur via a hydroxyl radical based mechanism. Other transformations included oxidation to ketones and cyclisations. Ion monitoring graphs for all experiments analysed showed that intermediates formed were still persistent after the 3 h irradiation period for the optimized photocatalytic experiments at 0.083 mM. This demonstrates that TiO_2 cannot fully mineralize degradation products alone and hydrogen peroxide or another oxidant may be required. Unfortunately, instrumental downtime did not allow the running of the optimized $\text{TiO}_2/\text{UV}/\text{H}_2\text{O}_2$ process in the case of Tamsulosin and Solifenacin, however HPLC chromatograms indicated that a much greater degree of mineralization occurs for the intermediates generated by all the pharmaceuticals with this combined process.

Chapter 5 - Development and Characterisation of Visible Light Sensitised Photocatalytic Materials and Evaluation of their Photocatalytic Activity with Famotidine

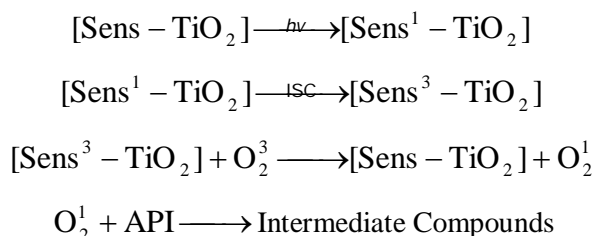
5.1 Introduction

Recent research involving TiO_2 has been focused around the development of visible light sensitised photocatalytic materials. Preparation of these materials will allow the use of cheaper light sources such as halogen lamps and/or natural sunlight which comes at no expense and is a sustainable energy source. The degradation mechanisms for sole TiO_2 photocatalysis have been well established and have previously been discussed in Chapter 1. The exact mechanism of photodegradation via sensitised TiO_2 is still unclear. A number of mechanisms have been proposed by various authors, which include electron transfer/injection with subsequent formation of reactive oxygen species (ROS), or directly via a sensitizer-only generated singlet oxygen mechanism.^{203,210,109} Both mechanisms occur upon absorption of a photon of light ($h\nu$) and in the case of the singlet oxygen mechanism, intersystem crossing (ISC) occurs from the sensitizer singlet state to the triplet state. Both mechanisms are presented in the following equations for Sens- TiO_2 :

Electron injection and formation of ROS:



Singlet oxygen mechanism:



Although both mechanisms are possible, electron injection from the sensitizer directly into the conduction band of TiO_2 is generally the most accepted mechanism.^{65,204}

This chapter concerns itself with the development, characterisation and photoactivity of new dye sensitised photocatalytic materials which incorporate TiO_2 , a sensitizer (or dye) with absorption into the visible region and a linker to bind both. Many of the most commonly used linkers for binding metal oxides to various dyes have already been detailed in Chapter 1. Of these, the following linkers were selected to develop visible light sensitised photocatalytic materials: (i) Acetylacetonate, (ii) Toluenediisocyanate, (iii) 3-aminopropylsilane, and (iv) carboxylate groups. The sensitising molecules chosen to bind to these linkers include porphyrins, phthalocyanines and metallo-phthalocyanines.

These composite materials have been prepared using a simple adsorbed method and are compared to other current literature methods. Characterisation of these materials was undertaken with both IR and UV-vis spectroscopy (DR and solution state). The photocatalytic performance of all composite materials have been evaluated with the pharmaceutical Famotidine as used in previous studies and in the case of the porphyrin/TiO₂ composite, the pharmaceuticals Tamsulosin and Solifenacin were also tested.

5.2 Results and Discussion

5.2.1 Synthesis of TCPP-TiO₂

In our attempts to synthesize visible light sensitised photocatalytic materials TPP was considered as a suitable sensitizer. An experiment was performed with non-functionalized TPP, to test whether the dye could simply be coated on to the TiO₂ and the reaction was simply left to stir in chloroform for 4 hours. This experiment yielded a white product indicating that no TPP had attached to the TiO₂. This demonstrated that functionalization of the dye would be required in order to anchor the dye to TiO₂. Its tetra acid analogue, TCPP (tetra-(4-carboxyphenyl)porphyrin) was chosen since it contains carboxylic acid groups which can potentially anchor the sensitizer to the TiO₂ surface. Two different methods were chosen to immobilize TCPP onto TiO₂.

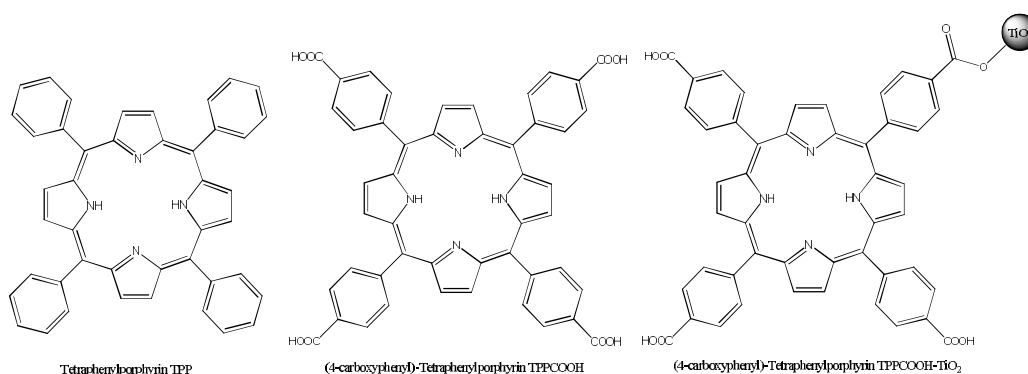


Figure 5.1: Structures of TPP, TCPP, and the porphyrin/TiO₂ composite.

In the first method, TCPP was immobilized by simple adsorption (reaction scheme 5). This method involved mild conditions and the product (A) was predicted to be attached via H-bonding, electrostatic or Van der Waals forces. The second method of preparation involved a reflux in DMF for 4 h, as previously described by Li *et al.* (reaction scheme 6).²⁰⁵ This method used much harsher conditions and was predicted to form a covalently bound product (B) i.e an ester linked product. Figure 5.2 shows examples of H-bonding, covalent bonding and electrostatic binding to TiO₂. Both methods yielded an identical product (a dark purple/brown powder, Figure 5.3). Given the previous failed experiment with non-functionalised TPP, it was

concluded that based on the product appearance alone that both methods were producing a chemically bound product.

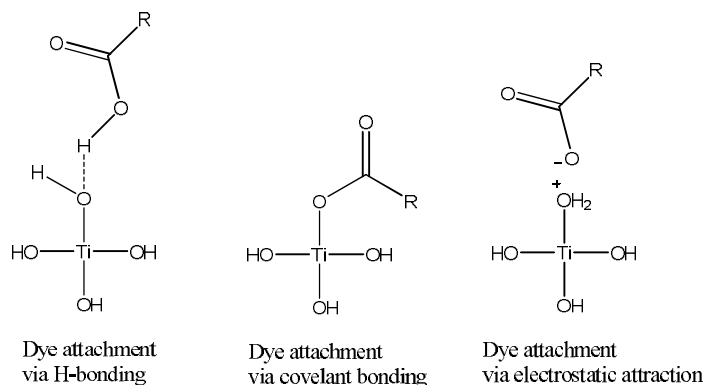


Figure 5.2: H-bonding vs. covalent bonding vs. electrostatic attraction of the dye to TiO_2 .

The synthetic procedures were repeated for both TCPP- TiO_2 -A and TCPP- TiO_2 -B with a soxhlet extraction performed on both to determine the residual porphyrin content and how much was bound to the surface of the TiO_2 (ie. the loading capacity). For TCPP- TiO_2 -A, 0.035 g was recovered via soxhlet from the original 0.050 g used in the reaction. This would indicate a maximum loading capacity of 0.015 g/1 g TiO_2 . For TCPP- TiO_2 -B, a total of 0.025 g was recovered from washings. A further soxhlet reaction of this composite generated a porphyrin plus contaminants which were believed to be from the DMF solvent used and which could not be separated. This was found also in a number of repeat experiments. Some additional porphyrin was attained although could not be accurately determined. With this in mind, an estimated loading not exceeding 0.025 g/1 g TiO_2 was concluded, which is close to that of Li *et al.* (0.021 g/1 g TiO_2).

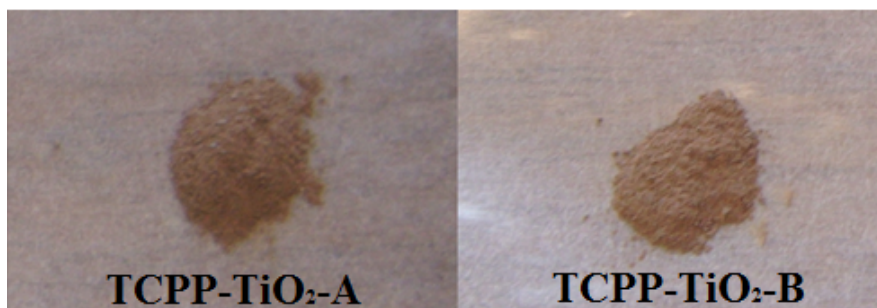


Figure 5.3: Photograph showing the appearance of ground TCPP- TiO_2 both bound and adsorbed.

5.2.2 Characterisation of TCPP- TiO_2

IR Spectroscopy

FT-IR analysis was performed on both TCPP- TiO_2 composite samples and also on, TiO_2 and TCPP alone. Titanium dioxide gave only two bands at 3340 cm^{-1} signifying the surface OH groups and a very broad stretch in the fingerprint region at 600 cm^{-1} representing the Ti-O-Ti

vibration. Stretches for the two composites and the porphyrin alone are shown in the Table 5.1 below. The major bands have been assigned to their principle functionalities.

Functional Group	TCPP		TCPP-TiO ₂ -A		TCPP-TiO ₂ -B	
TCPP, C=C-H stretch phenyl	3014	Weak	3740	Weak	3743	Weak
TiO ₂ , surface -OH groups			3391	Strong	3410	Strong
	2524	Weak	2923	Medium	2925	Medium
TCPP, C=O anchor	1685	Strong	1614	Medium	1621	Medium
TCPP, C=C	1604	Strong	o		o	
TCPP, C-H bend	1400	Medium	1383	Medium	1383	Weak
TCPP, C-O stretch	1222	Strong	1263	Weak	1263	Weak
TCPP, C ₆ H ₅ substituted	1174	Strong	1176	Weak	1176	Weak
TCPP, p-substituted C ₆ H ₅	1099	Strong	1110	Weak	1111	Weak
C-H pyrrole porphyrin ring system	o		1054	Weak	1055	Weak
TCPP, pyrrole C-H (rocking)	963	Strong	967	Weak	966	Weak
TiO ₂ , Ti-O-Ti vibration			636	Strong	667	Strong

Table 5.1: FT-IR samples for TCPP, TCPP-TiO₂-A and TCPP-TiO₂-B, o = overlap, stretches referenced from work by Thomas *et al.* and Jiang *et al.*^{206,118} Original IRs for these data can be found in the appendices (5A-4 -5A-6).

The $\nu(\text{C=O})$ band at 1685 cm^{-1} in TCPP, is shifted to lower wavenumbers at 1614 cm^{-1} and 1621 cm^{-1} for TCPP-TiO₂-A and TCPP-TiO₂-B respectively. The corresponding $\nu(\text{C-O})$ band which can normally appear at $1210\text{-}1320\text{ cm}^{-1}$, appears at 1222 cm^{-1} , and again shifted with the coated TiO₂ samples to 1263 cm^{-1} for both. These shifts were also noticed along with a decrease in the intensity of these bands, which is indicative of adsorption to TiO₂ according to work by Diaz-Urbe *et al.*²⁰⁷ TiO₂ bands are also clearly present in the spectra of the composite samples, and are now shifted to 3400 cm^{-1} for $\nu(\text{Ti-OH})$ and $\sim 650\text{ cm}^{-1}$ for the $\nu(\text{Ti-O-Ti})$ stretch.

UV-vis Spectroscopy

Figure 5.4 shows the UV-vis spectra of TCPP in methanol, where the Soret band can be seen clearly at 416 nm and Q bands at 512, 547, 589 and 643 nm. Solid state UV-vis (DR) spectra of the prepared photocatalytic materials were also attained. In addition to this we attained the UV-vis (DR) spectra for uncoated TiO₂ and TCPP. All samples are shown in Figure 5.5 and we can see that the bands of the porphyrin are not as clear in the diffuse reflectance spectra compared to the UV-vis in methanol. Samples were prepared with KBr, and differences in absorbance on the y-axis should be ignored due to varying concentrations in disc preparation. This is due to the difference in sampling techniques. In diffuse reflectance, the samples are prepared into densely

packed discs with KBr, whereas with solution phase UV, very dilute solutions are prepared so as to reduce aggregation and achieve well resolved bands.

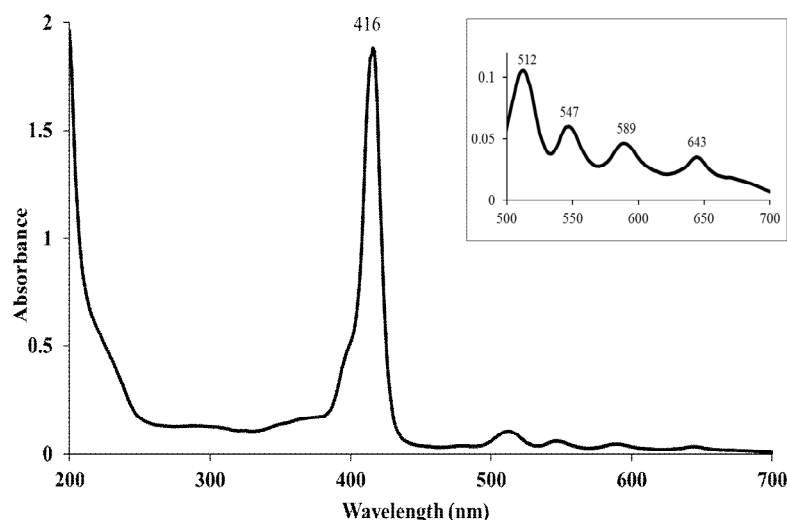


Figure 5.4: UV-vis spectra of TCPP in methanol with Q bands at 512, 547, 589, 643 nm and the Soret band at 416 nm.

TiO₂ absorbs in the UV region only below 400 nm, shown by the intense absorbance < 400 nm. TCPP-TiO₂-A, TCPP-TiO₂-B samples show almost identical spectra to each other and show Q bands at 523 nm, 560 nm, 597 nm 654 nm for TCPP-TiO₂-A and 523 nm, 561 nm, 598 nm and 655 nm for TCPP-TiO₂-B. The visible similarities in these spectra are a very promising sign that the much simpler preparation method of TCPP-TiO₂-A is just as effective as the TCPP-TiO₂-B method. As a control, a KBr disc containing TCPP alone was prepared (in Figure 5.5 also) and the UV-vis spectrum shows multiple bands both in the UV and visible region, the Q bands can be seen much more clearly than the Soret and appear at 523 nm, 560 nm, 596 nm and 654 nm.

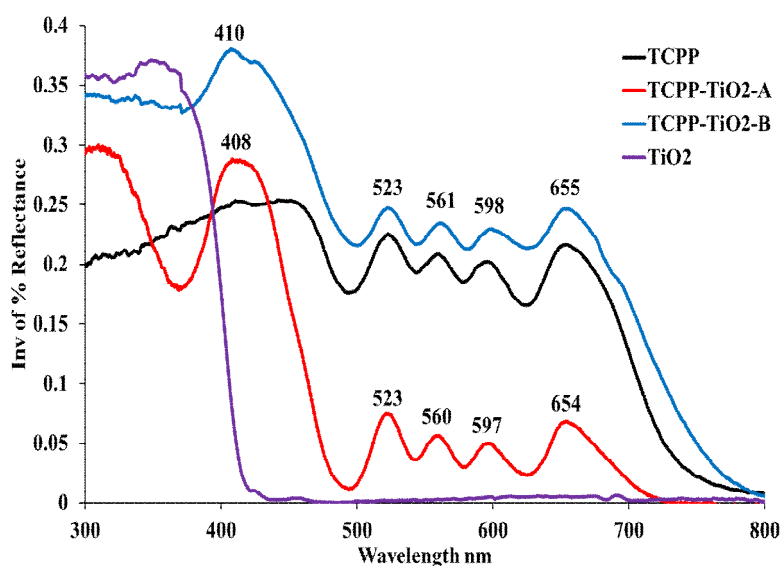


Figure 5.5: DR UV-vis Spectroscopy data for TCPP-TiO₂, TCPP and TiO₂

Table 5.2 contains the wavelengths of the Soret and Q bands for TCPP in methanol, literature wavelengths in ethanol and DMF, and those for the coated TiO₂ samples including the free TCPP. The difference in the intensities of the Q bands and the lack of major shifts compared to the coated TiO₂ samples was explained with the lack of solvent polarity effects which clearly influence the intensity and shifts of both the Soret and Q bands. Work by Diaz-Urbe *et al.* and Cherian *et al.* described a red shift for the coated TiO₂ samples when compared with the UV-vis in ethanol of TCPP.^{207,208} Diaz reported a shift of approximately 8 nm in the Q bands, whereas Cherain reported a shift of 5 nm for the lower energy bands and 10 nm for the higher energy bands albeit that their work was with coated TiO₂ electrodes. Ma *et al.* reported an average shift of 8 nm with their coated TiO₂ sample compared with the UV-vis of TCPP in DMF.²⁰⁹ Ma *et al.* also reported a decrease in intensity of the Soret band relative to the Q-bands which is similar to what has been observed in this work.

Sample	UV	Soret Band (nm)	Q bands(nm)			
TCPP-TiO ₂ -A	Solid	408	523	560	597	654
TCPP-TiO ₂ -B	Solid	410	523	561	598	655
TCPP	Solid	411	523	560	596	654
TCPP	Methanol	416	512	547	589	643
TCPP	Ethanol (lit.)	419	514	548	588	645
TCPP	DMF (lit.)	418	515	549	591	646

Table.5.2. Shifts in the UV-vis samples for TCPP-TiO₂-A, TCPP-TiO₂-B, TCPP.

SEM Imaging

SEM images were attained for both samples Figure 5.6 and Figure 5.7 and also for P-25 TiO₂. The highly mesoporous nature of the P-25 standard can be seen compared with the prepared coated TiO₂ samples. The prepared coated samples also show identical textures when compared to the P-25 sample.

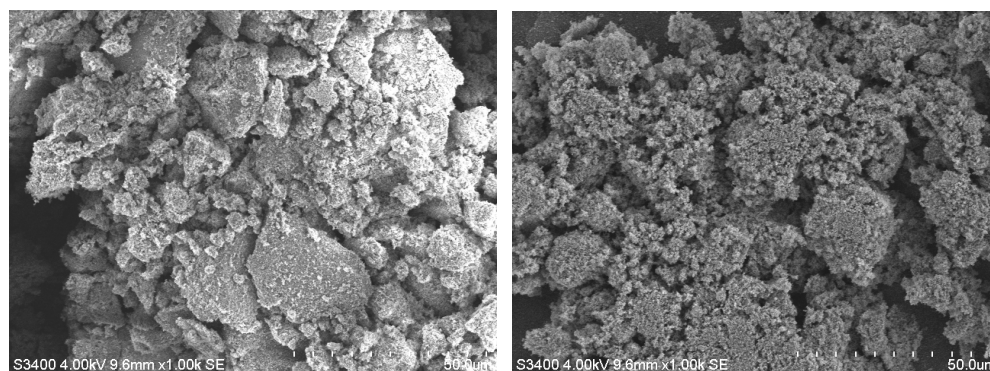


Figure 5.6: SEM image of TCPP-TiO₂ bound (Left) and P-25 TiO₂ (Right).

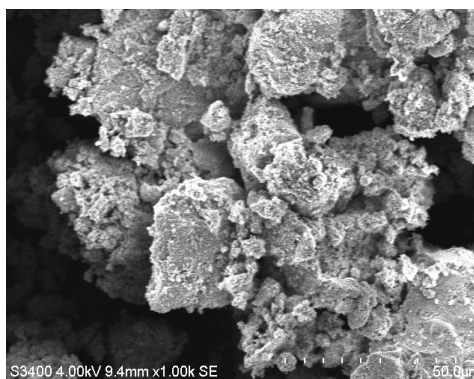


Figure 5.7: SEM image of TCPP-TiO₂ adsorbed

5.2.3 Examination of the Photocatalytic Efficiency of TCPP-TiO₂ in Famotidine Degradation with Visible Light.

5.2.3.1 Indoor Experiments

Both TCPP-TiO₂ photocatalysts were employed in the degradation of Famotidine using a halogen lamp. Halogen lamps are cheap, commercially available light sources and they emit only visible light. Halogen lamps will allow assessment of the photocatalytic efficiency of our porphyrin/TiO₂ composite. Famotidine is also a perfect candidate for testing of our visible light sensitised photocatalyst as it absorbs below 300 nm and is not sensitive to light above this wavelength. Figure 5.8 shows experiments in triplicate of each photocatalyst compared with controls of TiO₂ alone and photolysis (no photocatalyst). The experiments were monitored using HPLC analysis. Both photocatalysts show similar degradation profiles, with almost 100% elimination of Famotidine after 3 h. Both materials are also significantly better than the P-25 TiO₂, which only achieves 25% elimination after 3 h. This is more than would be expected because TiO₂ requires light below 400 nm to generate hydroxyl radicals. A slight tail of absorption over the 400 nm may be giving rise to this degradation seen by visible light (to approximately 425 nm, see UV-vis spectrum for TiO₂ Figure 5.5).

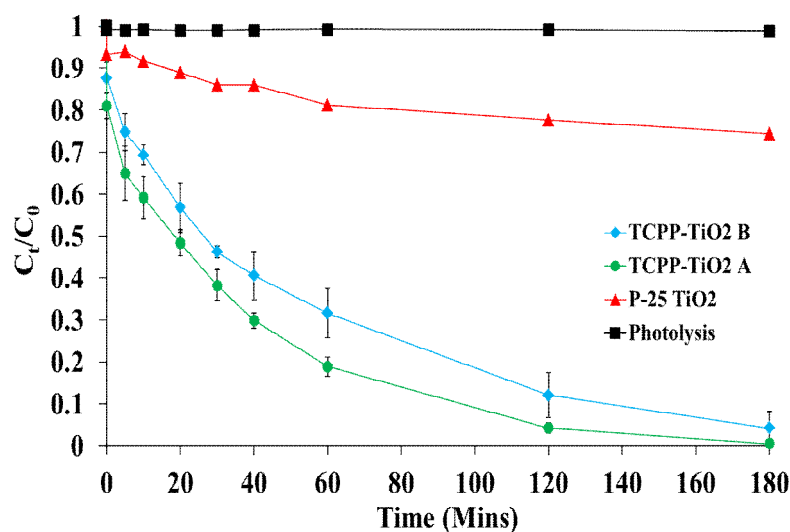


Figure 5.8: TCPP-TiO₂-A and TCPP-TiO₂-B photocatalytic experiments and controls with a Halogen Lamp for 3 h. [TCPP-TiO₂] = 0.031 g, [FAM] = 0.083 mM.

Further work in which a soxhlet extraction of the composite (post-synthesis) was performed, indicated that it had almost the same performance as non-soxhlet extracted TCPP-TiO₂ (Figure 5.9). A slightly improved performance by the soxhlet extracted composite could be explained by less aggregation affects which would be caused by over loading sensitizer onto TiO₂ or residual sensitizer on TiO₂. This effect was studied in work by Wang *et al.* 2010.²¹⁰

Two HPLC chromatograms are shown in Figure 5.10 of a sample at 0 mins vs. 180 mins, showing that no Famotidine is detected after 3 h irradiation. In the 180 mins sample early eluting intermediates are present in significant quantities. From intermediate studies performed on Famotidine (see Chapter 4), the largest intermediate peak in the chromatogram (at t_R = 3.2 mins) is most likely the intermediate m/z = 354 (Mw = 353 g/mol). This intermediate is the S-oxide of Famotidine. The presence of two to three other intermediates are apparent which may be photo-oxidative or photo-reductive intermediates. The large intensity of the S-oxide would indicate that the mechanism of degradation using this photocatalyst may be potentially selective as further mineralization of the degradation products does not appear to occur. These intermediates would need to be further characterized to identify these intermediates and hence the exact mechanism.

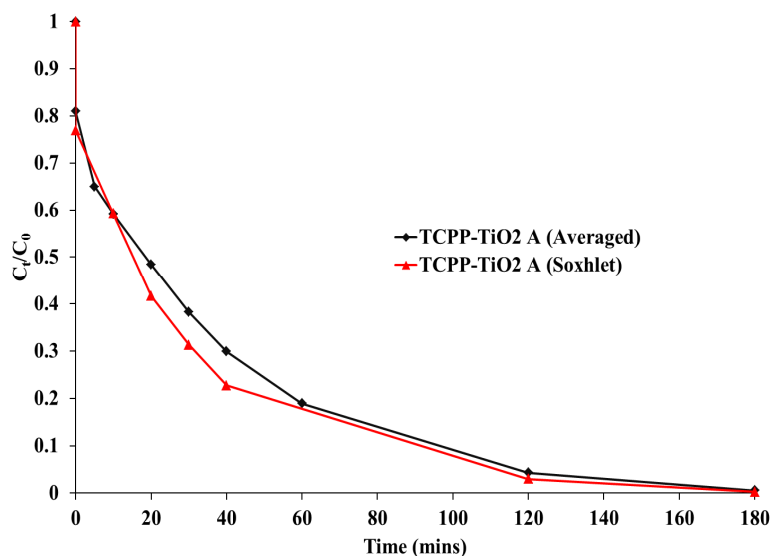


Figure 5.9: TCPP-TiO₂-A compared to a soxhlet extracted TCPP-TiO₂-A which shows almost identical performance. [TCPP-TiO₂] = 0.031 g, [FAM] = 0.083 mM.

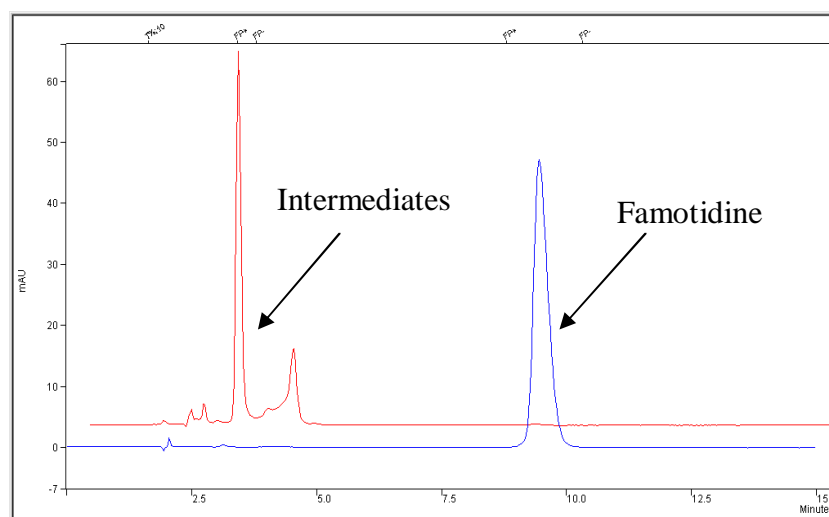


Figure 5.10: HPLC Chromatogram showing Famotidine, at 0 Mins (blue) and after 180 mins (red), in photocatalytic degradation by TCPP-TiO₂-A. [FAM] = 0.083 mM, TCPP-TiO₂-A = 0.031 g.

It was noticed that when placed in water the colour of the photocatalyst went from purple/brown to green. Odobel *et al.* noticed a colour change of the porphyrin from purple to green upon adsorption of the porphyrin to TiO₂ electrodes and attributed this effect to the interaction of the pyrrole nitrogens of the porphyrin with the hydroxyl groups on the surface of the TiO₂.²¹¹ Upon addition to the aqueous drug solution the same effect is occurring between the pyrrole nitrogens of the porphyrin and water molecules. This same effect also occurred in the presence of acid. Upon removal of water and addition of methanol to the photocatalyst, it reverted back to its purple colour.

5.2.3.2 Solar Experiments

A set of solar experiments were also conducted (22 June 2010) using both TCPP-TiO₂ photocatalysts, P-25 TiO₂ for comparison and one control experiment (photolysis) where no photocatalyst was added. A graph of the light intensity (in footcandles) recorded on a flux meter throughout the experiment can be found in the appendices (5A-1). The results shown in Figure 5.11 below are what would be expected under solar conditions. Both TCPP-TiO₂ photocatalysts work relatively similar to one another and show a good degradation profile which is improved from the indoor experiments. P-25 TiO₂ comparatively shows also a good degradation profile curve, although it is slower than both of the composite materials, and the control experiment with no photocatalyst (photolysis) shows insignificant degradation.

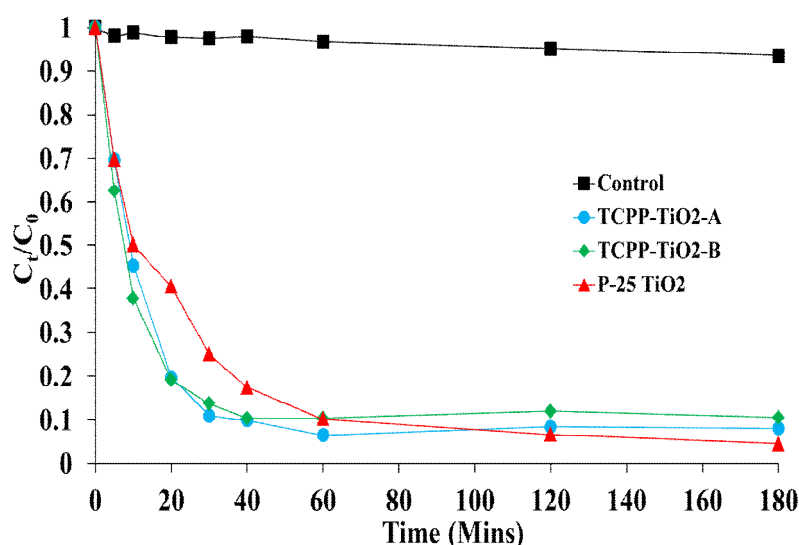


Figure 5.11: Solar reactions performed on 22-06-2010 with TiO₂, TCPP-TiO₂-A, TCPP-TiO₂-B, and photolysis.

The spectral irradiance data for a halogen (tungsten) lamp and the solar spectrum is shown in Figure 5.12. The spectrum for the halogen lamp used in our experiments can be found in appendix 5A-2. For the tungsten lamp, absorbance above 400 nm although minimal can be seen. Solar irradiance data covers the UV region unlike the tungsten halogen lamp, and degradation by both TiO₂ and the TCPP-TiO₂ samples can therefore be expected to be significantly improved. After 20 mins the composites can achieve 80% elimination of Famotidine, whereas, it takes 40 mins for TiO₂ to achieve the same elimination. The fact that both TCPP-TiO₂ materials show an improved activity over TiO₂ is a promising result as they were both prepared in different manners. HPLC traces for each solar experiment are shown in Figure 5.13 - 5.14. The presence of a greater quantity of intermediates in the traces of TCPP-TiO₂-A, is a testament to its better performance over the TCPP-TiO₂-B. TiO₂ shows a lower quantity of these intermediates. It can be noticed in these traces also that 100% degradation is not achieved.

Whereas, indoor experiments conducted do show complete disappearance (in the case of TCPP-TiO₂-A). This is possibly due to cloud coverage on the day these experiments were conducted which would lead to an inconsistent intensity of light reaching the sample. Despite these obvious disadvantages, solar energy is a more sustainable and cost-effective light source which has shown to be effective in combination with both prepared visible-light sensitised photocatalyst in the elimination of Famotidine.

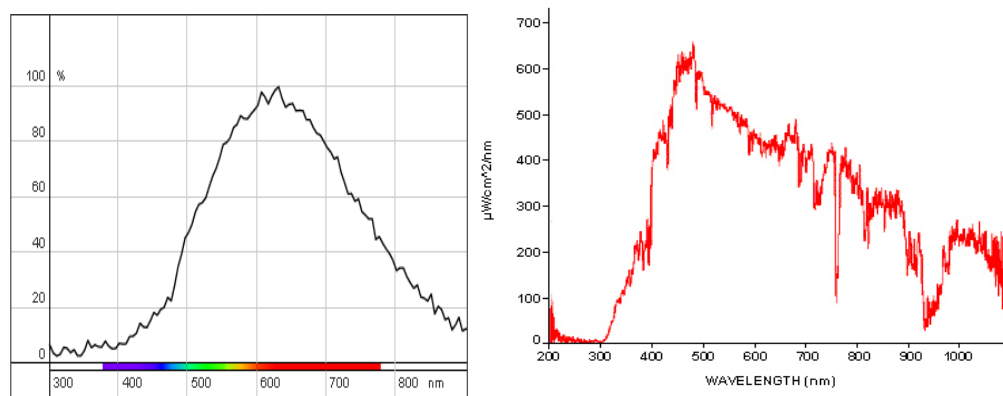


Figure 5.12 Spectral irradiance profile data for a typical Halogen (Tungsten) Lamp (left) versus the solar spectrum (right).^{212, 213}

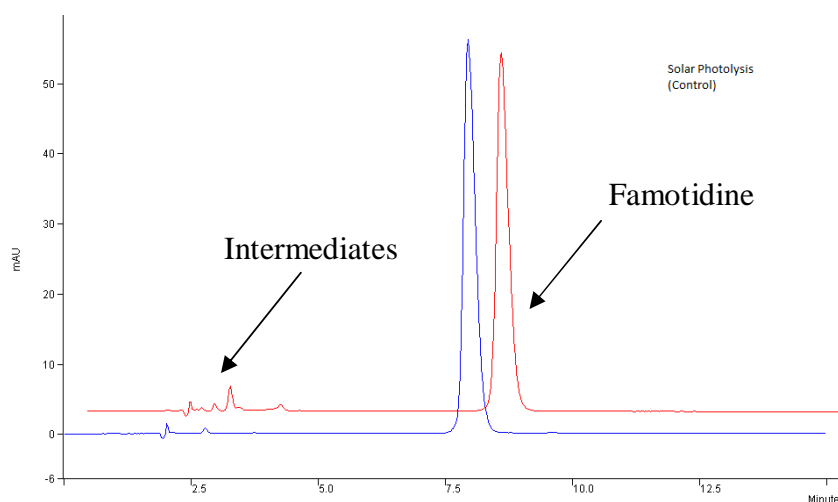


Figure 5.13: HPLC chromatogram of Famotidine at 0 Mins (blue) and 180 mins (red) showing the solar photolysis (control) of Famotidine.

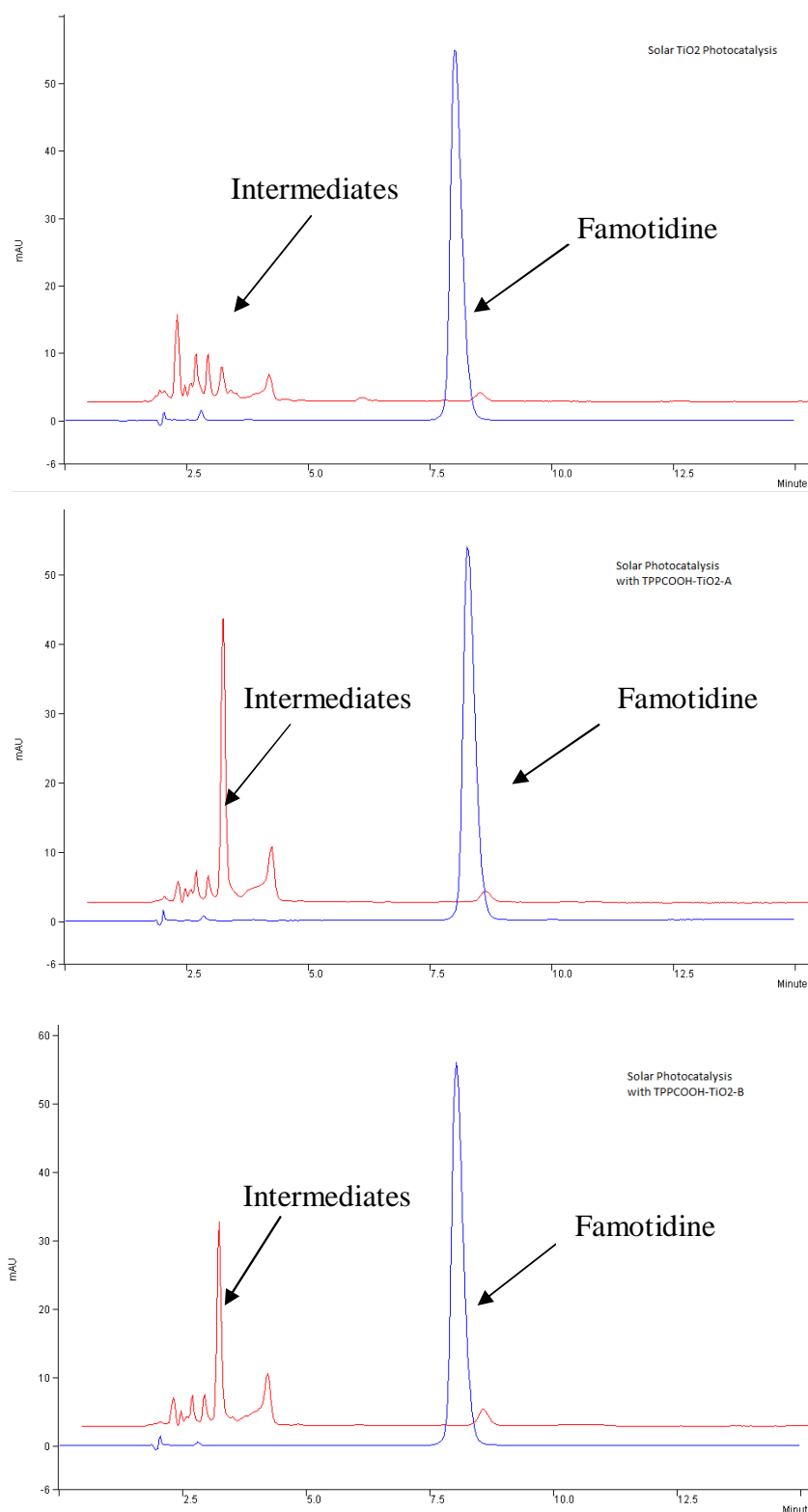


Figure 5.14: HPLC chromatograms of Famotidine at 0 mins (blue) and 180 mins (red) showing solar photocatalysis with TiO_2 and TCPP- TiO_2 -A and TCPP- TiO_2 -B.

5.2.3.3 Control Experiments

Figure 5.15 shows a series of additional control experiments which were conducted indoors with a halogen lamp. Two control experiments are shown with the sensitiser TCPP alone and

also the sensitiser TCPP in the presence of TiO_2 (both experiments were conducted in the presence of light). These are then compared with the performance of both composite materials. The amount of sensitiser used in these control experiments (0.001 g/1 g TiO_2) was more than double the amount coated onto 0.031 g of the composite. Considering a coating of 0.015 g/1 g TiO_2 as in TCPP- TiO_2 -A, in 0.031 g of TCPP- TiO_2 , there would be less than 0.0005 g of sensitiser. The sensitiser alone (TCPP) shows minimal degradation although degradation would have been expected due to singlet oxygen generation. TiO_2 alone also shows very poor degradation whilst in the presence of the sensitizer showing that binding of the sensitiser to the TiO_2 is required for photodegradation and that photodegradation is due to the composite material and not its individual components. An additional dark adsorption experiment was conducted and analysed with UV-vis spectroscopy and showed an expected initial adsorption after sonication and dispersion of the photocatalyst, but no further adsorption up to 1 h later. These data can be found in the appendices (5A-3).

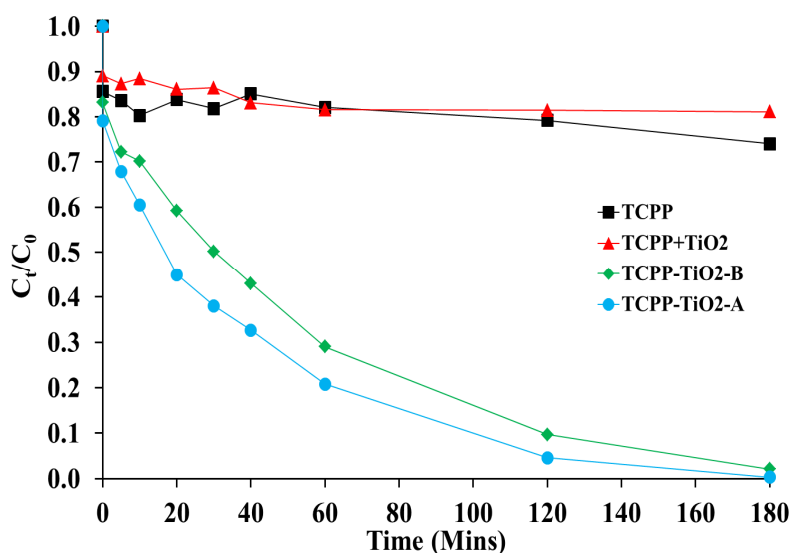


Figure 5.15: Indoor control experiments with a halogen lamp showing the degradation of pharmaceutical Famotidine with TCPP- TiO_2 -A, TCPP- TiO_2 -B, TCPP + TiO_2 (1 mg/100 mL) and TCPP (1 mg/100 mL). [TCPP- TiO_2] = 0.031 g, [FAM] = 0.083 mM. Controls performed by C. Saurel.

5.2.3.4 Recovery of the TCPP- TiO_2 materials and Stability

After solar and indoor experiments, the photocatalytic materials were recovered from the reaction solution. In the case of both TCPP- TiO_2 photocatalysts, the recovered photocatalysts were beige in colour (see Figure 5.16), differing in colour from the starting photocatalytic material. This led us to believe that a number of things may be happening, but that the TCPP- TiO_2 photocatalysts were unstable. Experiments were performed in which the reaction solution was simply sonicated for 10 min and then recovered the solution, to see if perhaps sonication was cleaving the TCPP from the TiO_2 prior to irradiation. In the case of both the recovered

photocatalysts, sonication had no visible effect on the photocatalyst although after centrifugation some residual TCPP was clouding the supernatant of TCPP-TiO₂-A, albeit, only slightly. The supernatant from TCPP-TiO₂-B was clear and thus, soxhlet extraction was clearly effective in removing residual porphyrin. Sonication, therefore was ruled out as a potential destruction method. Further control photo-degradation tests with the dye and TiO₂ separately placed in a schlenk flask and irradiated with a halogen lamp concluded that the dye was being degraded by TiO₂.

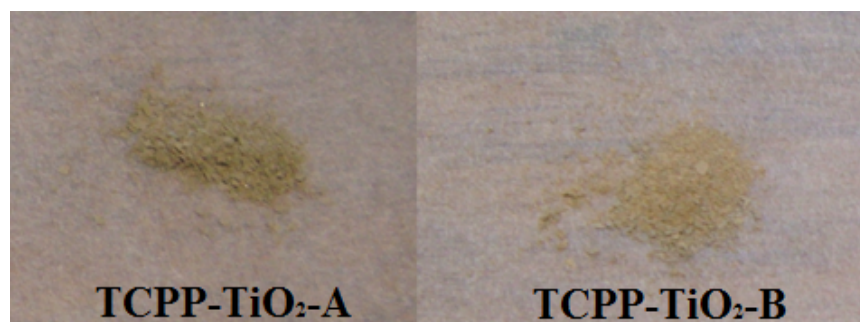


Figure 5.16: TCPP-TiO₂-A and TCPP-TiO₂-B post photoreaction.

FT-IR analysis was performed on the photocatalysts post-reaction (Figure 5.17) and there are some noticeable differences between the samples. The $\nu(\text{C}=\text{O})$ stretch which appeared at 1614 cm^{-1} and 1621 cm^{-1} for TCPP-TiO₂-A and TCPP-TiO₂-B respectively are now shifted to 1630 cm^{-1} and 1637 cm^{-1} . The three stretches typical of TCPP in the fingerprint region Figure 5.18a and 5.18b are also noticeably different in Figure 5.18c and Figure 5.18d. The three bands are now overlapped by one principle band at 1062 cm^{-1} which would indicate significant changes to the core π -ring system.

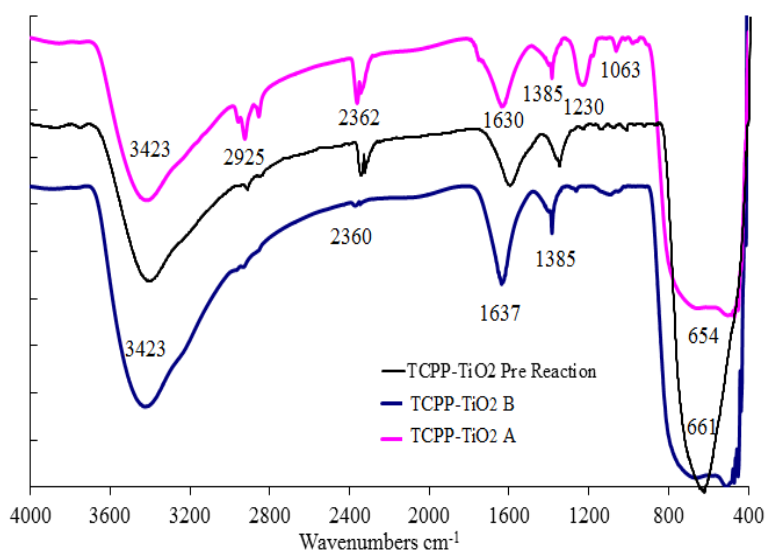


Figure 5.17: FT-IR of both adsorbed and bound TCPP-TiO₂ post photoreaction compared with TCPP-TiO₂-B pre-reaction.

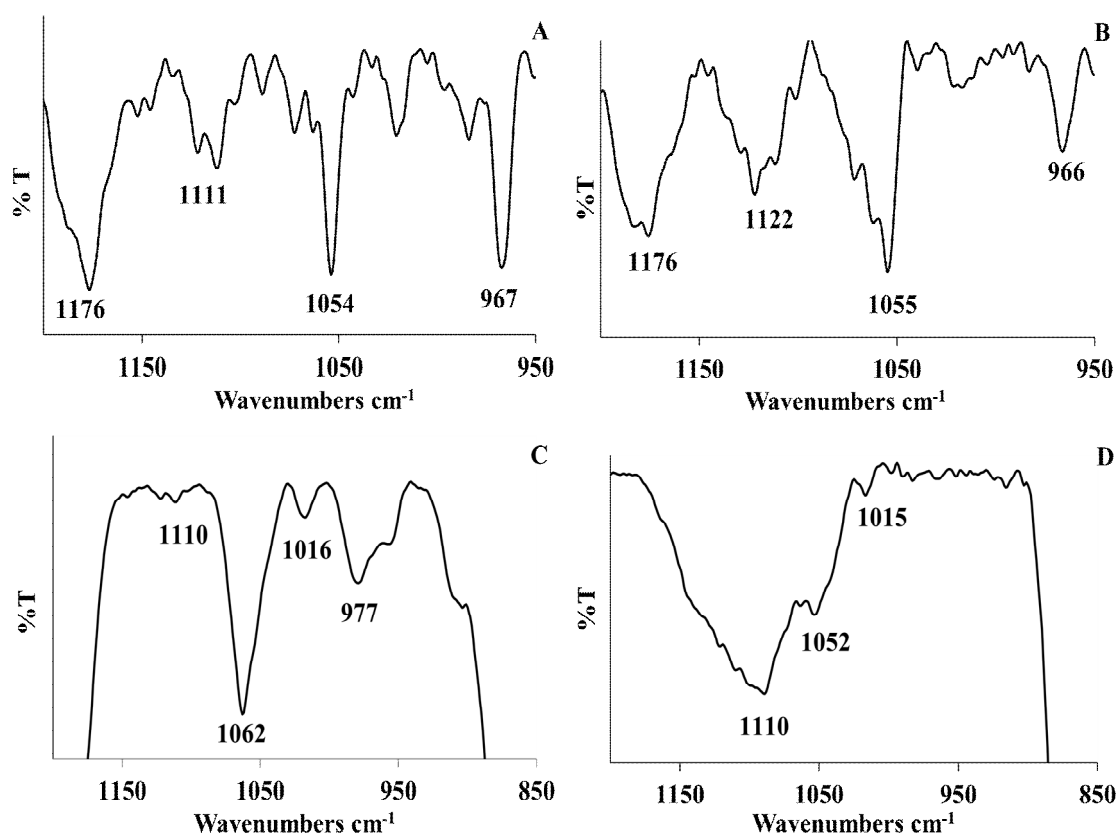


Figure 5.18: FT-IR showing the fingerprint region for TCPP-TiO₂ composites pre/post-photoreaction. (A): TCPP-TiO₂-A (pre) (B): TCPP-TiO₂-B, (pre) (C): TCPP-TiO₂-A (post) (D): TCPP-TiO₂-B (post).

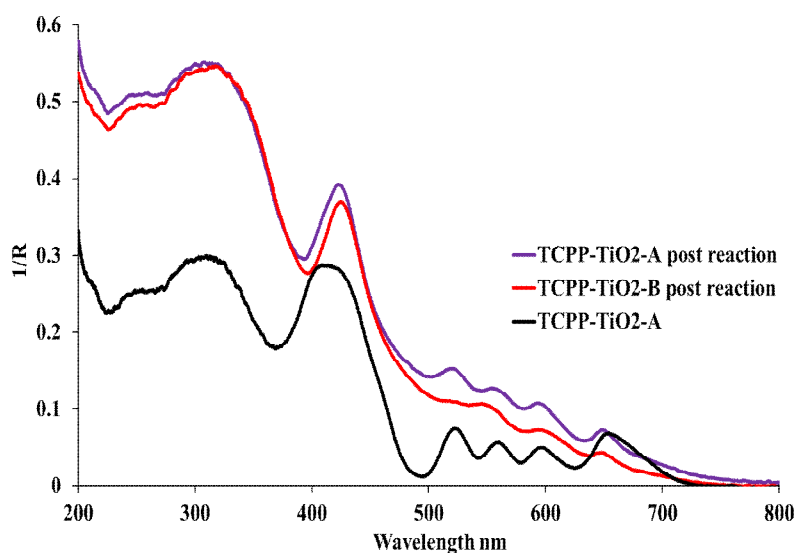


Figure 5.19: UV-vis analysis of TCPP-TiO₂-A and TCPP-TiO₂-B post reaction (photo-bleaching) compared with the original UV-vis profile for TCPP-TiO₂-A.

UV-vis analysis (Figure 5.19) of the coated materials post reaction would indicate that some of the sensitizer remains intact on the surface of the TiO₂ despite the changes in the FTIR spectra. These samples were further used in photocatalytic experiments to examine whether photoactivity was retained despite the photobleached product. Considering these findings, it was

concluded that dark storage of the photocatalyst would be required (to prevent degradation of the porphyrin dye on the TiO₂ surface by regular laboratory light or natural daylight sources).

5.2.3.5 Recyclability

After recovering the photocatalyst post reaction, it was washed, dried, and reintroduced into fresh Famotidine solution and the experiment was repeated. The results are shown in Figure 5.20. The photoactivity is shown to be significantly reduced, although it is still superior over the standard P-25 TiO₂ photocatalyst (not recycled) and photolysis with approximately 66% elimination of Famotidine after 3h for TCPPP-TiO₂-A and 34% elimination for TCPPP-TiO₂-B. The improved performance of TCPPP-TiO₂-A was again observed even in recycling.

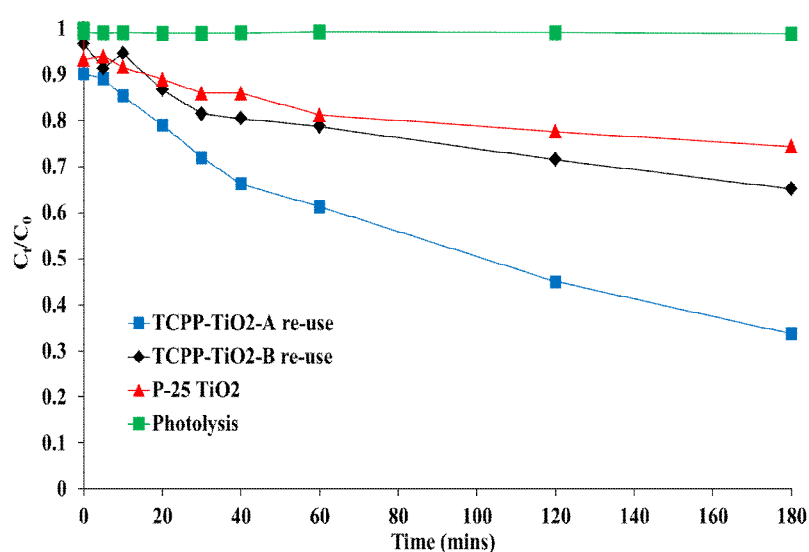


Figure 5.20: HPLC analysis of TCPPP-TiO₂-A and TCPPP-TiO₂-B recovered and reintroduced into fresh Famotidine solution compared with controls.

5.2.3.6 Applicability to other Pharmaceuticals (Tamsulosin and Solifenacin)

Further experiments were conducted with Tamsulosin and Solifenacin to examine the applicability of the photocatalyst to other types of pharmaceuticals. The results for Tamsulosin are shown in Figure 5.21 and for Solifenacin are shown in Figure 5.22. In the case of both pharmaceuticals the performance of the TCPPP-TiO₂ was not significantly superior over TiO₂. After sonication and prior to irradiation there is a drop in the concentration of pharmaceutical which we believe is due to the dispersion of the photocatalyst and adsorption of the pharmaceutical to the photocatalyst. However, at the point of exposure of the reaction solution to light irradiation there is no significant drop in concentration which indicates no photo-degradation is occurring.

Solifenacin and Tamsulosin both contain a number of aromatic rings which can be difficult to degrade, which may explain why the photocatalyst is superior in the case of Famotidine and not in the case of Tamsulosin and Solifenacin. In previous concentration variation studies (Chapter 3), the TiO_2/UV process was shown to be effective for high concentrations of the pharmaceuticals in the following order for 200 μM : Famotidine, Tamsulosin, Solifenacin. Solifenacin showed the poorest performance at higher concentrations, with Famotidine being the best. This may further reinforce the results obtained in these trial studies. Applicability of this photocatalyst can thus be considered to be unsuitable perhaps for drugs with significant aromatic/phenyl groups, although this would further have to be evaluated in follow-up studies. Time constraints did not allow further optimisation of the photodegradation process with all pharmaceuticals, although we believe that the process could be further optimised to ensure both a longer lifetime and a better performance of the photocatalyst.

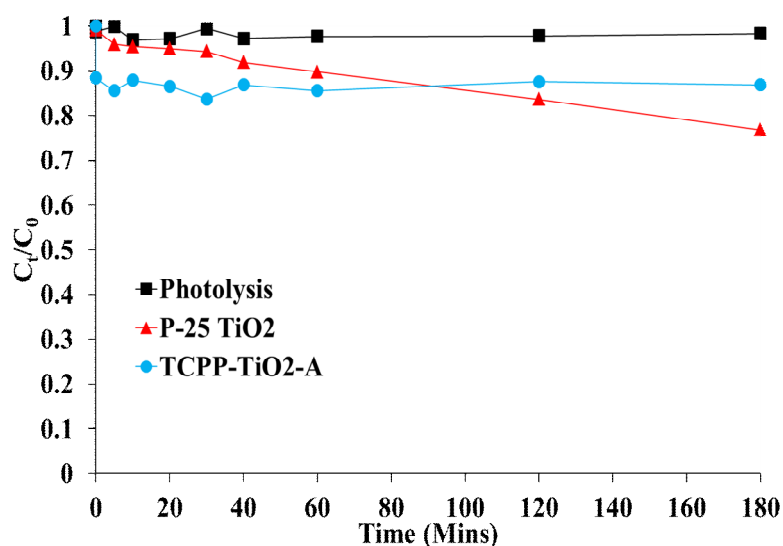


Figure 5.21 Indoor photocatalytic degradation experiments with TCPP- TiO_2 along with controls for Tamsulosin. $[\text{TCPP-TiO}_2] = 0.031 \text{ g}$, $[\text{TAM}] = 0.083 \text{ mM}$.

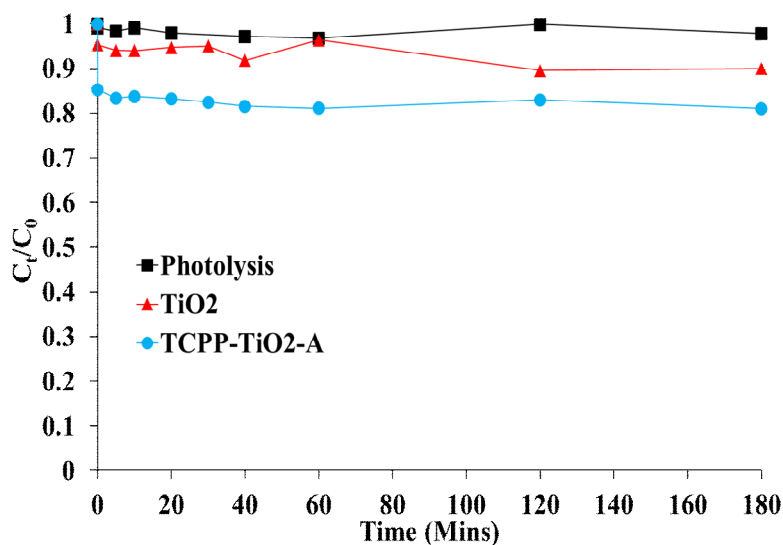


Figure 5.22 Indoor photocatalytic degradation experiments with TCPP-TiO₂ along with controls for Solifenacin. [TCPP-TiO₂] = 0.031 g, [SOL] = 0.083 mM.

5.2.4 Synthesis of Zn-Hexadecafluorophthalocyanine-TiO₂

Phthalocyanines are considered to be better sensitizers than porphyrins due to their intense absorption in the visible region (into the near IR) and also their high stability towards demetallation and chemical degradation.²¹⁴ In light of this and considering the occurrence of photo-bleaching in our previous composite and the success of the previous adsorbed method of coating sensitizers onto TiO₂, we attempted to coat a sensitizer of this nature onto TiO₂. Many novel phthalocyanine compounds have been synthesized in our group. The Zn-Hexadecafluorophthalocyanine (ZnHFpc) seen in Figure 5.23 (synthesized by B. Murphy) has substituted fluorines on the peripheral phenyl groups which ensure a highly stable species.

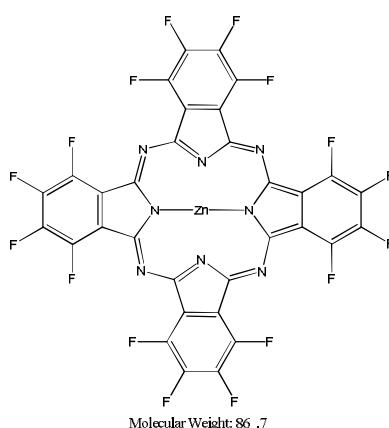


Figure 5.23: Structure of the Zn-Hexadecafluorophthalocyanine (ZnHFpc)

The ZnHFpc-TiO₂ was prepared in a similar manner to the previous TCPP-TiO₂ composite. The synthetic procedure was performed this time in chloroform and following adsorption to TiO₂, a soxhlet extraction in chloroform was then performed. After soxhlet extraction 0.011 g of the

original 0.045 g phthalocyanine was recovered leaving a loading of 0.034 g/1 g TiO₂. This material was dried and half of the material underwent a further soxhlet with acetone which removed more of the phthalocyanine resulting in a lighter coated composite (approximately 0.002 g/1 g TiO₂). This was later tested in comparison to the original composite.

5.2.5 Characterisation

5.2.5.1 UV-vis Spectroscopy

UV-vis analysis of the ZnHFpc yielded the spectrum shown in Figure 5.24. The λ_{max} at 677 nm (Q-band) shows another absorbance at 643 nm. A UV-vis spectrum was obtained at a higher concentration (inset) and showed that the ratio of this peak to the main Q-band peak increased meaning that this peak is due to co-facial aggregation of the phthalocyanine, a common property of phthalocyanine dyes.²¹⁵ Significant dimerization or aggregation results in Q-band shifts and band broadening.²¹⁶ Solid state UV-vis analysis was performed on the ZnHFpc-TiO₂ composites and the spectra are shown in Figure 5.25 with some interesting results.

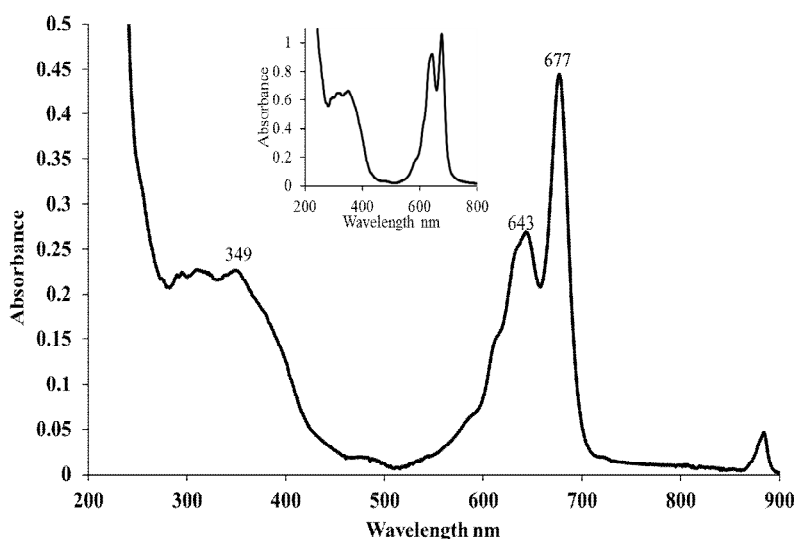


Figure 5.24: UV-vis spectrum of ZnHFpc in DCM showing the Q-band at 677 nm and the B-band at 349 nm. Inset is the UV-vis spectrum at a higher concentration.

The lighter coated composite showed a red shifted Q-band at 682 nm. Slight shifts can be expected due to the differences between UV-vis in the solid state vs. solution state, although this Q-band shift was found on both occasions of two separately prepared KBr discs. The order of intensity of the Q-bands also changes, with the most intense band now occurring at 647 nm. There is also significant band broadening which would signify aggregation of the dye on the TiO₂ surface. This would be seen as very unlikely as this composite contains a significantly lighter concentration of the dye on the surface of the TiO₂. The heavier coated sample shows even further band broadening and a greater red shift of the Q-band to 689 nm. These results

would indicate that the heavier coated composite has a higher degree of aggregation/dimerization than the lighter coated composite. Both composites are compared with the solid state UV-vis spectrum of TiO_2 . No absorbance due to TiO_2 can be determined with these samples as phthalocyanines have a B-band absorbance which occurs at approximately 350 nm (see UV-vis in Figure 5.24).

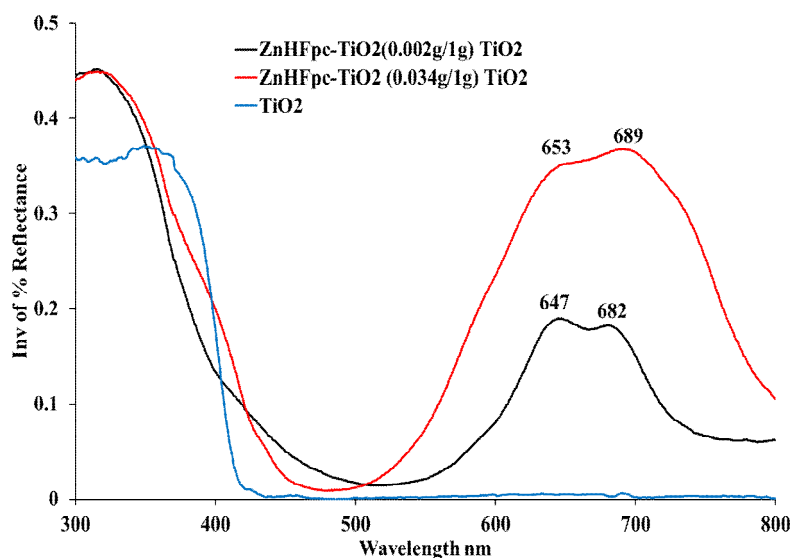


Figure 5.25: Diffuse reflectance spectra of the ZnHFphthalocyanine- TiO_2 compared to TiO_2 .

5.2.5.2 IR Spectroscopy

FT-IR analysis of the coated TiO_2 was compared to the free sensitizer. Presentation of the normalised spectra in Figure 5.26 (fingerprint region) show that there is no shift in any of the bands of the phthalocyanine once coated onto TiO_2 . This is indicative of a coating as opposed to a bound material. Although it may be difficult to observe with normalized spectra, the intensity of the bands also remain proportional to one another, indicating that coating to TiO_2 does not affect the stretching modes of functionalities within the sensitizer.

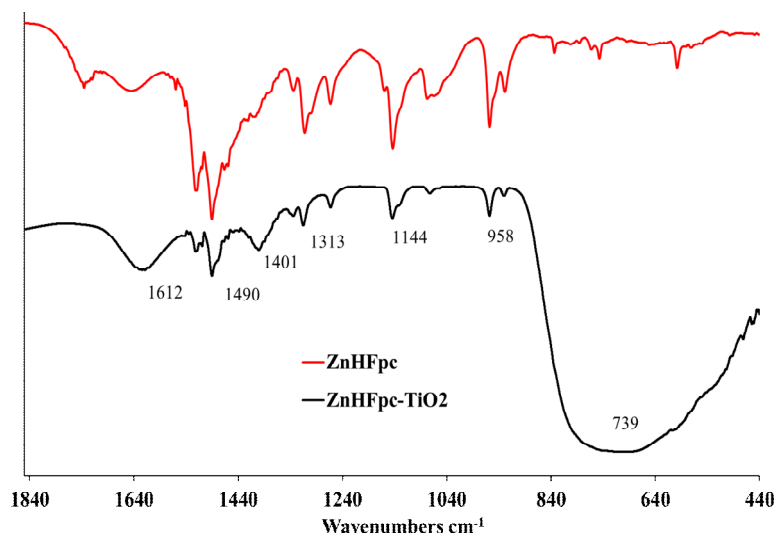


Figure 5.26: FT-IR spectra for ZnHFphthalocyanine and its TiO₂ composite, showing no shift in bands indicative of a coating as opposed to a binding.

5.2.6 Examination of the Photocatalytic Efficiency of ZnHFphthalocyanine-TiO₂ in Famotidine Degradation with Visible Light.

A preliminary photodegradation reaction of Famotidine with the ZnHFphthalocyanine-TiO₂ composite indicated that its photo-efficiency was not comparable to the porphyrin composite with some degradation seen, although nothing significant. The material was recovered after this 3 h photodegradation experiment and appeared to remain intact (Figure 5.27).

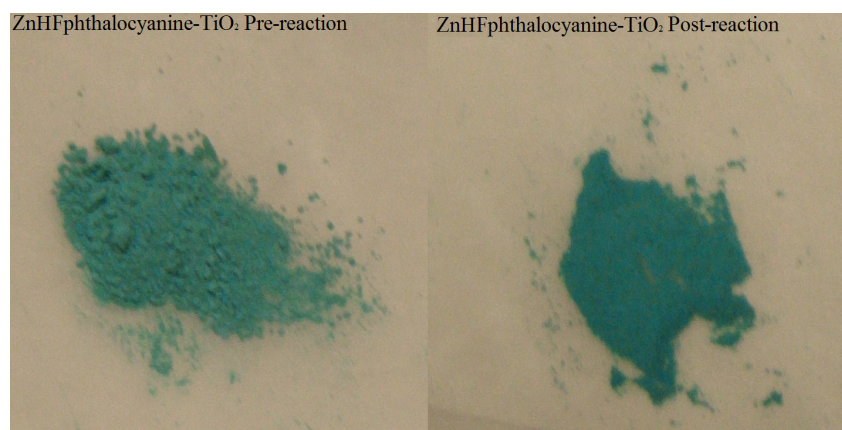


Figure 5.27: Photograph showing the ZnHFphthalocyanine-TiO₂ pre-photoreaction and post-photoreaction (3 h).

Although only some degradation of Famotidine was observed, the fact that the material was unchanged is a promising result since a more stable material can undergo longer irradiation times. Considering this, we decided to further test the composite with longer irradiation times and lab air purging. In addition, we attempted an experiment with both conditions

simultaneously (extended irradiation and lab air purging). Lab air purging provides oxygen necessary for singlet oxygen generation if this is the method of degradation followed by this composite. Various controls were also performed in order to ensure any degradation occurring was directly from the composite. Initial tests with the material are shown in Figure 5.28.

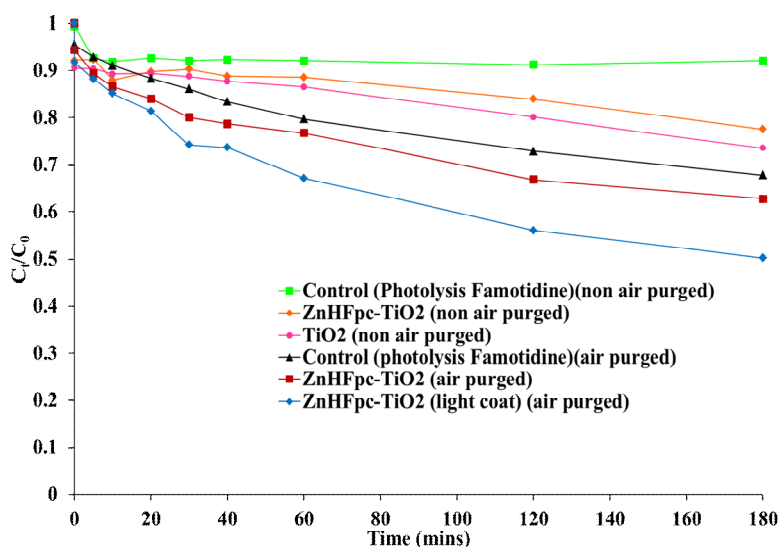


Figure 5.28: Indoor photocatalytic experiments with ZnHFpc-TiO₂ for 3 h with air purging compared with purged and non-purged control experiments. [ZnHFpc-TiO₂] = 0.031 g, [FAM] = 0.083 mM.

The control experiment (Famotidine photolysis) showed no degradation, and TiO₂ photocatalysis showed approximately 20% degradation as would be expected. The ZnHFphthalocyanine-TiO₂ composite performed slightly worse than TiO₂. This would indicate that the sensitizer coat may be simply hindering the performance of the TiO₂ by quenching any hydroxyl radicals generated. A high loading of the sensitizer can also cause aggregation which is a recurring problem reported with phthalocyanines caused by their planar structure. This problem can be resolved by using phthalocyanines with bulky peripheral substituents that sterically prevent aggregation. A short term solution would be to use a lighter coated composite.

The ZnHFphthalocyanine-TiO₂ composite which had a much lighter coat was tested in a parallel experiment with air purging and showed a slightly better performance than the heavier coated. However, the air purged control experiment (photolysis) we performed also showed an improved degradation over TiO₂ meaning that the lighter coat is only a slight improvement to the heavier coat. Further extended irradiation experiments were performed with the original composite to investigate the stability of the composite over this longer period, and to see if perhaps 100% elimination of Famotidine could be achieved with this material. The results of these experiments are shown in Figure 5.29.

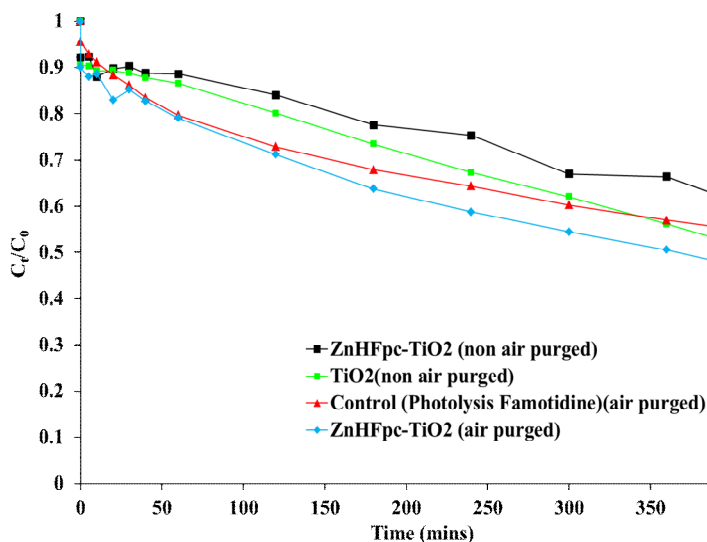


Figure 5.29: Extended irradiation photocatalytic experiments with ZnHFpc-TiO₂ for 7h with air purging compared with a non-purged experiment. [ZnHFpc-TiO₂] = 0.031 g/100 mL (0.0155 g/50 mL, air purged), [FAM] = 0.083 mM.

Even with an extended irradiation of 7 h (420 mins), the total elimination of Famotidine by ZnHFphthalocyanine-TiO₂ reaches only 55%. Without air purging the total elimination reaches 42% which is still out-performed by TiO₂ which reaches just over 50% after 7 h. Following these experiments, we deemed this composite, although photo-stable, to be an ineffective photocatalyst. Further to this we have concluded that a lighter loading of the phthalocyanine sensitizer showed an improved performance over the heavier coat which may indicate that aggregation is a cause for the inefficiencies with this material.

5.2.7 Preparation of 1,4-(tetrabenzaldehyde)phthalocyanine-TiO₂

Two non-metallated phthalocyanines prepared in our group (V. Peters *et al.*) were also considered as sensitizers for preparation of TiO₂ based composites. These phthalocyanines experience much less aggregation due to the presence of aromatic peripheral substituents. We considered first preparing a composite with the β -isomer (Figure 5.30) and if this proved successful, further preparation of a composite with the α -isomer. For this non-metallated phthalocyanine we decided to adopt a different synthetic strategy which other authors in this area have previously reported. Their method involves coating the sensitizer onto the TiO₂ by stirring for 5h and instead of filtering the composite to remove the solvent, removal under vacuum thereby forcing all of the sensitizer onto the TiO₂. A recent publication by Lu *et al.* 2010 showed that their metallo-porphyrin-TiO₂ composites could be recycled as much as six times in the degradation of nitrophenol without any dramatic loss in efficiency.¹⁶⁴ In the synthesis of this phthalocyanine-TiO₂ composite we adopted loading concentrations similar to Lu *et al.* (6 μ M, 0.006 g/1 g TiO₂) and also tested a higher loading (8 μ M, 0.008 g/1 g TiO₂) and

for comparison we also prepared a composite using the method previously adopted in our own work with TCPP-TiO₂ with a higher loading (0.022 g/1 g TiO₂). Photographs of these composites can be seen in Figure 5.31.

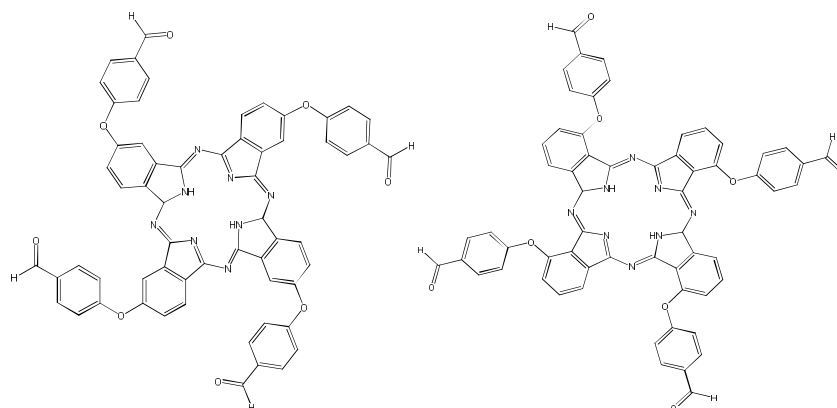


Figure 5.30: Structure of 1,4-(tetrabenzaldehyde)-phthalocyanine, β -isomer (left) and 1,3-(tetrabenzaldehyde)-phthalocyanine, α -isomer (right).

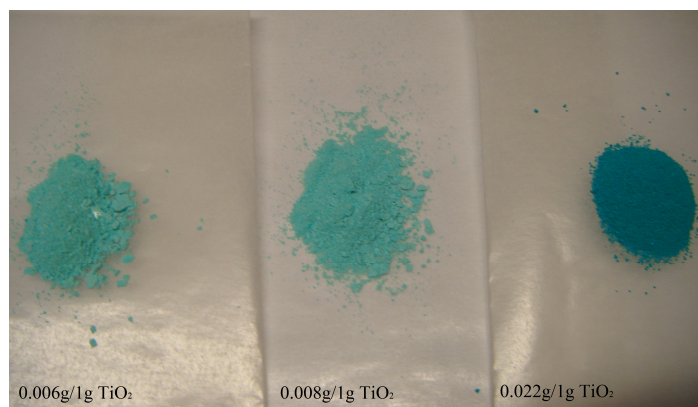


Figure 5.31: Photograph showing the β -(tetrabenzaldehyde)phthalocyanine-TiO₂ composites with various loadings: 0.006 g/1 g TiO₂, 0.008 g/1 g TiO₂, and 0.022 g/1 g TiO₂.

5.2.8 Characterisation

5.2.8.1 UV-vis Spectroscopy

The UV-vis spectrum of the β -(tetrabenzaldehyde)phthalocyanine in chloroform is shown in Figure 5.32. Also shown is its α -isomer. In non-metallated phthalocyanines the Q-band is split into two bands and for the β -isomer are seen at 702 nm and 666 nm, with the B-band arising at 329 nm. For the α -isomer there is a red shift of the Q-bands to 714 nm and 681 nm, the B-band in this case arising at 328 nm. UV-vis DR analysis was also obtained of the composite samples and the results are shown in Figure 5.33.

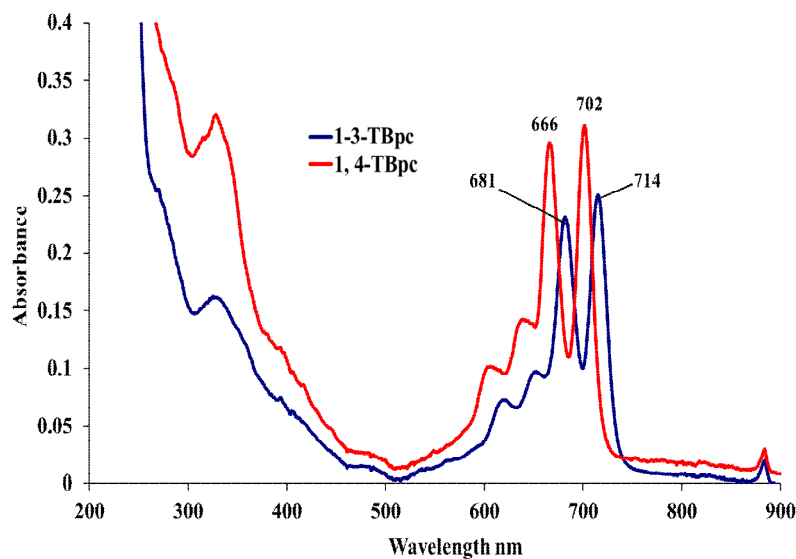


Figure 5.32: UV-vis spectra in chloroform of the α -(tetrabenzaldehyde)phthalocyanine and the β -(tetrabenzaldehyde)phthalocyanine.

Similar to the previous ZnHFphthalocyanine-TiO₂ composite materials, significant broadening of the bands arises with the solid state UV-vis for the β -tetrabenzaldehydephthalocyanine-TiO₂ composites. The order of the intensity of the bands in the visible region, as seen in the solution phase, has also reversed, and the most significant band in the spectrum arises at 638 nm. The shifts and broadening of the bands as previously discussed is dimerization/aggregation of the phthalocyanine on the surface. These effects appear to be enhanced somewhat in the solid state. Similar effects were observed in the solid state by Monahan *et al.* with Cu (II) phthalocyanine, who reported a close correspondence between the solution phase UV-vis of the dimer and the solid state spectrum of the dye.²¹⁷ More recent work to that for Cu(II)Pc by Seelan *et al.* reported red shifted broad bands with lower absorption coefficients in the solid state compared to narrow, sharp well resolved Q-bands in solution.²¹⁸

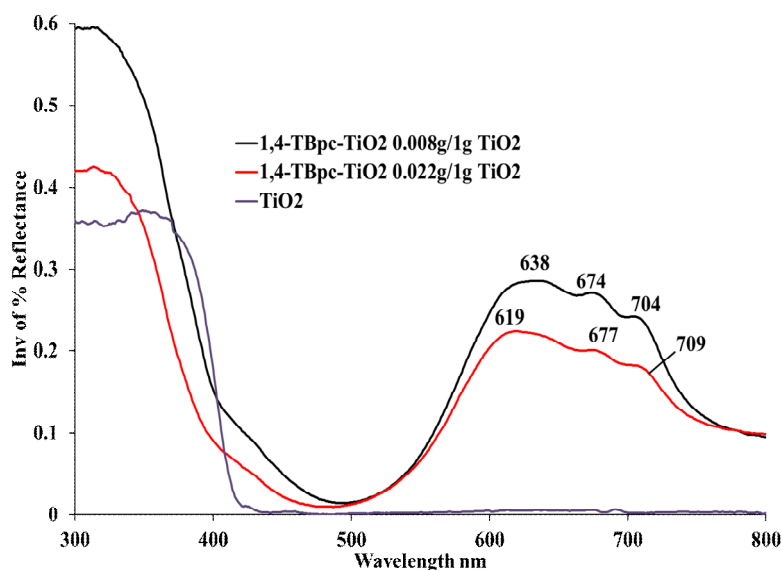


Figure 5.33: Diffuse reflectance UV-vis spectra of the β -tetrabenzaldehyde)phthalocyanine- TiO_2

5.2.8.2 IR spectroscopy

FT-IR of the composite and the sensitizer alone were obtained and the spectra are compared in Figure 5.34. The previous composite ZnHFpc-TiO_2 indicated a binding in the IR spectra based on identical shifts in the composite and the sensitizer. The spectra for β -tetrabenzaldehydephthalocyanine- TiO_2 show the absence of two stretches 1014 cm^{-1} and 1094 cm^{-1} and the appearance of a stretch at 1055 cm^{-1} .

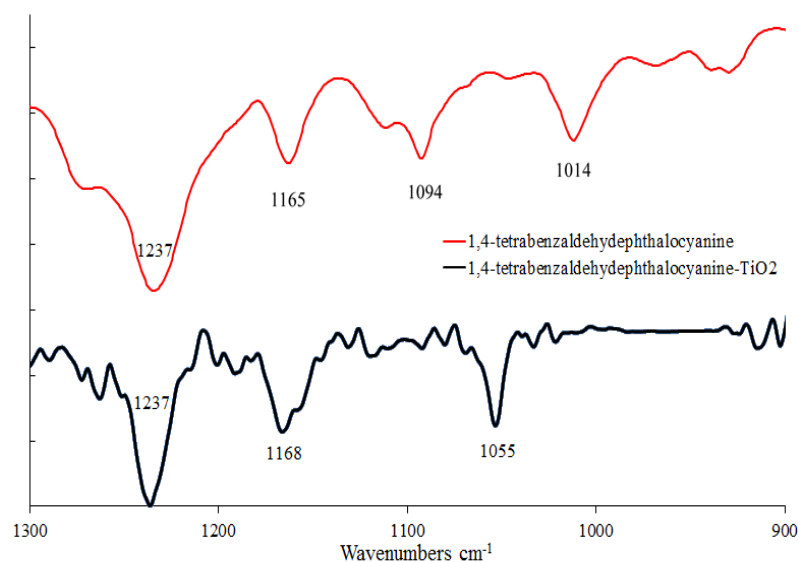


Figure 5.34: FT-IR spectra of β -(tetrabenzaldehyde)phthalocyanine- TiO_2 compared with the free sensitizer.

Shifts are generally indicative of a binding as previously discussed. Arguably, binding is possible via H-bonding of the TiO_2 surface with the aldehyde oxygen present on the peripheral substituents. Analysis of the full spectrum of stretches (see experimental for stretches) indicates

that the (C-O) band in the sensitiser, 1720 cm^{-1} , is shifted in the composite to 1650 cm^{-1} . This shift, along with the other shifts seen in Figure 5.34 would conclude that there is a binding of this sensitiser to the TiO_2 surface.

5.2.9 Examination of the Photocatalytic Efficiency of β -(tetrabenzaldehyde)-phthalocyanine- TiO_2 in Famotidine Degradation with Visible Light.

Photodegradation experiments on the degradation of Famotidine were conducted with the three composites with the various loadings. The experiments were conducted for 3 h and were not air purged. Figure 5.35 shows the degradation profiles for the three composites along with two controls (TiO_2 and photolysis). The performance of all 3 composites showed no significant degradation of Famotidine after 3 h and similar to the ZnHFphthalocyanine- TiO_2 composite, the coat may have been a hindrance to photodegradation by TiO_2 . Of the 3 coats the 8 mg/1 g TiO_2 performed the best, although achieving only 24% elimination of Famotidine.

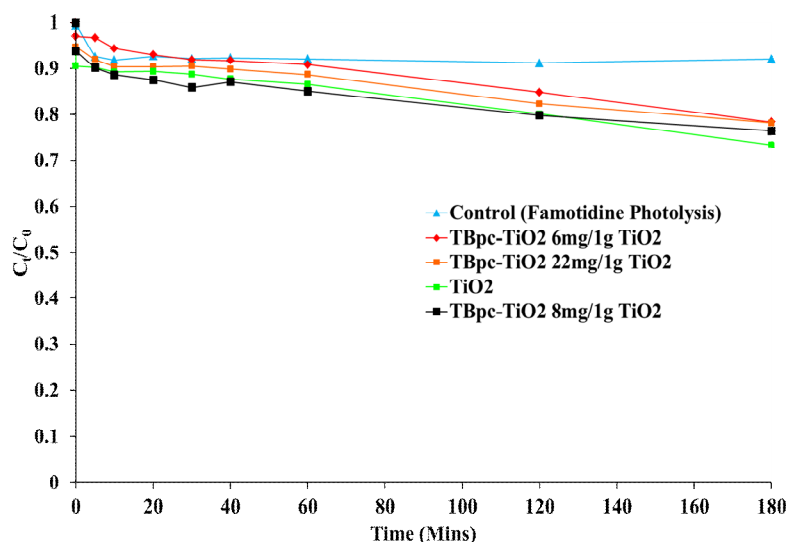


Figure 5.35: Indoor photocatalytic experiments with β -(tetrabenzaldehyde)phthalocyanine- TiO_2 (6 mg/1 g TiO_2 vs. 8 mg/1 g TiO_2 vs. 22 mg/1 g TiO_2) for 3 h compared with control experiments. $[\beta\text{-TBpc-TiO}_2] = 0.031\text{ g}$, $[\text{FAM}] = 0.083\text{ mM}$.

Unlike the previous sensitiser ZnHFpc, this phthalocyanine has considerably less aggregation and showed evidence of a binding to the TiO_2 which is desirable for an electron injection based photocatalytic degradation mechanism. This photocatalyst also showed considerable stability post reaction so it is not fully understood why very little elimination of Famotidine was observed. It may simply be the case that carboxylate linkers are more efficient electron transfer functionalities than aldehydes. It may be worthwhile to investigate metallated and non-metallated bulky substituted phthalocyanines with additional carboxylate functionalities present for anchorage to TiO_2 . Extended irradiation experiments were not performed with this

composite and based on the results obtained we did not proceed with coating and testing of the α -isomer.

5.2.10 Synthesis of Acetylacetonate linker (3-[4-benzoic acid] pentane-2,4-dione)

In reviewing current literature on linking groups, a recent study by McNamara *et al.*, reported the use of an acetylacetonate linker which they attached to TiO_2 and then subsequently attached this to a manganese sensitiser.¹⁶³ This linker was synthesized and a 60% yield of product was obtained (compared to the literature 62%). Column chromatography as stated in McNamara *et al.* cited a 1:1 Ethyl Acetate: Hexane, however this ratio was re-optimised and we found that 2:1 gave a more pure product.

5.2.11 Immobilisation onto TiO_2

McNamara *et al.* reported a high stability to hydrolysis and oxidation when this linker was used. Figure 5.36 shows the acetylacetonate linker and the positions at which it binds to the sensitiser and TiO_2 . The carboxylic acid functionality could in theory be bound to the sensitiser or TiO_2 . With this in mind, the linker should first be attached to the sensitiser followed by attachment to TiO_2 . In order to link a sensitiser to this carboxylic acid functionality, functionalised porphyrins/phthalocyanines would need to be synthesized and then attached to the linker. Unfortunately time restraints did not allow this work to be carried out. We do, however, envisage the use of this linker as a potential solution for the current instability problems and work of this kind to be an appropriate direction for this project.

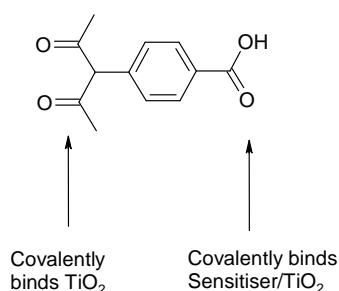


Figure 5.36 Acetylacetonate linker and its 2 possible linking sites for TiO_2 and a sensitiser.

5.2.12 Synthesis of TDI- TiO_2

Jiang *et al.* 2008 employed TDI (toluene diisocyanate) as a linker to attach a dye molecule to TiO_2 . The synthesis of TDI- TiO_2 was very straightforward method involving stirring in DCM for 2h under N_2 . This yielded a pale yellow solid material which was left to vacuum dry and collected.

5.2.13 Characterisation of TDI-TiO₂

5.2.13.1 IR Spectroscopy

FT-IR spectroscopy on the TDI-TiO₂ showed both stretches for the amide at 3300 cm⁻¹ and 1600 cm⁻¹, carbonyl moieties at 1644 cm⁻¹ and the isocyanate stretch at 2280 cm⁻¹ indicating that it has been coated onto TiO₂.

Sample	Wavenumber cm ⁻¹	Strength	Functional group
TDI-TiO ₂	3300	weak	N-H amide stretch
	2280	strong	O=C=N Isocyanate Stretch
	1644	strong	C=O
	1600	strong	N-H amide stretch

Table 5.3: Table of IR stretches and assigned functional groups for TDI-TiO₂.

5.2.13.2 UV-vis Spectroscopy

UV-vis analysis of the linked TiO₂ was undertaken and the data shown in Figure 5.37. The TDI linker has some conjugation and its yellow colour should predictably give rise to absorbance above 400 nm. A large tail of absorbance was found with this sample from 400 nm to as far as 600 nm indicating its conjugation to TiO₂.

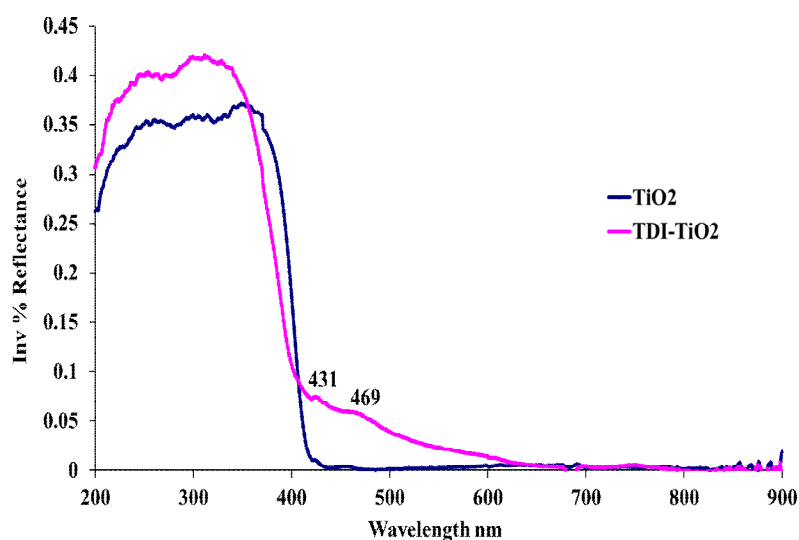


Figure 5.37: Diffuse Reflectance spectroscopy of TDI-TiO₂ compared with TiO₂

5.2.13.3 Immobilisation onto TiO₂

Figure 5.38 shows TDI-TiO₂ and the free isocyanate moiety to which a sensitizer can be bound. In order to link a sensitizer to this isocyanate moiety, functionalised sensitizers are required. Time constraints did not allow this although the use of this linked TiO₂ should be considered in the development of future visible light sensitised photocatalysts.

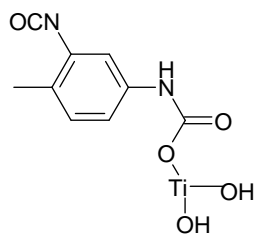


Figure 5.38: TDI attached to TiO_2 with a remaining thiocyanate group for linkage to a sensitiser.

5.2.14 Synthesis of APS- TiO_2

Silane coupling agents are commonly used to couple inorganic materials together with organic materials. Typical inorganic materials include metal oxides such as alumina, silica and titanium dioxide. Silane coupling agents generally exist as Y-R-SiX_3 where Y is a functional group such as an amine which can be used to attach various organic molecules with mild conditions.^{162,219} R is the space between the functional group and the silane group which can be a range of species but is generally a straight aliphatic chain. X is another functional group which can undergo hydrolysis to attach to the metal oxide/inorganic material. Silanised TiO_2 was prepared via a method by Ye *et al.* 2007.¹⁶² In this preparation method they used APTES, however, in our synthetic procedure APTMS was used instead. This procedure was also performed by a visiting student. The first product yielded a pale grey powder, the second product (synthesized by a visiting student), yielded a very wet product, which upon continued washing and vacuum drying did not yield a dry powder product similar to the first product. Follow-up analysis was performed on the former sample. Analysis for this linked TiO_2 included EDX, diffuse reflectance, and FTIR analysis which is described below.

5.2.15 Characterisation of APS- TiO_2

5.2.15.1 Energy Dispersive X-Ray Spectroscopy (EDX)

Energy dispersive X-ray spectroscopy is a technique used in conjunction with SEM and is a form of analysis which detects x-rays emitted from the sample which is first bombarded with an electron beam. This beam ejects electrons from the sample which are then replaced by higher energy electrons from the beam. X-ray energy is then released from the sample in order to balance the energy between the two electron states. X-ray beams of various energies are then detected (in keV) depending on the element.

EDX is an appropriate technique for solid samples which can be considered comparable to elemental analysis. Like elemental analysis it can generate information about the percentages of elements in a sample as well as the presence of certain elements. Since EDX is a very sensitive

technique it can only generate accurate results for rarer elements such as Ti, Fe, Si, etc. elements such as C, H, O and N cannot be determined. This technique was employed for the silane linked TiO_2 sample as only this sample has Si atoms.

The spectrum for a control TiO_2 sample is shown in Figure 5.39 along with the APS- TiO_2 sample. Ti appears in the spectra at 4.6 and 5 keV in both samples, with silicon appearing at 1.8 keV. A number of spectra were attained at various points in the sample, giving rise to mean values of abundances of certain elements which are found in Table 5.4. The approximate abundance found for silicon is 1.71%. A higher percentage of carbon is detected in the second sample due to the propyl chains on the linker. Carbon found in the control sample is due to contamination and for this reason this technique is only suitable for rarer elements.

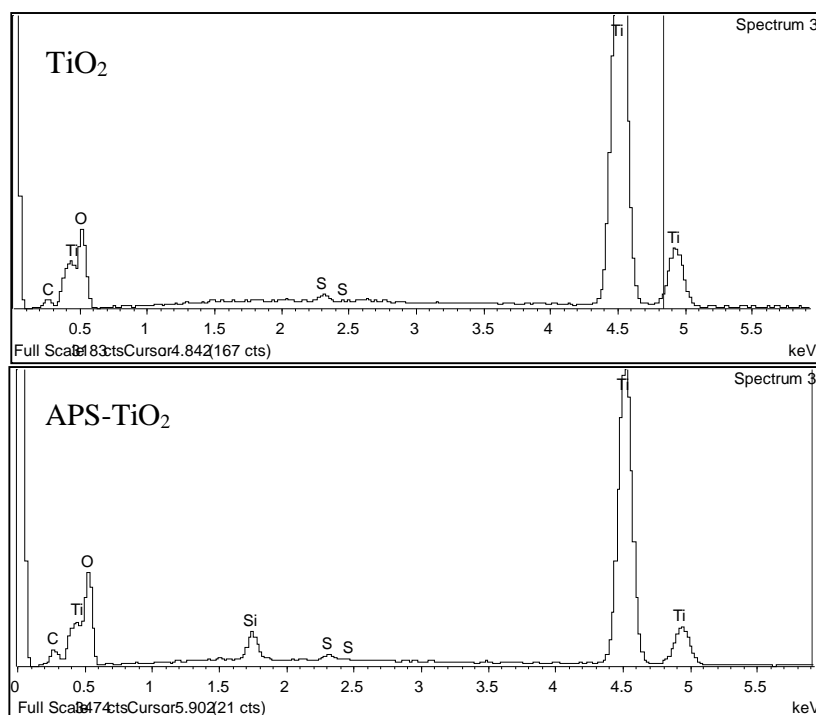


Figure 5.39: EDX spectra for TiO_2 and APS- TiO_2 showing clear signals for Ti and Si with the appearance of a peak for silica.

Atom	C	O	Ti	Si	S
Sample 1 (TiO_2) mean	1.97	40.85	56.76	0	0.42
Sample 2 (APS- TiO_2) mean	4.3	47.33	46.6	1.71	0.31

Table 5.4: Mean values of the percentages of elements in both the control P-25 sample and the APS- TiO_2 sample.

5.3.15.3 FT-IR spectroscopy

Characterisation of the APS-TiO₂ linker was carried out via FT-IR spectroscopy (Figure 5.41). Stretches for amine, Si and C-H moieties can be found. Most importantly is the weak Si-O-Ti stretch at 956 cm⁻¹. Amine stretches are found at 1666 cm⁻¹ and at ~3450 cm⁻¹. C-H stretches are also seen at 2937 cm⁻¹ and weaker bands around ~1400 cm⁻¹. Presence of these stretches confirm linkage of the aminopropyl silane chain to TiO₂.

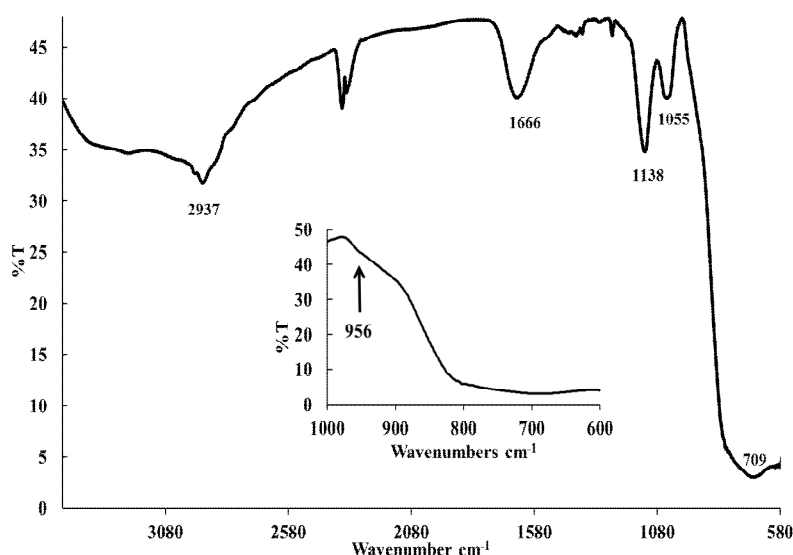


Figure 5.41: FT-IR spectrum of the APS-TiO₂, inset is a close up of the Si-O-Ti stretch.

5.2.15.4 Attachment of a sensitizer to APS-TiO₂

Figure 5.42 below shows a typical coupling method of our prepared linker with an acid chloride functionalized sensitizer, R. Time constraints did not allow synthesis of an acid chloride functionalized sensitizer to coat our prepared linker, although preparation of this type of material could be considered a worthwhile venture in the future to develop stable visible light sensitised TiO₂ materials.

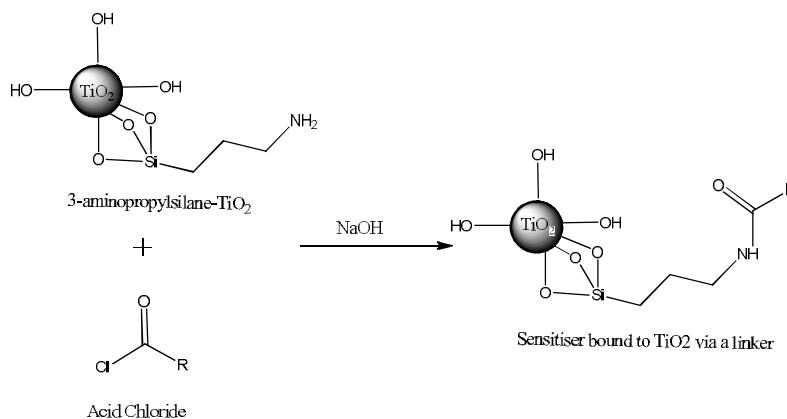


Figure 5.42: Coupling of the synthesized APS-TiO₂ linker to a functionalized sensitizer. (R= Sensitizer).

5.2.16 Visible Light Sensitised Photocatalyst Development Conclusions

Porphyrin Sensitised Photocatalysts: TCPP-TiO₂

Our first successfully prepared photocatalyst, TCPP-TiO₂, showed an impressive performance in the photocatalytic degradation of Famotidine with both indoor and solar light. However, the photocatalyst showed instability throughout irradiation and considerable quantities of intermediates were shown to be present in chromatogram traces, which may indicate simple conversion to an oxidised/reduced Famotidine molecule. UV-vis studies on the photocatalyst post-reaction indicated that sensitiser still remains on the TiO₂ surface and results have shown the possibility for re-use of the photocatalyst and also longer irradiation times which may have an effect on the performance of the photocatalyst. Further studies with other pharmaceuticals, Tamsulosin and Solifenacin indicated that the photocatalyst was less effective for these pharmaceuticals and it is clear that further studies should be performed with other types of pollutants to examine the exact nature of compounds which would be suitable candidates for this photocatalyst.

Metallated-Phthalocyanine Photocatalysts: ZnHFphthalocyanine-TiO₂

Our metallated Zn-phthalocyanine-TiO₂ composites showed a less impressive photodegradation of Famotidine compared to the porphyrin/TiO₂ composites. Various conditions were tested such as air purging, and extended irradiation, however, control studies indicated that air purging alone was effective for some removal of Famotidine. Despite the ineffectiveness of the photocatalyst it showed a good stability to degradation by light and TiO₂. The ineffectiveness of this photocatalyst was possibly due to the lack of a link/anchor between the TiO₂ and the sensitiser (which may explain the success of our previous composite), and it is also possible that intense aggregation due to its planar structure may be quenching any photo-excited states of the phthalocyanine which are generated. In order to confirm this, a Zn-phthalocyanine possessing bulky substituents would need to be developed and tested.

Our studies could not determine the exact mechanism of degradation for this composite as a singlet oxygen mechanism would be supported by an improved degradation with air purging. The lack of an anchor in the case of this composite may be of importance if a mechanism of 'electron injection' is followed. The presence of a functionality on the peripheral substituents may allow anchoring of the phthalocyanine which may then allow an 'electron injection' mechanism of degradation to proceed. Development of phthalocyanine based sensitisers with functionalities such as carboxylic acids, sulfonates and phosphonic acids could be considered, along with the presence of additional bulky substituents to prevent aggregation.

Work by Reddy *et al.* 2007, Giribabu *et al.* 2009 and more recently Mori *et al.* 2010 reported the use of unsymmetrical Znphthalocyanine sensitisers in DSSCs.^{220,221,222} They reported the synthesis of these sensitisers with various bulky peripheral substituents such as diphenylphenoxys, or *t*-butyl groups and one acid group to anchor to TiO₂ electrodes. They reported efficiencies of between 3.0-4.6% which are among the best achieved for MPc based DSSCs. Reddy *et al.* 2007 compared mono acid vs. tetra acid Zn phthalocyanine and found that the mono acid gave superior efficiencies due to the bulky *t*-butyl groups preventing aggregation and also creating 'directionality' in the excited state for electron injection to the TiO₂ conduction band. The current work by these groups and their respective success in synthesising unsymmetrical Zn-phthalocyanines by these various groups is encouraging.

Metal-free Phthalocyanine Photocatalysts: 1,4-(tetrabenzaldehyde)phthalocyanine-TiO₂.

Our characterisation of this composite indicated that the sensitiser was bound to the TiO₂ surface via the aldehyde peripheral substituents. These peripheral substituents reduce aggregation between phthalocyanine rings. The results on Famotidine photocatalytic degradation however indicated that no significant elimination was occurring compared to TiO₂. In the case of all loadings the elimination of Famotidine was less than that of TiO₂, which would indicate that sensitiser immobilisation is inhibiting TiO₂ photocatalysis. Given the evidence of binding, high photostability and reduced aggregation in this sensitiser the only explanation as to why this photocatalyst was not successful is that binding through an aldehyde functionality is just not as effective for electron injection as carboxylate anchors.

Chapter 6 - Thesis Conclusions/Future Work

The key aims of this thesis were four-fold.

1. To investigate the photolytic degradation of three regularly prescribed pharmaceuticals (Famotidine, Tamsulosin Hydrochloride and Solifenacin Succinate) using various light sources and reactors,
2. To examine the photocatalytic degradation of these pharmaceuticals with the photocatalyst titanium dioxide(TiO_2) and determine the effects of various parameters such as pH, TiO_2 concentration etc. on the photocatalytic process,
3. To identify and characterise any intermediates generated from these photodegradation studies using LC-MS/MS and determine the degradation pathways to these intermediates.
4. And finally, to develop and characterise new visible light sensitised photocatalytic materials such that visible/solar light could be harnessed and evaluate the performance of these materials with the 3 pharmaceutical targets.

Photolysis studies in Chapter 3 examined the contribution of light only in the degradation of the three target pharmaceuticals. These studies examined a variety of light sources (MP vs. LP Hg lamps), glass types (Quartz and Pyrex) and reactor types (Enviolet vs. immersion well). Large scale Enviolet photolysis studies showed that significant quantities of intermediates were generated for Tamsulosin and Solifenacin. The design of this reactor was also shown to be inefficient with issues relating to inadequate cooling, and the potential for build-up of nanoparticulate residues throughout the reactor. Pyrex photolysis studies conducted with each of the pharmaceuticals in the immersion well set-up indicated that Tamsulosin could be completely eliminated within the 3 h period. This can be attributed to its light-sensitive nature. Famotidine and Solifenacin showed an elimination of 25% and 20% elimination respectively in photolysis studies showing that they are relatively photo-stable.

Chapter 3 also showed the effects of photocatalytic degradation on each the pharmaceuticals. Titanium dioxide was employed as a photocatalyst in these studies and results showed that this photocatalyst can efficiently eliminate both Famotidine and Tamsulosin with complete removal within the three hour irradiation period. Solifenacin was not completely eliminated within the allotted irradiation time with approximately 80% removal. This was due to the formation of significant quantities of coloured intermediate products which can compete with Solifenacin for degradation and for light absorption. pH adjusted photocatalytic degradation studies indicated that the adsorption of each pharmaceutical is improved under alkaline conditions, however our studies with Solifenacin showed that this does not necessarily indicate a better photocatalytic performance as is documented in many literature articles.

Concentration variation studies indicated that the optimised TiO₂ process can completely eliminate relatively high concentrations of Famotidine (200 µM), and Tamsulosin (up to 200 µM). However, only low concentrations of Solifenacin could be completely eliminated (20 µM) with an appreciable 80% removal of concentrations at 83 µM. These concentrations are of course abnormally high and even environmentally relevant concentrations would be at more 'treatable' concentrations in the region of ng-µg/L. Further studies with the addition of hydrogen peroxide as an oxidant showed that each of the pharmaceuticals can be eliminated at a faster rate, and with effective mineralisation of intermediate compounds. The degradation and mineralisation achieved with the combined TiO₂/UV/H₂O₂ process within a relatively short time frame, makes it a practical option for the treatment of pharmaceutical compounds in industrial wastewater treatment plants. Future work in the field of TiO₂ photocatalysis is focused on two main aims: enhancing the visible light absorption of TiO₂ and the immobilisation of TiO₂. Immobilisation of the photocatalyst for ease of removal and the potential to recycle the photocatalyst would significantly reduce the cost of implementing the process.

Control experiments in Chapter 3 also showed some interesting effects of the reaction of Famotidine and sodium bisulfite.¹H NMR studies showed shifts which would indicate oxidation of the thiazole ring and also showed a complete conversion to this oxidised product. Oxidation of thiazole heterocycles are rare and compounds possessing these analogues are of particular interest as therapeutic agents.²²³ These oxidations generally employ harsh conditions, multiple steps and long reaction times.²²⁴ The effect observed in NMR experiments now warrants further study as it could be an alternative synthetic procedure for these analogues.

Chapter 4 investigated the intermediates generated from photo-degradation studies with each of the pharmaceuticals. In-house individual methods were developed for each of the pharmaceuticals and these methods were initially applied in monitoring the elimination of the pharmaceuticals. These methods were then transferred to an LC-MS/MS system for analysis and characterisation of intermediate structures. Intermediates from photocatalytic and photolytic studies were examined and various structures were proposed based on MS/MS analysis of fragments. Identification of these intermediates has further allowed us to understand the mechanism and propose routes of degradation for each of the pharmaceuticals. Degradation routes were found to be principally photo-oxidative, although photo-reductive mechanisms were also apparent.

In Chapter 5 new visible light sensitised photocatalytic composite materials were developed, characterised and evaluated with our pharmaceutical targets. These composite materials were based on titanium dioxide with porphyrin and phthalocyanine dyes. The performance of these

materials was evaluated initially with the pharmaceutical Famotidine and later with Tamsulosin and Solifenacin. The porphyrin/TiO₂ composite showed significant activity in the degradation of Famotidine in indoor experiments when compared to TiO₂ and photolysis. In solar studies with Famotidine, it outperformed TiO₂ once again owing to its absorption in the visible region. HPLC chromatograms indicated that the degradation of Famotidine observed with this composite could be a relatively selective oxidation or reduction (depending on the mechanism i.e singlet oxygen, electron transfer) compared to the mechanism of TiO₂ which is unselective. Additional studies with Tamsulosin and Solifenacin indicated that the composite was not effective for these pharmaceuticals. This may further indicate the selective degradation of Famotidine by this composite.

Additional composite materials based on phthalocyanine dyes were prepared and tested. These dyes are found to be more stable and absorb into the near-IR. These materials were prepared in different manners which were similar to recently adopted methods by other groups. The photocatalytic activity of these composites were also evaluated with Famotidine. However, these composites showed little photocatalytic activity in the degradation of Famotidine. Generally, novel dye sensitised TiO₂ materials are tested in the degradation of phenols and textile dyes and their elimination is monitored using UV-vis alone. This is the first use, to our knowledge, of dye sensitised TiO₂ composites to be tested with actual pharmaceuticals and to additionally monitor their elimination with HPLC analysis.

Further research with the porphyrin/TiO₂ composite should include the addition of additives which could aid in the stability and lifetime of the material. A variety of visible light sources could also be employed to exclude as much as possible the absorption of TiO₂ by the lamp. This may prevent photodegradation of the dye by TiO₂, however this would need to be done in conjunction with the synthesis of new porphyrin molecules which red-shift the Soret band as they currently overlap and if lamps are selected which do not irradiate in the region of this band absorption of light by the dye could be significantly hampered along with the photocatalytic performance of the material. In addition to this, various porphyrins and phthalocyanines should be synthesized. These, ideally, should contain additional peripheral substituents to inhibit aggregation and also a variety of linkers to attach to TiO₂. This should create optimum conditions for electron transport to TiO₂. Composites which are based on metallated porphyrins/phthalocyanines should continue to be employed as these will result in a very stable material and could significantly prolong the lifetime of the photocatalyst. Also, considering the findings of a possible selective oxidation/reduction with our porphyrin/TiO₂ composite, there may be potential for the use of this composite in synthetic organic chemistry. Generally oxidation and reduction reactions employ harsh and even dangerous reagents. Further work

could be done to investigate if this composite could be employed in selective photo-oxidation/photo-reduction reactions.

References

- ¹ Ellis, J.B., (2006), 'Pharmaceutical and Personal Care Products (PPCPs) in Urban Receiving Waters Environmental Pollution' 144 (1) 184-189.
- ² <http://www.ourstolenfuture.org/basics/chemlist.htm> (accessed: 06-01-2012)
- ³ Liu, Z., Kanjo, Y., Mizutani S., (2009) 'Removal Mechanisms for Endocrine Disrupting Compounds (EDCs) in Wastewater Treatment — Physical Means, Biodegradation, and Chemical Advanced Oxidation: A Review' *Science of The Total Environment* 407, 2, 731-748
- ⁴ http://ec.europa.eu/environment/water/water-framework/priority_substances.htm (accessed: 06-12-2012)
- ⁵ Kummerer, K., (2005) 'Pharmaceuticals in the Environment: Sources, Fate, Effects and Risks' *Springer publications*
- ⁶ Kummerer, K., (2004) 'Resistance in the Environment' *Journal of Antimicrobial Chemotherapy* 54(2), 311-320.
- ⁷ Khetan, S.K., Collins, T. J., (2007) 'Human Pharmaceuticals in the Aquatic Environment: A Challenge to Green Chemistry' *Chemical Reviews* 107, 2319-2364.
- ⁸ Kolpin, D. W., Furlong, E. T., Meyer, M. T., Thurman, E. M., Zaugg, S. D., Barber, L. B., Buxton, H. T., (2002) 'Pharmaceuticals, Hormones, and other Organic Wastewater Contaminants in U.S. streams, 1999-2000: A National Reconnaissance' *Environmental Science and Technology* 36, 1202.
- ⁹ Rabiet, M., Togola, A., Brissaud, F., Seidel, J.L., Budzinski, H., Elbaz-Poulichet, F., (2006) 'Consequences of Treated Water Recycling as Regards Pharmaceuticals and Drugs in Surface and Ground Waters of a Medium-Sized Mediterranean Catchment' *Environmental Science and Technology* 40, 5282-5288.
- ¹⁰ Zuccato, E., Calamari, D., Natangelo, M., Fanelli, R., (2000), 'Presence of Therapeutic Drugs in the Environment.' *Lancet* 355, 1789-1790.
- ¹¹ Tauber, R. (2003) 'Quantitative Analysis of Pharmaceuticals in Drinking Water from Ten Canadian Cities' Enviro-Test Laboratories/Xeno-Test Division, Canada.
- ¹² Esplugas, S., Bila, D. M., Krause, L. G. T., Dezotti, M., (2007) 'Ozonation and Advanced Oxidation Technologies to Remove Endocrine Disrupting Chemicals (EDCs) and Pharmaceuticals and Personal Care Products (PPCPs) in Water Effluents' *Journal of Hazardous Materials* 149, 631–642.
- ¹³ Langford, K. H., Reid, M., Thomas, K. V., (2011) 'Multi-residue Screening of Prioritised Human Pharmaceuticals, Illicit Drugs and Bactericides in Sediments and Sludge' *Journal of Environmental Monitoring*, 13, 2284.
- ¹⁴ Oaks, J., Gilbert, M., Virani, M., Watson, R., Meteyer, C., Rideout, B., Shivaprasad, H., Ahmed, S., Iqbal Chaudhry, M., Arshad, M., Mahmood, S., Ali, A., Khan, A., (2004) 'Diclofenac Residues as the Cause of Vulture Population Decline in Pakistan' *Nature* 427, 630-633.
- ¹⁵ R. B. Bringolf, R. M. Heltsley, T. J. Newton, C. B. Eads, S. J. Fraley, D. Shea, W. G. Cope (2010) 'Environmental Occurrence and Reproductive Effects of the Pharmaceutical Fluoxetine in Native Freshwater Mussels' *Environmental Toxicology and Chemistry*, 29, 6, 1311–1318.

-
- ¹⁶ Rizzo, L., Meric, S., Guida, M., Kassinos, D., Belgiorno, V., (2009), 'Heterogenous Photocatalytic Degradation Kinetics and Detoxification of an Urban Wastewater Treatment Plant Effluent Contaminated with Pharmaceuticals' *Water Research* 43, 16, 4070-4078.
- ¹⁷ Snyder, S. A., Adham, S., Redding, A. M., Cannon, F. S., DeCarolis, J., Oppenheimer, J., Wert, E. C., Yoon, Y., (2007) 'Role of Membranes and Activated Carbon in the Removal of Endocrine Disruptors and Pharmaceuticals' *Desalination* 202 156–181.
- ¹⁸ Herberer, T., Mechlinski, A., Fanck, B., Knappe, A., Massmann, G., Pekdeger, A., Fritz, Field, B., (2004) 'Studies on the Fate and Transport of Pharmaceutical Residues in Bank Filtration', *Ground Water Monitoring and Remediation* 24 70-77.
- ¹⁹ K.M. Hiscock, T. Grischek (2002) 'Attenuation of Groundwater Pollution by Bank Filtration' *Journal of Hydrology* 266 139–144.
- ²⁰ Pokhrel, D., Viraraghavan, T., (2009) 'Biological Filtration for Removal of Arsenic from Drinking Water' *Journal of Environmental Management* 90 1956–1961.
- ²¹ Huisman, L., Wood, W.E., (1974) 'Slow Sand Filtration' World Health Organisation www.who.int/water (accessed: 06-01-2012)
- ²² Bolong, N., Ismail, A.F., Salim, M.R., Matsuura, T., (2009) 'A Review of the Effects of Emerging Contaminants in Wastewater and Options for their Removal' *Desalination* 239, 229–246.
- ²³ Schafer, A.I., Nghiem, L. D., Waite, T.D., (2003) 'Removal of the Natural Hormone Estrone from Aqueous Solutions Using Nanofiltration and Reverse Osmosis' *Environmental Science and Technology* 37, 182-188.
- ²⁴ Fox, P., Houston, S., Westerhoff, P., (2001) 'Soil Aquifer Treatment for Sustainable Water Reuse' *American Waterworks Association*
- ²⁵ Idelovitch, E., Michail, M., (1984) 'Soil-Aquifer Treatment: A New Approach to an Old Method of Wastewater Reuse' *Water Pollution Control Federation* 56, 8.
- ²⁶ Drewes, J. E., Quanrud, D. M., Amy, G. L., Westerhoff, P. K., (2006) 'Character of Organic Matter in Soil-Aquifer Treatment Systems' *Journal of Environmental Engineering* 1447-1458.
- ²⁷ Mendez-Arriaga, F., Torres-Palma, R.A., Petriera, C., Esplugas S., Gimenez, J., Pulgarin, C., (2008) 'Ultrasonic Treatment of Water Contaminated with Ibuprofen' *Water Research* 42, 4243-4248.
- ²⁸ Hartmann, J., Bartels, P., Mau, U., Witter, M., Tümpling, W.v., Hofmann, J., Nietzsche, E., (2008) 'Degradation of the Drug Diclofenac in Water by Sonolysis in presence of Catalysts' *Chemosphere* 70, 453-461.
- ²⁹ Torres, R., Peatrier, C., Combet, E., Moulet, F., Pulgarin, C., (2007) 'Bisphenol A Mineralization by Integrated Ultrasound-UV-Iron (II) Treatment' *Environmental Science and Technology* 41, 297-302.
- ³⁰ Glassmaker, T., Shoemaker, J. A., (2005) 'Effects of Chlorination on the Persistence of Pharmaceuticals in the Environment' *Bulletin of Environmental Contamination and Toxicology* 74, 24-31.
- ³¹ Bedner, M., Maccreehan, W.A., (2004) 'Transformation of Acetaminophen by Chlorination Produces the Toxins 1,4-Benzoquinone, N-acetyl-p-benzoquinone Imine' *Environmental Science and Technology* 40, 516-52.

-
- ³² Westerhoff, P., Yoon, Y., Snyder, S., Wert, E., (2005) 'Fate of Endocrine-Disruptor, Pharmaceutical, and Personal Care Product Chemicals during Simulated Drinking Water Treatment Processes' *Environmental Science and Technology* 39(17), 6649-6663.
- ³³ De Witte, B., Dewulf, J., Demeestere, K., Van Langenhove, H., (2009) 'Ozonation and Advanced Oxidation by the Peroxone Process of Ciprofloxacin in Water' *Journal of Hazardous Materials* 161, 701–708.
- ³⁴ McDowell, D.C., Huber, M.M., Wagner, M., Von Gunten, U., Ternes, T.A., (2005) 'Ozonation of Carbamazepine in Drinking Water: Identification and Kinetic Study of Major Oxidation Products' *Journal of Environmental Science and Technology* 39, 8014-8022.
- ³⁵ Lee, Y., Escher, B. I., Von Gunten, U., (2008) 'Efficient Removal of Estrogenic Activity during Oxidative Treatment of Waters Containing Steroid Estrogens' *Journal of Environmental Science and Technology*, 42(17), 6333-6339.
- ³⁶ Huber, M. M., Canonica, S., Park, G., Von Gunten, U., (2003) 'Oxidation of Pharmaceuticals during Ozonation and Advanced Oxidation Processes' *Journal of Environmental Science and Technology* 37(5), 1016-1024.
- ³⁷ Kemsley, J., (2007) 'Bromate in Los Angeles Water' *Chemical and Engineering News*, 85 (9).
- ³⁸ Dasani (2004) 'Voluntary Withdrawal of Dasani in the UK' Available at: <http://www.thecoca-colacompany.com> (accessed 25-10-11).
- ³⁹ Von Gunten, U., (2003) 'Ozonation of Drinking Water: Part I. Oxidation Kinetics and Product Formation' *Water Research* 37, 1443–1467.
- ⁴⁰ Esplugas, S., Gimenez, J., Contreras, S., Pascual, E., Rodriguez, M., (2002) 'Comparison for Different Advanced Oxidation Processes for Phenol Degradation' *Water Research* (36) 1034-1042.
- ⁴¹ Rivas, F.J., Encinas, A., Acedo, B., Beltran, F J., (2009) 'Mineralization of Bisphenol A by Advanced Oxidation Processes' *Journal of Chemical Technology and Biotechnology* 84, 589–594.
- ⁴² Haque, M.M., Muneer, M., (2007) 'Photodegradation of Norfloxacin in Aqueous Suspensions of Titanium Dioxide' *Journal of Hazardous Materials* 145, 51–57.
- ⁴³ Yang, L., Yua, L. E., Ray, M. B., (2008) 'Degradation of Paracetamol in Aqueous Solutions by TiO₂ Photocatalysis' *Water Research* 42, 3480 – 3488.
- ⁴⁴ Shemer, H., Kunukcu, Y.K., Linden, K.G., (2006) 'Degradation of the Pharmaceutical Metronidazole via UV, Fenton and Photo-Fenton Processes' *Chemosphere* 63, 269–276.
- ⁴⁵ Diebold, U., (2003) 'The Surface Science of Titanium Dioxide' *Surface Science Reports*, 48, 53-229.
- ⁴⁶ Arslan-Alaton, I., Gurses, F., (2004) 'Photo-Fenton-like and Photo-Fenton-like Oxidation of Procaine Penicillin G Formulation Effluent' *Journal of Photochemistry and Photobiology A: Chemistry* 165, 165-175.
- ⁴⁷ Shemer, H., Kunukcu, Y. K., Linden, K.G., (2006) 'Degradation of the Pharmaceutical Metronidazole via UV, Fenton and Photo-Fenton processes' *Chemosphere* 63, 269-276.
- ⁴⁸ Molinari, R., Argurio, P., Poerio, T., Bonaddio, F., (2007) 'Photo Assisted Fenton in a Batch and a Membrane Reactor for Degradation of Drugs in Water' *Separation Science and Technology* 42, 1597–1611.

-
- ⁴⁹ Pera-Titus, M., Garcia-Molina, V., Banos, M.A., Gimenez, J., Esplugas, S., (2004) 'Degradation of Chlorophenols by Advanced Oxidation Processes: A General Review' *Applied Catalysis B: Environmental* 47, 219-256.
- ⁵⁰ Yuan, F., Hu, C., Hu, X., Qu, J., Yang, M., (2009) 'Degradation of Selected Pharmaceuticals in Aqueous Solution with UV and UV/H₂O₂' *Water Research* 43, 1766-1774.
- ⁵¹ Pereira, V. J., Linden, K. G., Weinberg, H. S., (2007) 'Evaluation of UV Irradiation for Photolytic and Oxidative Degradation of Pharmaceutical Compounds in Water' *Water Research* 41, 4413 – 4423.
- ⁵² Vogna, D., Marotta, R., Napolitano, A., Andreozzi, R., d'Ischia M., (2004) 'Advanced Oxidation of the Pharmaceutical Drug Diclofenac with UV/H₂O₂ and Ozone' *Water Research* 38, 414–422.
- ⁵³ Balcioglu, I. A., Ötöker, M., (2004) 'Pre-Treatment of Antibiotic Formulation Wastewater by O₃, O₃/H₂O₂, and O₃/UV Processes' *Turkish Journal of Engineering and Environmental Science* 28, 325-331.
- ⁵⁴ Ternes, T. A., Ueber, J. S., Herrmann, N., McDowell, D., Ried, A., Kampmann, M., Teiser, B., (2003) 'Ozonation: a Tool for Removal of Pharmaceuticals, Contrast Media and Musk Fragrances from Wastewater?' *Water Research* 37, 1976–1982.
- ⁵⁵ Rivas, F. J., Encinas, A., Acedo, B., Beltran, F. J., (2009) 'Mineralization of Bisphenol A by Advanced Oxidation Processes' *Journal of Chemical Technology and Biotechnology* 84, 589–594.
- ⁵⁶ Ravina, M., Campanella, L., Kiwi, J., (2002) 'Accelerated Mineralization of the Drug Diclofenac via Fenton Reactions in a Concentric Photo-Reactor' *Water Research* 36, 3553–3560.
- ⁵⁷ Perez-Estrada, L. A., Malato, S., Agüera, A., Fernandez-Alba, A. R., (2007) 'Degradation of Dipyrone and its Main Intermediates by Solar AOPs Identification of Intermediate Products and Toxicity Assessment' *Catalysis Today* 129(1-2), 207-214.
- ⁵⁸ Bautitz, I. R., Nogueira, R.F.P., (2007) 'Degradation of Tetracycline by Photo-Fenton Process—Solar Irradiation and Matrix Effects' *Journal of Photochemistry and Photobiology A: Chemistry* 187, 33–39.
- ⁵⁹ Arslan-Alaton, I., Dogruel, S., (2004) 'Pre-treatment of Penicillin Formulation Effluent by Advanced Oxidation Processes' *Journal of Hazardous Materials B* 112, 105–113.
- ⁶⁰ Beltran-Heredia, J., Torregrosa, J., Dominaguez, J.R., Perez, J.A., (2001) 'Comparison of the Degradation of p-hydroxybenzoic Acid in Aqueous Solution by Several Oxidation Processes' *Chemosphere* 42, 351-359.
- ⁶¹ http://www.enva.com/News/Enva_Ireland_News/Enva_Delivers_Advanced_UV_Solution_for_WestWstm.html (accessed: 28-10-2011)
- ⁶² O'Connor, K., Martin, C.P., Jensen, J.N., Holtz, K., (2004) 'Evaluation of Ultraviolet (UV) Radiation Disinfection Technologies for Wastewater Treatment Plant Effluent' (for the New York State Research and Development Authority) *Report 04-07* December
- ⁶³ <http://www.esemag.com/archive/1105/lethbridge.html> (accessed: 28-10-2011)
- ⁶⁴ www.iupac.org (accessed: 28-10-2011)
- ⁶⁵ Linsebigler, A.L., Lu, G., Yates, J.T., (1995) 'Photocatalysis on TiO₂ Surfaces: Principles, Mechanisms, and Selected Results' *Chemical Reviews*, 95, 735-758.
- ⁶⁶ Fujishima, A., Honda, K., (1972) 'Electrochemical Photolysis of Water at a Semiconductor Electrode' *Nature* 238, 37-38.

-
- ⁶⁷ Peral, J., Cascado, J., Domenesch, J., (1988) 'Light Induced Oxidation of Phenol over ZnO Powder' *Journal of Photochemistry and Photobiology A: Chemistry* 44, 209-217.
- ⁶⁸ Oppenlander, T. (2003) 'Photochemical Purification of Water and Air: Advanced Oxidation Processes (AOPs): Principles, Reaction Mechanisms, Reactor Concepts' *Wiley-VCH*, Weinheim.
- ⁶⁹ Hermann, J. M., (2005) 'Heterogeneous Photocatalysis: State of the Art and Present Applications' *Topics in Catalysis* 34, 49-65.
- ⁷⁰ Hoffmann, M. R., Martin, S. T., Choi, W., Bahnemann, D. W., (1995) 'Environmental Applications of Semiconductor Photocatalysis' *Chemical Reviews* 95, 69-96.
- ⁷¹ Kaniou, S., Pitarikis, K., Barlagianni, I., Poullos, I., (2005) 'Photocatalytic Oxidation of Sulfamethazine' *Chemosphere* 60, 372-380.
- ⁷² Mills, A., Le Hunte, S., (1997) 'An Overview of Semiconductor Photocatalysis' *Journal of Photochemistry and Photobiology A: Chemistry* 108, 1-35.
- ⁷³ Legrini, O., Oliveros, E., Braun, A. M., (1993) 'Photochemical Processes for Water Treatment' *Chemical Reviews* 93, 671-698.
- ⁷⁴ Monllor-Satoca, D., Gomez, R., Gonzalez-Hidalgo, M., Salvador, P., (2007) 'The Direct-Indirect Model: An Alternative Kinetic Approach in Heterogeneous Photocatalysis Based on the Degree of Interaction of Dissolved Pollutant Species with the Semiconductor Surface' *Catalysis Today* 129, 247-255.
- ⁷⁵ Rajeshwar, K., Chenthamarakshan, C.R., Goeringer, S., Djukic, M., (2001) 'Titania based Heterogeneous Photocatalysis: Materials Mechanistic Issues and Implications for Environmental Remediation' *Pure and Applied Chemistry* 73(12), 1849-1860.
- ⁷⁶ Pecci, G., Reyes, R., Sanhueza, P., Villase-nor, J., (2003) 'Photocatalytic Degradation of Pentachlorophenol on TiO₂-Sol Gel Catalysts' *Chemosphere* 41, 141-146.
- ⁷⁷ Lopez, T., Gomez, R., Pecci, G., Reyes, P., Bokhimi, X., Novaro, O., (1999) 'Effect of pH on the Incorporation of Platinum into the Lattice of Sol-Gel Titania Phases' *Materials Letters* 40, 59-65.
- ⁷⁸ <http://en.wikipedia.org/wiki/Anatase> (accessed: 12-01-2012)
- ⁷⁹ <http://en.wikipedia.org/wiki/Rutile> (accessed: 12-01-2012)
- ⁸⁰ Theurich, J., Lindner, M., Bahnemann, D. W., (1996) 'Photocatalytic Degradation of 4-Chlorophenol in Aerated Aqueous Titanium Dioxide Suspensions: A Kinetic and Mechanistic Study' *Langmuir* 12, 6368-6376.
- ⁸¹ Hurum, D., Agrios, A., Gray, K., Rajh T., Thurnauer, M., (2003) 'Explaining the Enhanced Photocatalytic Activity of Degussa P25 Mixed Phase TiO₂ Using EPR' *Journal of Physical Chemistry B* 107, 4545-4549.
- ⁸² Sunada, K., Watanabe, T., Hashimoto, K. (2003) 'Studies on Photokilling of Bacteria on TiO₂ Thin Film' *Journal of Photochemistry and Photobiology A: Chemistry* 156, 227-23.
- ⁸³ Ochuma, I. J., Osibo, O. O., Fishwick, R. P., Pollington, S., Wagland, A., Wood, J., Winterbottom, M., (2007) 'Three-Phase Photocatalysis Using Suspended Titania and Titania Supported on a Reticulated Foam Monolith for Water Purification' *Catalysis Today* 128, 100-107.

- ⁸⁴ Alinsafi, A., Evenou, F., Abdulkarim, E.M., Pons, M.N., Zahraa, O., Benhammou, A., Yaacoubi, A., Nejmeddine, A., (2007) 'Treatment of Textile Industry Wastewater by Supported Photocatalysis' *Dyes and Pigments* 74, 439-445.
- ⁸⁵ Lizama, C., Bravo, C., Caneo, C., Ollino, M., (2005) 'Photocatalytic Degradation of Surfactants with Immobilised TiO₂: Comparing Two Reaction Systems' *Environmental Technology* 26, 909-914.
- ⁸⁶ Fernández, J., Kiwi, J., Baeza, J., Freer, J., Lizama, C., Mansilla, H.D., (2004) 'Orange II Photocatalysis on Immobilised TiO₂ Effect of the pH and H₂O₂' *Applied Catalysis B: Environmental* 48, 205-211.
- ⁸⁷ Zhang, Y., Crittenden, J. C., Hand, D. W., Perram, D. L., (1994) 'Fixed-Bed Photocatalysts for Solar Decontamination of Water' *Environmental Science and Technology* 28(3), 435-442.
- ⁸⁸ Coleman, H. M., Eggins, B. R., Byrne, J. A., Palmer, F. L., King, E., (2000) 'Photocatalytic Degradation of 17- β -oestradiol on Immobilised TiO₂' *Applied Catalysis B: Environmental* 24, L1-L5.
- ⁸⁹ Fernandez, A., Lassaletta, G., Jimknez, V.M., Justo, A., GonzSlez-Elipse, A.R., Herrmann, J.M., Tahiri, H., Ait-Ichou, Y. (1995) 'Preparation and Characterization of TiO₂ Photocatalysts Supported on Various Rigid Supports (Glass, Quartz and Stainless Steel). Comparative Studies of Photocatalytic Activity in Water Purification' *Applied Catalysis B: Environmental* 7, 49-63.
- ⁹⁰ Choi, Y., Kim, B., (2000) 'Photocatalytic Disinfection of *E coli* in a UV/TiO₂-Immobilised Optical-Fibre Reactor' *Journal of Chemical Technology and Biotechnology* 75, 1145-1150.
- ⁹¹ Byrne, J.A., Eggins, B.R., Brown, N.M.D., McKinney, B., Rouse, M., (1998) 'Immobilisation of TiO₂ Powder for the Treatment of Polluted Water' *Applied Catalysis B: Environmental* 17, 25-36.
- ⁹² Araña, J., González Diaz, O., Doña Rodriguez, J.M., Herrera Melián, J.A., Garriga i Cabo, C., Pérez Peña, J., Carmen Hidalgo, M., Navio-Santos, J. A., (2003) 'Role of Fe³⁺/Fe²⁺ as TiO₂ Dopant Ions in Photocatalytic Degradation of Carboxylic Acids' *Journal of Molecular Catalysis A: Chemistry* 197, 157-171.
- ⁹³ Ou, H., Lo, S., (2007) 'Effect of Pt/Pd-Doped TiO₂ on the Photocatalytic Degradation of Trichloroethylene' *Journal of Molecular Catalysis A: Chemical* 275, 200-205.
- ⁹⁴ Seery, M.K., George, R., Floris, P., Pillai, S.C., (2007) 'Silver Doped Titanium Dioxide Nanomaterials for Enhanced Visible Light Photocatalysis' *Journal of Photochemistry and Photobiology A: Chemistry* (189) 258-263.
- ⁹⁵ http://www.antonine-education.co.uk/physics_gcse/Unit_1/Topic_5/em_spectrum.jpg (accessed: 28-10-2011)
- ⁹⁶ Paz, Y., (2006) 'Preferential Photodegradation – Why and How?' *Comptes Rendus Chimie* 9, 774-787.
- ⁹⁷ Qiu, R., Song, L., Zhang, D., Mo, Y., Brewer, E., Huang, X., (2008) 'Characterization of Conjugated Polymer Poly(fluorene-co-thiophene) and Its Application as Photosensitizer of TiO₂' *International Journal of Photoenergy* 1-5.
- ⁹⁸ Liao, G., Chen, S., Quan, X., Chen, H., Zhang, Y., (2010) 'Photonic Crystal Coupled TiO₂/Polymer Hybrid for Efficient Photocatalysis under Visible Light Irradiation' *Environmental Science and Technology* 44, 3481-3485.

- ⁹⁹ Xu, S., Li, S., Wei, Y., Zhang, L., Xu, F. (2010) 'Improving the Photocatalytic Performance of Conducting Polymer Polythiophene Sensitized TiO₂ Nanoparticles under Sunlight Irradiation' *Reaction Kinetics, Mechanisms and Catalysis* 101, 237–249.
- ¹⁰⁰ Jiang, D., Xu, Y., Wu, D., Sun, Y., (2008) 'Visible-light Responsive Dye-Modified TiO₂ Photocatalyst' *Journal of Solid State Chemistry* 181, 593–602.
- ¹⁰¹ Chatterjee, D, Mahata, A. (2002) 'Visible Light Induced Photodegradation of Organic Pollutants on Dye Adsorbed TiO₂ Surface' *Journal of Photochemistry and Photobiology A: Chemistry* 153, 199–204.
- ¹⁰² Wang, C., Yang, G., Li, J., Mele, G., Slota, R., Broda, M. A., Duan, M., Vasapollo, G., Zhang, X., Zhang, F., (2009) 'Novel Meso-Substituted Porphyrins: Synthesis, Characterization and Photocatalytic Activity of their TiO₂-based Composites' *Dyes and Pigments* 80, 321–328.
- ¹⁰³ Ali, H., Lier, J. E., (1999) 'Metal Complexes as Photo- and Radiosensitizers' *Chemical Reviews* 99, 2379–2450.
- ¹⁰⁴ De la Torre, G., Vazquez, P., Agullo-Lopez, F., Torres, T., (2004) 'Role of Structural Factors in the Nonlinear Optical Properties of Phthalocyanines and Related Compounds' *Chemical Reviews* 104, 3723–3750.
- ¹⁰⁵ Mele, G., Del Sole, R., Vasapollo, G., García-López, E., Palmisano, L., Schiavello, M. (2003) 'Photocatalytic Degradation of 4-Nitrophenol in Aqueous Suspension by using Polycrystalline TiO₂ Impregnated with Functionalized Cu(II)–Porphyrin or Cu(II)–Phthalocyanine' *Journal of Catalysis* 217, 334–342.
- ¹⁰⁶ Lü, X., Li, J., Wang, C., Duan, M., Luo, Y., Yao, G., Wang, J., (2010) 'Enhanced Photoactivity of CuPp-TiO₂ Photocatalysts under Visible Light Irradiation' *Applied Surface Science* 257, 795–801.
- ¹⁰⁷ Sun, Q., Xu, Y., (2009) 'Sensitization of TiO₂ with Aluminum Phthalocyanine: Factors Influencing the Efficiency for Chlorophenol Degradation in Water under Visible Light' *Journal of Physical Chemistry: C* 113, 12387–12394.
- ¹⁰⁸ Machado, A.E.H., Franca, M.D., Velani, V., Magnino, G.A., Velani, H.M.M., Freitas, F.S., Muller P. S., Sattler, C., Schmucker, M., (2008) 'Characterization and Evaluation of the Efficiency of TiO₂/Zinc Phthalocyanine Nanocomposites as Photocatalysts for Wastewater Treatment Using Solar Irradiation' *International Journal of Photoenergy* 1–12.
- ¹⁰⁹ Huang, H., Gu, X., Zhou, J., Ji, K., Liu, H., Feng, Y., (2009) 'Photocatalytic Degradation of Rhodamine B on TiO₂ Nanoparticles Modified with Porphyrin and Iron-Porphyrin' *Catalysis Communications* 11, 58–61.
- ¹¹⁰ Anderson, N.A., Ai, X., Chen, D., Mohler, D.L., Lian, T., (2003) 'Bridge Assisted Ultrafast Interfacial Electron Transfer to Nanocrystalline SnO₂ Thin Films' *Journal of Physical Chemistry B* 107, 14231–14239.
- ¹¹¹ Galoppini, E., (2004) 'Linkers for Anchoring Sensitizers to Semiconductor Nanoparticles' *Coordination Chemistry Reviews* 248, 1283–1297.
- ¹¹² Grätzel, M., (2003) 'Dye-Sensitized Solar Cells' *Journal of Photochemistry and Photobiology C: Photochemistry* 4, 145–153.

-
- ¹¹³ She, C., Guo, J., Irle, S., Morokuma, K., Mohler, D. L., Zabri, H., Odobel, F., Youm, K.T, Liu, F., Hupp, J. T., Lian, T., (2007) 'Comparison of Interfacial Electron Transfer through Carboxylate and Phosphonate Anchoring Groups' *Journal of Physical Chemistry A* 111, 6832-6842.
- ¹¹⁴ Qu, Q. Geng, H., Peng, R., Cui, Q., Gu, X., Li, F., Wang, M. (2010) 'Chemically Binding Carboxylic Acids onto TiO₂ Nanoparticles with Adjustable Coverage by Solvothermal Strategy' *Langmuir* 26(12), 9539-9546.
- ¹¹⁵ Lin, J., Siddiqui, J.A., Ottenbrite, R. M., (2001) 'Surface Modification of Inorganic Oxide Particles with Silane Coupling Agent and Organic Dyes' *Polymers for Advanced Technologies* 12, 285-292.
- ¹¹⁶ Ye, L., Pelton, R., Brook, M. A. (2007) 'Biotinylation of TiO₂ Nanoparticles and Their Conjugation with Streptavidin' *Langmuir* 23, 5630-5637.
- ¹¹⁷ Heimer, T.A., D'Arcangelis, S.T., Farzad, F., Stipkala, J.M., Meyer, G.J., (1996) 'An Acetylacetonate-Based Semiconductor-Sensitizer Linkage' *Inorganic Chemistry* 35, 5319-5324.
- ¹¹⁸ Jiang, D., Xu, Y., Hou, B., Wu, D., Sun, Y., (2007) 'Synthesis of Visible Light-Activated TiO₂ Photocatalyst via Surface Organic Modification' *Journal of Solid State Chemistry* 180, 1787-1791.
- ¹¹⁹ Chen, F., Zou, W., Qu, W., Zhang, J. (2009) 'Photocatalytic Performance of a Visible Light TiO₂ Photocatalyst Prepared by a Surface Chemical Modification Process' *Catalysis Communications* 10, 1510-1513.
- ¹²⁰ Notestein, J. M., Iglesia, E., Katz, A., (2007) 'Photoluminescence and Charge-Transfer Complexes of Calixarenes Grafted on TiO₂ Nanoparticles' *Chemistry Materials*, 19, 4998-5005.
- ¹²¹ Altobello, S., Bignozzi, C.A., Caramori, S., Larramona, G., Quici, S., Marzanni, Rajae, G., Lakhmiri, R., (2004) 'Sensitization of TiO₂ with Ruthenium Complexes Containing Boronic Acid Functions' *Journal of Photochemistry and Photobiology A: Chemistry* 166, 91-98.
- ¹²² Haarstrick, A., Kut, O. M., Heinzle, E., (1996) 'TiO₂-Assisted Degradation of Environmentally Relevant Organic Compounds in Wastewater Using a Novel Fluidized Bed Photoreactor' *Environmental Science and Technology* 30, 817-824.
- ¹²³ Lee, B.N., Liaw, W.D, Lou, J.C., (1999) 'Photocatalytic Decolorisation of Methylene Blue in Aqueous TiO₂ Suspensions' *Environmental Engineering Science* 16(3), 165-175.
- ¹²⁴ Pujara, K., Kamble, S.P., Pangarkar, V.G., (2007) 'Photocatalytic Degradation of Phenol-4-Sulfonic Acid Using an Artificial UV/TiO₂ System in a Slurry Bubble Column Reactor' *Industrial and Engineering Chemistry Research* 46, 4257-4264.
- ¹²⁵ Fox, M., Dulay, M., (1993) 'Heterogeneous Photocatalysis' *Chemical Reviews* 93, 341-357.
- ¹²⁶ Jiang, J., Oberdörster, G., Biswas, P., (2009) 'Characterization of Size, Surface Charge, and Agglomeration State of Nanoparticle Dispersions for Toxicological Studies' *Journal of Nanoparticle Research* 11, 77-89.
- ¹²⁷ Kaniou, S., Pitarakis, K., Barlagianni, I., Poulis, I., (2005) 'Photocatalytic Oxidation of Sulfamethazine' *Chemosphere* 60, 372-380.
- ¹²⁸ Augugliaro, V., Davi, E., Palmisano, L., Schiavello, M., Sclafani, A., (1990) 'Influence of Hydrogen Peroxide on the Kinetics of Phenol Photodegradation in Aqueous Titanium Dioxide Dispersion' *Applied Catalysis* 65, 101-116.

-
- ¹²⁹ Adan, C., Coronado, J.M., Bellod, R., Soria, J., Yamaoka, H. (2006) 'Photochemical and Photocatalytic Degradation of Salicylic Acid with Hydrogen Peroxide over TiO₂/SiO₂ Fibres' *Applied Catalysis A: General* 303(2), 199-206.
- ¹³⁰ Carraway, E.R., Hoffman, A.J., Hoffmann, M.R., (1994) 'Photocatalytic Oxidation of Organic Acids on Quantum sized Semiconductor Colloids' *Environmental Science and Technology* 28, 786-793.
- ¹³¹ Kormann, C., Bahnemann, D.W., Hoffmann, M.R., (1988) 'Photocatalytic Production of H₂O₂ and Organic Peroxides in Aqueous Suspensions of TiO₂, ZnO, and Desert Sand' *Environmental Science and Technology* 22(7), 798-806.
- ¹³² Mills, A., Valenzuela, M.A., (2004) 'The Photo-Oxidation of Water by Sodium Persulfate, and other Electron Acceptors, Sensitised by TiO₂' *Journal of Photochemistry and Photobiology A: Chemistry* 165 25-34
- ¹³³ Drug Index <http://www.rxlist.com/pepcid-drug.htm> (accessed: 28-10-2011)
- ¹³⁴ Data sourced from SymphonyIRI Group Inc,
- ¹³⁵ Lee, K.W., Kayser, S.R., Hongo, R.H., Tseng, Z.H., Scheinman, M.M., (2004) 'Famotidine and Long QT Syndrome' *American Journal of Cardiology* 93, 1325-1327.
- ¹³⁶ Gros, M., Petrović, M., Ginebreda, A., Barceló, D., (2010) 'Removal of Pharmaceuticals during Wastewater Treatment and Environmental Risk Assessment using Hazard Indexes' *Environment International* 36, 15-26.
- ¹³⁷ Radjenovic, J., Petrović, M., Barceló, D., (2009) 'Fate and Distribution of Pharmaceuticals in Wastewater and Sewage Sludge of the Conventional Activated Sludge (CAS) and Advanced Membrane Bioreactor (MBR) Treatment' *Water Research* 43, 831 – 841.
- ¹³⁸ Fatta-Kassinos, D., Hapeshi, E., Achilleos, A., Meric, S., Gros, M., Petrović, M., Barceló, D., 'Existence of Pharmaceutical Compounds in Tertiary Treated Urban Wastewater that is Utilized for Reuse Applications' (2011) *Water Resources Management* 25, 1183-1193.
- ¹³⁹ Kakinoki, K., Yamane, K., Teraoka, R., Otsuka, M., Matsuda, Y., (2004) 'Effect of Relative Humidity on the Photocatalytic Activity of Titanium Dioxide and Photostability of Famotidine' *Journal of Pharmaceuticals Sciences* 93, 582-589.
- ¹⁴⁰ Karpinska, J., Sokol, A., Kobeszko, M., Starczewska, B., Czyzewska, U., Hryniewicka, M., (2010) 'Study on Degradation Process of Famotidine Hydrochloride in Aqueous Samples' *Toxicological & Environmental Chemistry* 92(8), 1409 – 1422.
- ¹⁴¹ Wu, Y., Fassihi, R. (2005) 'Stability of Metronidazole, Tetracycline HCl and Famotidine and in Combination' *International Journal of Pharmaceuticals* (290) 1-13.
- ¹⁴² Junnarkar, G.H, Stavchansky, S., (1995) 'Isothermal and Nonisothermal Decomposition of Famotidine in Aqueous Solution', *Pharmaceutical Research* 12, 599-604.
- ¹⁴³ Singh, S., Kumar, S., Sharda, N., Chakraborti, A.K., (2002) 'New Findings on Degradation of Famotidine Under Basic Conditions: Identification of a Hitherto Unknown Degradation Product and the Condition for Obtaining the Propionamide Intermediate in Pure Form' *Journal of Pharmaceutical Sciences* 91, 253-257.
- ¹⁴⁴ www.chemspider.com (accessed: 25-10-2011)

- ¹⁴⁵ Noguchi, Y., Ohtake, A., Suzuki, M., Sasamata, M. (2008) 'In Vivo Study of the Effects of Alpha1-adrenoceptor Antagonists on Intraurethral Pressure in the Prostatic Urethra and Intraluminal Pressure in the Vas Deferens in Male Dogs' *European Journal of Pharmacology* (580) 256-261.
- ¹⁴⁶ Sourced from www.drugs.com/top200 (accessed: 25-10-2011)
- ¹⁴⁷ Prasaja, B., Harahap, Y., Lusthom, W., Setiawan, E.C., Ginting, M.B., Lipin, H., (2011) 'A Bioequivalence study of Two Tamsulosin Sustained-Release Tablets in Indonesian Healthy Volunteers' *European Journal of Drug Metabolites and Pharmacokinetics* 36, 109-113.
- ¹⁴⁸ Zhang, Z., Yang, G., Liang, G., Liu, H., Chenc, Y., (2004) 'Chiral Separation of Tamsulosin Isomers by HPLC Using Cellulose Tris (3,5-dimethylphenylcarbamate) as a Chiral Stationary Phase' *Journal of Pharmaceutical and Biomedical Analysis* 34, 689–693.
- ¹⁴⁹ Lehtonen, M., Keski-Rahkonen, S.A.P., Parssinen, O., Leppanen, E., Mauriala, T., (2007) 'Determination of Tamsulosin in Human Aqueous Humor and Serum by Liquid Chromatography–Electrospray ionization Tandem Mass Spectrometry' *Journal of Pharmaceutical and Biomedical Analysis* 43, 606–612.
- ¹⁵⁰ Nirogi, R.V.S., Kandikere, V., Shrivastava, W., Mudigonda, K., Maurya, S., Ajjala, D., (2007) 'Quantification of Pramipexole in Human Plasma by Liquid Chromatography Tandem Mass Spectrometry Using Tamsulosin as Internal Standard' *Biomedical Chromatography* 21, 1151–1158.
- ¹⁵¹ Yanagihara, T, Aoki, T., Soeishi, Y., Iwatsubo, T. (2007) 'Determination of Solifenacin Succinate, a Novel Muscarinic Receptor Antagonist, and its Major Metabolites in Rat Plasma by Semi-Micro High Performance Liquid Chromatography' *Journal of Chromatography B* 859(2), 241-245.
- ¹⁵² Maniscalco, M. Singh-Franco, D., Wolowich, W.R., Torres-Colón. R. (2006) 'Solifenacin Succinate for the Treatment of Symptoms of Overactive Bladder' *Clinical Therapeutics* 28(9), 1247-1272.
- ¹⁵³ Krauwinkel, W.J., Smulders, R.A., Mulder, H., Swart, P.J., Taekema-Roelvink, M.E., (2005) Effect of Age on the Pharmacokinetics of Solifenacin in Men and Women. *International Journal of Clinical Pharmacology and Therapeutics* 43, 227-238.
- ¹⁵⁴ Mistri, H. N., Jangid, A. G., Pudage, A., Rathod, D. M., Shrivastav, P. S. (2008) 'Highly Sensitive and Rapid LC–ESI-MS/MS Method for the Simultaneous Quantification of Uroselective α_1 -blocker, Alfuzosin and an Antimuscarinic Agent, Solifenacin in Human Plasma' *Journal of Chromatography B* 876(2), 236–244.
- ¹⁵⁵ Calza, P., Sakkas, V.A., Medana, C., Baiocchi, C., Dimou, A., Pelizzetti, E., Albanis, T., (2006) 'Photocatalytic Degradation Study of Diclofenac over Aqueous TiO₂ Suspensions' *Applied Catalysis B: Environmental* (67) 197-205.
- ¹⁵⁶ Perez-Estrada, L. A., Maldonado, M.I., Gernjak, W., Aguera, A., Fernandez-Alba, A.R., Ballesteros, M. M., Malato, S., (2005) 'Decomposition of Diclofenac by Solar Driven Photocatalysis at Pilot Plant Scale' *Catalysis Today* 101, 219-226.
- ¹⁵⁷ Deegan, A., (2011) 'Pharmaceuticals in Industrial Wastewater and their Removal using Photo-Fenton's Oxidation' PhD Thesis Dublin City University
- ¹⁵⁸ <http://www.epa.gov/oppt/nano/ev32.pdf> (accessed: 05-01-2012)

- ¹⁵⁹ http://www.sigmaaldrich.com/catalog/ProductDetail.do?lang=en&N4=232033|ALDRICH&N5=SEARCH_CONCAT_PNO|BRAND_KEY&F=SPEC (accessed: 05-01-2012)
- ¹⁶⁰ Yao, Y. Li, G. Gray K. A., Lueptow, R. M., (2008), 'Single-Walled Carbon Nanotube-Facilitated Dispersion of Particulate TiO₂ on ZrO₂ Ceramic Membrane Filters' *Langmuir* 24, 7072-7075.
- ¹⁶¹ Segura, C., Zaror, C., Mansilla, H. D., Mondaca, M., (2008) 'Imidacloprid Oxidation by Photo-Fenton Reaction' *Journal of Hazardous Materials* 150, 3, 679-686.
- ¹⁶² Ye, L., Pelton, R., Brook, M., (2007) 'Biotinylation of TiO₂ Nanoparticles and Their Conjugation with Streptavidin', *Langmuir* 23(10), 5630-5637.
- ¹⁶³ McNamara, R., Snoeberger III, R. C., Li, G., Schleicher, J. M., Cady, C.W., Poyatos, M., Schmuttenmaer, C. A. Crabtree, R. H., Brudvig, G.W., Batista, V. S., (2008) 'Acetylacetonate Anchors for Robust Functionalisation of TiO₂ Nanoparticles with Mn (II)-Terpyridine Complexes' *Journal of the American Chemical Society*, 130(43), 14329-14338.
- ¹⁶⁴ Lu, X., Li, J., Wang, C., Duan, M., Luo, Y., Yao, G., Wang, J., (2010) 'Enhanced Photoactivity of Cu-PP-TiO₂ Photocatalysts under Visible Light Irradiation' *Applied Surface Sciences* 257, 795-801.
- ¹⁶⁵ http://www.ardeenvironment.info/medium_pressure.html (accessed: 04-01-2012)
- ¹⁶⁶ http://www.ardeenvironment.info/low_pressure.html (accessed: 04-01-2012)
- ¹⁶⁷ Optical Building Blocks Cooperation <http://www.obb1.com> (accessed: 04-01-2012)
- ¹⁶⁸ Herrmann, J. M., (1999) 'Heterogeneous Photocatalysis: Fundamentals and Applications to the Removal of Various Types of Aqueous Pollutants' *Catalysis Today* 53, 115-119.
- ¹⁶⁹ Reyes, C., Fernandez, J., Freer, J., Mondaca, M.A., Zaror, C., Malato, S., Mansilla, H.D., (2006) 'Degradation and Inactivation of Tetracycline by TiO₂ Photocatalysis' *Journal of Photochemistry and Photobiology A: Chemistry* 184, 141-146.
- ¹⁷⁰ Hu, L., Flanders, P. M., Miller, P. L. Strathmann, T. J., (2007) 'Oxidation of Sulfamethoxazole and Related Antimicrobial Agents by TiO₂ Photocatalysis', *Water Research* 41, 2612 – 2626.
- ¹⁷¹ Molinari, R. Pirillo, F., Loddò, V., Palmisano, L. (2006) 'Heterogeneous Photocatalytic Degradation of Pharmaceuticals in Water by Using Polycrystalline TiO₂ and a Nanofiltration Membrane Reactor' *Catalysis Today* 118, 205–213.
- ¹⁷² Keyes, T.E., Vos, J.G., Kolnaar, J.A., Haasnoot, J. G., Reedijk, J., Hage R., (1996) 'Tuning of the Photostability of Bis (2,2'-biquinoline) Ruthenium (II) Complexes Containing Pyridyltriazole Ligands by Variation of pH' *Inorganica Chimica Acta* 245, 237-242.
- ¹⁷³ Anzenbacherova, E., Filipova, K., Nobilis, M., Anzenbacher, P., (2003) 'Selective Determination of Famotidine in Human Plasma by High Performance Liquid Chromatography in Alkaline Media with Solid Phase Extraction' *Journal of Separation Science* 26(8), 722-726.
- ¹⁷⁴ Molinari, R. Caruso, A., Argurio, P., Poerio, T., (2008) 'Degradation of the Drugs Gemfibrozil and Tamoxifen in Pressurized and De-Pressurized Membrane Photoreactors using Suspended Polycrystalline TiO₂ as Catalyst' *Journal of Membrane Science* 319, 54–63.
- ¹⁷⁵ Rengaraj, S. Li, X.Z., Tanner, P.A., Pan, Z.F., Pang, G.K.H., (2005) 'Photocatalytic Degradation of Methylparathion—An Endocrine Disruptor by Bi³⁺-doped TiO₂' *Journal of Molecular Catalysis A: Chemical* 247, 36–43

- ¹⁷⁶ D'Oliveira, J., Al-Sayyed, G., Pichat, P. (1990) 'Photodegradation of 2- and 3-Chlorophenol in TiO₂ Aqueous Suspensions' *Environmental Science Technology* 24(7), 990-996.
- ¹⁷⁷ Sohrabi, M.R., Ghavami, M. (2008) 'Photocatalytic Degradation of Direct Red 23 Dye using UV/TiO₂: Effect of Operational Parameters' *Journal of Hazardous Materials* 153, 1235-1239.
- ¹⁷⁸ Zhang, Y.J., Zhou, L., Ning, B., (2007) 'Photodegradation of Estrone and 17 β -estradiol in Water' *Water Research* 41, 19-26.
- ¹⁷⁹ Bancroft W. D., Murphy, N.F., (1935) 'Oxidation and Reduction with Hydrogen Peroxide.' *Journal of Physical Chemistry* 39(3), 377-398.
- ¹⁸⁰ Product Monograph for Flomax (Tamsulosin Hydrochloride) (2007) 1-26. Attained from: (http://www.boehringer-ingelheim.ca/en/human_health/our_products.html) (accessed:28-10-2011)
- ¹⁸¹ Erdemoglu, S., Aksu, S.K., Sayilkan, F., Izgi, B., Asilturk, M., Sayilkan, H., Frimmel, F., Gucer, S., (2008) 'Photocatalytic Degradation of Congo Red by Hydrothermally Synthesized Nanocrystalline TiO₂ and Identification of Degradation Products by LC-MS' *Journal of Hazardous Materials* 155, 469-476.
- ¹⁸² Addamo, M. Auguliaro, V., Di Paola, A., Garcia-Lopez, E., Loddo, V., Marci, G., Palmisano, L., (2005) 'Removal of Drugs in Aqueous Systems by Photoassisted Degradation' *Journal of Applied Electrochemistry* 35: 765-774.
- ¹⁸³ Abellan, M.N., Bayarri, B., Gimenez, J., Costa, J., (2007) 'Photocatalytic Degradation of Sulfamethoxazole in Aqueous Suspension of TiO₂' *Applied Catalysis B: Environmental* 74, 233-241.
- ¹⁸⁴ Jiao, S., Zheng, S., Yin, D., Wang, L., Chen, L., (2008) 'Aqueous Oxytetracycline Degradation and the Toxicity Change of Degradation Compounds in Photoirradiation Process' *Journal of Environmental Sciences* 20, 806-813.
- ¹⁸⁵ Achilleos, A., Hapeshi, E., Xekoukoulotakis, N. P., Mantzavinos, D., Fatta-Kassinosa, D., (2010) 'Factors Affecting Diclofenac Decomposition in Water by UV-A/TiO₂ Photocatalysis' *Chemical Engineering Journal* 161, 53-59.
- ¹⁸⁶ Sirtori, C., Zapata, A., Malato, S. Gernjak, W., Fernández-Alba, A. R., Agüera, A., (2009), 'Solar Photocatalytic Treatment of Quinolones: Intermediates and Toxicity Evaluation' *Photochemical & Photobiological Sciences* 8, 644-651.
- ¹⁸⁷ Paul, T., Miller, P. L., Strathmann, T. J., (2007) 'Visible-Light-Mediated TiO₂ Photocatalysis of Fluoroquinolone Antibacterial Agents' *Environmental Science and Technology* 41, 4720-4727.
- ¹⁸⁸ Lambropoulou, D.A., Hernando, M.D., Konstantinou, I.K., Thurman, E.M., Ferrer, I., Albanis, T. A., Fernández-Alba, A.R., (2008) 'Identification of Photocatalytic Degradation Products of Bezafibrate in TiO₂ Aqueous Suspensions by Liquid and Gas Chromatography' *Journal of Chromatography A*, 1183 38-48.
- ¹⁸⁹ Radjenovic, J., Sirtori, C. Petrovic, M., Barceló, D., Malato, S., (2010) 'Characterization of Intermediate Products of Solar Photocatalytic Degradation of Ranitidine at Pilot-Scale' *Chemosphere* 79, 368-376.
- ¹⁹⁰ Sentellas, S., Puignou, L., Moyano, E. Galceran, M.T., (2000) 'Determination of Ebrotidine and its Metabolites by Capillary Electrophoresis with UV and Mass Spectrometry Detection' *Journal of Chromatography A*, 1-2, (4) 281-292.

-
- ¹⁹¹ Rozman, E., Galcerán, M.T., Albet, C., (1997) 'Determination of Ebrotidine and its Metabolites in Human Urine by Reversed-Phase Ion-Pair High-Performance Liquid Chromatography' *Journal of Chromatography B* 688, 107-115.
- ¹⁹² Tran, J.C., Doucette, A.A., (2006) 'Cyclic Polyamide Oligomers Extracted from Nylon 66 Membrane Filter Disks as a Source of Contamination in Liquid Chromatography/Mass Spectrometry' *Journal of American Society of Mass Spectrometry* 17, 652-656.
- ¹⁹³ Kamel, A., Colizza, K., Jeanville, P., (2007) 'Mechanisms of Ion Formation for Famotidine and Azithromycin using Hydrogen/Deuterium Exchange and High Resolution Mass Measurements' *Thermo Scientific Application Note* 374.
- ¹⁹⁴ Rahman, N., Kashif, M., (2003) 'Kinetic Spectrophotometric Determination of Famotidine in Commercial Dosage Forms' *Analytical Sciences* 19, 907-911.
- ¹⁹⁵ <http://www.freepatentsonline.com/7094414.html> (accessed: 04-01-2012)
- ¹⁹⁶ Calza, P., Medana, C., Baiocchi, C., Pelizzetti, E., (2004) 'Photocatalytic Transformations of Aminopyridines on TiO₂ in Aqueous Solution' *Applied Catalysis B: Environmental* 52, 267-274.
- ¹⁹⁷ SMILES calculated using EPIsuite. Estimation Programme Interface (EPIsuite) version 4.1. Downloaded from <http://www.epa.gov/oppt/exposure/pubs/episuiteld.htm> (accessed: 27-12-2011)
- ¹⁹⁸ VCCLAB: The Virtual Computational Chemistry Laboratory, ALlogPs 2.1 LogP Online Calculation Software. <http://146.107.217.178/lab/alogps/index.html> (accessed: 27-12-2011)
- ¹⁹⁹ Konstantinou, I.K., Sakkas, V.A., Albanis, T.A., (2001) 'Photocatalytic Degradation of the Herbicides Propanil and Molinate over Aqueous TiO₂ Suspensions: Identification of Intermediates and the Reaction Pathway' *Applied Catalysis B: Environmental* 34, 227-239.
- ²⁰⁰ Buth J.M., Arnold, W.A., McNeill, K., (2007) 'Unexpected Products and Reaction Mechanisms of the Aqueous Chlorination of Cimetidine' *Environmental Science and Technology* 41, 6228-6233.
- ²⁰¹ Taguchi, K., Saitoh, M., Sato, S., Asano, M., Michel, M.C., (1997) 'Effects of Tamsulosin Metabolites at Alpha-1 Adrenoceptor Subtypes' *The Journal of Pharmacology and Experimental Therapeutics* 280, 1-5.
- ²⁰² Nudelman, N. S., Cabrera, C.G., (2002) 'Isolation and Structural Elucidation of Degradation Products of Alprazolam: Photostability Studies of Alprazolam Tablets', *Journal of Pharmaceutical Sciences* 91, 5.
- ²⁰³ Duan, M., Li, J., Mele, G., Wang, C., Lu, X., Vasapollo, G., Zhang, F., (2010), 'Photocatalytic Activity of Novel Tin Porphyrin/TiO₂ Based Composites' *Journal of Physical Chemistry C*. 114 (2010) 7857-7862.
- ²⁰⁴ Zhang, J., Zhang, L., Li, X., Kang, S., Mu, J., (2011) 'Visible Light Photocatalytic Activity of Porphyrin Tin(IV) Sensitized TiO₂ Nanoparticles for the Degradation of 4-Nitrophenol and Methyl Orange' *Journal of Dispersion Science and Technology*, 32, 943-947.
- ²⁰⁵ Li, D., Dong, W., Sun, S., Shi, Z., Feng, S., (2008) 'Photocatalytic Degradation of Acid Chrome Blue K with Porphyrin-Sensitized TiO₂ under Visible Light' *Journal of Physical Chemistry C*. 112, 14878-14882.
- ²⁰⁶ Thomas, D.W., Martell, A.E., (1956) 'Absorption Spectra of Para-Substituted Tetraphenylporphyrins' *Journal of the American Chemical Society* 78, 1338-1343.

- ²⁰⁷ Diaz-Urbe, C.E., Daza, M.C., Martínez, F., Paez-Mozo, E.A., Guedes, C.L.B., Di Mauro, E., 2010 'Visible Light Superoxide Radical Anion Generation by Tetra(4-carboxyphenyl)Porphyrin/TiO₂: EPR Characterisation' *Journal of Photochemistry and Photobiology A: Chemistry* 215, 172-178.
- ²⁰⁸ Cherian, S., Wamser, C., (2000) 'Adsorption and Photoactivity of Tetra(4-carboxyphenyl)porphyrin TCP on Nanoparticulate TiO₂' *Journal of Physical Chemistry B* 104, 3624-3629.
- ²⁰⁹ Ma, T., Inoue, K., Noma, H., Yao, K., Abe, E., (2002) 'Effect of Functional Group on Photochemical Properties and Photosensitization of TiO₂ Electrode Sensitized by Porphyrin Derivatives' *Journal of Photochemistry and Photobiology A : Chemistry* 152, 207-212.
- ²¹⁰ Wang, C., Mele, G., Duan, M., Lu, X., Palmisano, L., Vasapollo, G., Zhang, F., (2010) 'The Photocatalytic Activity of Novel, Substituted Porphyrin/TiO₂ Based Composites' *Dyes and Pigments*, 84, 183-189.
- ²¹¹ Odobel, F., Blart, E., Lagree, M., Villieras, M., Boujtita, H., El Murr, N., Caramori, S., Bignozzi, C. A., (2003) 'Porphyrin Dyes for TiO₂ Sensitization' *Journal of Materials Chemistry* 13, 502-510.
- ²¹² http://www.erco.com/guide_v2/guide_2/lighting_te_94/tungsten_ha_1617/en/en_tungsten_ha_physic_1.php (accessed: 28-10-2011)
- ²¹³ <http://www.oceanoptics.com/products/hr4000cg.asp> (accessed: 28-10-2011)
- ²¹⁴ Darwent, J. R., Douglas, P., Harriman, A., Porter, G., Richoux, M., (1982) 'Phthalocyanines and Porphyrins as Photosensitizers for Reduction of Water to Hydrogen' *Coordination Chemistry Reviews* 44, 83-126.
- ²¹⁵ Ogata, H., Higashi, R., Kobayashi, N., (2003) 'Electronic Absorption Spectra of Substituted Phthalocyanines in Solution and as Films' *Journal of Porphyrins and Phthalocyanines* 7, 551-557.
- ²¹⁶ Speirs, N.M., Ebenezer, W.J., Jones, A.C., (2002) 'Observation of a Fluorescent Dimer of a Sulfonated Phthalocyanine' *Photochemistry and Photobiology* 76(3), 247-251.
- ²¹⁷ Monahan, A.R., Brado, J.A., DeLuca, A.F., (1979) 'The Dimerization of a Copper (II)-Phthalocyanine Dye in Carbon Tetrachloride and Benzene' *The Journal of Physical Chemistry* 76(3), 446-449.
- ²¹⁸ Seelan, S., Agashe, M.S., Srinivas, D., Sivasanker, S., (2001) 'Effect of Peripheral Substitution on Spectral and Catalytic Properties of Copper Phthalocyanine Complexes' *Journal of Molecular Catalysis A: Chemical* 168, 61-68.
- ²¹⁹ <http://www.tciamerica.com/product/materials-chem/F014.shtml> (accessed: 28-10-2011)
- ²²⁰ Reddy, P.Y., Giribabu, L., Lyness, C., Snaith, H.J., Vijaykumar, C. Chandrasekharam, M., Lakshmikantam, M., Yum, J., Kalyanasundaram, K., Grätzel, M., Nazeeruddin, M.K., (2007) 'Efficient Sensitization of Nanocrystalline TiO₂ Films by a Near IR Absorbing Unsymmetrical Zinc Phthalocyanine' *Angewandte Chemie International Edition* 46, 373-376.
- ²²¹ Giribabu, L., Kumar, C., Reddy, P., Yum, J., Grätzel, M., Nazeeruddin, M.K., (2009) 'Unsymmetrical Extended π -conjugated Zinc Phthalocyanine for Sensitization of Nanocrystalline TiO₂ Films' *Journal of Chemical Sciences* 121(1), 75-82.
- ²²² Mori, S., Nagata, M., Nakahata, Y., Yasuta, K., Goto, R., Kimura, M. Taya, M., (2010) 'Enhancement of Incident Photon-to-Current Conversion Efficiency for Phthalocyanine-Sensitized Solar Cells by 3D Molecular Structuralization' *Journal of the American Chemical Society* 132, 4054-4055.

-
- ²²³ Höfle, G., Glaser, N., Leibold, T., Sefkow, M., (1999) 'Epothilone A-D and their thiazole-modified analogs as novel anticancer agents' *Pure and Applied Chemistry* 71, (11) 2019-2024.
- ²²⁴ Amir, E., Rozen, S., (2006) 'Easy Access to the Family of Thiazole N-oxides using HOF.CH₃CN' *Chemical Communications*, 2262–2264.

Appendices

In order of appearance:

Chapter 2 Appending Data

2A-1. Methods adopted for monitoring prior to our method development (developed by A. Deegan 2011)

2A-2. HPLC Chromatogram of Famotidine Standards 0-100 μM

2A-3. Standard Curve of Famotidine Standards

2A-4. HPLC Chromatogram of Tamsulosin Standards 0-100 μM

2A-5. HPLC Chromatogram of Tamsulosin 10 μM

2A-6. Standard Curve of Tamsulosin Standards

2A-7. HPLC Chromatogram of Solifenacin Standards 0-100 μM

2A-8. Standard Curve of Solifenacin Standards

2A-9. HPLC Chromatogram of Solifenacin in MeOH

2A-10. HPLC Chromatogram of Solifenacin Standards in MeOH

2A-11. Famotidine Standard Curve with Final HPLC-PDA Method

2A-12. Tamsulosin Standard Curve with Final HPLC-PDA Method

2A-13. Solifenacin Standard Curve with Final HPLC-PDA Method

Chapter 3 Appending Data

3A-1. UV-vis of Photocatalysis of Famotidine at pH3 (Sigma TiO_2)

3A-2. UV-vis of Photocatalysis of Famotidine at pH5 (Sigma TiO_2)

3A-3. UV-vis of Photocatalysis of Famotidine at pH6 (Sigma TiO_2)

3A-4. UV-vis of Photocatalysis of Famotidine at pH5 (P-25 TiO_2)

3A-5. UV-vis of Photocatalysis of Famotidine at pH9 (P-25 TiO_2)

3A-6. UV-vis of Photocatalysis of Famotidine at pH10 (P-25 TiO_2)

3A-7. UV-vis of Photocatalysis of Famotidine at pH4 (P-25 TiO_2)

3A-8. UV-vis of Photocatalysis of Tamsulosin at pH3 (P-25 TiO_2)

3A-9. UV-vis of Photocatalysis of Tamsulosin at pH3 (SA TiO_2)

3A-10. UV-vis degradation profiles showing studies with Famotidine and Tamsulosin in the Enviolet reactor vs. Low pressure Hg Lamp Studies vs. Quartz Immersion Well Studies.

3A-11. UV-vis degradation profiles showing studies for Solifenacin in the Enviolet reactor vs. Low pressure Hg Lamp Studies vs. Quartz Immersion Well Studies with Quartz. Profiles are based on the increase in absorbance seen in the case of Solifenacin.

3A-12. UV-vis analysis of an adsorption isotherm for Famotidine after 16 h of shaking (foil-covered). [FAM] = 0-100 μM , SA TiO_2 = 0.05 g/50 mL, Time = 16 h.

3A-13. UV-vis analysis of an adsorption isotherm for Famotidine after 48 h of shaking (foil-covered). [FAM] = 0-100 μM , SA TiO_2 = 0.05 g/50 mL, Time = 48 h.

3A-14. Charts showing adsorption (0.5 h) relative to degradation for different pHs for Famotidine (pre-illumination) by Sigma TiO_2 at different pHs.

3A-15. Charts showing adsorption (0.5 h) relative to degradation for different pHs for Famotidine (pre-illumination) by P-25 TiO₂ at different pHs.

Chapter 4 Appending Data

4A-1. Table of masses and intensities found in DI-MS studies of a Famotidine photocatalysis experiment
Most significant and consistent masses in colour.

4A-2. DI-Mass spectrum of $m/z = 352$, a Famotidine intermediate found only in DI-MS studies.

4A-3. DI-Mass spectrum of $m/z = 370$, a Famotidine intermediate found in DI-MS studies and LC-MS studies.

4A-4. DI-Mass spectrum of $m/z = 171$, a Famotidine intermediate found in both DI-MS and LC-MS studies.

4A-5. DI-Mass spectrum of $m/z = 173$, a Famotidine intermediate found in both DI-MS and LC-MS.

4A-6. $m/z = 350$ found in Famotidine DI-MS studies of a photocatalytic experiment.

4A-7. $m/z = 403$ found in Famotidine DI-MS studies of a photocatalytic experiment.

4A-8. $m/z = 365$ found in Famotidine DI-MS studies of a photocatalytic experiment.

4A-9. $m/z = 392$ found in Famotidine DI-MS studies of a photocatalytic experiment.

4A-10. EIC chromatograms of a photocatalytic reaction showing the development of $m/z = 365$.
Photocatalysis [FAM] = 1 mM, 0.1 g/320 mL TiO₂.

4A-11. EIC chromatograms of a photocatalytic reaction showing the development of $m/z = 392$.
Photocatalysis [FAM] = 1 mM, 0.1 g/320 mL TiO₂.

4A-12. EIC of a 50 μ M standard of Famotidine showing the presence of the potassium adduct at $m/z = 376$ in the MS. Inset MS (top) and MS/MS (bottom) spectra.

4A-13. Ions detected by LC-MS in the photocatalytic degradation of Famotidine. [FAM] = 0.083 mM, TiO₂ = P-25 0.1 g/320 mL.

4A-14. Ions detected by LC-MS in photolytic degradation of Famotidine with Pyrex glassware. [FAM] = 0.083 mM.

4A-15. Ions detected by LC-MS in photolytic degradation of Famotidine with Quartz glassware. [FAM] = 0.083 mM.

4A-16. Ions detected by LC-MS in photocatalytic degradation of Famotidine. [FAM] = 1 mM, TiO₂ = P-25 0.1 g/320 mL.

4A-17. Masses between 40-120 mins found in DI-MS of a photocatalytic experiments of Tamsulosin.

4A-18. Ions detected by LC-MS in the photocatalytic degradation of Tamsulosin. [TAM] = 0.083 mM, TiO₂ = P-25 0.2 g/320 mL

4A-19. Ions detected by LC-MS in the photolytic degradation of Tamsulosin with Pyrex glassware. [TAM] = 0.083 mM.

4A-20. Ions detected by LC-MS in the photolytic degradation of Tamsulosin with Quartz glassware. [TAM] = 0.083 mM.

4A-21. Ions detected by LC-MS in the photocatalytic degradation of Tamsulosin. [TAM] = 1 mM, TiO₂ = P-25 0.2 g/320 mL

4A-22. 15 possible structural isomers for m/z = 395.

4A-23. MS of m/z = 395 at 18.9 mins and respective MS/MS spectra.

4A-24. MS of m/z = 379 at 11.8 mins and 24.6 mins and their respective MS/MS spectra.

4A-25. Ions detected by LC-MS in the photocatalytic degradation of Solifenacin. [SOL] = 0.083 mM, TiO₂ = P-25 0.1 g/320 mL.

4A-26. Ions detected by LC-MS in the photolytic degradation of Solifenacin with Pyrex glassware. [SOL] = 0.083 mM.

4A-27. Ions detected by LC-MS in the photolytic degradation of Solifenacin with Quartz glassware. [SOL] = 0.083 mM.

4A-28. Ions detected by LC-MS in the photocatalytic degradation of Solifenacin. [SOL] = 1 mM, TiO₂ = P-25 0.1 g/320 mL.

4A-29. Table of MS parameters for Famotidine DI-MS and LC-MS Studies.

4A-30. Table of MS parameters for Tamsulosin DI-MS and LC-MS Studies.

4A-31. Table of MS parameters for Solifenacin DI-MS and LC-MS Studies.

Chapter 5 Appending Data

5A-1. Light Intensity in Footcandles recorded on 22-06-2010 during solar experiments with TPPCOOH-TiO₂ photocatalysts.

5A-2. Spectral irradiance profile data for our Halogen (Tungsten) Lamp which was used in indoor photocatalytic reactions with visible light sensitised materials.

5A-3. UV-vis profile of the adsorption of Famotidine onto TCPP-TiO₂ in the dark. [FAM] = 0.083 mM, TCPP-TiO₂ = 0.031 g/100 mL, Time = 1 h.

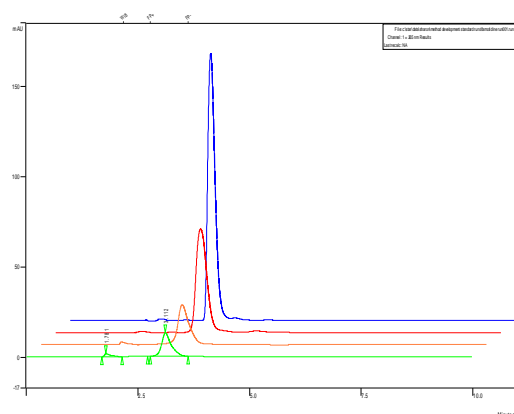
5A-4. FT-IR analysis of TCPP-TiO₂-A composite, inset the fingerprint region. This data is presented in Table 5.1 in the main thesis.

5A-5. FT-IR analysis of TCPP-TiO₂-B composite, inset the fingerprint region. This data is presented in Table 5.1 in the main thesis.

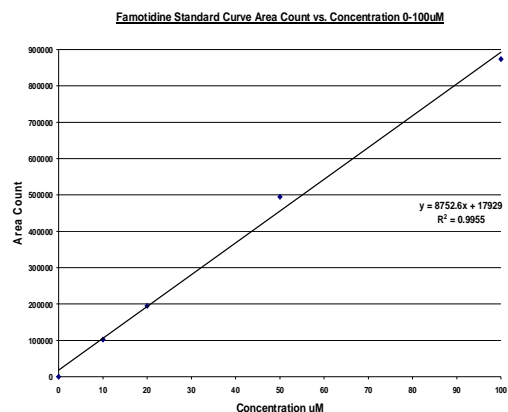
5A-6. ATR-IR analysis of TCPP. This data is presented in Table 5.1 in the main thesis.

API	Solvent System	Inj. Vol. (μL)	Wavelength (nm)	t _R (mins)	R.T. (mins)
Famotidine	10 % ACN: H ₂ O (0.1% ammonium acetate buffer)	50	205	5.2	10
Tamsulosin	35 % ACN: H ₂ O (0.1% ammonium acetate buffer)	50	205	7.5	10

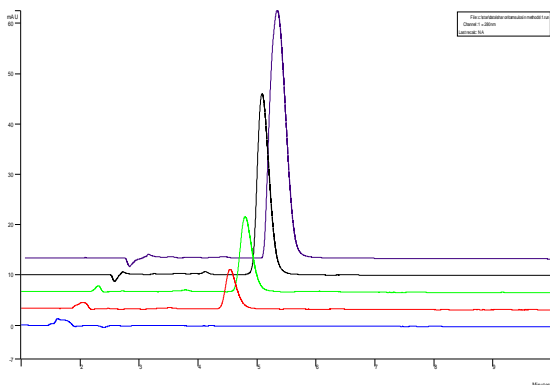
2A-1. Methods adopted for monitoring prior to our method development (developed by A. Deegan 2011)



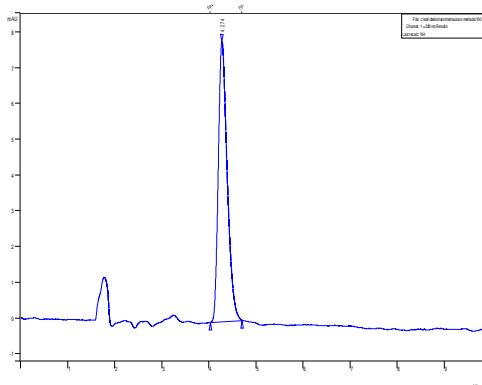
2A-2. Famotidine Standards 0-100 µM (offset)



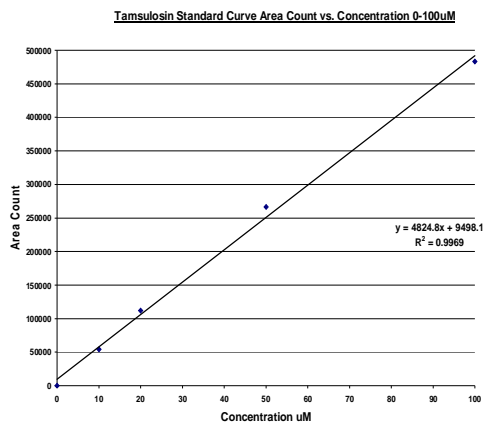
2A-3. Standard Curve Famotidine



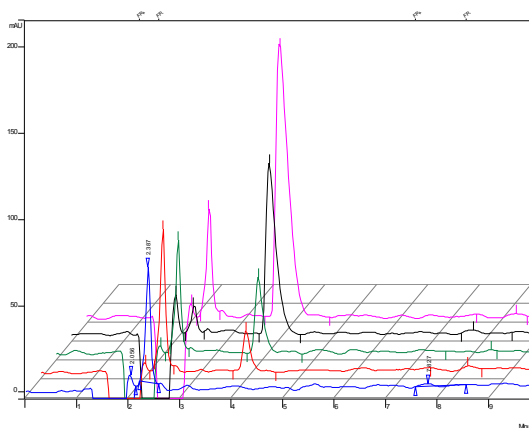
2A-4. Tamsulosin Standards 0-100 µM (offset)



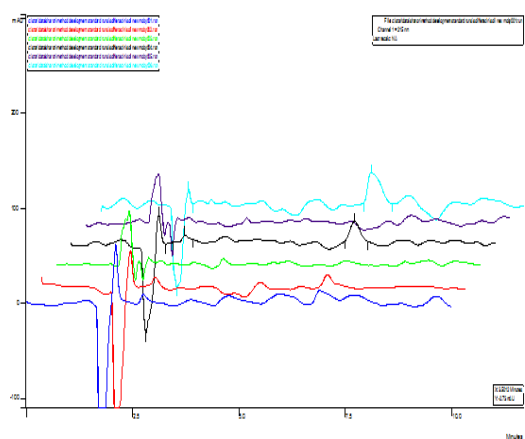
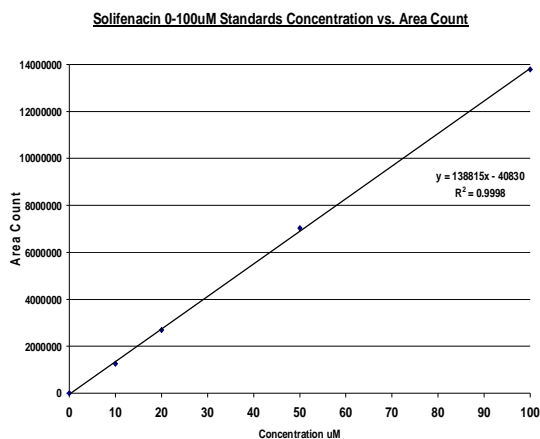
2A-5. Tamsulosin 10 µM standard



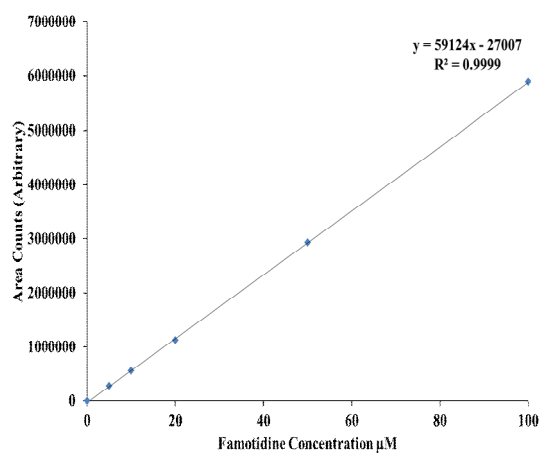
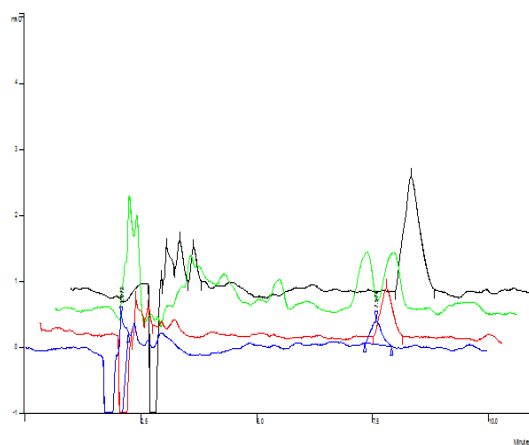
2A-6. Tamsulosin Standard Curve



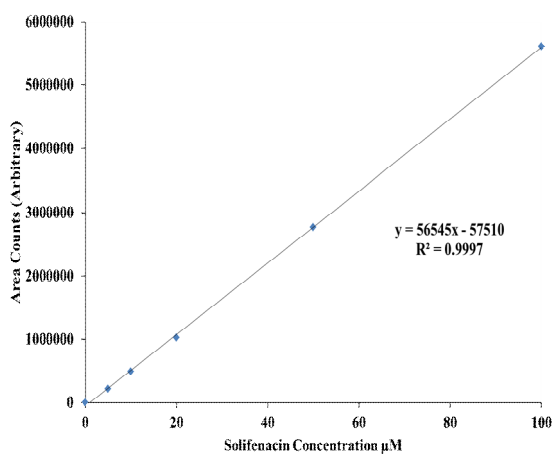
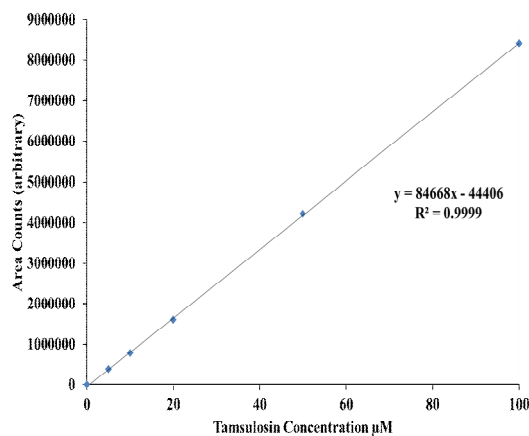
2A-7. Solifenacin Standards (offset)



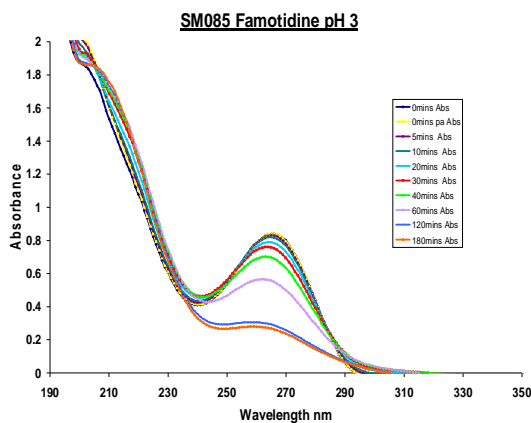
2A-8. Solifenacin Standard Curve with ACN method **2A-9. Solifenacin standards (70:30 MeOH:H₂O) 215 nm**



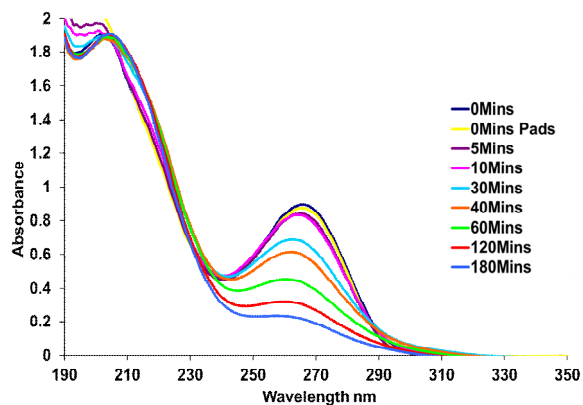
2A-10. Solifenacin standards (70:30 MeOH:H₂O) 260 nm **2A-11. Famotidine Standard Curve Final Method**



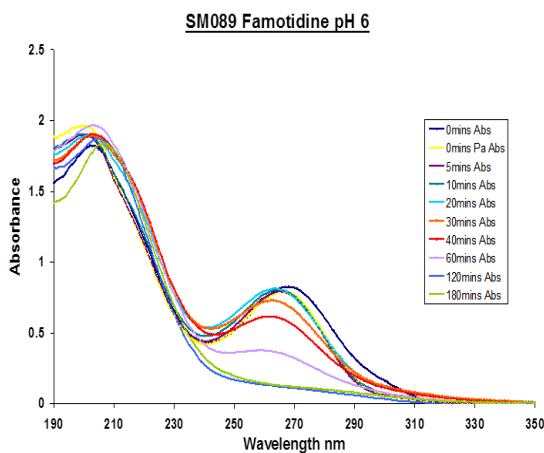
2A-12. Tamsulosin Standard Curve Final Method **2A-13. Solifenacin Standard Curve Final Method**



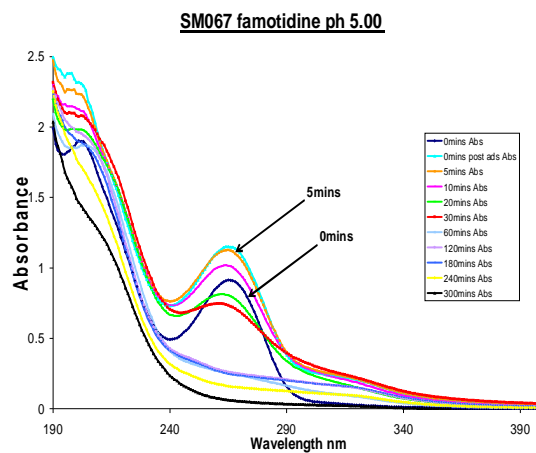
3A-1. FAM Photocatalysis at pH 3 SA-TiO₂



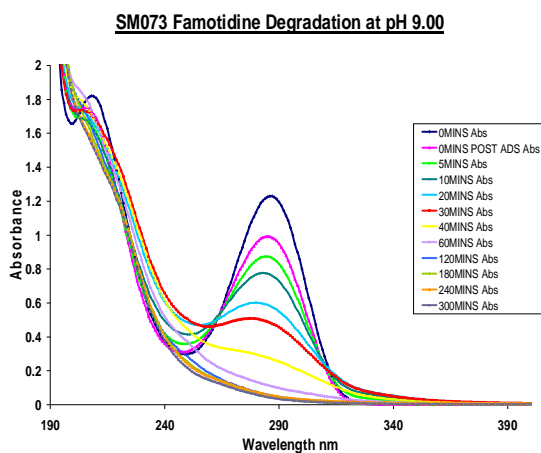
3A-2. FAM Photocatalysis at pH 5 SA-TiO₂



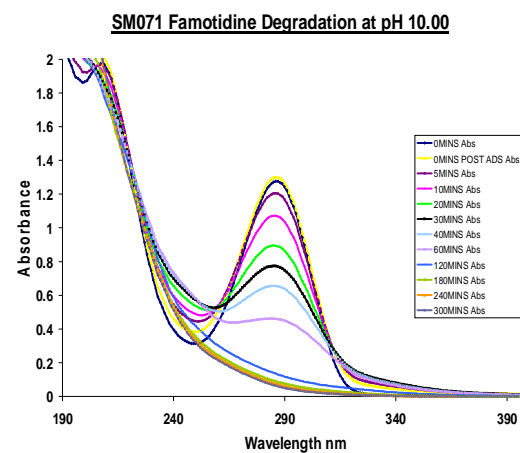
3A-3. FAM Photocatalysis at pH 6 SA-TiO₂



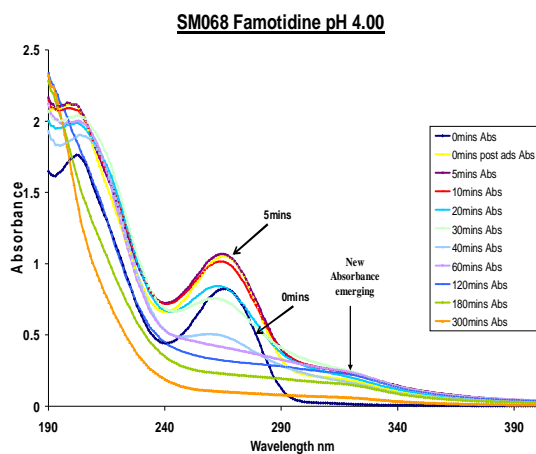
3A-4. FAM Photocatalysis at pH 5 P-25 TiO₂



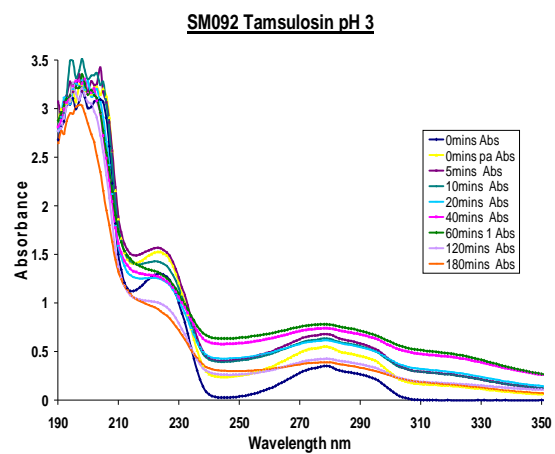
3A-5. FAM Photocatalysis at pH 9 P-25TiO₂



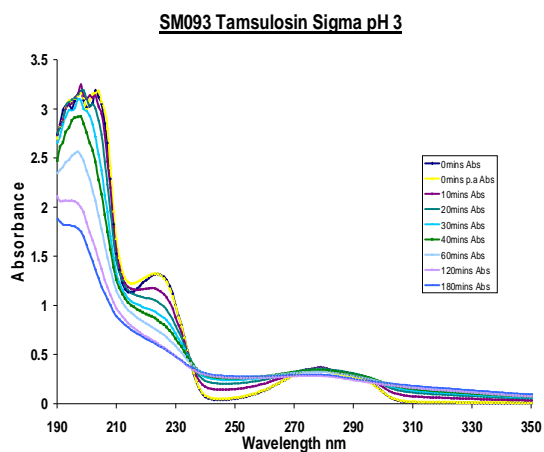
3A-6. FAM Photocatalysis at pH 10 P-25TiO₂



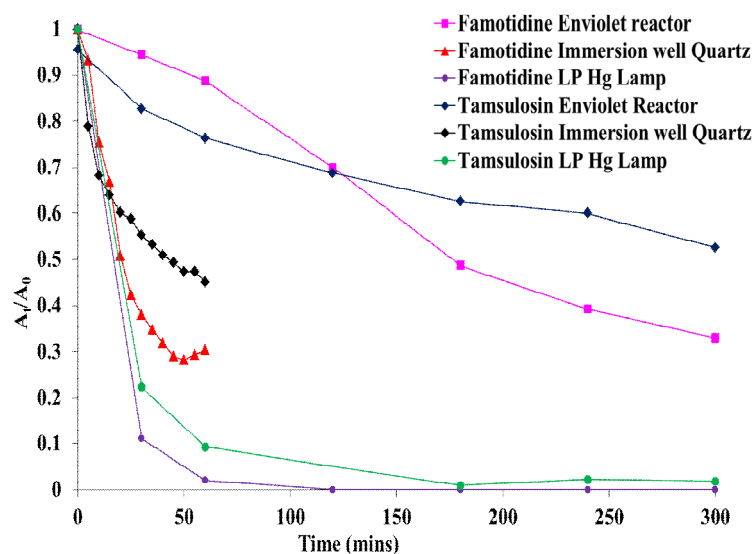
3A-7. FAM Photocatalysis at pH4 P-25TiO₂



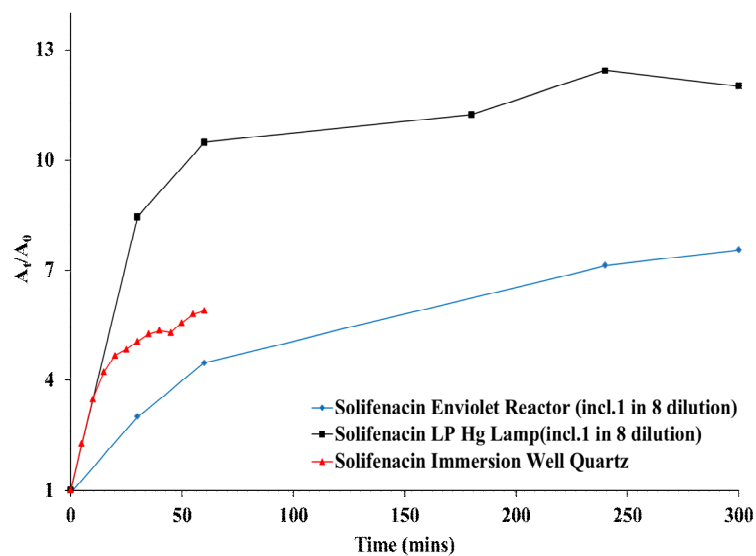
3A-8. TAMS Photocatalysis at pH 3 P-25TiO₂



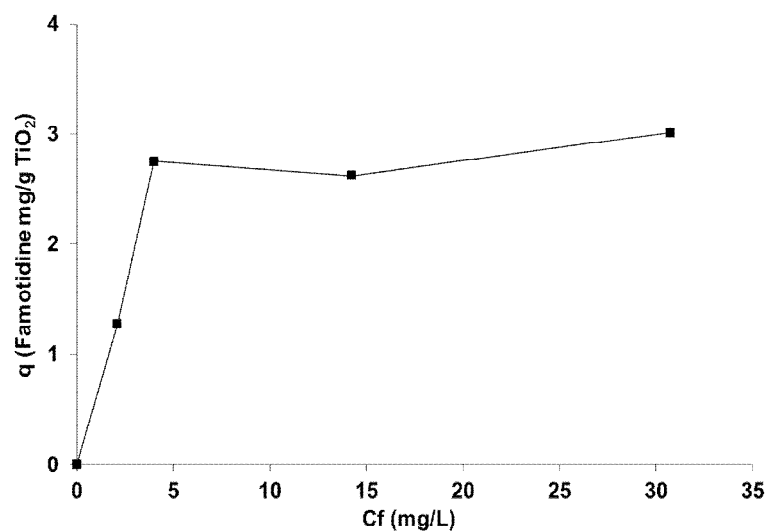
3A-9. TAMS Photocatalysis at pH 3 SA-TiO₂



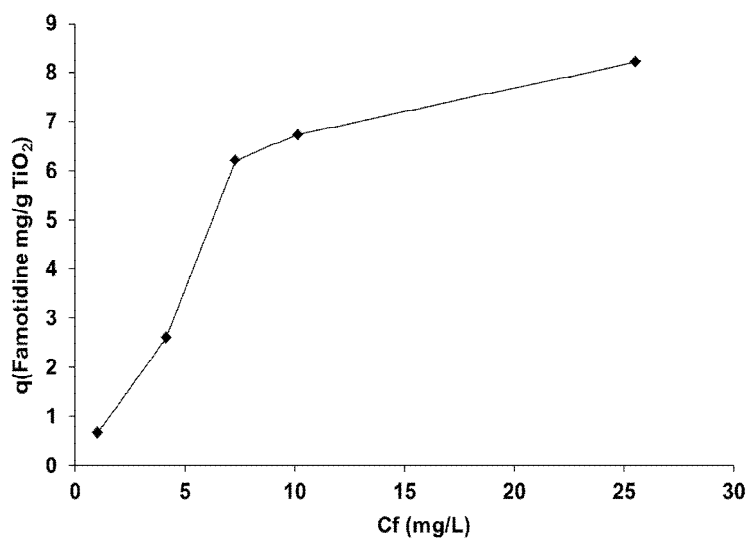
3A-10. UV-vis degradation profiles showing studies with Famotidine and Tamsulosin in the Enviolet reactor vs. Low pressure Hg Lamp Studies vs. Quartz Immersion Well Studies. [FAM], [TAM] = 0.083 mM, Time = 1 or 5 h.



3A-11. UV-vis degradation profiles showing studies for Solifenacin in the Enviolet reactor vs. Low pressure Hg Lamp Studies vs. Quartz Immersion Well Studies with Quartz. Profiles are based on the increase in absorbance seen in the case of Solifenacin. [SOL] = 1 mM, Time = 1 or 5 h.

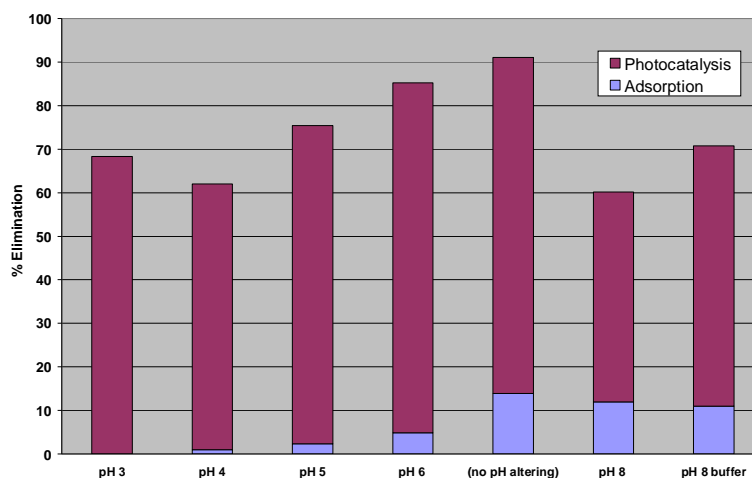


3A-12. UV-vis analysis of an adsorption isotherm for Famotidine after 16 h of shaking (foil-covered). [FAM] = 0-100 μ M, SA TiO₂ = 0.05 g/50 mL, Time = 16 h.



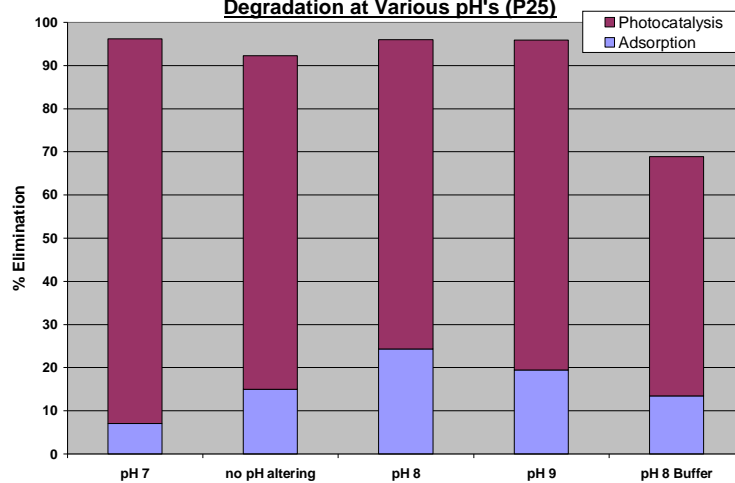
3A-13. UV-vis analysis of an adsorption isotherm for Famotidine after 48 h of shaking (foil-covered). [FAM] = 0-100 μ M, SA TiO₂ = 0.05 g/50 mL, Time = 48 h.

**Adsorption and Photocatalytic Contributions to Famotidine
Degradation at Various pHs**



3A-14. Charts showing adsorption (0.5 h) relative to degradation for different pHs for Famotidine (pre-illumination) by Sigma TiO_2 at different pHs.

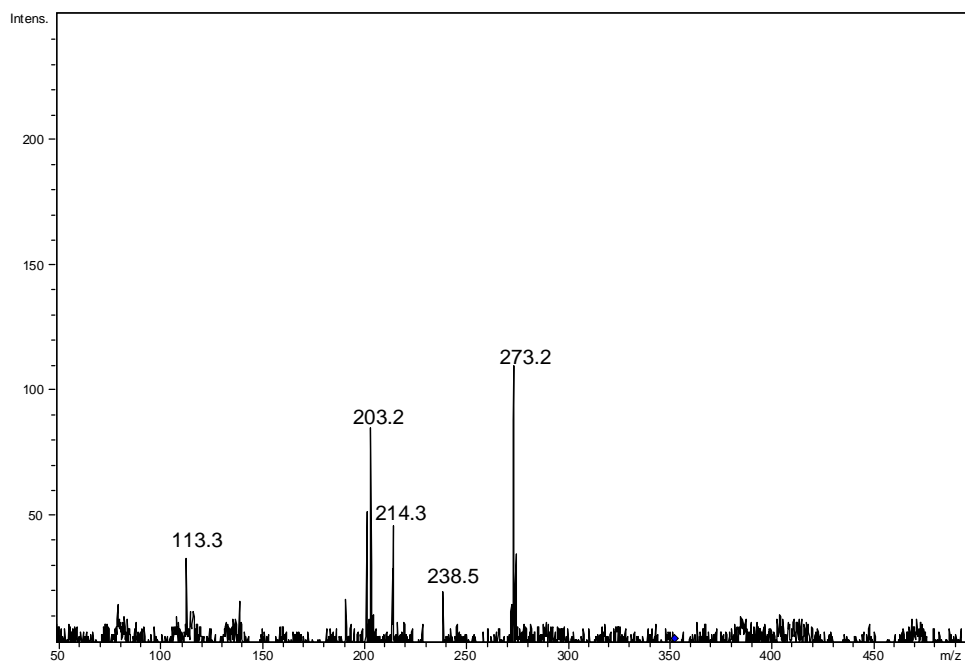
**Adsorption and Photocatalytic contributions to Famotidine
Degradation at Various pH's (P25)**



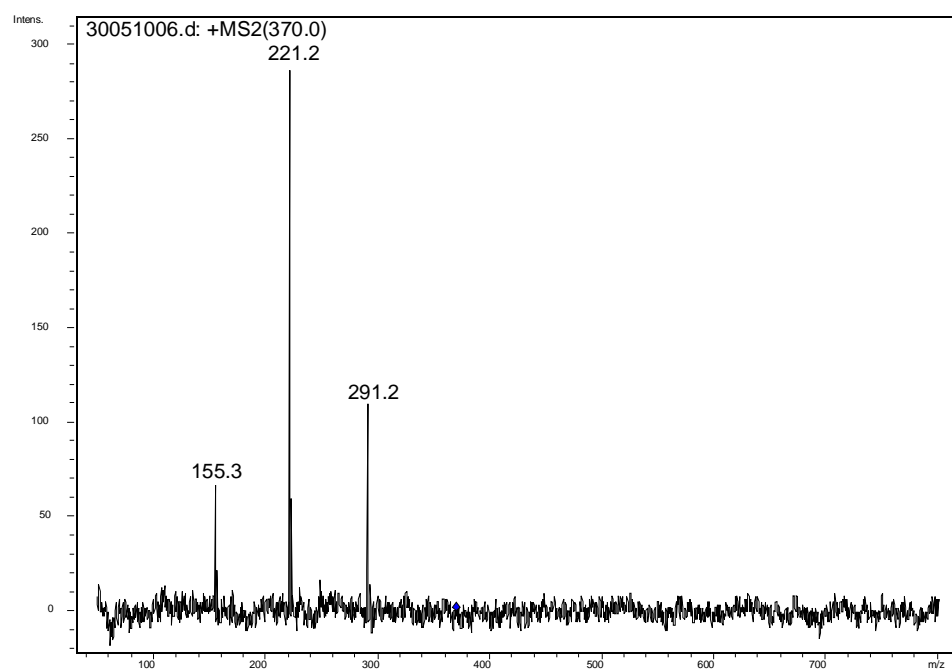
3A-15. Charts showing adsorption (0.5 h) relative to degradation for different pHs for Famotidine (pre-illumination) by P-25 TiO_2 at different pHs.

0 mins p.a.		10mins		20mins		30mins		40mins		60mins		120mins		180mins	
m/z	Intens %	m/z	Intens %	m/z	Intens %	m/z	Intens %	m/z	Intens %	m/z	Intens %	m/z	Intens %	m/z	Intens %
376	3	359	11	359	21	397	10	360	22	360	57	379.4	7	360	3
340	12	338	100	354	21	360	31	360	15	359.5	55	373.6	6	359.4	15
339	11	246	8	340	12	359	34	359	44	355.1	15	370.5	7	351.5	6
338	100	117	2	339	11	354	34	355	24	354.1	28	363.5	10	346.2	3
337	10	77.5	2	338	100	351	11	354	42	351.6	19	360	10	342.5	5
260	2			246	10	341	27	353	10	349.6	9	359.5	10	341.9	5
				187	9	340	61	352	17	345.1	9	356.5	6	340.6	100
				170	4	339	17	340	82	341.1	44	352.2	6	300.4	7
				159	2	338	100	339	27	340.6	100	351.7	7	294.3	3
				145	4	246	10	338	100	339.6	8	348.1	9	279.5	3
				119	3	187	21	337	16	338.6	8	341.5	21	246.6	4
				117	2	117	22	336	10	320.1	8	340.6	100	218.4	3
								246	19	246.4	11	338.3	9	175.4	4
								223	14	220.6	8	300.5	7	159.4	8
								187	39	201.4	17	291.5	6	145.4	4
								145	11	191.3	11	234.4	6	143.5	4
								119	14	175.4	12	228.3	8	117.4	2
								117	28	173.5	11	159.4	11	101.4	2
										159.4	14	117.4	5		
										135.4	8				
										117.4	39				
										99.5	9				

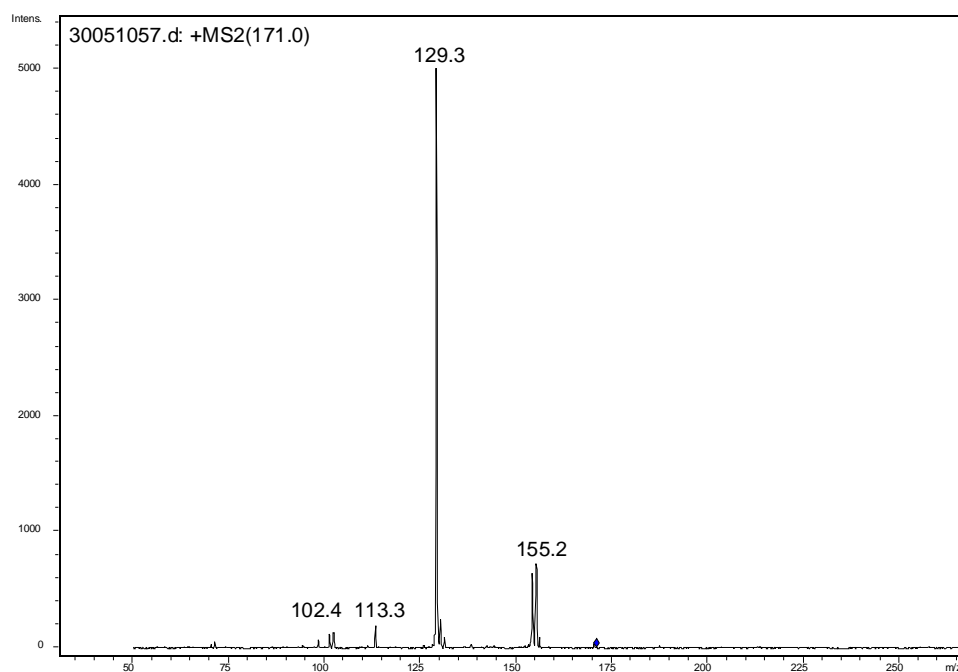
4A-1. Masses in Famotidine mass spectra. Most significant and consistent masses in colour.



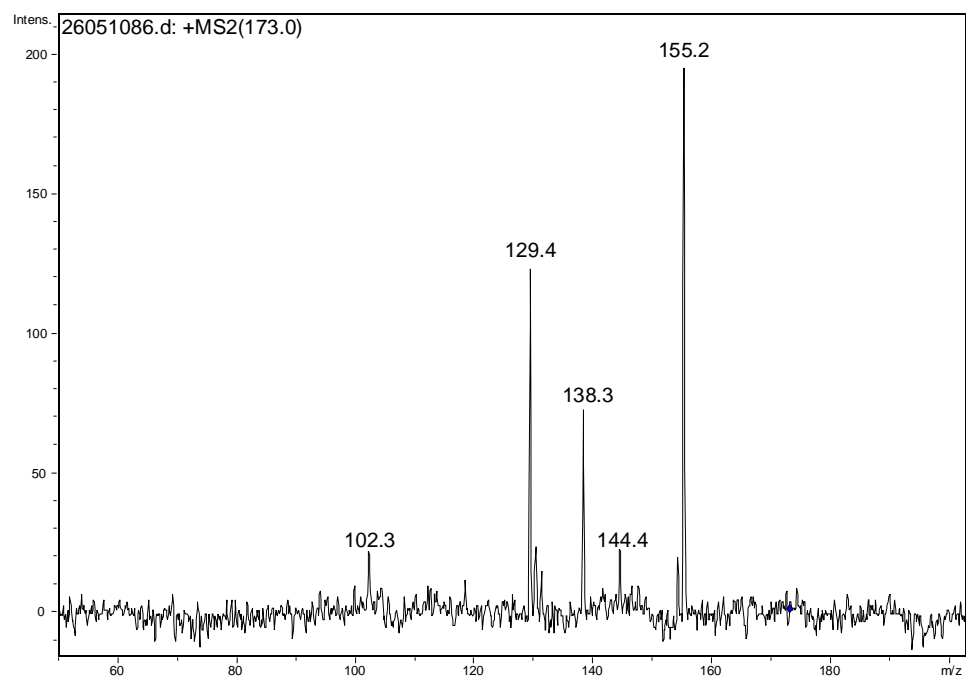
4A-2. DI mass spectrum of m/z = 352 a Famotidine intermediate found in DI-MS studies.



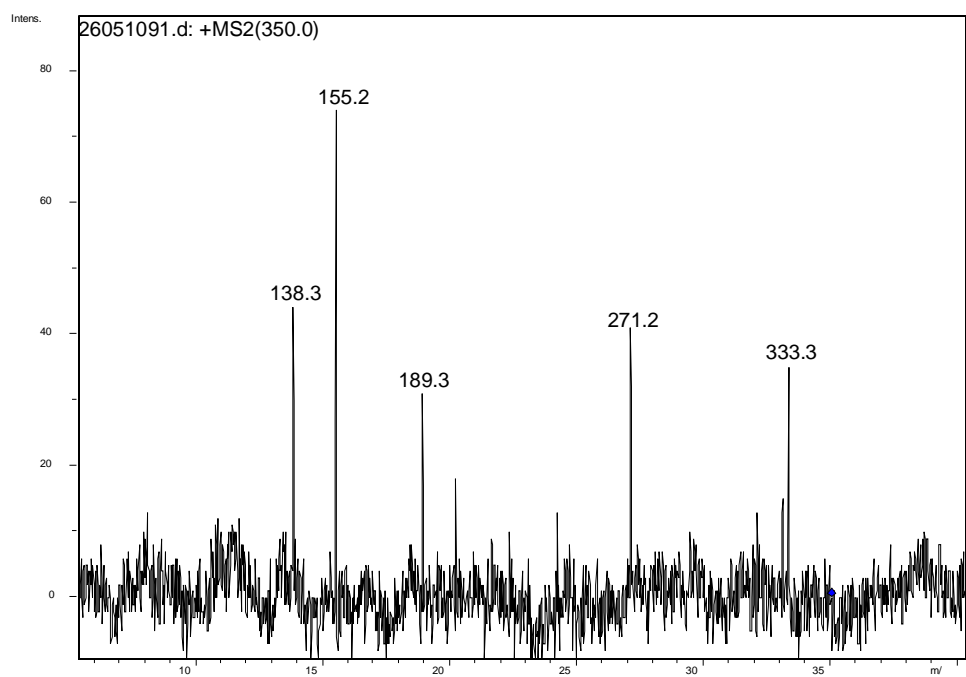
4A-3. DI-Mass spectrum of $m/z = 370$, a Famotidine intermediate found in DI-MS studies and LC-MS studies.



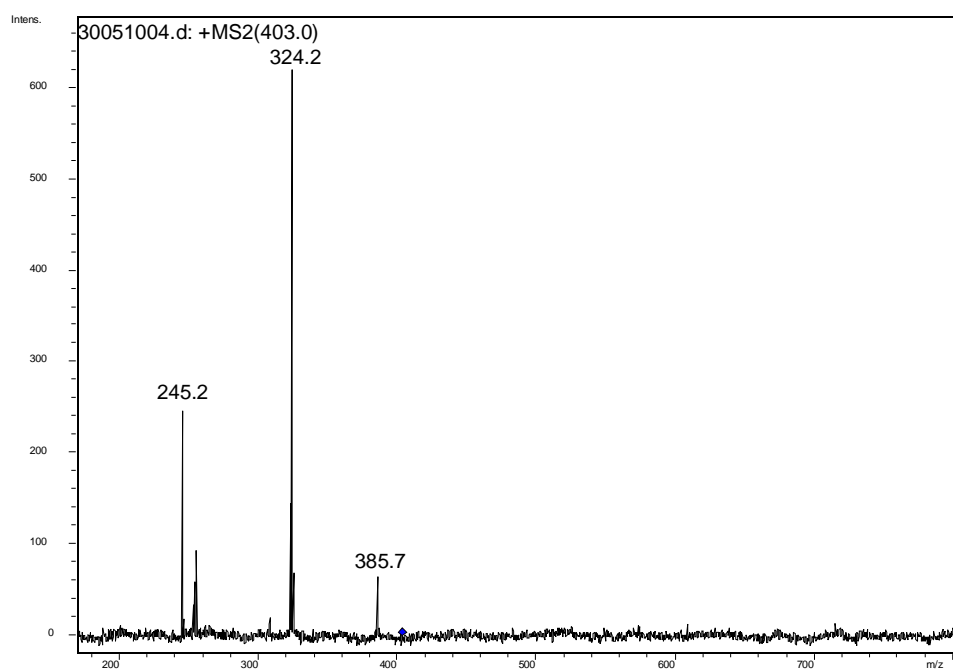
4A-4. DI-Mass spectrum of $m/z = 171$, a Famotidine intermediate found in both DI-MS and LC-MS studies.



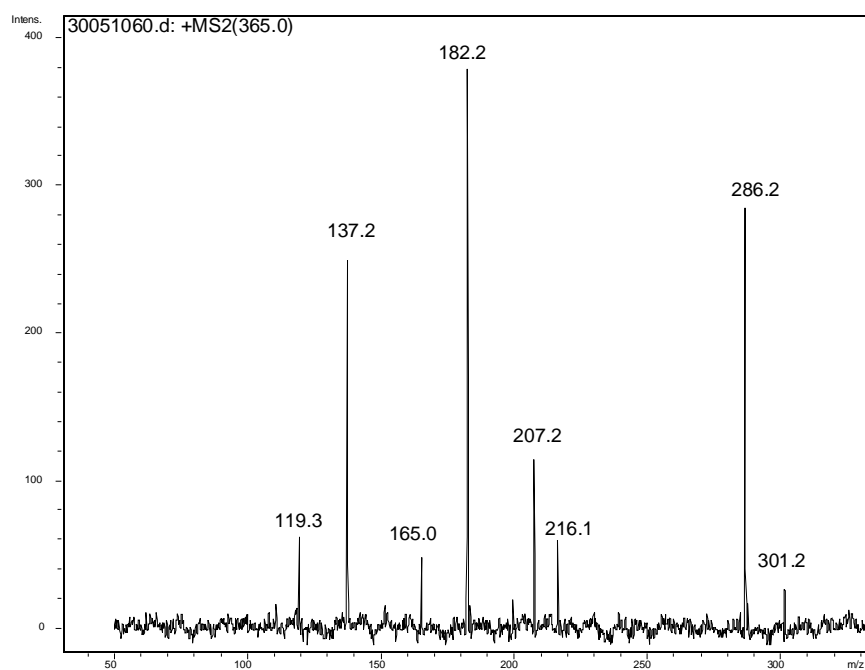
4A-5. DI-Mass spectrum of $m/z = 173$, a Famotidine intermediate found in both DI-MS and LC-MS



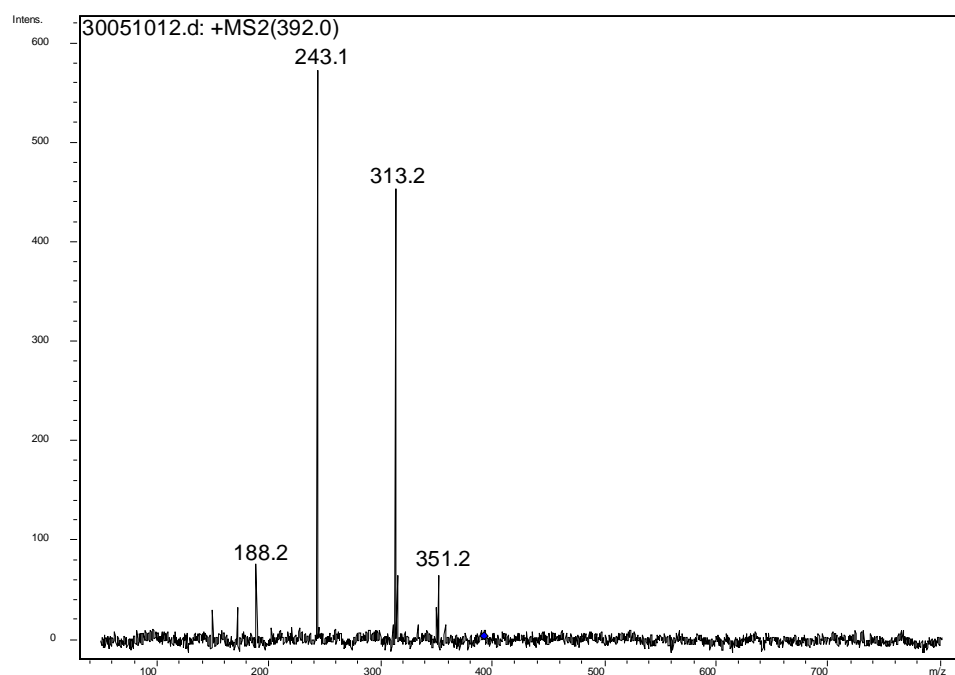
4A-6. $m/z = 350$ found in Famotidine DI-MS studies of a photocatalytic experiment.



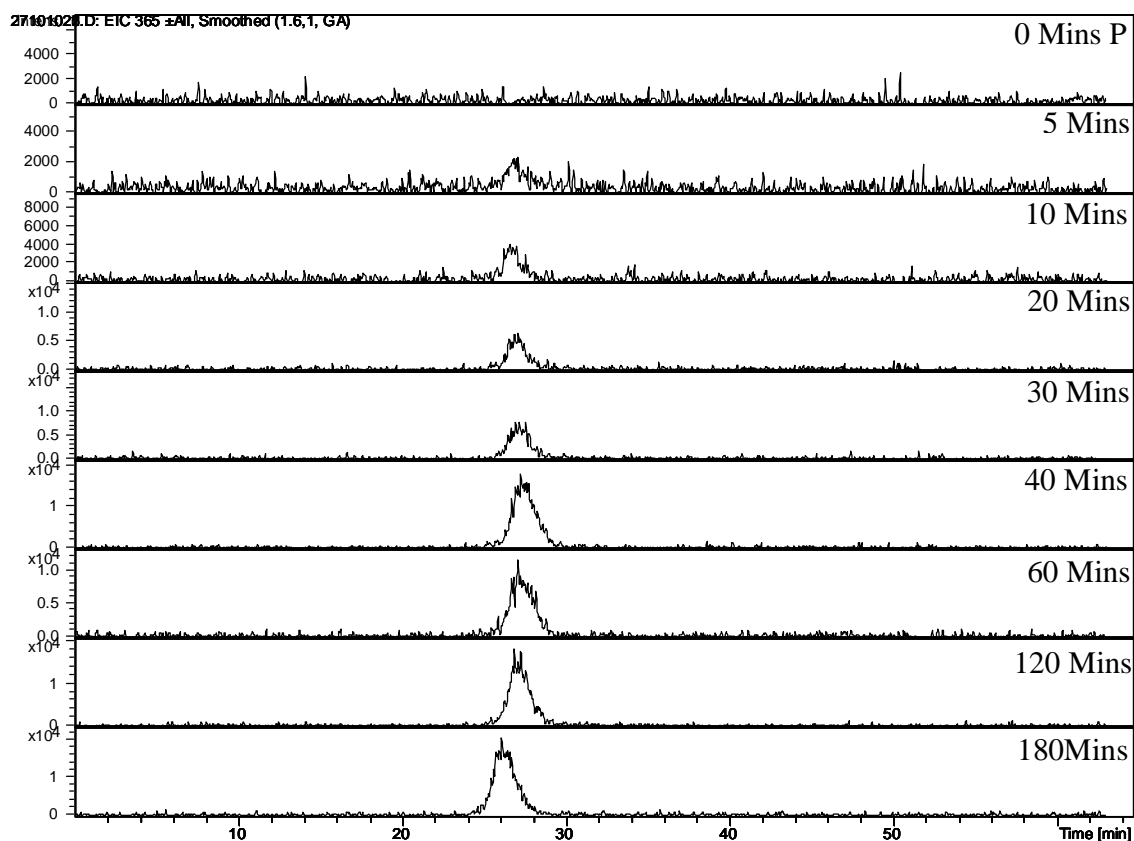
4A-7. $m/z = 403$ found in Famotidine DI-MS studies of a photocatalytic experiment.



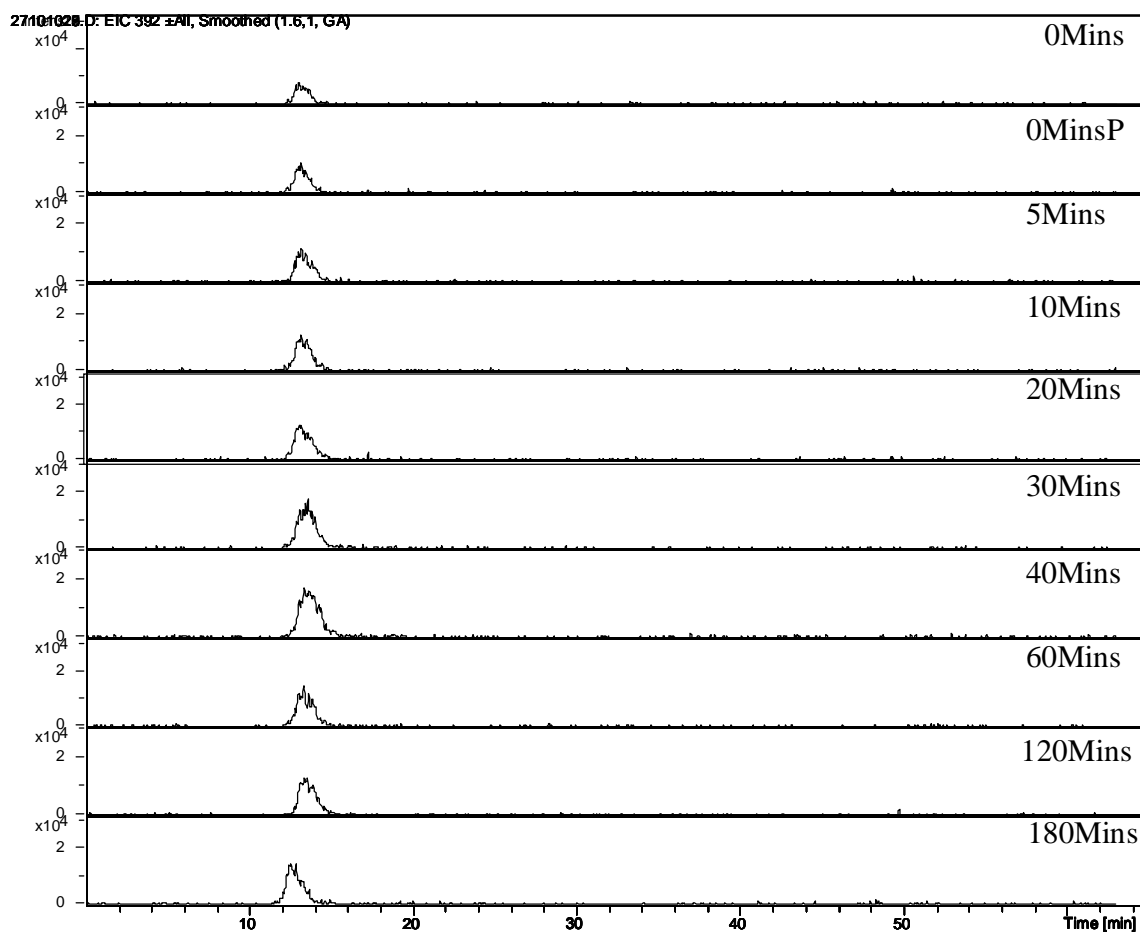
4A-8. $m/z = 365$ found in Famotidine DI-MS studies of a photocatalytic experiment.



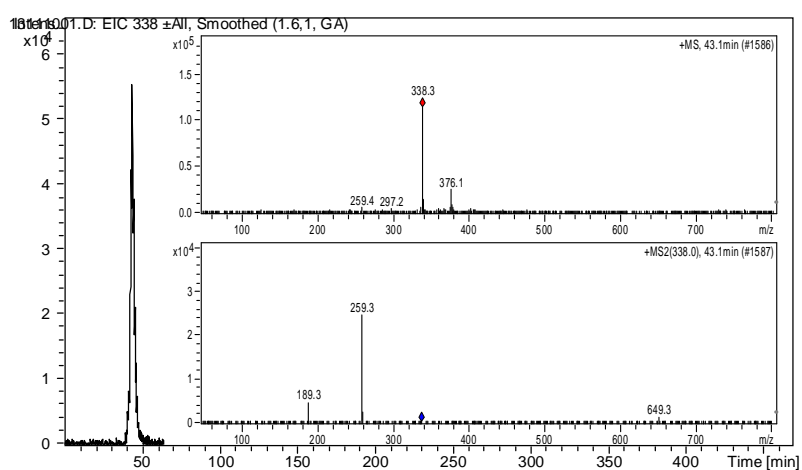
4A-9. $m/z = 392$ found in Famotidine DI-MS studies of a photocatalytic experiment.



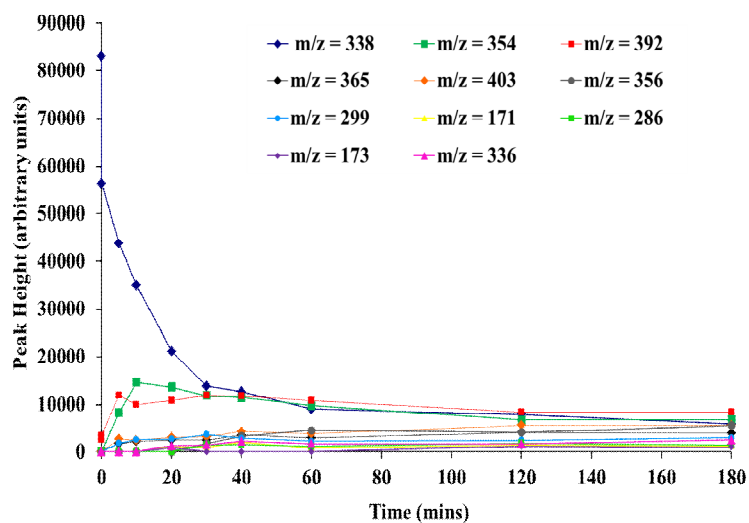
4A-10. EIC chromatograms of a photocatalytic reaction showing the development of $m/z = 365$.
Photocatalysis [FAM] = 1mM, 0.1g/320ml TiO_2



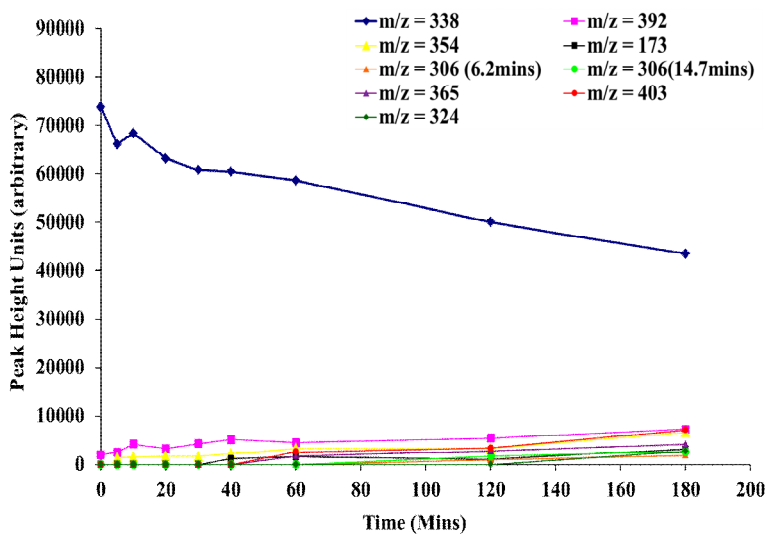
4A-11. EIC chromatograms of a photocatalytic reaction showing the development of $m/z = 392$. Photocatalysis [FAM] = 1mM, 0.1g/320ml TiO_2



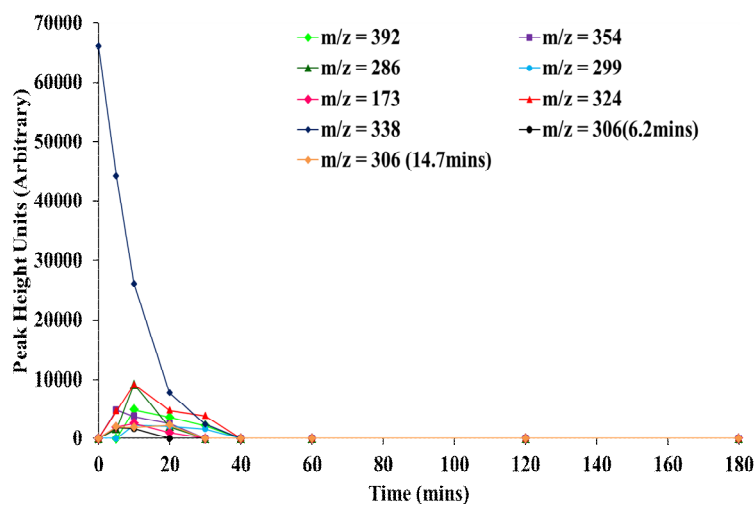
4A-12. EIC of a $50\mu\text{M}$ standard of Famotidine showing the presence of the potassium adduct at $m/z = 376$ in the MS. Inset MS (top) and MS/MS (bottom) spectra.



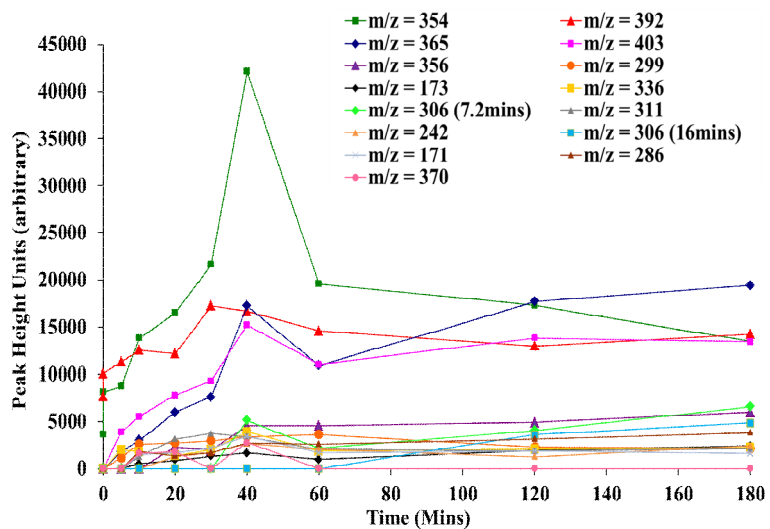
4A-13. Ions detected by LC-MS in the photocatalytic degradation of Famotidine. [FAM] = 0.083mM, TiO_2 = P-25 0.1g/320mLs



4A-14. Ions detected by LC-MS in photolytic degradation of Famotidine with Pyrex glassware. [FAM] = 0.083mM.



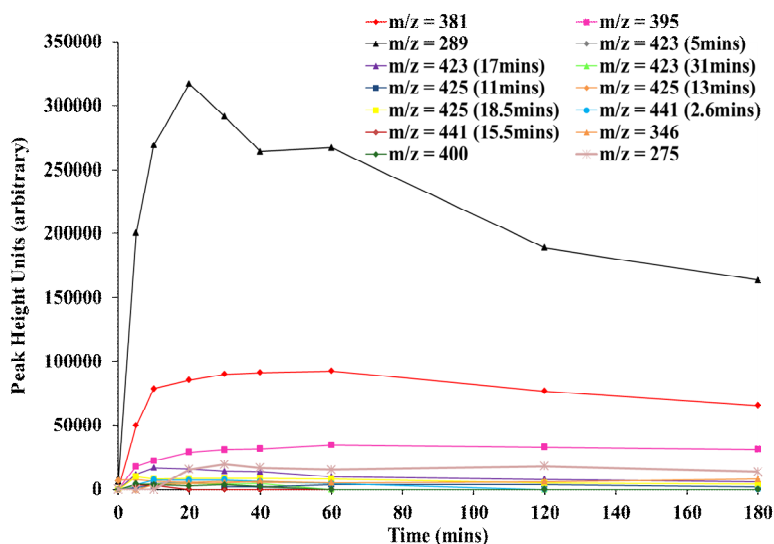
4A-15. Ions detected by LC-MS in photolytic degradation of Famotidine with Quartz glassware. [FAM] = 0.083mM.



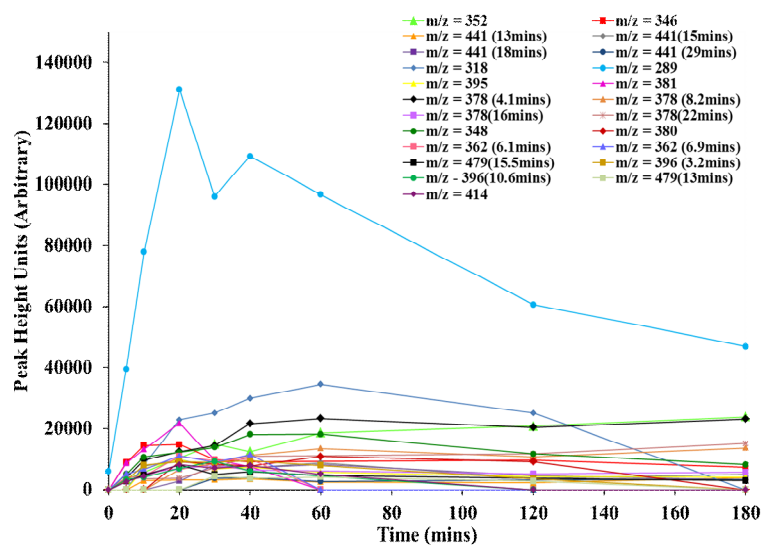
4A-16. Ions detected by LC-MS in photocatalytic degradation of Famotidine. [FAM] = 1mM, TiO_2 = P-25 0.1g/320mLs.

40mins			60mins									120mins								
m/z	I	I%	m/z	I	I%	m/z	I	I%	m/z	I	I%	m/z	I	I%	m/z	I	I%	m/z	I	I%
409.5	26700	100	362.8	2268	8	409.5	18939	100	358.4	2739	14	409.5	18939	100	343.7	2628	14			
410.4	7508	28	397.4	2007	8	441.3	7767	41	449.5	2743	14	441.3	7767	41	358.4	2739	14			
441.4	7573	28	436.4	2185	8	289.5	7175	38	489.7	2678	14	289.5	7175	38	449.5	2743	14			
289.5	7022	26	438.4	2082	8	410.6	6721	35	531.2	2589	14	410.6	6721	35	489.7	2678	14			
425.6	6664	25	443.4	2179	8	277.1	5796	31	675.6	2712	14	277.1	5796	31	531.2	2589	14			
367.5	4527	17	449.4	2075	8	423.5	5575	29	681.6	2667	14	423.5	5575	29	675.6	2712	14			
381.4	4108	15	450.8	2248	8	378.4	5276	28	227.4	2466	13	378.4	5276	28	681.6	2667	14			
395.4	4096	15	520.4	2106	8	359.5	4961	26	269.6	2510	13	359.5	4961	26	227.4	2466	13			
475.5	3973	15	682	2013	8	455.6	4935	26	303.5	2459	13	455.6	4935	26	269.6	2510	13			
332.4	3428	13	275.5	1777	7	228.4	4782	25	396.7	2426	13	228.4	4782	25	303.5	2459	13			
355.6	3455	13	327.6	1947	7	381.5	4436	23	426.6	2548	13	381.5	4436	23	396.7	2426	13			
368.3	3374	13	345	1832	7	452.7	4370	23	436.6	2436	13	452.7	4370	23	426.6	2548	13			
350.6	3075	12	346.5	1888	7	441.7	4231	22	439.4	2536	13	441.7	4231	22	436.6	2436	13			
411.4	3179	12	346.7	1796	7	701.5	4005	21	467.6	2449	13	701.5	4005	21	439.4	2536	13			
441	3083	12	347.6	1896	7	360.2	3709	20	500.2	2502	13	360.2	3709	20	467.6	2449	13			
228.4	2829	11	394.5	1984	7	365.5	3696	20	292.5	2261	12	365.5	3696	20	500.2	2502	13			
305.5	2844	11	423.5	1883	7	412.6	3847	20	340.7	2217	12	412.6	3847	20	292.5	2261	12			
227.6	2731	10	449.6	1886	7	475.9	3785	20	392.5	2343	12	475.9	3785	20	340.7	2217	12			
359.5	2586	10	472.7	1914	7	382.4	3638	19	401.4	2331	12	382.4	3638	19	392.5	2343	12			
383.5	2646	10	545.4	1846	7	476.5	3624	19	425.6	2238	12	476.5	3624	19	401.4	2331	12			
414.6	2639	10	683.5	1888	7	502.4	3444	18	491.7	2231	12	502.4	3444	18	425.6	2238	12			
424.9	2572	10	218.5	1515	6	286.5	3303	17	252.3	2055	11	286.5	3303	17	491.7	2231	12			
491.4	2753	10	300.5	1572	6	376.7	3168	17	262.7	2067	11	376.7	3168	17	252.3	2055	11			
321.4	2532	9	318.5	1729	6	318.5	3051	16	319.3	2010	11	318.5	3051	16	262.7	2067	11			
351.6	2432	9	326.5	1491	6	346.4	2961	16	335.4	2072	11	346.4	2961	16	319.3	2010	11			
369.4	2454	9	330.6	1545	6	374.4	2996	16	383.3	2017	11	374.4	2996	16	335.4	2072	11			
455.4	2479	9	336.1	1524	6	340	2755	15	413.2	2106	11	340	2755	15	383.3	2017	11			
461.5	2276	9	338.5	1590	6	368.4	2878	15	486.2	2007	11	368.4	2878	15	413.2	2106	11			
544.3	2310	9	343.3	1583	6	395.5	2902	15	505.3	2173	11	395.5	2902	15	486.2	2007	11			
186.5	2064	8	346.1	1664	6	402.6	2883	15	505.7	2020	11	402.6	2883	15	505.3	2173	11			
285.5	2140	8	352.1	1543	6	435.6	2837	15	524.2	2160	11	435.6	2837	15	505.7	2020	11			
291.4	2032	8	353.1	1700	6	533.3	2847	15				533.3	2847	15	524.2	2160	11			
329.3	2101	8	389.4	1730	6	180.5	2739	14				180.5	2739	14						
			390.5	1726	6	343.7	2628	14												

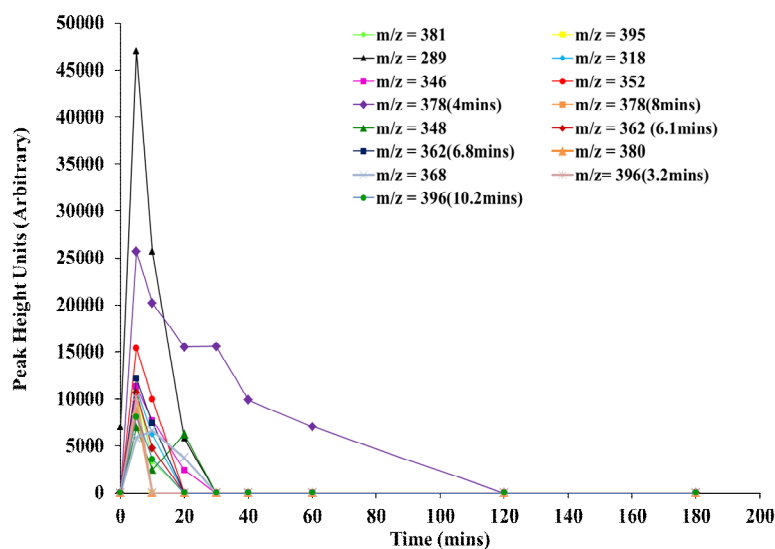
4A-17. Masses between 40-120mins found in DI-MS of a photocatalytic experiment of Tamsulosin.



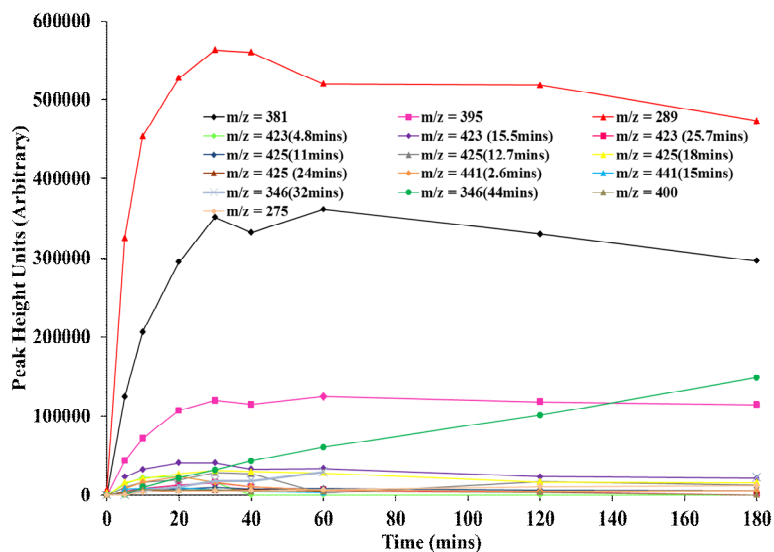
4A-18 Ions detected by LC-MS in the photocatalytic degradation of Tamsulosin. [TAM] = 0.083mM, TiO₂ = P-25 0.2g/320mLs



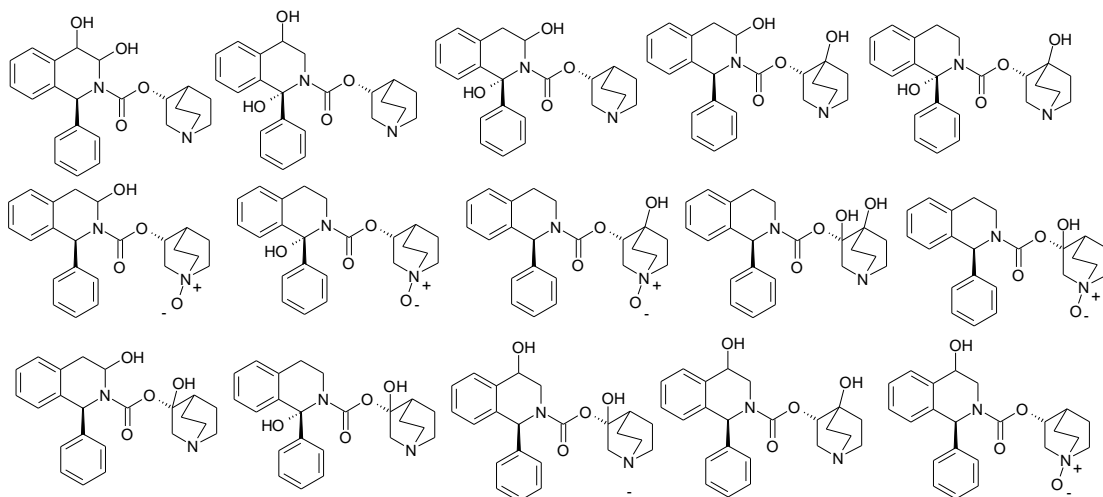
4A-19. Ions detected by LC-MS in the photolytic degradation of Tamsulosin with Pyrex glassware. [TAM] = 0.083mM.



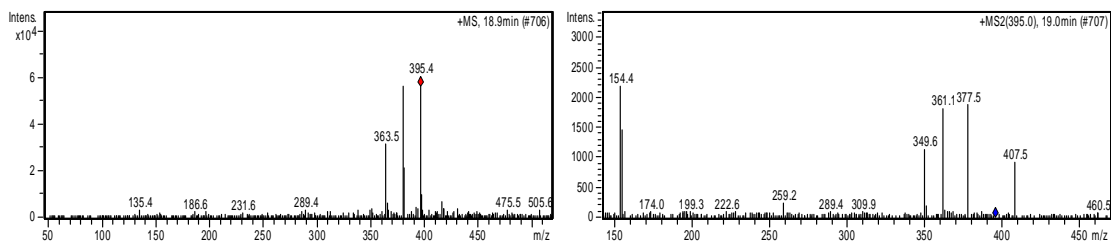
4A-20. Ions detected by LC-MS in the photolytic degradation of Tamsulosin with Quartz glassware. [TAM] = 0.083mM.



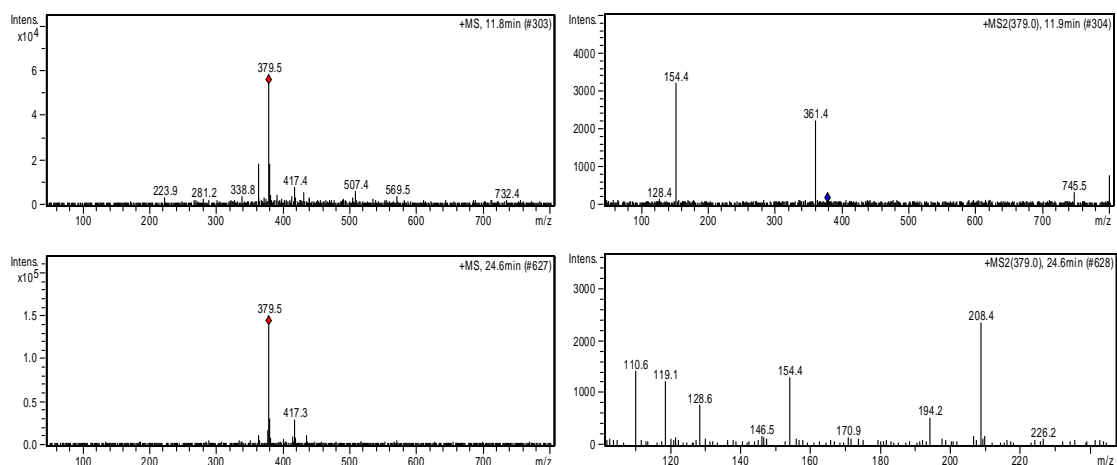
4A-21. Ions detected by LC-MS in the photocatalytic degradation of Tamsulosin. [TAM] = 1mM, TiO₂ = P-25 0.2g/320mLs



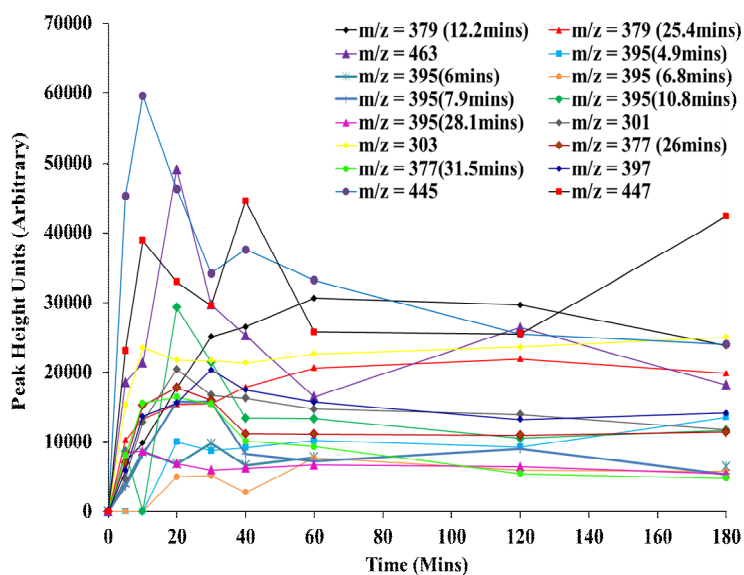
4A-22. 15 possible structural isomers for m/z = 395.



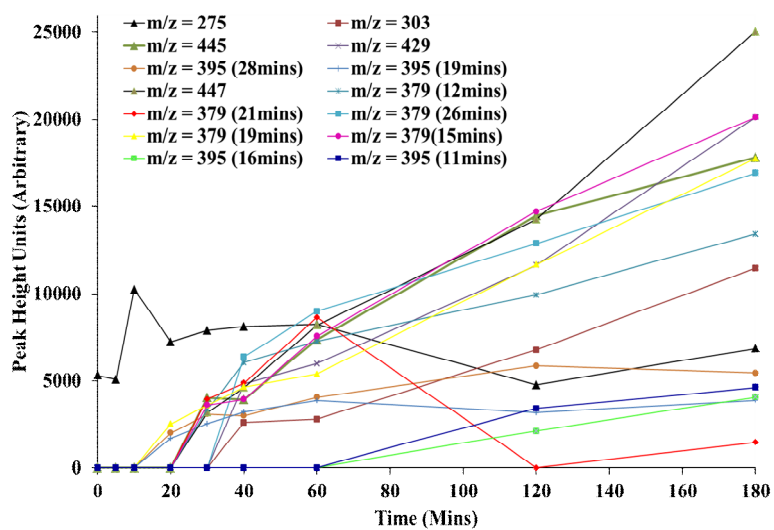
4A-23. MS of m/z = 395 at 18.9mins and respective MS/MS spectra.



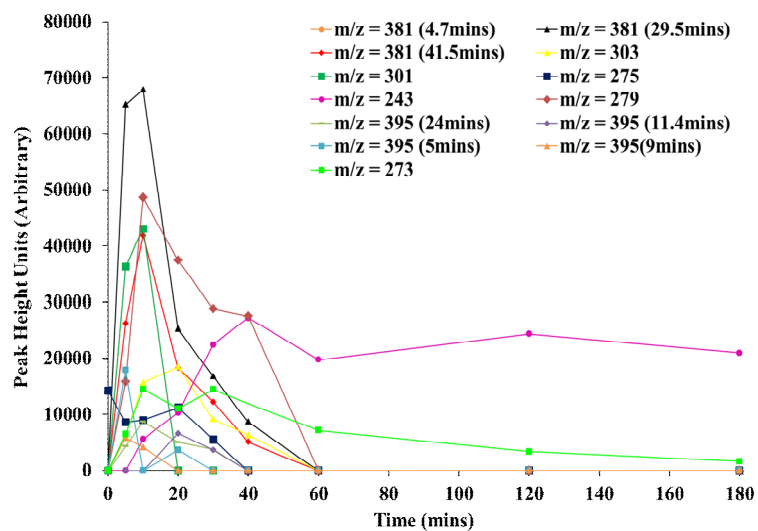
4A-24. MS of $m/z = 379$ at 11.8mins and 24.6mins and their respective MS/MS spectra.



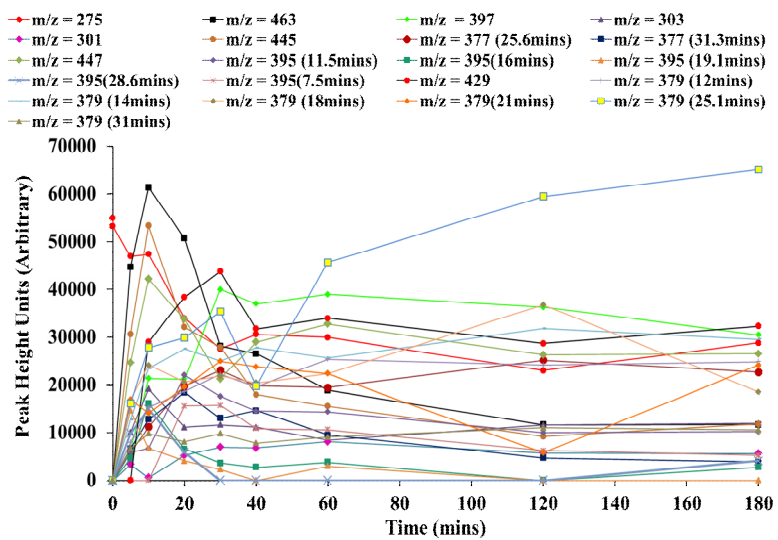
4A-25. Ions detected by LC-MS in the photocatalytic degradation of Solifenacin. [SOL] = 0.083mM, TiO_2 = P-25 0.1g/320mLs



4A-26. Ions detected by LC-MS in the photolytic degradation of Solifenacin with Pyrex glassware. [SOL] = 0.083mM



4A-27. Ions detected by LC-MS in the photolytic degradation of Solifenacin with Quartz glassware. [SOL] = 0.083mM



4A-28. Ions detected by LC-MS in the photocatalytic degradation of Solifenacin. [SOL] = 1mM, TiO₂ = P-25 0.1g/320mLs

	FAM DI-MS	FAM LC-MS		FAM DI-MS	FAM LC-MS
MODE			TRAP		
Mass Range Mode	STD/Normal	STD/Normal	Scan Begin	50 m/z	50 m/z
Ion Polarity	Positive	Positive	Scan End	800 m/z	800 m/z
Ion Source Type	ESI	ESI	Averages	5 Spectra	5 Spectra
Current Alternating Ion Pol	N/A	N/A	Charge Control	ON	ON
Alternating Ion Polarity	N/A	N/A	ICC Target	20000	20000
DETECTOR AND BLOCK VOLTAGES			ICC Actual	6278	491
Multiplier Voltage	1750 V	1850 V	Accumulation		
Dynode Voltage	7 kV	7 kV	Time	1814 μ s	50000 μ s
Scan Delay	0 μ s	0 μ s	Max. Acc. Time	50000 μ s	50000 μ s
Skimmer 1 Block	100 V	100 V	MS/MS MANUAL MODE		
Skimmer 2 Block	300 V	300 V	Fast Calc	ON	ON
TUNE SOURCE			ISTD	OFF	OFF
Trap Drive	32.9	50.1	MS/MS AUTOMATIC		
Skim 1	34.9 V	15 V	Auto MS/MS	OFF	ON
Skim 2	6 V	8.1 V	ROLLING AVERAGING		
Octopole RF amplitude	150 Vpp	177.1 Vpp	Rolling	ON 2cts	OFF
Octopole delta	2.4 V	2.05 V	COMPRESSED SPECTRA		
Lens 1	-5 V	-2.2 V	Compressed		
Lens 2	-60 V	-49.5 V	Spectra	OFF	OFF
OCtopole	2.49 V	5 V			
Capillary Exit	108.2 V	65 V			
Cap Exit Offset	73.2 V	50 V			
HV endplate Offset	-500 V	-500 V			
Current Endplate	237.671 nA	1327.5 nA			
HV Capillary	4000 V	4500 V			
Current Capillary	41.605 nA	91.938 nA			
Dry Temp (measured)	302°C	327°C			
Dry Gas (measured)	5 L/min	8.01 L/min			
Nebuliser (measured)	15.14 psi	50.5 psi			

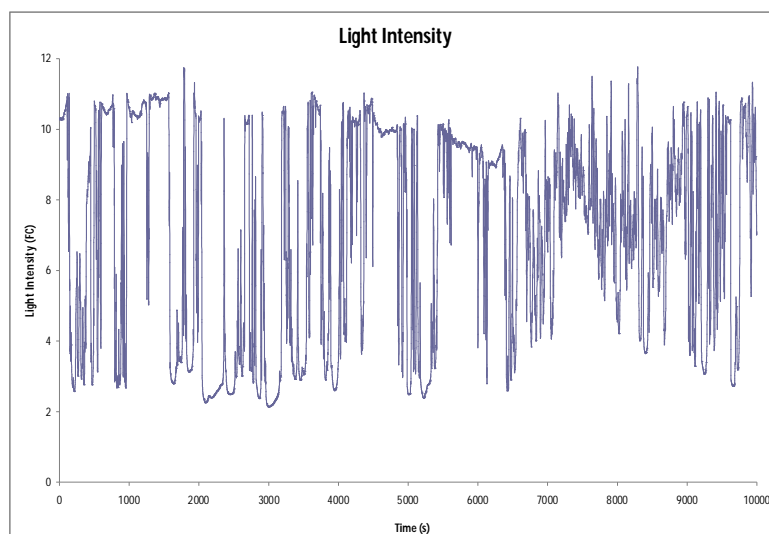
4A-29. Table of MS parameters for Famotidine DI-MS and LC-MS Studies

	TAMS DI-MS	TAMS LC-MS		TAMS DI-MS	TAMS LC-MS
MODE			TRAP		
Mass Range Mode	STD/Normal	STD/Normal	Scan Begin	50 m/z	50 m/z
Ion Polarity	Positive	Positive	Scan End	850 m/z	850 m/z
Ion Source Type	ESI	ESI	Averages	5 Spectra	5 Spectra
Current Alternating			Charge Control	ON	ON
Ion Pol	N/A	N/A	ICC Target	20000	20000
Alternating Ion Polarity	N/A	N/A	ICC Actual	16857	350
DETECTOR AND BLOCK VOLTAGES			Accumulation Time	702 μ s	50000 μ s
Multiplier Voltage	1750 V	1850 V	Max. Acc. Time	50000 μ s	50000 μ s
Dynode Voltage	7 kV	7 kV	MS/MS MANUAL MODE		
Scan Delay	0 μ s	0 μ s	Fast Calc	ON	ON
Skimmer 1 Block	100 V	100 V	ISTD	OFF	OFF
Skimmer 2 Block	300 V	300 V	MS/MS AUTOMATIC		
TUNE SOURCE			Auto MS/MS	OFF	ON
Trap Drive	35.9	38.4	ROLLING AVERAGING		
Skim 1	38.8 V	19.2 V	Rolling	ON 2cts	OFF
Skim 2	6 V	6.2 V	COMPRESSED SPECTRA		
Octopole RF amplitude	150 V _{pp}	201.6 V _{pp}	Compressed Spectra	OFF	OFF
Octopole delta	2.4 V	1.93 V			
Lens 1	-5 V	-4.1 V			
Lens 2	-60 V	-46.1 V			
Octopole	2.55 V	2.51 V			
Capillary Exit	113.7 V	95.4 V			
Cap Exit Offset	75 V	76.2 V			
HV endplate Offset	-500 V	-1200 V			
Current Endplate	281.33 nA	1147.018 nA			
HV Capillary	4000 V	4500 V			
Current Capillary	40.679 nA	155.035 nA			
Dry Temp (measured)	303 L/min	327 L/min			
Dry Gas (measured)	5°C	8.01°C			
Nebuliser (measured)	15.19 psi	50.51 psi			

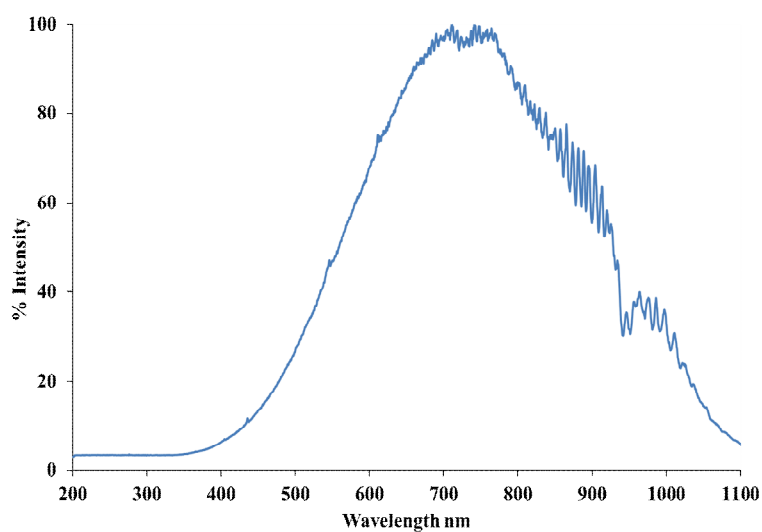
4A-30. Table of MS parameters for Tamsulosin DI-MS and LC-MS Studies

	SOL DI-MS	SOL LC-MS		SOL DI-MS	SOL LC-MS
MODE			TRAP		
Mass Range Mode	STD/Normal	STD/Normal	Scan Begin	50 m/z	50 m/z
Ion Polarity	Positive	Positive	Scan End	2200 m/z	800 m/z
Ion Source Type	ESI	ESI	Averages	5 Spectra	5 Spectra
Current Alternating Ion Pol	N/A	N/A	Charge Control	ON	ON
Alternating Ion Polarity	N/A	N/A	ICC Target	20000	20000
DETECTOR AND BLOCK VOLTAGES			ICC Actual	13835	485
Multiplier Voltage	1850 V	1850 V	Accummulation Time	333 μ s	50000 μ s
Dynode Voltage	7 kV	7 kV	Max. Acc. Time	50000 μ s	50000 μ s
Scan Delay	0 μ s	0 μ s	MS/MS MANUAL MODE		
Skimmer 1 Block	100 V	100 V	Fast Calc	ON	ON
Skimmer 2 Block	300 V	300 V	ISTD	OFF	OFF
TUNE SOURCE			MS/MS AUTOMATIC		
Trap Drive	34	38.5	Auto MS/MS	OFF	ON
Skim 1	36.3 V	31.7 V	ROLLING AVERAGING		
Skim 2	6 V	15 V	Rolling	ON 2cts	OFF
Octopole RF amplitude	150 Vpp	205.7 Vpp	COMPRESSED SPECTRA		
Octopole delta	2.4 V	2.05 V	Compressed Spectra	OFF	OFF
Lens 1	-5 V	-4.7 V			
Lens 2	-60 V	-50.7 V			
Octopole	2.51 V	2.64 V			
Capillary Exit	110.2 V	81.7 V			
Cap Exit Offset	73.8 V	50 V			
HV endplate Offset	-500 V	-752 V			
Current Endplate	144.921 nA	1420.181 nA			
HV Capillary	4000 V	4451 V			
Current Capillary	32.488 nA	135.468 nA			
Dry Temp (measured)	301°C	328°C			
Dry Gas (measured)	4.99 L/min	8.01 L/min			
Nebuliser (measured)	15.14 psi	50.61 psi			

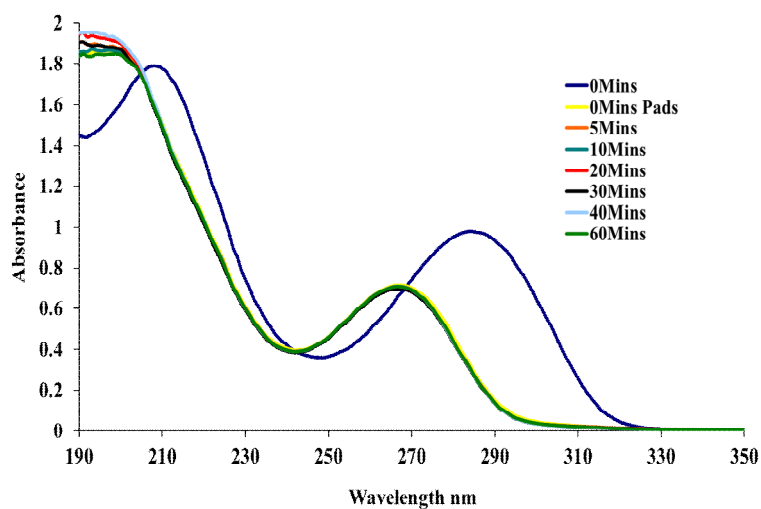
4A-31. Table of MS parameters for Solifenacin DI-MS and LC-MS Studies



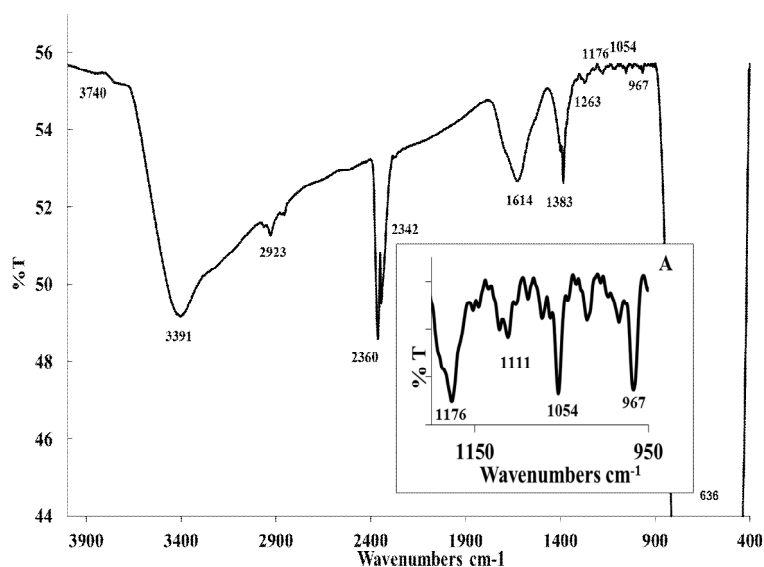
5A-1. Light Intensity in Footcandles recorded on 22-06-2010 during solar experiments with TCPP-TiO₂ photocatalysts



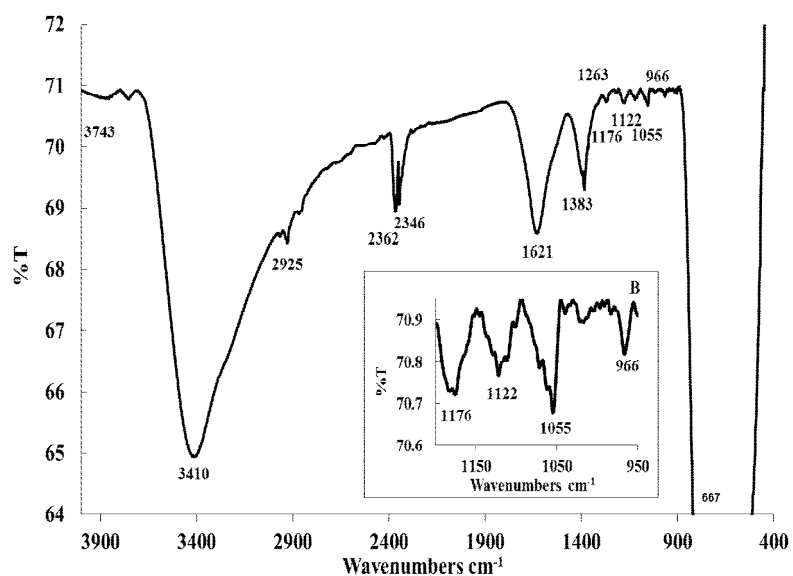
5A-2. Spectral irradiance profile data for our Halogen (Tungsten) Lamp which was used in indoor photocatalytic reactions with visible light sensitised materials.



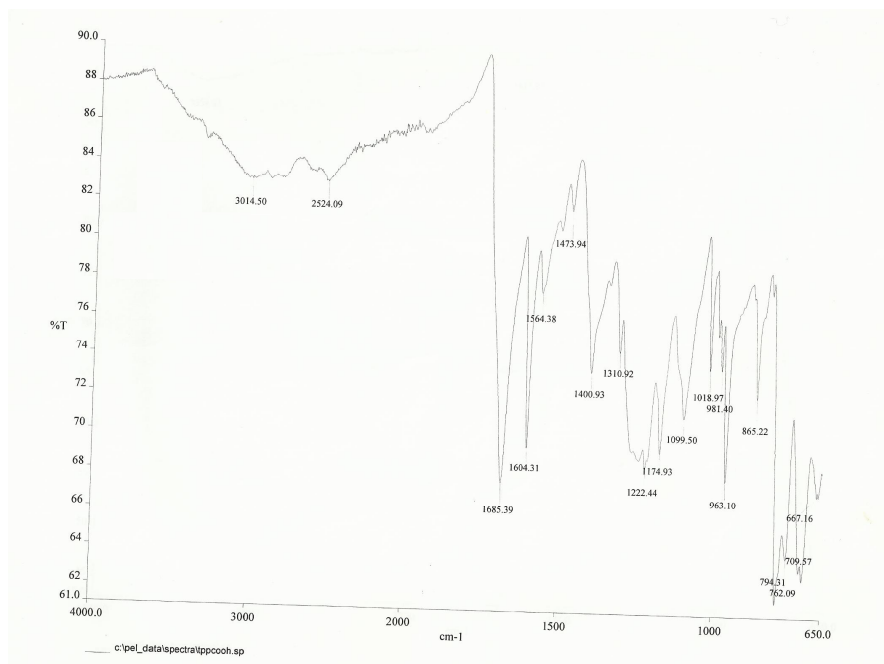
5A-3. UV-vis analysis of the adsorption of Famotidine onto TCPP-TiO₂-A(soxhleted) in the dark. [FAM] = 0.083mM, TCPP-TiO₂-A = 0.031g/100mL, Time = 1h.



5A-4. FT-IR analysis of TCPP-TiO₂-A composite, inset the fingerprint region. This data is presented in Table 5.1 in the main thesis.



5A-5. FT-IR analysis of TCPP-TiO₂-B composite, inset the fingerprint region. This data is presented in Table 5.1 in the main thesis.



5A-6. ATR-IR analysis of TCPP. This data is presented in Table 5.1 in the main thesis.